ERDC/CHL TR-13-7

US Army Corps
of Engineers®
Engineer Research and
Development Center

Hydrodynamic and Salinity Transport Modeling of the Morganza to the Gulf of Mexico Study Area

Tate O. McAlpin, Joseph V. Letter, Jr., Gaurav Savant, and
Fulton C. Carson

August 2013

Coastal and Hydraulics Laboratory

The US Army Engineer Research and Development Center (ERDC) solves the nation's toughest engineering and environmental challenges. ERDC develops innovative solutions in civil and military engineering, geospatial sciences, water resources, and environmental sciences for the Army, the Department of Defense, civilian agencies, and our nation's public good. Find out more at www.erdc.usace.army.mil.

To search for other technical reports published by ERDC, visit the ERDC online library at http://acwc.sdp.sirsi.net/client/default.

ERDC/CHL TR-13-7
August 2013

Hydrodynamic and Salinity Transport Modeling of the Morganza to the Gulf of Mexico Study Area

Tate O. McAlpin, Joseph V. Letter, Jr., and Fulton C. Carson

Coastal and Hydraulics Laboratory
US Army Engineer Research and Development Center
3909 Halls Ferry Road
Vicksburg, MS 39180

Gaurav Savant

Dynamic Solutions, LLC
6421 Deane Hill Drive, Suite 1
Knoxville, TN 37919

Final report

Prepared for US Army Corps of Engineers, New Orleans District
New Orleans, LA 70118-3651

Under Military Interdepartmental Purchase Request (MIPR) W42HEM03376317, dated 1 May 2012

Abstract

This report documents the development of a hydrodynamic and salinity transport model for the Morganza to the Gulf of Mexico study area. The model domain encompasses a significant portion of the Louisiana coastline, extending from Bayou Lafourche (eastern boundary) to the Vermilion Bay (western boundary). This report details the creation of the mesh and all boundary conditions. Also included are model-versus-field comparisons, exhibiting the model's ability to accurately represent the behavior of the system. The validated model (for hydrodynamics and salinity) detailed in this report was utilized to determine approximate base-versus-plan differences for the proposed Morganza to the Gulf of Mexico levee system, including the impacts associated with sea-level rise.

Contents

Figures and Tables

Figures

Tables

Preface

This investigation was conducted for the US Army Engineer District, New Orleans (CEMVN), under Military Interdepartmental Purchase Request (MIPR) W42HEM03376317, "Systemwide Model – TABS Run 3," dated 1 May 2012.

The work was performed during the period of October 2007 through October 2011 by the Coastal and Hydraulics Laboratory, US Army Engineer Research and Development Center (ERDC-CHL), Vicksburg, MS. A portion of the study was performed under contract by Dr. Guarav Savant of Dynamic Solutions, LLC, Knoxville, TN. The work was executed under the general supervision of Dr. William D. Martin, Director, CHL and Jose Sanchez, Deputy Directory, CHL. Direct supervision was provided by Dr. Ty Wamsley, Chief, Flood and Storm Protection Division, HF and Dr. Robert McAdory, Chief of the Estuarine Engineering Branch, HF-E.

The authors would like to acknowledge the contributions made by Amena Henville and Danielle Washington, CEMVN-ED-H, for their efforts in coordinating the logistics of this project at New Orleans District. Henville and Washington organized the data collected by the New Orleans District and provided it to ERDC for use in the validation of the numerical model. The authors also acknowledge the contributions of Elaine Stark, who organized meetings between the modelers and the local sponsors, and also provided the funding for this work.

The authors wish to acknowledge the efforts by Patrick Williams (NOAA) and Ronald Paille (US Fish and Wildlife Service). The previously mentioned members of the Project Delivery Team (and others) provided reviews of the numerical model mesh and model results. These comments were utilized to improve the model results.

COL Jeffrey R. Eckstein was the Commander of ERDC, and Dr. Jeffery P. Holland was the Director.

Unit Conversion Factors

Multiply	By	To Obtain
cubic feet	0.02831685	cubic meters
cubic inches	1.6387064 E-05	cubic meters
cubic yards	0.7645549	cubic meters
degrees (angle)	0.01745329	Radians
Feet	0.3048	Meters
foot-pounds force	1.355818	Joules
Inches	0.0254	Meters
inch-pounds (force)	0.1129848	newton meters
Knots	0.5144444	meters per second
miles (nautical)	1,852	Meters
miles (US statute)	1,609.347	Meters
miles per hour	0.44704	meters per second
Slugs	14.59390	Kilograms
square feet	0.09290304	square meters
square inches	6.4516 E-04	square meters
square miles	2.589998 E+06	square meters
square yards	0.8361274	square meters
Yards	0.9144	Meters

1 Introduction

1.1 Background

In the aftermath of Hurricane Katrina, many new levee systems are being constructed to reduce the risk of flooding induced by hurricane storm surge. One such example is the Morganza to the Gulf of Mexico (MTOG) levee system, shown as a red line shown in Figure 1, which is designed as a hurricane protection system for Terrebonne and Lafourche Parishes. The project will protect over 150,000 people and 130 square miles of saline and freshwater marshes, farmlands, heavy and light industry, residential property, and other developed areas (Project Fact Sheet 2008). New Orleans District (MVN) intends for the Morganza levee system to reduce surge-induced flooding while simultaneously improving the surrounding marshland habitat.

Figure 1. Proposed Morganza to the Gulf of Mexico levee alignment.

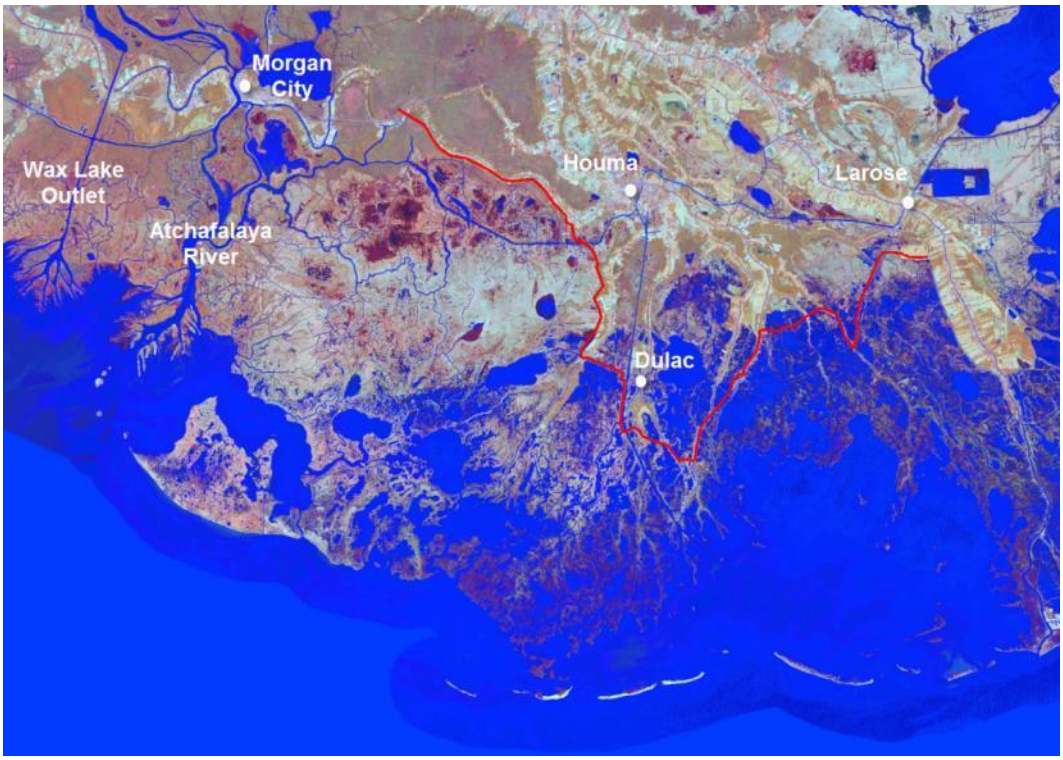

The study area for this project consisted primarily of the areas immediately to the north and south of the proposed levee system. To determine the impacts of the proposed levee system on the study area's

habitat and navigation conditions, MVN requested that the Engineer Research and Development Center (ERDC) perform several numerical model studies to investigate the hydrodynamic and salinity behavior in the MTOG study area. Adaptive Hydraulics (AdH) numerical model studies were previously performed to investigate the proper sizing for the navigation structures to be located along the proposed levee system (McAlpin et al. 2009 and McAlpin et al. 2011). A previous TABS-MDS numerical model study was completed to investigate the impacts of the proposed levee system on the salinity regime for the post-construction system (McAlpin et al. 2012). The primary limitation of these previous model studies was the inability to investigate the impacts of sea-level rise for the pre- and post-construction system. Therefore, a new AdH numerical model capable of investigating hydrodynamics and salinity impacts associated with sea-level rise was developed and validated.

1.2 Objective

The objective of this study was to create and validate a numerical model of the Morganza area for hydrodynamics and salinity transport, and then use the numerical model to investigate the impacts of the proposed levee system on the hydrodynamics and salinity transport in the area of interest. This includes impacts associated with sea-level rise.

1.3 Approach

This report documents the validation of the numerical model that will be applied to investigate the levee system's expected impacts on salinity and circulation in the study area, including the impacts associated with sea-level rise. The available water-surface elevation, discharge, and salinity data used in the model validation are detailed in Chapter 2 with the development of the Adaptive Hydraulics (AdH) numerical model detailed in Chapter 3. The model validation, including model-versus-field comparisons, is included in Chapter 4. The plan alternative configurations are detailed in Chapter 5, and the base-versus-plan comparisons are presented in Chapter 6. The summary and conclusions for the model study are included in Chapter 7.

1.4 Description of project location

The project area is located south of Houma, LA, on the southern coast of the state. The study area includes portions of Terrebonne and Lafourche

Parishes, and consists primarily of waterways, lakes, and marsh areas. The primary inflows to the system are the Atchafalaya River and the Wax Lake Outlet, with lesser inflows from Bayou Lafourche and Bayou Boeuf. The tidal signal for the area comes from the Gulf of Mexico, making it a diurnal, micro-tidal system (~ 2 ft spring tide range). Figure 2 shows the project location in relation to the state of Louisiana.

Figure 2. Project location (image obtained from MVN web page).

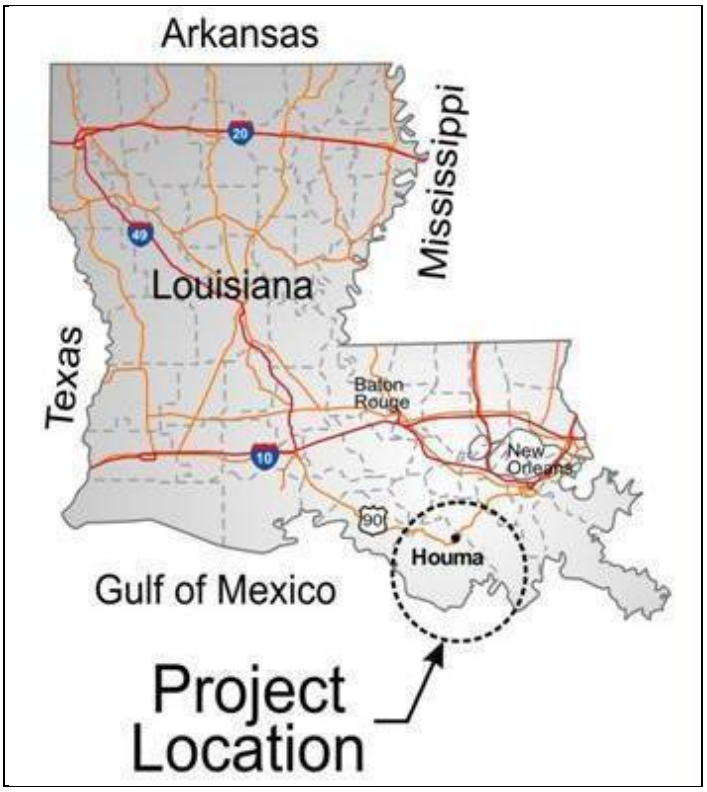

2 Field Data

2.1 Water-surface elevation data

There are ample water-surface elevation (WSE) data for the numerical model validation. The US Geological Survey (USGS) provided data from numerous gages, as listed in Table 1 and shown in Figure 3. This USGS coverage was augmented with additional gages deployed by MVN, as listed in Table 2 and shown in Figure 4. The validation period for the model was 1 January 2004 to 1 January 2005. It should be noted that varying amounts of data were available for gages during the validation period; some gages recorded data for the entire period while others recorded for shorter durations during the observation period. These WSE gages were essential to the hydrodynamic validation of the model.

Table 1. USGS gages.

Gage Description	Gage Longitude	Gage Latitude
Wax Lake Outlet (USGS 07381590)	-91.37278	29.69778
GIWW at Mile 103 (USGS 073816202)	-91.30417	29.64944
Lower Atchafalaya River (USGS 07381600)	-91.20194	29.70250
Bayou Penchant (USGS 073816503)	-91.15528	29.58556
Bayou Boeuf (USGS 073814675)	-91.09972	29.66830
Caillou Lake (USGS 073813479)	-90.92111	29.24917
Caillou Bay (USGS 073813498)	-90.87139	29.07806
Houma Navigation Canal (USGS 07381328)	-90.72972	29.38500
Bayou Grand Caillou (USGS 07381324)	-90.71528	29.38278
GIWW at Houma (USGS 07381331)	-90.71000	29.59806
Bayou Petit Caillou, Upstream (USGS 07381343)	-90.61803	29.38697
Bayou Petit Caillou, Downstream (USGS 07381343)	-90.61803	29.38697
Bayou Terrebonne, Upstream (USGS 073813375)	-90.58778	29.38889
Bayou Terrebonne, Downstream (USGS 073813375)	-90.58778	29.38889

Gage Description	Gage Longitude	Gage Latitude
Company Canal, Lockport (USGS 07381355)	-90.55767	29.62733
Company Canal, Salt Barrier (USGS 07381350)	-90.54472	29.64500
GIWW West of Bayou Lafourche (USGS 07381235)	-90.38083	29.57722

Table 2. MVN gages.

Gage Description	Gage Longitude	Gage Latitude
GIWW West of Minors canal (MG 01)	-90.80661	29.53520
Falgout Canal (MG 02)	-90.79279	29.41628
Bayou Dularge (MG 03)	-90.78622	29.40918
Bayou Grand Caillou (MVN) (MG 04)	-90.76538	29.26600
Houma Navigation Canal (MVN) (MG 13)	-90.73187	29.33399
Cocodrie (MG 06)	-90.66792	29.23324
Bayou Petit Caillou (MG 05)	-90.64756	29.28970
Bush Canal (MG 07)	-90.61771	29.37979
Lake Boudreaux (MG 16)	-90.62372	29.38732
Bayou Terrebonne (MG 08)	-90.58866	29.38745
Madison Bay (MG 15)	-90.54851	29.39785
Humble Canal (MG 09)	-90.56549	29.43782
Pointe Aux Chenes (MG 10)	-90.43497	29.40661
Grand Bayou Canal (MG 11)	-90.40227	29.53359

Figure 3. USGS WSE gage locations (red line indicates proposed levee alignment).

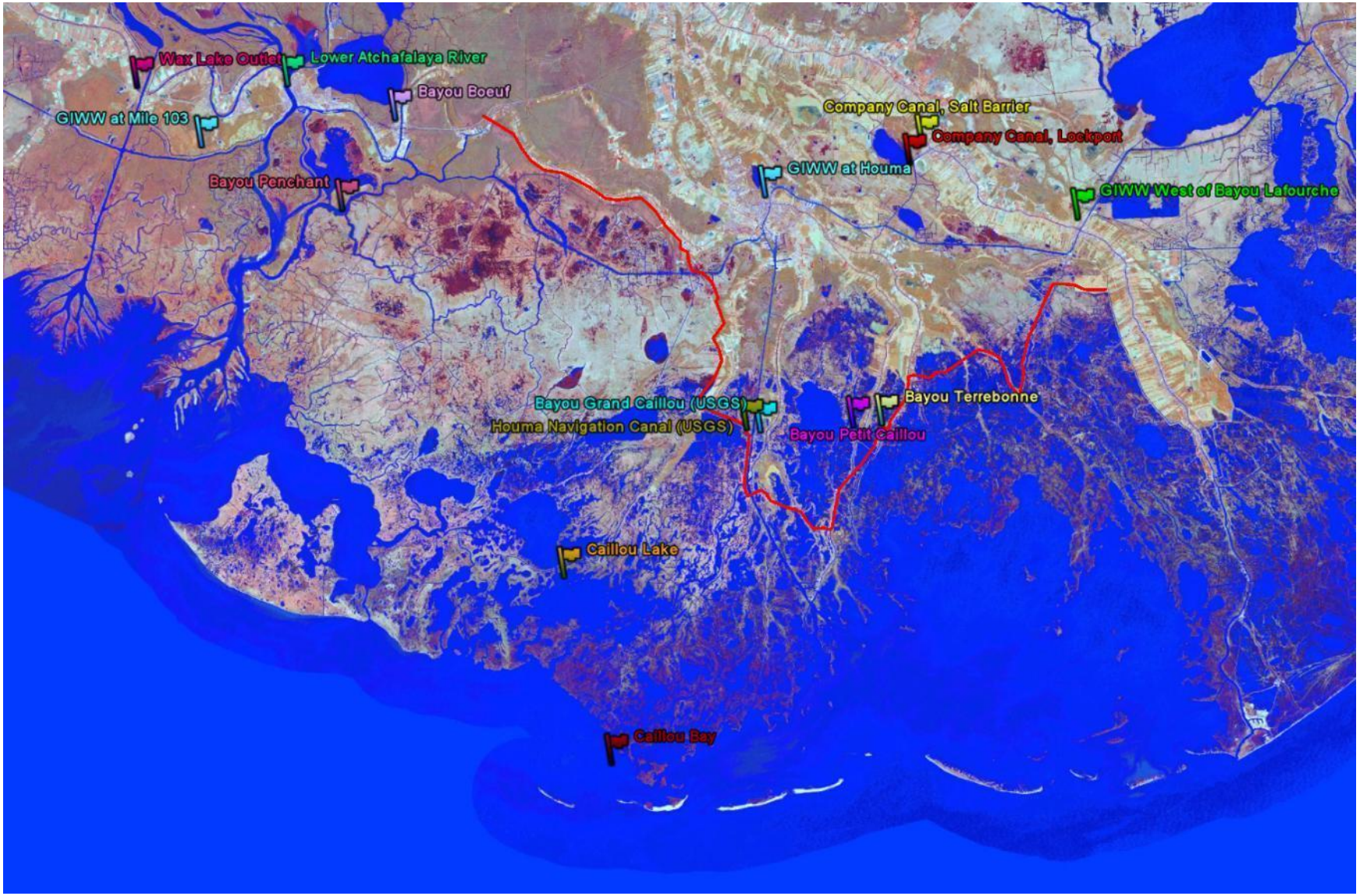

Figure 4. MVN WSE gage locations (red line indicates proposed levee alignment).

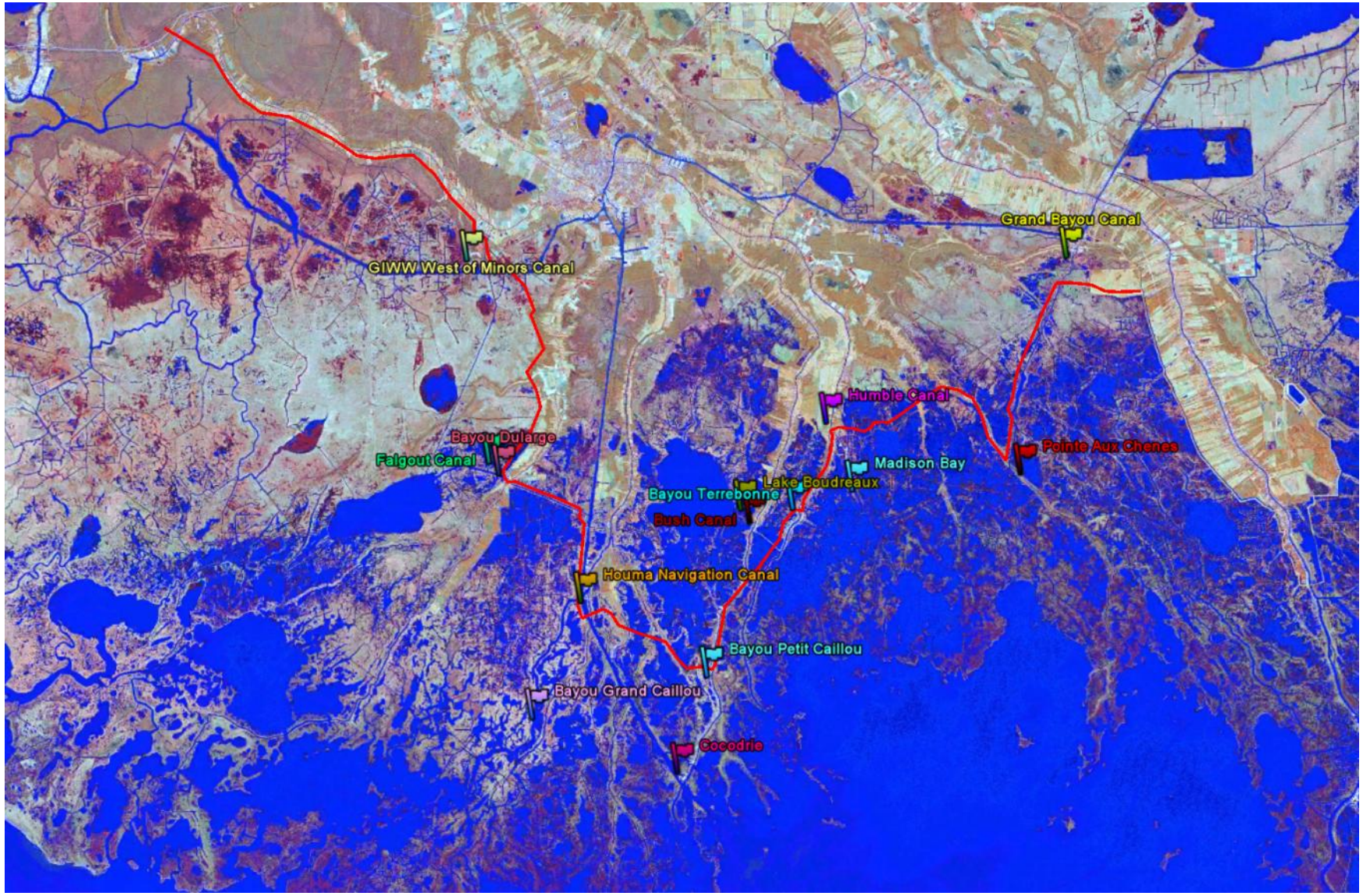

2.2 Discharge data

In addition to the WSE gages, some USGS and MVN discharge measurements (locations listed in Table 3 and shown in Figure 5) were available. Compared to WSE measurements, significantly fewer discharge measurements were available. These discharge measurements were used to validate the flow separation for different areas of the model. As with the WSE gages, a varying amount of data were available to the gages during the validation time period because some gages recorded data for the entire time period and others recorded for shorter durations.

Table 3. Discharge gages.

Gage Description	Gage Longitude	Gage Latitude
Bayou Penchant (USGS 073816503)	-91.15528	29.58560
Houma Navigation Canal (USGS 07381328)	-90.72972	29.38500
Bayou Grand Caillou (USGS 07381324)	-90.71500	29.38281
GIWW at Houma (USGS 07381331)	-90.71000	29.59810
GIWW West of Bayou Lafourche (USGS 07381235)	-90.38083	29.57722
GIWW West of Minors canal (MG 01)	-90.80661	29.53520
GIWW Near Bay Wallace (USGS 073816505)	-91.04528	29.62694

Figure 5. Discharge gage locations (red line indicates proposed levee alignment).

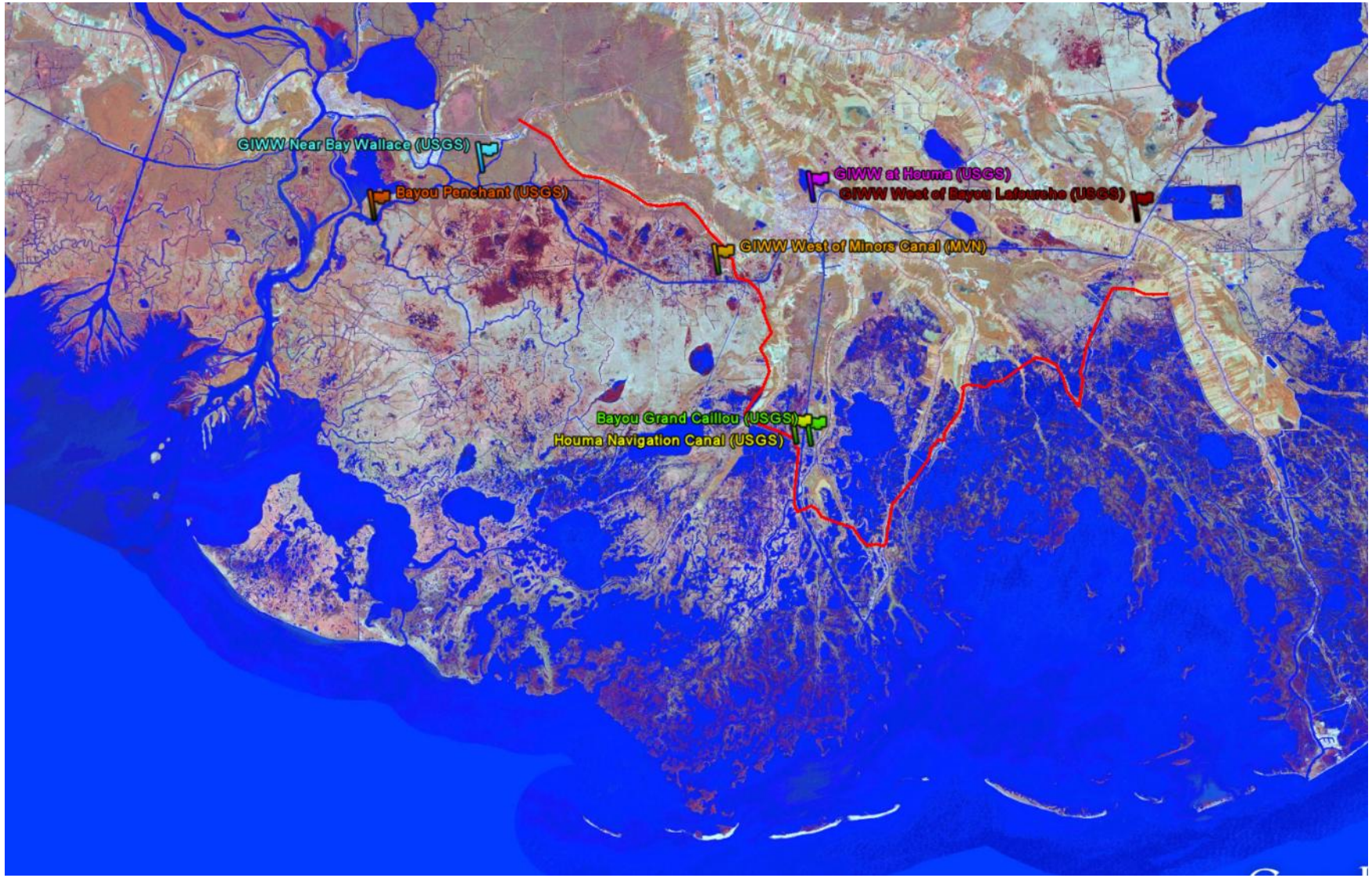

2.3 Salinity data

Salinity data were available from a combination of USGS and MVN gages (locations listed in Table 4 and shown in Figure 6). The salinity coverage is significantly less extensive than the WSE coverage. There is also a much greater occurrence of gaps in the measured data.

Table 4. Salinity gages.

Gage Description	Gage Longitude	Gage Latitude
Caillou Lake (USGS 073813479)	-90.92167	29.25220
Caillou Bay (USGS 073813498)	-90.87139	29.07810
Houma Navigation Canal (USGS 07381328)	-90.72972	29.38500
Bayou Grand Caillou (USGS 07381324)	-90.71500	29.38281
GIWW at Houma (USGS 07381331)	-90.71000	29.59810
Company Canal, Lockport (USGS 07381355)	-90.55767	29.62730
Company Canal, Salt Barrier (USGS 07381350)	-90.54462	29.64491
GIWW West Minors canal (MG 01)	-90.80661	29.53520
Falgout Canal (MG 02)	-90.79279	29.41628
Bayou Dularge (MG 03)	-90.78622	29.40918
Bayou Grand Caillou (MVN) (MG 04)	-90.76538	29.26600
Bayou Petit Caillou (MG 05)	-90.64756	29.28970
Bayou Terrebonne (MG 08)	-90.58866	29.38745
Humble Canal (MG 09)	-90.56549	29.43782
Pointe Aux Chenes (MG 10)	-90.43497	29.40661
Grand Bayou Canal (MG 11)	-90.40227	29.53359

Figure 6. Salinity gage locations (red line indicates proposed levee alignment).

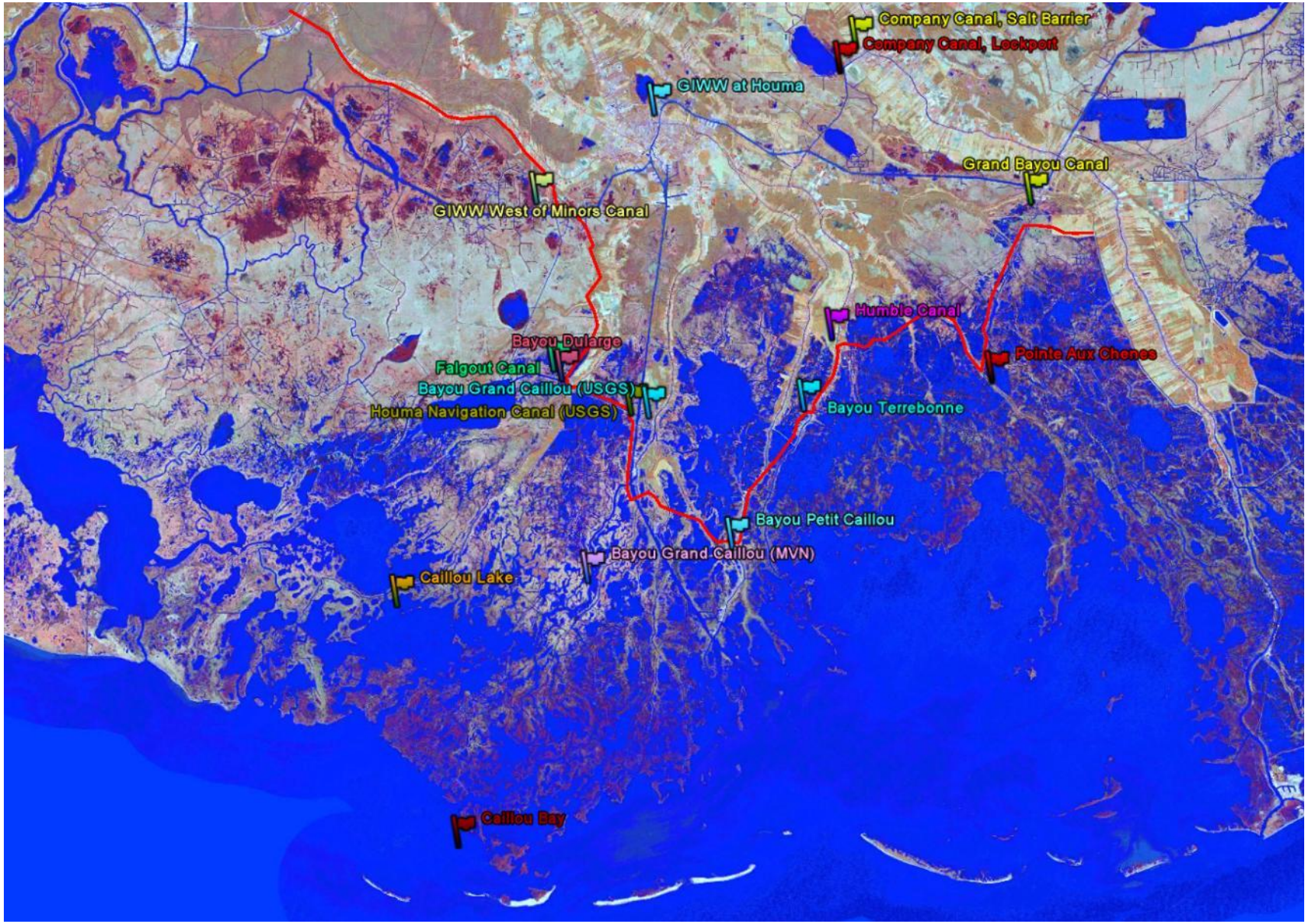

3 Model Development

This modeling study is an additional application of AdH to the numerous ones already completed. AdH has been utilized to study varied phenomena such as dam break (Savant et al. 2010), estuarine circulation (McAlpin et al. 2009; Martin et al. 2010; Tate et al. 2010; McAlpin et al. 2011), riverine flow (Stockstill and Vaughan 2009; Stockstill et al. 2010), and others. A brief discussion of the AdH model is provided in Appendix A, and more information is available at https://adh.usace.army.mil.

Due to the shallowness of the bays and bayous in the system, along with the significant winds common for southern Louisiana, a high degree of mixing is prevalent in the system, resulting in vertical homogeneity for the majority of the study area. Wang (1988) indicated that the Houma Navigational Canal can be partially to highly stratified, but the majority of the data shown in Wang (1988), USACE (2008), and USGS (2008) indicate a partially stratified Houma Navigational Canal, with rare periods of high stratification. McAlpin et al. (2012) performed studies to determine the impact of performing 3D model simulations versus 2D simulations for the Houma Navigational Canal. These sensitivity tests indicated that the stratification was limited in occurrence (temporally), and primarily located in the southernmost extents of the canal. Therefore, the 2D approach was considered adequate for the purpose of determining the impacts of the levee system on the regional salinity regime.

3.1 Mesh development

Several existing numerical model meshes were available, but none included both the required mesh extents and proper resolution. Therefore, a new mesh was created with bathymetry being utilized from a variety of sources. The mesh boundaries were created using high-resolution aerial photography. This allowed the mesh to be created with the elements oriented parallel to the flow pathways, and also allowed the resolution to be reduced for areas that are not channelized (i.e., inside large bays with minimal variation in bathymetry and flat marsh areas that experience wetting/drying). The AdH numerical model mesh was generated using the Surface-water Modeling System, or SMS (Aquaveo 2009). Due to the extensive model domain and numerous small channels, the numerical

model mesh required approximately 325,000 nodes and 650,000 triangular elements to properly resolve the model domain.

The bathymetry data for this numerical model came from a variety of sources. The previous model studies (McAlpin et al. 2009; McAlpin et al. 2011; McAlpin et al. 2012) were used as the bathymetry source for the wetted areas (channels and bays). The ADCIRC (Advanced CIRCulation Model) mesh (sl15v3_2007_r09a) (Cialone et al. 2010) was used for the non-wetted areas, since the previous studies did not include these areas within the model domain. The existing conditions mesh domain and bathymetry are shown in Figure 7.

Figure 7. Existing-conditions mesh domain and bathymetry.

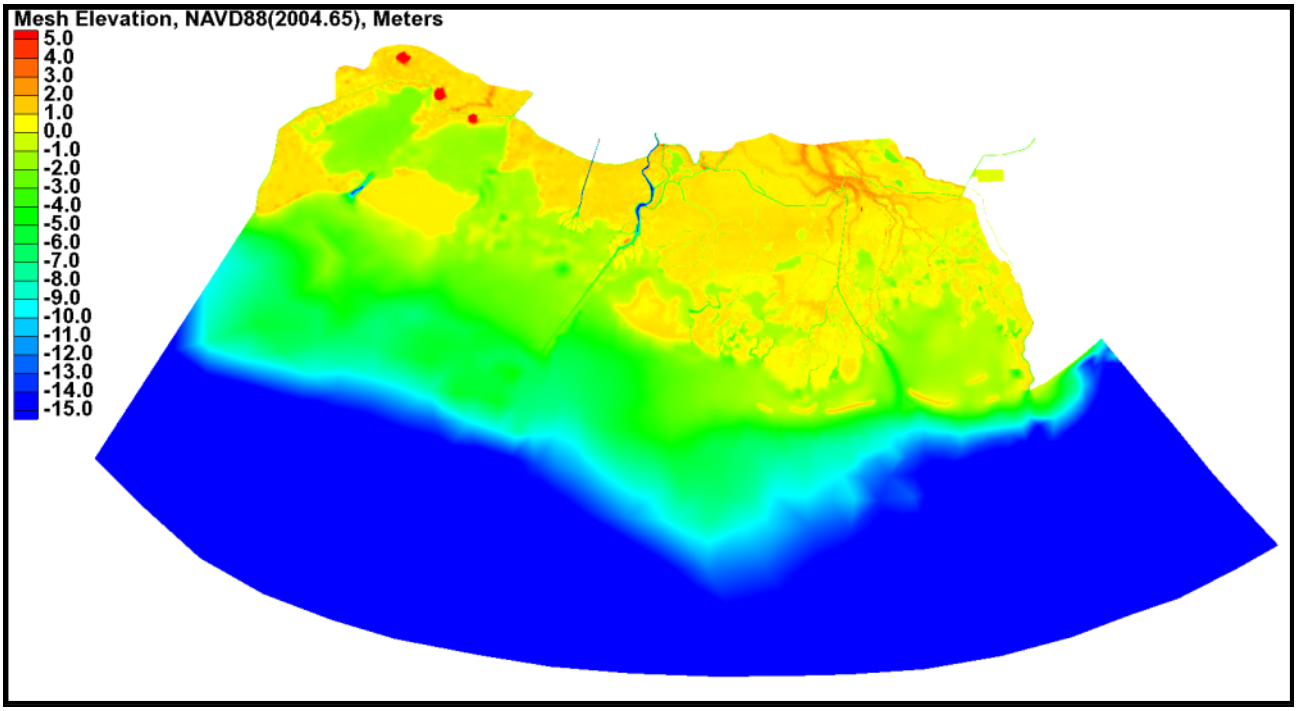

3.2 Boundary conditions development

3.2.1 Tidal boundary

The tidal boundary applied to the model was obtained from the National Oceanic and Atmospheric Administration (NOAA) Port Fourchon gage (Station ID: 8762075). A frequency filter was used to remove any component of the measured signal with a period of less than 4 hours to create a more numerically stable tidal signal. Figure 8 shows a comparison of a pre- and post-filtered signal. The Port Fourchon signal used for the model tidal boundary is shown in Figure 9, with the tidal boundary shown

in Figure 10. The salinity applied at the tidal boundary was a constant 30 parts per thousand (ppt). Water flowing out of the model domain exited with the salinity present for that water, but water entering the model domain at the ocean boundary did so with a salinity of 30 ppt.

Figure 8. Pre- and post-filtered Port Fourchon tidal signal.

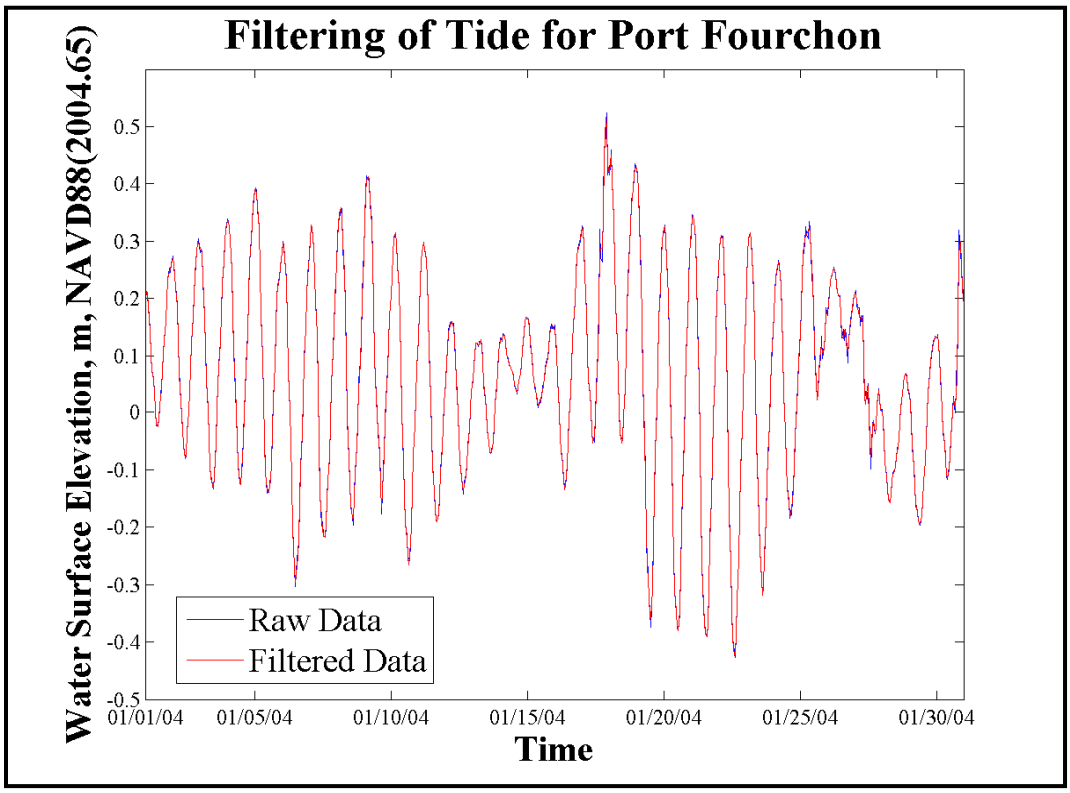

The Gulf of Mexico exhibits certain regional circulation patterns (Blumberg and Mellor 1985; Oey et al. 2005; Sturges et al. 2001; Johnson 2008) that can only be reproduced by including the entire Gulf of Mexico in the model domain. Because this model does not include the entire Gulf of Mexico, the tidal boundary was modified to create the prevalent currents present in the northern Gulf of Mexico as reported by Johnson (2008). The pertinent circulation behavior was accomplished by applying a head difference along the tidal boundary. The head difference along the boundary was a time-varying function since the magnitude and direction of the velocity pattern varies depending on the time of year. The monthly averaged velocity values for January, July, and September are shown in Figure 11 – Figure 13. These values, and additional monthly values from Johnson (2008), were used with Manning's equation to determine a time-varying head difference to be applied along the boundary to create the desired flow patterns (Figure 14). Acceptable results were obtained by

applying 10 % of the head difference to the eastern boundary of the model and the remaining 90 % to the western boundary. A distance-based linear interpolation was used for boundary points between the eastern and western boundaries to prevent any sharp gradients in the tidal boundary specification.

Figure 9. Port Fourchon tide signal.

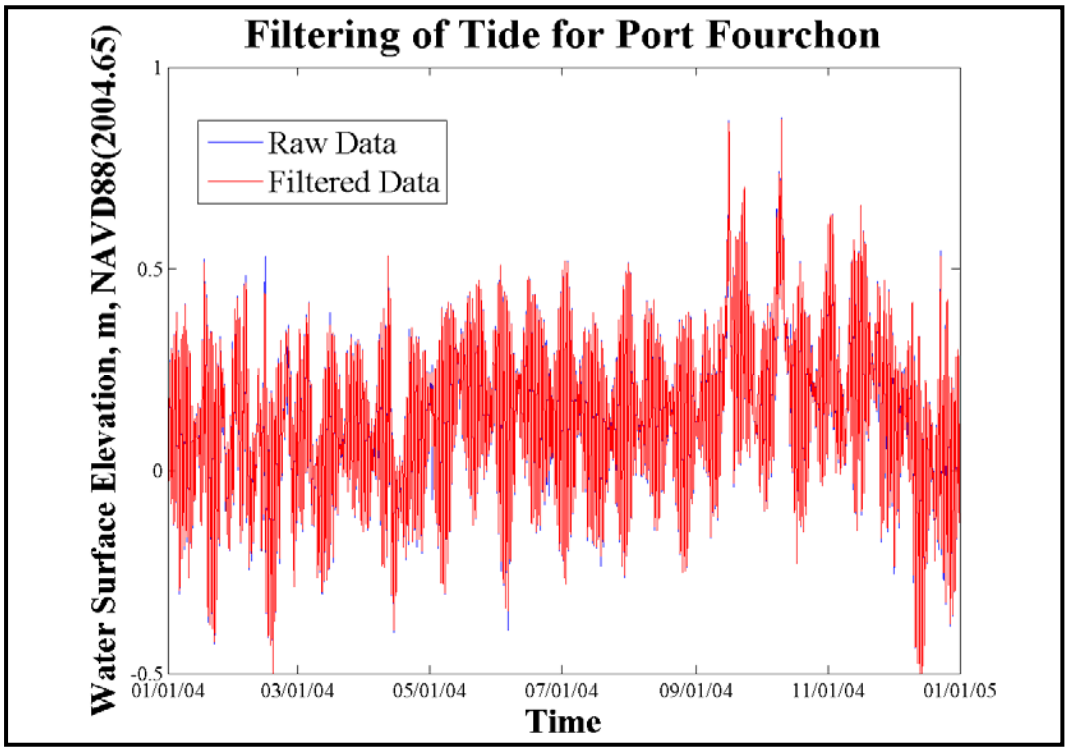

Figure 10. Tidal boundary specification.

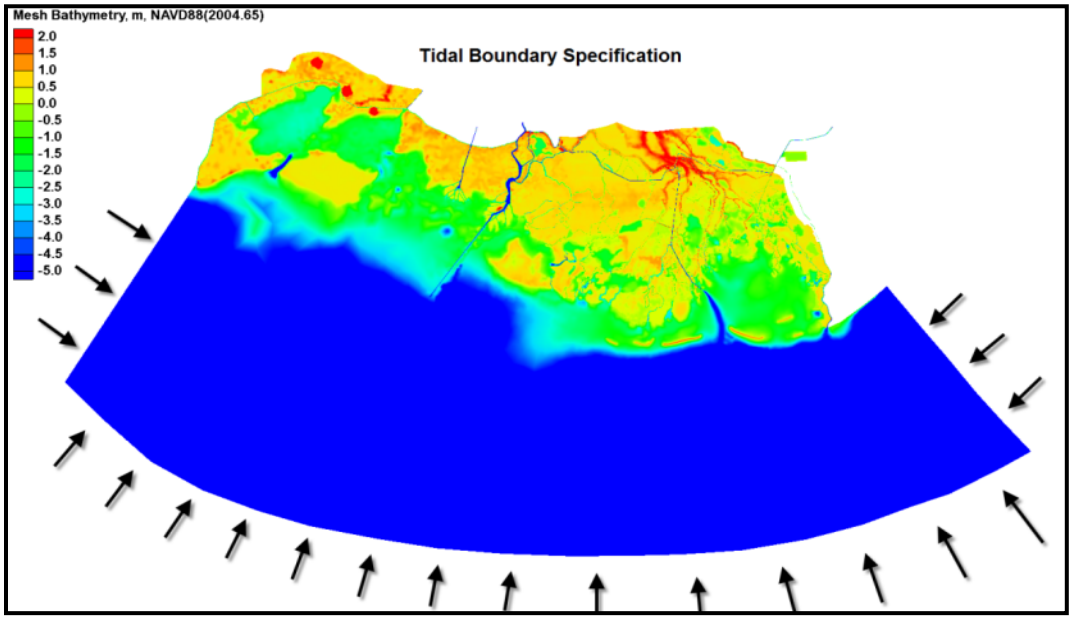

Figure 11. Average currents for the northern Gulf of Mexico for January (Johnson 2008).

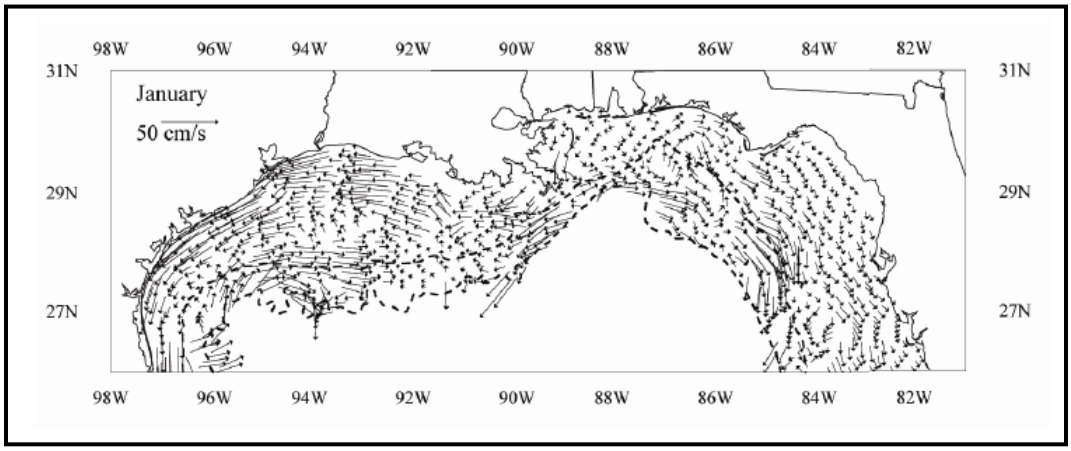

Figure 12. Average currents for the northern Gulf of Mexico for July (Johnson 2008).

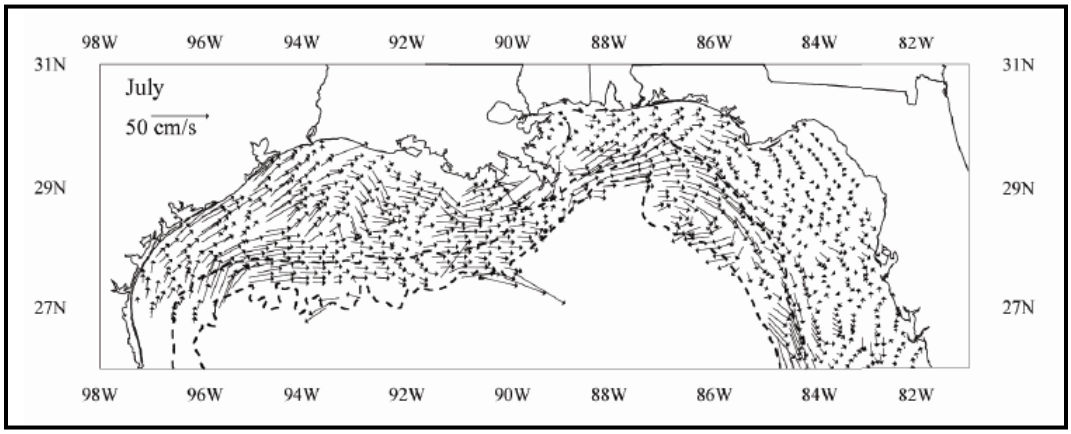

Figure 13. Average currents for the northern Gulf of Mexico for September (Johnson 2008).

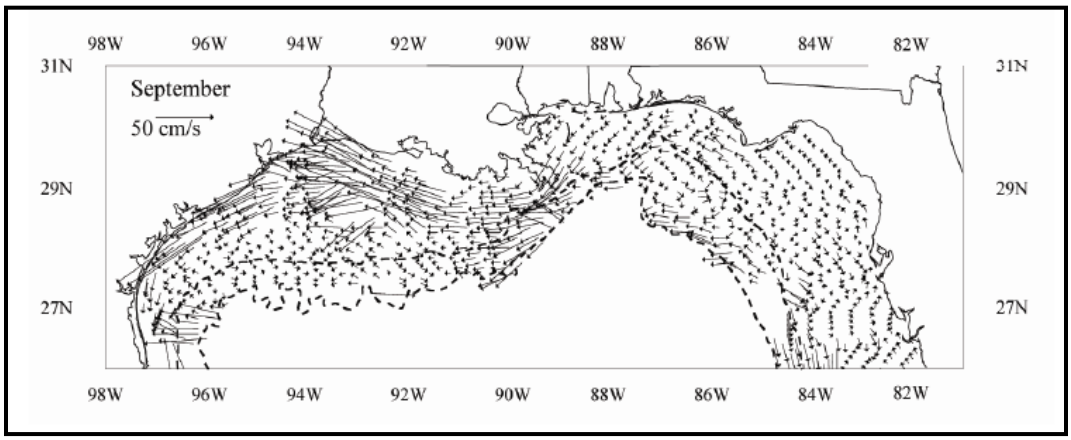

Figure 14. Head difference function applied along the tidal boundary.

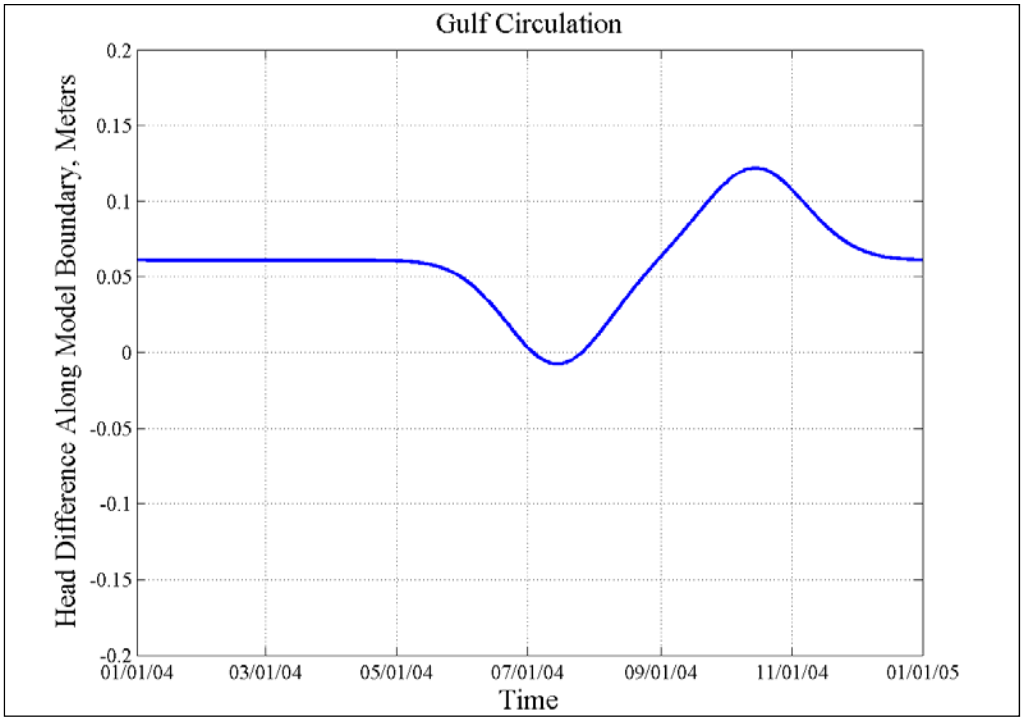

The primary reason for including this phenomenon is to force the freshwater inflow from the Atchafalaya River and Wax Lake Outlet to the west and away from the study area, as occurs in the field. Without this current, the large freshwater inflows dominate the salinity in the system. Therefore, this circulation pattern must be accounted for to obtain accurate salinity results for this area and, thus, a better boundary condition for the interior waters of interest in the study. However, uncertainty in this specification could also explain some of the discrepancies in the salinity validation (see section 4.4).

Another water-level specification was applied for the eastern boundary of the Gulf Intracoastal Waterway (GIWW). This boundary was initially specified using measured discharge values, but due to the introduction of the GIWW at Larose structure as part of the proposed plan conditions and the desire to perform sea-level rise simulations, it was imperative the boundary be extended to the east and specified with a water level using the water level values for the USGS GIWW West of Bayou Lafourche (USGS 07381235) gage, which is at Larose. This specification allows the model to determine the appropriate flow response to the new structure and sea-level rise scenarios, whereas a discharge specification would have forced the given flow through the structure regardless of its size. The location of this water-level specification is shown in Figure 15. A frequency filter was

also applied to this tidal boundary (Figure 16) to remove portions of the signal that have a period of less than 30 hours. A higher cutoff frequency was used for this location (compared to the Gulf of Mexico boundary) to make the flow in/out of this boundary more a function of the water levels in the system than the tidal signal being applied.

Figure 15. GIWW eastern boundary specification (red line indicates model boundary).

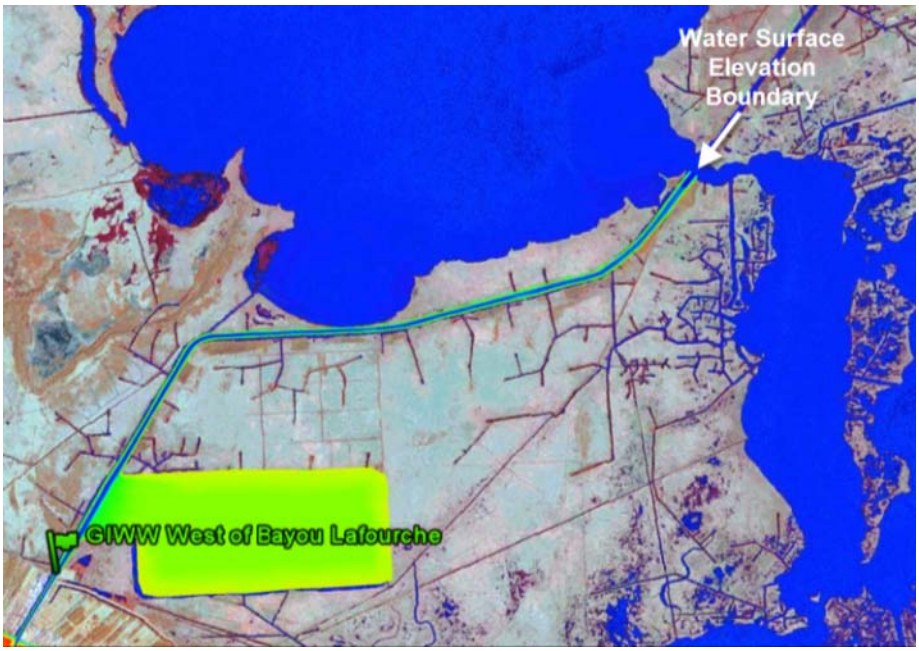

Figure 16. GIWW West of Bayou Lafourche tidal signal for 2004.

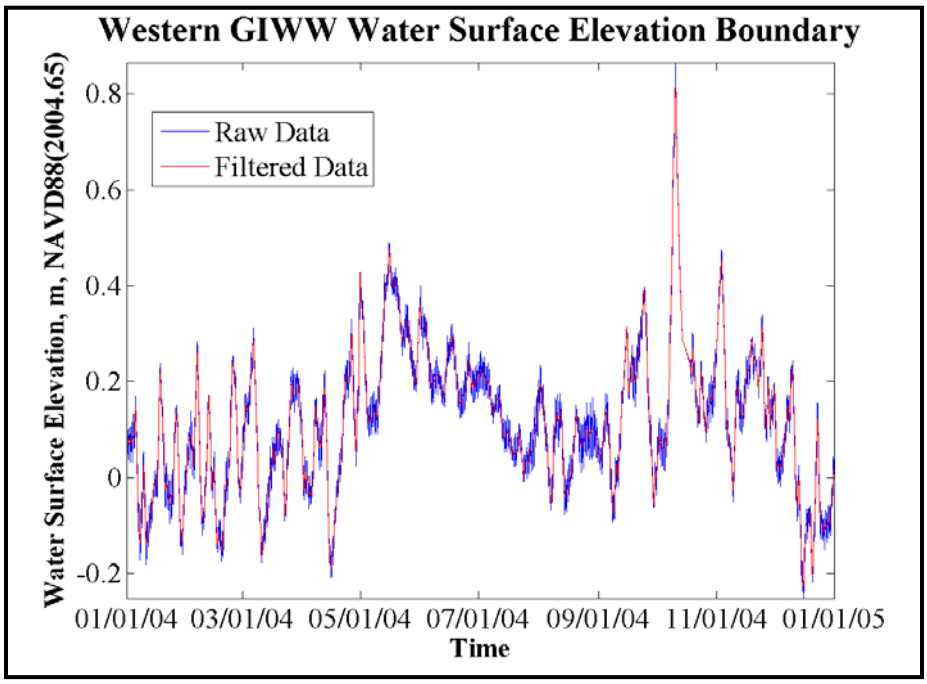

3.2.2 Inflows

The primary freshwater inflows to the system are the Atchafalaya River and the Wax Lake Outlet. Additional smaller inflows (Bayou Boeuf and Bayou Lafourche) were also included in the boundary-condition specification. Inflow locations are shown in Figure 17. The inflow data used to drive the model are shown in Figure 18 and Figure 19. A linear interpolation was performed to fill any gaps in the inflow data. A running-average filter was applied to smooth the values in an effort to reduce the noise in the signal while maintaining the cumulative flow.

Figure 17. Model inflow locations.

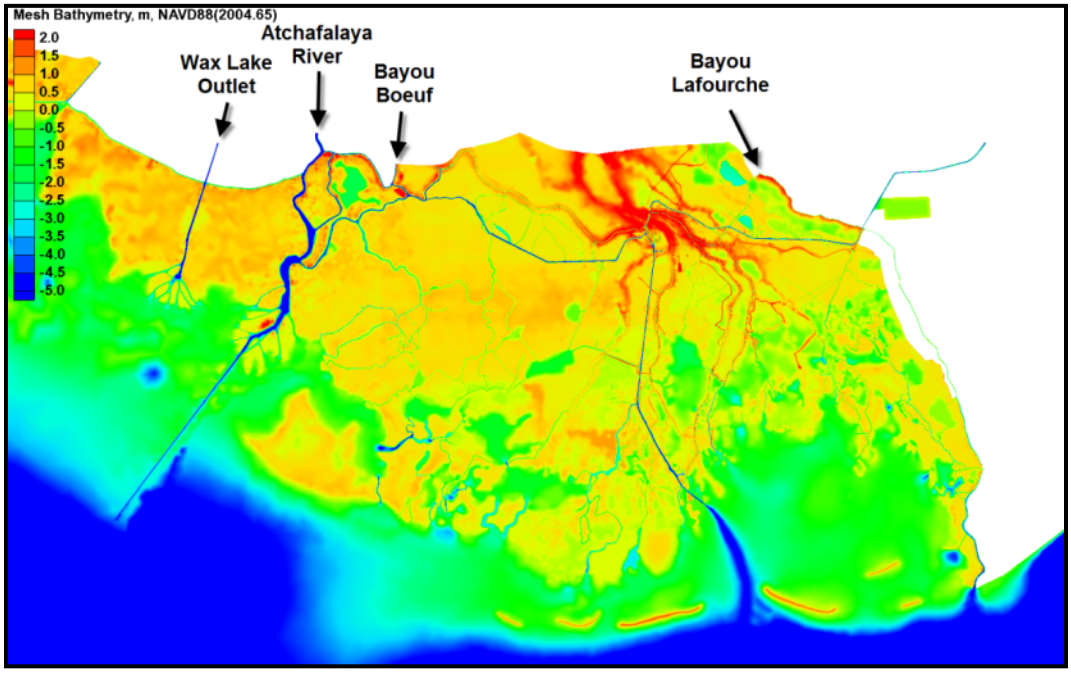

Figure 18. Large inflows for 2004.

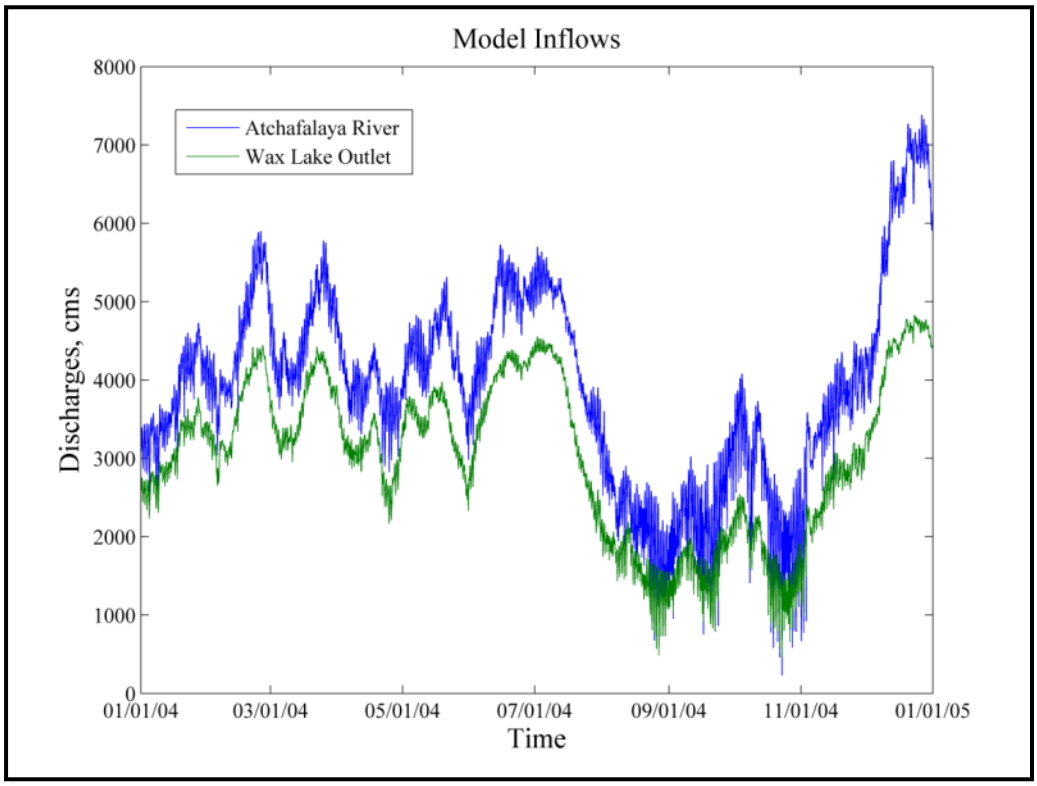

Figure 19. Smaller inflows for 2004.

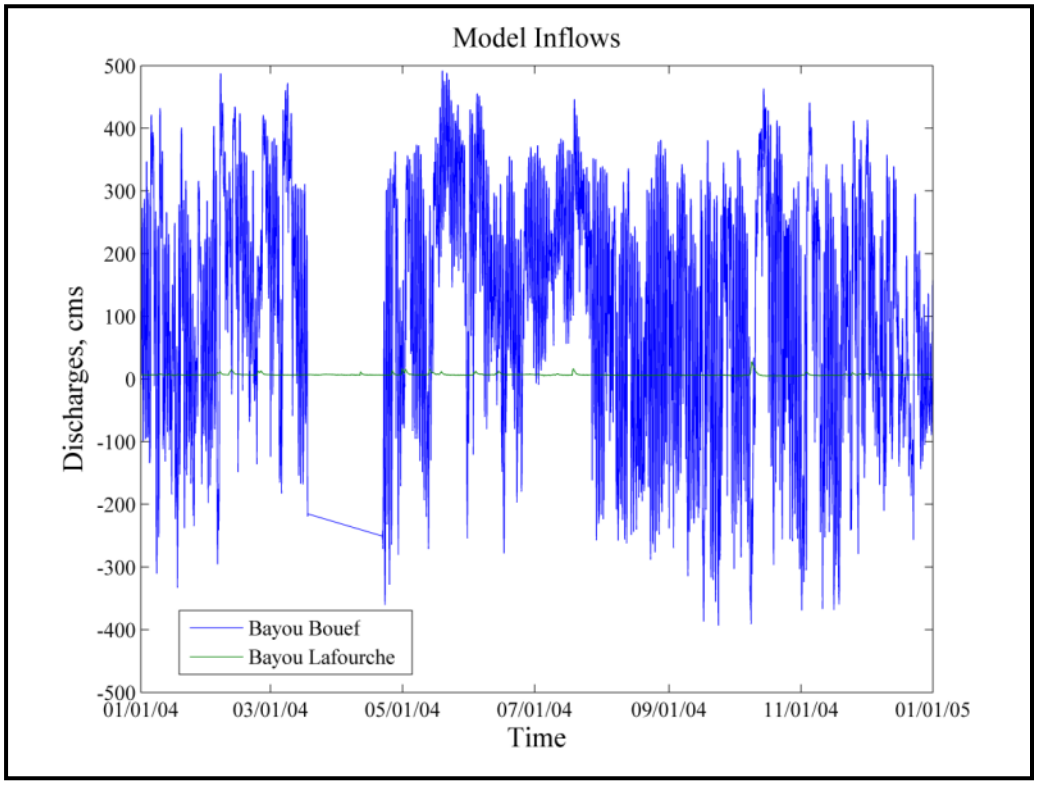

3.2.3 Wind data

The wind data used to drive the model were obtained from the Caillou Bay USGS gage (USGS 073813498), the Houma Navigational Canal USGS gage (USGS 07381328), and the Bayou Petit Caillou USGS gage (USGS 07381343) (locations previously shown in Figure 3). The wind direction and magnitudes were separated into northern (y) and eastern (x) components. These components were interpolated and filtered to remove the portions of the signal that have a period of less than 4 hours in order to reduce noise in the wind signal. Examples of pre- and post-filtered wind components are shown in Figure 20 (positive component values represent toward the east or north).

Figure 20. Pre- and post-filtered wind components for Caillou Bay.

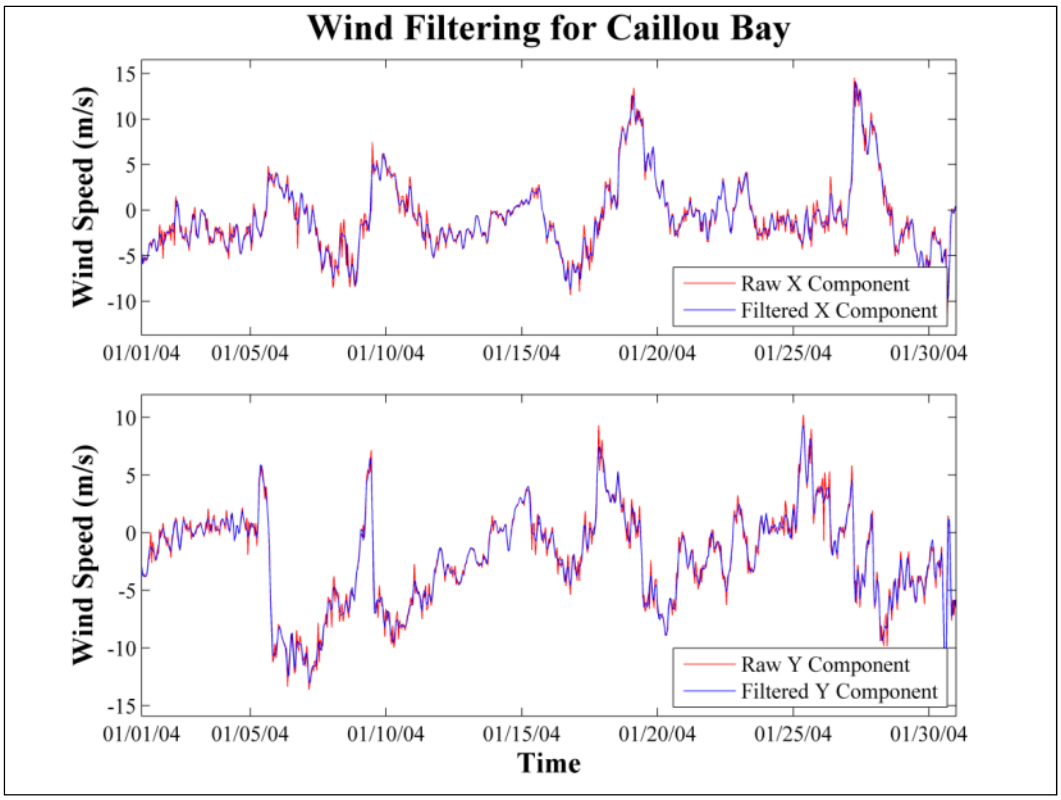

The figure shows a smoothing of the wind signal, resulting in a more numerically stable wind field. The x and y component raw and filtered wind signals for all three USGS gages are presented in Figure 21 – Figure 23.

Figure 21. Raw and filtered wind signal applied in the numerical model for Caillou Bay.

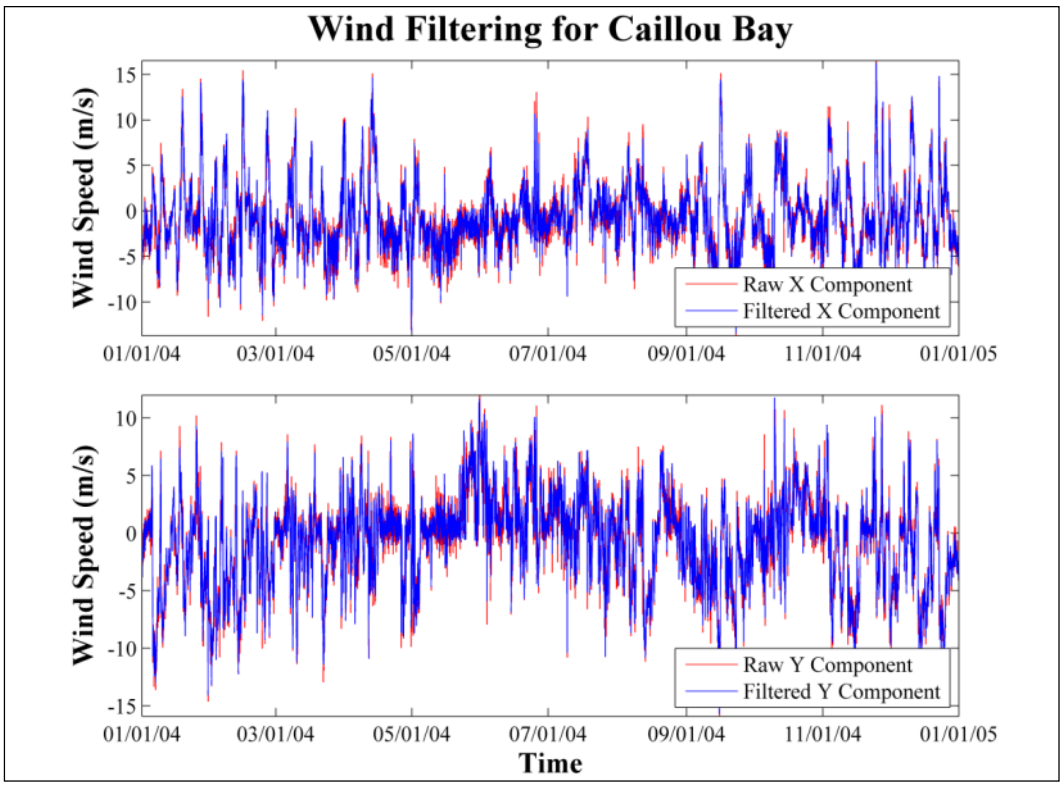

Figure 22. Raw and filtered wind signal applied in the numerical model for the Houma Navigation Canal.

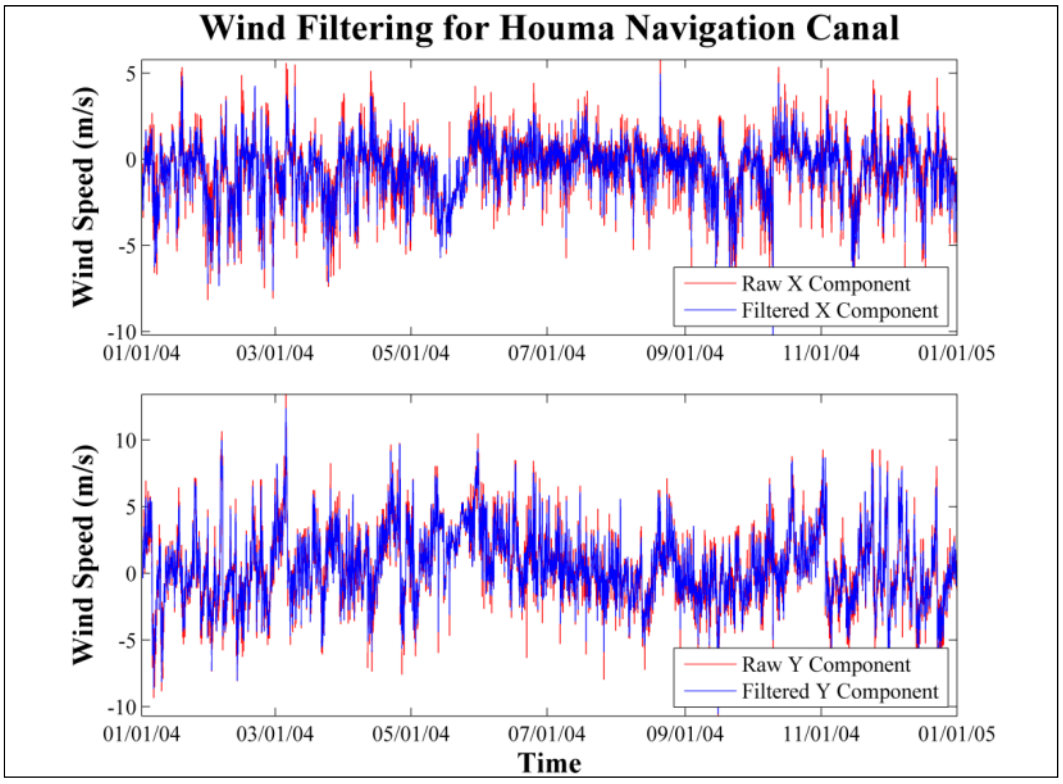

Figure 23. Raw and filtered wind signal applied in the numerical model for Bayou Petit Caillou.

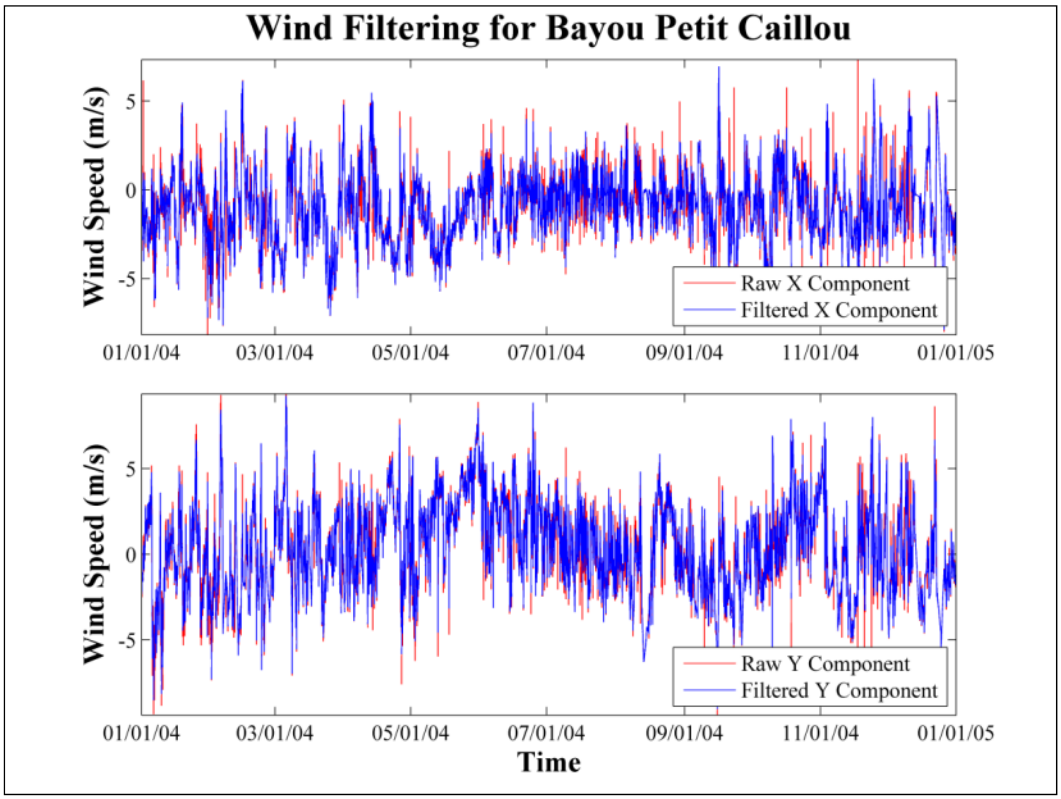

3.3 Computational environment

The numerical modeling was executed on the ERDC High-Performance Computing (HPC) Cray XE6 (Garnet) parallel processing supercomputer. The numerical model meshes contained approximately 325,000 nodes and 650,000 elements. The model was executed on 512 parallel processors and required approximately 4 days of computation time to simulate 1 year of model time. A time step of 500 seconds was used, with the ability to reduce the time step as needed for model stability and model accuracy. The AdH numerical model is significantly faster computationally than the TABS-MDS simulation times reported in McAlpin et al. (2012), which required approximately 1 month to simulate a single year versus approximately 4 days for the AdH model.

4 Model Validation

The purpose of model validation is to ensure that the developed model represents the system adequately for the purpose of making useful comparisons between existing conditions and proposed alternatives. This chapter compares the model results with the WSE, discharge, and salinity data, supporting a conclusion that the model represents the system well.

4.1 Error metrics used in model validation

In an effort to determine a quantitative measure of the model accuracy, certain error metrics were calculated. In the following error metric equations, x represents observed values and y represents model values. N is the total number of values compared and n is a specific value.

One of these metrics was the root mean square error ($RMSE$), which was derived using Equation 1.

$$RMSE = \sqrt{\frac{\sum_{n=1}^{N}(x_n - y_n)^2}{N}} \quad \text{Eq 1}$$

Lower values for $RMSE$ represent a lower error in the model-to-field data comparison, whereas higher values represent a larger error in the model's ability to replicate the field data (McLaughlin et al. 2003). This parameter provides an indication of the average accuracy of the model.

The correlation coefficients were calculated using Equation 2.

$$Correlation\ Coefficient = \frac{N\sum_{n=1}^{N} x_n y_n - \left(\sum_{n=1}^{N} x_n\right)\left(\sum_{n=1}^{N} y_n\right)}{\sqrt{N\left(\sum_{n=1}^{N} x_n^2\right) - \left(\sum_{n=1}^{N} x_n\right)^2}\sqrt{N\left(\sum_{n=1}^{N} y_n^2\right) - \left(\sum_{n=1}^{N} y_n\right)^2}} \quad \text{Eq 2}$$

The correlation coefficient provides a single number that indicates how closely one variable is related to another (Taylor 1997). Values for the correlation coefficients range from +1 to -1, with a value of +1 representing a direct correlation between two data sets.

4.2 Water-surface elevation validation

The model-calculated WSE values were validated through comparison with the data for 1 January 2004 to 1 January 2005. USGS and MVN had numerous WSE gages in and around the study area, as previously shown in Figure 3 and Figure 4. Those gages were of vital importance in the validation process.

Water-surface elevation comparison plots are provided in Appendix B. They consist of year-long time series comparisons for 2004, zoomed comparisons for varying three-month periods (depending on data availability), and model-versus-field box plots. For the box plots, points lying on the 45 degree black line represent an exact replication of the field by the model. Points below the line represent calculated model results below the observed field values, and points above the line represent calculated model results above the observed field values.

Table 5 (USGS) and Table 6 (MVN) include the error metric values discussed in the previous section. These tables also indicate whether a gage location is considered to be within the project study area. If a gage was located within the study area, then additional effort was made to obtain satisfactory comparisons. Gages located outside of the study area were deemed less important given the goals of the modeling effort and, therefore, less-than-ideal comparisons at these locations were not considered to be a cause for concern.

Table 5. USGS WSE metrics.

Gage Description	Correlation Coefficient	Root Mean Square Error, m	Within Primary Area of Interest
Wax Lake Outlet (USGS 07381590)	0.95	0.13	No
GIWW at Mile 103 (USGS 073816202)	0.87	0.11	No
Lower Atchafalaya River (USGS 07381600)	0.86	0.17	No
Bayou Penchant (USGS 073816503)	0.84	0.08	No
Bayou Boeuf (USGS 073814675)	0.81	0.09	No
Caillou Lake (USGS 073813479)	0.82	0.11	Yes
Caillou Bay (USGS 073813498)	0.85	0.12	No
Houma Navigation Canal (USGS 07381328)	0.86	0.08	Yes
Bayou Grand Caillou (USGS 07381324)	0.86	0.07	Yes
GIWW at Houma (USGS 07381331)	0.85	0.07	Yes
Bayou Petit Caillou, Upstream (USGS 07381343)	0.83	0.09	Yes

Gage Description	Correlation Coefficient	Root Mean Square Error, m	Within Primary Area of Interest
Bayou Petit Caillou, Downstream (USGS 07381343)	0.87	0.08	Yes
Bayou Terrebonne, Upstream (USGS 073813375)	0.86	0.09	Yes
Bayou Terrebonne, Downstream (USGS 073813375)	0.87	0.09	Yes
Company Canal, Lockport (USGS 07381355)	0.84	0.08	No
Company Canal, Salt Barrier (USGS 07381350)	0.84	0.08	No
GIWW West of Bayou Lafourche (USGS 07381235)	0.92	0.05	Yes

Table 6. MVN WSE metrics.

Gage Description	Correlation Coefficient	Root Mean Square Error, ft	Within Primary Area of Interest
GIWW West of Minors Canal (MG 01)	0.84	0.06	Yes
Falgout Canal (MG 02)	0.88	0.08	Yes
Bayou Dularge (MG 03)	0.88	0.07	Yes
Bayou Grand Caillou (MVN) (MG 04)	0.82	0.09	Yes
Houma Navigation Canal (MVN) (MG 13)	0.84	0.08	Yes
Cocodrie (MG 06)	0.90	0.08	Yes
Bayou Petit Caillou (MG 05)	0.91	0.08	Yes
Bush Canal (MG 07)	0.84	0.08	Yes
Lake Boudreaux (MG 16)	0.66	0.14	Yes
Bayou Terrebonne (MG 08)	0.87	0.09	Yes
Humble Canal (MG 09)	0.86	0.09	Yes
Madison Bay (MG 15)	0.86	0.07	Yes
Pointe Aux Chenes (MG 10)	0.79	0.09	Yes
Grand Bayou Canal (MG 11)	0.89	0.06	Yes

The model tide range for Lake Boudreaux (Figure 24) is significantly lower than that observed in the field. Upon further analysis, it was observed that the field data indicated a larger tide range for Lake Boudreaux than for the surrounding areas. The Lake Boudreaux, Bayou Petit Caillou, Houma Navigation Canal, and Bayou Grand Caillou gages (shown in Figure 25) had continuous data for 20 February 2004 to 27 May 2004. The average tide ranges over this time period were 0.25 m for Lake Boudreaux, 0.16 m for Bayou Petit Caillou; 0.15 m for the Houma Navigation Canal; and 0.11 m for Bayou Grand Caillou. Since Bayou Grand Caillou and Bayou Petit Caillou are the two primary means for flow to enter Lake Boudreaux, it is hypothesized that the tide measurements in Lake Boudreaux are overestimated in the field observations. Bayou Petit Caillou and Lake

Boudreaux are separated by less than 0.75 km, making this significant increase in tide range for Lake Boudreaux unlikely.

Figure 24. Lake Boudreaux WSE comparison plot.

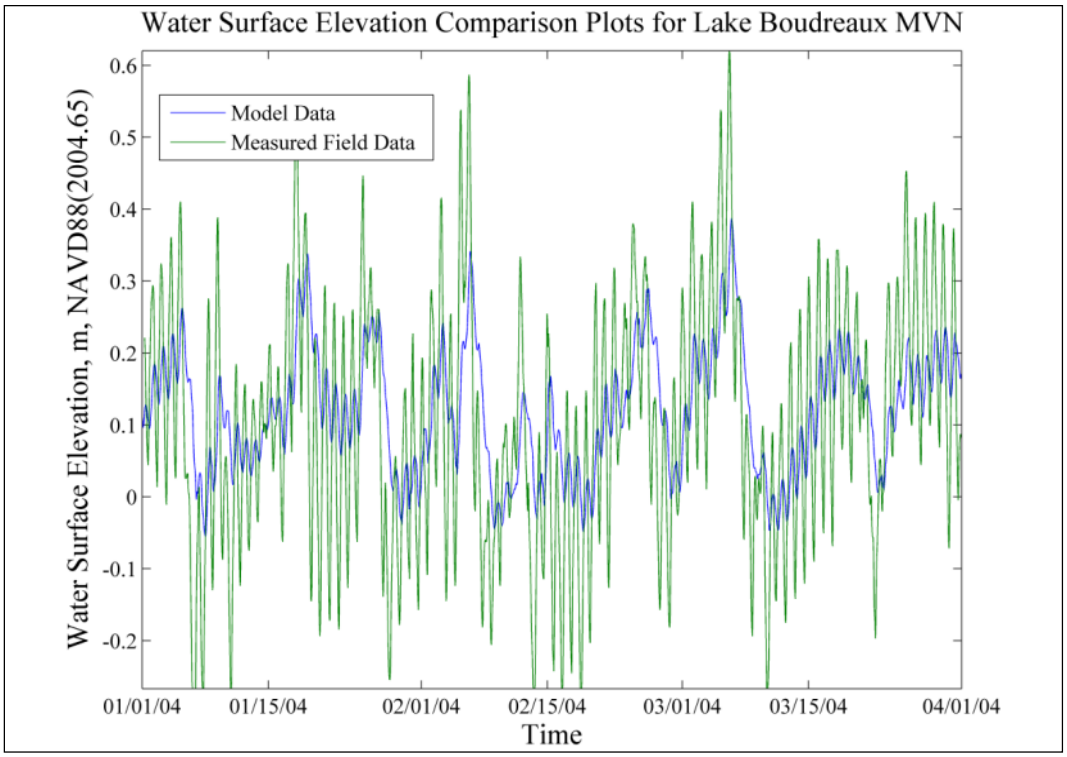

Figure 25. Location of gages near Lake Boudreaux.

The beginning and end of 2004 consist of several frontal passage events. These more extreme events consist of large increases and decreases (several tenths of a meter) in the water-surface elevations over short time periods, and therefore are extremely challenging to model. The numerical model replicates the occurrence of these events, but the magnitudes of the individual events are sometimes slightly over/under estimated. The magnitude of these events and the accuracy with which the model replicates them can be observed in Figure 26 – Figure 28, with additional examples in Appendix B. These comparisons illustrate an adequate replication of the observed values in the model given the numerous phenomena (wind data, bathymetry data, topography data, wetting/drying, etc.) that impact the water-surface elevations observed in the field. The accuracy of the model is also exemplified in the root mean square errors (average value of 0.09 m and median value of 0.08 m) and the correlation coefficients (average value of 0.85 and median value of 0.86) for the gages located within the study area (see Table 5 and Table 6).

Figure 26. GIWW at Houma WSE comparison plot.

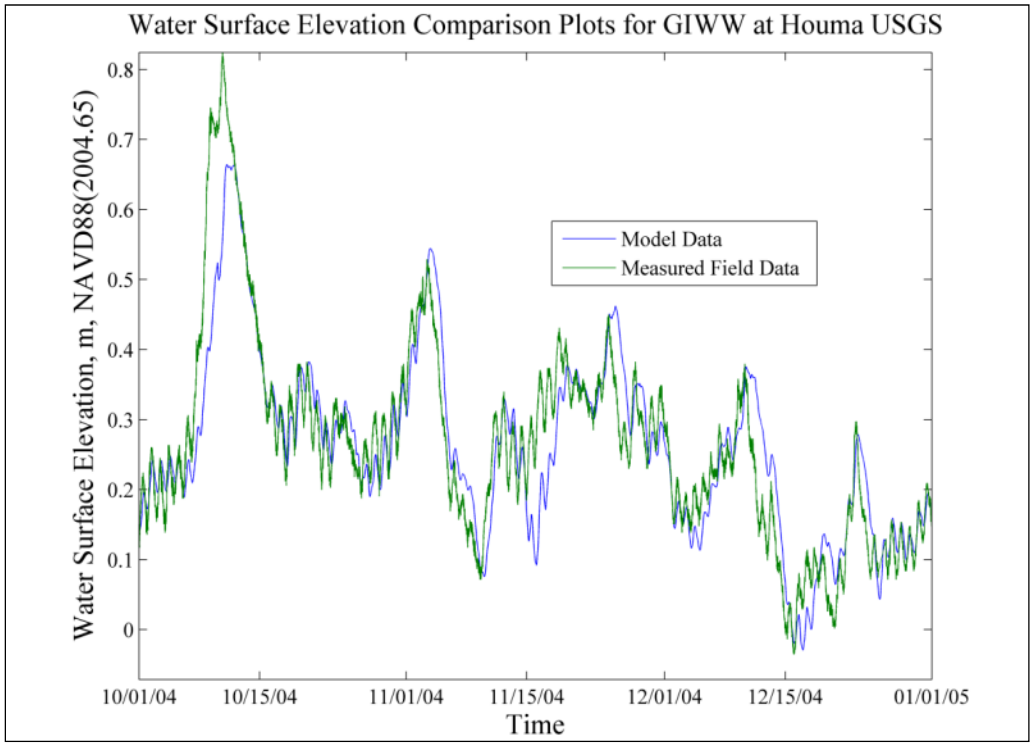

Figure 27. Falgout Canal WSE comparison plot.

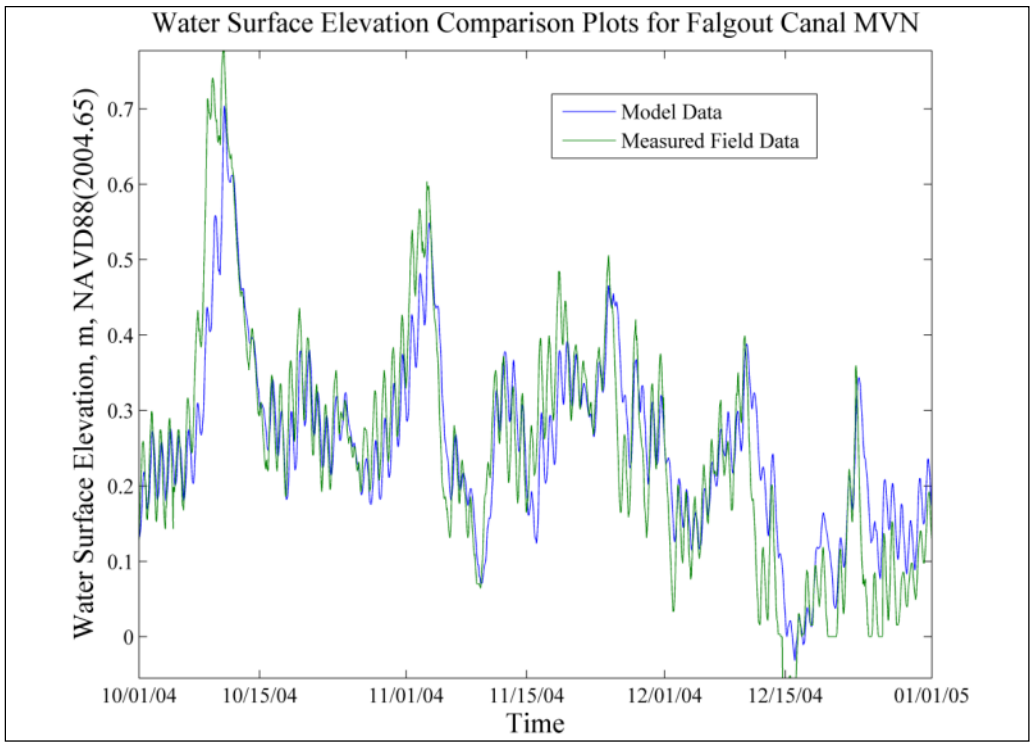

Figure 28. Madison Bay WSE comparison plot.

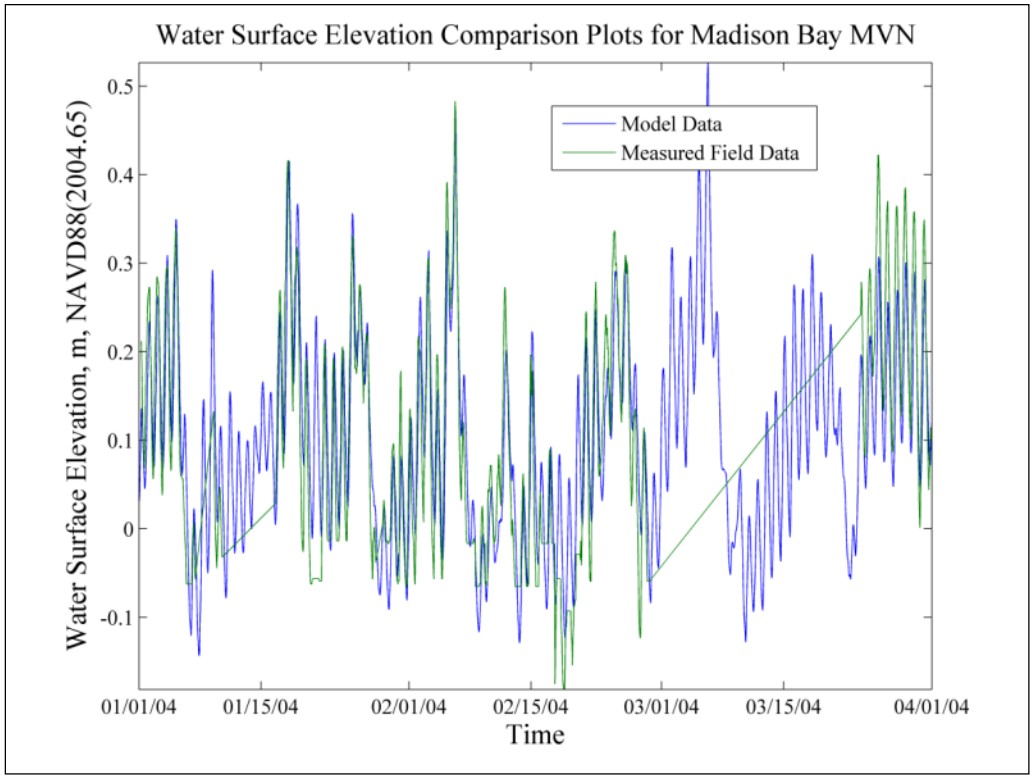

4.3 Discharge validation

Model discharge was validated through comparisons with the measured discharge from 1 January 2004 to 1 January 2005. The measurement locations were shown and discussed in Chapter 2. The discharge comparison plots are provided in Appendix C. Similar to the water-surface elevations, the discharge comparison plots consist of year-long time series comparisons, comparison plots for varying three-month periods (depending on data availability), and box plot comparisons that include data for the entire 2004 calendar year. Table 7 provides a list of the error metrics and an indication of whether a gage location was considered to be within the primary model study area. Inherently, there is a larger uncertainty in discharge measurements than WSE measurements, so the observed-versus-field discharge comparisons are not expected to be as favorable as the WSE comparisons.

Table 7. Discharge comparison error metrics.

Gage Description	Correlation Coefficient	Root Mean Square Error, cms	Mean Field Discharge, cms	Mean Model Discharge, cms	Within Primary Area of Interest
Bayou Penchant (USGS 073816503)	0.68	48	93	77	No
Houma Navigation Canal (USGS 07381328)	0.90	81	112	63	Yes
Bayou Grand Caillou (USGS 07381324)	0.70	6	2	2	Yes
GIWW at Houma (USGS 07381331)	0.60	39	43	56	Yes
GIWW West of Bayou Lafourche (USGS 07381235)	0.65	54	45	64	Yes
GIWW West of Minors Canal (MG 01)	0.78	121	-30	-146	Yes
GIWW Near Bay Wallace* (USGS 073816505)	0.42	43	189	206	No

*The correlation coefficient and root mean square error for GIWW Near Bay Wallace were determined using daily averaged field measurements (and corresponding model daily averaged values) instead of the more frequent measurements utilized for the other gages. This was done as more frequent measurements were unavailable for the GIWW Near Bay Wallace gage.

The GIWW West of Minors Canal comparison plot (Figure 29) shows the right trend but with a vertical offset in the values. In an effort to determine if the comparisons are indicative of a problem with the model or with the observed measurements, a flow analysis was performed.

Figure 29. GIWW West of Minors Canal discharge comparison.

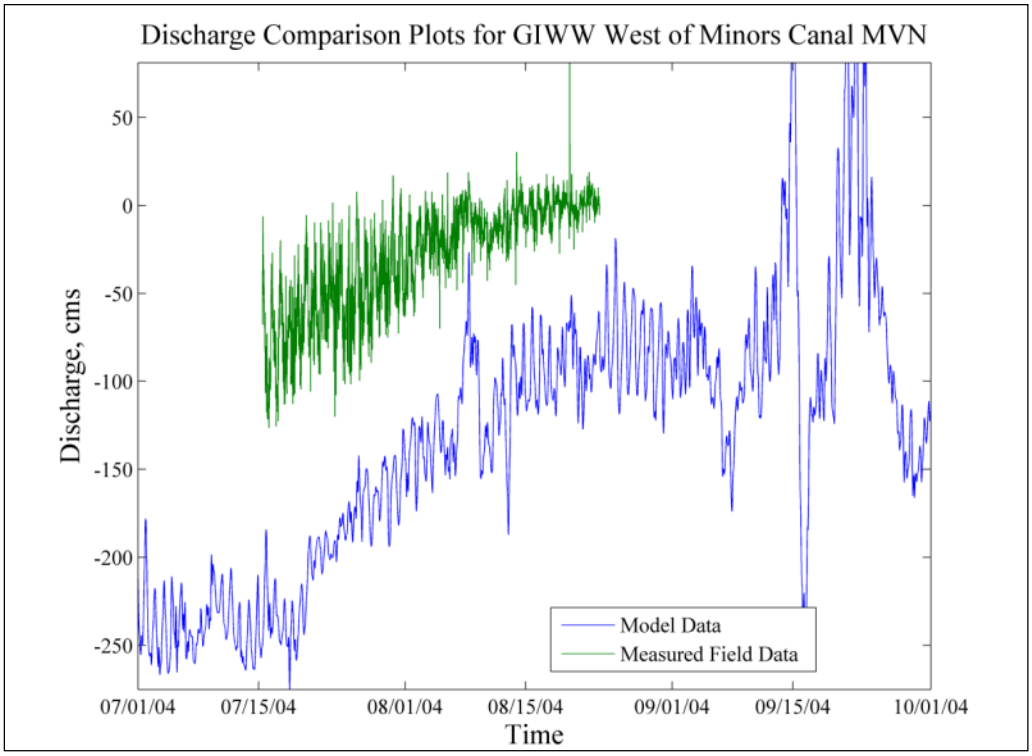

The gages shown in Figure 30 should capture the flow separation occurring at the confluence of the Houma Navigation Canal and the GIWW. Other channels are connected to these larger waterways, but most of the flow should be in the GIWW and Houma Navigation Canal. Therefore, an analysis assuming conservation of mass can be applied to determine if there is a significant error in the observed discharge measurements. Since the GIWW West of Minors Canal gage only had a subset of data for the entire year, the analysis was only performed for data observed during that time period (17 July 2004 to 21 August 2004). The blue arrows in Figure 30 indicate the dominant flow directions for the given locations. Flow toward the northeast at the GIWW at Houma location plus flow toward the south at the Houma Navigation Canal location should be approximately equal to the eastward flow at the GIWW West of Minors Canal location. Using the average discharges for the observed field data from 17 July 2004 to 21 August 2004, the flow in at the GIWW West of Minors Canal location was 30 cubic meters per second (cms), with the total flow out (GIWW at Houma plus Houma Navigation Canal) being almost 156 cms. This would indicate a significant unaccounted-for source of water (~126 cms) which is unlikely. Therefore, the GIWW West of Minors Canal observations are viewed with much skepticism. The favorable correlation coefficient value would indicate that

the magnitude of the observed measurements should be increased, but without additional information the factor of increase could not be definitively determined.

Figure 30. Residual flow directions for discharge gages on the GIWW and Houma Navigation Canal.

The model does a good job reproducing the mean-flow measurement at Bayou Penchant, Bayou Grand Caillou, GIWW at Houma, GIWW at Bayou Lafourche and GIWW at Bay Wallace (Table 7). The Houma Navigation Canal (Figure 31), Bayou Grand Caillou (Figure 32), GIWW at Houma (Figure 33) and GIWW West of Bayou Lafourche (Figure 34) discharge measurements are influenced by the passage of several frontal events. The field data for these events include large increases/decreases in the field measurements. These events are replicated adequately in the Houma Navigation Canal (Figure 31) and Bayou Grand Caillou (Figure 32)

locations, but less so at the GIWW at Houma (Figure 33) and GIWW West of Bayou Lafourche (Figure 34) locations.

Figure 31. Houma Navigation Canal discharge comparison.

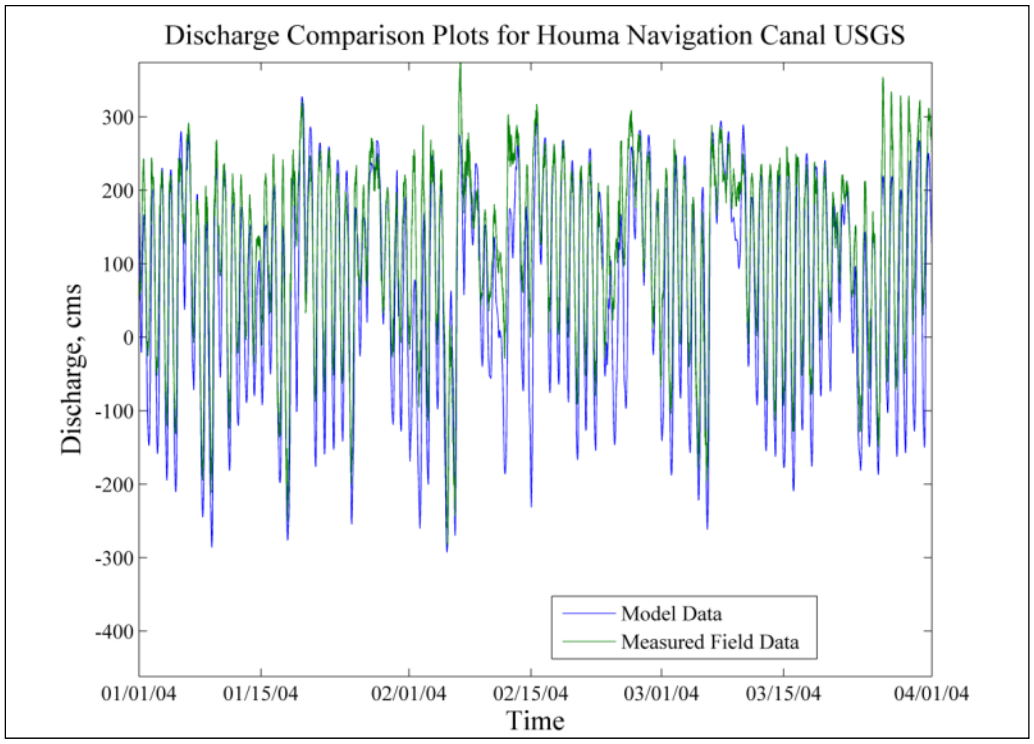

Figure 32. Bayou Grand Caillou discharge comparison.

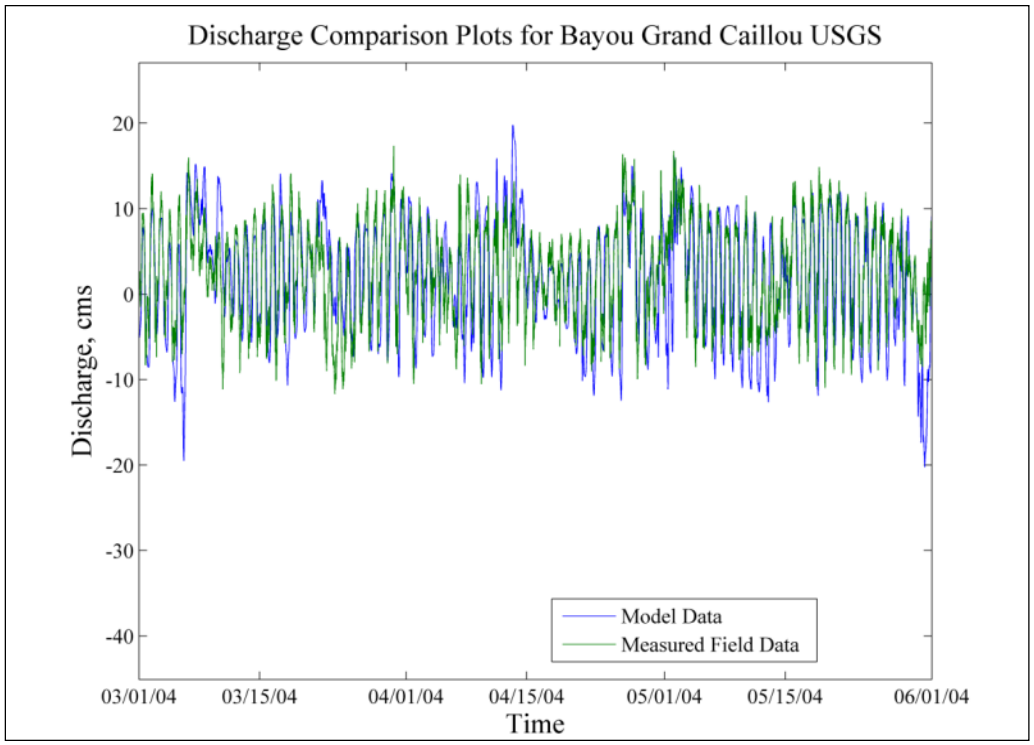

Figure 33. GIWW at Houma discharge comparison.

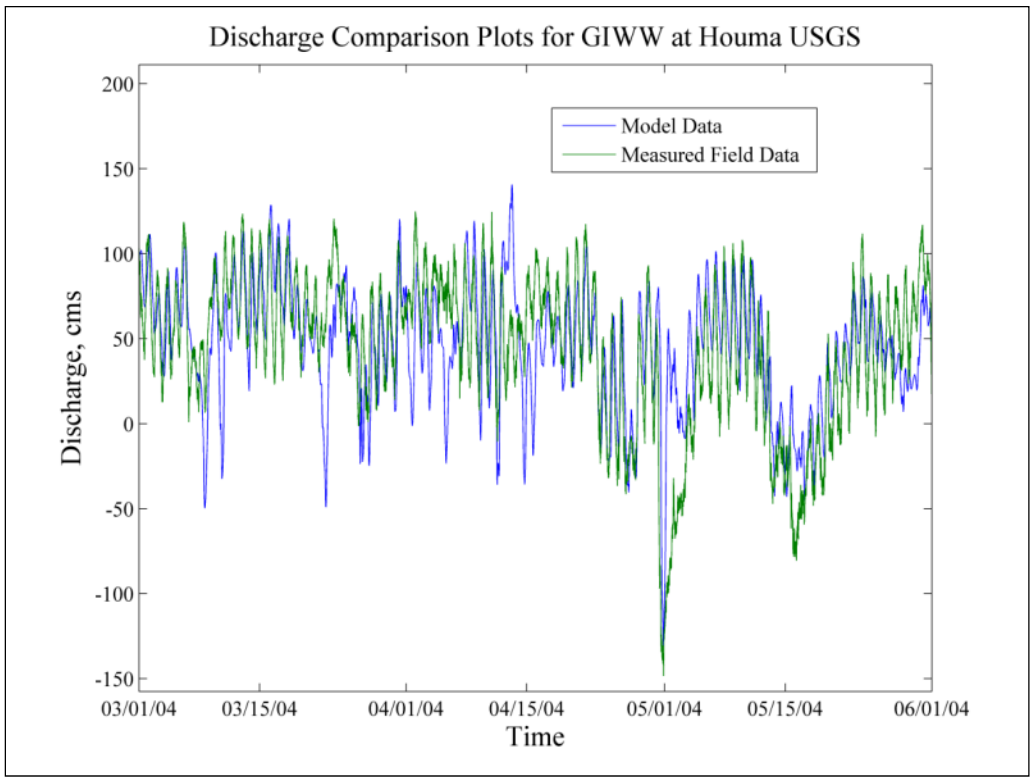

Figure 34. GIWW West of Bayou Lafourche discharge comparison.

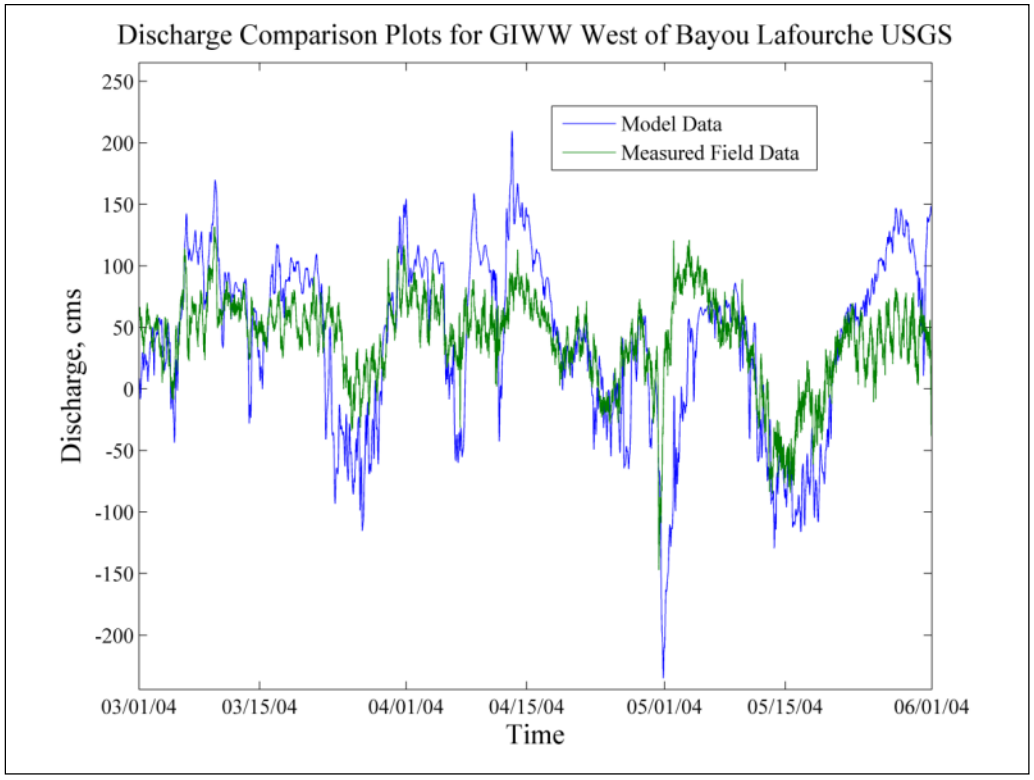

As expected, the error metrics for the discharge values are not as favorable as the water-surface elevations, but they are still acceptable given the goals for this study, with average values of 0.73 for the correlation coefficient and 60 cms for the *RMSE* for gages considered to be within the primary study area (Table 7). The GIWW West of Minors Canal values were not included in the averages due to the previously discussed concerns about the accuracy of this gage's measurements.

4.4 Salinity validation

Model salinity results were validated through comparisons with the measured salinity values taken from 1 January 2004 to 1 January 2005. The measurement locations were those shown and described in Chapter 2. The comparison plots are provided in Appendix D. Table 8 provides a list of the error metrics, as previously calculated for the water-surface elevations and discharges.

Table 8. Salinity performance metrics.

Gage Description	Correlation Coefficient	Root Mean Square Error, ppt	Observed Mean Value, ppt	Model Mean Value, ppt	Within Primary Area of Interest
Caillou Lake (USGS 073813479)	0.36	10.4	10.49	1.00	Yes
Caillou Bay (USGS 073813498)	0.31	13.8	23.24	13.42	No
Houma Navigational Canal (USGS 07381328)	0.80	2.9	2.33	1.78	Yes
Bayou Grand Caillou (USGS 07381324)	0.55	4.7	4.79	1.52	Yes
GIWW at Houma (USGS 07381331)	0.39	0.7	0.20	0.13	Yes
Company Canal, Lockport (USGS 07381355)	0.40	0.1	0.16	0.09	No
Company Canal, Salt Barrier (USGS 07381350)	0.10	0.3	0.21	0.02	No
Minors Canal (MG 01)	0.20	0.4	0.19	0.00	Yes
Falgout Canal (MG 02)	0.79	2.9	3.22	1.48	Yes
Bayou Dularge (MG 03)	0.74	2.8	2.35	0.97	Yes
Bayou Grand Caillou (MG 04)	0.71	4.3	10.18	7.92	Yes
Bayou Petit Caillou (MG 05)	0.46	4.2	9.45	6.65	Yes
Bayou Terrebonne (MG 08)	0.40	2.1	3.26	3.51	Yes
Humble Canal (MG 09)	0.41	2.6	1.20	2.78	Yes
Pointe Aux Chenes (MG 10)	-0.12	6.2	7.47	12.13	Yes
Grand Bayou Canal (MG 11)	0.24	3.8	0.36	2.67	Yes

The numerical model underestimates the salinity intrusion into Caillou Lake (Figure 35) and Caillou Bay (Figure 36). The salinity comparisons for the Houma Navigation Canal (Figure 37) show a good representation of the types of events (sudden spikes in salinity and quick returns to fresh water) that occur for this area. The magnitudes of the events are sometimes overestimated or underestimated, but the events occurring in the field are replicated to some degree in the model. The salinities for the eastern portion of the model (Pointe Aux Chenes [Figure 38] and Grand Bayou Canal [Figure 39]) are over-estimated in the model.

Figure 35. Caillou Lake salinity comparison.

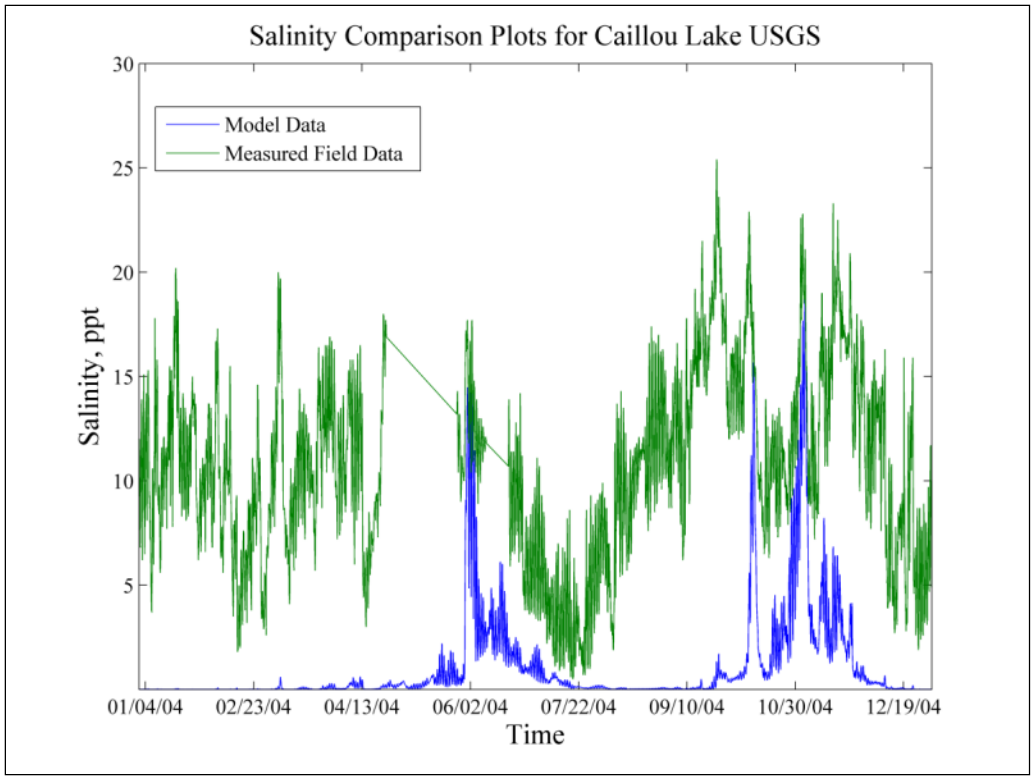

Figure 36. Caillou Bay salinity comparison.

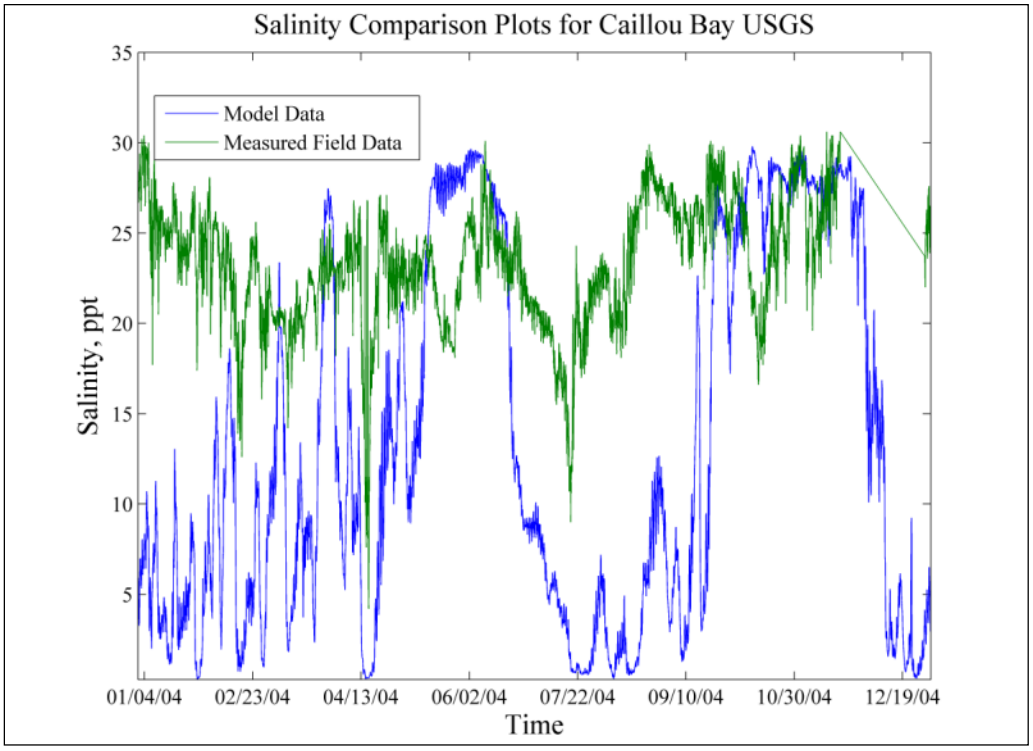

Figure 37. Houma Navigation Canal salinity comparison.

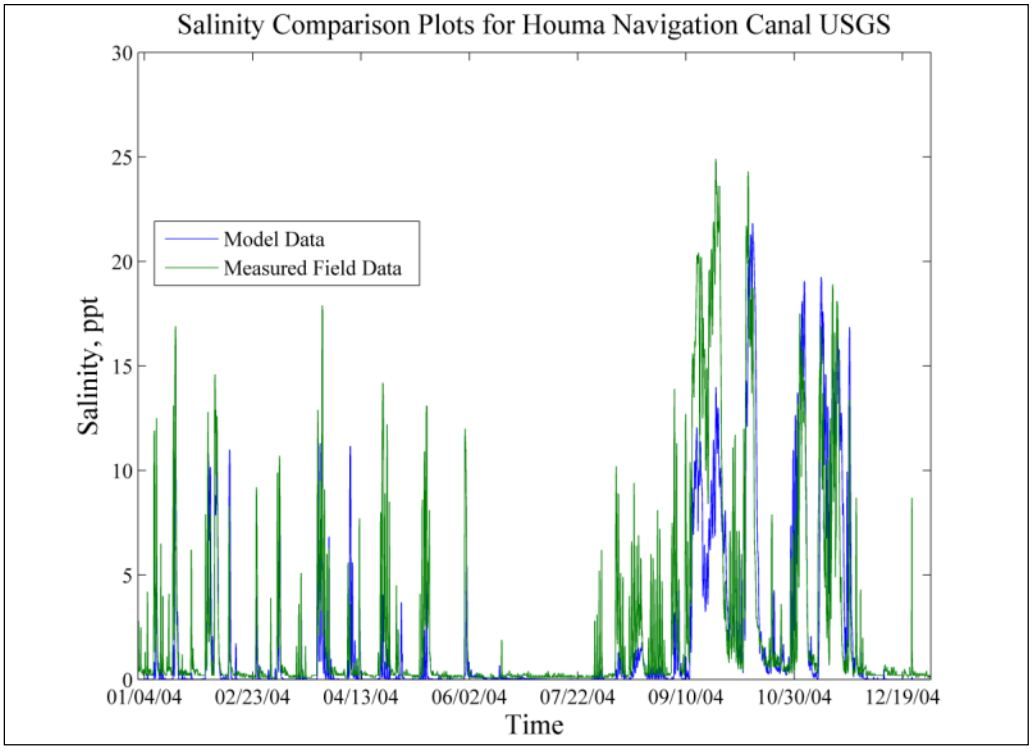

Figure 38. Pointe Aux Chenes salinity comparison.

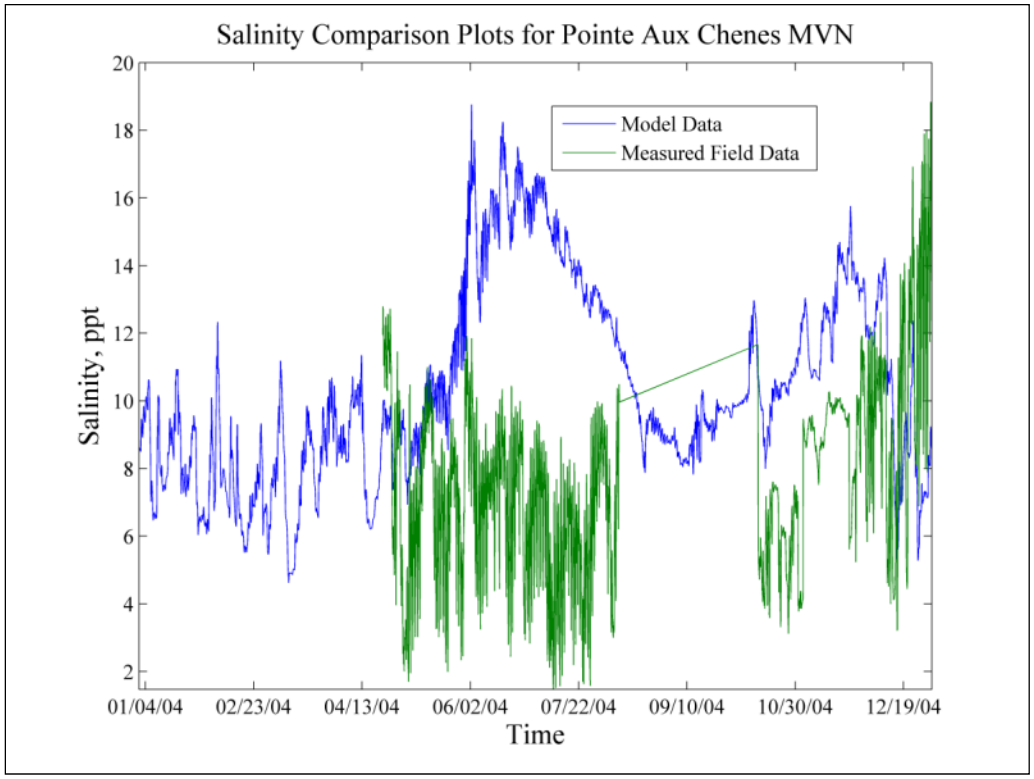

Figure 39. Grand Bayou Canal salinity comparison.

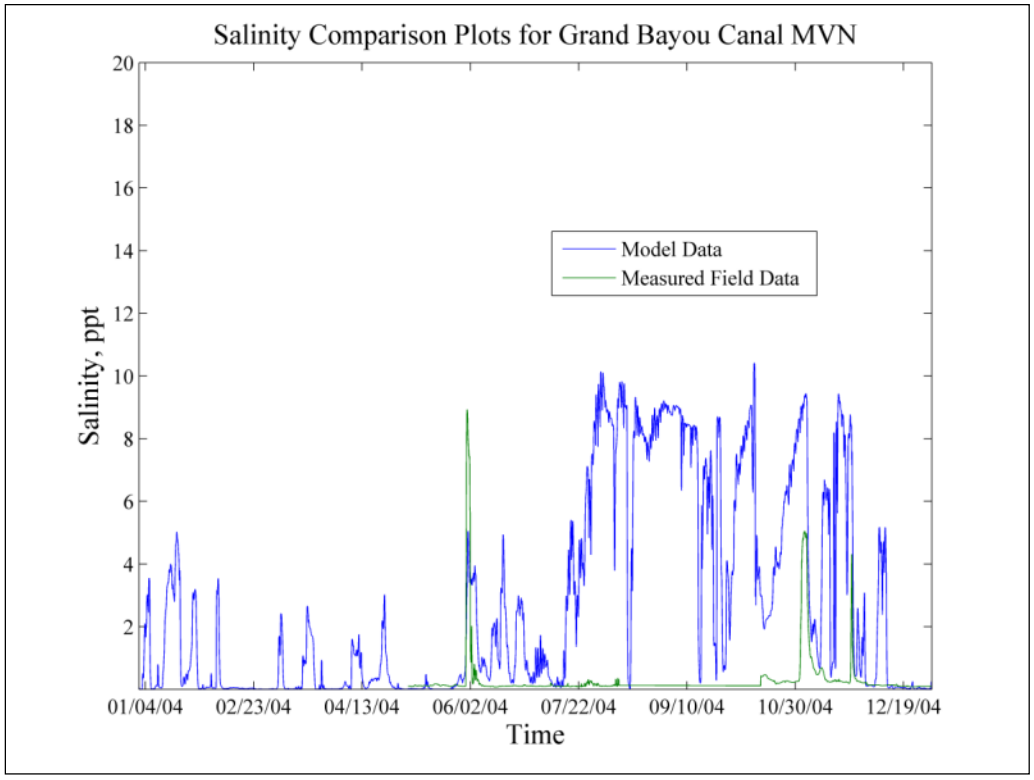

The global trends are replicated in the numerical model. This includes the significant freshening of the entire system during July along with the salinity increase that occurs in late August/early September. The freshening is due to the large inflows for the Atchafalaya River and the Wax Lake Outlet along with the reversed head difference along the boundary driving flow toward the study area to the east (refer back to Figure 14). The increase in salinity in both the model and the field in the September – December time period is due to a combination of phenomena. The offshore currents return to the dominant western direction carrying the Atchafalaya River and Wax Lake Outlet freshwater flows away from the study area (Figure 14). There is a significant reduction in the freshwater flows from these two major inflows as well, leading to a reduced freshwater flow (refer back to Figure 18) eastward along the GIWW to the Houma Navigation Canal. The Port Fourchon tidal boundary (see Figure 9) also contains periods of increased water-surface elevations for the September to December time period, leading to increased flow from offshore to fill the increased tidal storage. The combination of these three phenomena leads to a significant increase in the salinity measurements during the latter part of 2004.

The observed trends in the salinities tend to be simulated accurately in the model, especially for the gages located within the primary study area. Pointe Aux Chenes and Grand Bayou Canal salinities are less accurately represented. The numerical model overestimates the freshening during July and the subsequent increase in salinity, but the general behavior is reproduced. The reason for the error in the model is most likely the uncertainty in the tidal boundary conditions. The head difference applied along the boundary was created in an effort to replicate the general behavior reported in Johnson (2008). The measurements reported by Johnson (2008) were monthly average currents over a 23-year period, and therefore may not be as accurate representing the system behavior for 2004. Since detailed 2004 boundary salinities, tides, and littoral flows, which bring Mississippi River flow into the system as well as sweeping Atchafalaya River flow away from the system offshore, are not known in detail, precise agreement between model and field results was not expected. The trends, however, are represented. For purposes of comparing the existing conditions to the alternate plans, the numerical model is sufficiently validated.

5 Plan Alternatives

The validated AdH mesh (hydrodynamics and salinity) was used as the starting point for generating the plan condition meshes. The existing conditions/without project mesh (domain shown previously in Figure 7) was modified to include the impermeable levee along with all proposed structures to be located along the levee.

The levee system along with all planned structures is shown in Figure 40. The environmental structures consist of collections of culverts. The navigation structures consist of different configurations of sluice and sector gates. Plan 1 has all structures in the open-flow position. Plan 2 has all the navigation structures in the open position, with all the environmental structures in the no-flow (closed) position. Plan 3 has all structures in the open position except for the Houma Navigational Canal structure and lock (both closed).

It should be noted that the environmental structures (culverts) located along the proposed levee system were modeled as reversible culverts. The top elevation of the culverts was enforced using a pressure penalty term within the AdH numerical code to obtain the proper WSE (and wetted area) for the culvert. Additional information on this pressure penalty term can be found in Berger et al. (2010).

Table 9 and Table 10 provide the structure sizes, bottom elevations, and opened/closed status for the three plan alternative configurations. A more detailed description of the plan alternatives along with figures showing the incorporation of the levee system into the numerical model is provided in Appendix E.

In summary the three plan conditions are:

Plan 1: All navigation and environmental structures in the open position.

Plan 2: All navigation structures (green flags in Figure 40 and green circles in Figure 115 – Figure 137 [Appendix E]) in the open position, with all environmental structures (red flags in Figure

40 and red circles in Figure 115 – Figure 137 [Appendix E]) in the closed position.

Plan 3: All navigation and environmental structures in the open position with the exception of the Houma Navigation Canal structure and lock (blue flag in Figure 40 and green circle in Figure 125 [Appendix E]) in the closed position.

Figure 40. Location of proposed structures along the proposed Morganza to the Gulf of Mexico levee system.

Note: Green flags are navigation structures, red flags are environmental structures, and the blue flag is the Houma Navigation Canal structure.

Table 9. Navigation structure sizes and bottom elevations.

Structure	Invert, m (ft) NAVD88(2004.65)	Sector Gate Width, m (ft)	Number Sluice Gates	Sluice Gate Width, m (ft)	Sluice Gate Invert, ft NAVD88(2004.65)	Plan 1	Plan 2	Plan 3
Black Bayou (S-1)	-3.66 (-12)	17.07 (56)	0	N/A	N/A	Open	Open	Open
Shell Canal West (S-2)	-3.05 (-10)	10.67 (35)	0	N/A	N/A	Open	Open	Open
Shell Canal East (S-3)	-3.66 (-12)	17.07 (56)	0	N/A	N/A	Open	Open	Open
Elliot Jones Canal (S-4)	-2.44 (-8)	6.10 (20)	0	N/A	N/A	Open	Open	Open
NAFTA (S-5)	-3.66 (-12)	17.07 (56)	0	N/A	N/A	Open	Open	Open
Minors Canal (S-6)	-2.74 (-9)	17.07 (56)	0	N/A	N/A	Open	Open	Open
GIWW West of Houma (S-7)	-4.88 (-16)	53.34 (175)	6	4.88 (16)	-3.96 (-13)	Open	Open	Open
Marmande Canal (S-8)	-1.83 (-6)	9.14 (30)	0	N/A	N/A	Open	Open	Open
Falgout Canal (S-9)	-2.74 (-9)	17.07 (56)	9	4.88 (16)	-2.74 (-9)	Open	Open	Open
Bayou Dularge (S-10)	-2.13 (-7)	17.07 (56)	0	N/A	N/A	Open	Open	Open
Bayou Grand Caillou (S-11)	-3.66 (-12)	17.07 (56)	9	4.88 (16)	-3.66 (-12)	Open	Open	Open
Houma Navigational Canal (S-12)	-5.49 (-18)	76.20, 33.53 Lock (250, 110 Lock)	10	3.05 (10)	-2.13 (-7)	Open	Open	Closed
Bayou Fourpoints (S-13)	-2.44 (-8)	9.14 (30)	0	N/A	N/A	Open	Open	Open
Bayou Petit Caillou (S-14)	-2.44 (-8)	17.07 (56)	6	4.88 (16)	-2.44 (-8)	Open	Open	Open
Placid Canal (S-15)	-2.44 (-8)	17.07 (56)	6	4.88 (16)	(-8)	Open	Open	Open
Bush Canal (S-16)	-3.66 (-12)	17.07 (56)	9	4.88 (16)	-3.66 (-12)	Open	Open	Open
Bayou Terrebonne (S-17)	-2.74 (-9)	17.07 (56)	0	N/A	N/A	Open	Open	Open
Humble Canal (S-18)	-2.74 (-9)	17.07 (56)	0	N/A	N/A	Open	Open	Open
Pointe Aux Chenes (S-19)	-1.83 (-6)	17.07 (56)	0	N/A	N/A	Open	Open	Open
Grand Bayou (S-20)	-2.74 (-9)	17.07 (56)	9	4.88 (16)	-2.74 (-9)	Open	Open	Open
GIWW at Larose (S-21)	-4.88 (-16)	53.34 (175)	3	4.88 (16)	-3.05 (-10)	Open	Open	Open

Table 10. Environmental structure sizes and bottom elevations.

Structure	Total Structure Width, m (ft)	Structure Bottom Invert, m (ft) NAVD88(2004.65)	Plan 1	Plan 2	Plan 3
Reach E, West Structure (E-1)	9 x (1.83 m x 1.83 m) = 16.5 (54)	-1.37 (-4.5)	Open	Closed	Open
Reach E, East Structure (E-2)	9 x (1.83 m x 1.83 m) = 16.5 (54)	-1.37 (-4.5)	Open	Closed	Open
Reach G (E-3)	6 x (1.83 m x 1.83 m) = 11.0 (36)	-1.37 (-4.5)	Open	Closed	Open
Reach H, Bayou Sale Structure (E-4)	4 x (1.83 m x 1.83 m) =7.3 (24)	-1.37 (-4.5)	Open	Closed	Open
Reach H, Second from West Structure (E-5)	4 x (1.83 m x 1.83 m) = 7.3 (24)	-1.37 (-4.5)	Open	Closed	Open
Reach H, Third from West Structure (E-6)	1 x (1.83 m x 1.83 m) = 1.8 (6)	-1.37 (-4.5)	Open	Closed	Open
Reach H, East Structure (E-7)	6 x (1.83 m x 1.83 m) = 11.0 (36)	-1.37 (-4.5)	Open	Closed	Open
Reach J-2, West Structure (E-8)	4 x (1.52 m x 3.05 m) = 12.2 (40)	-1.07 (-3.5)	Open	Closed	Open
Reach J-2, Center Structure (E-9)	4 x (1.52 m x 3.05 m) = 12.2 (40)	-1.07 (-3.5)	Open	Closed	Open
Reach J-2, East Structure (E-10)	5 x (1.52 m x 3.05 m) = 15.2 (50)	-1.07 (-3.5)	Open	Closed	Open
Reach K, South West Structure (E-11)	2 x (1.83 m x 1.83 m) = 3.7 (12)	-1.37 (-4.5)	Open	Closed	Open
Reach K, Middle Structure (E-12)	2 x (1.83 m x 1.83 m) = 3.7 (12)	-1.37 (-4.5)	Open	Closed	Open
Reach K, North East Structure (E-13)	6 x (1.83 m x 1.83 m) = 11.0 (36)	-1.37 (-4.5)	Open	Closed	Open

6 Base Condition versus Plan Comparisons

6.1 Boundary conditions

Each of the three plan alternatives discussed in Chapter 5, including the base conditions (i.e., without a project configuration), was simulated for three sea level values: existing sea level; 0.738 m (2.42 ft) of sea-level rise; and 1.45 m (4.75 ft) of sea-level rise. A total of 12 simulations were performed. The existing sea level represents the conditions for calendar year 2004 and uses identical forcing conditions (winds, inflows, and water-level specifications) as those previously discussed under "Model Validation" in section 4.2. The sea-level rise scenarios consist of the same forcing conditions as the existing sea level simulations (winds and inflows), with the exception of the WSE boundary conditions. The WSE boundaries were increased by 0.738 m (2.42 ft) and 1.45 m (4.75 ft) for sea-level rise scenarios 1 and 2, respectively. No alterations were made to the numerical model meshes for the various sea level simulations. Since the original (base) mesh included all areas that would be inundated by future sea-level rise scenarios, the mesh bathymetry was left unchanged for all sea level amounts. Bathymetric changes due to sedimentation were neglected. Although this assumption is conservative, it is thought that the area of interest (green area of Figure 41) is sediment starved.

6.2 Comparison of alternatives

Extensive base (existing conditions/without project) versus plan comparisons were performed. These comparisons were separated into the following categories:

1. comparisons of the inundation/wetted area and tidal prism between all alternatives for the area inside the proposed levee system
2. comparison of the average salinities for the entire model domain with comparisons between the alternatives and the without project configuration
3. comparison of the water-surface elevations and salinities for a number of discrete locations
4. comparison of the velocities in the proposed structures for all alternatives.

These comparisons illustrate the impact of the proposed levee system for the existing sea level and for two sea-level rise amounts: 0.738 m (2.42 ft) and 1.45 m (4.75 ft).

6.3 Comparison of inundations and tidal prisms

The inundation/wetted area and tidal prism were determined for the areas within the levee system (green area in Figure 41). This was done to determine how the levee system would impact inundation amounts and tidal exchange.

Figure 41. The area in green is considered "protected" by the proposed levee system.

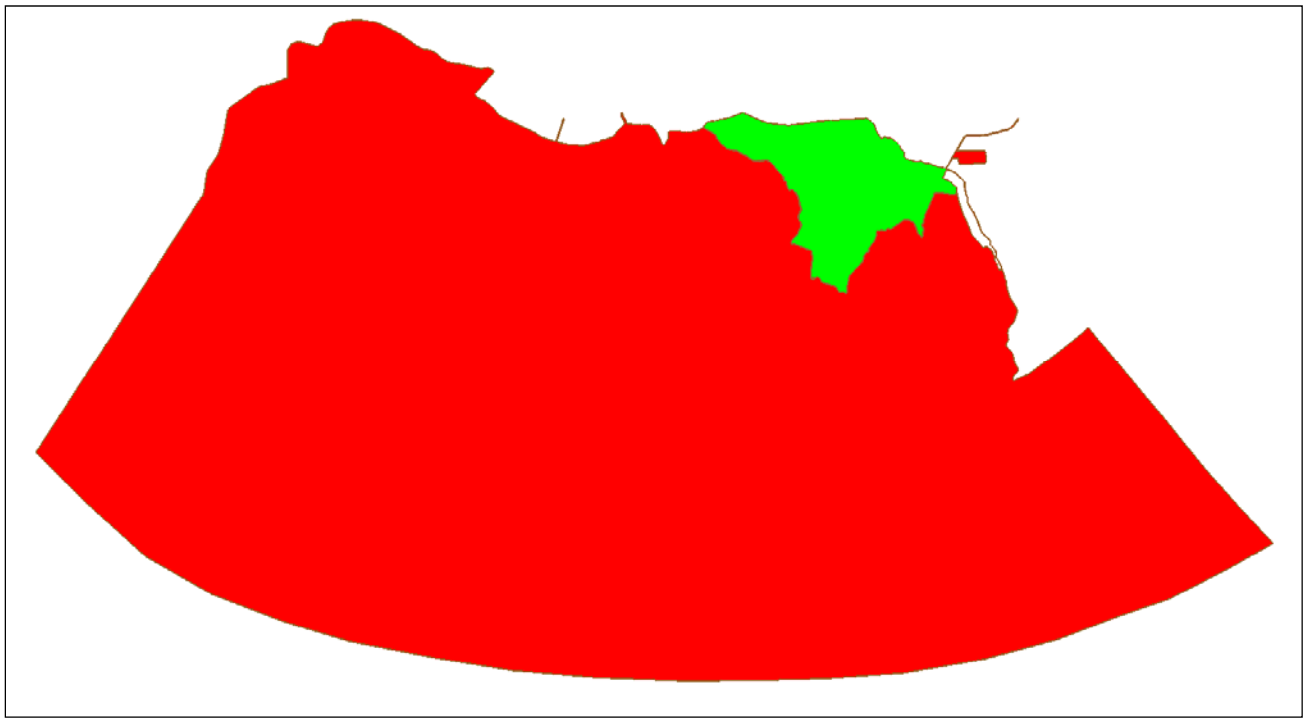

Figure 42 to Figure 47 are time series plots and inundation images (for plan 1) of the wetted area inside the levee system for the three sea-level rise amounts (existing sea level, sea-level rise scenario 1 and sea-level rise scenario 2). Figure 48 is a bar plot of the average wetted area and Figure 49 is a bar plot of the average tidal prism for all modeled scenarios.

Figure 42. Wetted area for the area within the proposed levee system for the existing sea level.

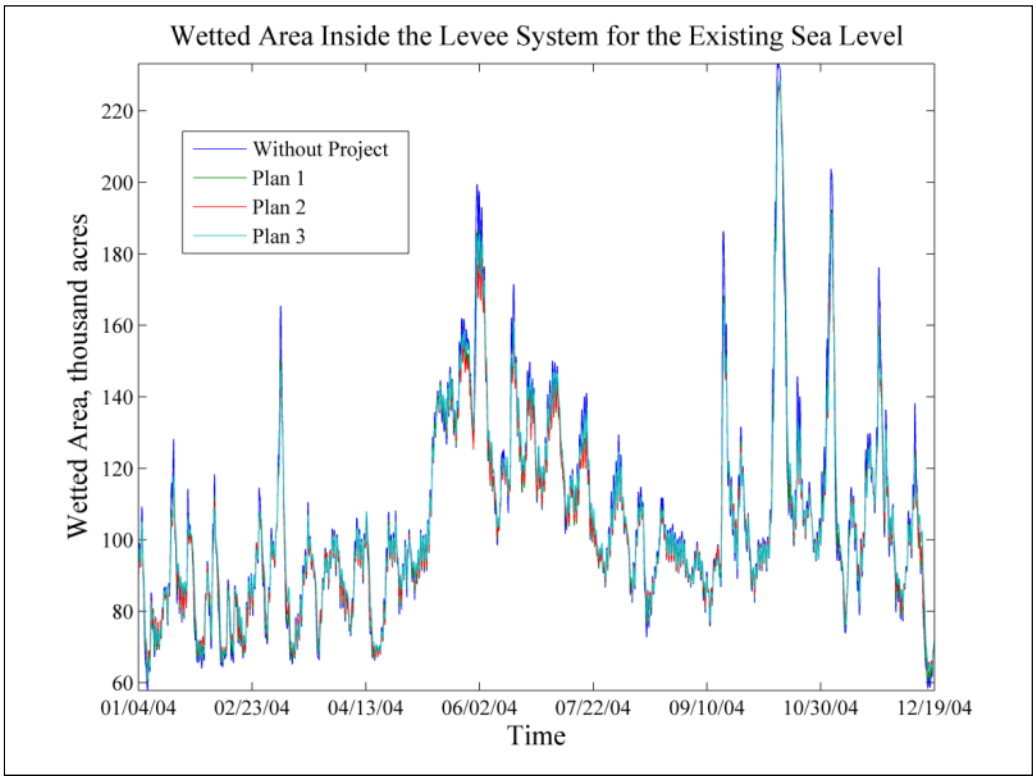

Figure 43. Median depths for the plan 1 alternative for the existing sea level.

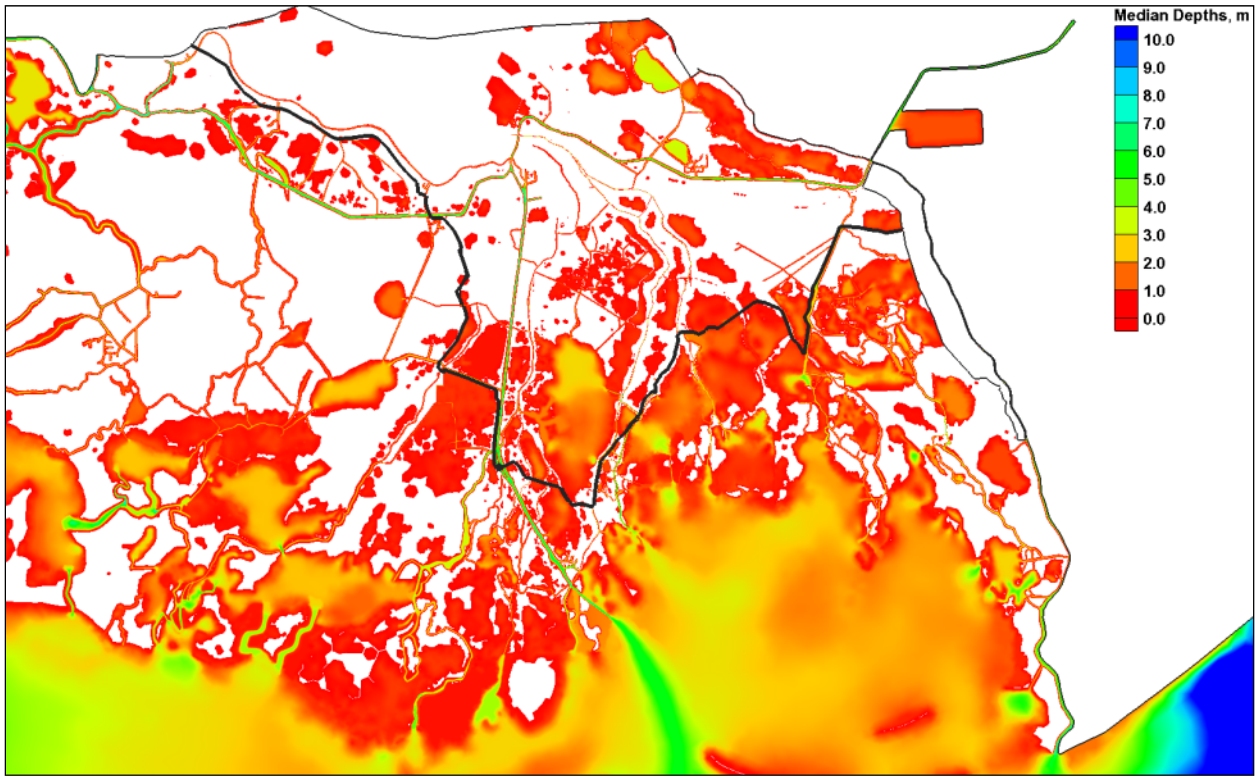

Figure 44. Wetted area for the area within the proposed levee system for the sea-level rise 1 scenario.

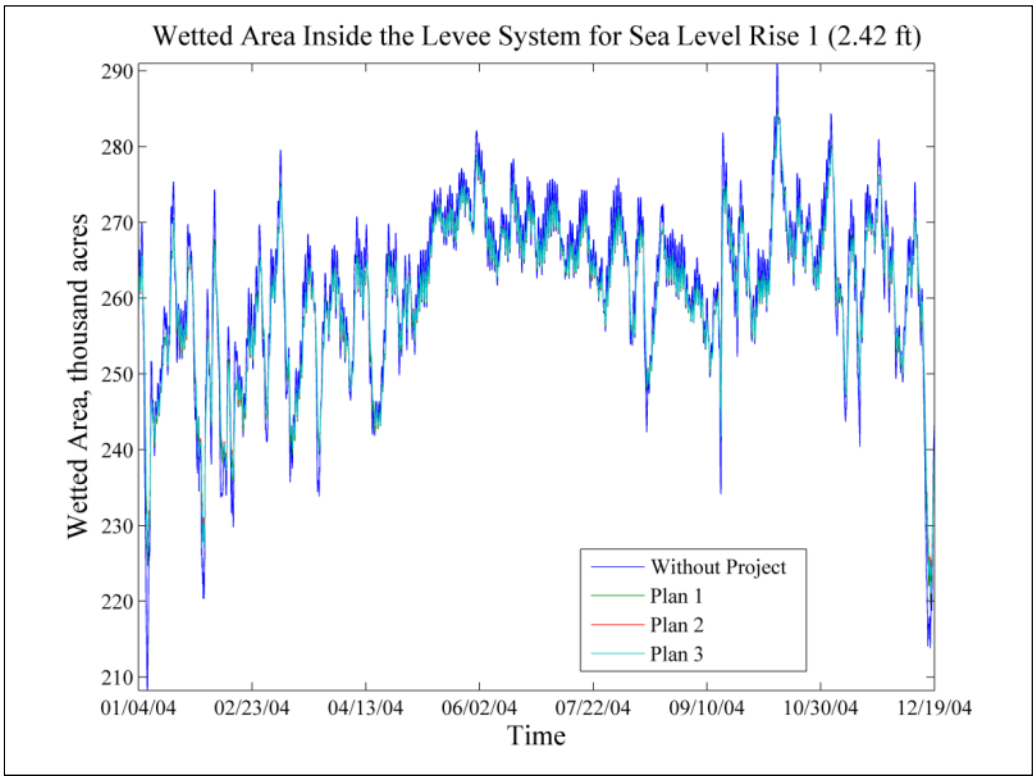

Figure 45. Median depths for the plan 1 alternative for the sea-level rise 1 scenario.

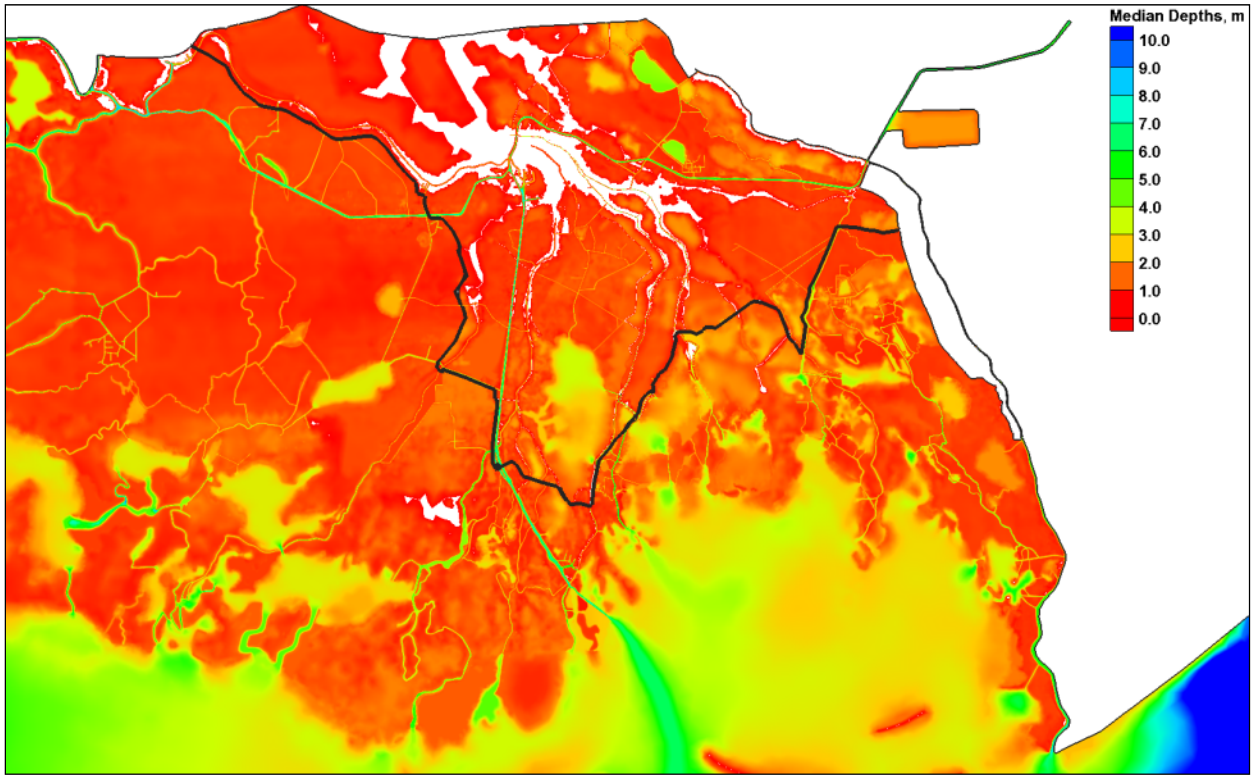

Figure 46. Wetted area for the area within the proposed levee system for the sea-level rise 1 scenario.

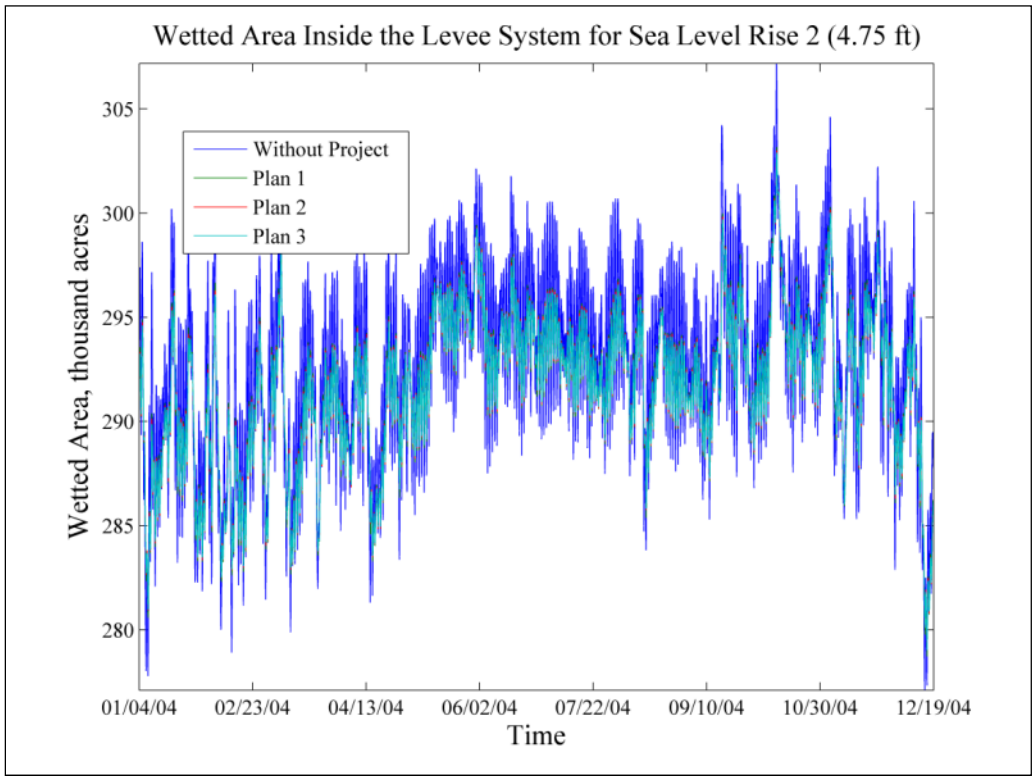

Figure 47. Median depths for the plan 1 alternative for the sea-level rise 2 scenario.

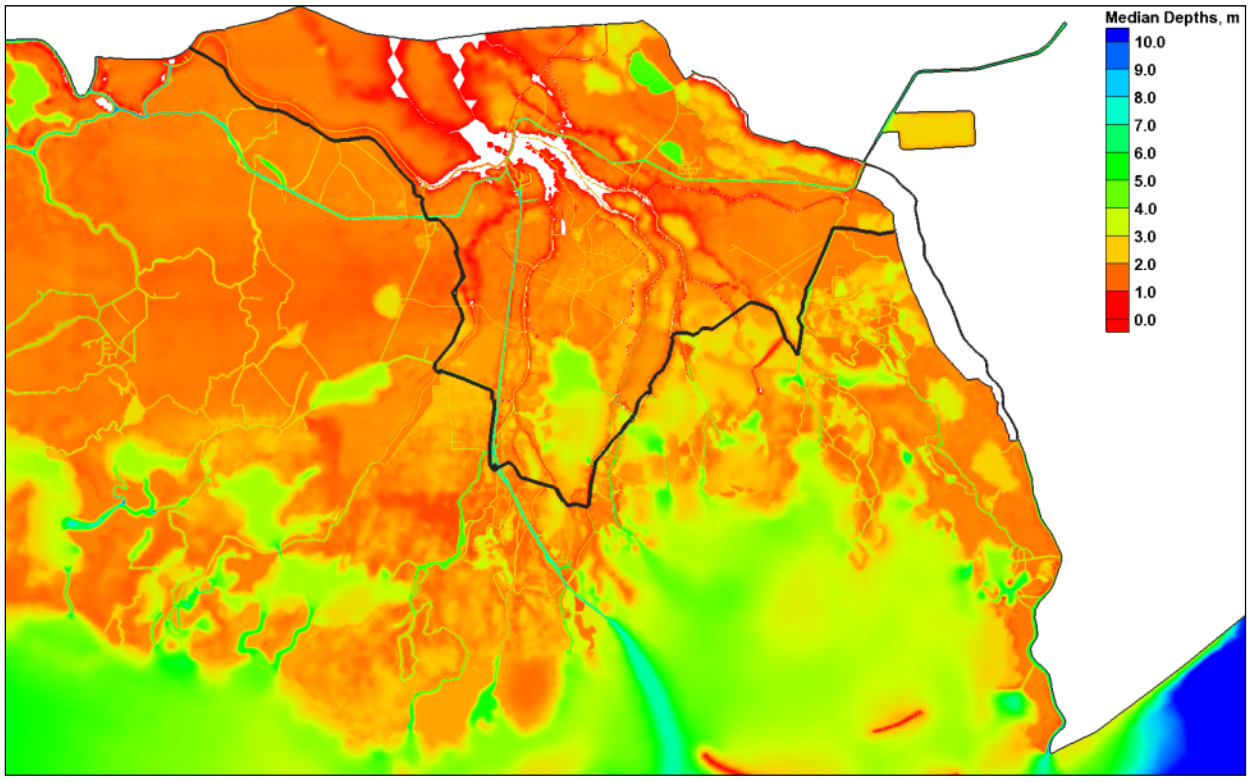

Figure 48. Bar plot of the average wetted area inside the proposed levee system (green area in Figure 41).

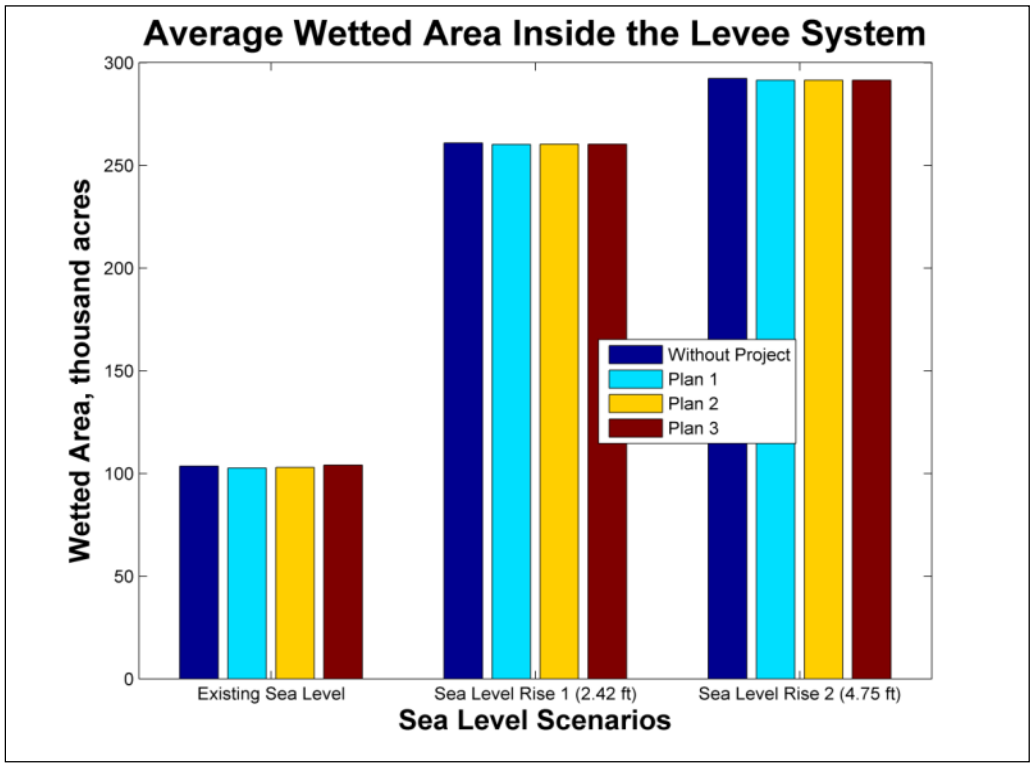

Figure 49. Bar plot of the average tidal prisms inside the proposed levee system (green area in Figure 41).

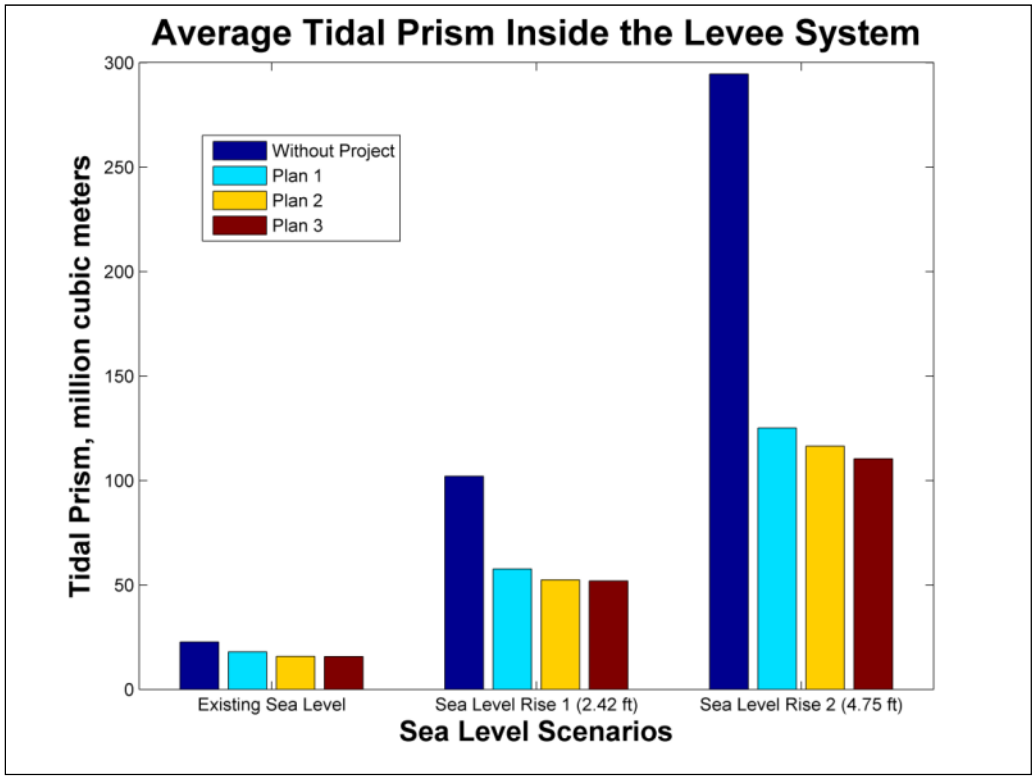

Figure 42 indicates that for the existing sea level, the proposed levee system has a minimal impact on the wetted area for the area inside the proposed levee system. Some of the peaks in Figure 42 are associated with frontal passage events that produced large increases in water level. These events are damped for the with-project configurations, but the wetted areas for the normal tidal time periods are similar for all four mesh configurations. Thus, the levee system will reduce the influx of water during a frontal passage type event but will not impact the wetted area/tidal exchange during normal tidal conditions. This is exemplified by the similar average wetted areas (Figure 48) and tidal prisms (Figure 49) for the existing water level for all four mesh configurations.

The impact of the levee system on the wetted area and tidal prism increases for the sea-level rise 1 scenario, and increases again, significantly, for the sea-level rise 2 scenario. The wetted areas for the sea-level rise 1 scenario show a reduction in the normal wetting/drying occurring inside the proposed levee system as compared to the base conditions mesh configuration (see Figure 44). This indicates that the levee system is now impeding the normal tidal exchange for the system. This can also be observed in the tidal prism plot in Figure 49, which indicates the tidal prism has on average been reduced by approximately 50 %, or 60 million cubic meters. The minimal difference in the average wetted area (Figure 48) indicates no significant set up/down of the mean water levels inside the levee system.

The wetted area for the sea-level rise 2 scenario indicates a significant reduction in the wetting/drying occurring over a given tidal cycle as compared to the without project mesh configuration (see Figure 46). Therefore, for this sea-level rise amount, the proposed levee system would significantly impede the tidal exchange for the protected areas. The reduction in the tidal prism (Figure 49) is similar to the sea-level rise 1 scenario from a percentage standpoint (approximately 50 %), but the magnitude reduction is now over 150 million cubic meters. The minimal difference in the average wetted area (Figure 48) for the sea-level rise 2 scenario also indicates no significant change of the mean water levels inside the levee system.

6.4 Comparison of average salinities

A comparison was performed on the average salinity values for the base and plan conditions. These comparisons were performed for the vegetative

growing season, March 1 to November 30, along with yearly averaged values (see Appendix F for figures). These comparisons show that the changes in the average salinity values due to the new levee system for the existing sea level are less than 1 ppt in most areas for plans 1 and 2. Plan 3 does have some larger impacts compared to the base conditions (changes of several ppt) associated with the diversion of a significant amount of fresh water from the Houma Navigation Canal. The salinity impacts of the plan alternatives become larger when considering the occurrence of sea-level rise.

The average salinities and salinity differences indicate several impacts associated with the construction of the proposed levee system. The patterns for the salinity differences are similar for both the annual average and the averages for the growing season, and therefore the remaining discussion in this section will not distinguish between these two averages.

Plan 1 has all the environmental and navigation structures open, and therefore it is the closest alternative to the base configuration. The plan 1 salinity averages are similar to the base salinities for the existing sea level, and therefore have minimal differences. The sea-level rise 1 scenario has increased differences between the plan 1 and base salinities with some increased salinities (less than 1 ppt) along the Houma Navigation Canal north of the levee system along with some slight increases in the salinities in Terrebonne Bay. The sea-level rise 2 scenario has significant and widespread differences between the plan 1 and base configurations. This includes widespread freshening of the system of up to 4 ppt for the plan 1 configuration, as compared to the without-project sea-level rise 2 scenario. These differences for the sea-level rise 2 scenario are due to the large difference in the tidal prism for these two mesh configurations (see Figure 49). This significant reduction in tidal exchange has a large impact on the salinity results for the system.

Plan 2 has all the navigation structures open and all the environmental structures closed. The plan 2 average salinities are similar to the plan 1 and base salinities for the existing sea level, with some localized differences of up to 1 ppt. For the sea-level rise 1 scenario, the plan 2 salinities are higher by up to 0.3 ppt as compared to the plan 1 and base salinities for the Lake Boudreaux area. The sea-level rise 2 scenario has significant and widespread differences between the plan 2 and without-project configurations. This includes widespread freshening of the system

of up to 4 ppt for the plan 2 configuration as compared to the without-project sea-level rise 2 scenario similar to that observed for the plan 1 configuration.

Plan 3 has all the navigation and environmental structures open with the exception of the Houma Navigation Canal structure, which is closed. This significantly alters the freshwater flow down the Houma Navigation Canal and, therefore, has significant and spatially widespread impacts to the salinity field. For the existing water level, plan 3 freshens large areas located within the levee system and areas south of Falgout Canal, but has an increase (~4 ppt) in salinity south of the Houma Navigation Canal structure compared to the without-project configuration. For the sea-level rise 1 scenario, plan 3 continues to create a freshening of large areas inside the levee system and south of Falgout Canal, with an increase in salinity south of the Houma Navigation Canal structure as compared to the base configuration. For the sea-level rise 2 scenario, plan 3 is similar to plans 1 and 2, but without the slight increase in salinity along the Houma Navigation Canal north of the Houma Navigation Canal structure.

6.5 Comparison of WSE and salinity time series

For a discrete number of points (74), WSE and salinity comparisons were performed for all four mesh configurations and all three sea level scenarios. The water-surface elevations and salinity values were extracted and compared at these points (listed in Table 11 and shown in Figure 50 – Figure 54). Water-surface elevation and salinity comparison plots are provided in Appendix G.

Table 11. Comparison point locations.

Point Number	Longitude	Latitude
1	-90.669289	29.232544
2	-90.696510	29.271372
3	-90.720001	29.311825
4	-90.734276	29.354900
5	-90.713273	29.487288
6	-90.705704	29.551195
7	-90.710228	29.598242
8	-90.742813	29.563219
9	-90.795364	29.535259
10	-90.859489	29.534847
11	-90.682999	29.211962
12	-90.734451	29.214161
13	-90.743507	29.258171
14	-90.765388	29.287666
15	-90.835564	29.229433
16	-90.914894	29.241508
17	-90.748650	29.327631
18	-90.791359	29.327898
19	-90.768036	29.385658
20	-90.830704	29.350513
21	-90.954147	29.309168
22	-91.069054	29.340000
23	-90.865356	29.396051
24	-90.828331	29.465212
25	-90.799728	29.494301
26	-90.782867	29.412148
27	-90.748647	29.398956
28	-90.614204	29.276691
29	-90.643066	29.275499
30	-90.679398	29.288996
31	-90.700685	29.313726
32	-90.726975	29.361813
33	-90.708484	29.396500
34	-90.700394	29.337360
35	-90.665726	29.339334
36	-90.646193	29.312269
37	-90.621788	29.335306
38	-90.591003	29.351389
39	-90.610283	29.359966
40	-90.624900	29.355133
41	-90.610618	29.375199
42	-90.649330	29.401537

Point Number	Longitude	Latitude
43	-90.546906	29.395597
44	-90.554833	29.428279
45	-90.566921	29.438565
46	-90.540465	29.438770
47	-90.529289	29.430525
48	-90.514122	29.437250
49	-90.517497	29.449620
50	-90.557330	29.475600
51	-90.493858	29.441000
52	-90.469307	29.454262
53	-90.456008	29.428505
54	-90.446549	29.417391
55	-90.449570	29.397507
56	-90.392864	29.374581
57	-90.339157	29.382310
58	-90.310722	29.376612
59	-90.368669	29.423328
60	-90.418222	29.430971
61	-90.441849	29.438925
62	-90.451340	29.449686
63	-90.436241	29.468834
64	-90.407928	29.468994
65	-90.393173	29.480741
66	-90.363884	29.480225
67	-90.419031	29.503221
68	-90.424371	29.502626
69	-90.411591	29.517609
70	-90.402870	29.529966
71	-90.399260	29.539948
72	-90.443922	29.556538
73	-90.390852	29.556832
74	-90.377167	29.581756

Figure 50. Points located along the GIWW and the Houma Navigation Canal.

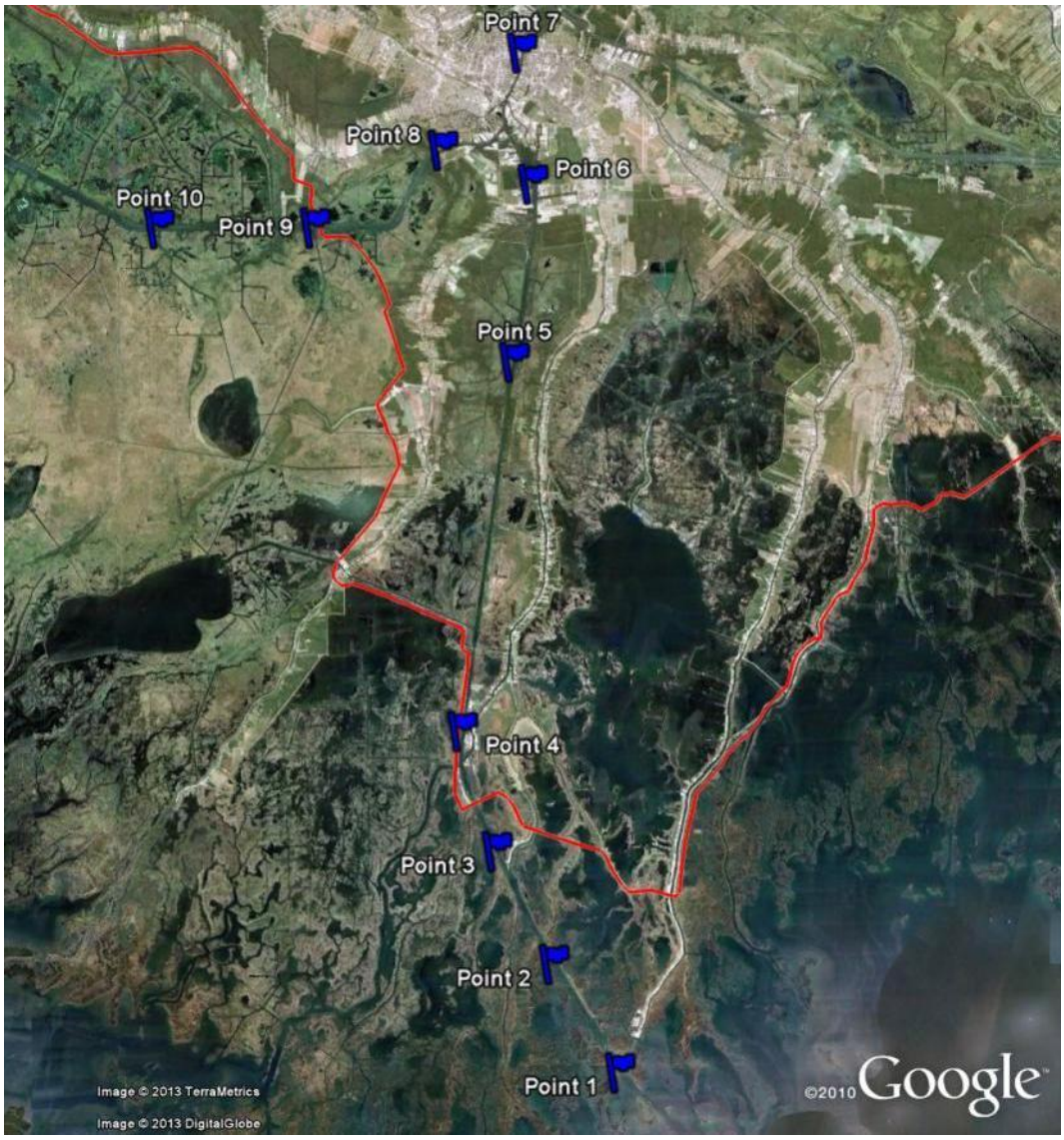

Figure 51. Points located to the west of the Houma Navigation Canal.

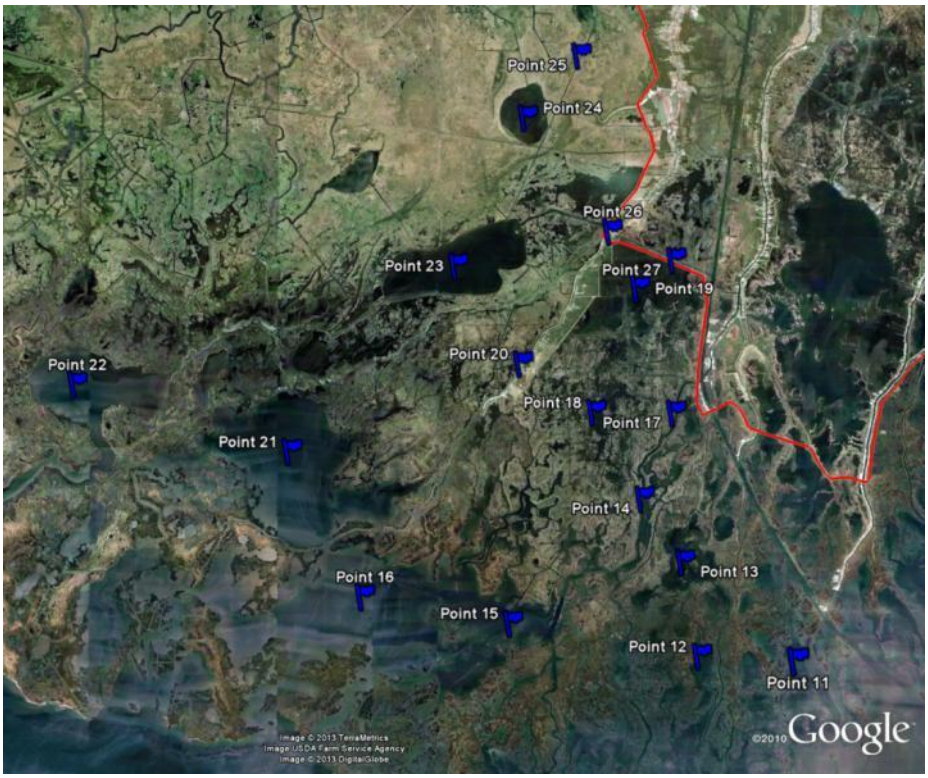

Figure 52. Points located to the east of the Houma Navigation Canal.

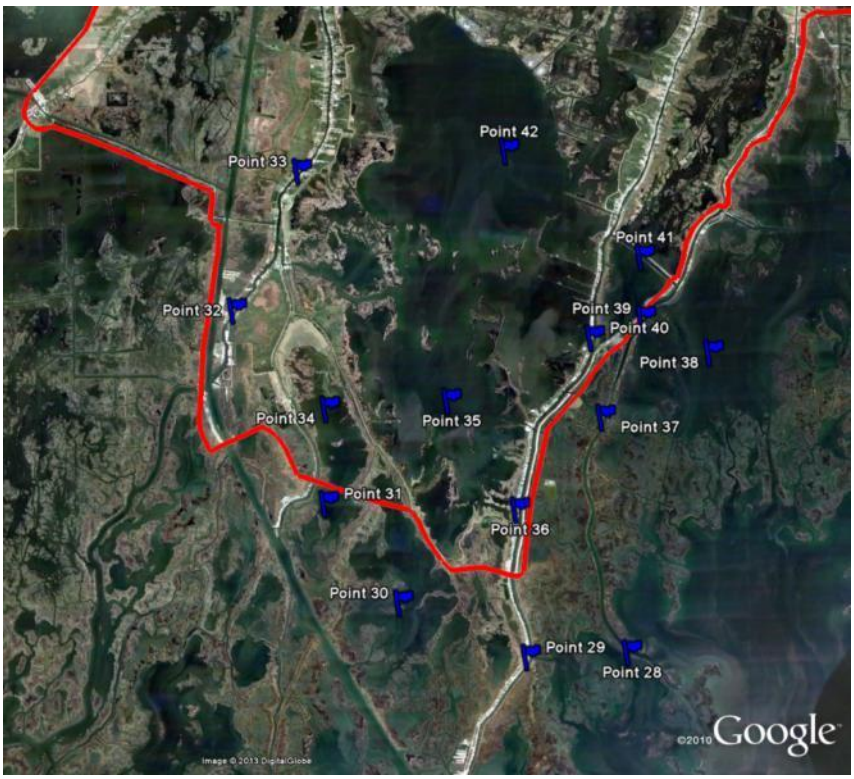

Figure 53. Points located to the west of Pointe Aux Chenes and east of Bayou Terrebonne.

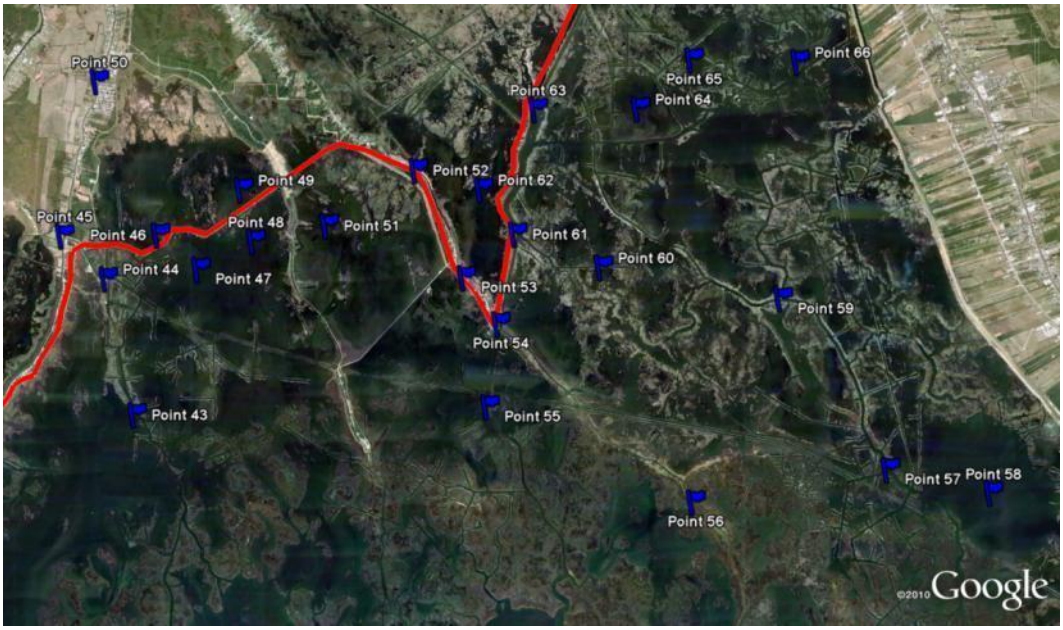

Figure 54. Points located to the east of Pointe Aux Chenes.

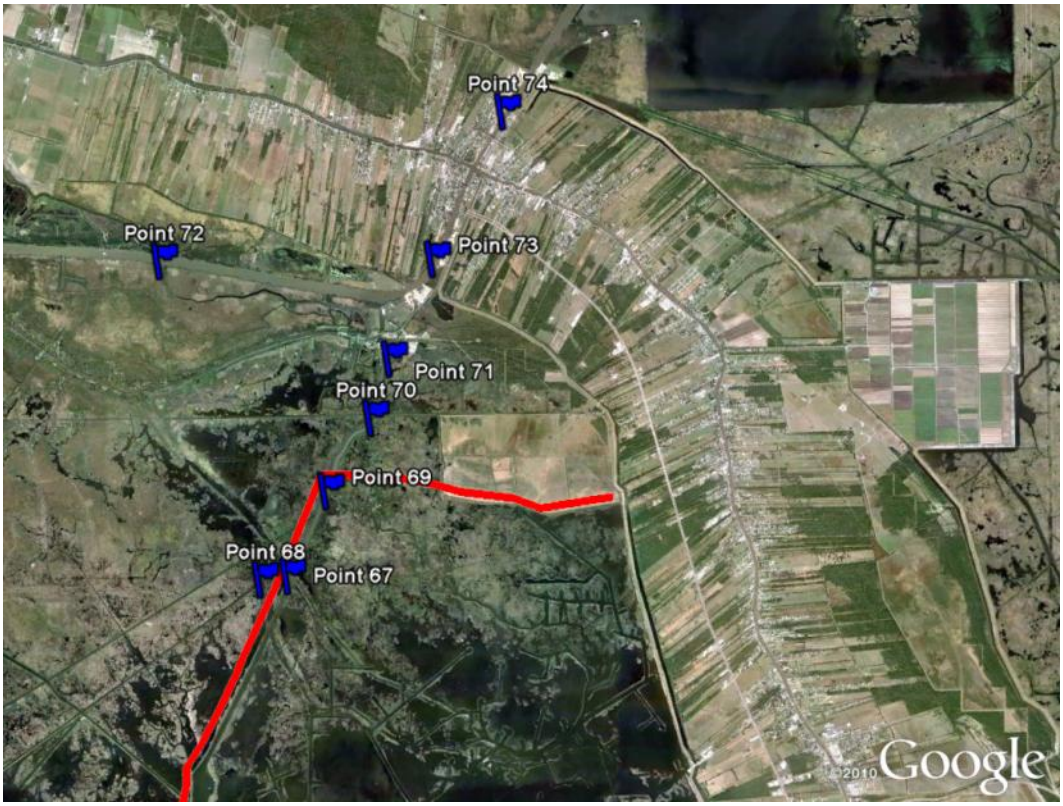

Some general statements can be made concerning the impact of the proposed levee system on the tidal signal of the system. The tide ranges

just outside of the levee system are sometimes amplified (more so with the higher sea-level scenarios), with this impact being reduced farther from the levee system. The tide ranges just inside of the levee system are sometimes damped (more so with the higher sea-level scenarios). For the existing water level, the tidal damping tends to be minimal, with damping primarily being associated with frontal passage events and not normal tidal exchange. This damping increases for the sea-level rise scenarios to include damping of the normal tidal exchange.

The point location comparisons illustrate how the average salinities increase consistently for the higher-water-level scenarios. This is due to the increased tidal prism (Figure 49). The increased tidal prism leads to an inflow of more water from the Gulf of Mexico and, correspondingly, more salinity for the system. The point comparisons in Appendix G indicate the impact of the levee system on the minimum, average, and maximum salinities. Some locations may experience lower average salinities but higher maximum salinities. This result, which is most prevalent in the plan 3 alternative, is due to an alteration of the flow pathways. Closing the Houma Navigation Canal structure significantly alters the way water enters and exits the levee system, thereby altering the flow of fresh water out of the levee system (resulting in lower average salinities for these new flow paths) and the flow of salt water into the levee system (resulting in the higher maximum salinities for these new flow paths and adjacent areas).

6.6 Comparison of velocities in the navigation structures

There were 1,574 motorized vessels greater than 25 feet in length registered in Terrebonne Parish in 2009 (USACE 2013), with many additional vessels less than 25 feet in length. The large numbers of both commercial and recreational vessels for this area require that the proposed levee system have several means of entry and exit. There are certain velocity restrictions in place for a structure to be considered safe for navigation (1.34 m/s, or 3 mph). A percentile analysis was performed on the model results to determine the 50^{th} and 10^{th} percentile velocities (i.e., velocities expected to exceed these values 50% and 10% of the time, respectively) for each mesh configuration and sea-level amount. These results are provided in Figure 55 – Figure 60.

Figure 55. 50th percentile exceedance velocity comparisons for plan 1, plan 2, and the without-project configuration for the existing sea level.

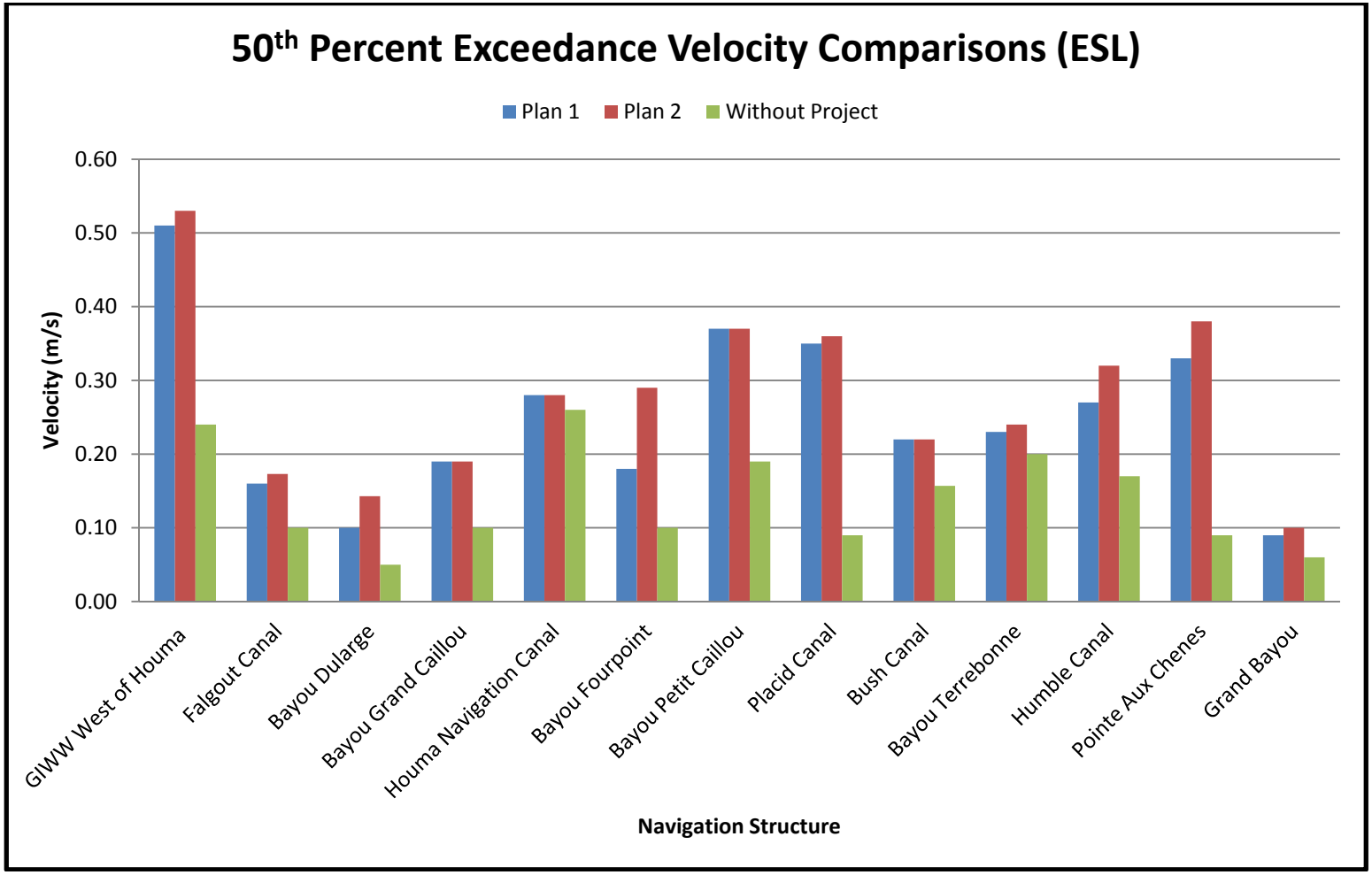

Figure 56. 10th percentile exceedance velocity comparisons for plan 1, plan 2, and the without-project configuration for the existing sea level.

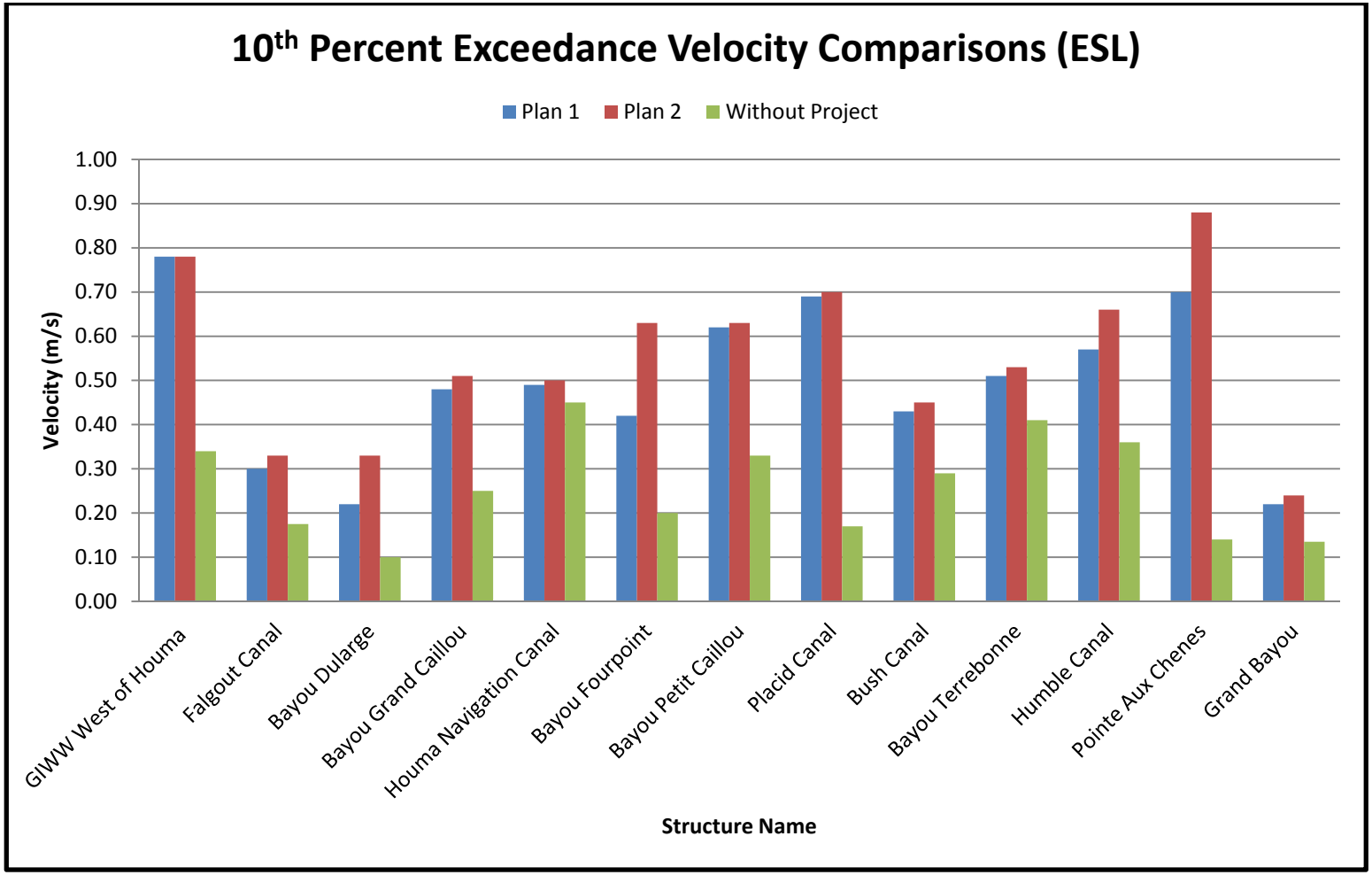

Figure 57. 50th percentile velocity comparisons for plan 1, plan 2, and the without-project configuration for the sea-level rise 1 scenario.

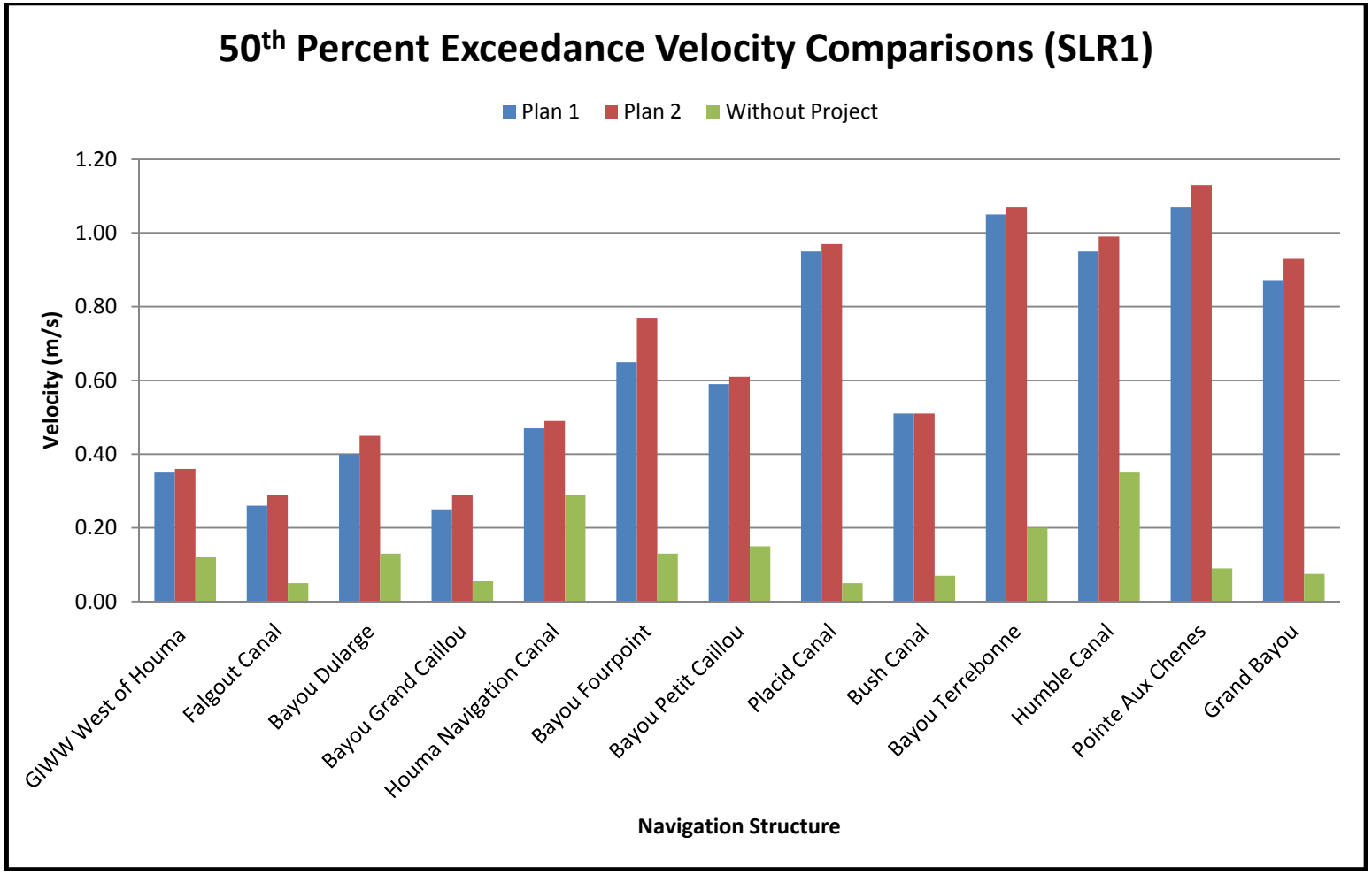

Figure 58. 10th percentile velocity comparisons for plan 1, plan 2, and the without-project configuration for the sea-level rise 1 scenario.

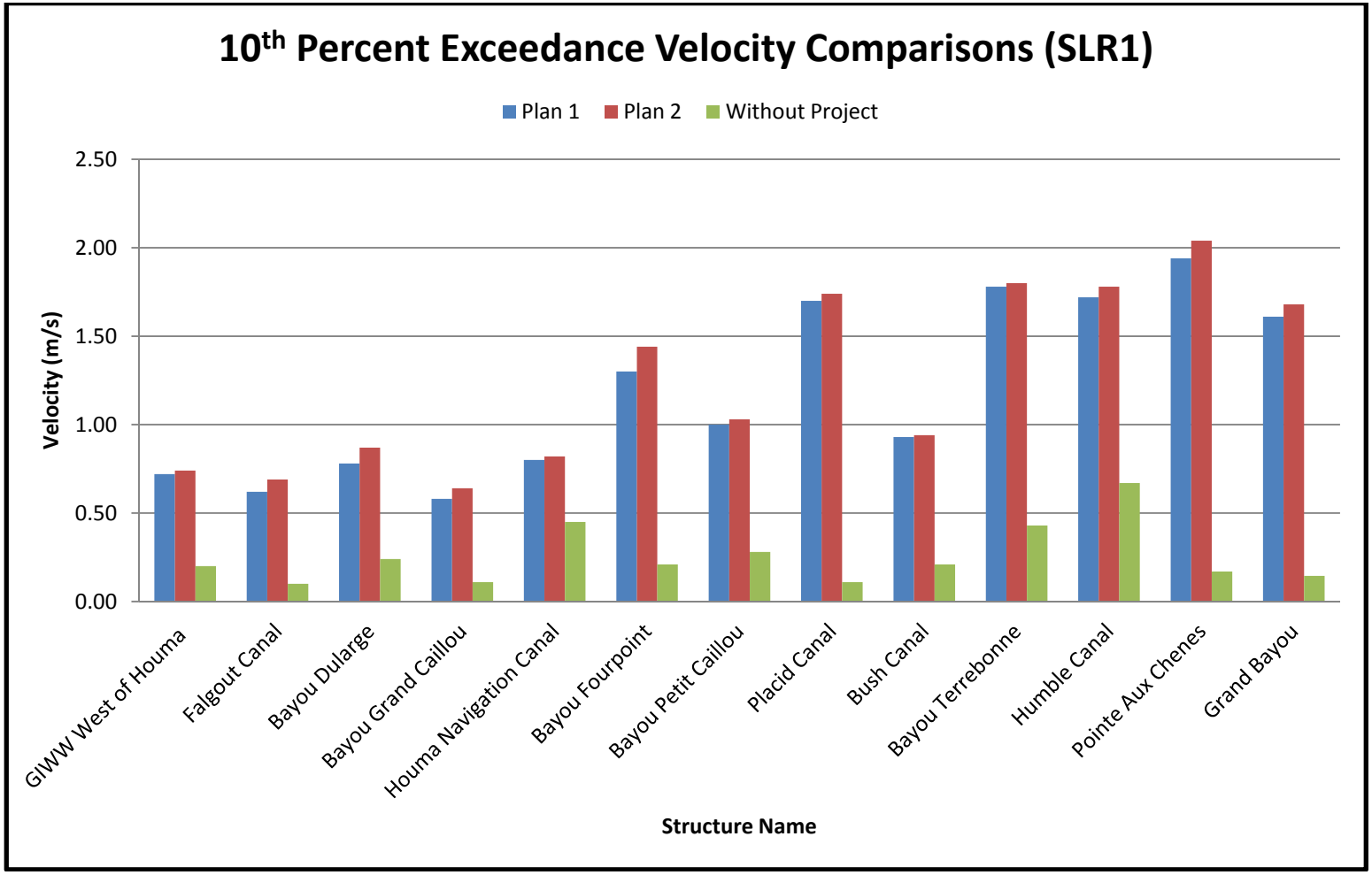

Figure 59. 50th percentile velocity comparisons for plan 1, plan 2, and the without-project configuration for the sea-level rise 2 scenario.

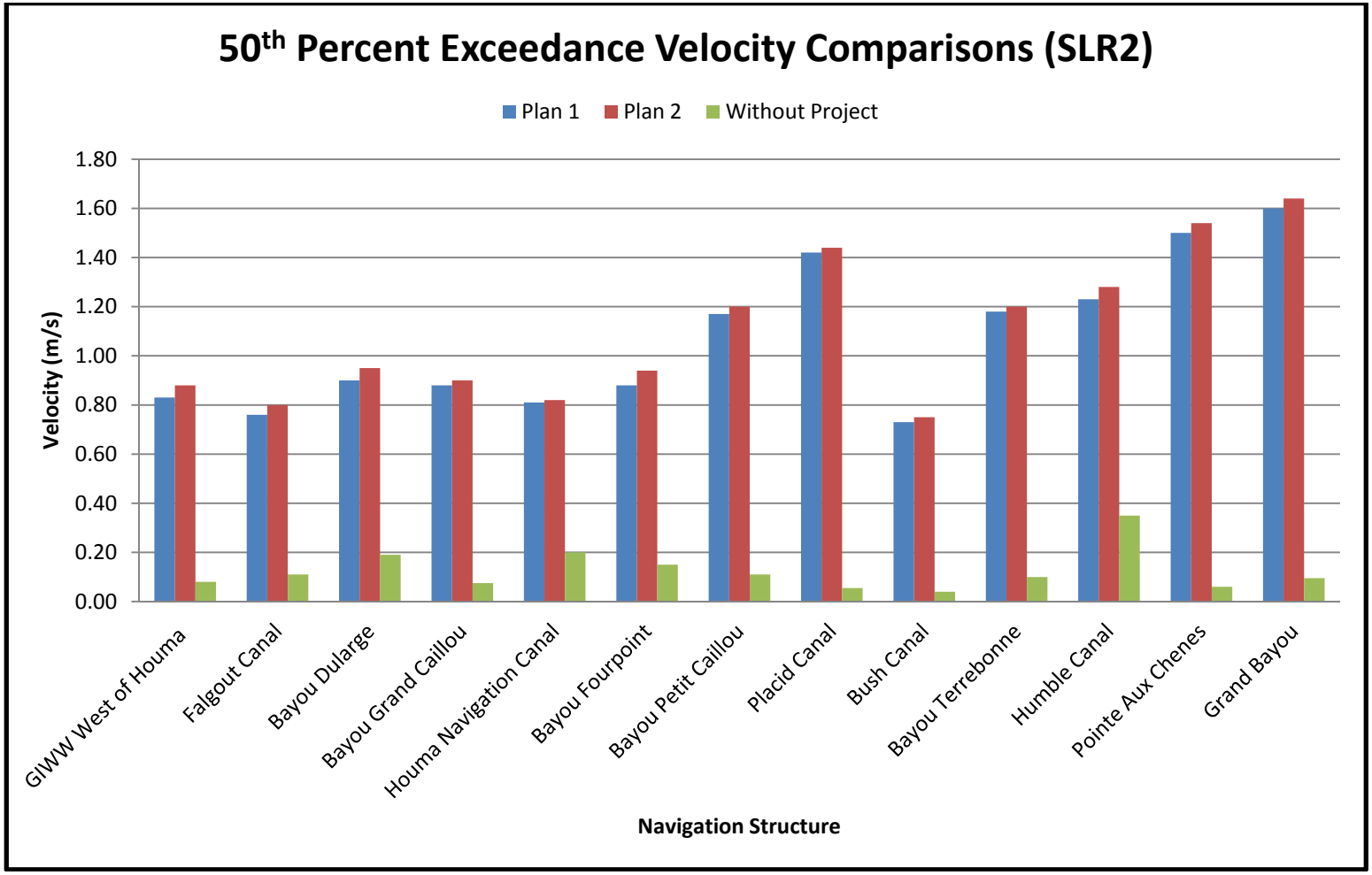

Figure 60. 10th percentile velocity comparisons for plan 1, plan 2, and the without-project configuration for the sea-level rise 2 scenario.

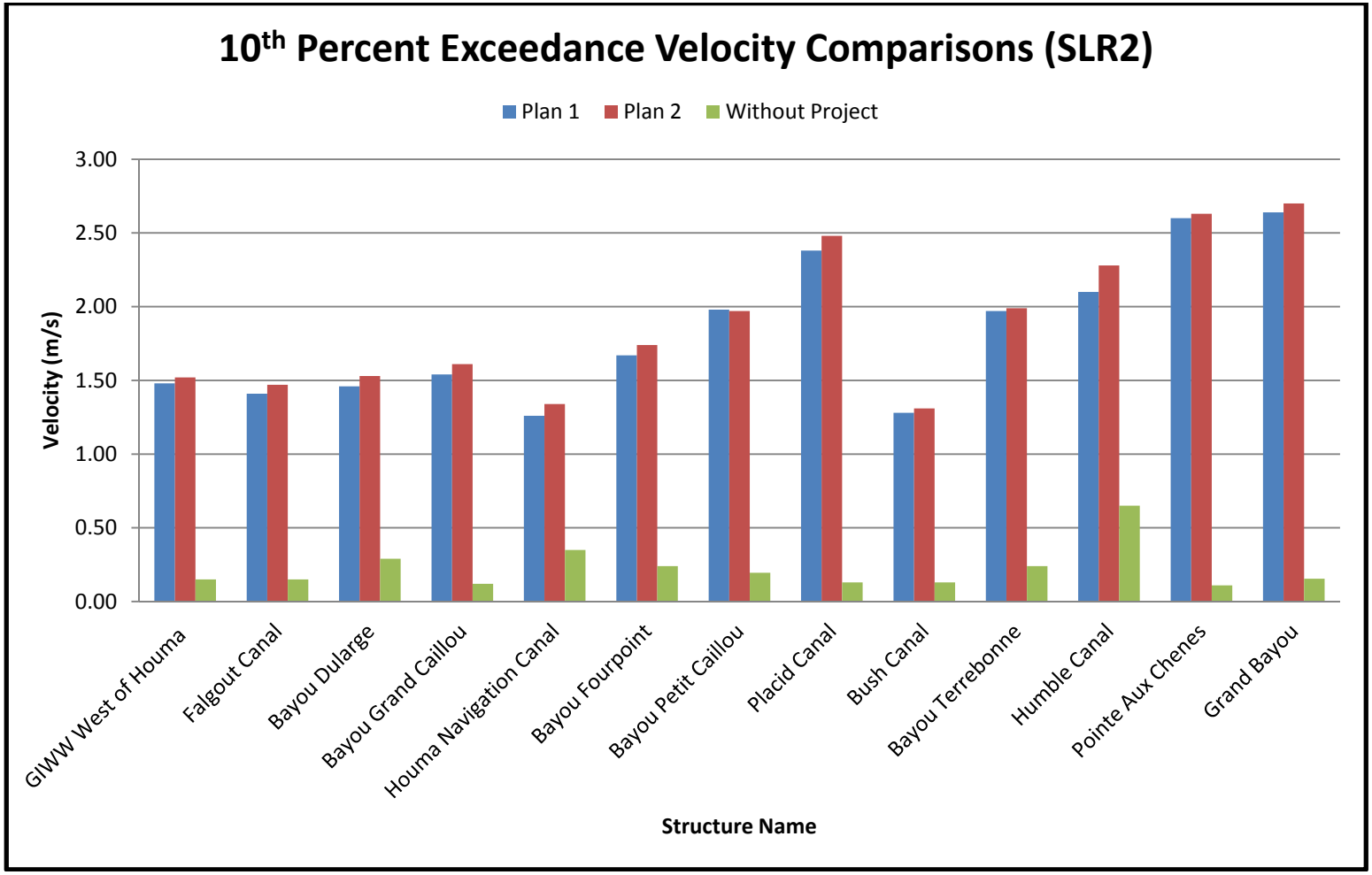

To prevent excessive navigational dangers, the New Orleans District designs structures to prevent velocities in excess of 1.34 m/s (3 mph). Figure 55 and Figure 56 indicate that exceedance of this velocity criterion would be rare for the existing sea level. The sea-level rise 1 scenario (Figure 57 and Figure 58) contains a significantly increased risk of unsafe navigation conditions. The 10th percentile exceedance velocities in Figure 58 indicate that six structures (Bayou Fourpoint, Placid Canal, Bayou Terrebonne, Humble Canal, Pointe Aux Chenes, and Grand Bayou) will have excessive velocities (greater than 1.34 m/s) at least 10% of the time. The sea-level rise 2 scenario (Figure 59 and Figure 60) has three structures (Placid Canal, Pointe Aux Chenes, and Grand Bayou) that are expected to have velocities exceeding the 1.34 m/s criteria at least 50% of the time, indicating significant restrictions on navigation and expectation that every structure will exceed the velocity criteria at least 10 % of the time. For the sea-level rise 1 and 2 scenarios, the without-project velocities are significantly lower than the plan alternatives due to the extensive overland flooding for these alternatives, which allows additional avenues for flow to enter the system beyond just these few locations.

7 Summary and Conclusions

7.1 Model validation

The comparison plots and error metrics (average *RMSE* value of 0.09 m and an average correlation coefficient of 0.85) for the water-surface elevations indicate an accurate representation of the field by the numerical model. This is especially exemplified in the WSE comparisons for the previously mentioned frontal passage events. Accurate replication of these events is highly challenging due to the extreme increases and decreases in water level over short time periods and the complexity of channel connectivity in the system. The accuracy with which the model reproduces this behavior significantly increases the confidence in the numerical model in predicting water-surface elevations.

As expected, the model-versus-field discharge comparisons are not as accurate as those for the water-surface elevations. They are, however, acceptable given the objectives of this study, with average values of 0.71 for the correlation coefficient and *RMSE* value of 45 cms for the gages located within the primary study area (excluding the GIWW at Minors Canal gage due to the previously discussed possible errors associated with this gage). The two gages located nearest the proposed levee alignment (Houma Navigation Canal and Bayou Grand Caillou) have the best error metrics, indicating a favorable representation of the field by the model for these important locations.

While the model's salinity values are sometimes higher or lower than the measured values, the type of activity prevalent in the system is replicated. Several gages located in the study area (Houma Navigation Canal, Bayou Grand Caillou, Humble Canal, etc.) experience sudden spikes in salinity and quick returns to freshwater conditions. The numerical model does an adequate job reproducing this behavior even if the exact salinity values differ. The model also reproduces the regional trends observed in the field, as evidenced by the freshening of the entire system during July and the subsequent increase in salinity from September – December. The numerical model contains all of the dominant processes leading to this increase in salinity (lower freshwater inflows, increased westerly offshore currents and increased offshore water levels). There are uncertainties associated with the specification of each of these important boundary

conditions, but the largest uncertainties are the magnitude and direction of the offshore currents, as these are extremely difficult phenomena to replicate without modeling the entire Gulf of Mexico. These currents are important for the salinity conditions in the Gulf of Mexico portion of the model. Since we are using averaged offshore currents and a constant 30 ppt on the boundary, the salinity boundary conditions in the model are less accurate for 2004 in particular, but they do represent trends and the types of behavior present and, so, the model is adequate for making base-versus-plan comparisons or looking at differences in salinity.

The purpose of the validation was to produce a numerical model that can be applied to compare a base (without-project) condition to alternative plan conditions for hydrodynamic and salinity changes in the model study area. Validation is challenging given the vast domain of the model, the numerous uncertainties present in the boundary-condition specification, and the complexities of the system. The documented validation indicates that the model responds to forcings in a manner similar to that observed in the field, and is sufficient to make base-versus-plan comparisons.

7.2 Base-versus-plan alternative comparisons

The tide ranges just outside of the levee system are sometimes amplified (more so with the higher-sea-level scenarios), with this impact being reduced farther from the levee system. The tide ranges just inside of the levee system are sometimes damped (more so with the higher-sea-level scenarios) due to the reduced connectivity to the Gulf of Mexico due to the limited number of environmental and navigation structures. For the existing water level, the tidal damping tends to be minimal, with damping primarily associated with frontal passage events with extreme increases and decreases in water level over short periods of time (Figure 42). This damping increases for the sea-level rise scenarios, and is expanded to include damping of the normal tidal exchange.

The proposed levee system has minimal impacts to the wetted area for the existing sea level. Some peaks in wetted area associated with frontal passage events are reduced for the alternative configurations, but the difference in the average wetted areas is minimal. This indicates the levee system will reduce the influx of water during a frontal passage event but will not impact the wetted areas/tidal exchange during normal tidal conditions. This is exemplified by the similar average wetted areas (Figure

48) and tidal prisms (Figure 49) for the existing water level for all four mesh configurations.

The impact of the levee system on the wetted area and tidal prism increases for the sea-level rise 1 and increases significantly for the sea-level rise 2 scenario. The wetted areas for the sea-level rise 1 scenario (see Figure 44) show a reduction in the normal wetting/drying occurring inside the proposed levee system as compared to the base mesh configuration. This indicates that the levee system is impeding the normal tidal exchange for the system. This can also be observed in the tidal prism plot in Figure 49, which indicates the tidal prism has been reduced by approximately 50%, or 60 million cubic meters.

The wetted area for the sea-level rise 2 scenario (see Figure 46) indicates a significant reduction in the wetting/drying occurring over a given tidal cycle as compared to the base mesh configuration. Therefore, for this sea-level rise amount, the proposed levee system would significantly impede the tidal exchange for the protected areas. The reduction in the tidal prism (Figure 49) is similar to the sea-level rise 1 scenario from a percentage standpoint (approximately 50 %), but the size of the reduction is now over 150 million cubic meters.

The salinity results indicate several impacts associated with the construction of the proposed levee system, depending on the sea level and particular alternative configuration. The average salinities increase consistently for the higher-water-level scenarios due to the increased tidal prism (Figure 49). The increased tidal prism leads to an inflow of more water from the Gulf of Mexico and, correspondingly, more salinity for the system. The higher water levels also allow more Atchafalaya River fresh water to exit the system by means other than the GIWW/Houma Navigation Canal path, resulting in reduced freshwater inflows for the higher-water-level scenarios.

The plan 1 and plan 2 salinity averages are similar to the without-project salinities for the existing sea level, and thus, have minimal differences. Plan 3 freshens large areas located within the levee system and areas south of Falgout Canal, but has a larger (~4 ppt) increase in salinity south of the Houma Navigation Canal structure as compared to the without project configuration.

The sea-level rise 1 scenario has increased salinity differences between plan 1 and the base mesh, with some increased salinities (less than 1 ppt) along the Houma Navigation Canal north of the levee system along with some slight increases in the salinities in Terrebonne Bay. The plan 2 average salinities are similar to those for plan 1 and the base mesh for the existing sea level, with some small localized differences. The salinities inside the levee system are higher for plans 1 and 2 due to trapping of salinity within the levee system. After salinity enters the system, it can take significantly longer to get flushed out for plans 1 and 2 as compared to the base configuration. For the sea-level rise 1 scenario, the plan 2 salinities are slightly higher than the plan 1 and base-configuration salinities for the Lake Boudreaux area. Plan 3 continues to have a freshening of large areas inside the levee system and south of Falgout Canal with an increase in salinity south of the Houma Navigation Canal structure as compared to the base configuration.

The sea-level rise 2 scenario has significant and widespread differences between plans 1 and 2 and the base configuration. These include widespread freshening of the system of up to 4 ppt for both plans 1 and 2. Plan 3 is similar to plans 1 and 2, but without the slight increase in salinity along the Houma Navigation Canal north of the Houma Navigation Canal structure. This freshening of the system for the plan alternatives is due to the significant reduction in tidal prism (see Figure 49), resulting in a corresponding reduction in the exchange of water and salinity from off shore. The reduction in salinity and water exchange with the Morganza area results in lower salinities for the plan alternatives as compared to the base configuration.

The percent exceedance plots in section 6.6 indicate that for the existing water level, the safe navigation velocity (1.34 m/s or 3 mph) would rarely be exceeded, but it would be exceeded occasionally for the sea-level rise 1 scenario and regularly exceeded for the sea-level rise 2 scenario. This indicates that for the higher sea level amounts, there will be a significant impact on the passage of vessels into and out of the protected areas.

References

Berger, R.C., Tate J.N., Brown, G.L., and Savant G. (2010). "Adaptive Hydraulics: Users Manual." Vicksburg, MS: US Army Engineer Research and Development Center. https://adh.usace.army.mil/.

Blumberg, Alan F. and Mellor, George L. (1985). "A Simulation of the Circulation in the Gulf of Mexico." *Israel Journal of Earth Sciences*, Vol. 34, pp 122-144.

Cialone, M. A., Wamsley, T.V., Sleath, A., Thomas, L., Tubman, M., Smith, J., McAlpin, T. and Resio, D. (2010). *Morganza to the Gulf Summary Report*. US Army Engineer Research and Development Center Letter Report.

Johnson, Donald R. (2008). "Ocean Surface Current Climatology in the Northern Gulf of Mexico." Gulf Coast Research Laboratory. Ocean Springs, MS.

Martin, S.K., Savant, G., and McVan, DC. (2010). *Lake Borgne Surge Barrier Study*. Technical Report ERDC/CHL TR-10-10. Vicksburg, MS: US Army Engineer Research and Development Center.

McAlpin, T.O., Berger, R.C., and Henville, A.M. (2009). *Bush Canal Floodgate Study*. Technical Report ERDC/CHL TR-09-09. Vicksburg, MS: US Army Engineer Research and Development Center.

McAlpin, T.O., Floyd, I.E., Callegan, C.J., Pratt, T.C. and Washington, D.M. (2011). *Morganza to the Gulf of Mexico Floodgate Study*. Technical Report ERDC/CHL TR-11-6. Vicksburg, MS: US Army Engineer Research and Development Center.

McAlpin, T.O., Letter Jr., J.V. and Carson, F.C. (2012). *Validation of the Morganza to the Gulf of Mexico TABS-MDS Numerical Model*. Technical Report ERDC/CHL TR-12-12. Vicksburg, MS: US Army Engineer Research and Development Center.

McLaughlin, J.W., Bilgili, A. and Lynch, D.R. (2003). "Numerical Modeling of Tides in the Great Bay Estuarine System: Dynamical Balance and Spring-Neap Residual Modulation." *Estuarine, Coastal and Shelf Science*. Vol. 57, No. 1 – 2, pp 283 – 296.

Oey, L.-Y., Ezer, T. and Lee, H.-C. (2005). "Loop Current, Rings and Related Circulation in the Gulf of Mexico; A Review of Numerical Models and Future Challenges." *Circulation in the Gulf of Mexico: Observations and Models*, Geophysical Monograph Series, Vol. 161, pp 31-56. Washington, DC.

Project Fact Sheet: Morganza to the Gulf of Mexico Hurricane Protection Project. http://www.mvn.usace.army.mil/prj/mtog/project_fact_sheet___morganza.asp . Updated 22 February 2008. New Orleans, LA: New Orleans District.

Savant, G., Berger, R.C., McAlpin, T.O., and Tate, J.N. (2010). "An Efficient Implicit Finite Element Hydrodynamic Model for Dam and Levee Breach." *Journal of Hydraulic Engineering*, ASCE. Doi:10.1061/(ASCE)HY.1943-7900.0000372.

Stockstill, R.L. and Vaughan, J.M. (2009). *Numerical Model Study of the Tuscarawas River below Dover Dam, Ohio*. Technical Report ERDC/CHL TR-09-17. Vicksburg, MS: US Army Engineer Research and Development Center.

Stockstill, R.L., Vaughan, J.M., and Martin, S.K. (2010). *Numerical Model of the Hoosic River Flood-Control Channel, Adams, MA*. Technical Report ERDC/CHL TR-10-01. Vicksburg, MS: US Army Engineer Research and Development Center.

Sturges, W., Niiler, P.P. and Weisberg, R.H. (2001). *Northeastern Gulf of Mexico Inner Shelf Circulation Study*. Final Report, MMS Cooperative Agreement 14-35-0001-=30787. OCS Report MMS 2001 – 103, US Minerals Management Service, Herndon, VA.

Surface-water Modeling System (SMS), Version 10.1. Computer software. Provo, UT: Aquaveo.

Tate, J.N., Lackey, T.C., and McAlpin, T.O. (2010). Seabrook Fish Larval Transport Study. Technical Report ERDC/CHL TR-10-12. Vicksburg, MS: US Army Engineer Research and Development Center.

Taylor, J.R. (1997). "An Introduction to Error Analysis: The Study of Uncertainties in Physical Measurements." Sausalito, CA: University Science Books.

US Army Corps of Engineers (2008). *Assessment of Houma Navigation Canal Deepening on Flow Distribution and Salinity Intrusion on its Major Tributaries and Distributaries*. New Orleans, LA: New Orleans District.

US Army Corps of Engineers (2013). "Morganza to the Gulf of Mexico, Louisiana, Post-Authorization Change Report (PAC)." New Orleans, LA: New Orleans District.

US Geological Survey (2008). *Influence of the Houma Navigation Canal on Salinity Patterns and Landscape Configuration in Coastal Louisiana*. US Department of the Interior. Open-File Report 2008-1127.

Wang, F.C. (1988). "Dynamics of Saltwater Intrusion in Coastal Channels." *Journal of Geophysical Research*, 93 (C6), 6937-6946.

Appendix A: Description of the Adaptive Hydraulics (AdH) Model

AdH is a state-of-the-art code developed by the US Army Engineer Research and Development Center (ERDC) to simulate both saturated and unsaturated groundwater, overland flow, three-dimensional Navier-Stokes flow, and 2D or 3D shallow water problems (Berger et al. 2010).

The 2D shallow-water equations are a result of the vertical integration of the equations of mass and momentum conservation for incompressible flow under the hydrostatic pressure assumption (Berger and Lee 2004). Written in conservative form, the 2D shallow water equations are:

$$\frac{\partial \boldsymbol{U}}{\partial t} + \frac{\partial \boldsymbol{F}}{\partial x} + \frac{\partial \boldsymbol{G}}{\partial y} + \boldsymbol{H} = 0$$

where

$$\mathbf{U} = \begin{Bmatrix} h \\ uh \\ vh \end{Bmatrix}$$

$$\mathbf{F} = \begin{Bmatrix} uh \\ u^2h + \frac{1}{2}gh^2 - h\frac{\sigma_{xx}}{\rho} \\ uvh - h\frac{\sigma_{yx}}{\rho} \end{Bmatrix}$$

$$\mathbf{G} = \begin{Bmatrix} vh \\ uvh - h\frac{\sigma_{xy}}{\rho} \\ v^2h + \frac{1}{2}gh^2 - h\frac{\sigma_{yy}}{\rho} \end{Bmatrix}$$

and

$$\mathbf{H} = \begin{Bmatrix} 0 \\ gh\dfrac{\partial z_b}{\partial x} + \tau_{bed_x} \\ gh\dfrac{\partial z_b}{\partial y} + \tau_{bed_y} \end{Bmatrix}$$

where ρ is the fluid density, g is the gravitational acceleration, z_b is the bed elevation, τ_{bed_i} is the bed shear stress drag where the subscript (i) indicates the direction (x and y), h is the flow depth, u is the x component of velocity, v is the y component of velocity, and σ represents the Reynolds stresses due to turbulence, where the first subscript indicates the direction, and the second indicates the face on which the stress acts.

The Reynolds stresses are determined using the Boussinesq approach to the gradient in the mean currents:

$$\sigma_{xx} = 2\rho v_t \frac{\partial u}{\partial x}$$

$$\sigma_{yy} = 2\rho v_t \frac{\partial v}{\partial y}$$

And

$$\sigma_{xy} = \sigma_{yx} = \rho v_t \left(\frac{\partial u}{\partial y} + \frac{\partial v}{\partial x}\right)$$

where v_t = kinematic eddy viscosity (which varies spatially).

The AdH shallow-water equations are placed in conservative form to ensure mass balance and balance of momentum and pressure across an interface. This results in a locally mass-conservative model (Berger and Howington 2002).

The equations are coded in a finite-element approach with the velocities and depth being represented as linear polynomials on each element. AdH utilizes a streamline-upwind Petrov-Galerkin (SUPG) scheme similar to that reported in Berger and Stockstill (1995) and patterned after previous work by Hughes and Brooks (1982), Moretti (1979), Gabutti (1983), and Steger and Warming (1981). Since the finite-element scheme is not the

primary focus of this paper, a more in-depth description of this method is omitted.

AdH contains other essential features such as wetting and drying, completely coupled sediment and salt transport, and wind effects. A series of modularized libraries make it possible for AdH to include vessel movement, friction descriptions, as well as a host of other features. AdH can run in parallel or on a single processor and runs on both Windows systems and UNIX based systems.

References

Berger, R.C. and Howington, S.E. (2002). "Discrete Fluxes and Mass Balance in Finite Elements." Journal of Hydraulic Engineering, ASCE, 128 (1), 87 – 92.

Berger, R.C. and Lee, L.M. (2004) "Multidimensional Numerical Modeling of Surges Over Initially Dry Land", Coastal and Hydraulics Engineering Technical Report, ERDC/CHL TR-04-10. Vicksburg, MS: US Army Engineer Research and Development Center.

Berger, R.C., Tate J.N., Brown, G.L., and Savant G. (2010). "Adaptive Hydraulics: Users Manual." Vicksburg, MS: US Army Engineer Research and Development Center. https://adh.usace.army.mil/.

Berger, R.C. and Stockstill, R.L. (1995). "Finite element model for high-velocity channels." Journal of Hydraulic Engineering ASCE, 121(10), 710–716.

Gabutti, B. (1983). "On two upwind finite difference schemes for hyperbolic equations in non-conservative form." Computers and Fluids, 11(3), 207-230.

Hughes, T.J.R., and Brooks, A.N. (1982). "A theoretical framework for Petrov-Galerkin methods with discontinuous weighting functions: applications to the streamline-upwind procedures." Finite Elements in Fluids, R. H. Gallagher et al. eds., J. Wiley & Sons, Inc., London, England, Vol. 4, 47 – 65.

Moretti, G. (1979). "The λ-scheme." Computers and Fluids, 7(3), 191 – 205.

Steger, J.L., and Warming, R.F. (1981). "Flux vector splitting of the inviscid gas dynamics equations with applications to finite difference methods." Journal of Computational Physics, Vol. 40, 263 – 293.

Appendix B: Water-Surface Elevation Comparisons

Water-surface elevation comparison plots consist of year-long time series comparisons for 2004, zoomed comparisons for varying three-month periods (depending on data availability), and model-versus-field box plots. For the box plots, points lying on the 45 degree black line represent an exact replication of the field by the model. Points below the line represent calculated model results below the observed field values, and points above the line represent calculated model results above the observed field values. These comparison plots are included as Figure 61 – Figure 91.

Figure 61. Wax Lake WSE comparison plots.

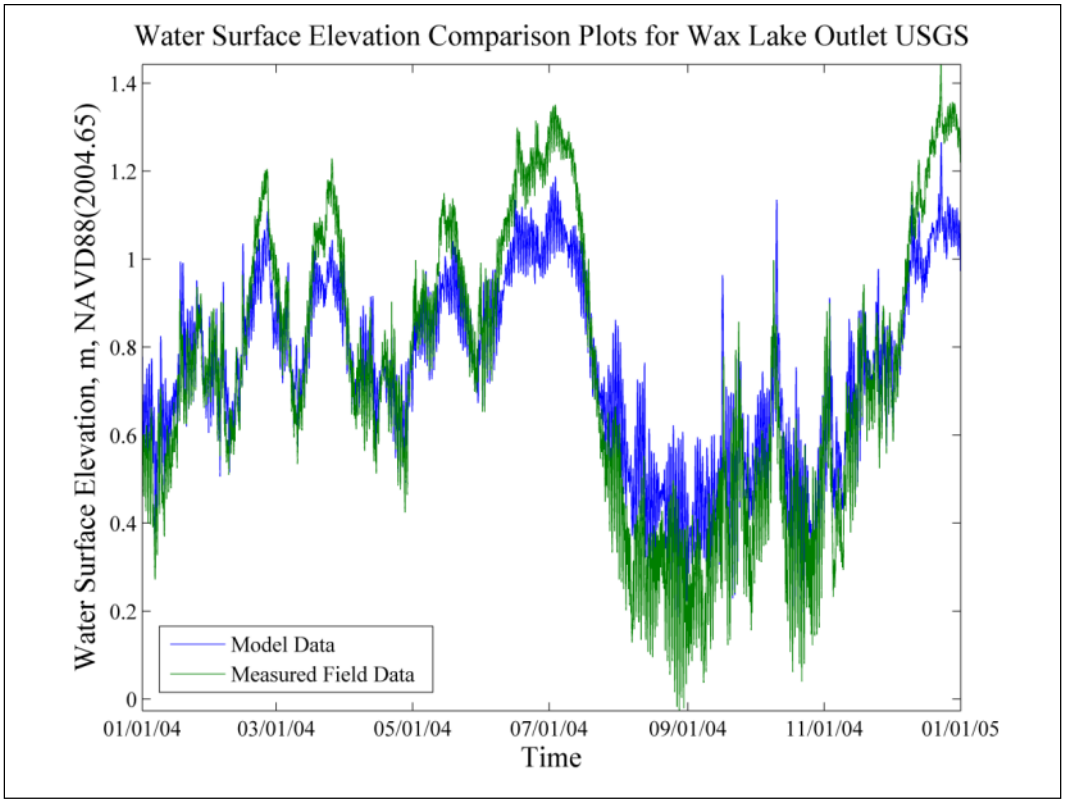

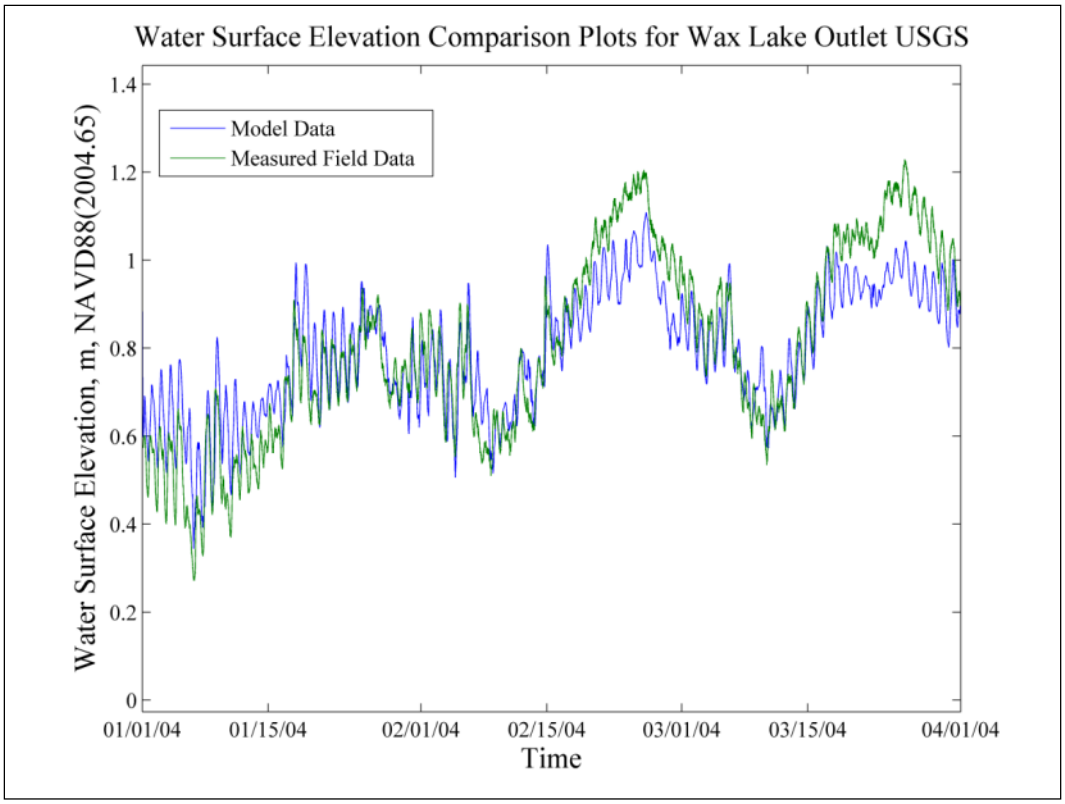

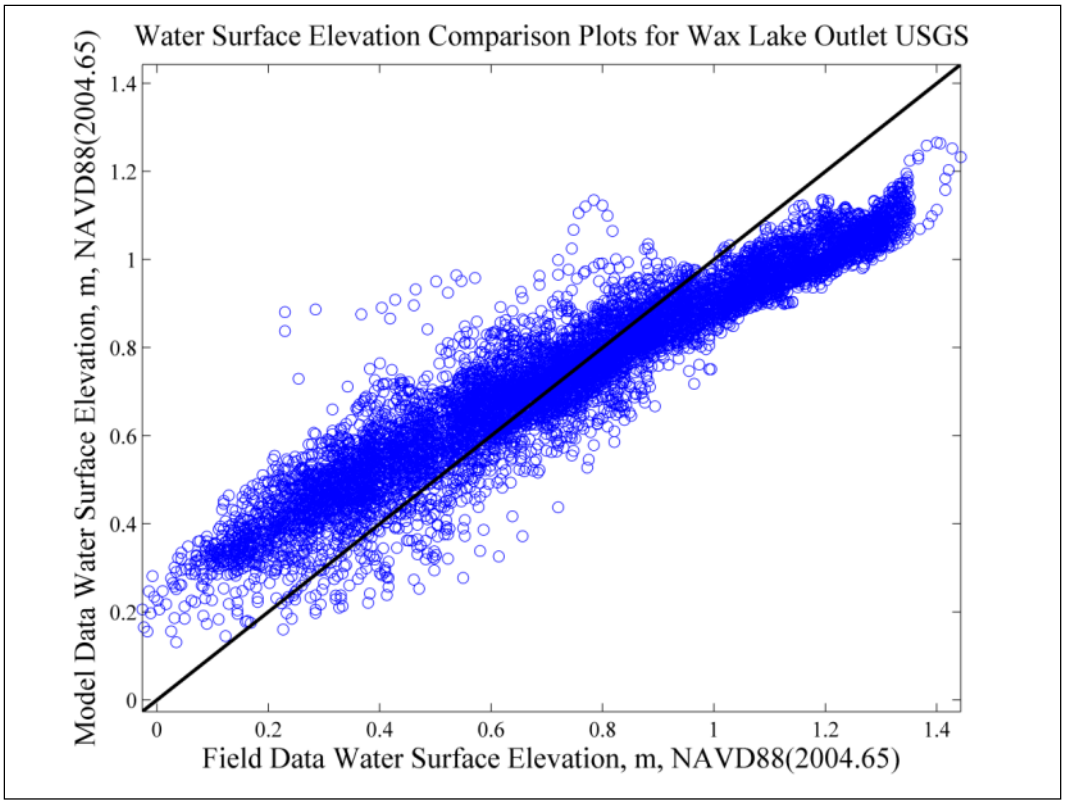
Water Surface Elevation Comparison Plots for Wax Lake Outlet USGS
Model Data Water Surface Elevation, m, NAVD88(2004.65)
Field Data Water Surface Elevation, m, NAVD88(2004.65)
0
0.2
0.4
0.6
0.8
1
1.2
1.4

Figure 62. GIWW at mile 103 WSE comparison plots.

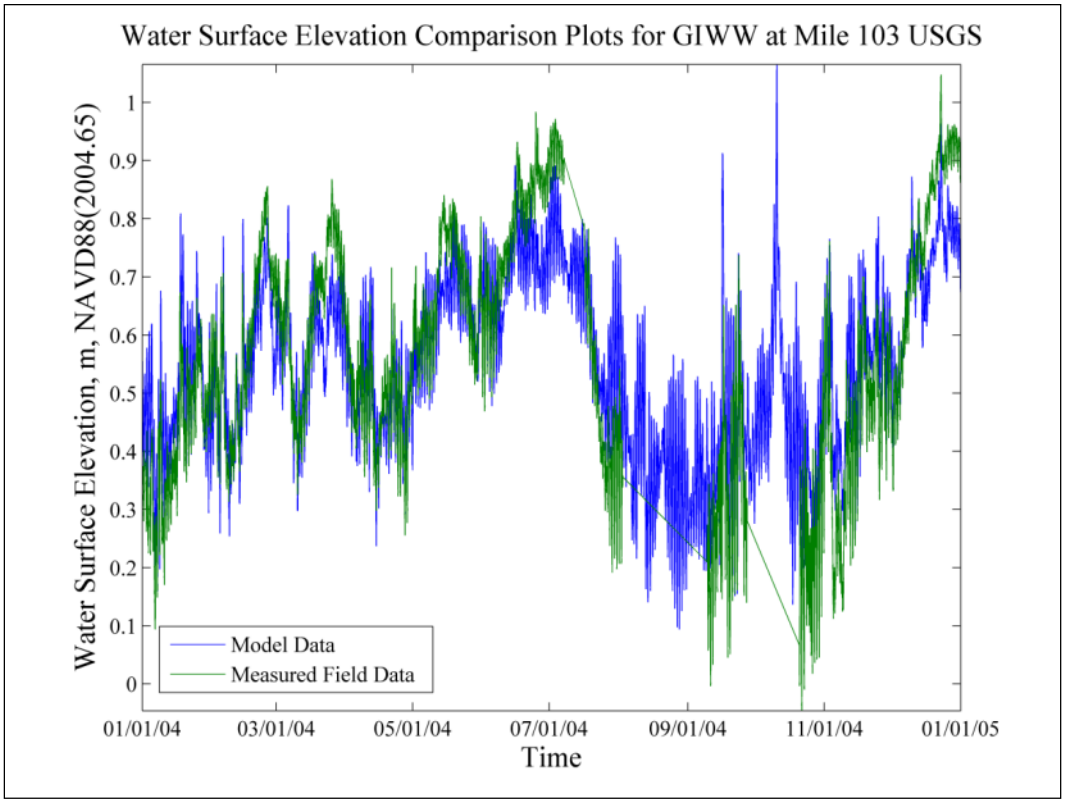

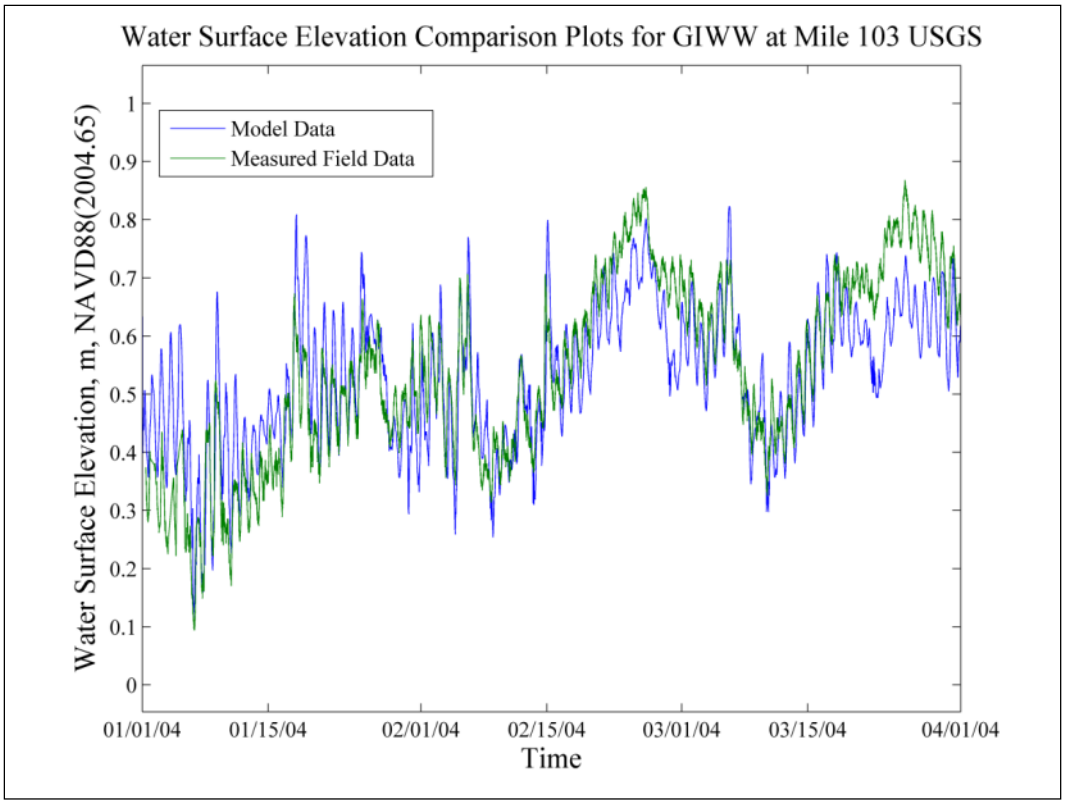

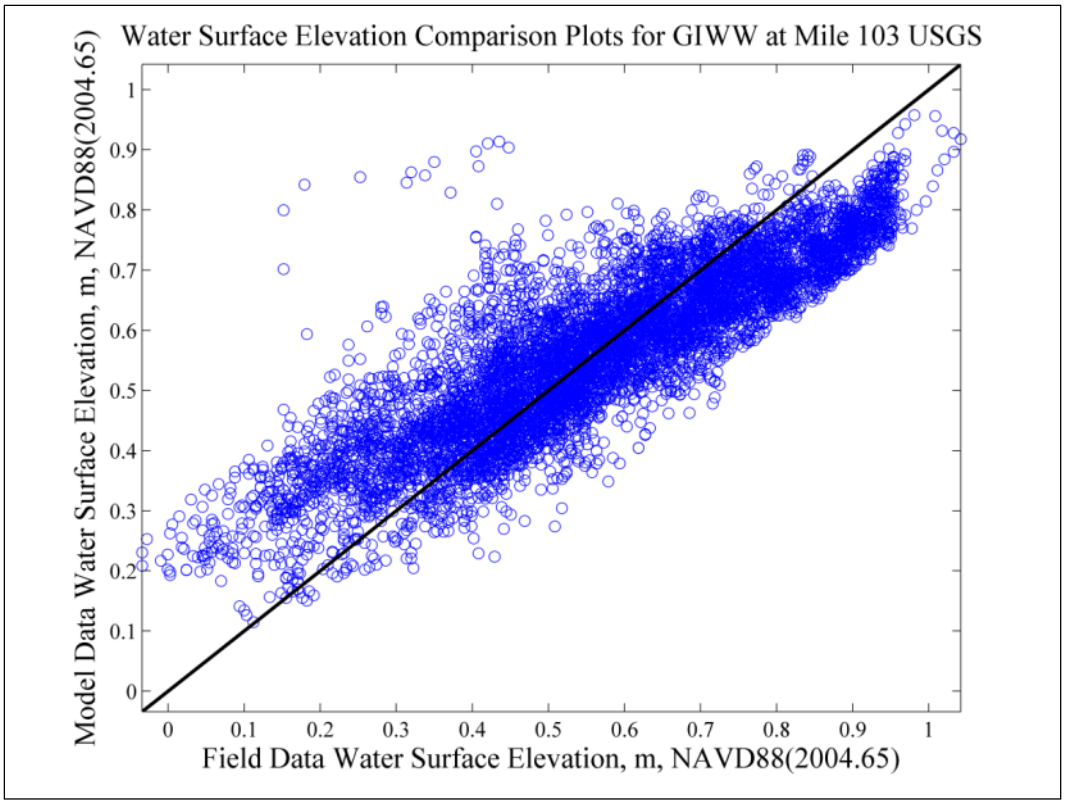
Water Surface Elevation Comparison Plots for GIWW at Mile 103 USGS
Model Data Water Surface Elevation, m, NAVD88(2004.65)
Field Data Water Surface Elevation, m, NAVD88(2004.65)
0
0.1
0.2
0.3
0.4
0.5
0.6
0.7
0.8
0.9
1

Figure 63. Lower Atchafalaya River WSE comparison plots.

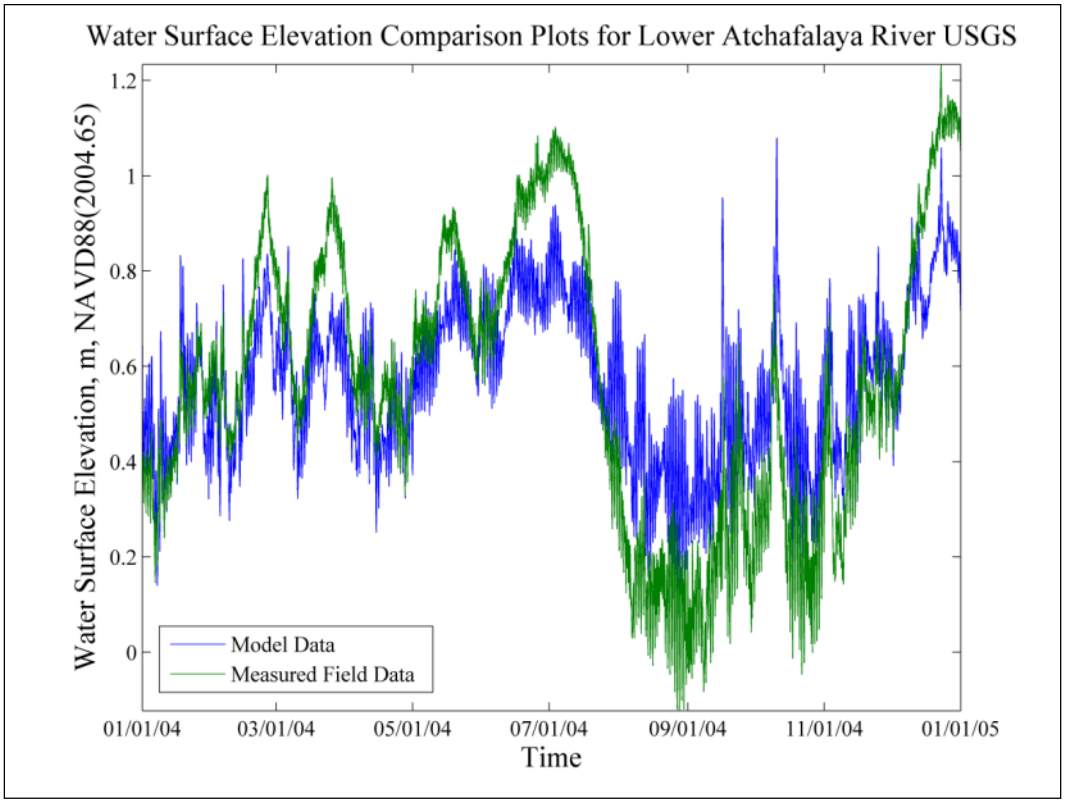

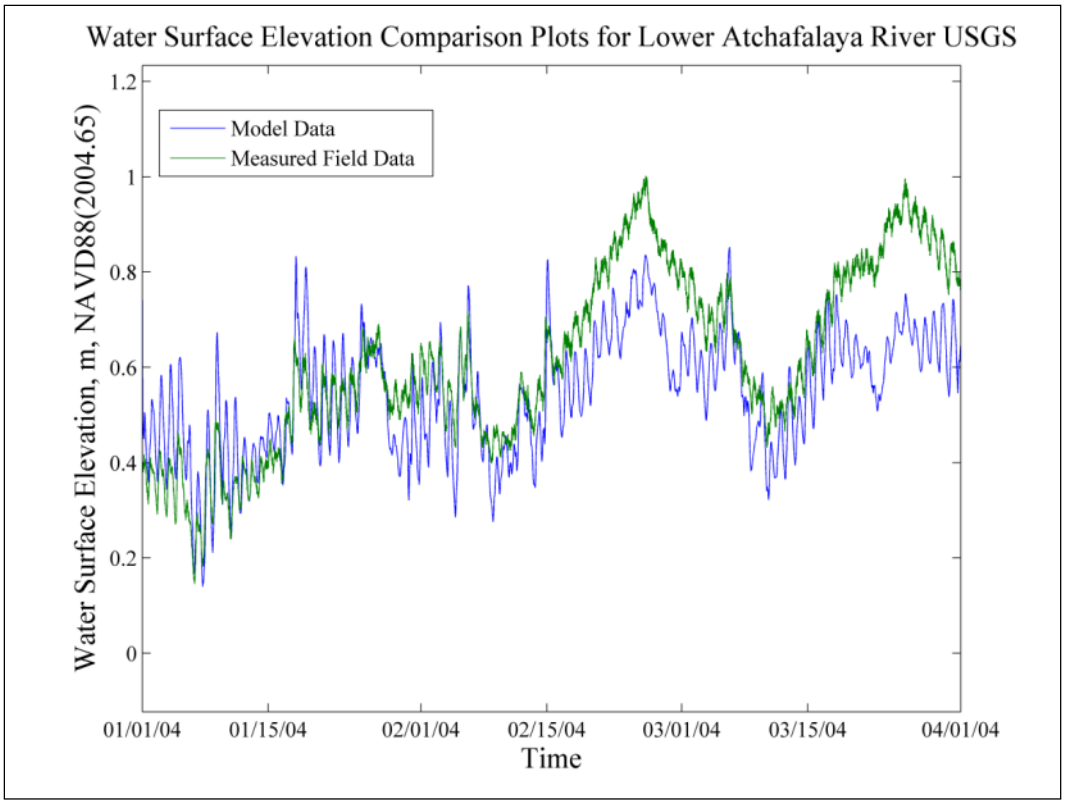

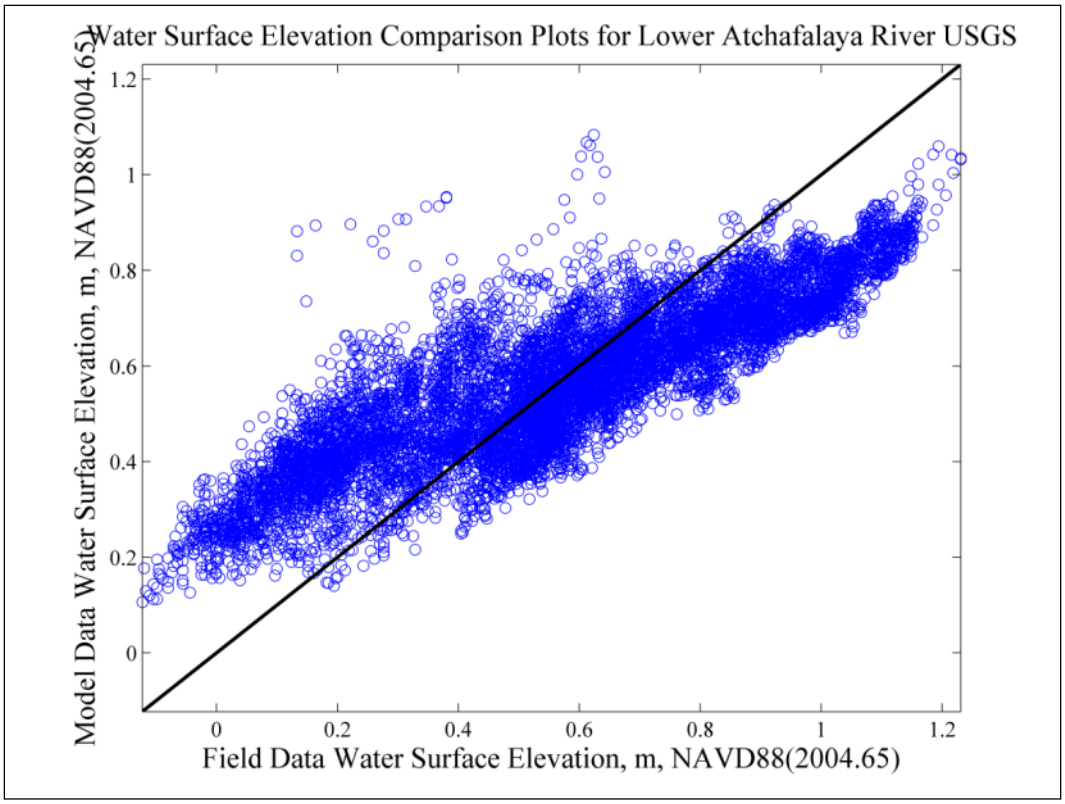
Water Surface Elevation Comparison Plots for Lower Atchafalaya River USGS
Model Data Water Surface Elevation, m, NAVD88(2004.65)
Field Data Water Surface Elevation, m, NAVD88(2004.65)
0
0.2
0.4
0.6
0.8
1
1.2

Figure 64. Bayou Penchant WSE comparison plots.

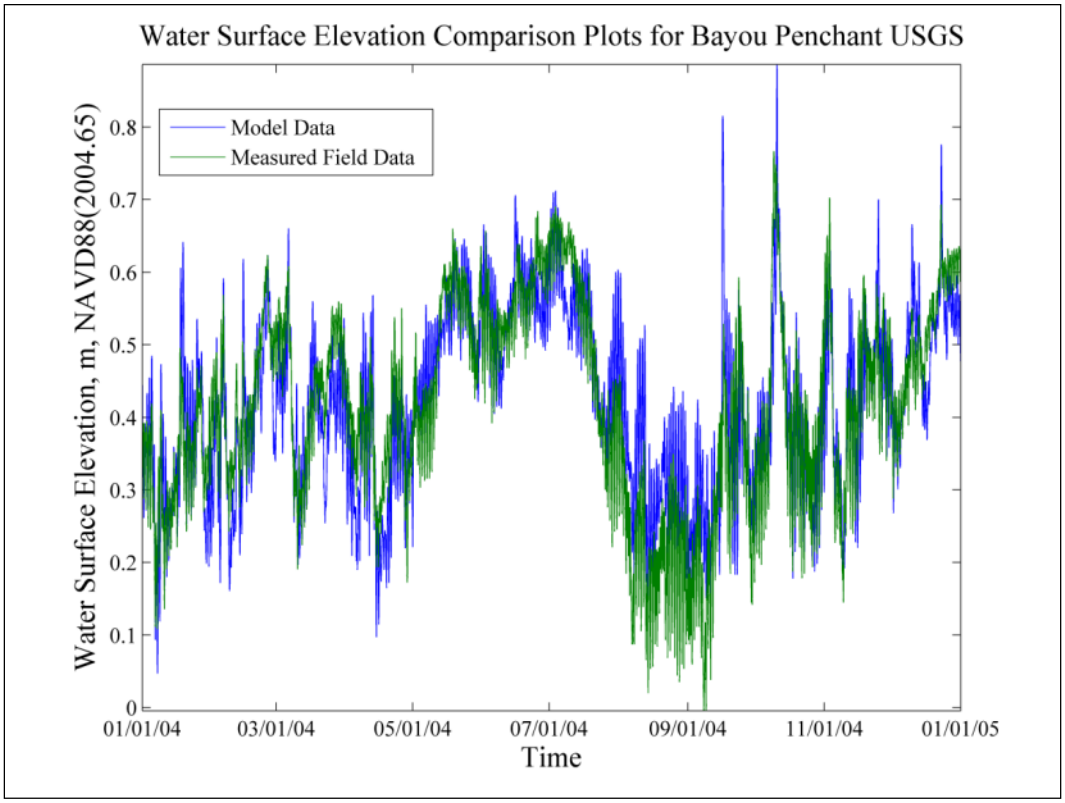

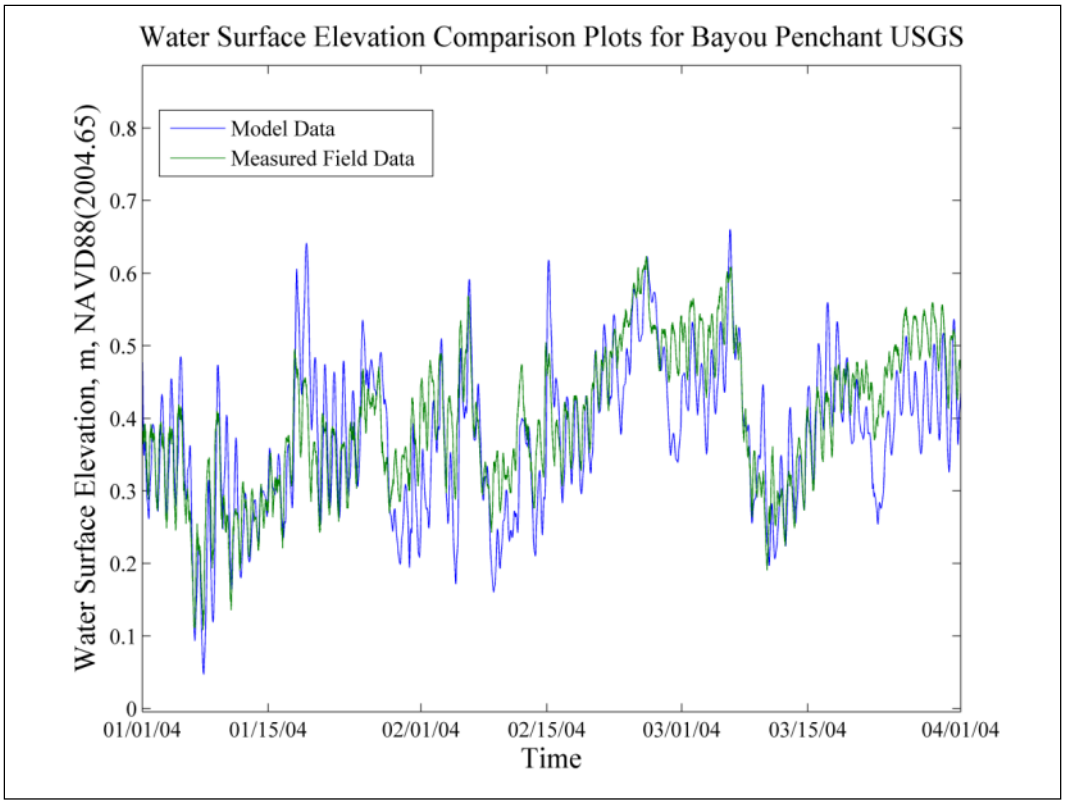

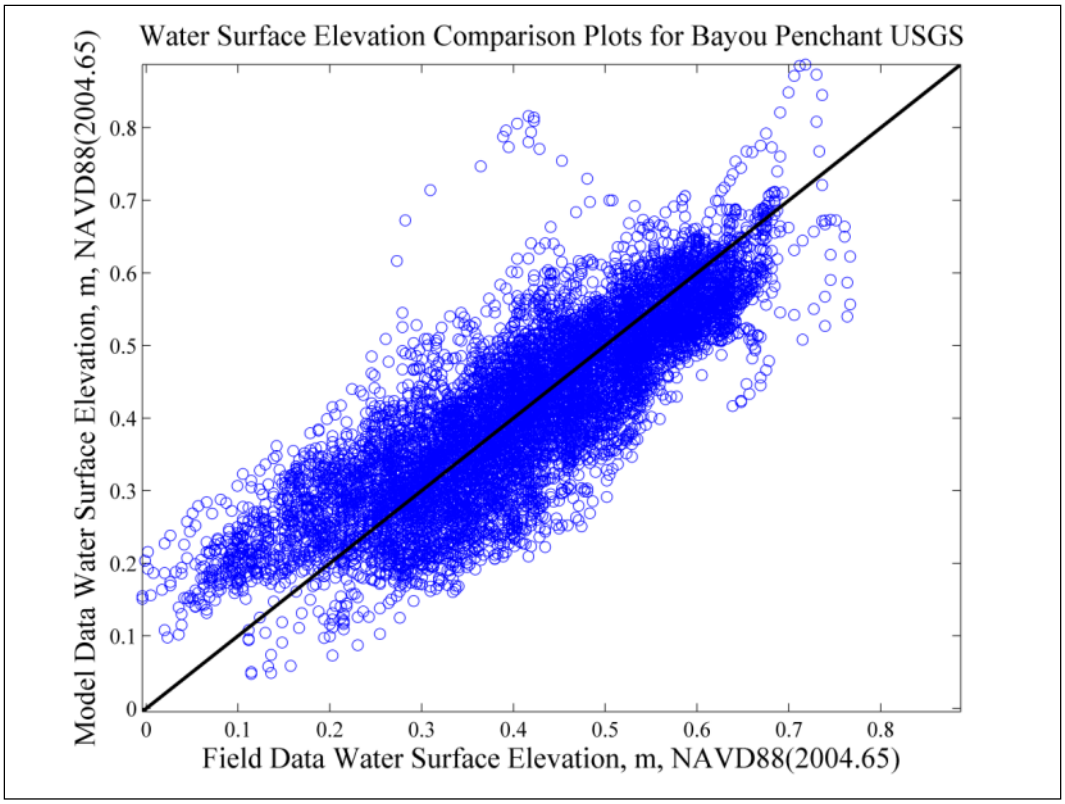
Water Surface Elevation Comparison Plots for Bayou Penchant USGS
Model Data Water Surface Elevation, m, NAVD88(2004.65)
Field Data Water Surface Elevation, m, NAVD88(2004.65)
0
0.1
0.2
0.3
0.4
0.5
0.6
0.7
0.8

Figure 65. Bayou Boeuf WSE comparison plots.

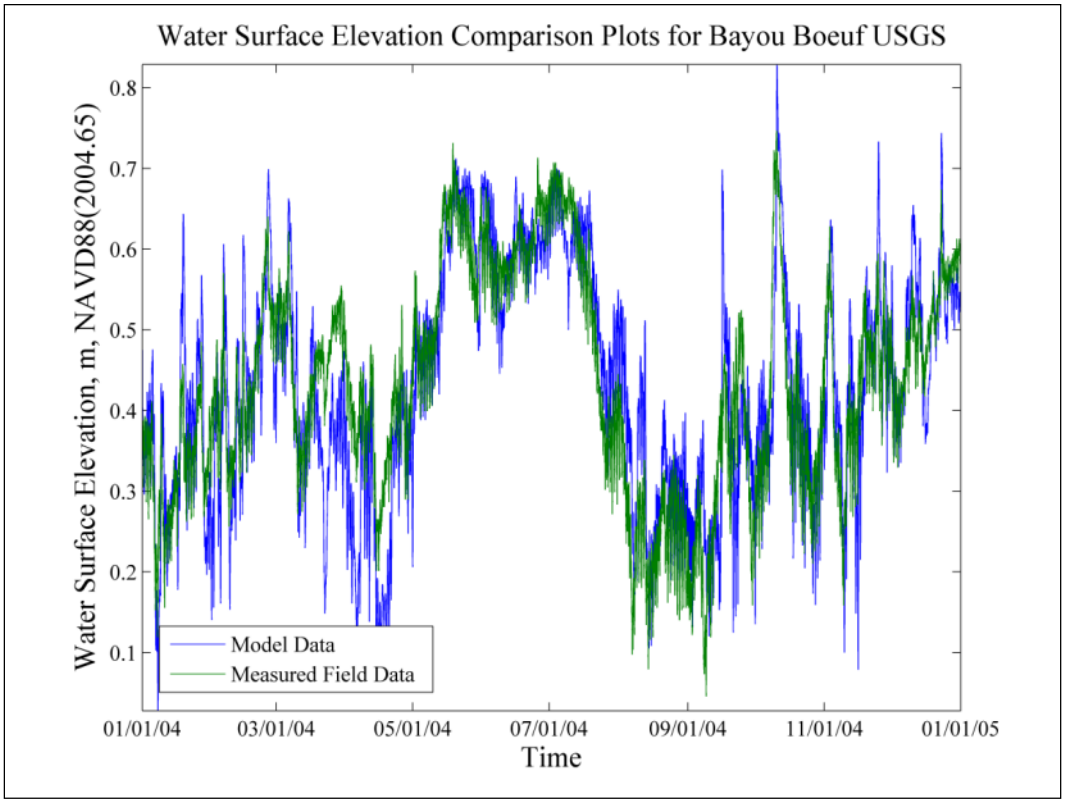

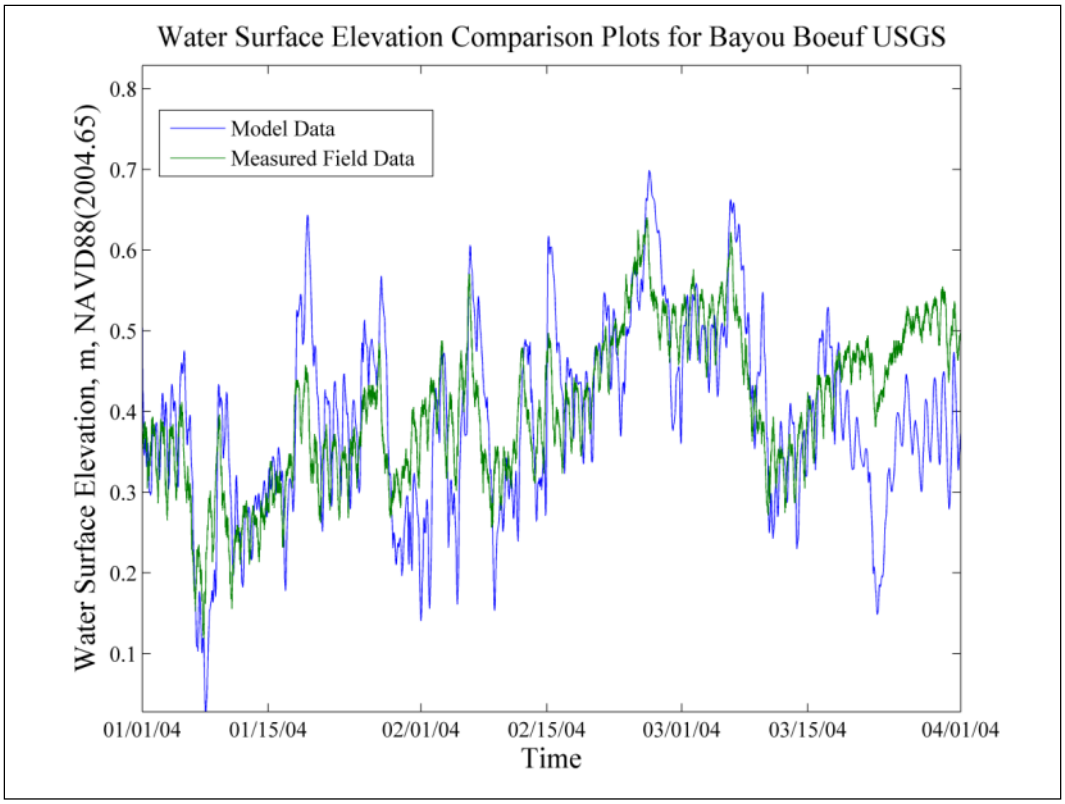

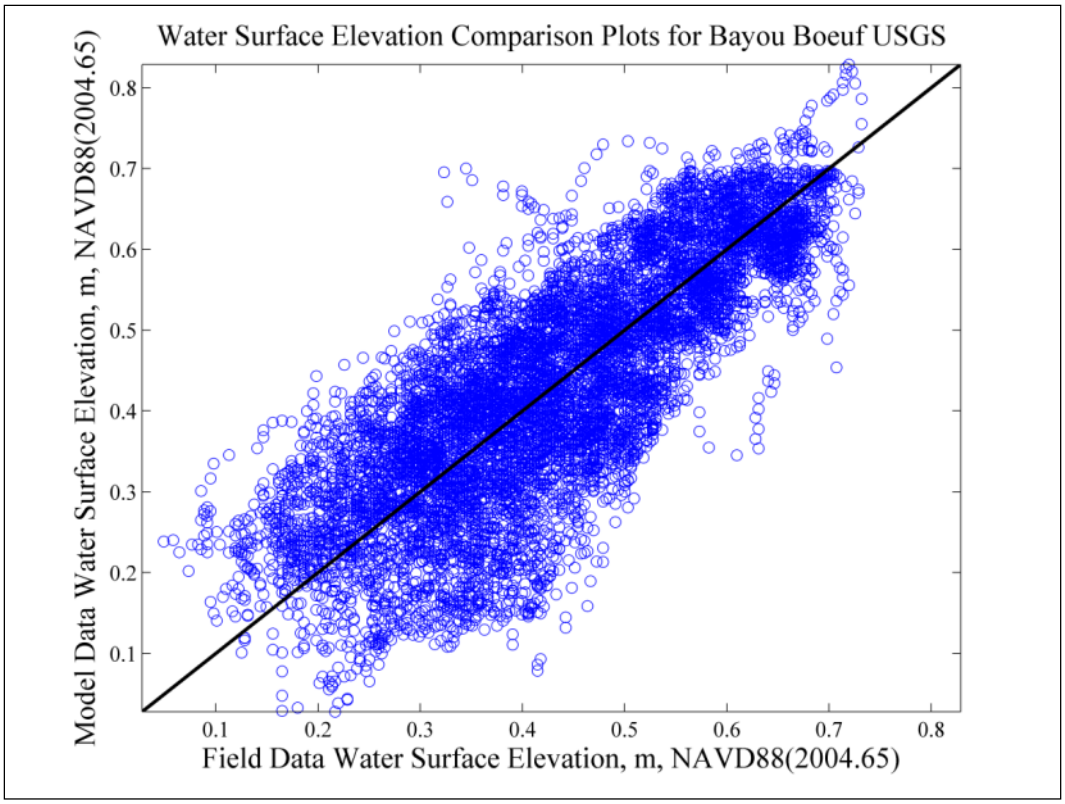
Water Surface Elevation Comparison Plots for Bayou Boeuf USGS
Model Data Water Surface Elevation, m, NAVD88(2004.65)
Field Data Water Surface Elevation, m, NAVD88(2004.65)
0.1
0.2
0.3
0.4
0.5
0.6
0.7
0.8

Figure 66. Caillou Lake WSE comparison plots.

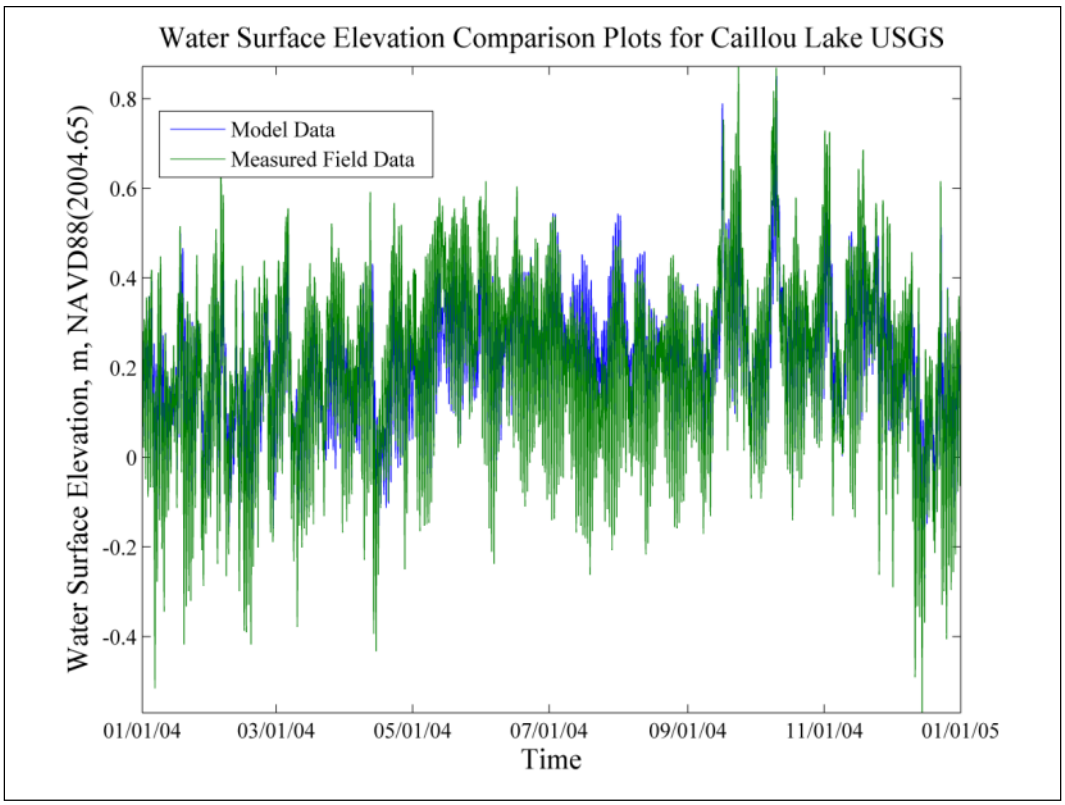

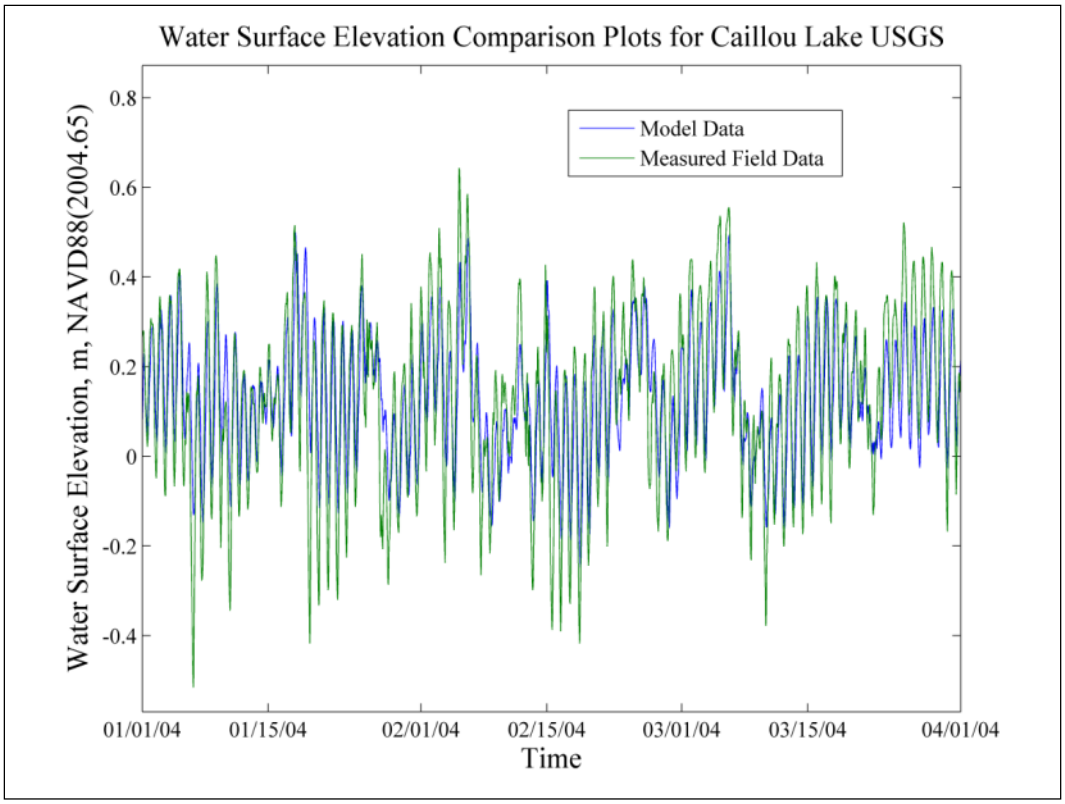

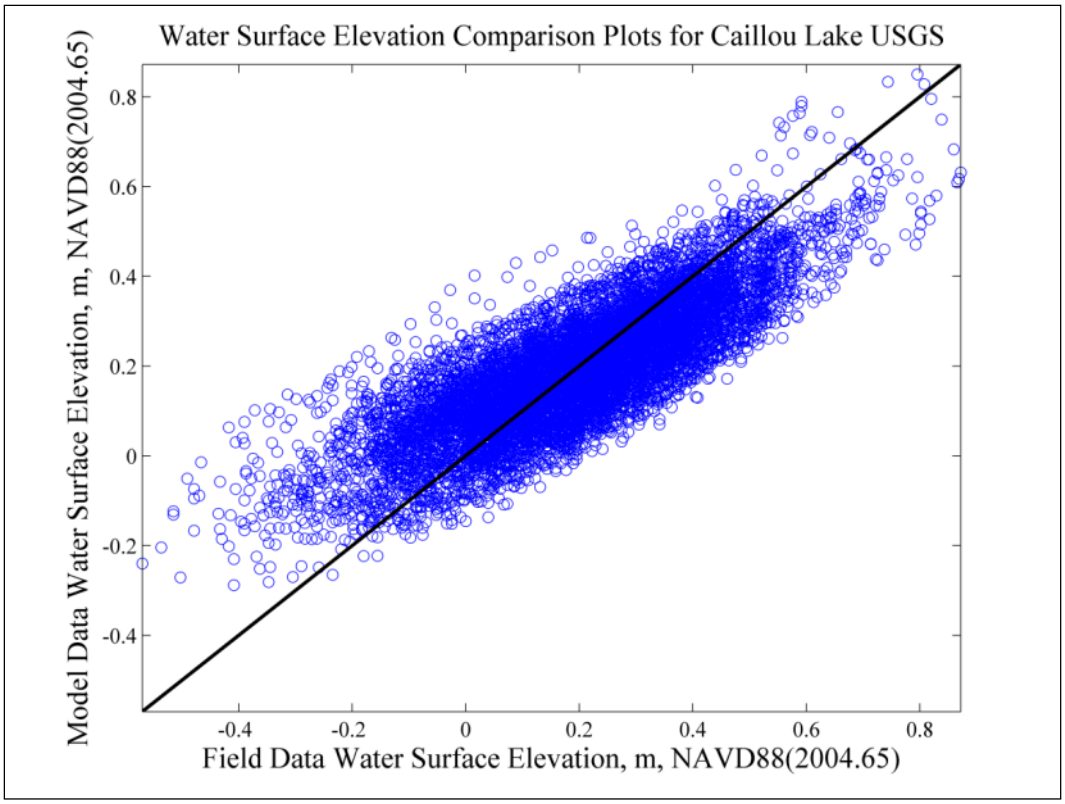
Water Surface Elevation Comparison Plots for Caillou Lake USGS
Model Data Water Surface Elevation, m, NAVD88(2004.65)
Field Data Water Surface Elevation, m, NAVD88(2004.65)
0.8
0.6
0.4
0.2
0
-0.2
-0.4
-0.4
-0.2
0
0.2
0.4
0.6
0.8

Figure 67. Caillou Bay WSE comparison plots.

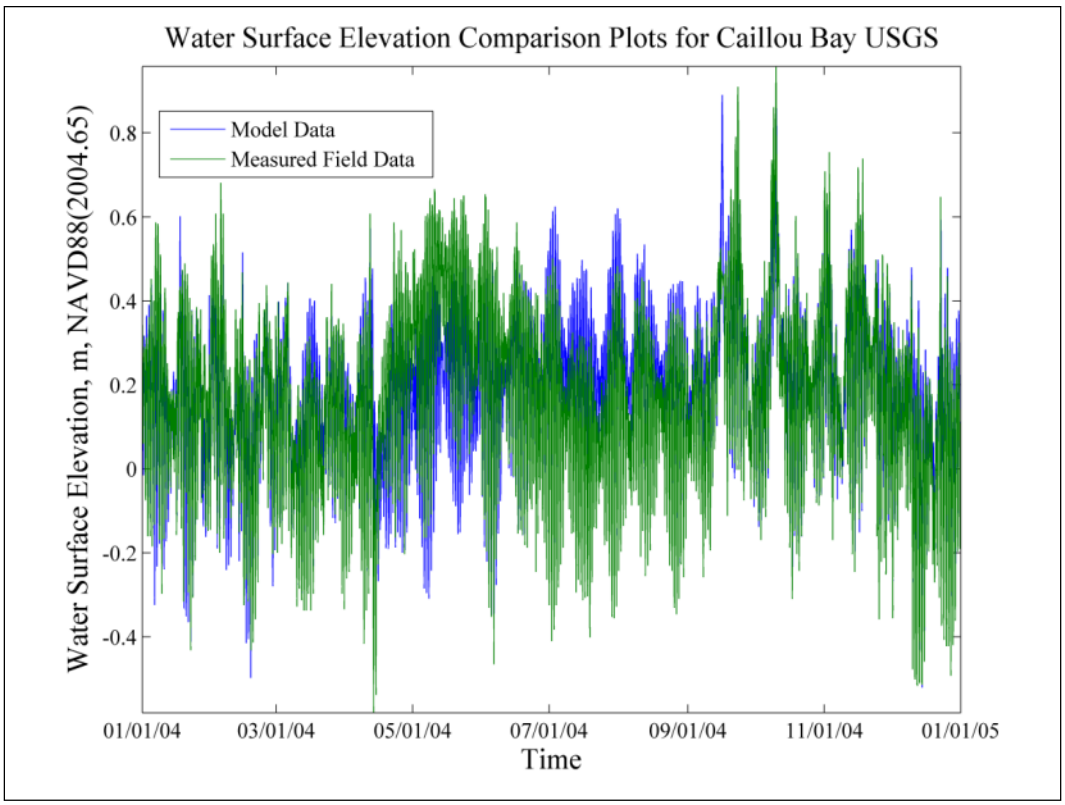

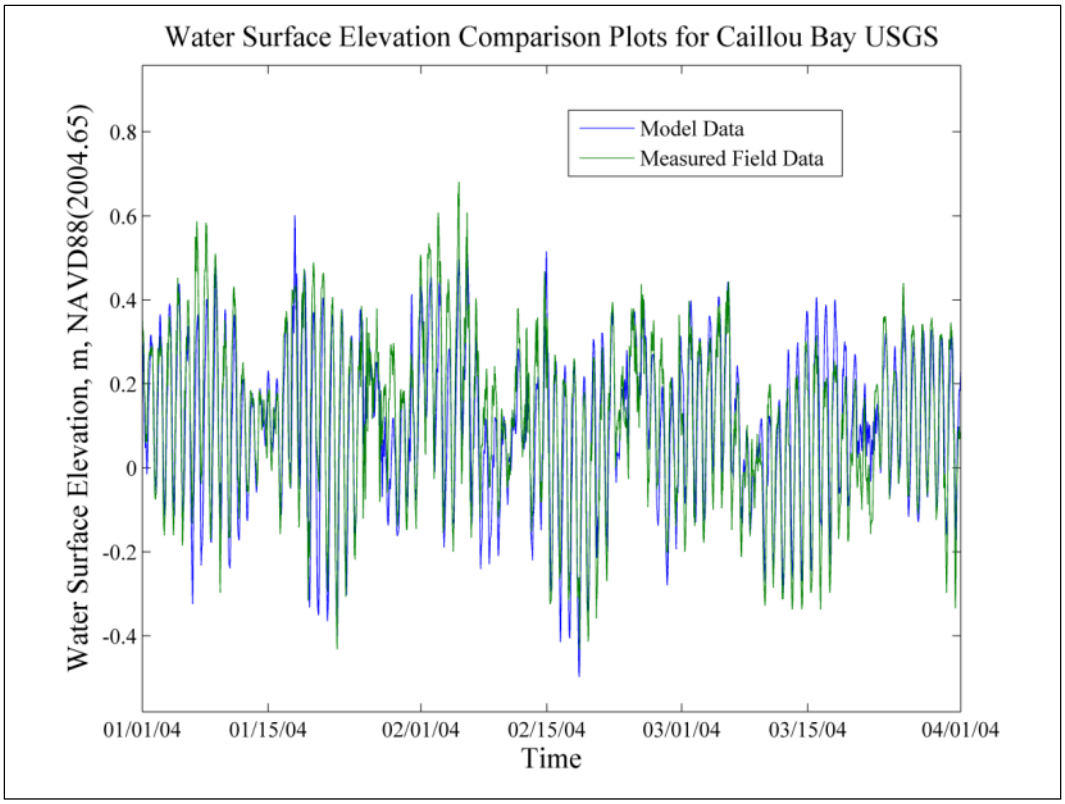

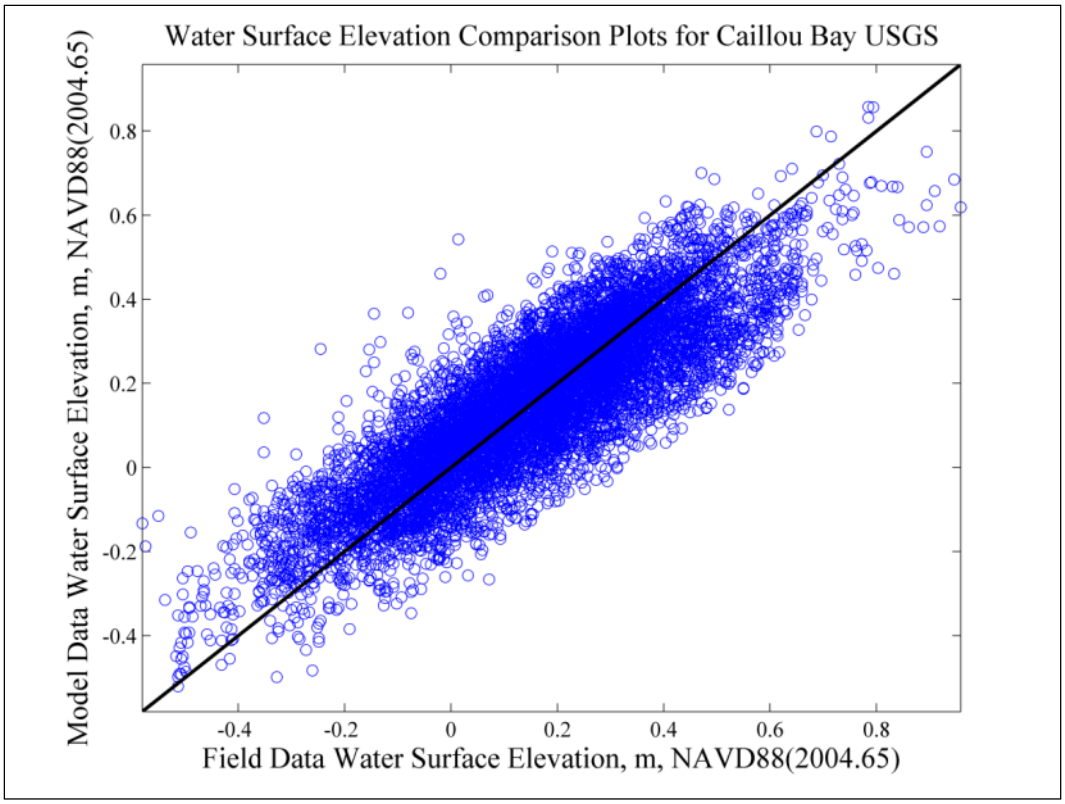
Water Surface Elevation Comparison Plots for Caillou Bay USGS
Model Data Water Surface Elevation, m, NAVD88(2004.65)
Field Data Water Surface Elevation, m, NAVD88(2004.65)
0.8
0.6
0.4
0.2
0
-0.2
-0.4
-0.4
-0.2
0
0.2
0.4
0.6
0.8

Figure 68. Houma Navigation Canal WSE comparison plots.

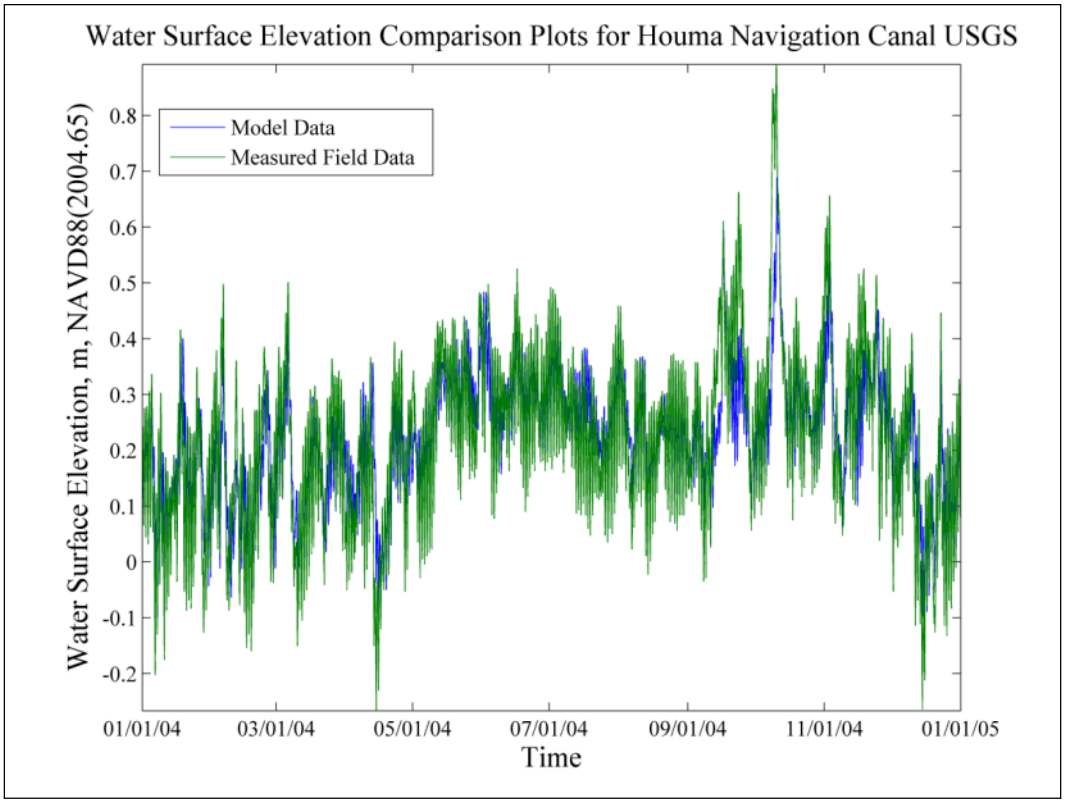

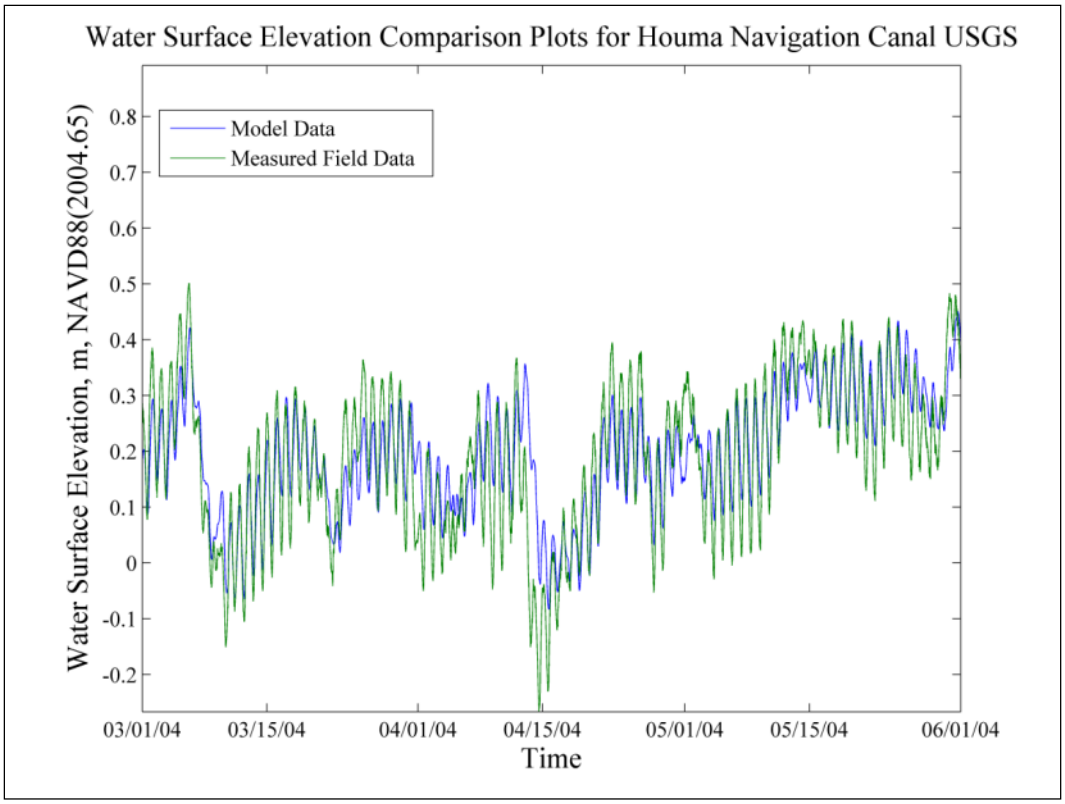

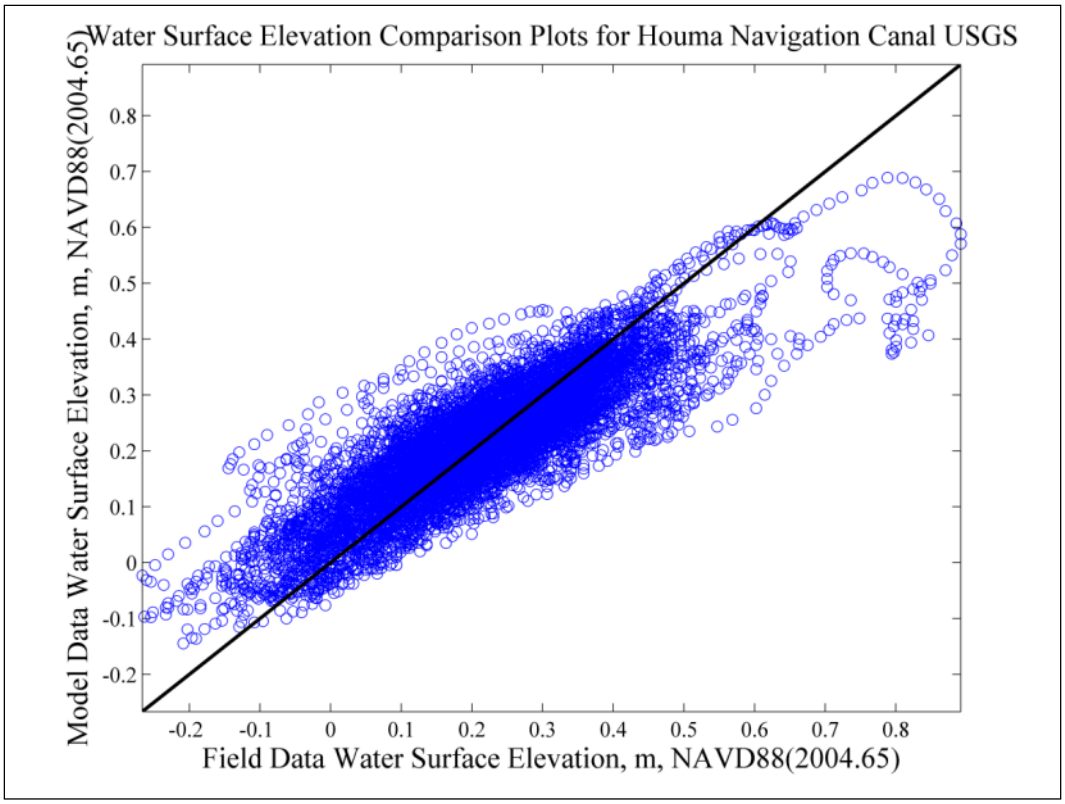
Water Surface Elevation Comparison Plots for Houma Navigation Canal USGS
Model Data Water Surface Elevation, m, NAVD88(2004.65)
Field Data Water Surface Elevation, m, NAVD88(2004.65)
0.8
0.7
0.6
0.5
0.4
0.3
0.2
0.1
0
-0.1
-0.2
-0.2
-0.1
0
0.1
0.2
0.3
0.4
0.5
0.6
0.7
0.8

Figure 69. Bayou Grand Caillou WSE comparison plots.

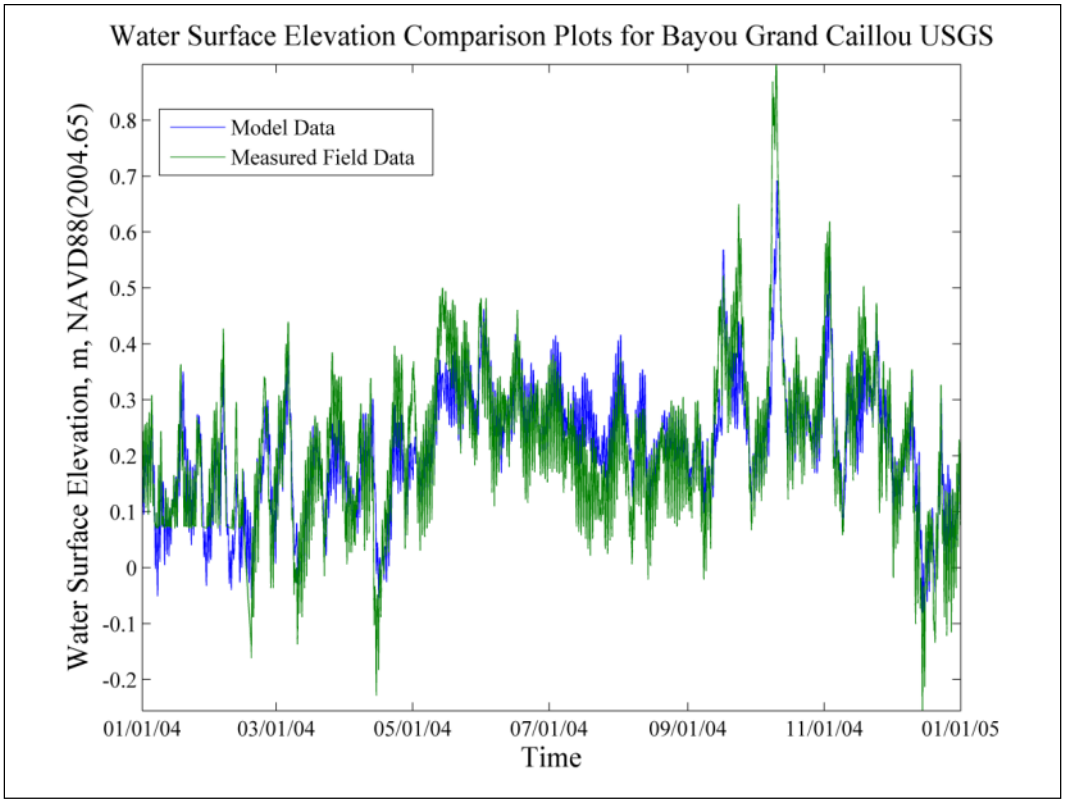

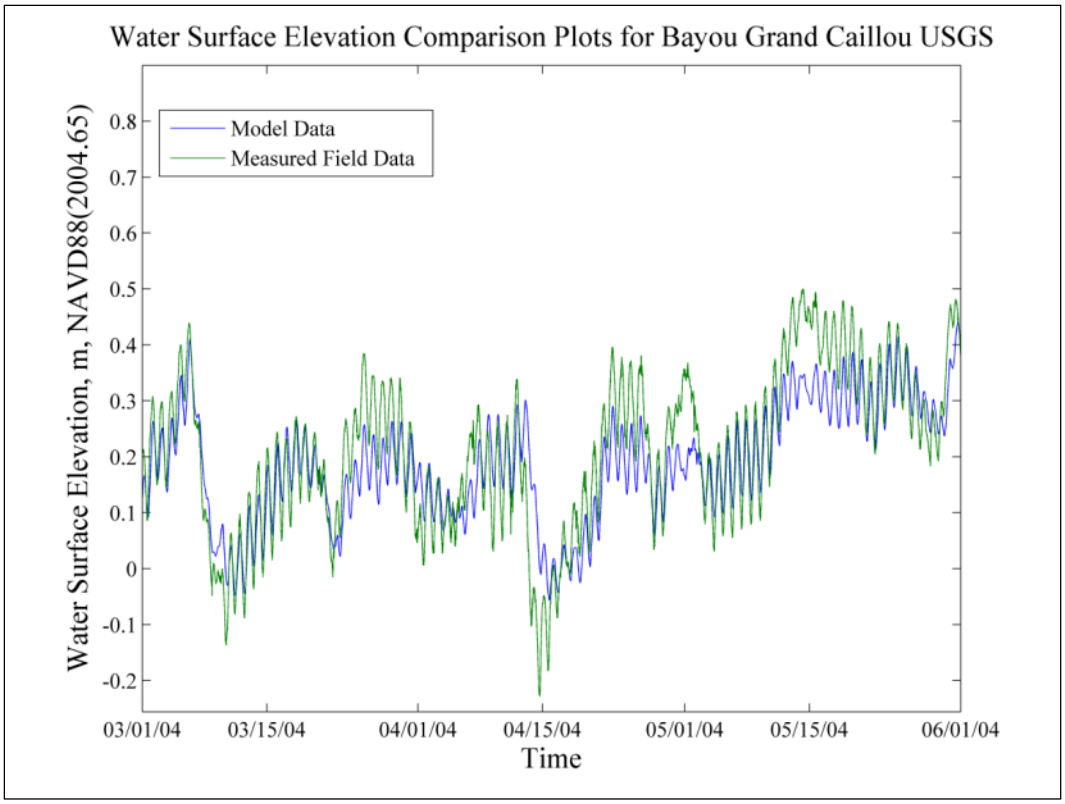

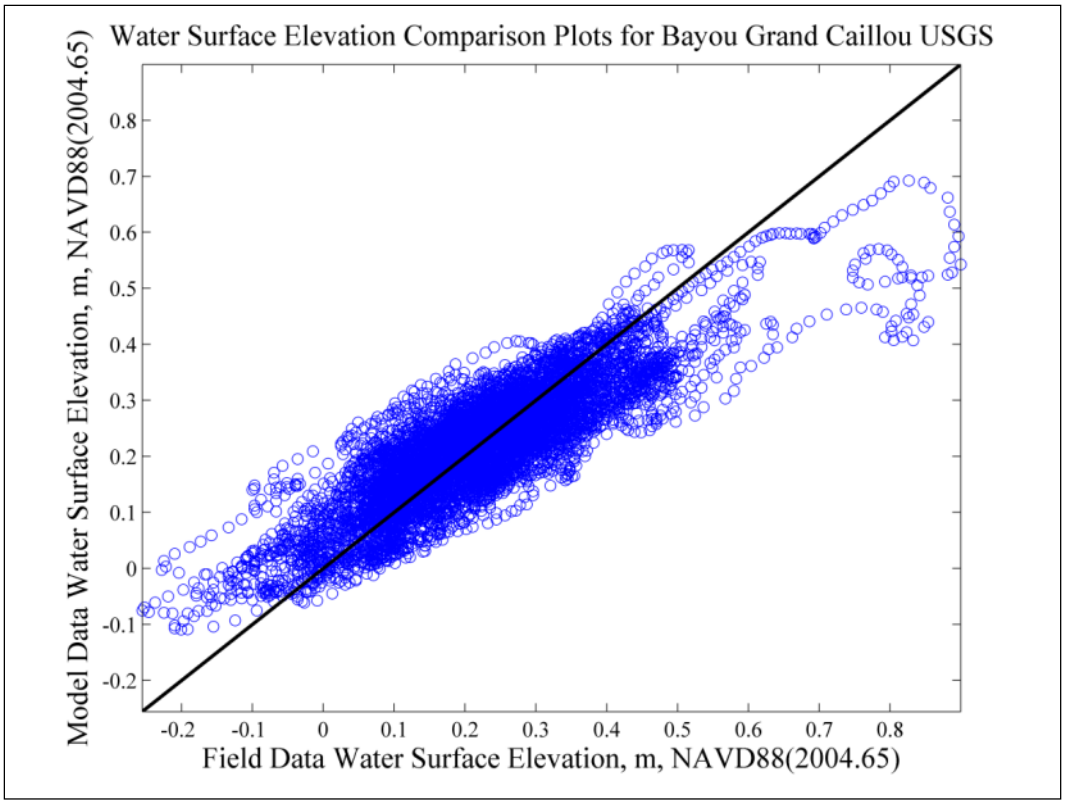
Water Surface Elevation Comparison Plots for Bayou Grand Caillou USGS
Model Data Water Surface Elevation, m, NAVD88(2004.65)
Field Data Water Surface Elevation, m, NAVD88(2004.65)
0.8
0.7
0.6
0.5
0.4
0.3
0.2
0.1
0
-0.1
-0.2
-0.2
-0.1
0
0.1
0.2
0.3
0.4
0.5
0.6
0.7
0.8

Figure 70. GIWW at Houma WSE comparison plots.

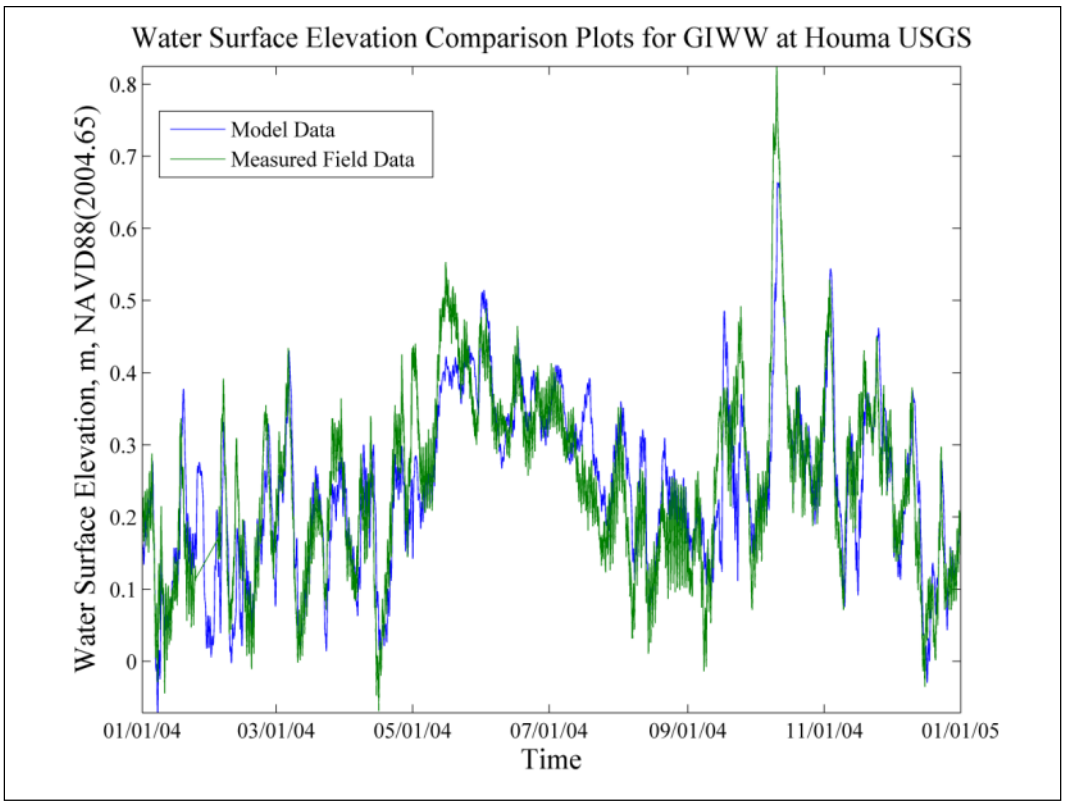

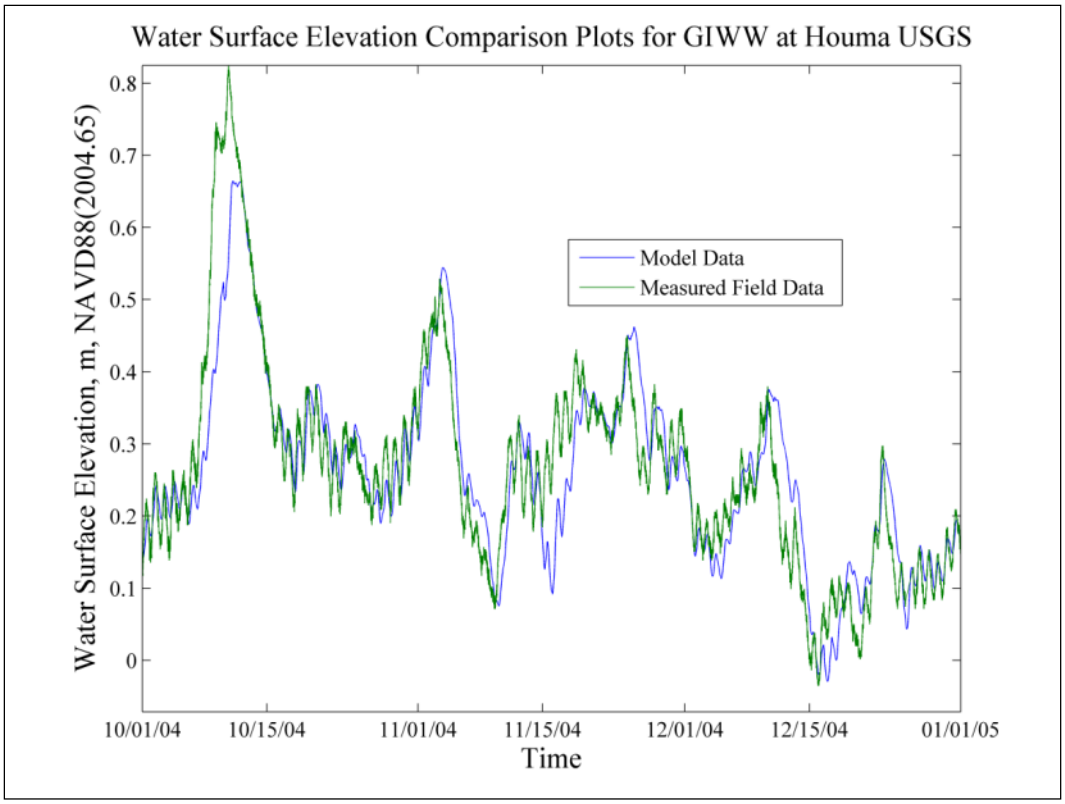

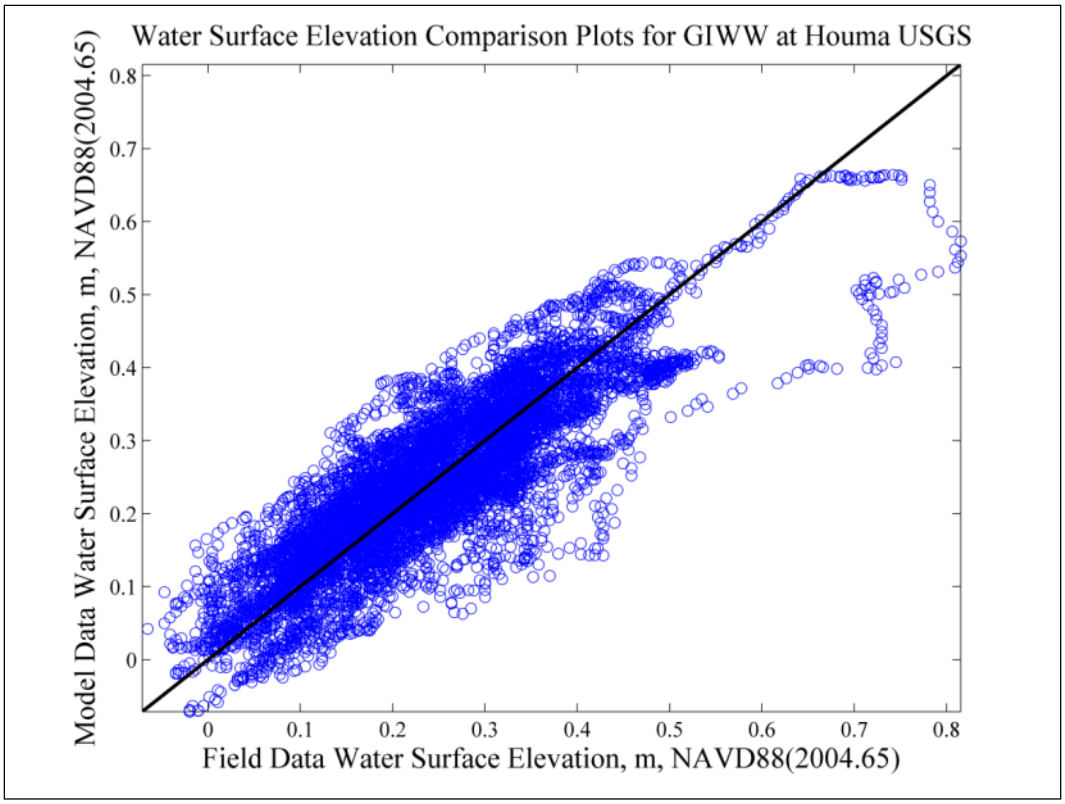
Water Surface Elevation Comparison Plots for GIWW at Houma USGS
Model Data Water Surface Elevation, m, NAVD88(2004.65)
Field Data Water Surface Elevation, m, NAVD88(2004.65)
0
0.1
0.2
0.3
0.4
0.5
0.6
0.7
0.8

Figure 71. Bayou Petit Caillou upstream WSE comparison plots.

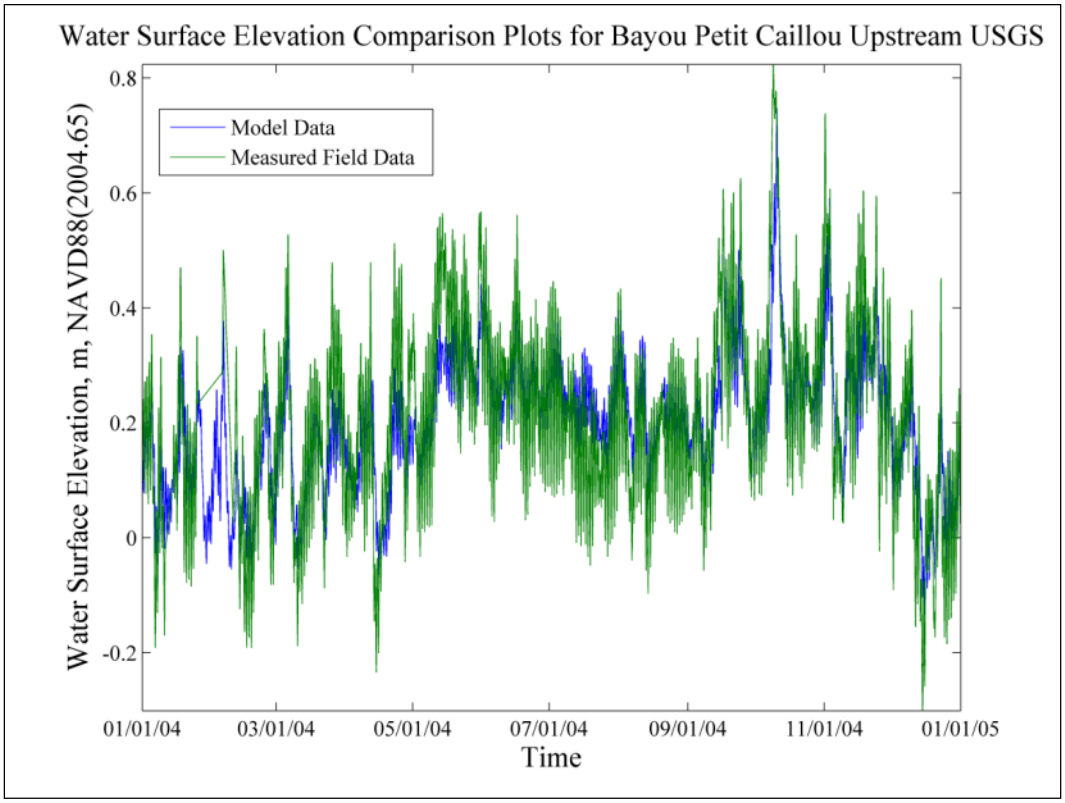

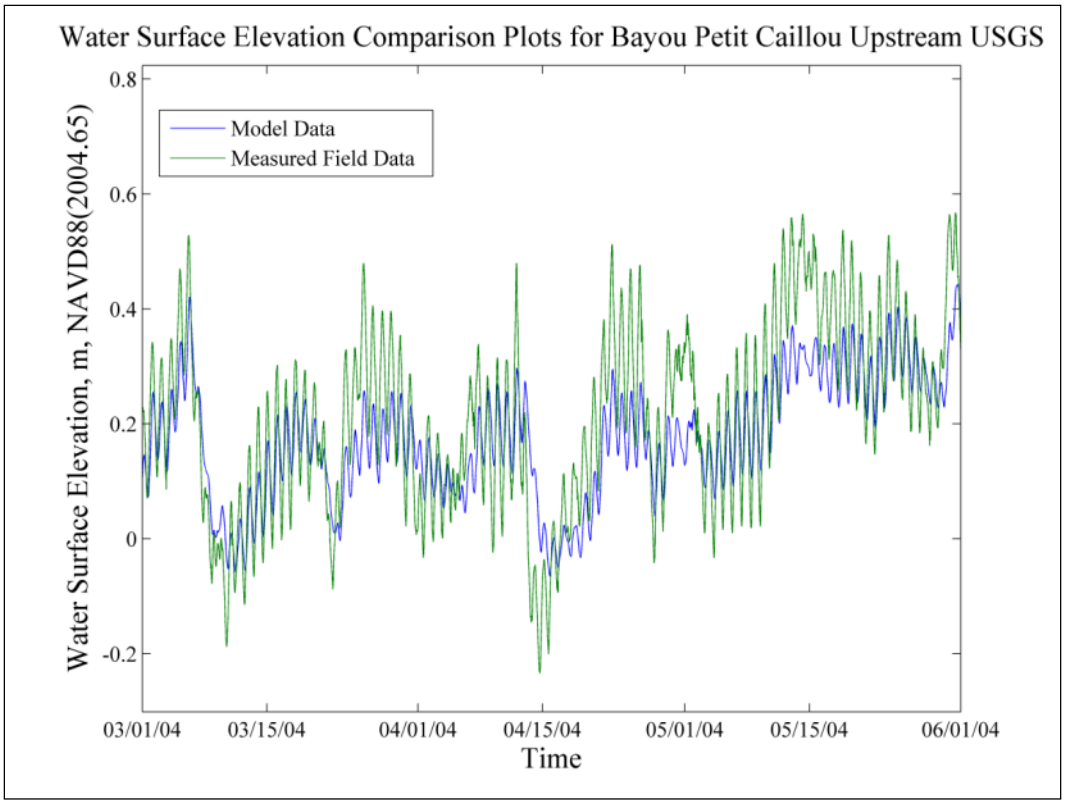

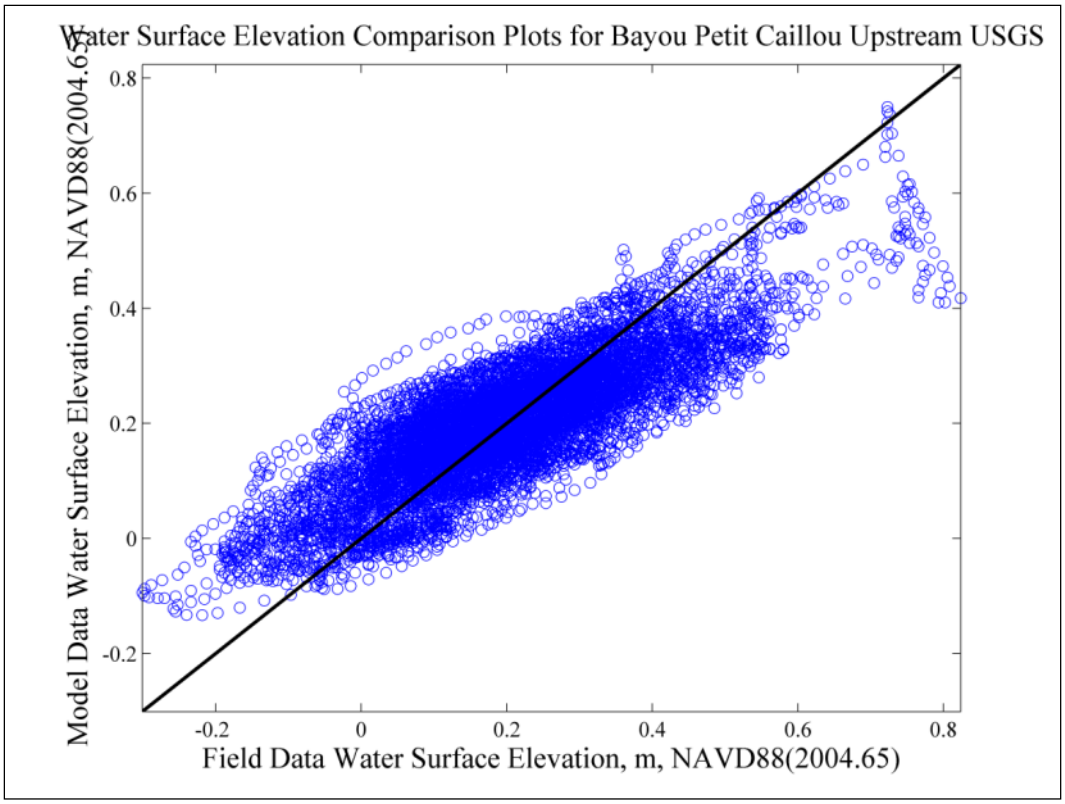
Water Surface Elevation Comparison Plots for Bayou Petit Caillou Upstream USGS
Model Data Water Surface Elevation, m, NAVD88(2004.65)
Field Data Water Surface Elevation, m, NAVD88(2004.65)
0.8
0.6
0.4
0.2
0
-0.2
-0.2
0
0.2
0.4
0.6
0.8

Figure 72. Bayou Petit Caillou downstream WSE comparison plots.

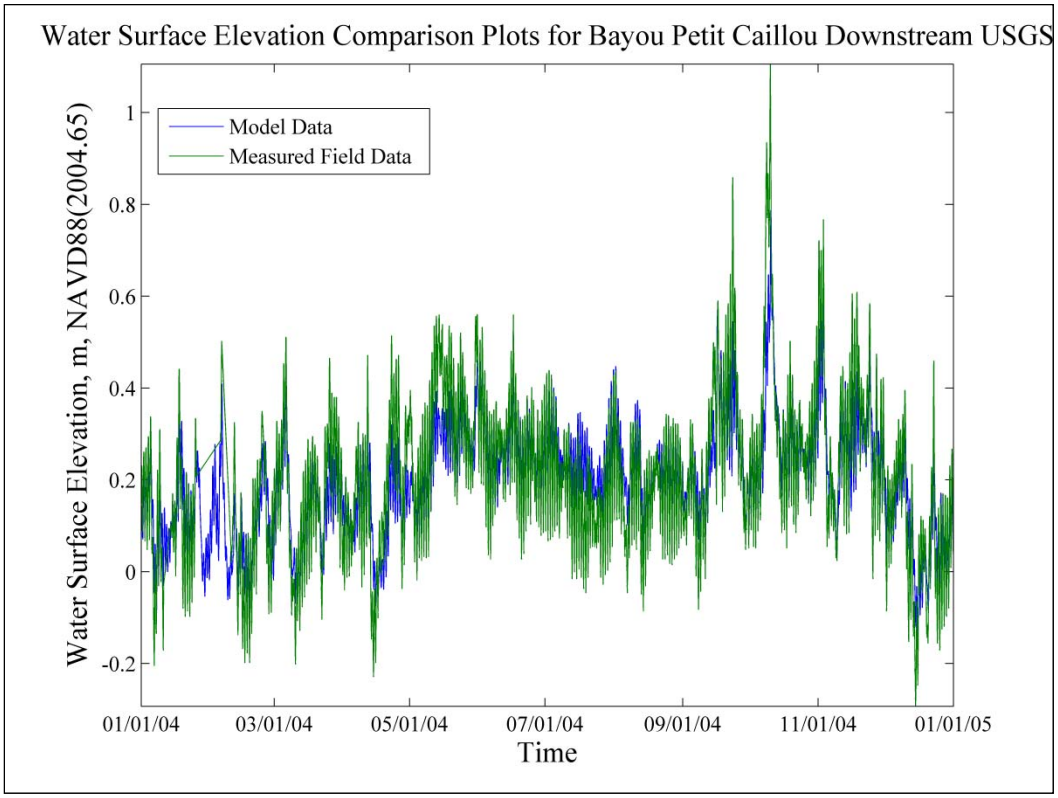

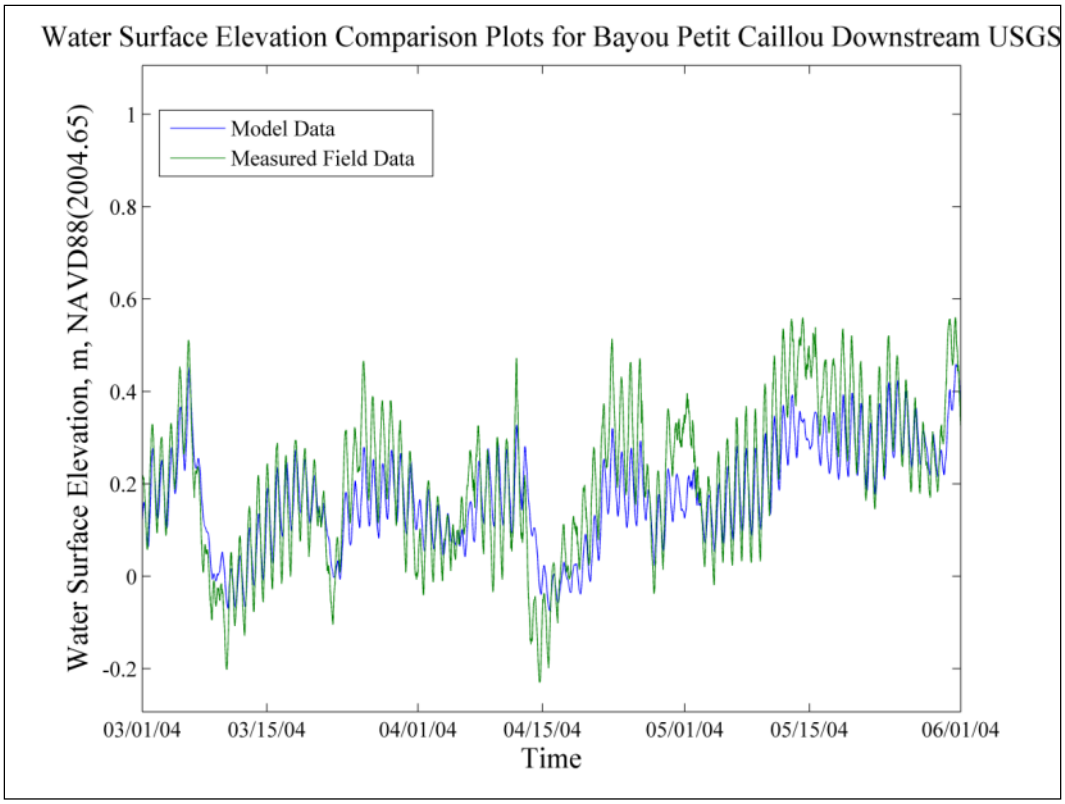

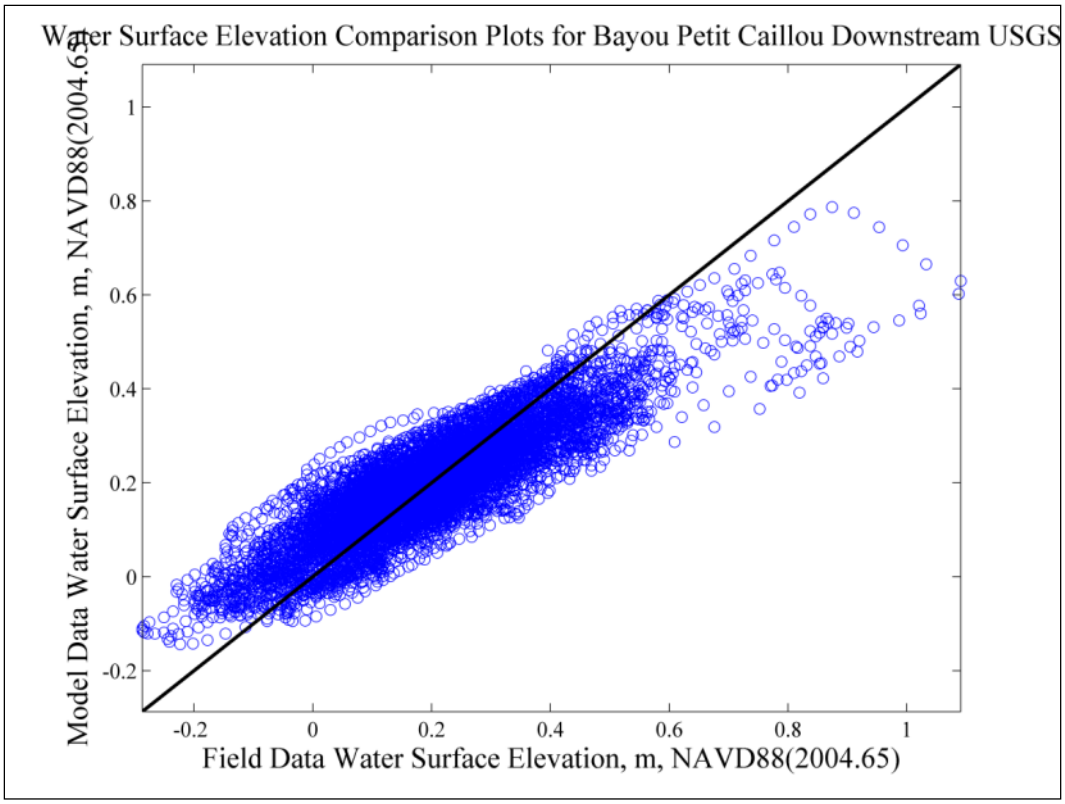
Water Surface Elevation Comparison Plots for Bayou Petit Caillou Downstream USGS
Model Data Water Surface Elevation, m, NAVD88(2004.65)
Field Data Water Surface Elevation, m, NAVD88(2004.65)
1
0.8
0.6
0.4
0.2
0
-0.2
-0.2
0
0.2
0.4
0.6
0.8
1

Figure 73. Bayou Terrebonne upstream WSE comparison plots.

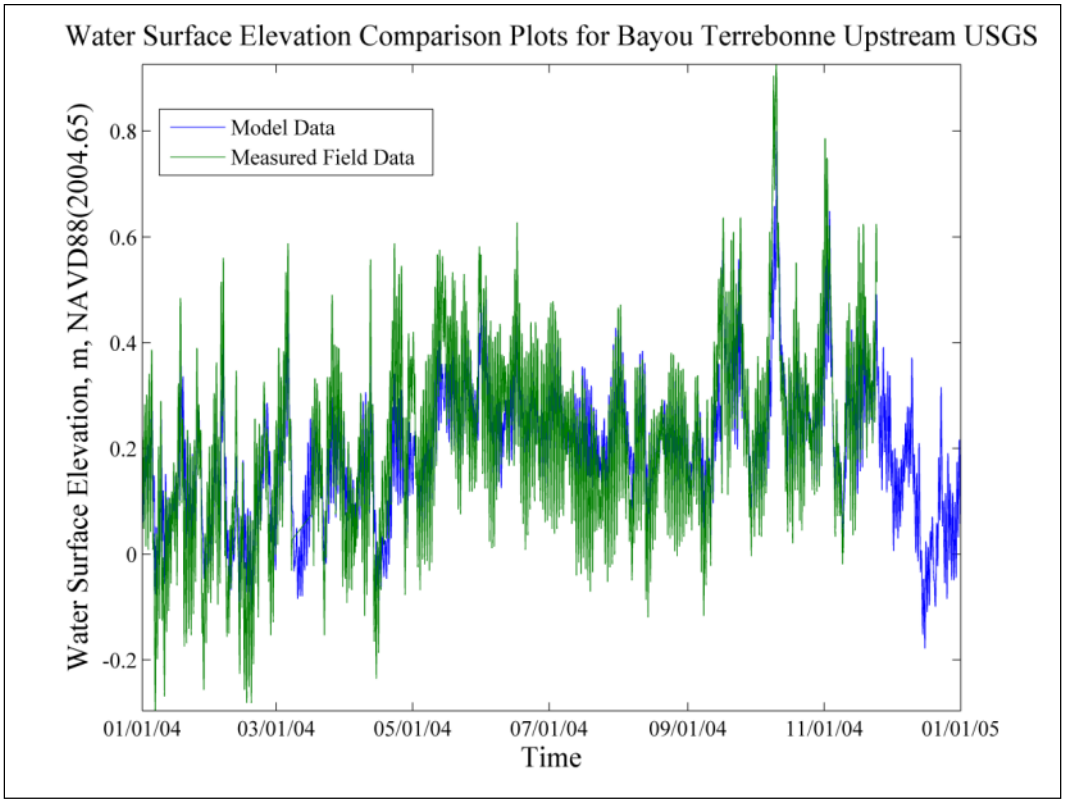

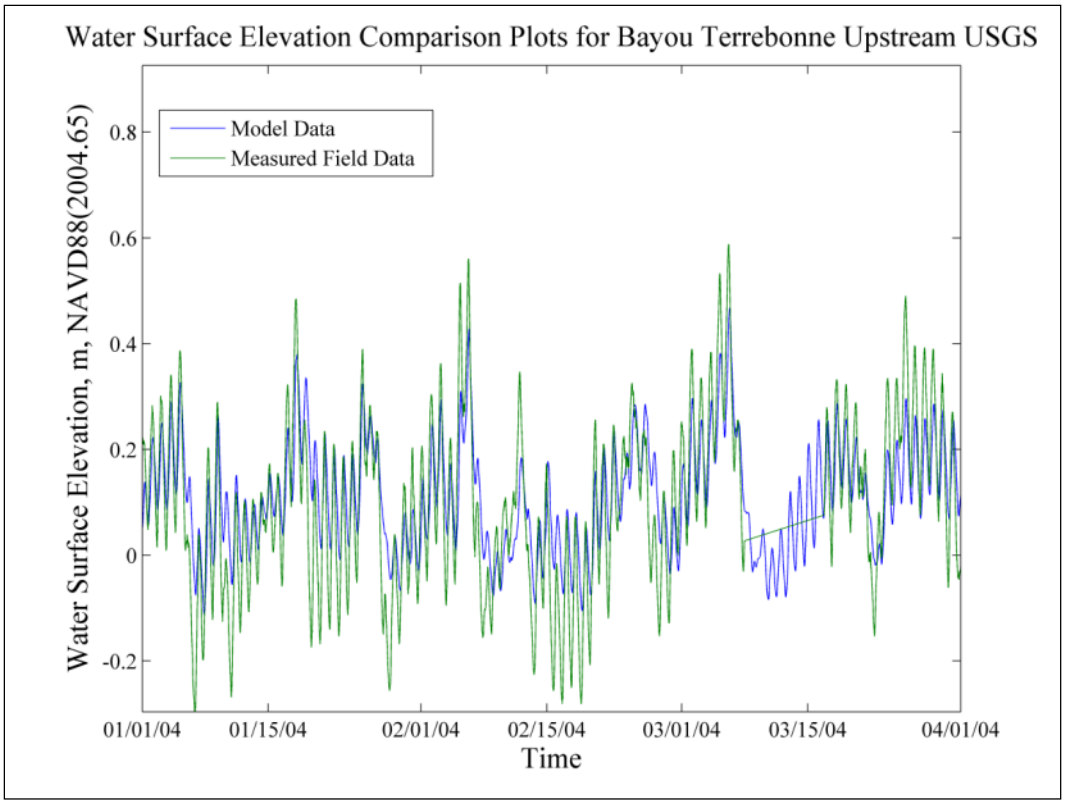

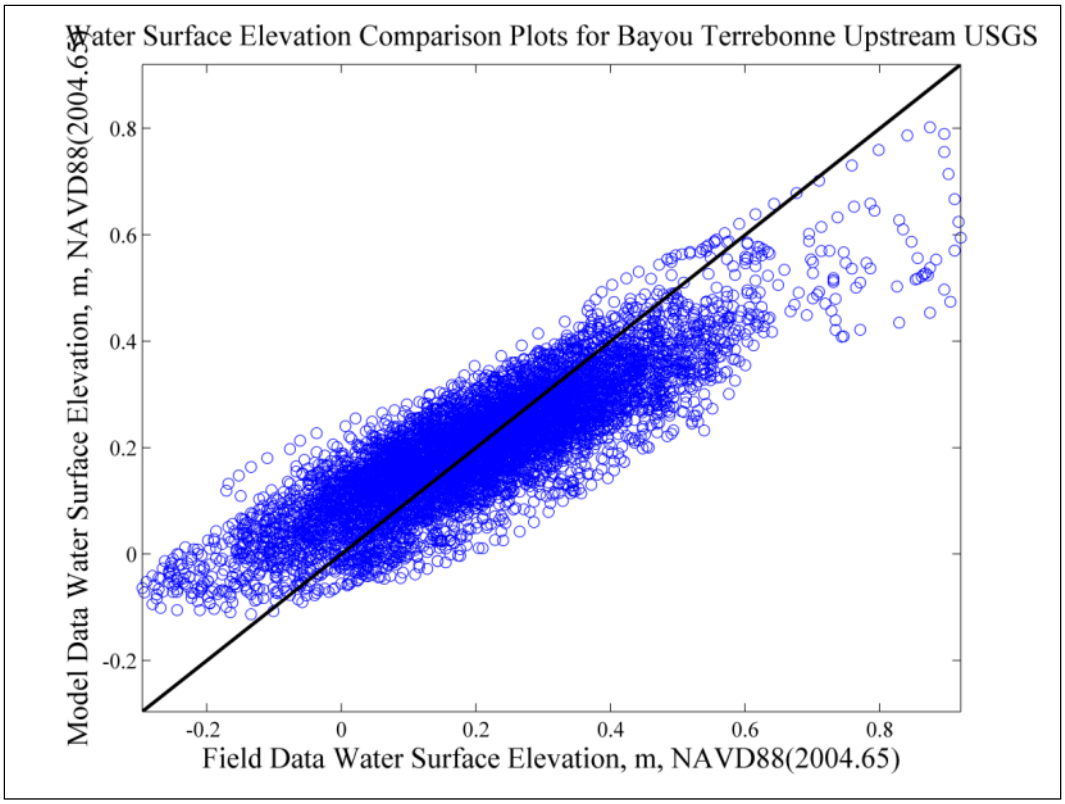
Water Surface Elevation Comparison Plots for Bayou Terrebonne Upstream USGS
Model Data Water Surface Elevation, m, NAVD88(2004.65)
Field Data Water Surface Elevation, m, NAVD88(2004.65)
0.8
0.6
0.4
0.2
0
-0.2
-0.2
0
0.2
0.4
0.6
0.8

Figure 74. Bayou Terrebonne downstream WSE comparison plots.

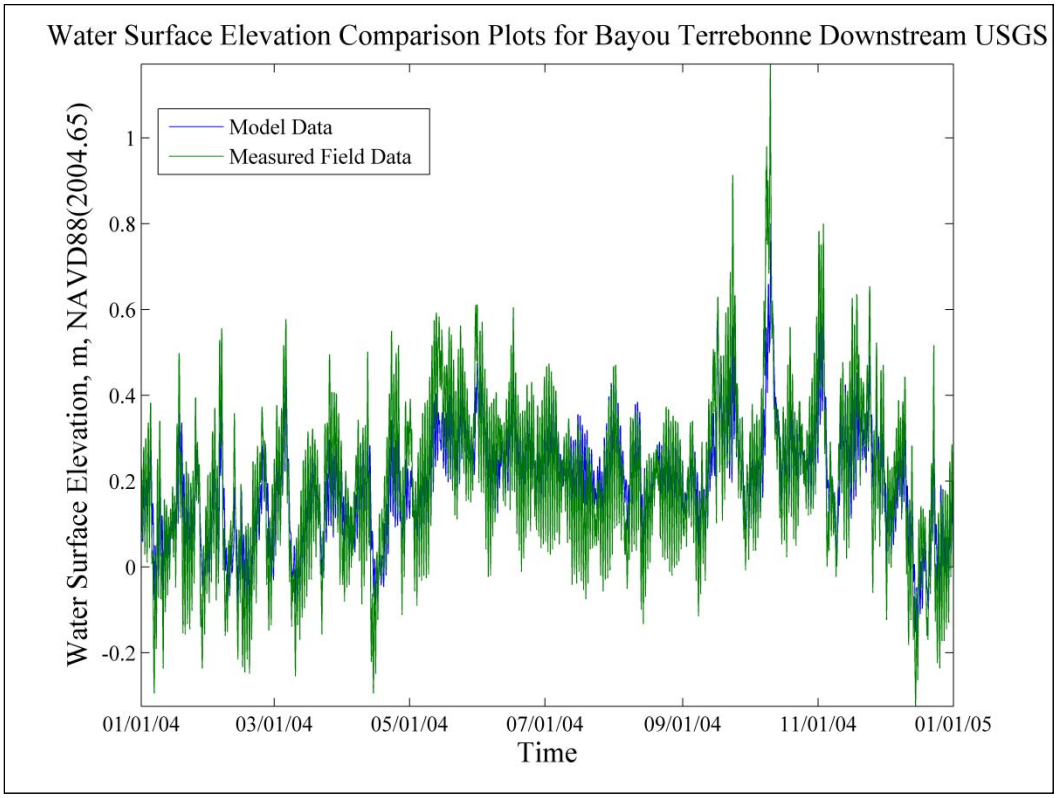

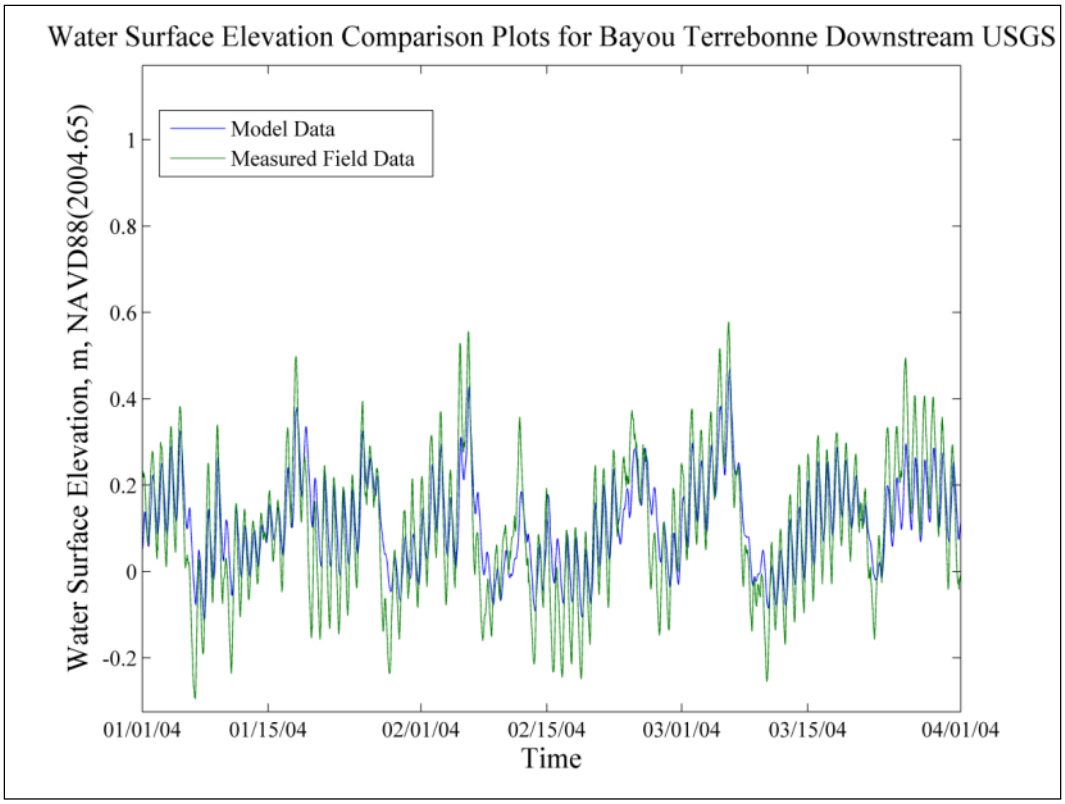

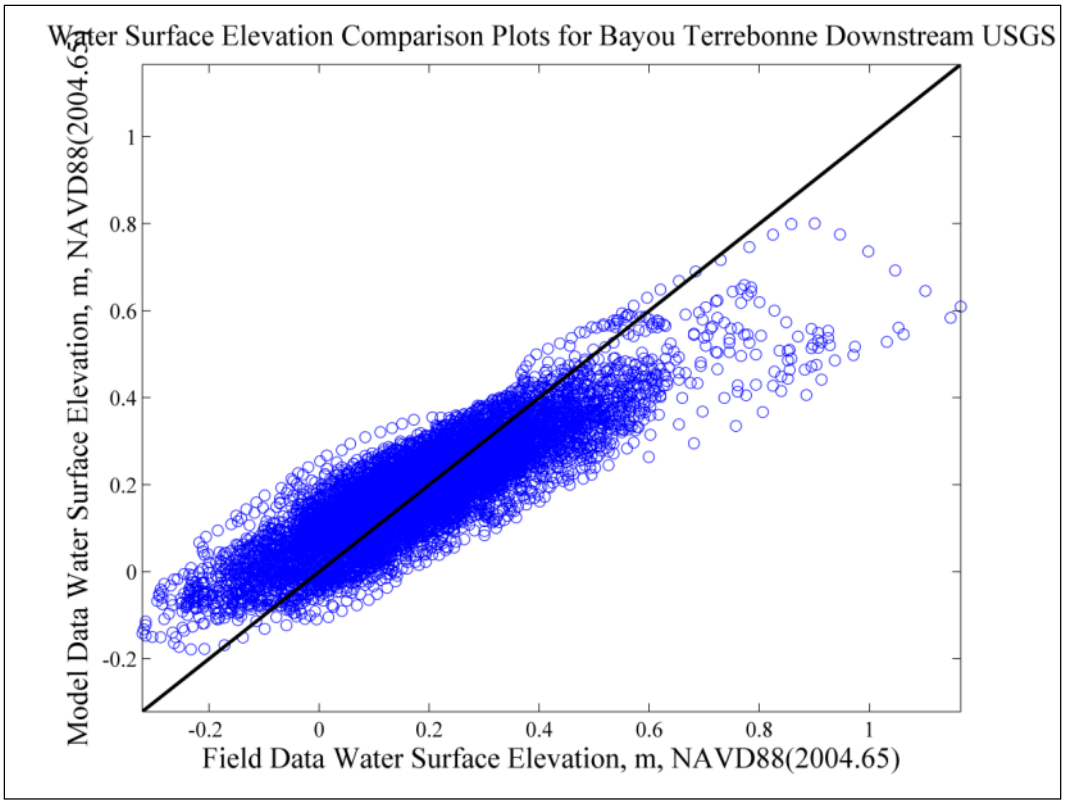
Water Surface Elevation Comparison Plots for Bayou Terrebonne Downstream USGS
Model Data Water Surface Elevation, m, NAVD88(2004.65)
Field Data Water Surface Elevation, m, NAVD88(2004.65)
1
0.8
0.6
0.4
0.2
0
-0.2
-0.2
0
0.2
0.4
0.6
0.8
1

Figure 75. Company Canal, Lockport WSE comparison plots.

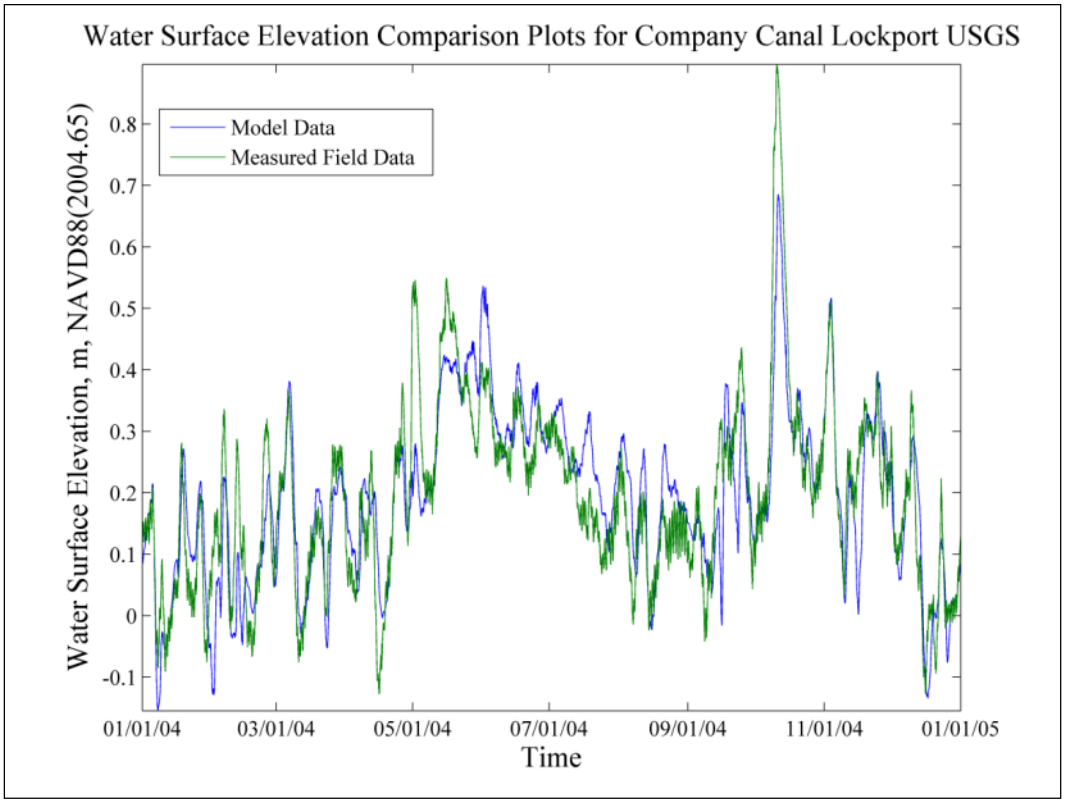

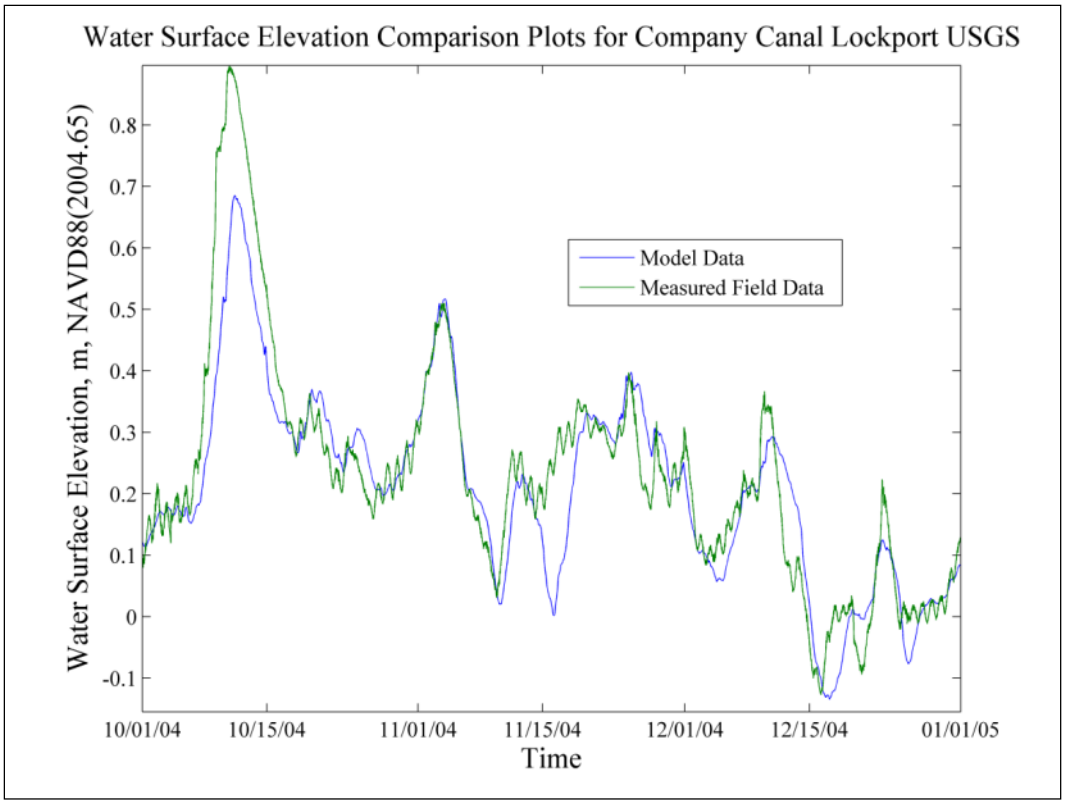

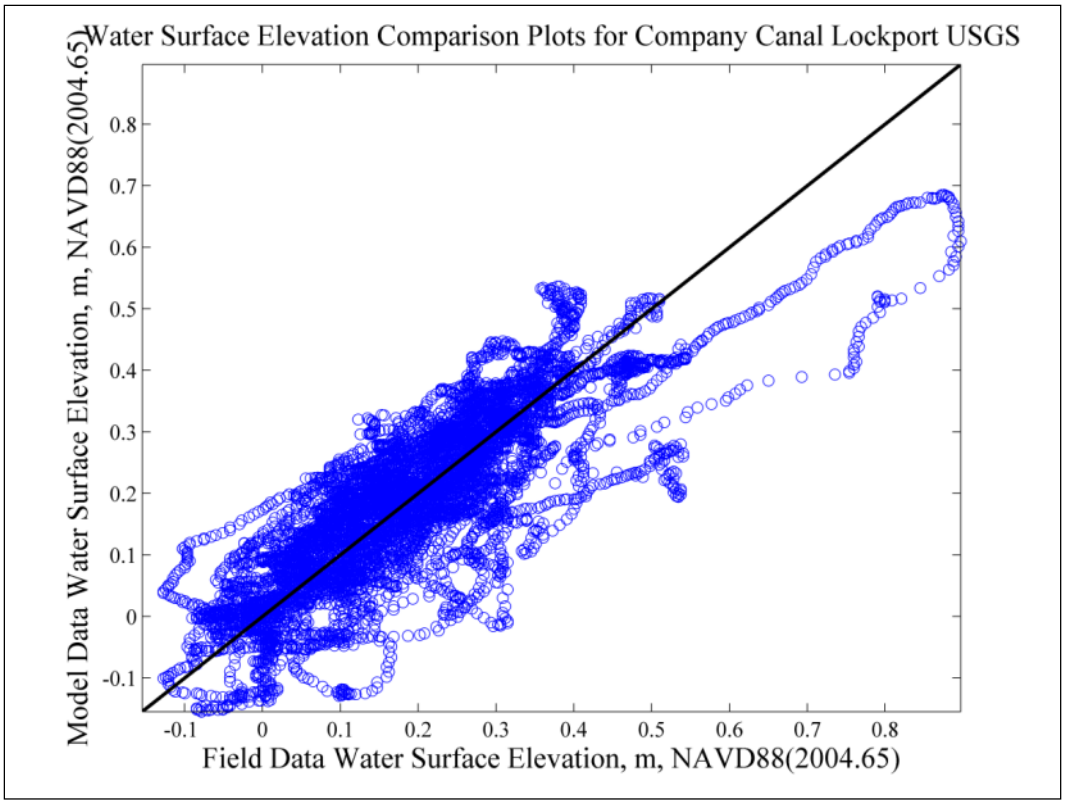
Water Surface Elevation Comparison Plots for Company Canal Lockport USGS
Model Data Water Surface Elevation, m, NAVD88(2004.65)
Field Data Water Surface Elevation, m, NAVD88(2004.65)
0.8
0.7
0.6
0.5
0.4
0.3
0.2
0.1
0
-0.1
-0.1
0
0.1
0.2
0.3
0.4
0.5
0.6
0.7
0.8

Figure 76. Company Canal, Salt Barrier WSE comparison plots.

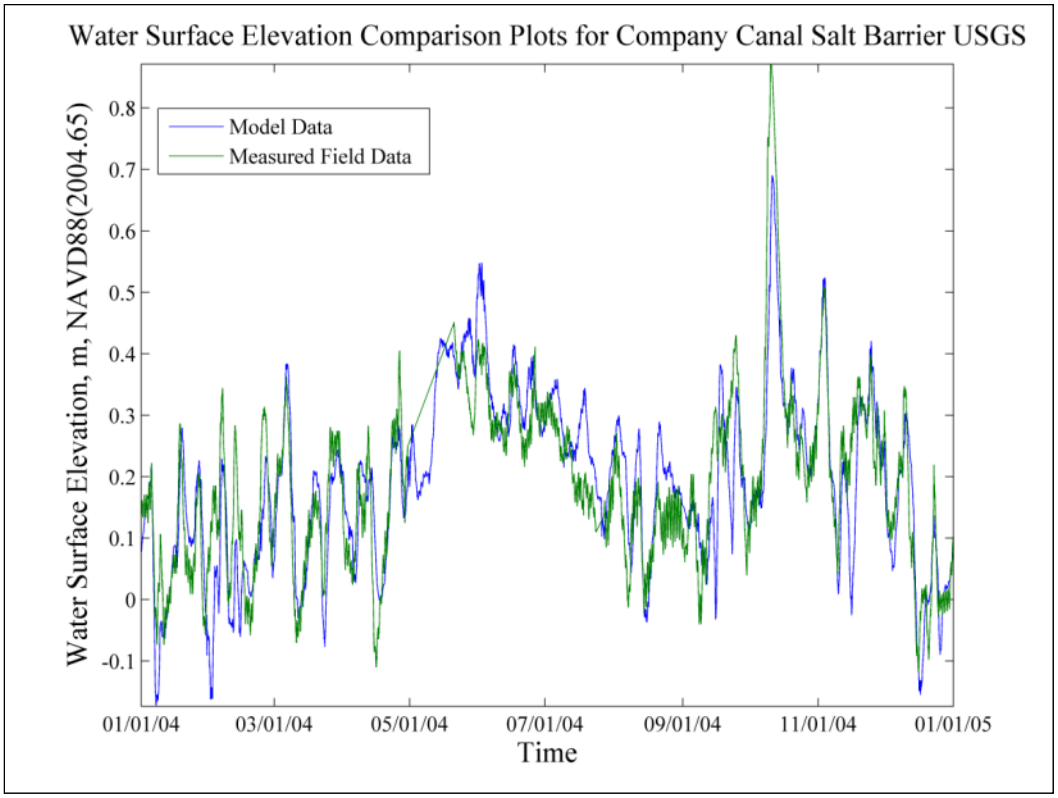

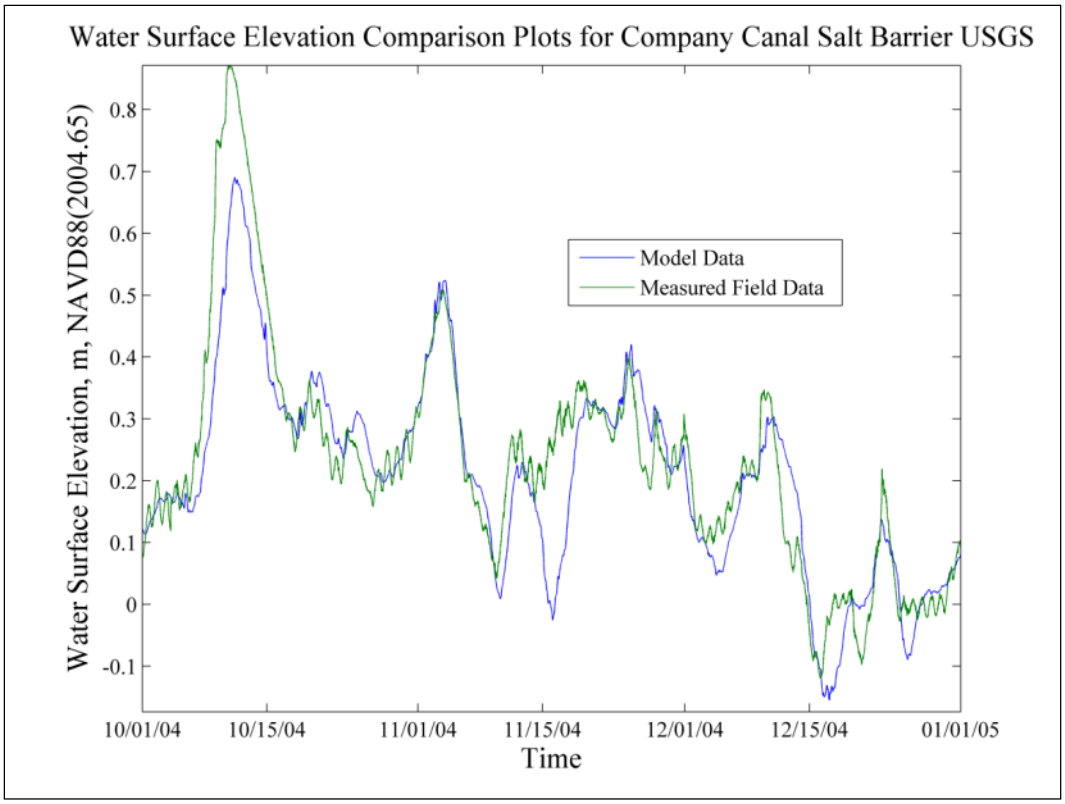

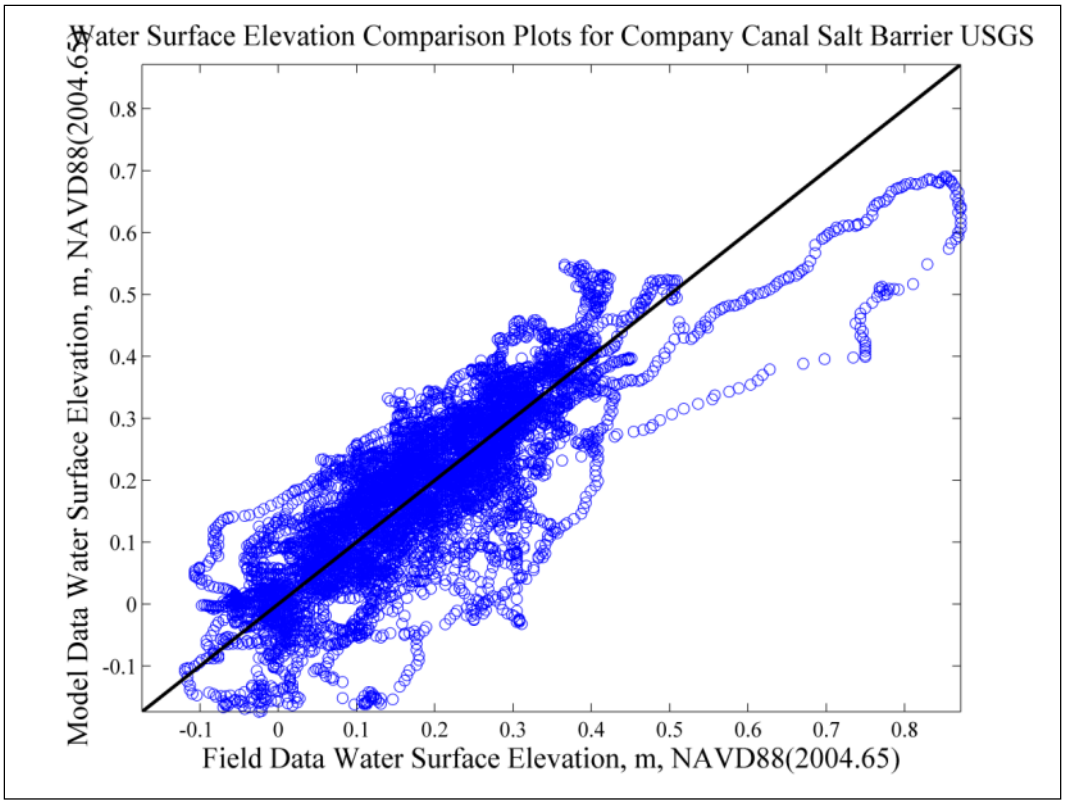
Water Surface Elevation Comparison Plots for Company Canal Salt Barrier USGS
Model Data Water Surface Elevation, m, NAVD88(2004.65)
Field Data Water Surface Elevation, m, NAVD88(2004.65)
0.8
0.7
0.6
0.5
0.4
0.3
0.2
0.1
0
-0.1
-0.1
0
0.1
0.2
0.3
0.4
0.5
0.6
0.7
0.8

Figure 77. GIWW West of Bayou Lafourche WSE comparison plots.

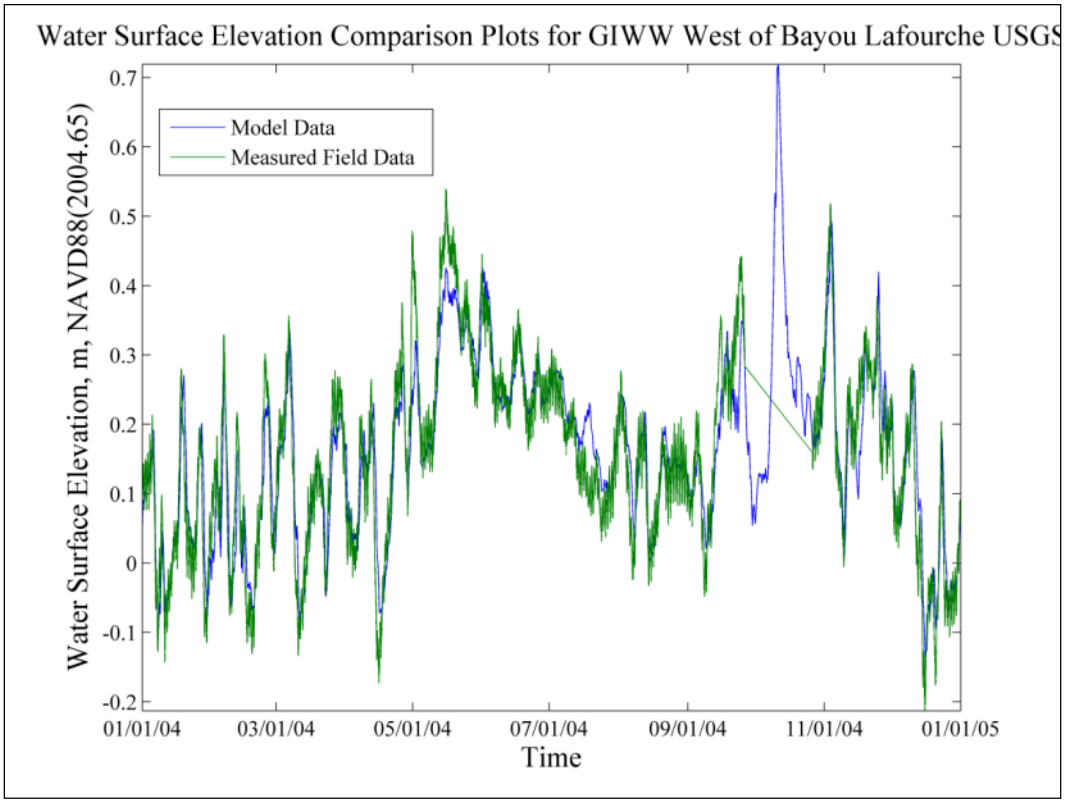

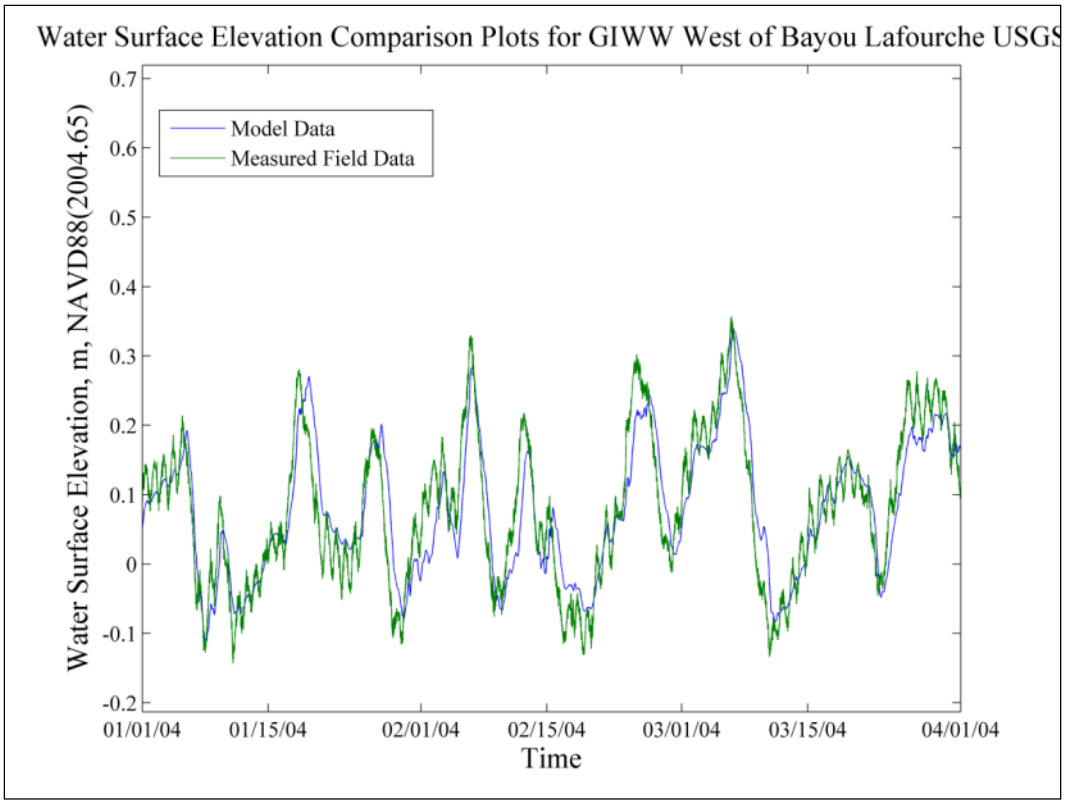

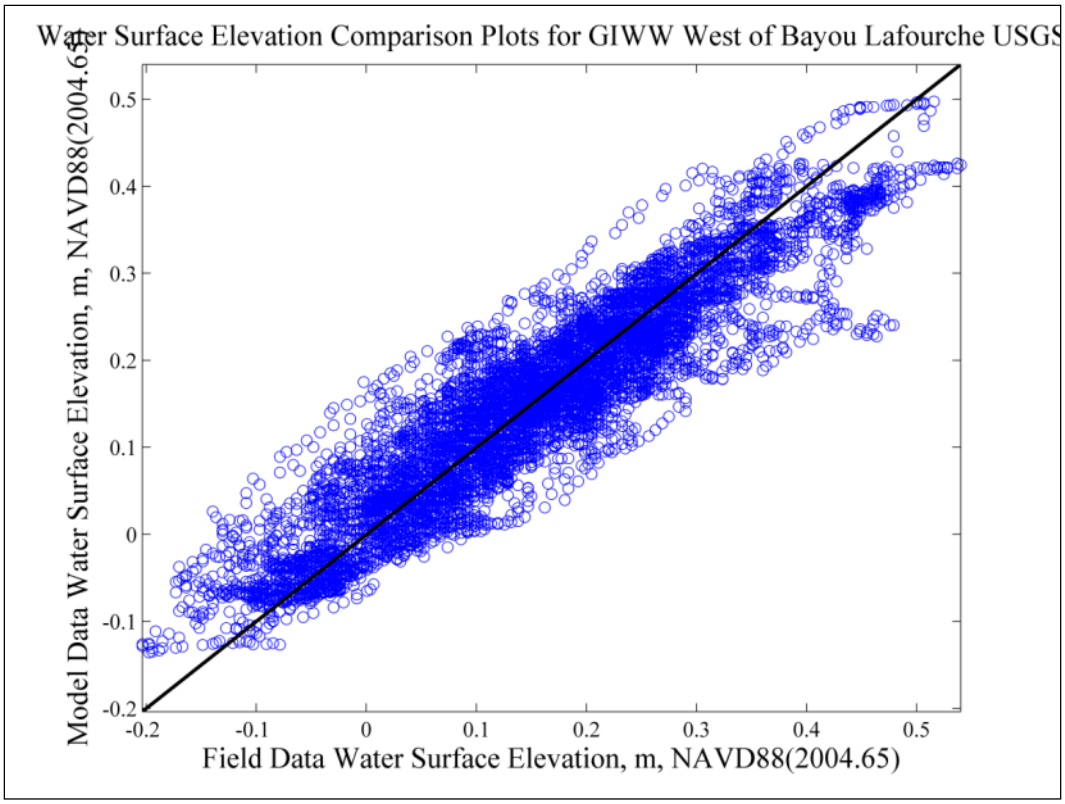
Water Surface Elevation Comparison Plots for GIWW West of Bayou Lafourche USGS
Model Data Water Surface Elevation, m, NAVD88(2004.65)
Field Data Water Surface Elevation, m, NAVD88(2004.65)
0.5
0.4
0.3
0.2
0.1
0
-0.1
-0.2
-0.2
-0.1
0
0.1
0.2
0.3
0.4
0.5

Figure 78. GIWW West of Minors Canal WSE comparison plots.

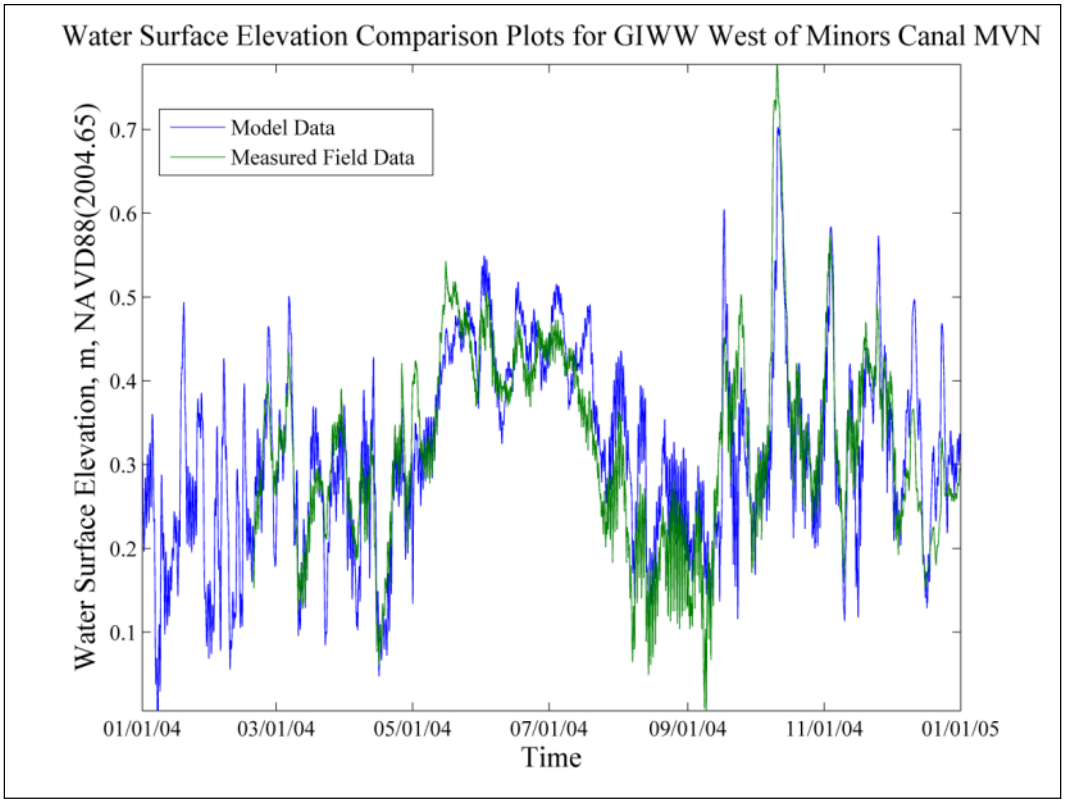

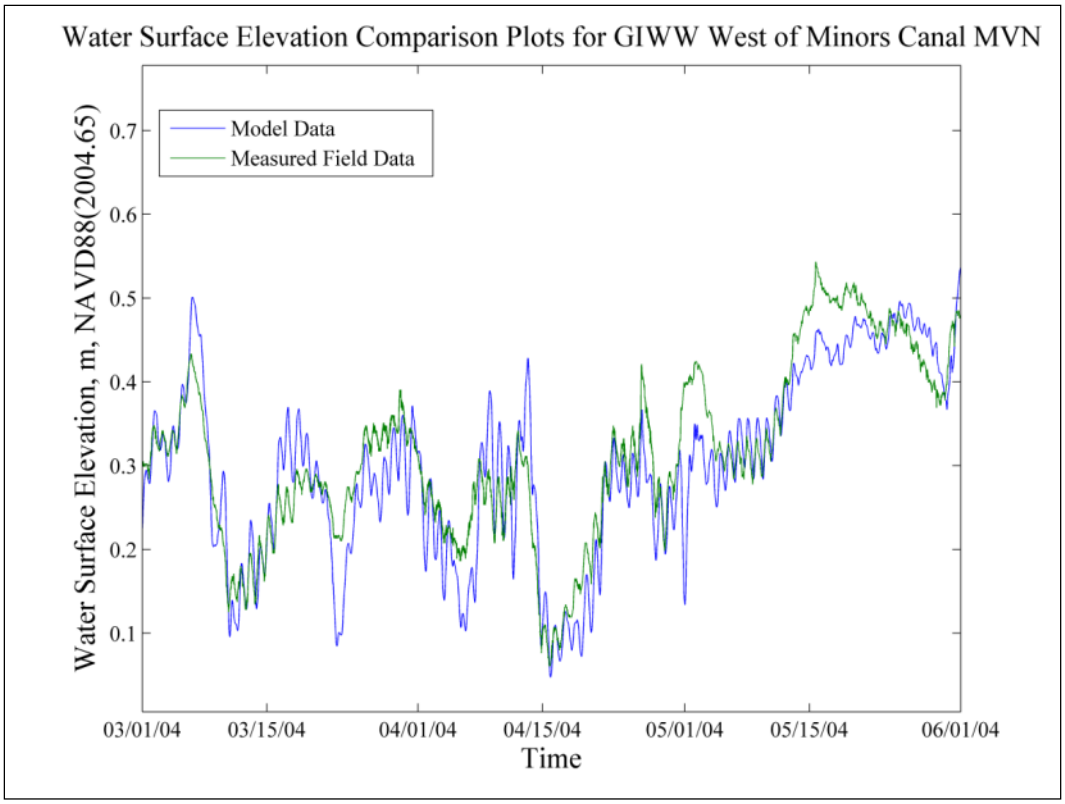

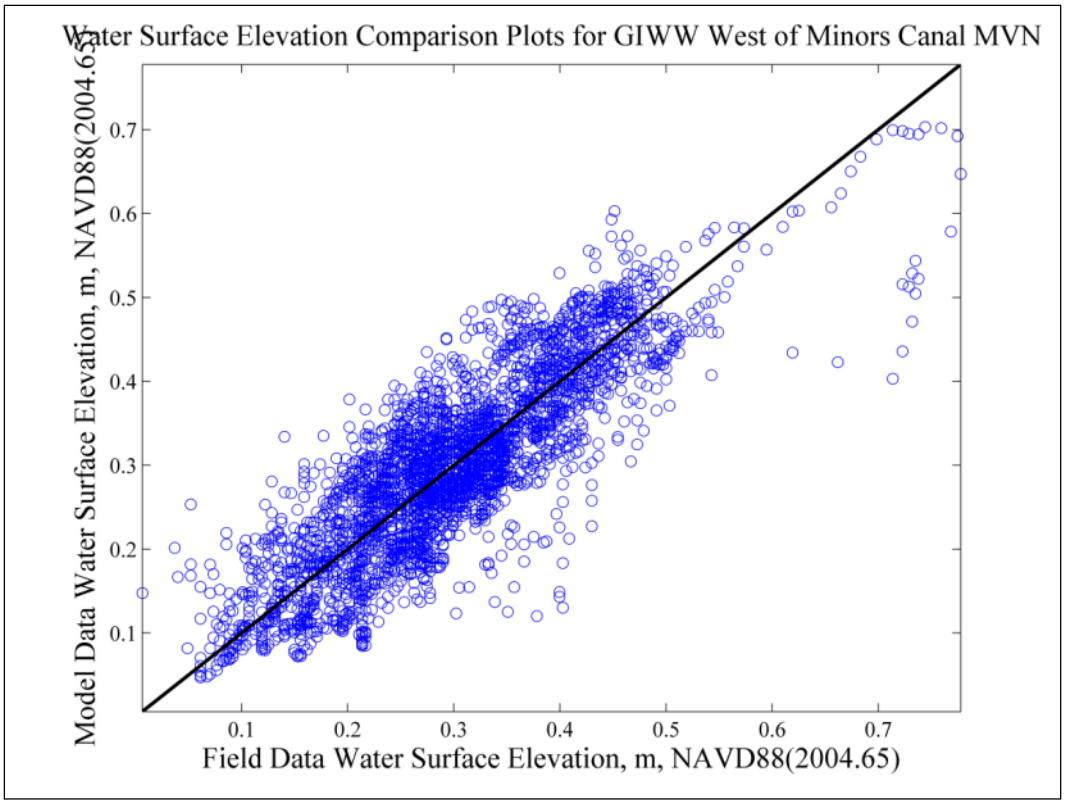
Water Surface Elevation Comparison Plots for GIWW West of Minors Canal MVN
Model Data Water Surface Elevation, m, NAVD88(2004.65)
Field Data Water Surface Elevation, m, NAVD88(2004.65)
0.1
0.2
0.3
0.4
0.5
0.6
0.7

Figure 79. Falgout Canal WSE comparison plots.

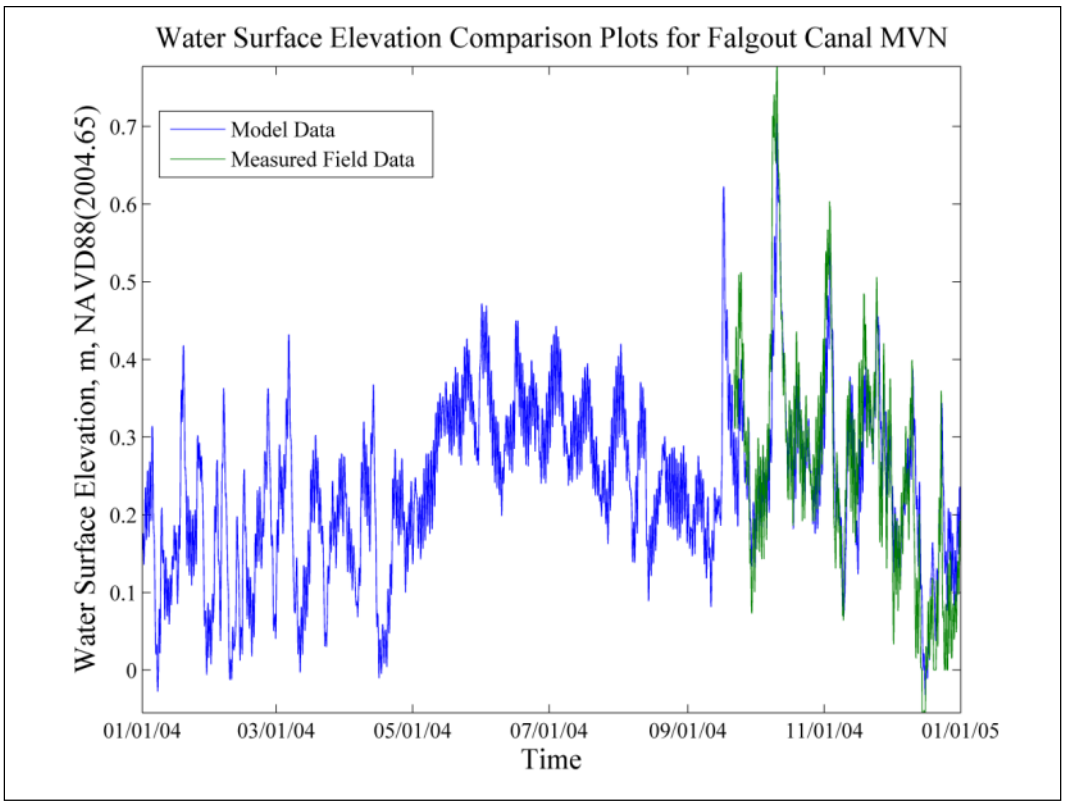

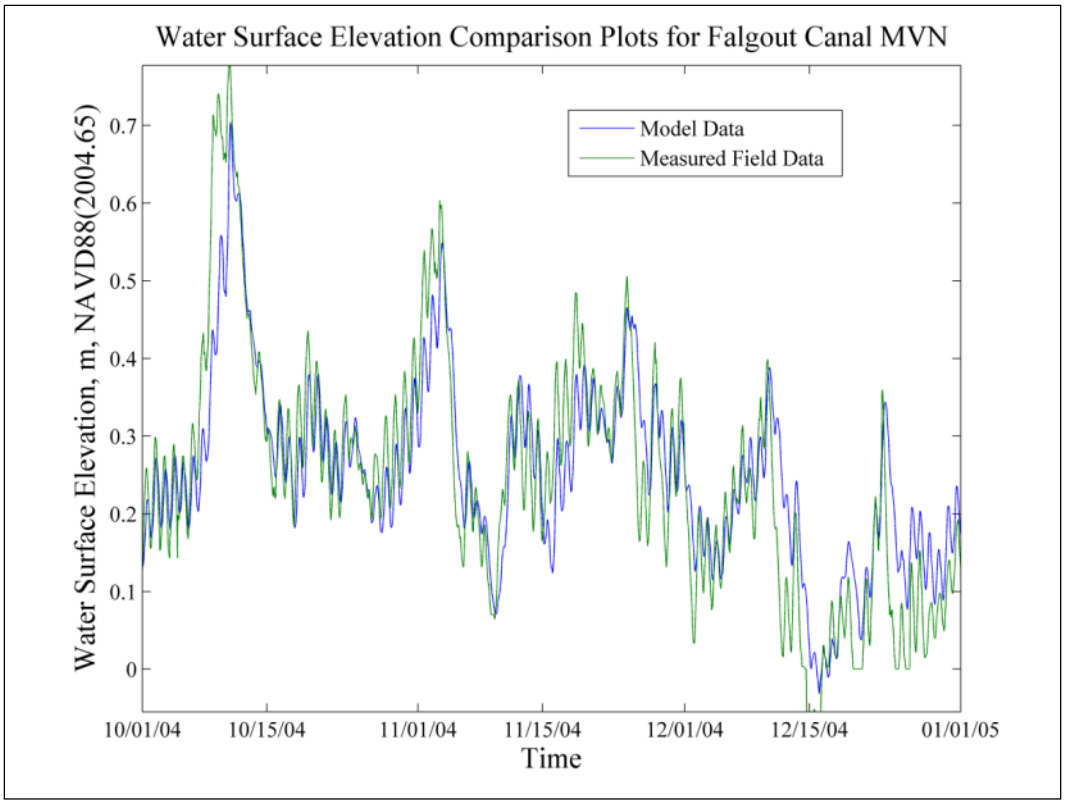

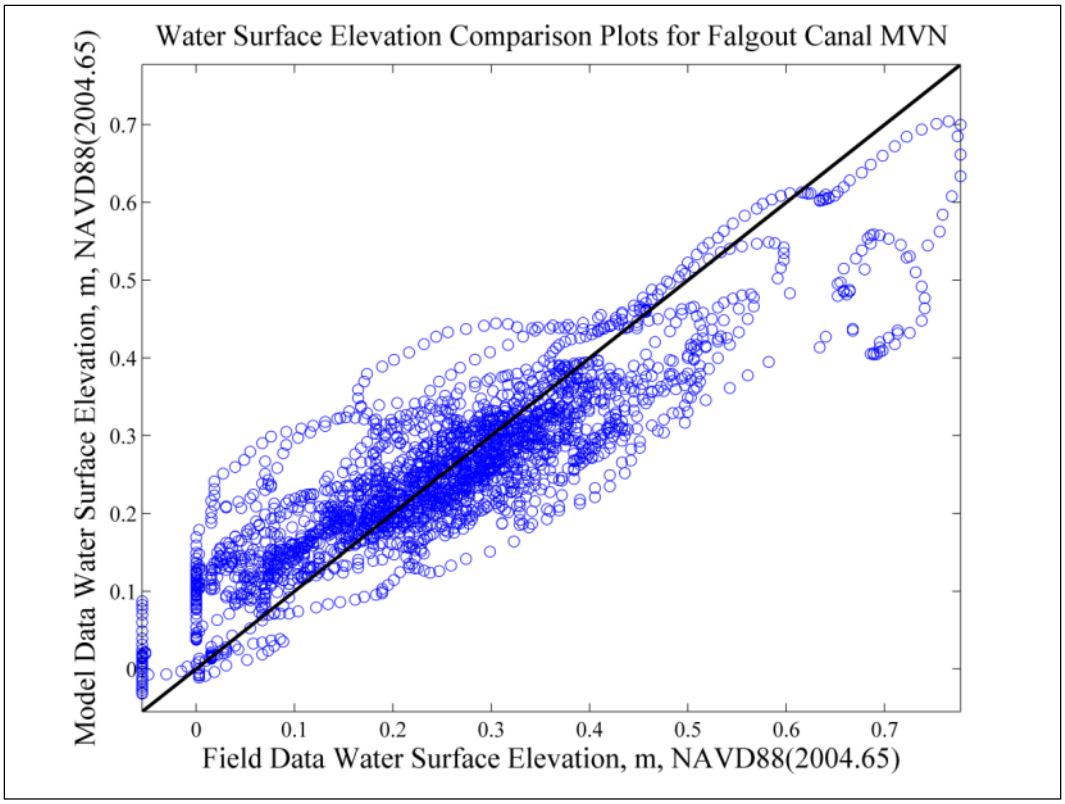
Water Surface Elevation Comparison Plots for Falgout Canal MVN
Model Data Water Surface Elevation, m, NAVD88(2004.65)
Field Data Water Surface Elevation, m, NAVD88(2004.65)
0
0.1
0.2
0.3
0.4
0.5
0.6
0.7

Figure 80. Bayou Dularge WSE comparison plots.

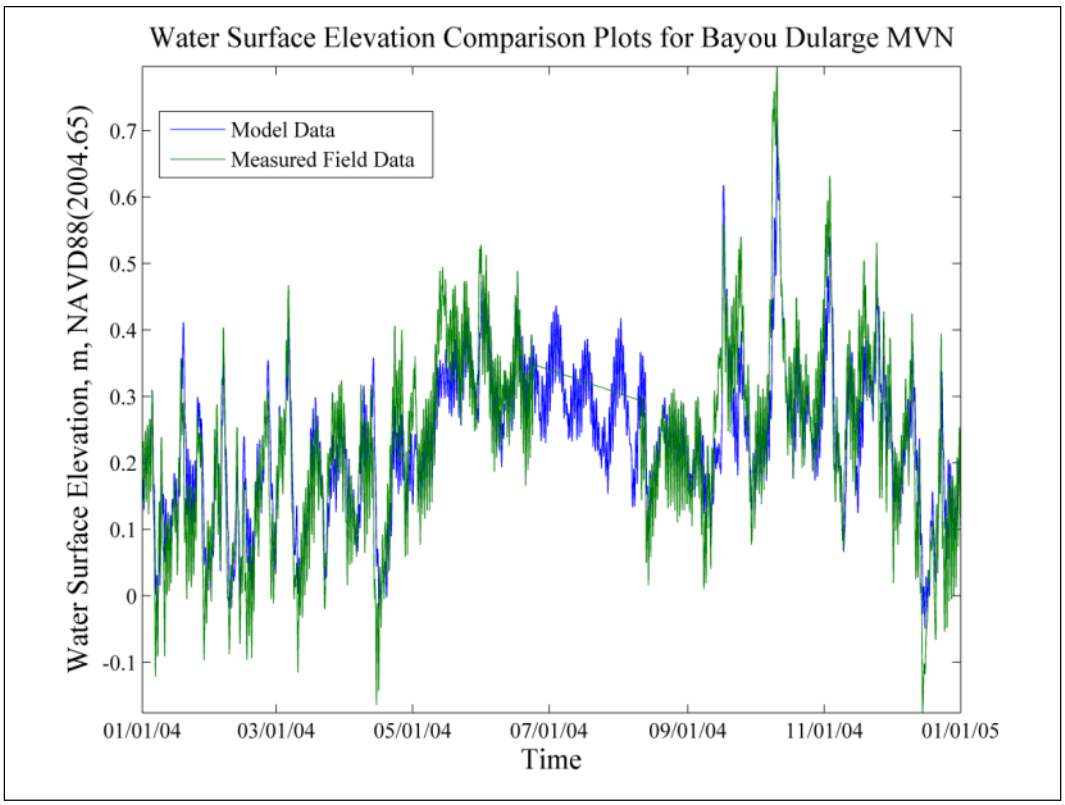

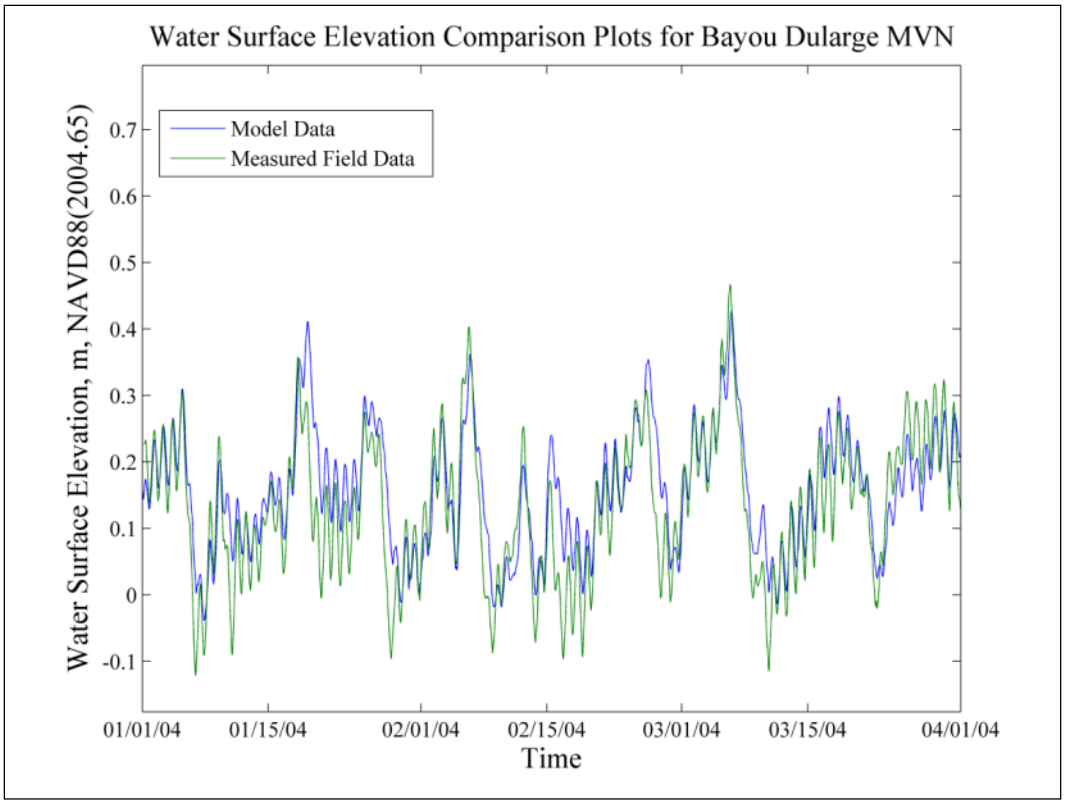

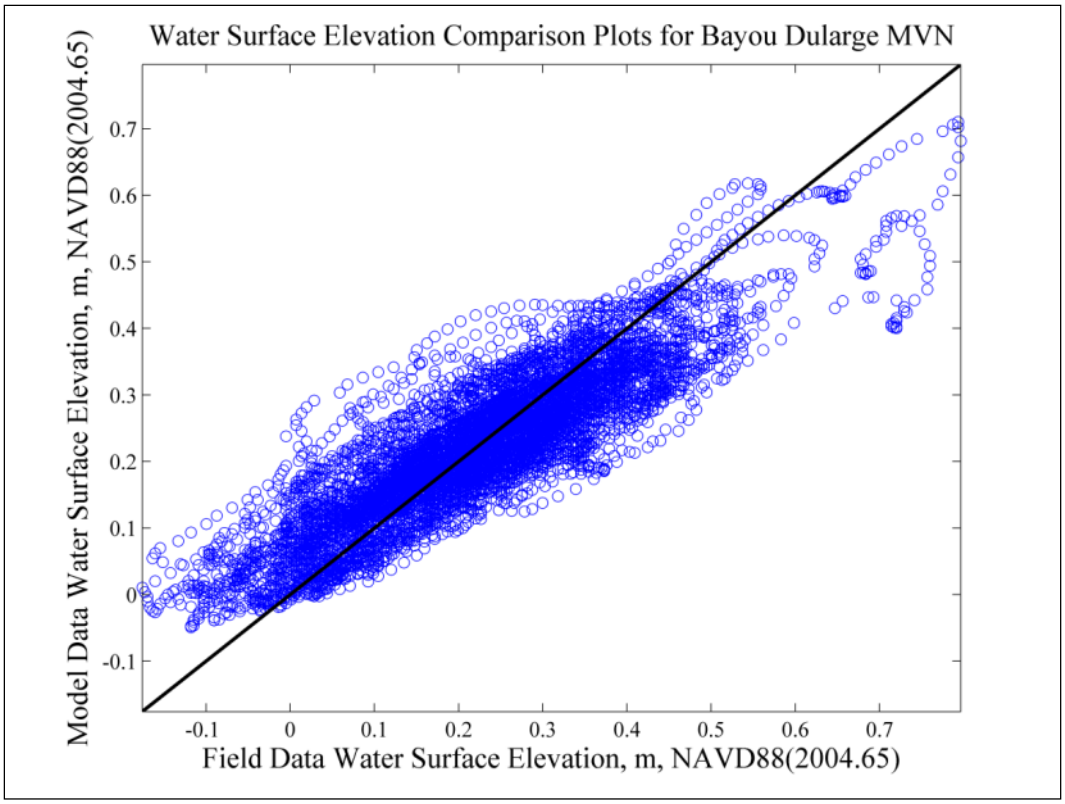
Water Surface Elevation Comparison Plots for Bayou Dularge MVN
Model Data Water Surface Elevation, m, NAVD88(2004.65)
Field Data Water Surface Elevation, m, NAVD88(2004.65)
0.7
0.6
0.5
0.4
0.3
0.2
0.1
0
-0.1
-0.1
0
0.1
0.2
0.3
0.4
0.5
0.6
0.7

Figure 81. Bayou Grand Caillou WSE comparison plots.

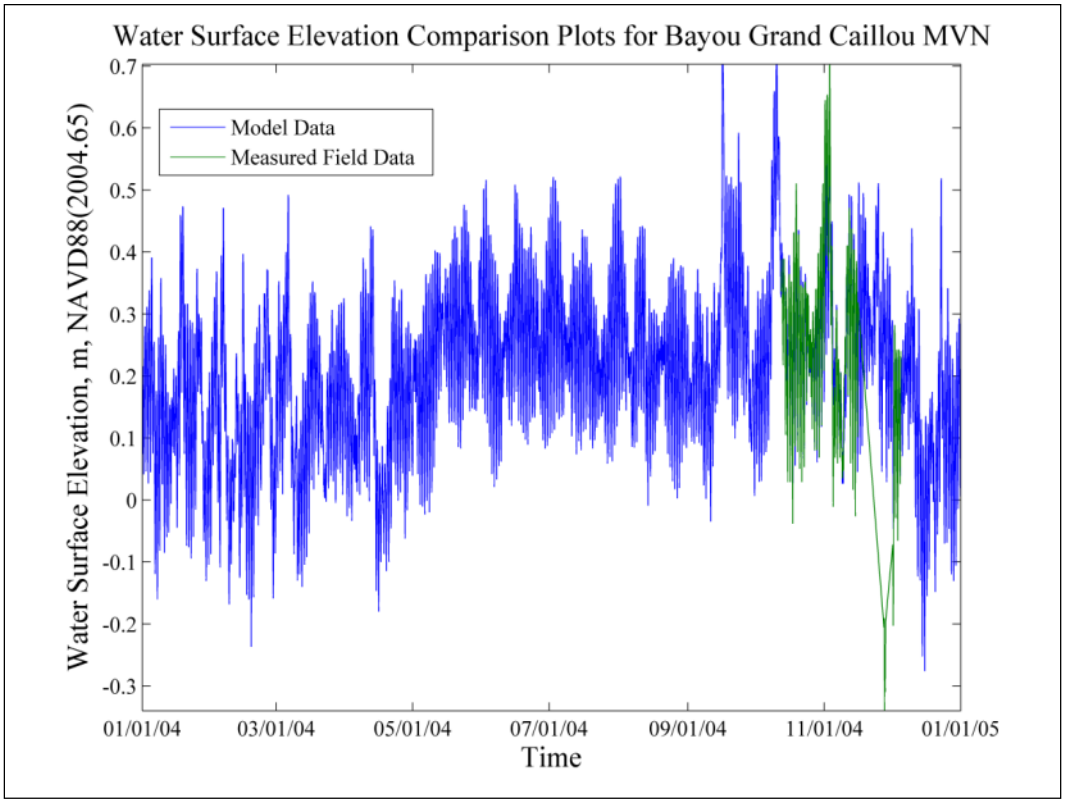

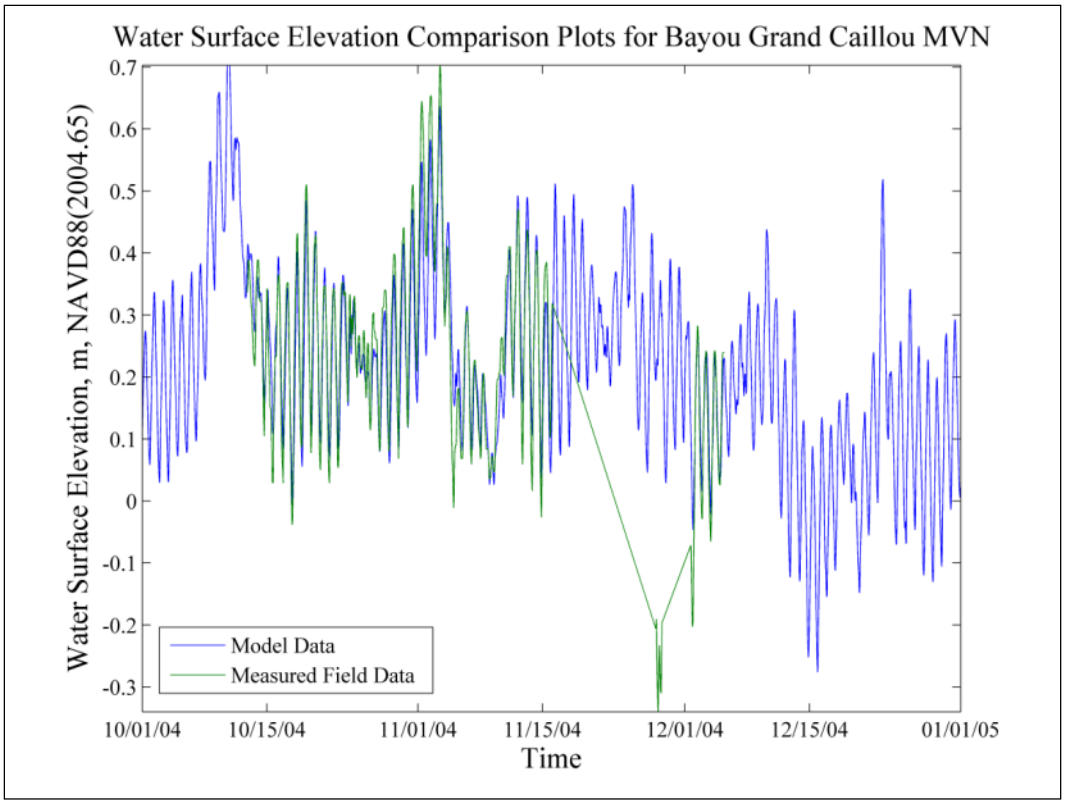

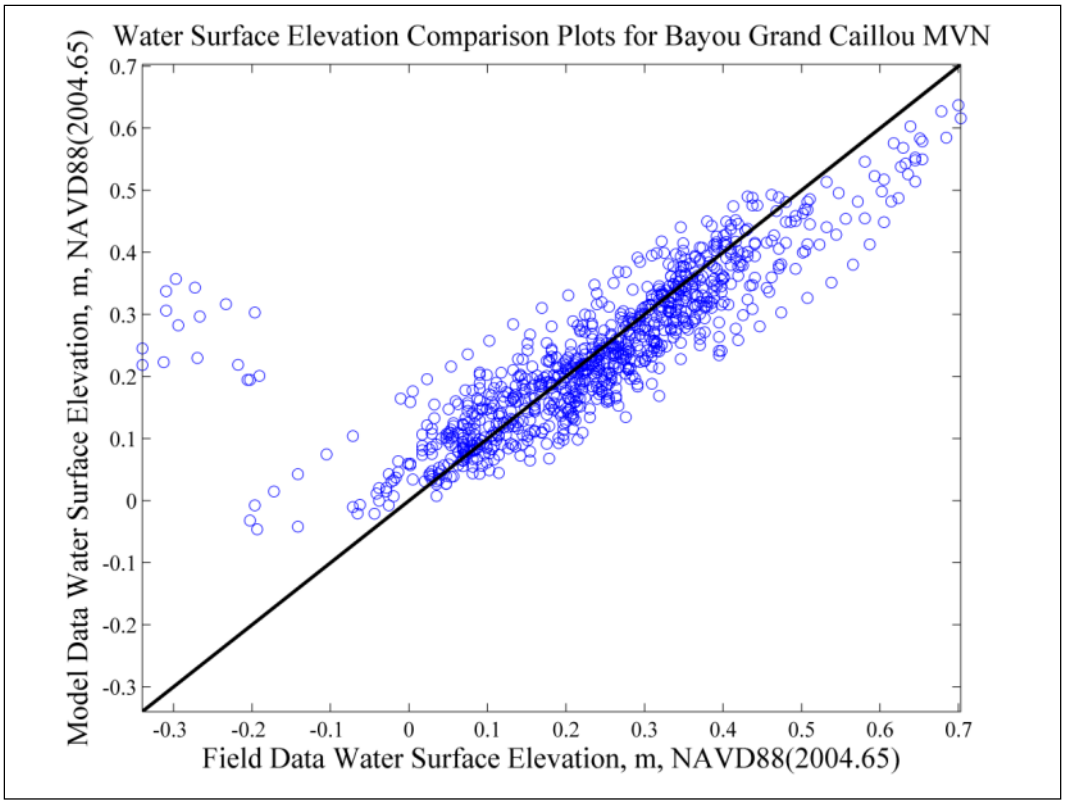
Water Surface Elevation Comparison Plots for Bayou Grand Caillou MVN
Model Data Water Surface Elevation, m, NAVD88(2004.65)
Field Data Water Surface Elevation, m, NAVD88(2004.65)
0.7
0.6
0.5
0.4
0.3
0.2
0.1
0
-0.1
-0.2
-0.3
-0.3
-0.2
-0.1
0
0.1
0.2
0.3
0.4
0.5
0.6
0.7

Figure 82. Houma Navigation Canal WSE comparison plots.

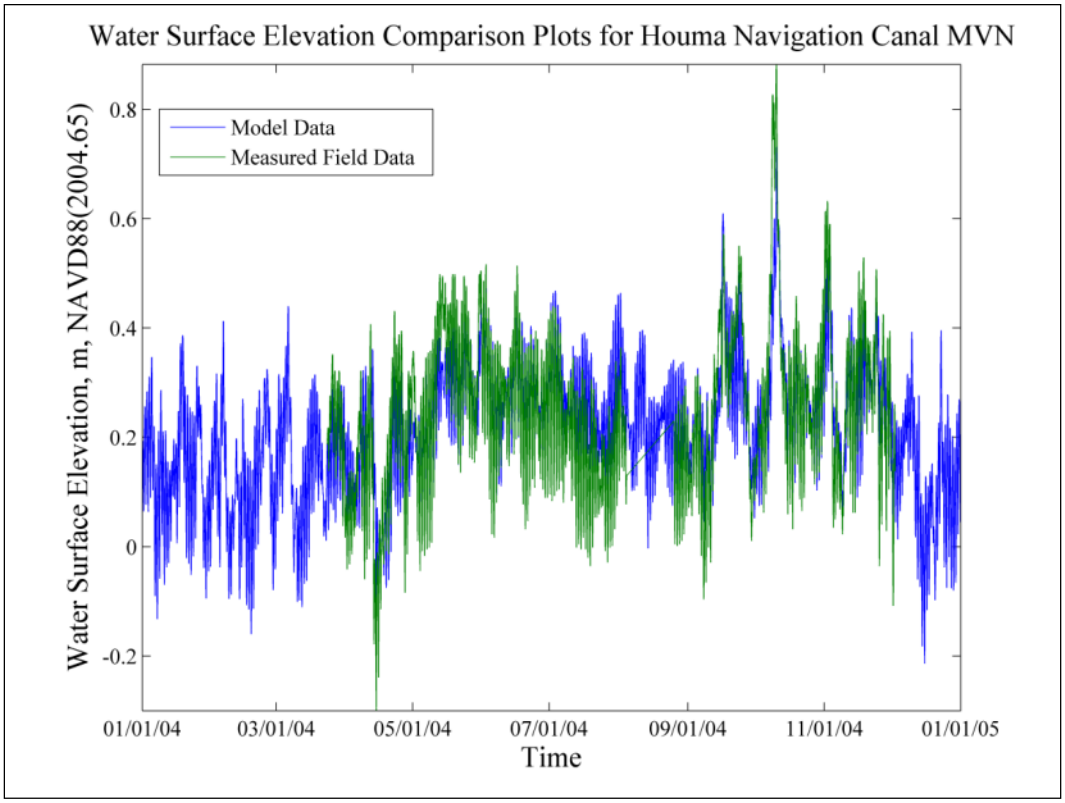

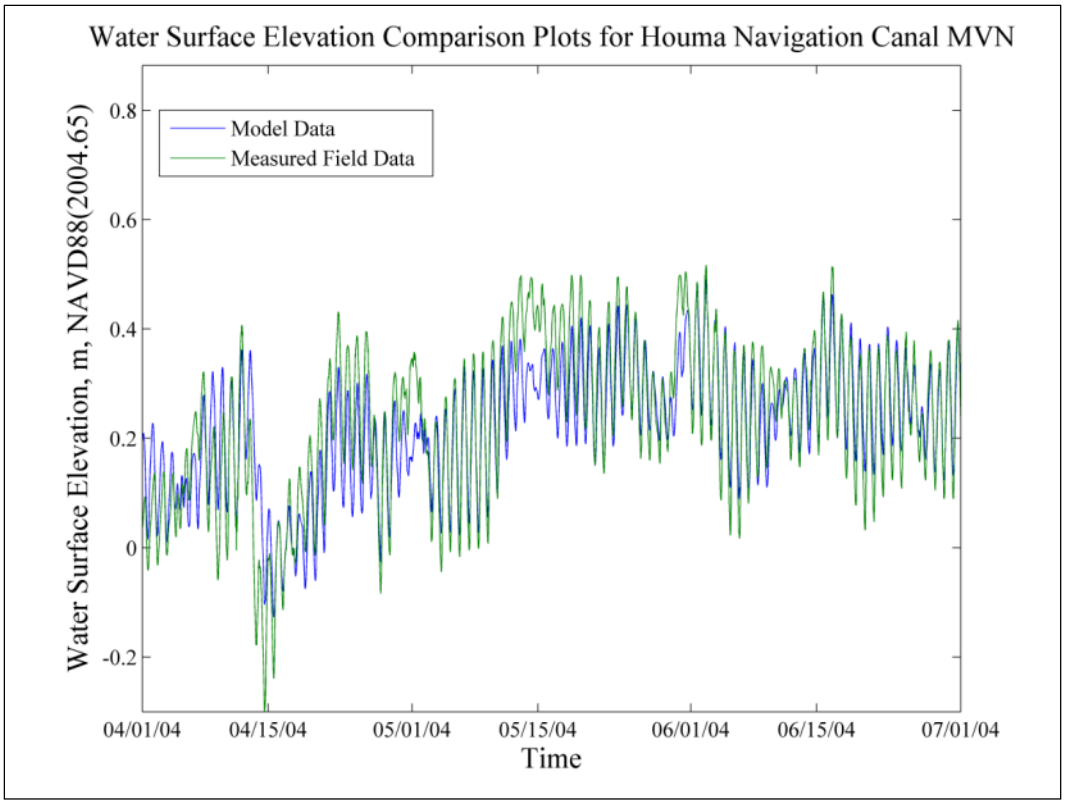

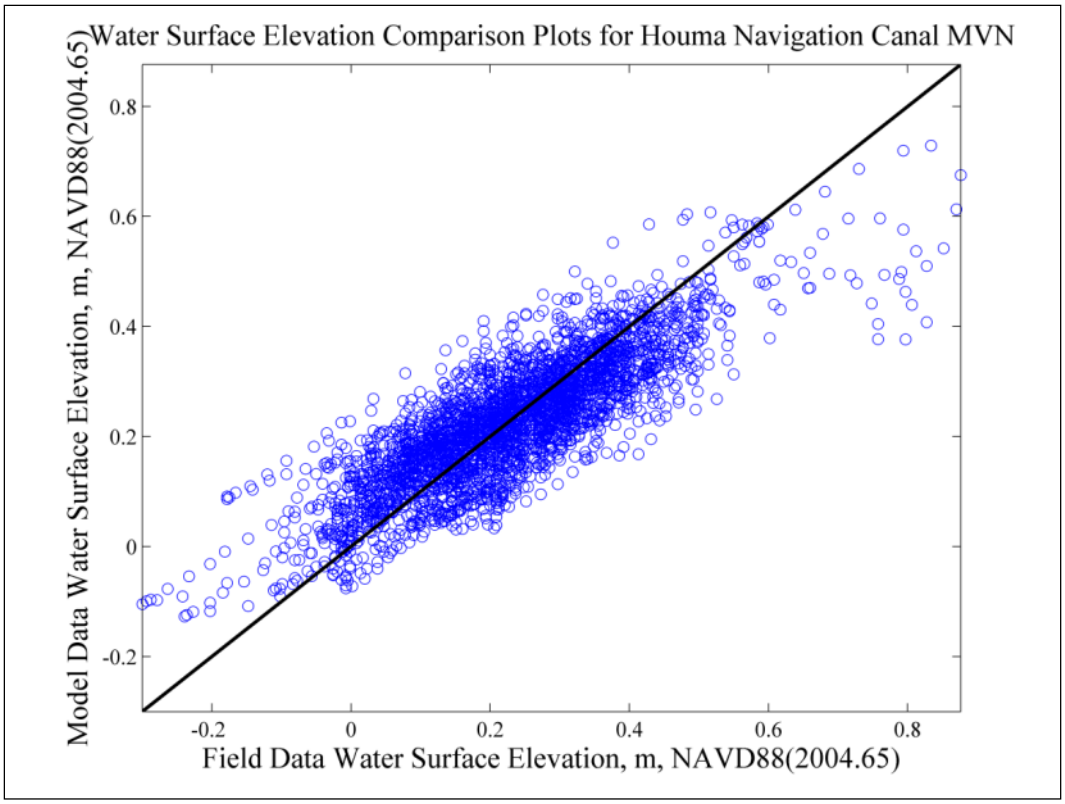
Water Surface Elevation Comparison Plots for Houma Navigation Canal MVN
Model Data Water Surface Elevation, m, NAVD88(2004.65)
Field Data Water Surface Elevation, m, NAVD88(2004.65)
0.8
0.6
0.4
0.2
0
-0.2
-0.2
0
0.2
0.4
0.6
0.8

Figure 83. Cocodrie WSE comparison plots.

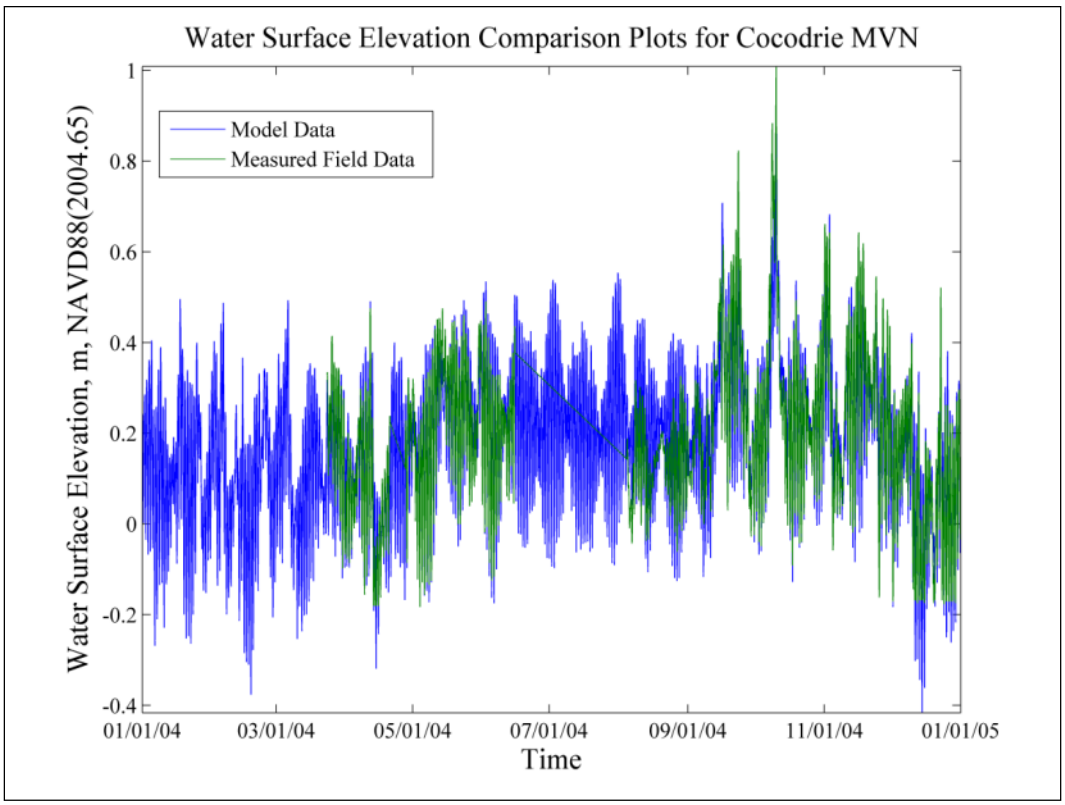

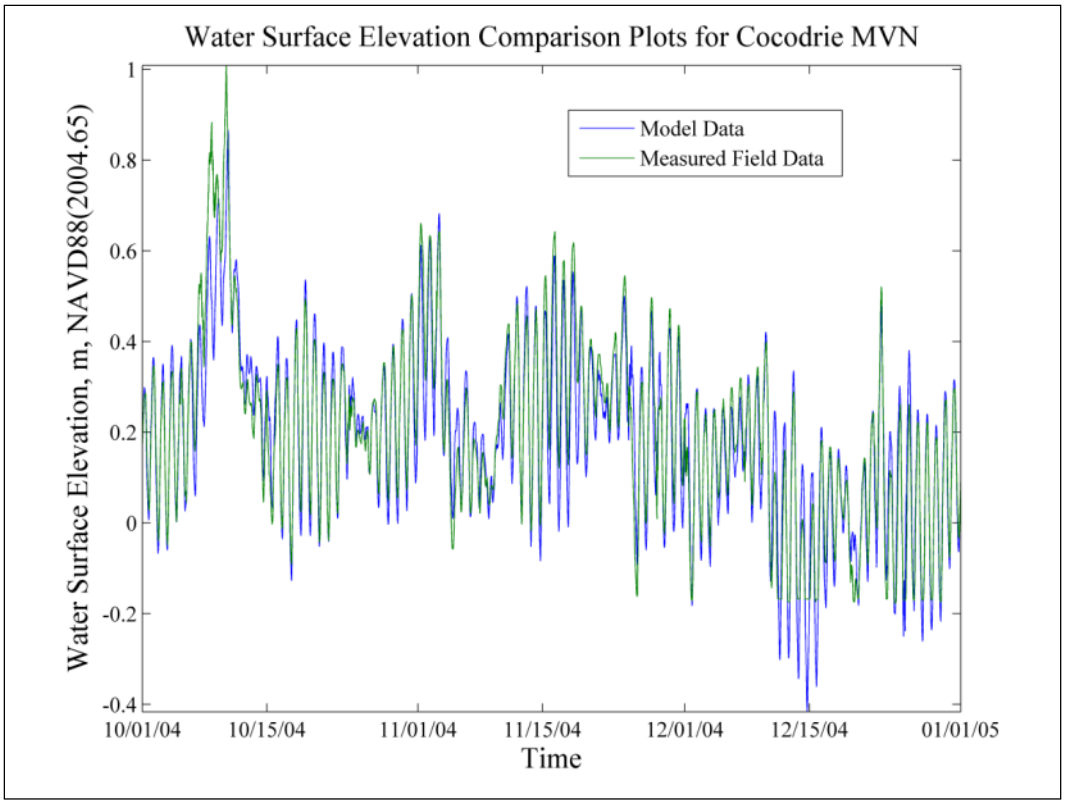

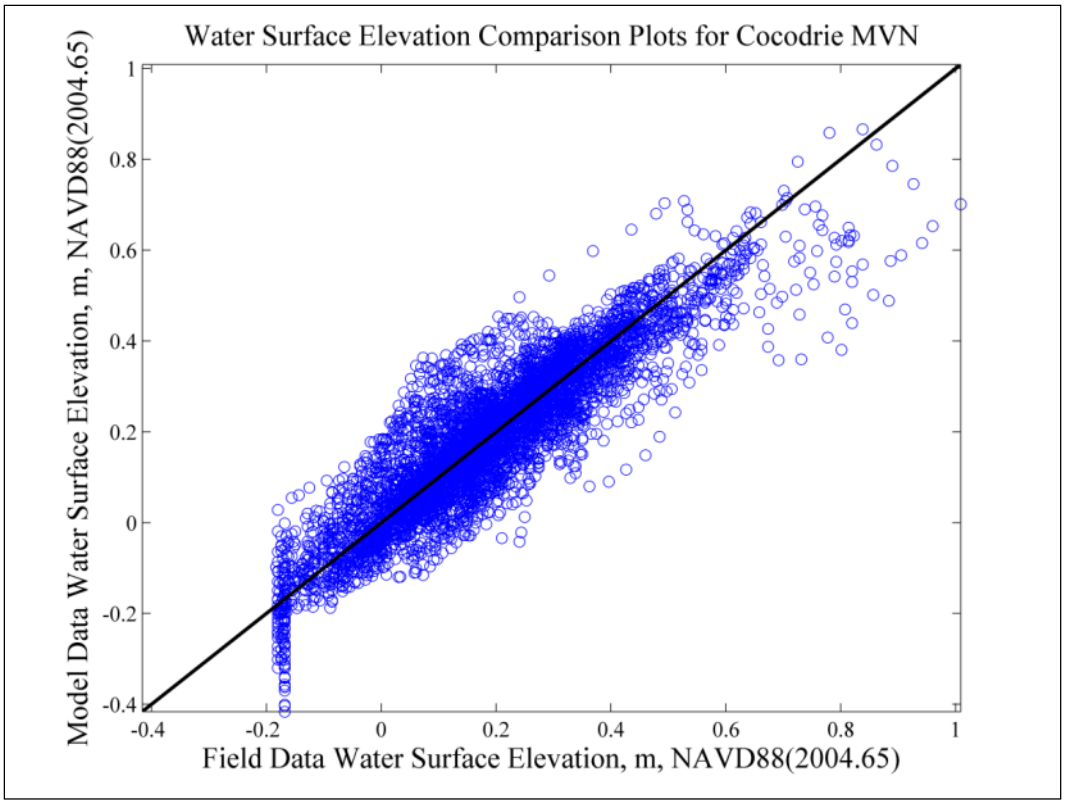
Water Surface Elevation Comparison Plots for Cocodrie MVN
Model Data Water Surface Elevation, m, NAVD88(2004.65)
Field Data Water Surface Elevation, m, NAVD88(2004.65)
1
0.8
0.6
0.4
0.2
0
-0.2
-0.4
-0.4
-0.2
0
0.2
0.4
0.6
0.8
1

Figure 84. Bayou Petit Caillou WSE comparison plots.

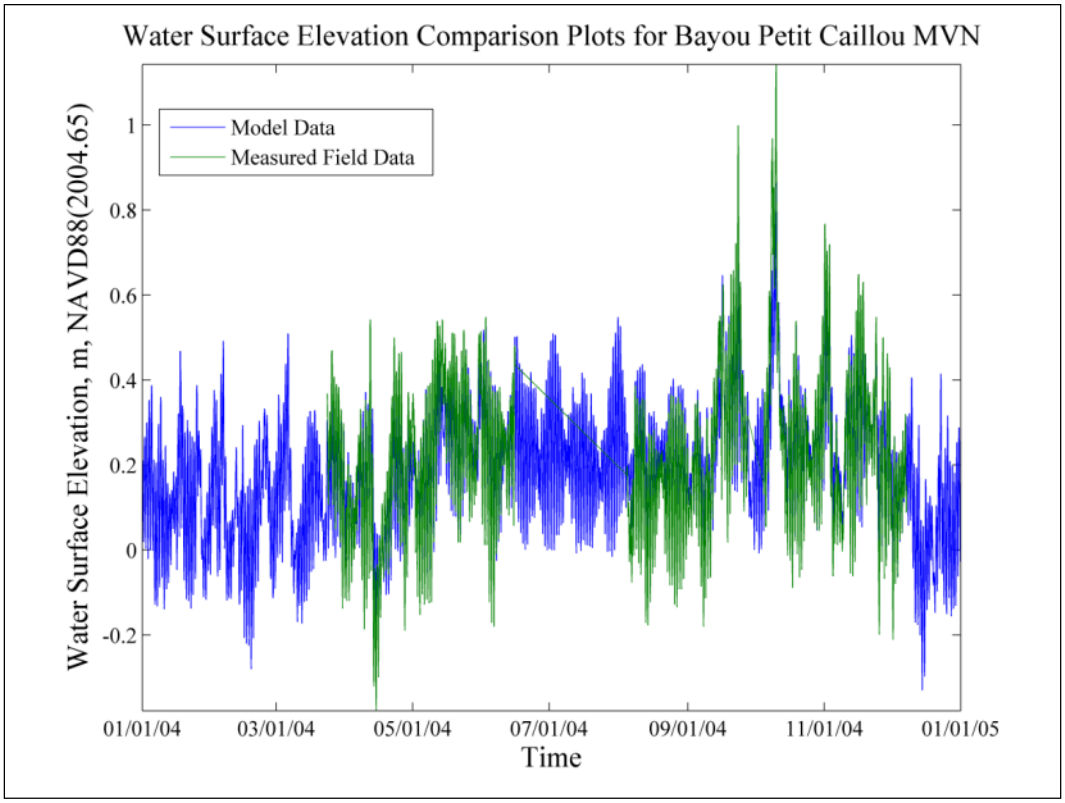

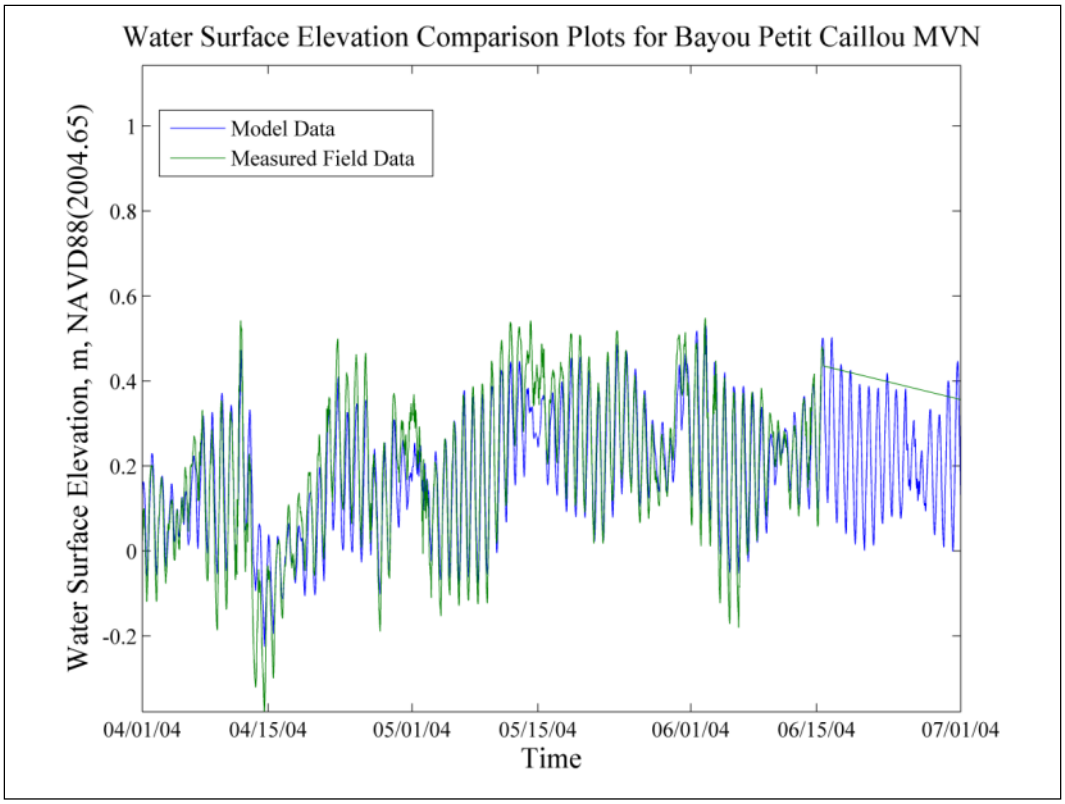

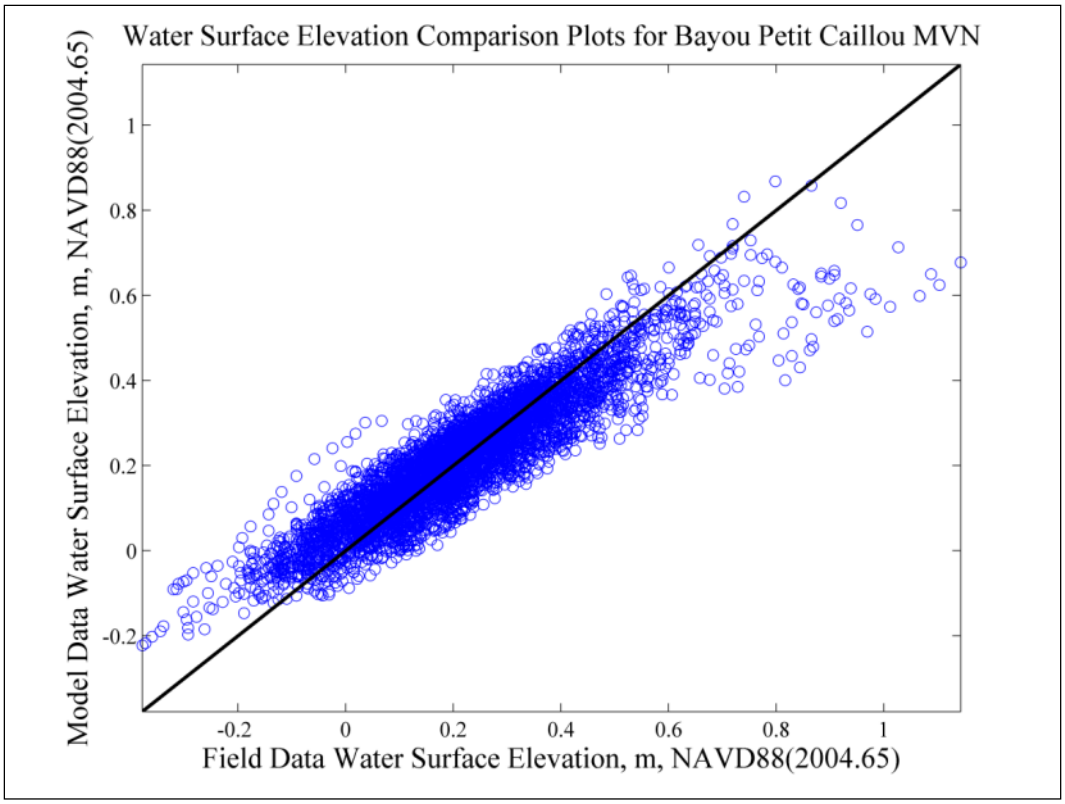
Water Surface Elevation Comparison Plots for Bayou Petit Caillou MVN
Model Data Water Surface Elevation, m, NAVD88(2004.65)
Field Data Water Surface Elevation, m, NAVD88(2004.65)
1
0.8
0.6
0.4
0.2
0
-0.2
-0.2
0
0.2
0.4
0.6
0.8
1

Figure 85. Bush Canal WSE comparison plots.

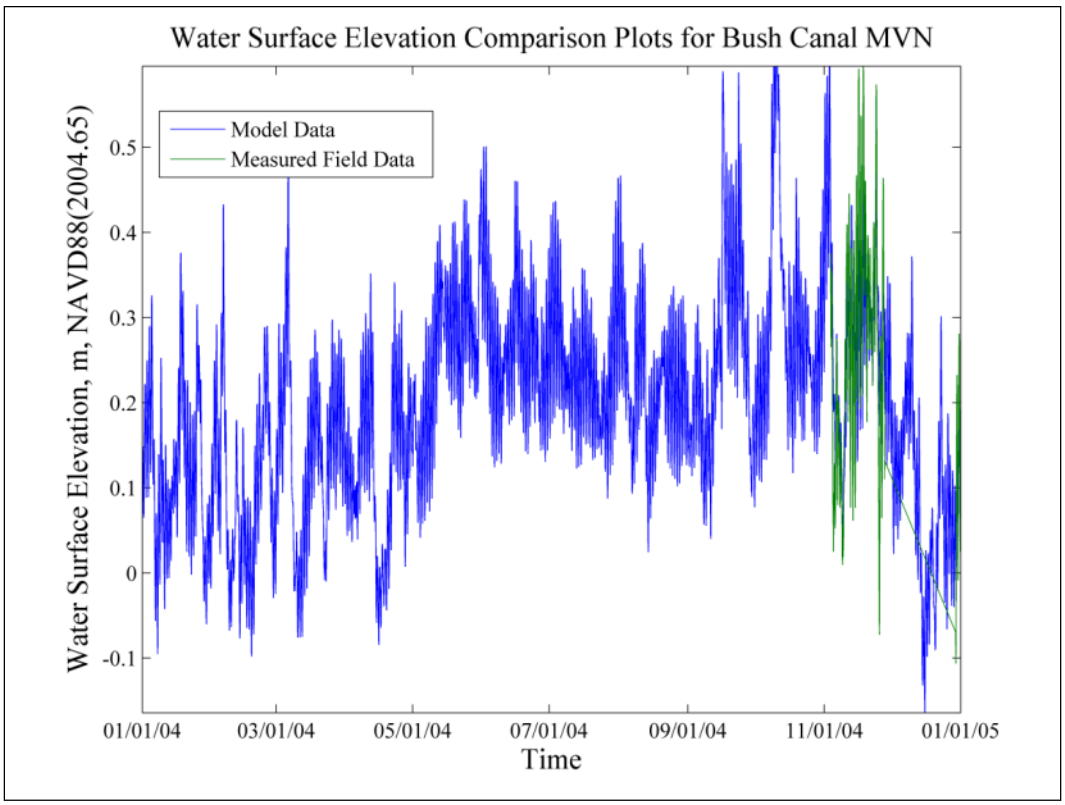

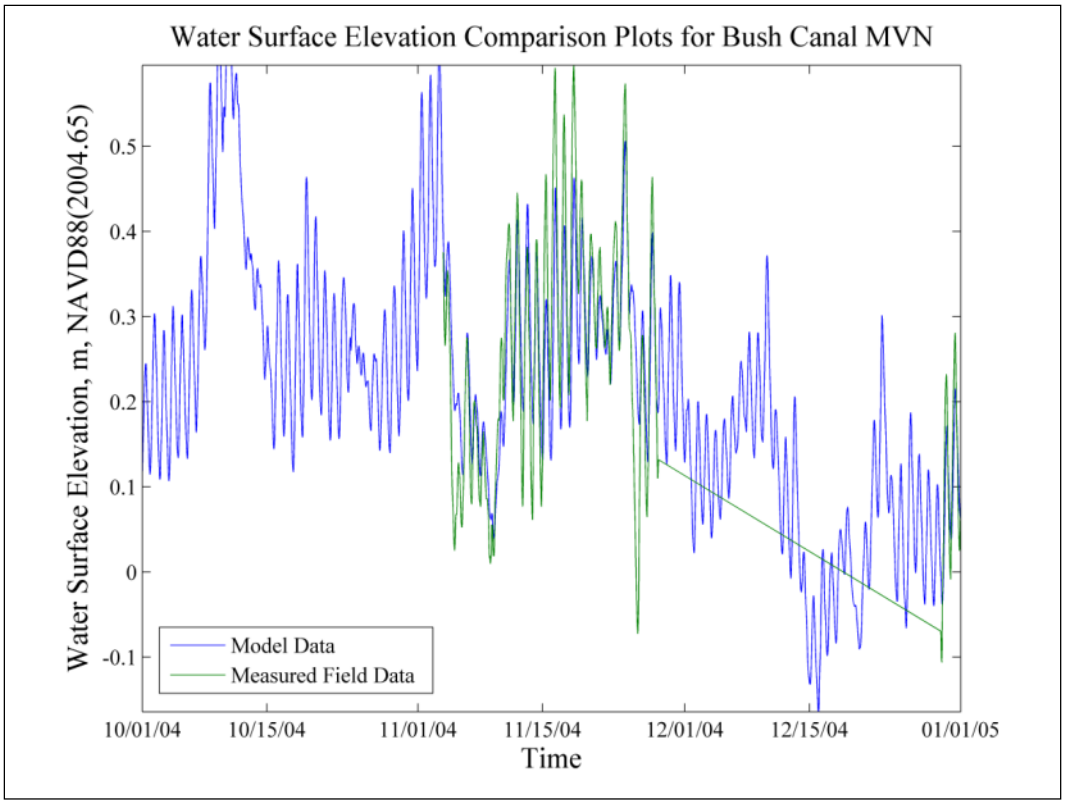

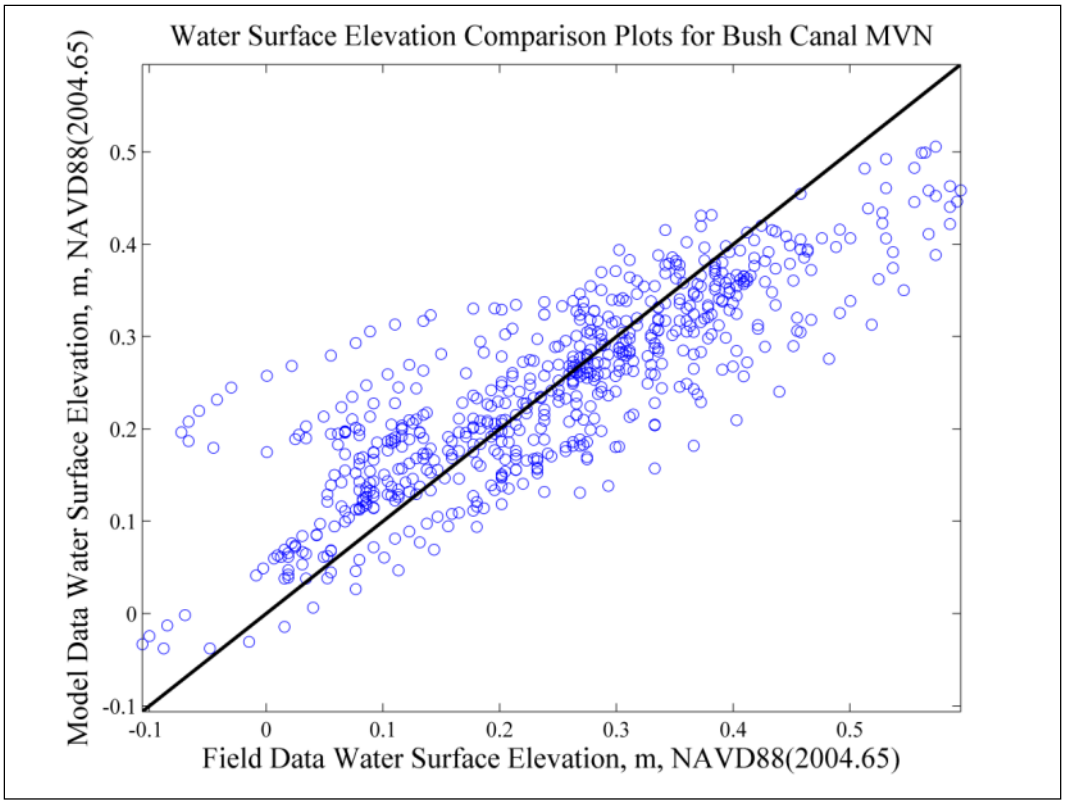
Water Surface Elevation Comparison Plots for Bush Canal MVN
Model Data Water Surface Elevation, m, NAVD88(2004.65)
Field Data Water Surface Elevation, m, NAVD88(2004.65)
-0.1
0
0.1
0.2
0.3
0.4
0.5

Figure 86. Lake Boudreaux WSE comparison plots.

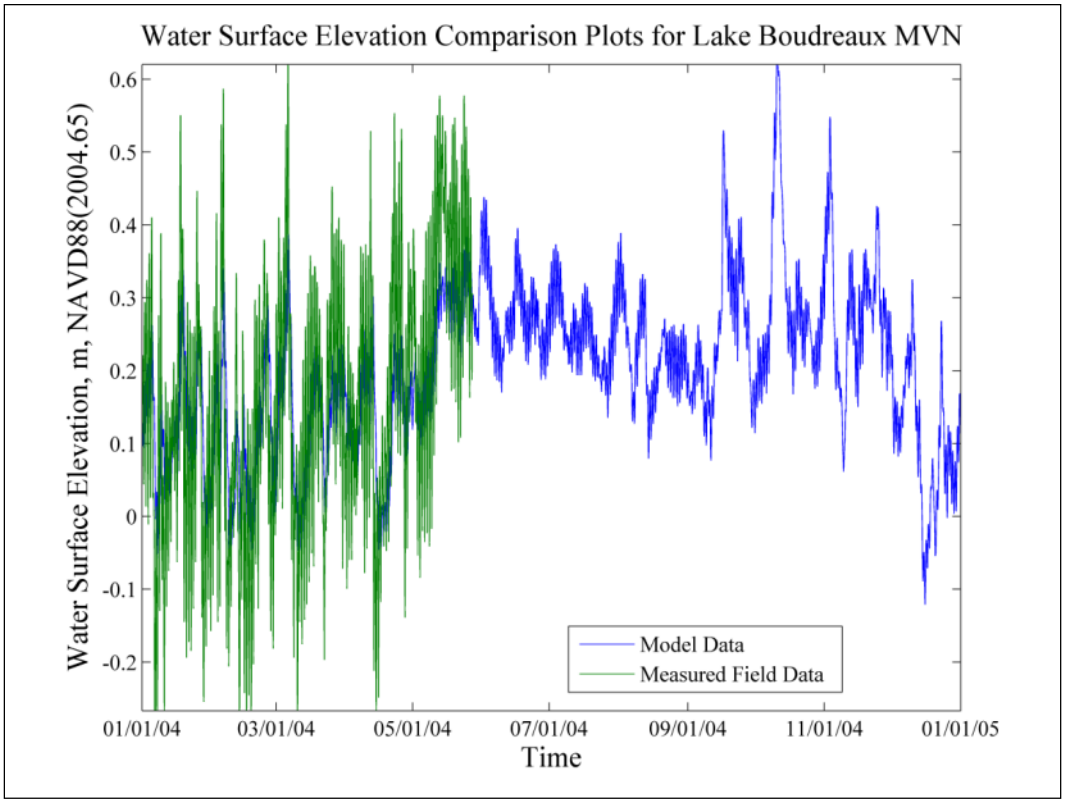

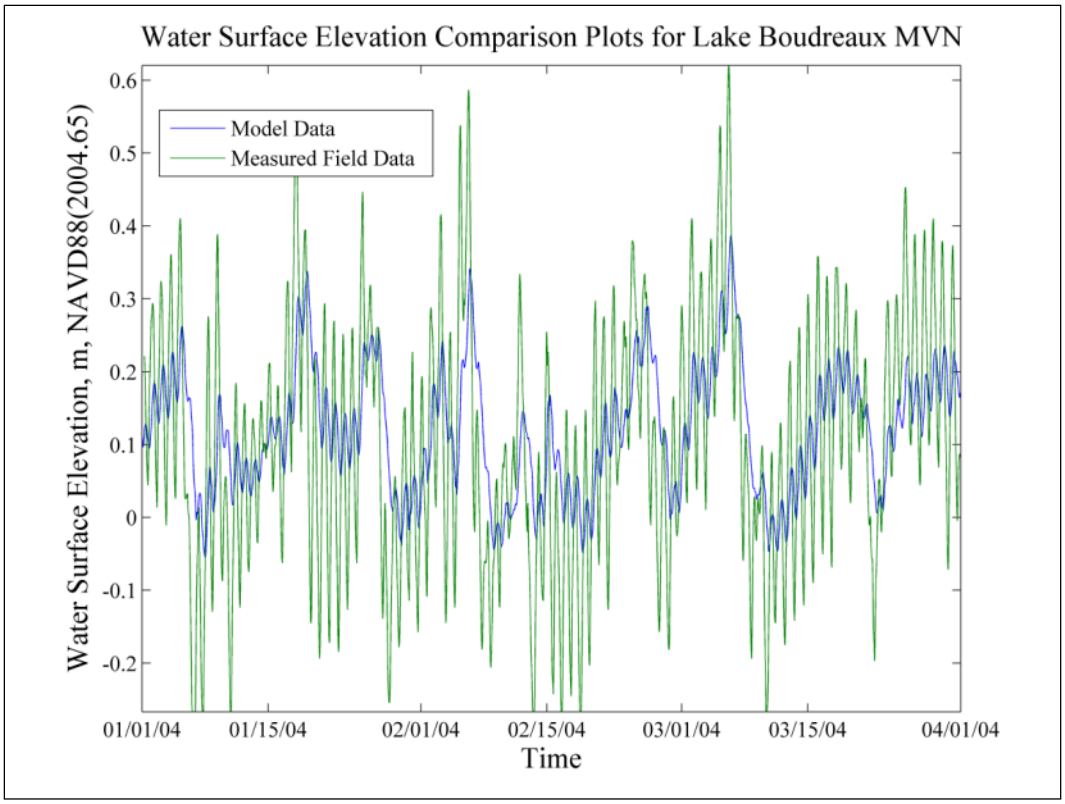

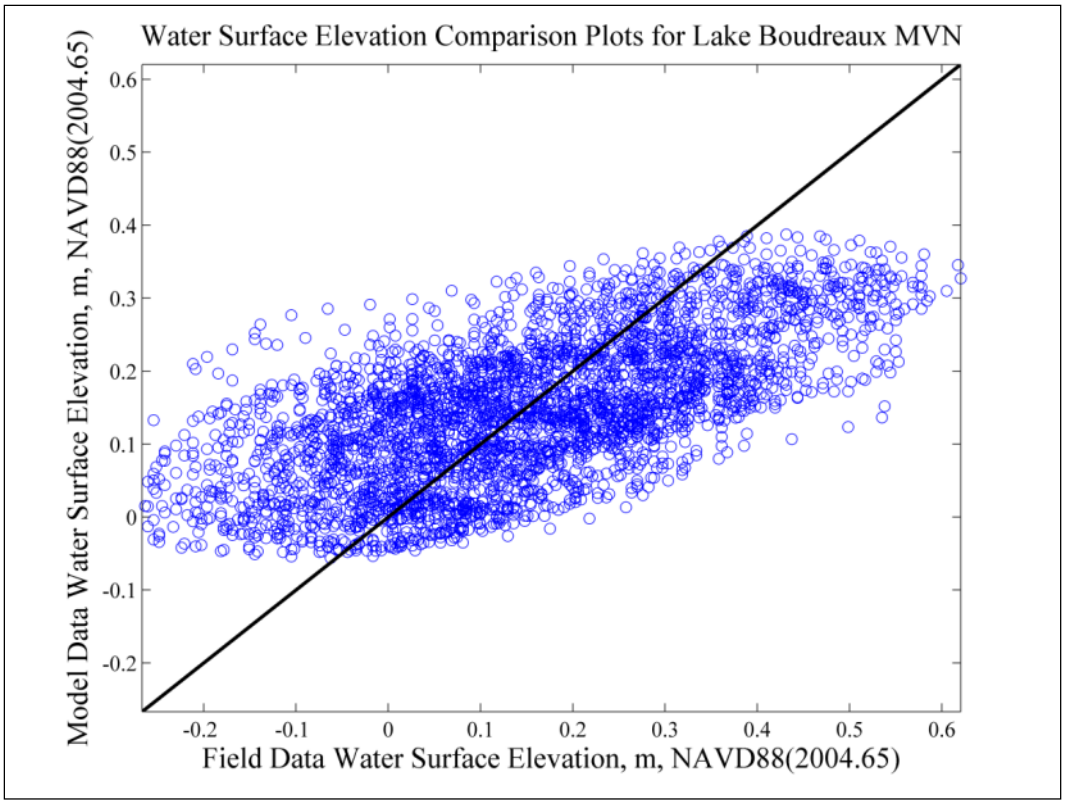
Water Surface Elevation Comparison Plots for Lake Boudreaux MVN
Model Data Water Surface Elevation, m, NAVD88(2004.65)
Field Data Water Surface Elevation, m, NAVD88(2004.65)
0.6
0.5
0.4
0.3
0.2
0.1
0
-0.1
-0.2
-0.2
-0.1
0
0.1
0.2
0.3
0.4
0.5
0.6

Figure 87. Bayou Terrebonne WSE comparison plots.

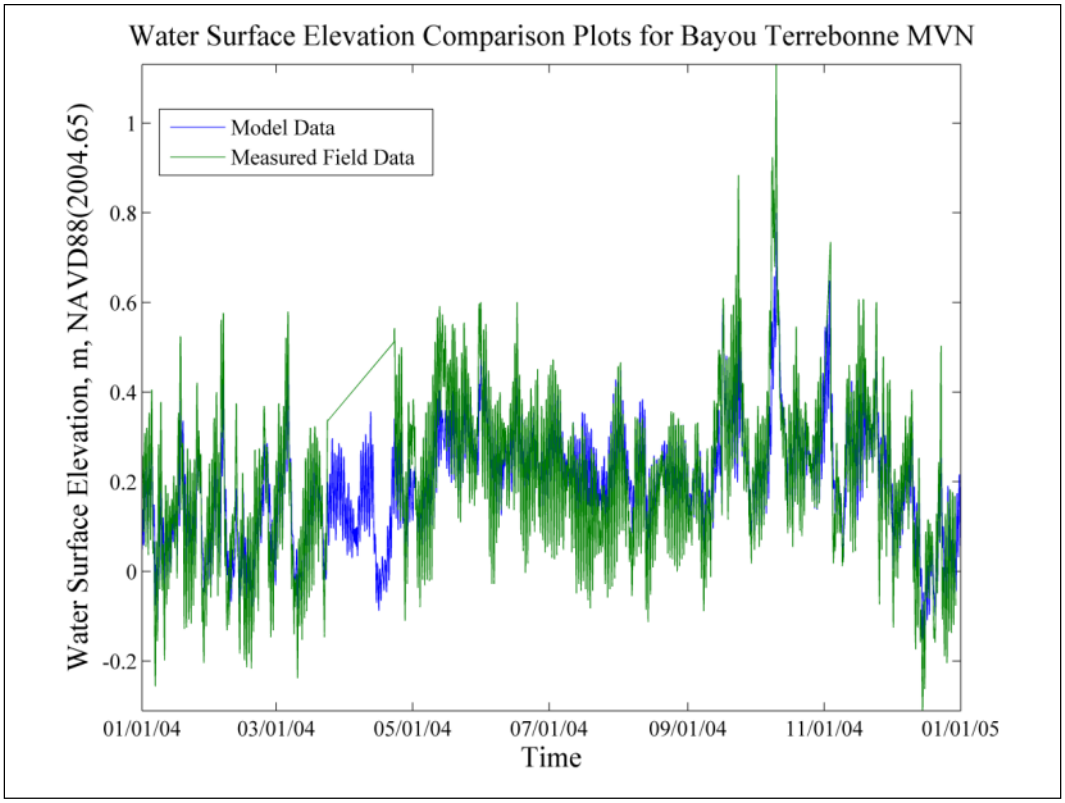

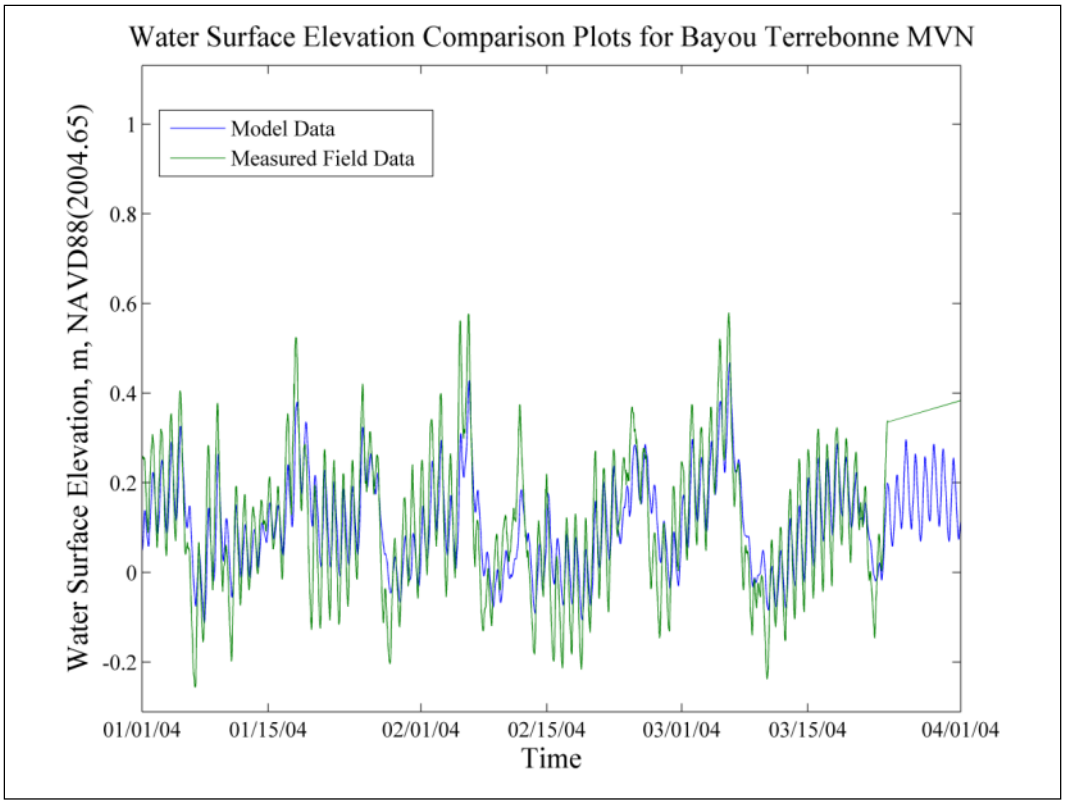

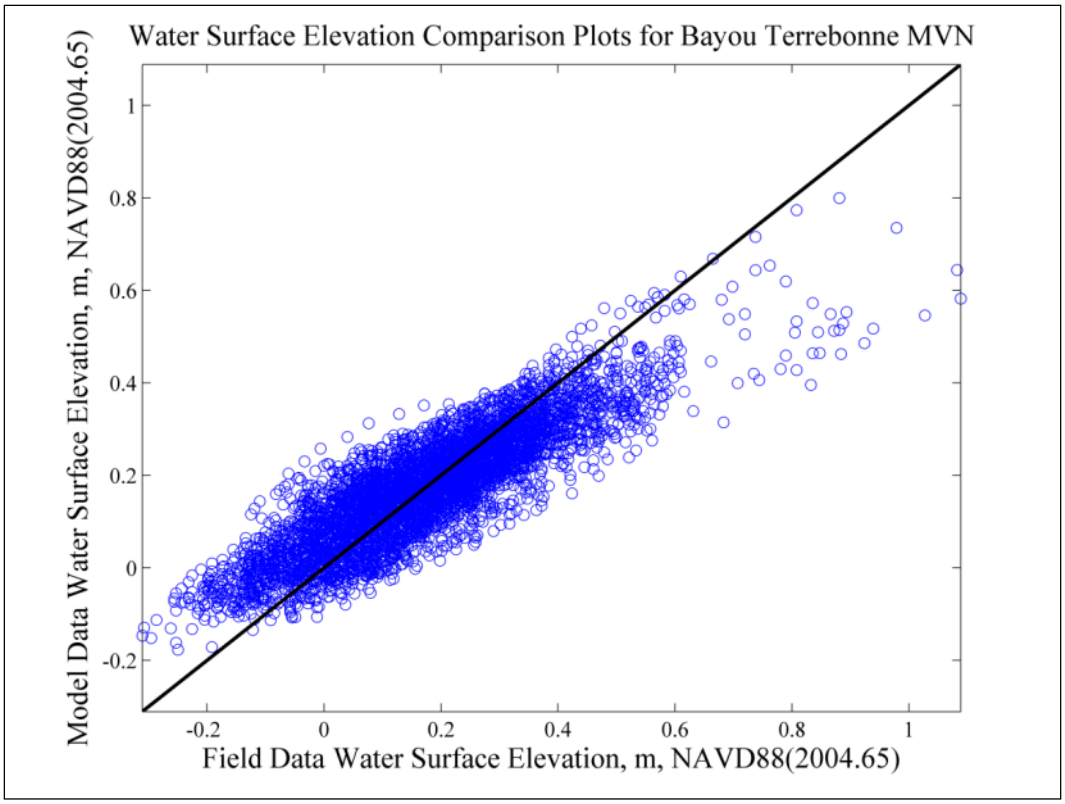
Water Surface Elevation Comparison Plots for Bayou Terrebonne MVN
Model Data Water Surface Elevation, m, NAVD88(2004.65)
Field Data Water Surface Elevation, m, NAVD88(2004.65)
1
0.8
0.6
0.4
0.2
0
-0.2
-0.2
0
0.2
0.4
0.6
0.8
1

Figure 88. Humble Canal WSE comparison plots.

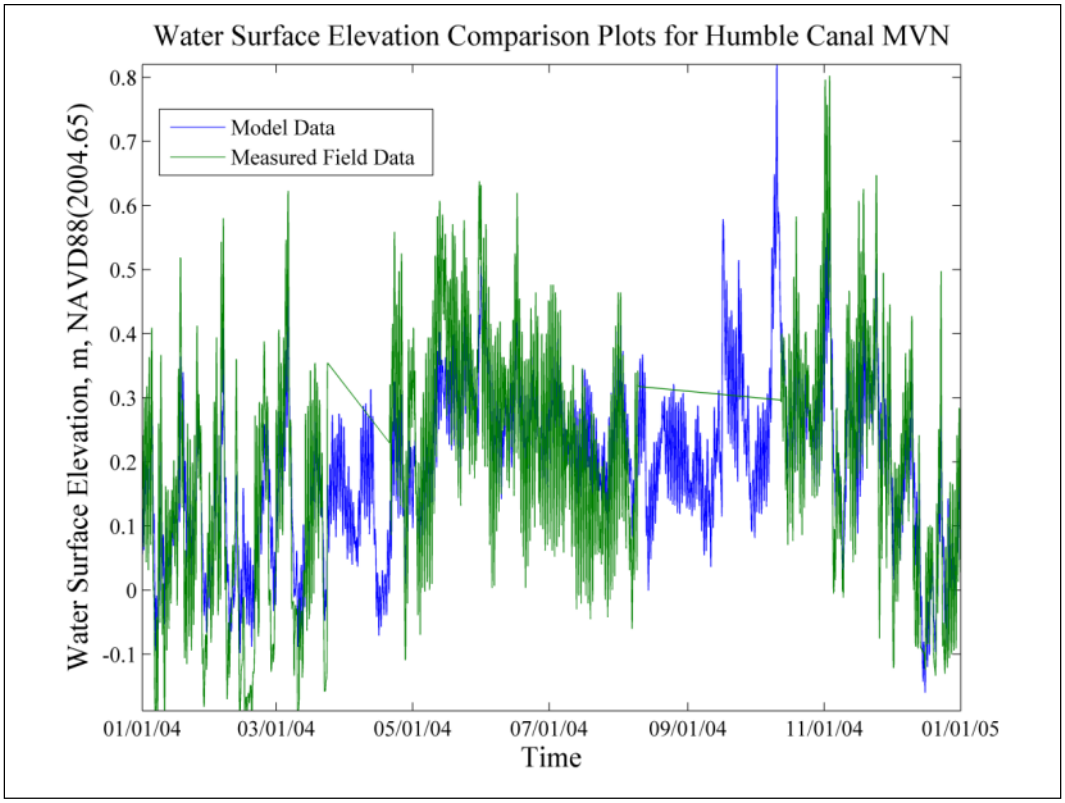

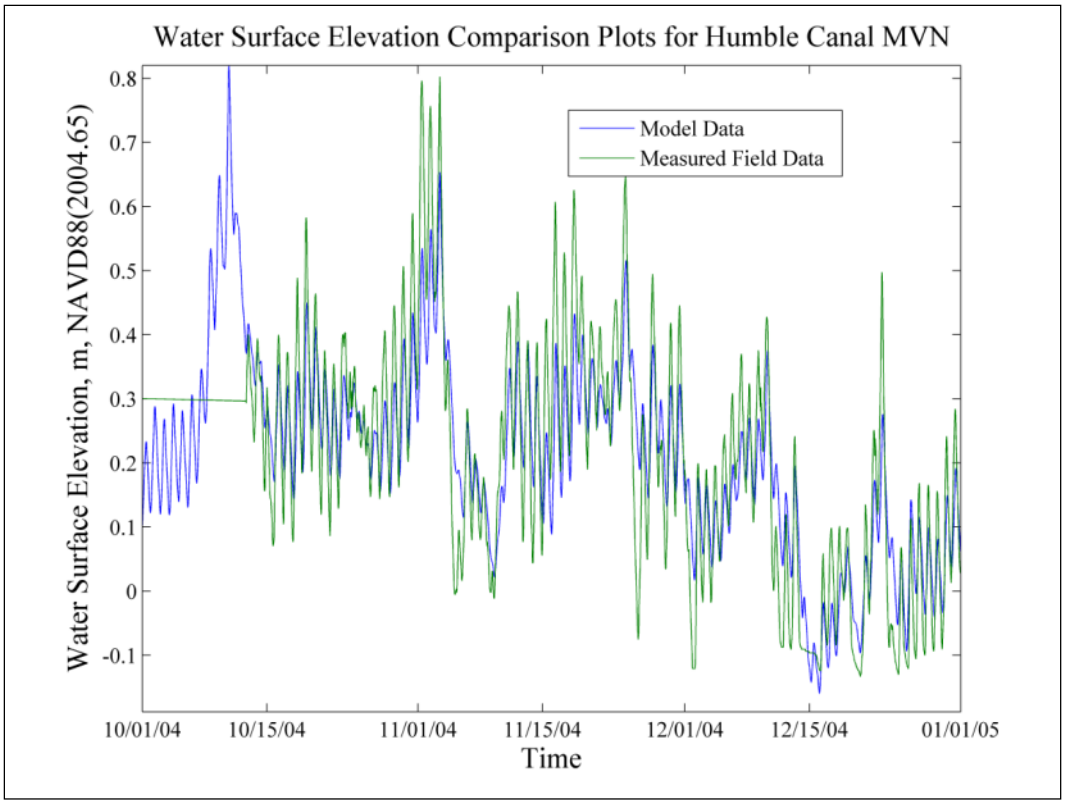

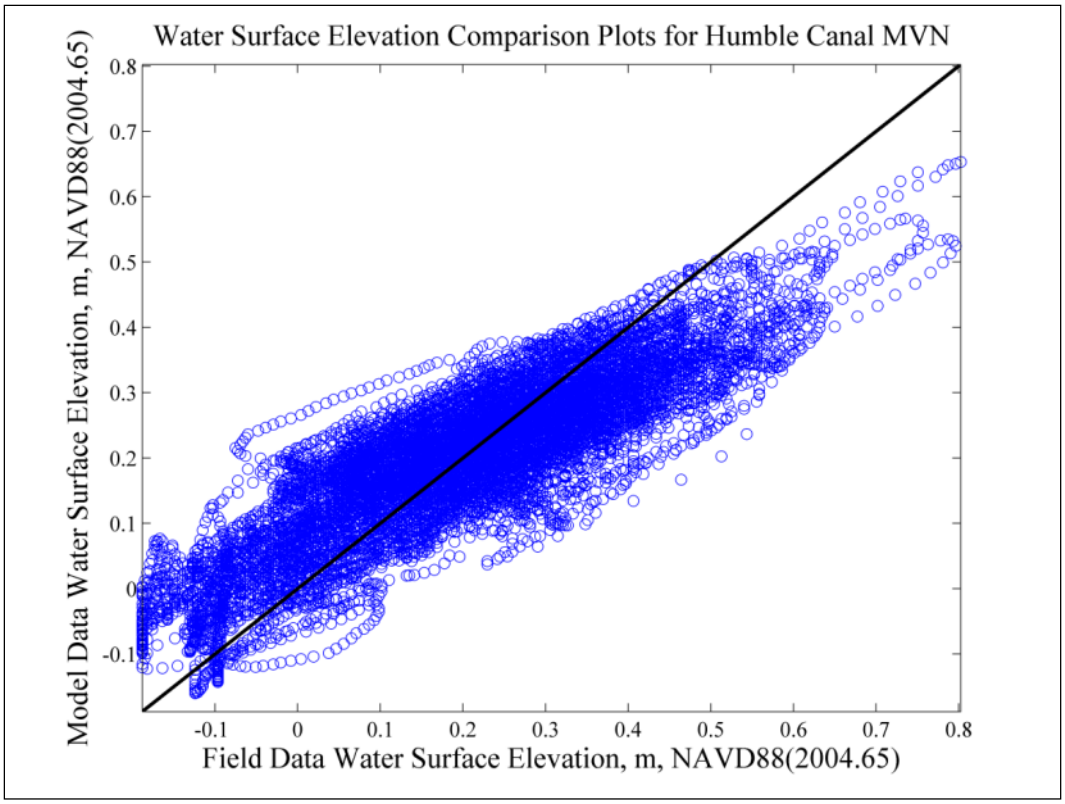
Water Surface Elevation Comparison Plots for Humble Canal MVN
Model Data Water Surface Elevation, m, NAVD88(2004.65)
Field Data Water Surface Elevation, m, NAVD88(2004.65)
0.8
0.7
0.6
0.5
0.4
0.3
0.2
0.1
0
-0.1
-0.1
0
0.1
0.2
0.3
0.4
0.5
0.6
0.7
0.8

Figure 89. Madison Bay WSE comparison plots.

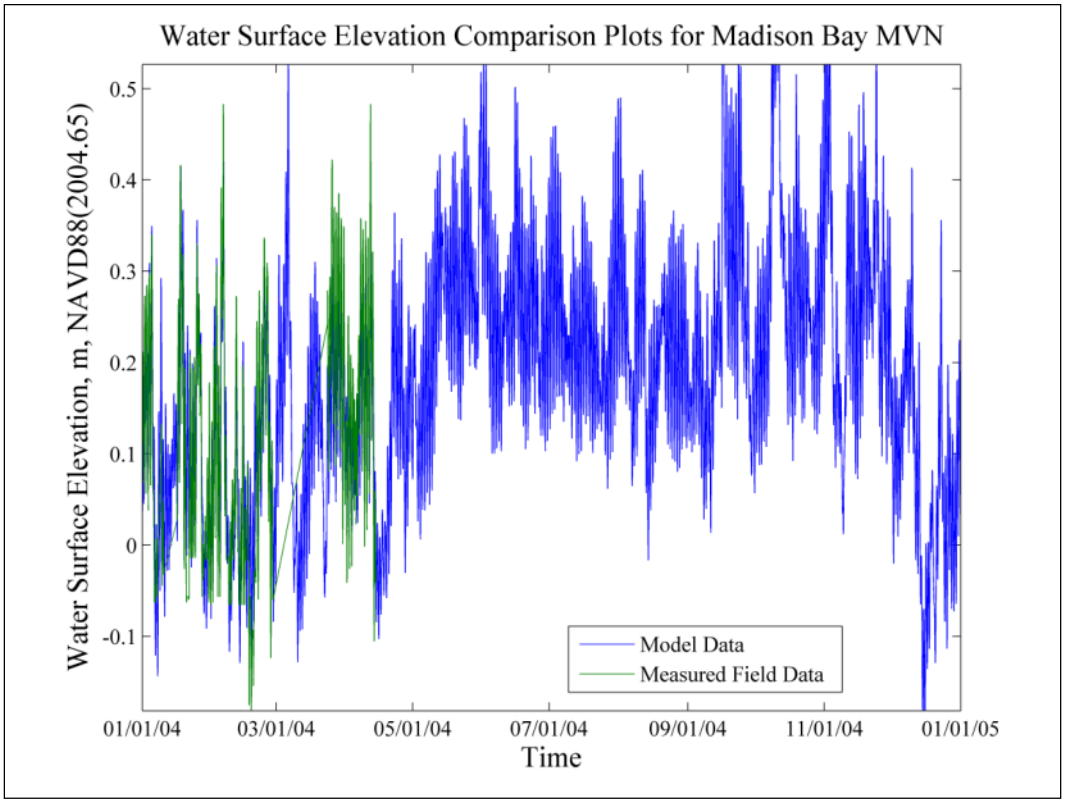

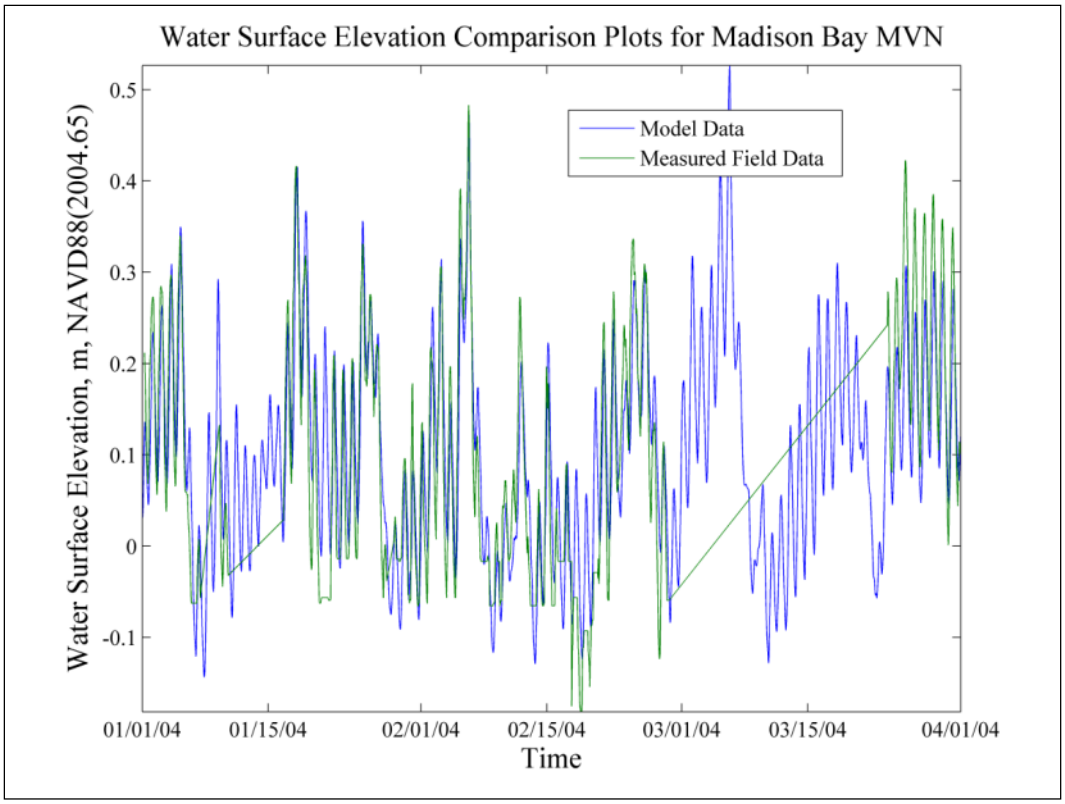

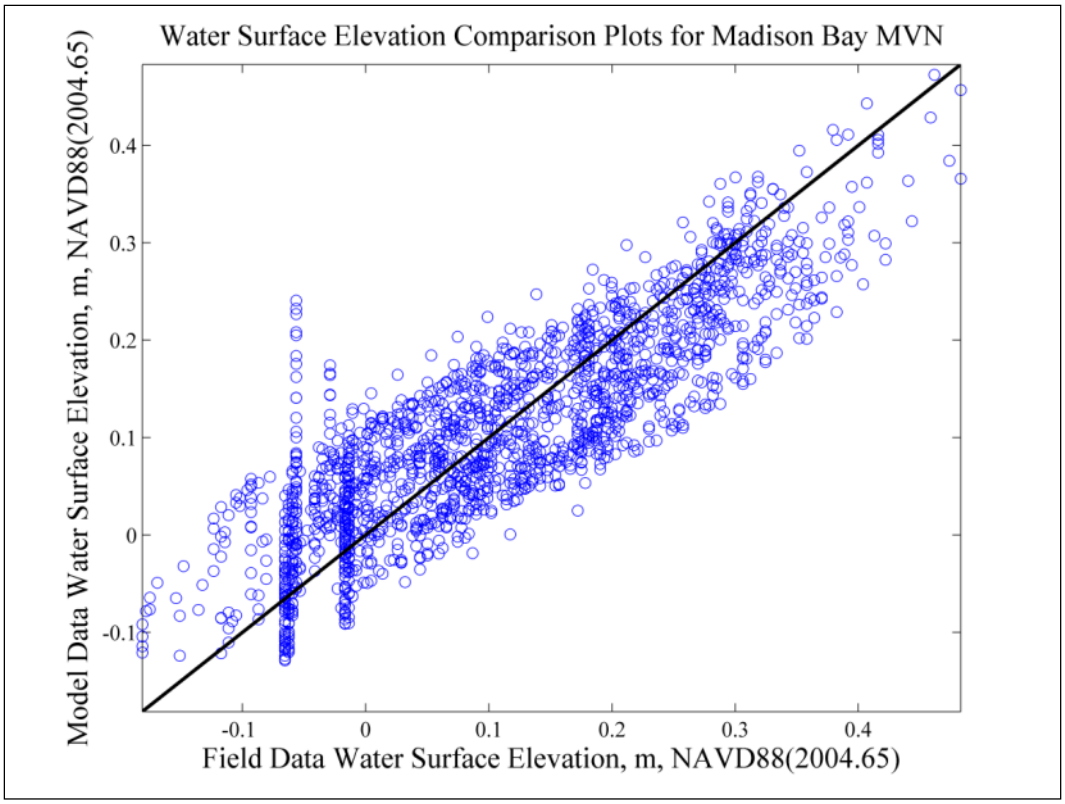
Water Surface Elevation Comparison Plots for Madison Bay MVN
Model Data Water Surface Elevation, m, NAVD88(2004.65)
Field Data Water Surface Elevation, m, NAVD88(2004.65)
0.4
0.3
0.2
0.1
0
-0.1
-0.1
0
0.1
0.2
0.3
0.4

Figure 90. Pointe Aux Chenes WSE comparison plots.

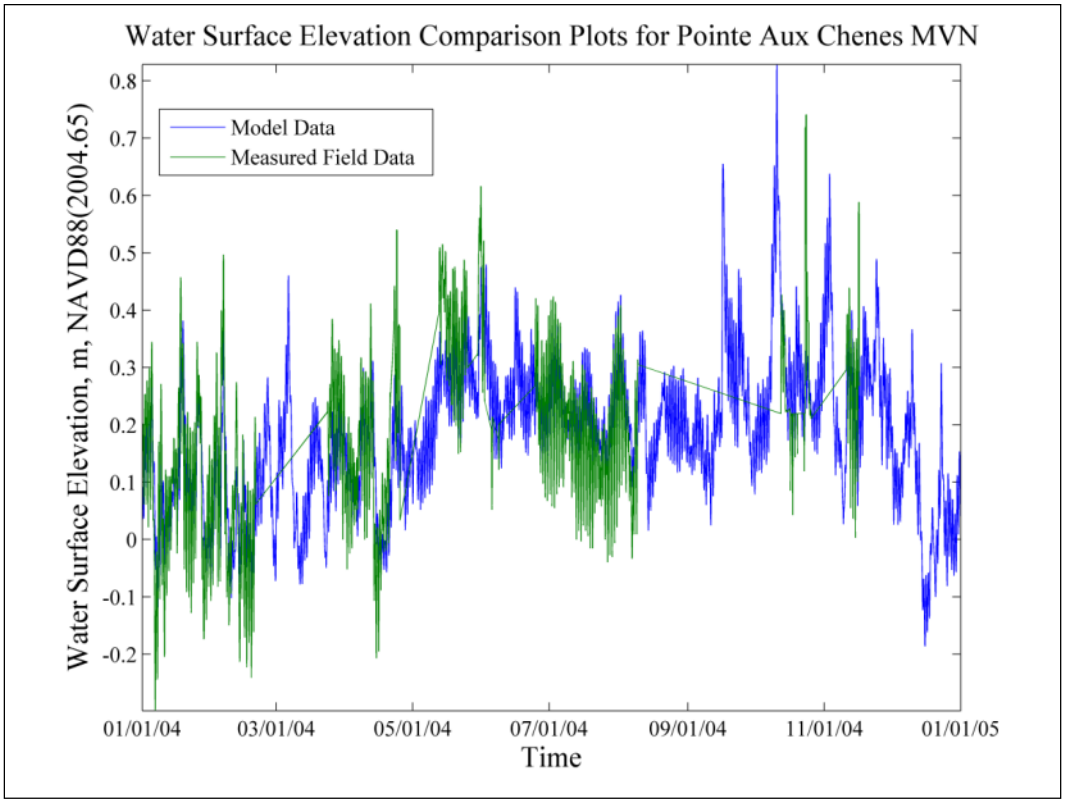

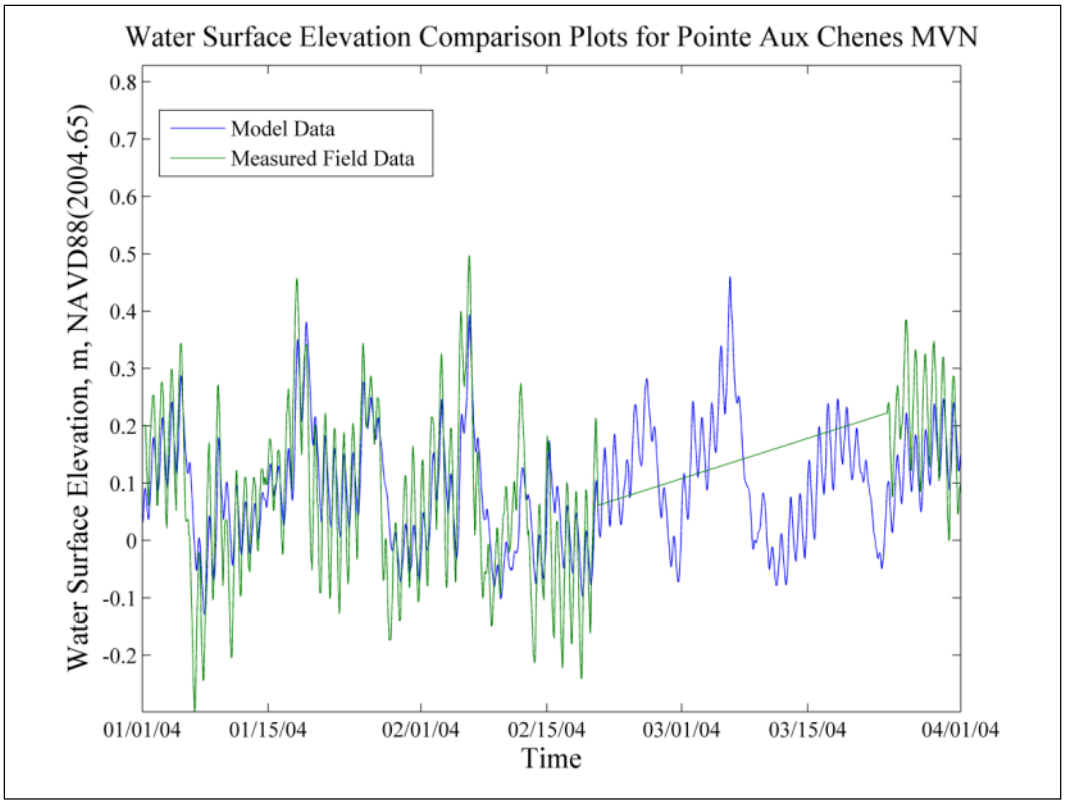

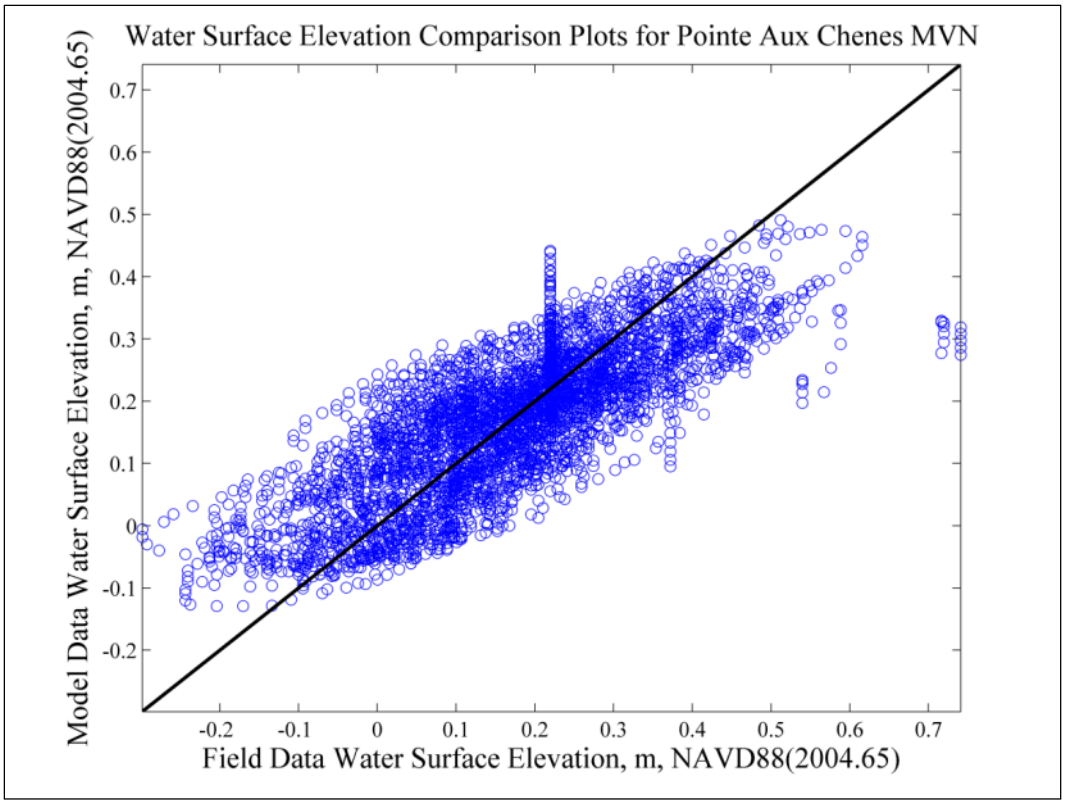
Water Surface Elevation Comparison Plots for Pointe Aux Chenes MVN
Model Data Water Surface Elevation, m, NAVD88(2004.65)
Field Data Water Surface Elevation, m, NAVD88(2004.65)
0.7
0.6
0.5
0.4
0.3
0.2
0.1
0
-0.1
-0.2
-0.2
-0.1
0
0.1
0.2
0.3
0.4
0.5
0.6
0.7

Figure 91. Grand Bayou Canal WSE comparison plots.

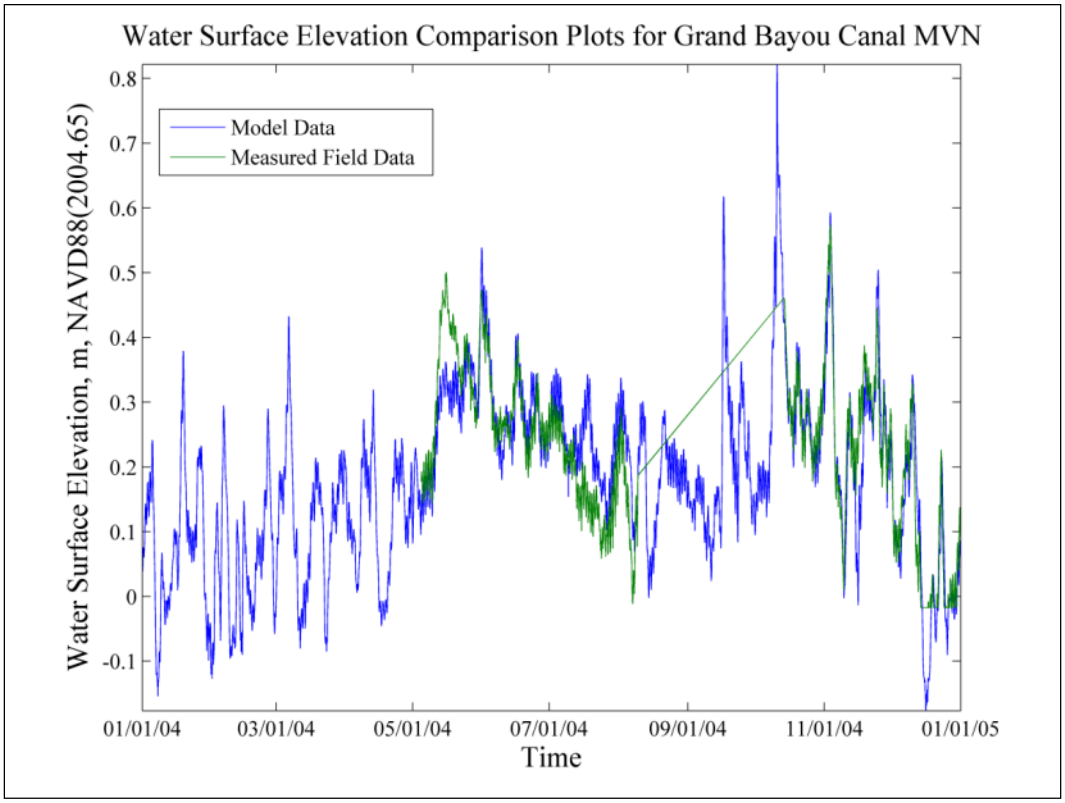

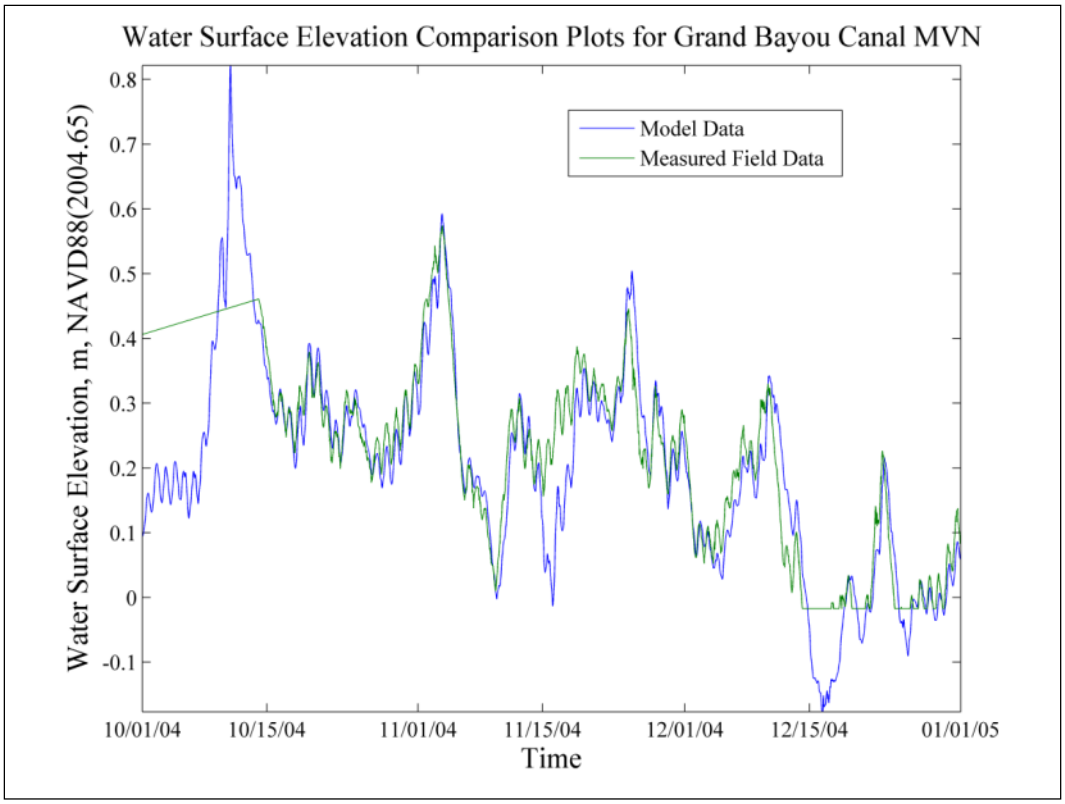

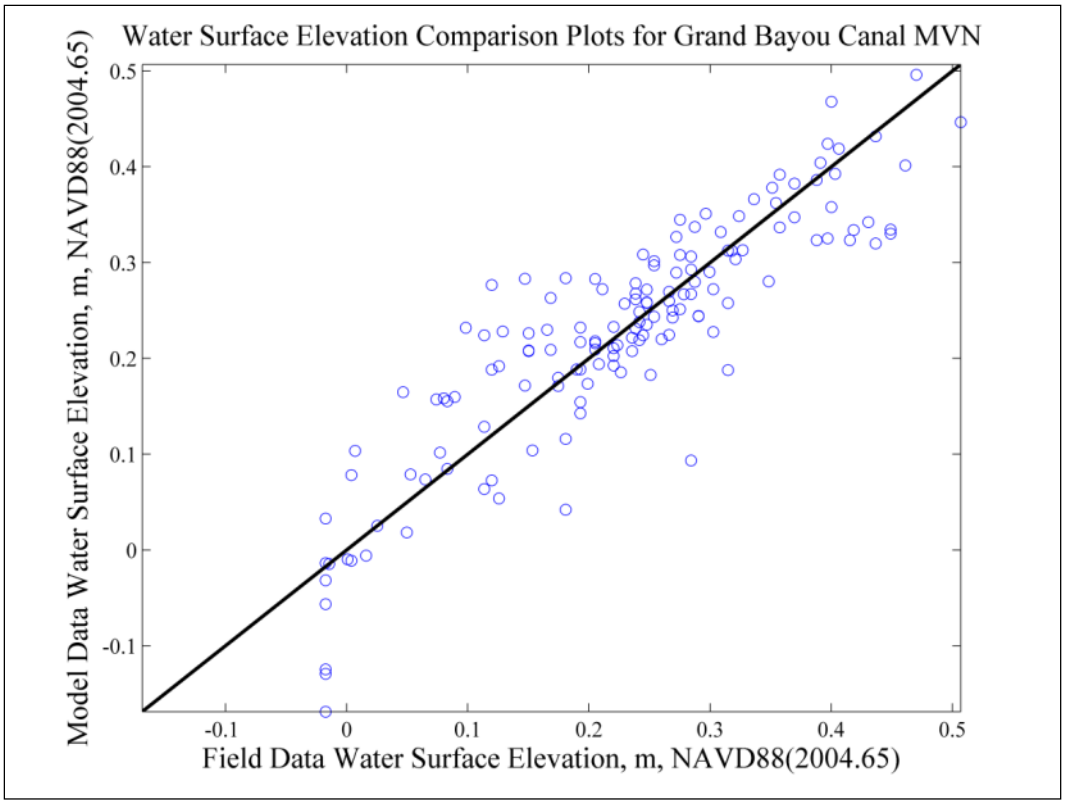
Water Surface Elevation Comparison Plots for Grand Bayou Canal MVN
Model Data Water Surface Elevation, m, NAVD88(2004.65)
Field Data Water Surface Elevation, m, NAVD88(2004.65)
0.5
0.4
0.3
0.2
0.1
0
-0.1
-0.1
0
0.1
0.2
0.3
0.4
0.5

Appendix C: Discharge Comparisons

Similar to the WSE comparison plots in Appendix B, the discharge comparison plots consist of year-long time series comparisons for 2004, zoomed comparisons for varying three-month periods (depending on data availability), and model-versus-field box plots. For the box plots, points lying on the 45 degree black line represent an exact replication of the field by the model. Points below the line represent calculated model results below the observed field values, and points above the line represent calculated model results above the observed field values. These comparison plots are included as Figure 92 – Figure 98.

Figure 92. Bayou Penchant discharge comparison plots.

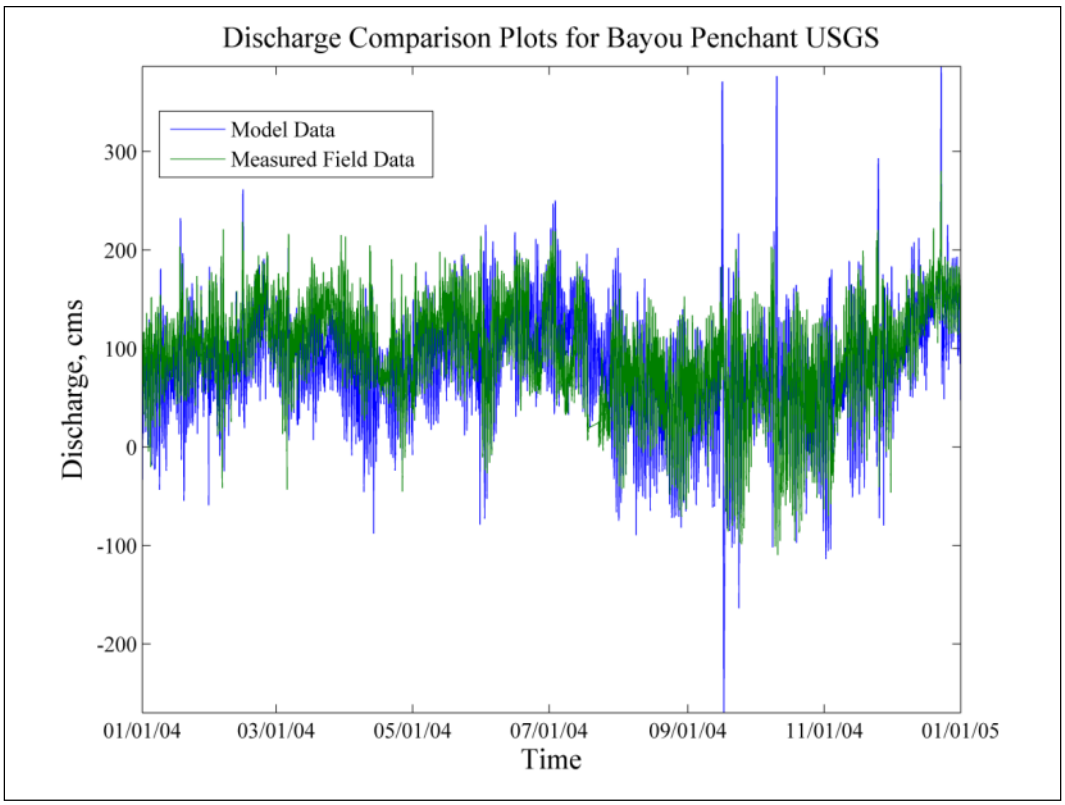

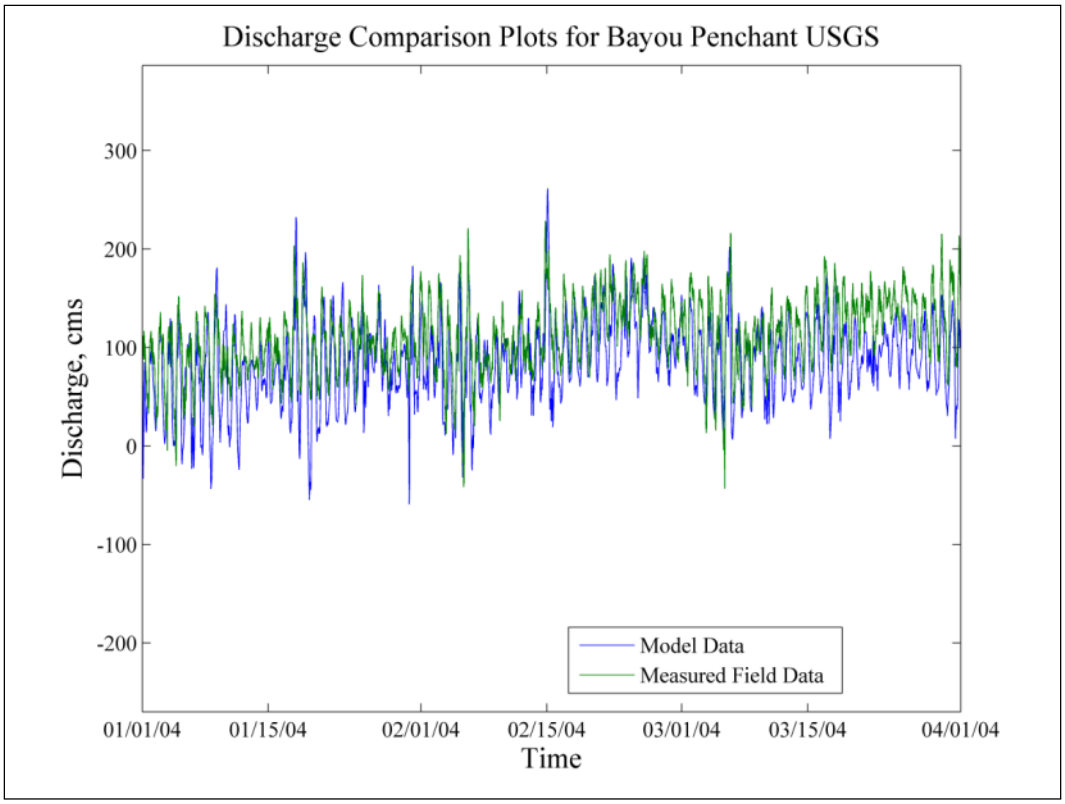

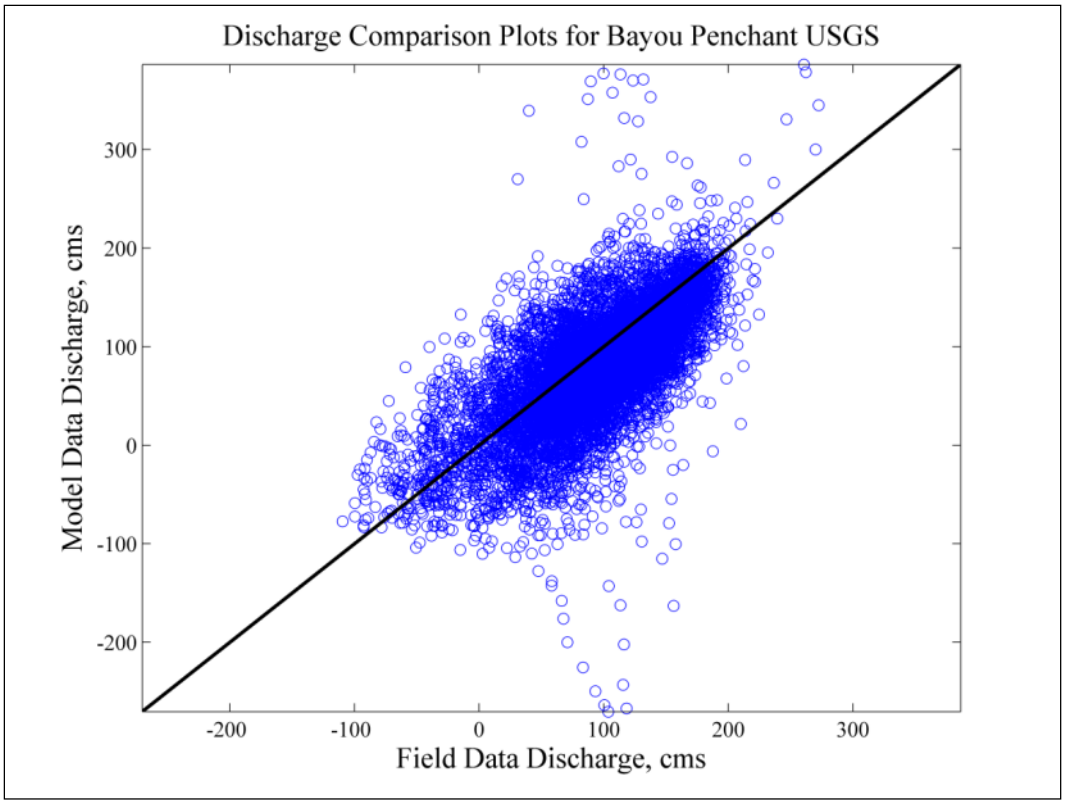
Discharge Comparison Plots for Bayou Penchant USGS
Model Data Discharge, cms
Field Data Discharge, cms
300
200
100
0
-100
-200
-200
-100
0
100
200
300

Figure 93. Houma Navigation Canal discharge comparison plots.

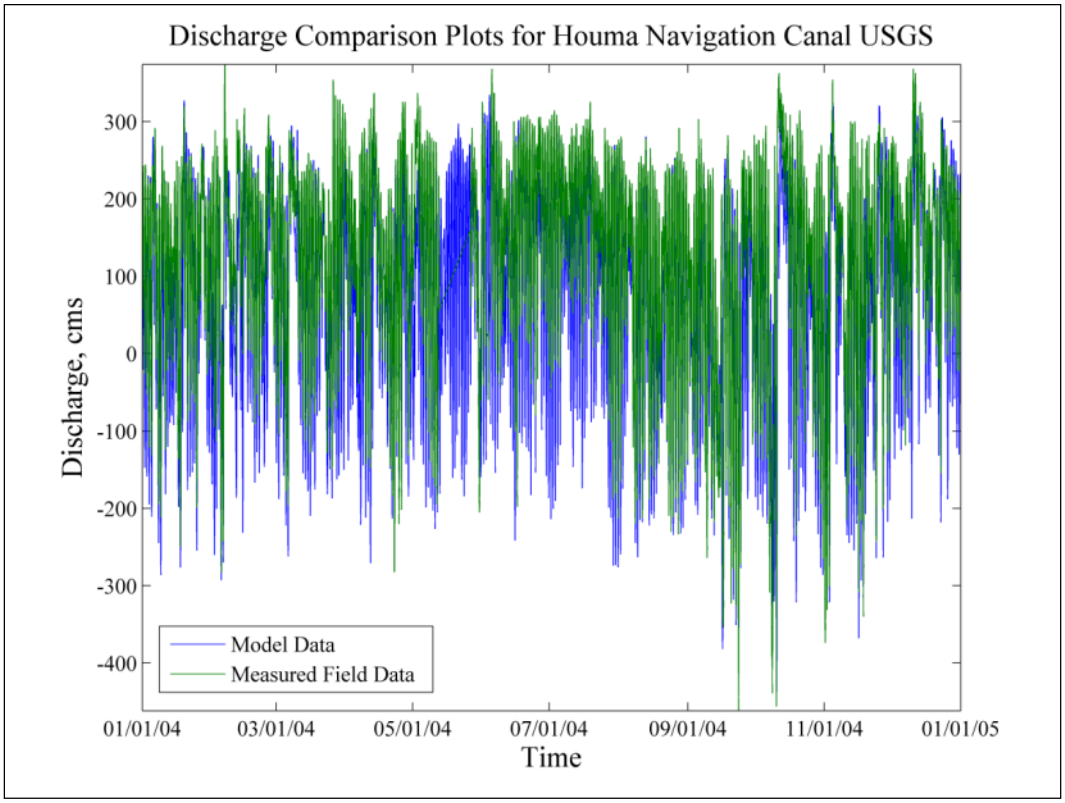

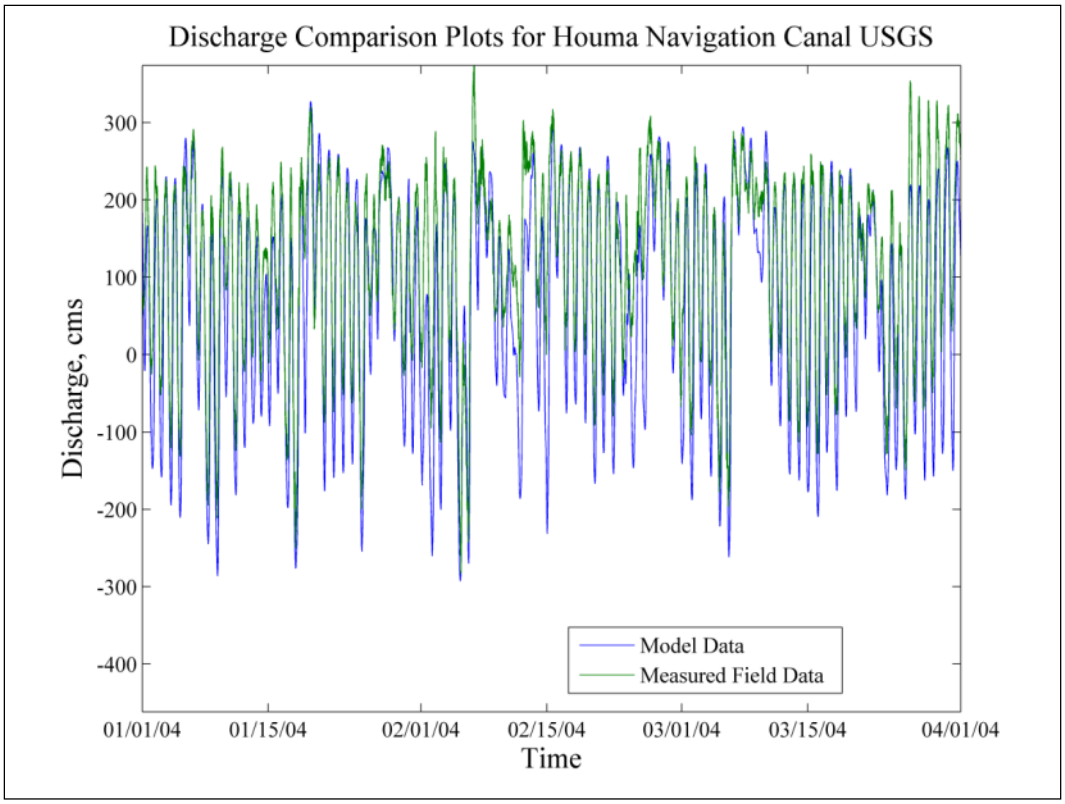

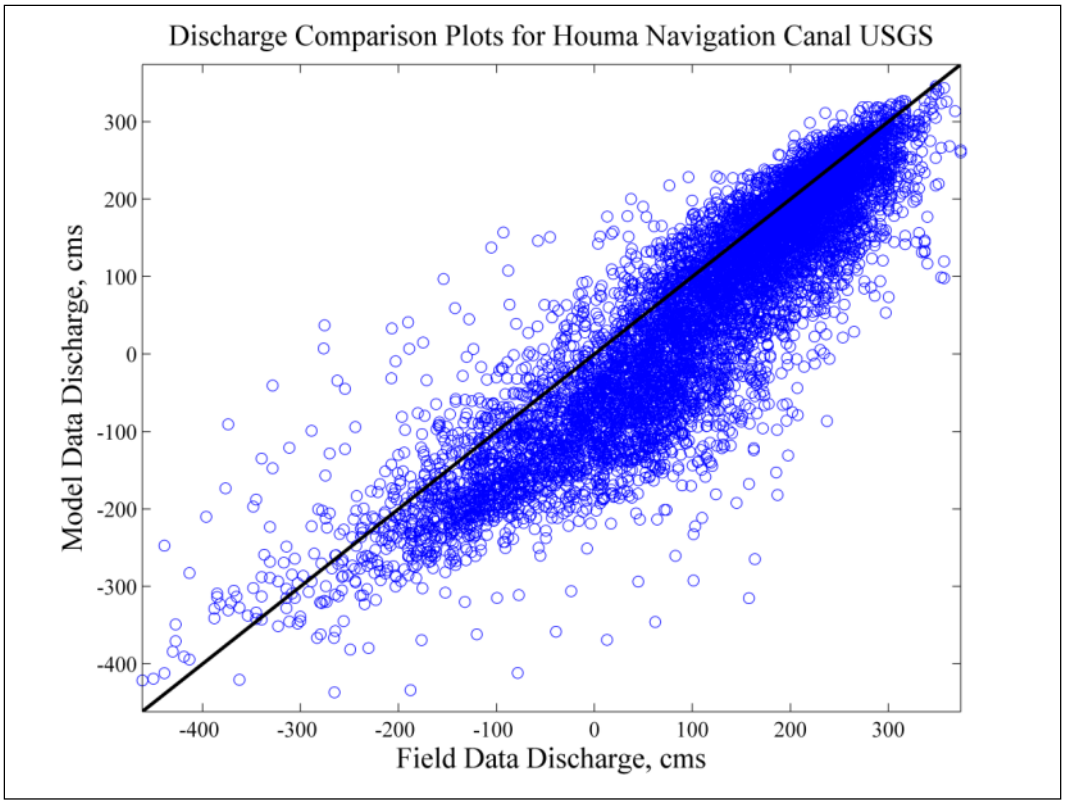
Discharge Comparison Plots for Houma Navigation Canal USGS
Model Data Discharge, cms
Field Data Discharge, cms
300
200
100
0
-100
-200
-300
-400
-400
-300
-200
-100
0
100
200
300

Figure 94. Bayou Grand Caillou discharge comparison plots.

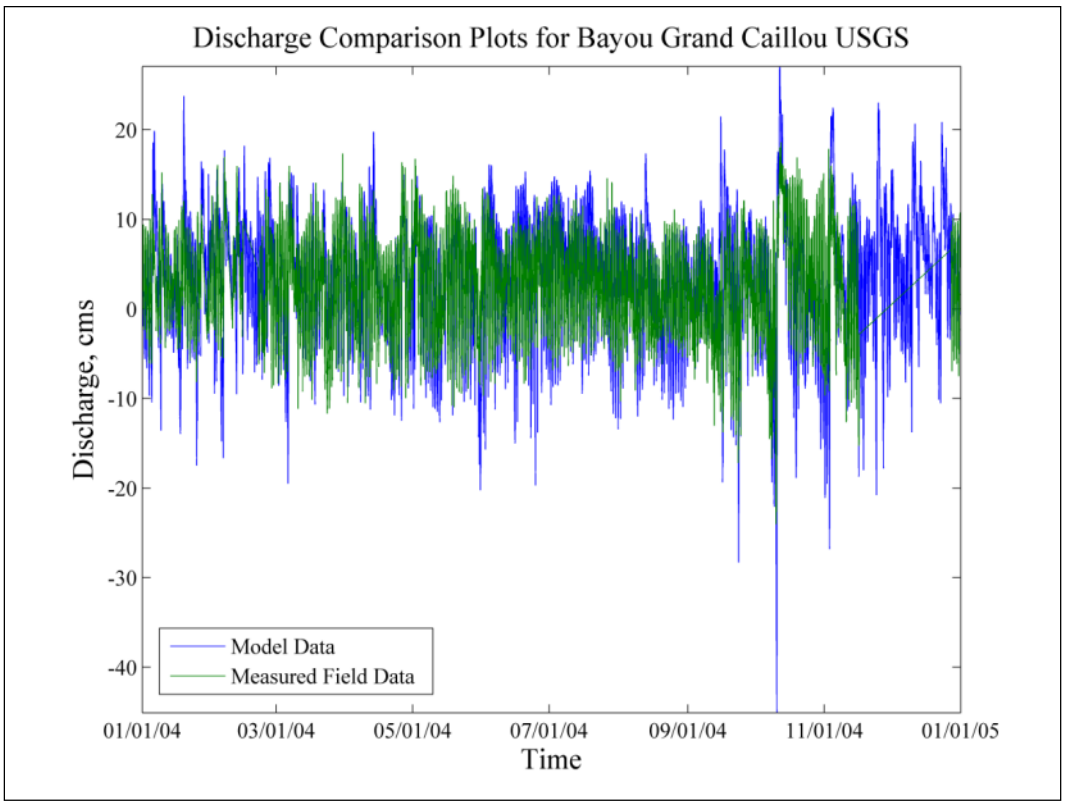

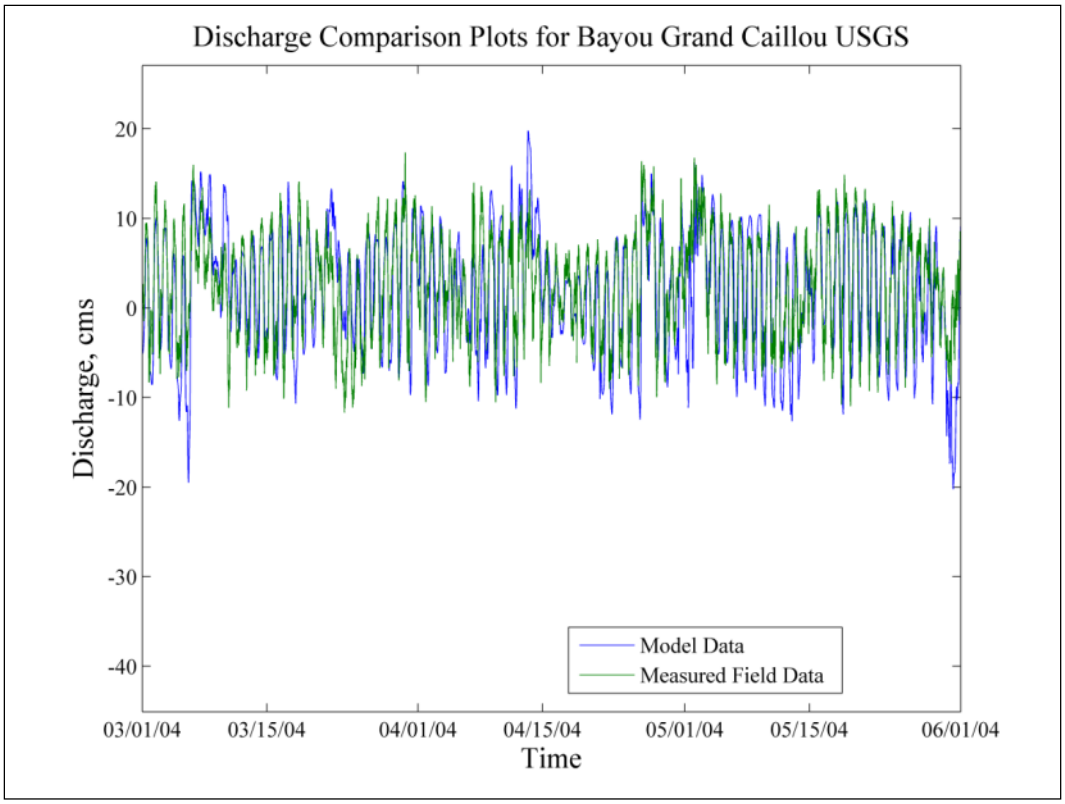

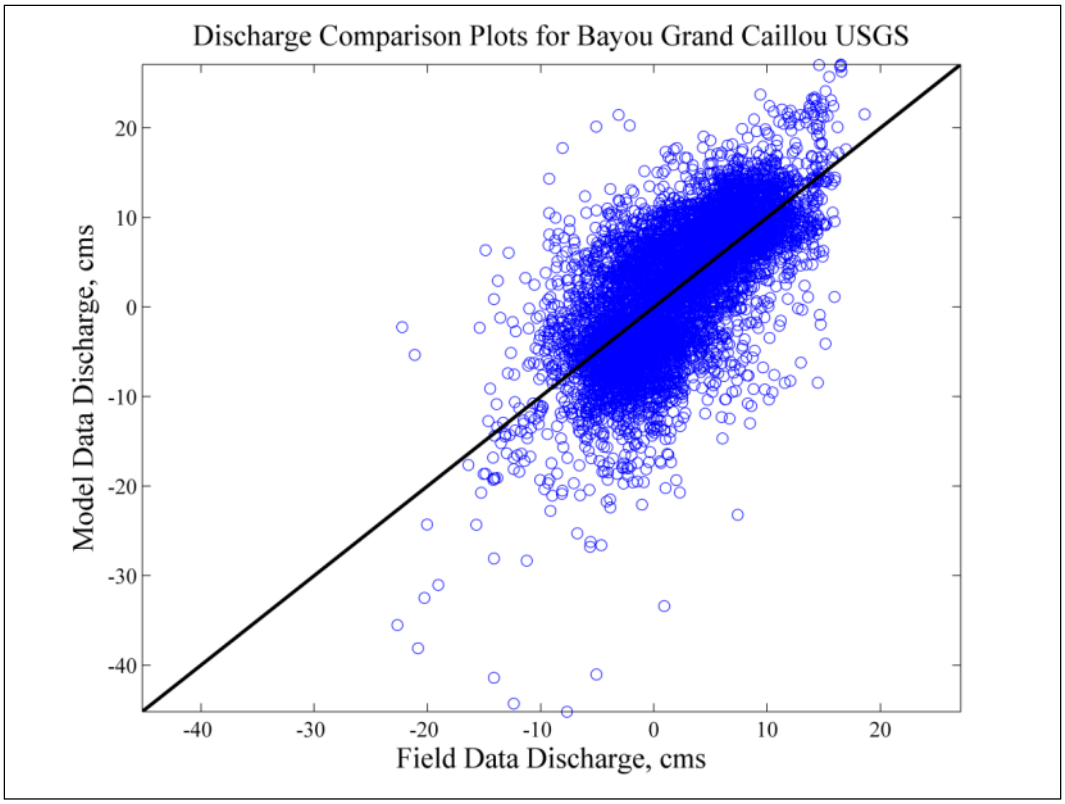
Discharge Comparison Plots for Bayou Grand Caillou USGS
Model Data Discharge, cms
Field Data Discharge, cms
20
10
0
-10
-20
-30
-40
-40
-30
-20
-10
0
10
20

Figure 95. GIWW at Houma discharge comparison plots.

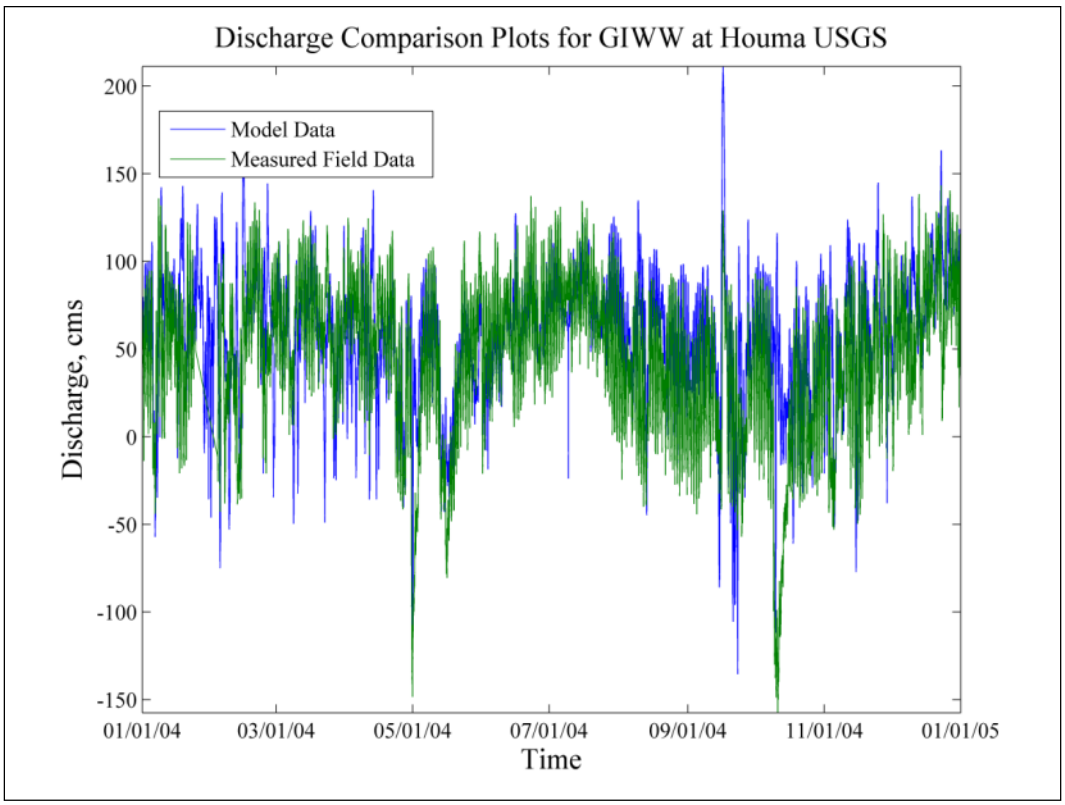

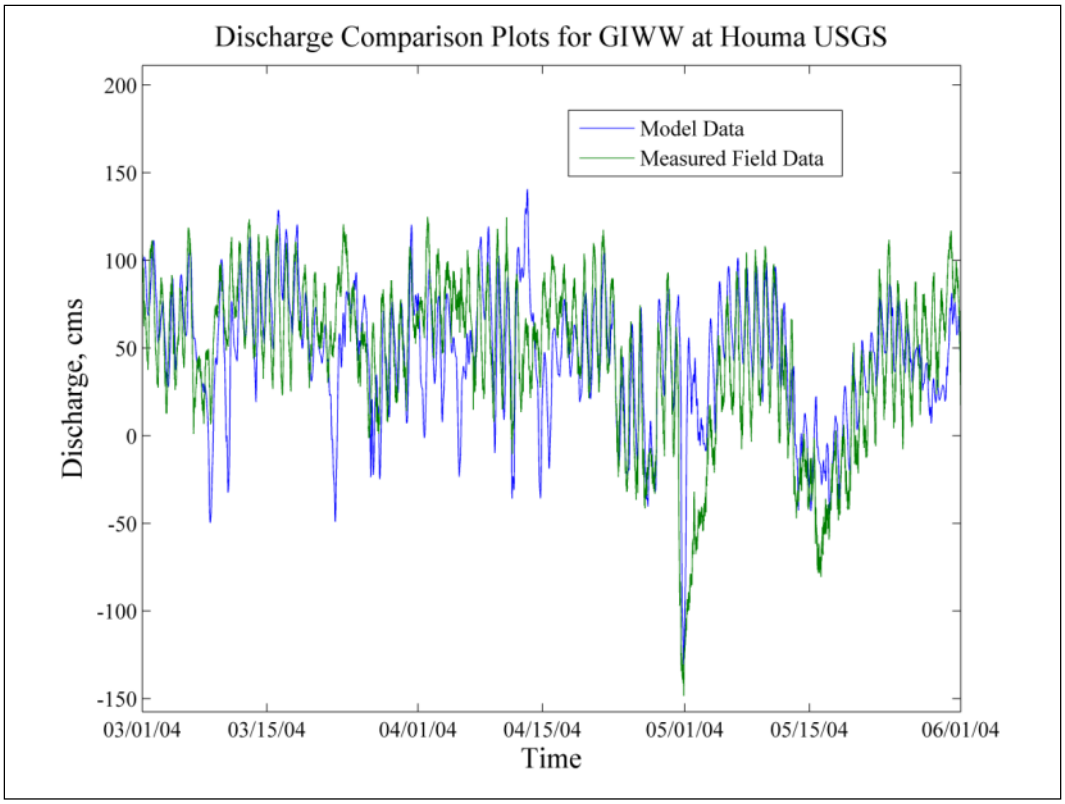

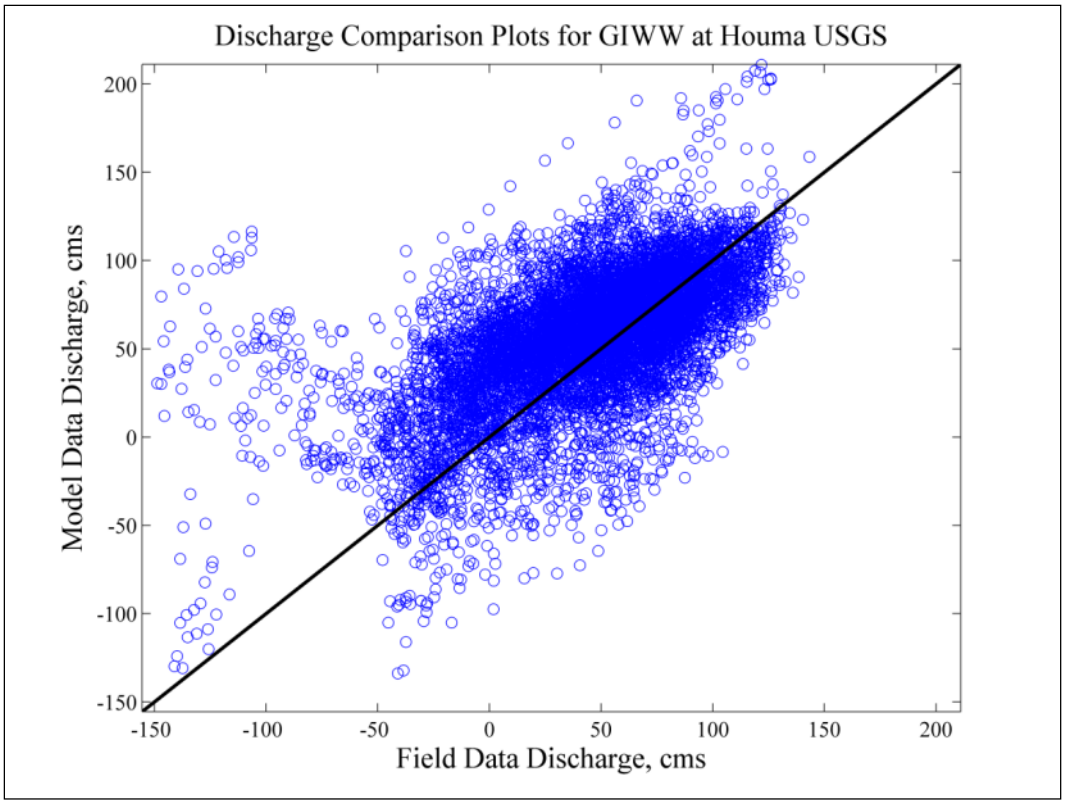
Discharge Comparison Plots for GIWW at Houma USGS
Model Data Discharge, cms
Field Data Discharge, cms
200
150
100
50
0
-50
-100
-150
-150
-100
-50
0
50
100
150
200

Figure 96. GIWW West of Bayou Lafourche discharge comparison plots.

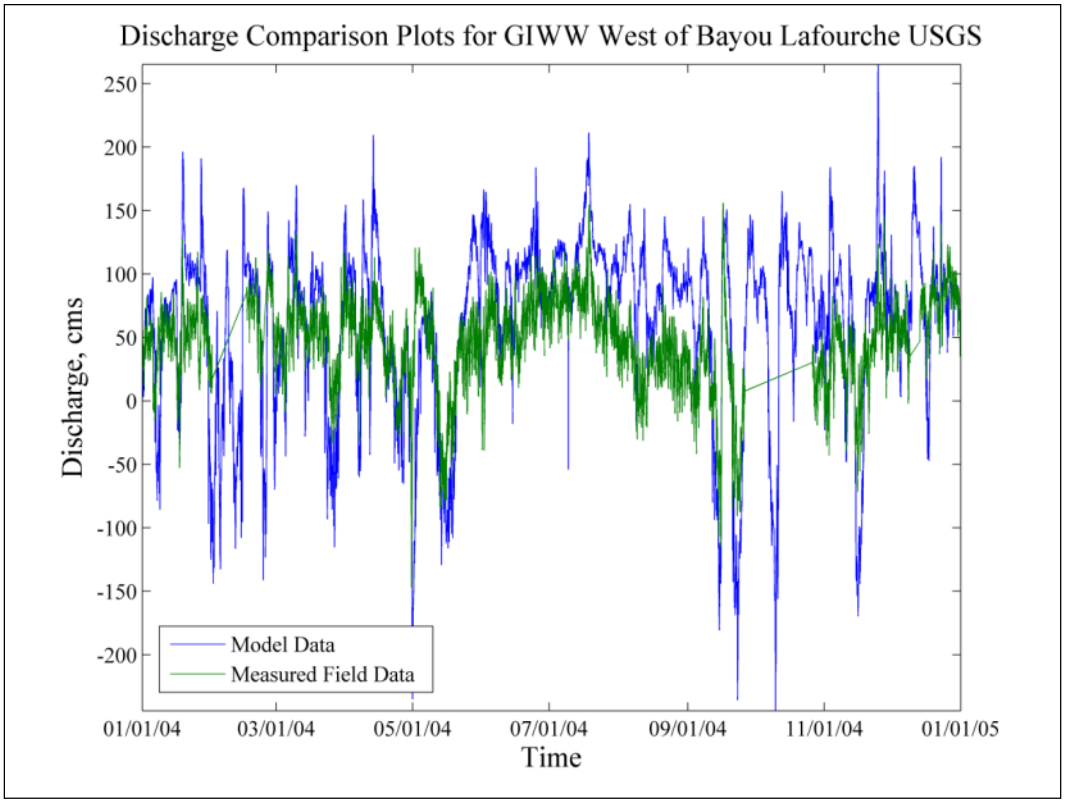

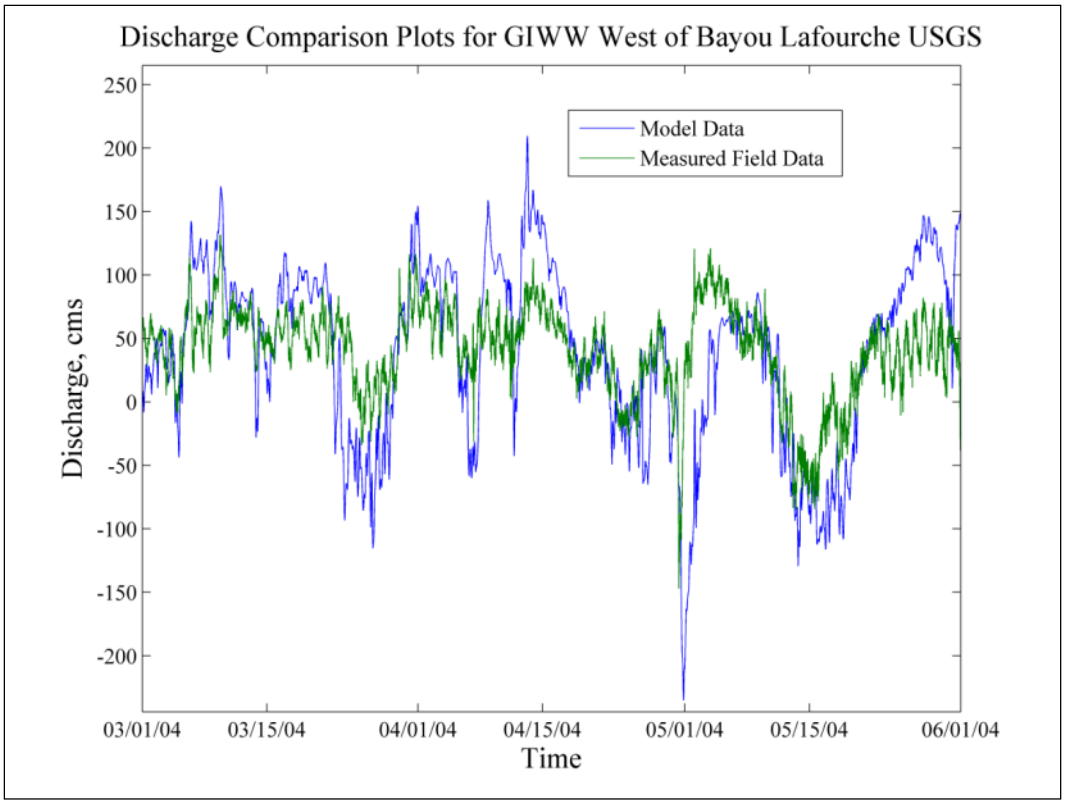

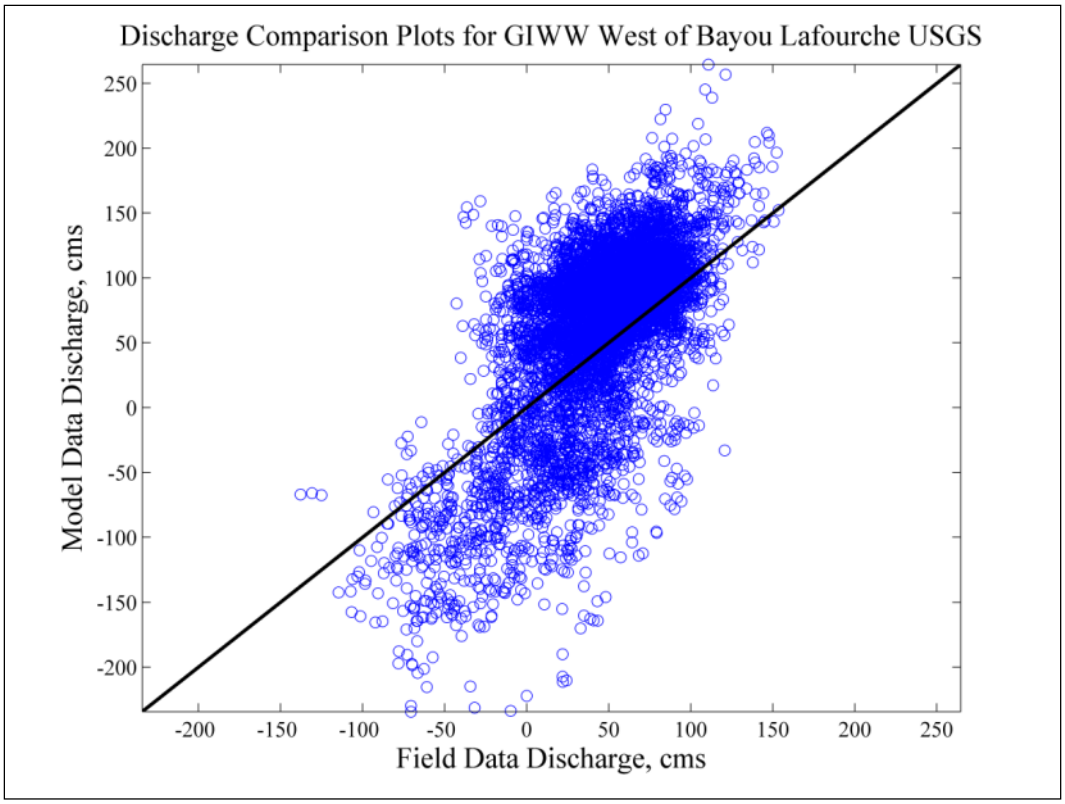
Discharge Comparison Plots for GIWW West of Bayou Lafourche USGS
Model Data Discharge, cms
Field Data Discharge, cms
250
200
150
100
50
0
-50
-100
-150
-200
-200
-150
-100
-50
0
50
100
150
200
250

Figure 97. GIWW West of Minors Canal discharge comparison plots.

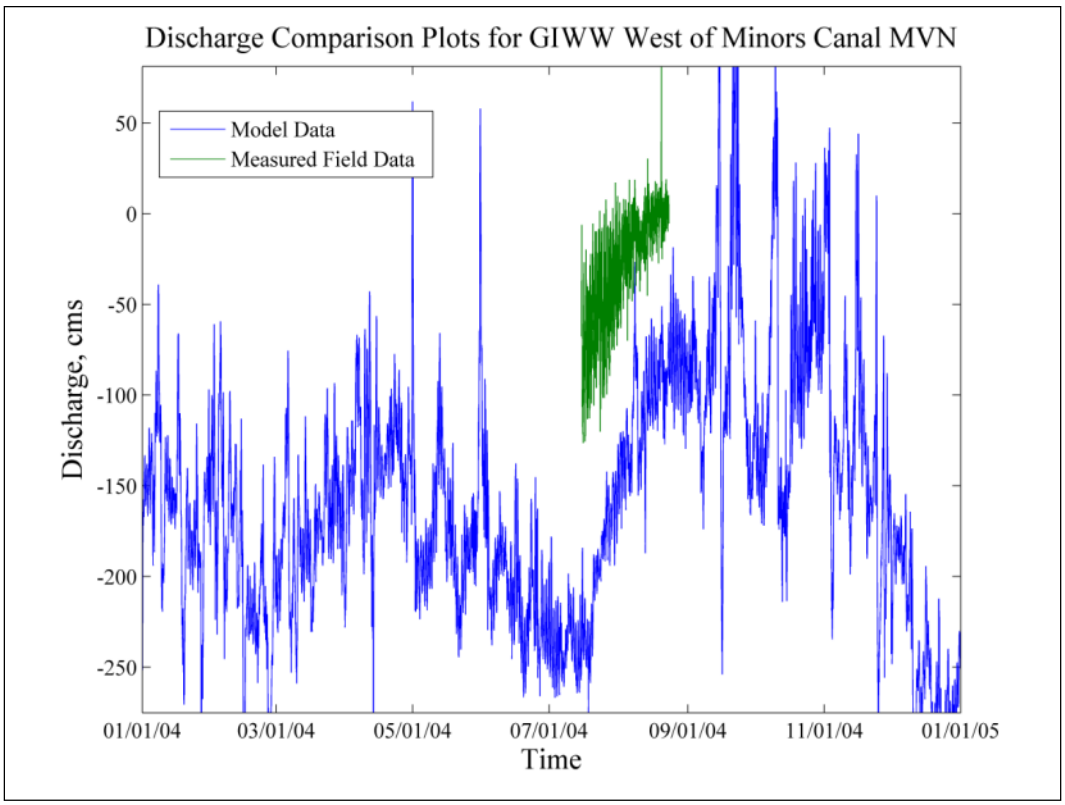

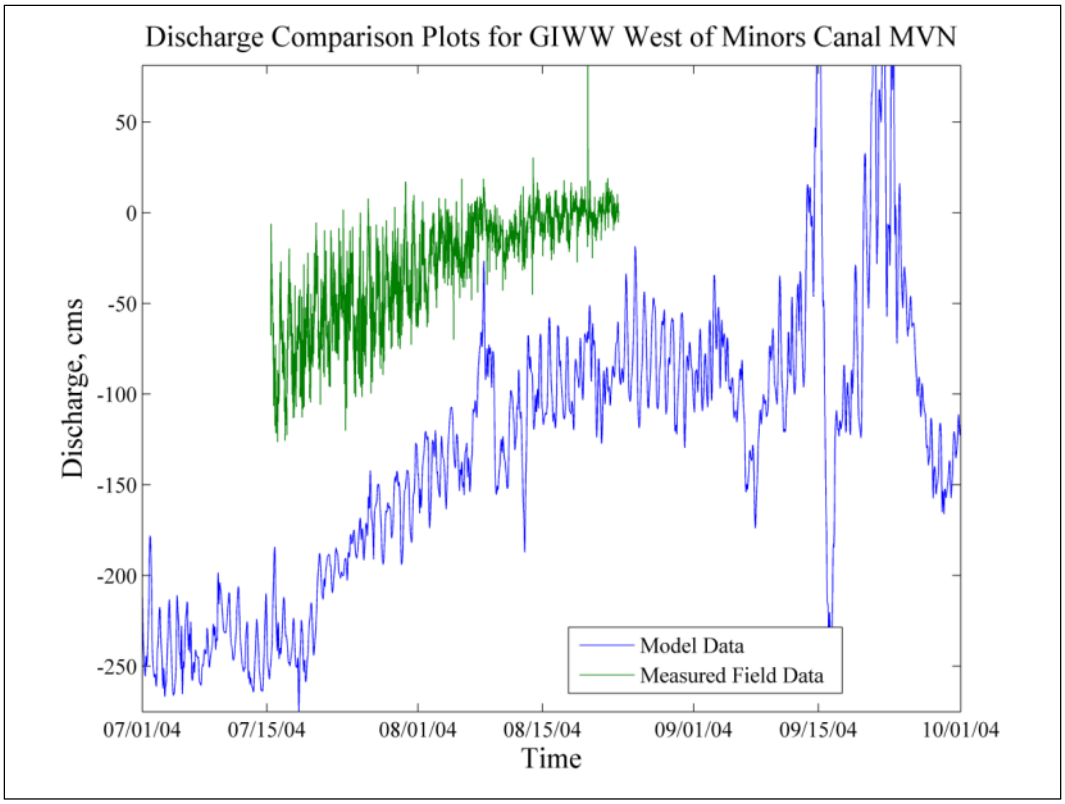

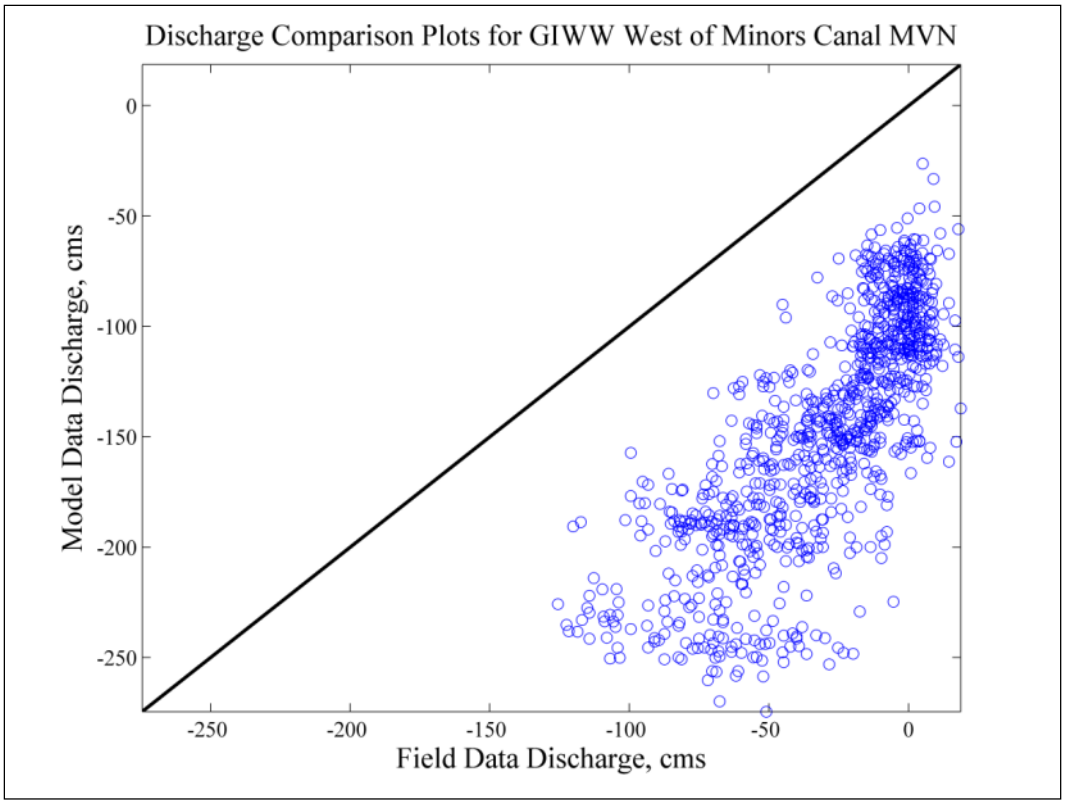
Discharge Comparison Plots for GIWW West of Minors Canal MVN
Model Data Discharge, cms
Field Data Discharge, cms
0
-50
-100
-150
-200
-250
-250
-200
-150
-100
-50
0

Figure 98. GIWW near Bay Wallace discharge comparison plots. (Field data represent averaged daily values, providing insufficient data to generate a useful box plot.)

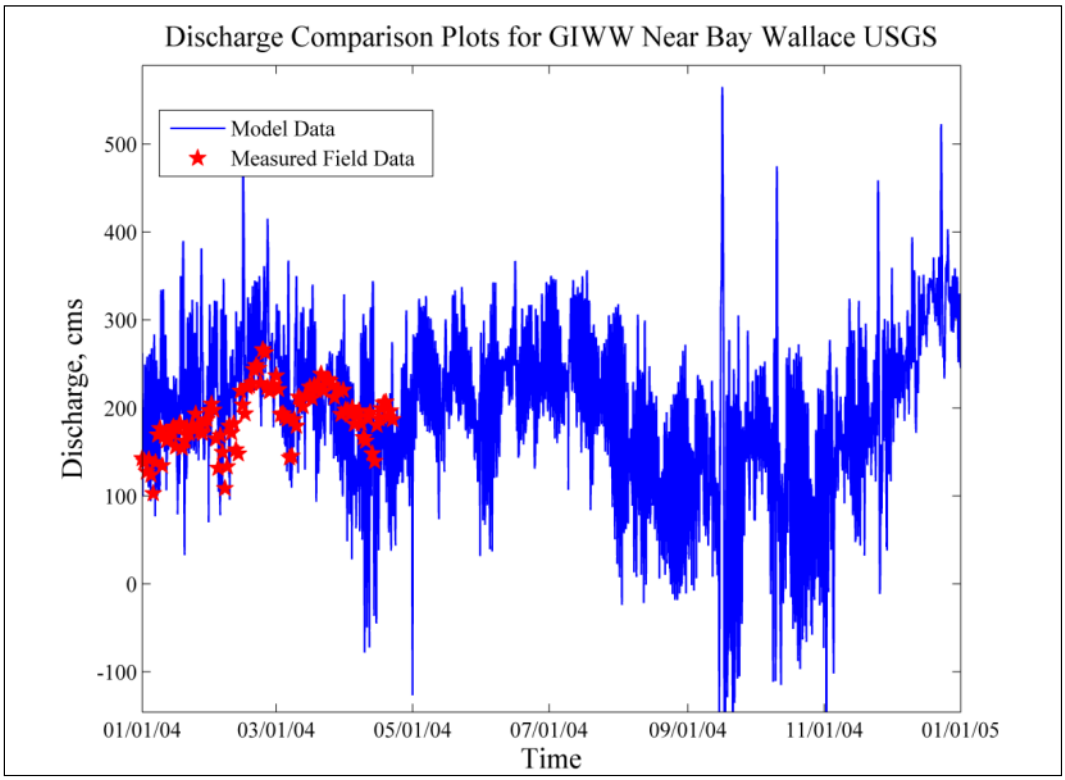

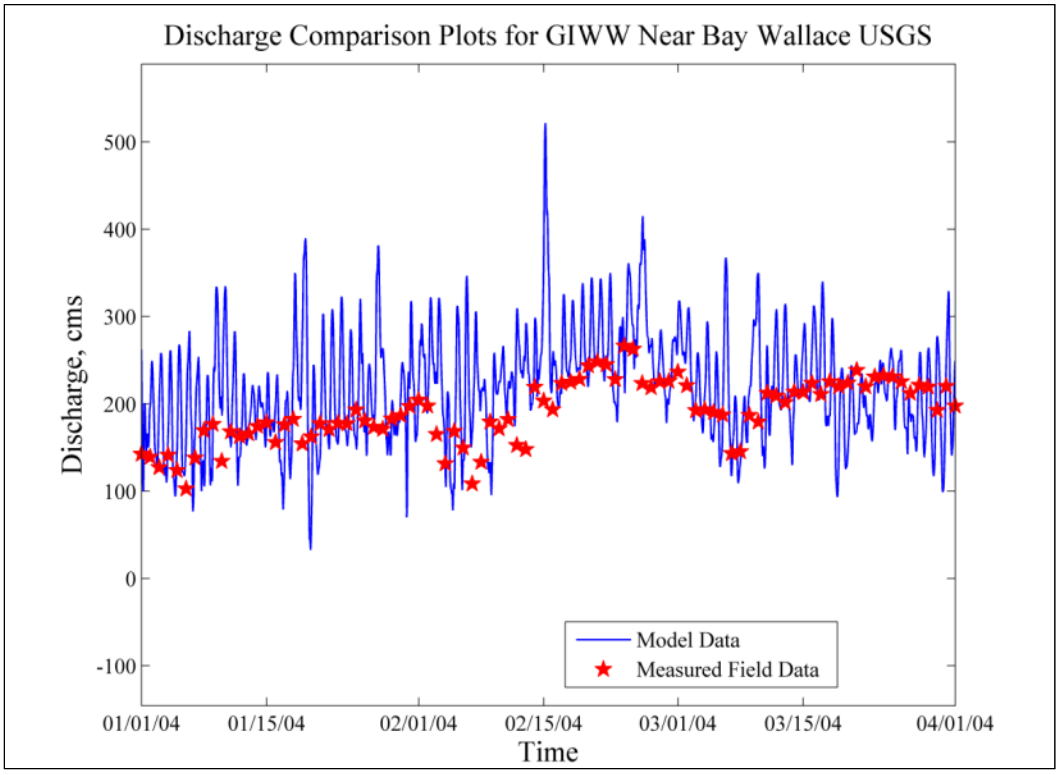

Appendix D: Salinity Comparisons

The salinity comparisons plots consist of year-long time series comparisons for the 2004 calendar year. These comparison plots are included as Figure 99 – Figure 114.

Figure 99. Caillou Lake salinity comparisons.

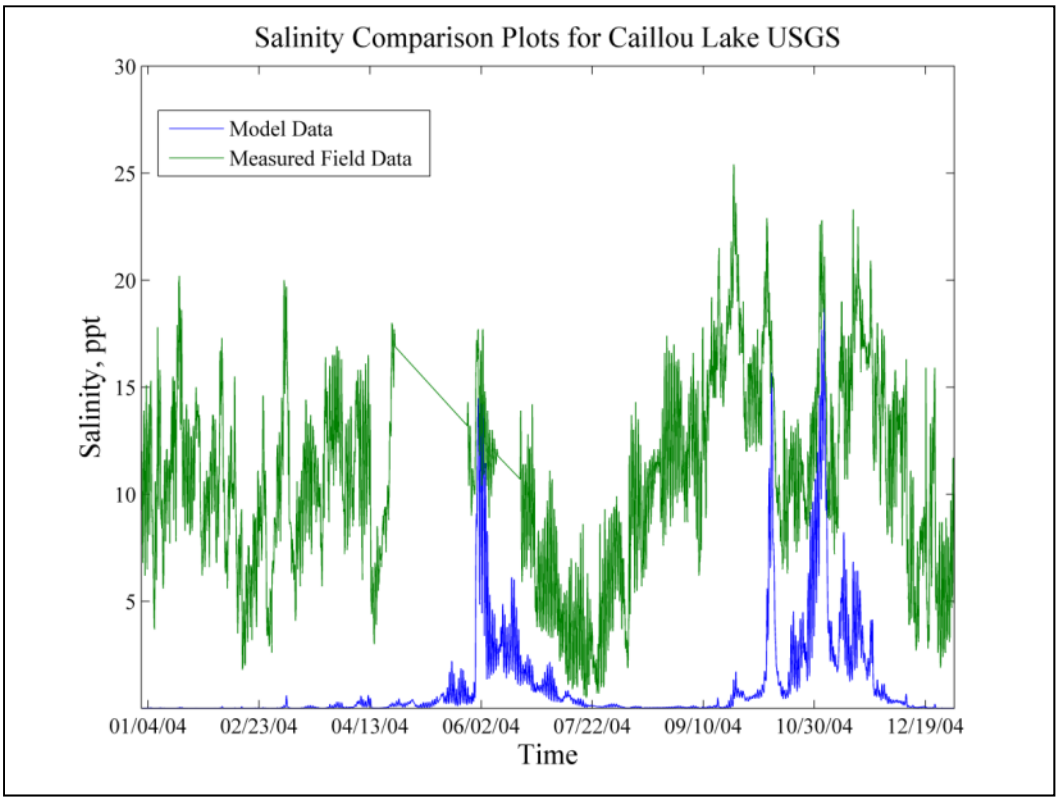

Figure 100. Caillou Bay salinity comparisons.

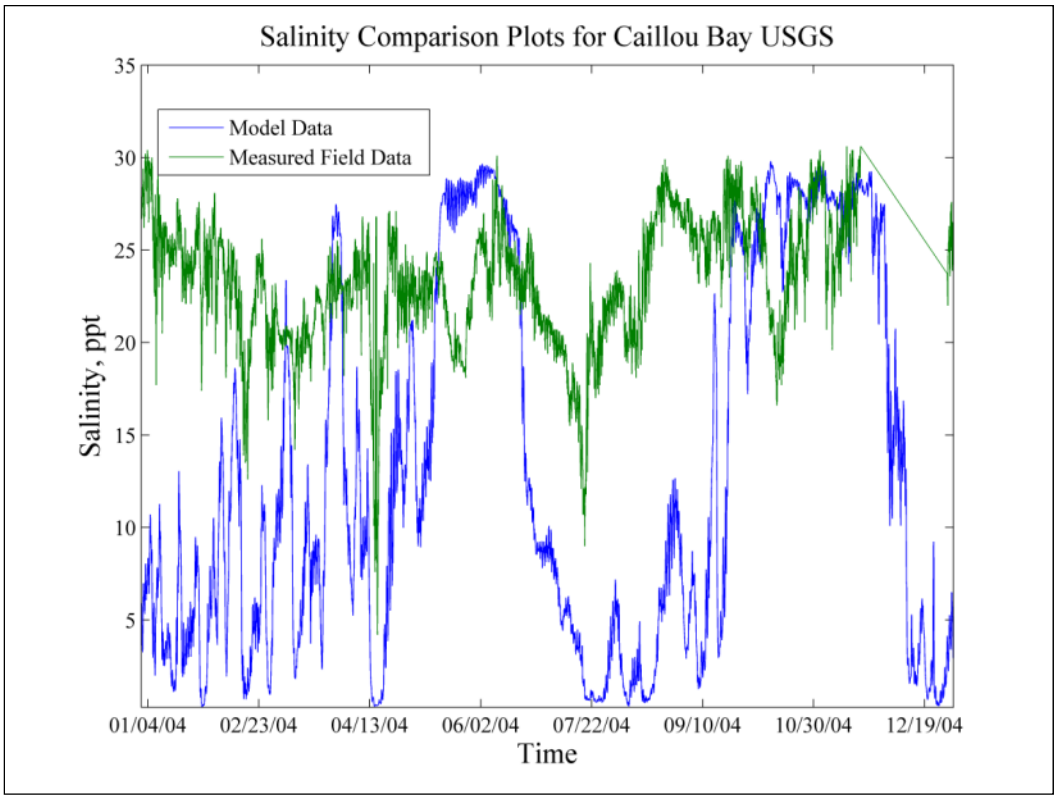

Figure 101. Houma Navigation Canal salinity comparisons.

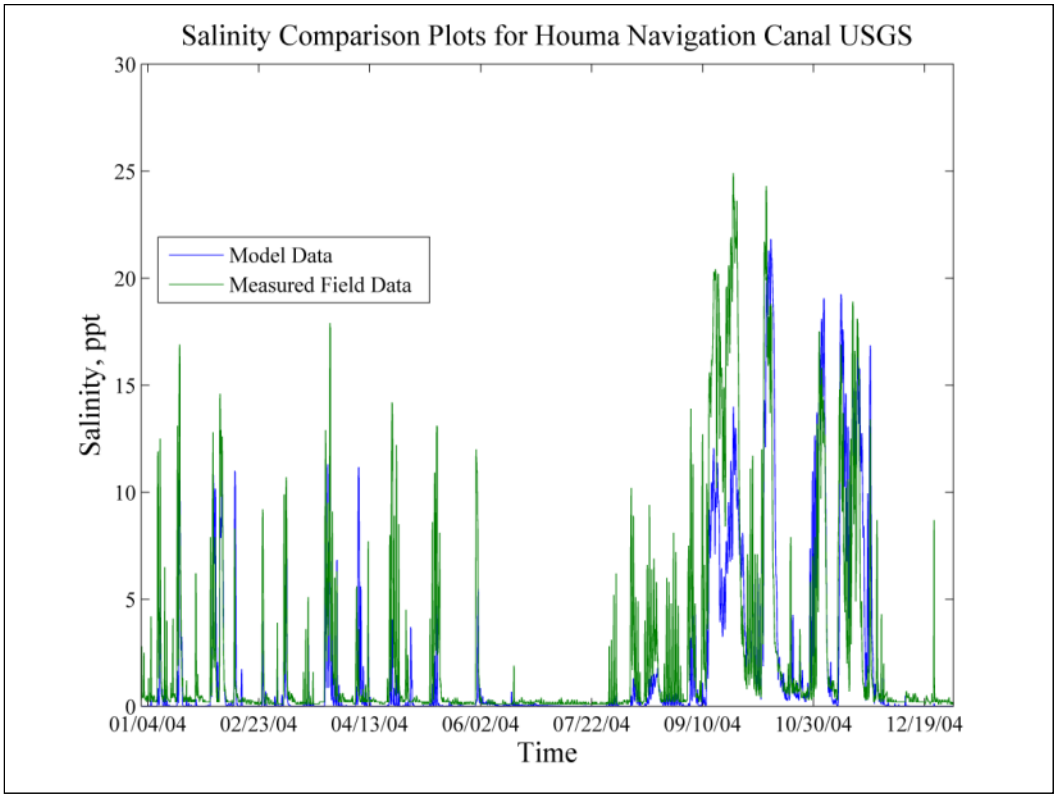

Figure 102. Bayou Grand Caillou salinity comparisons.

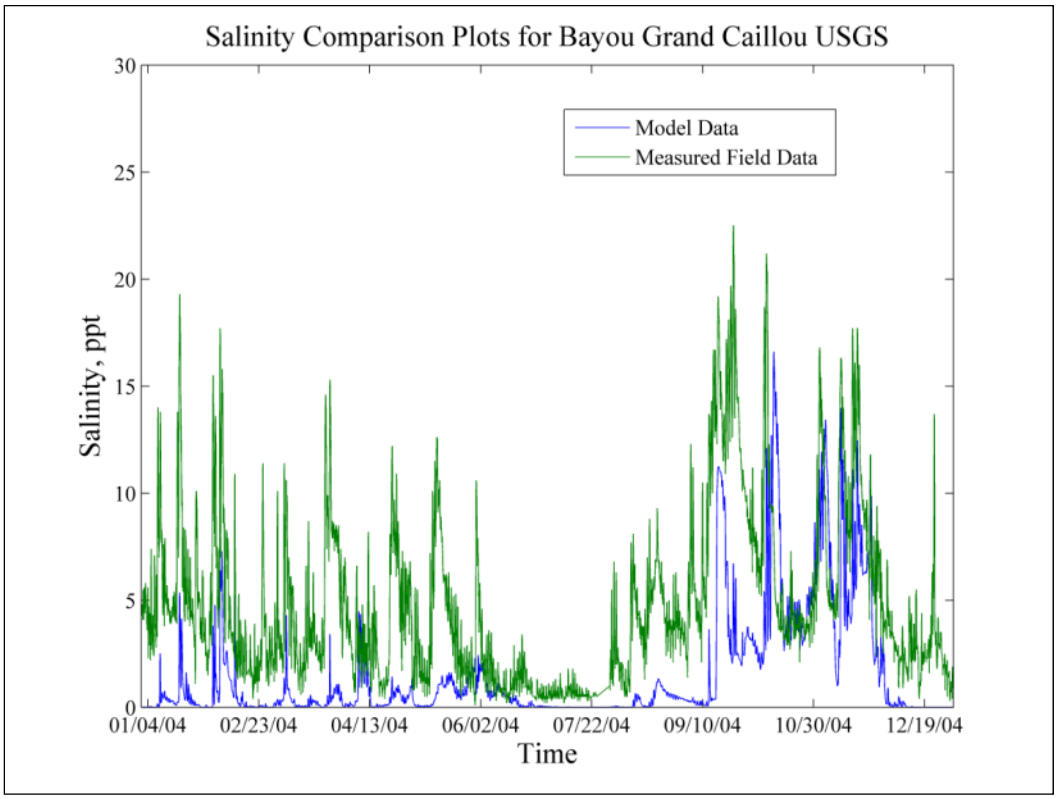

Figure 103. GIWW at Houma salinity comparisons.

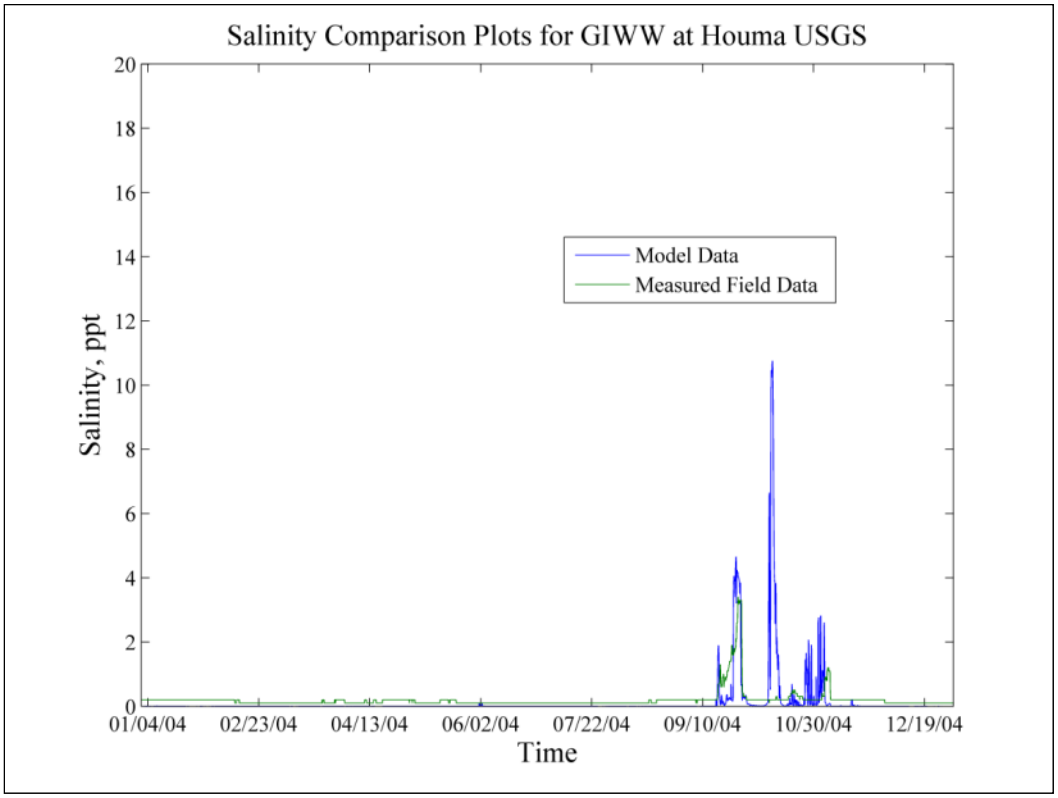

Figure 104. Company Canal, Lockport salinity comparisons.

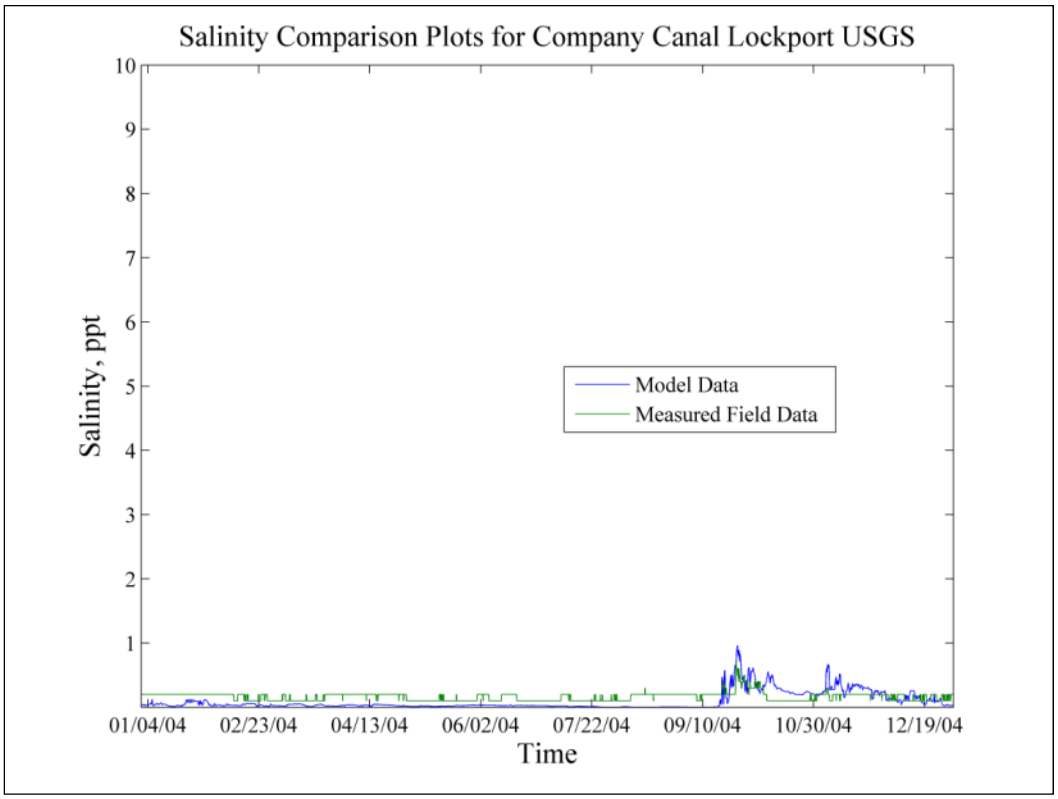

Figure 105. Company Canal, Salt Barrier salinity comparisons.

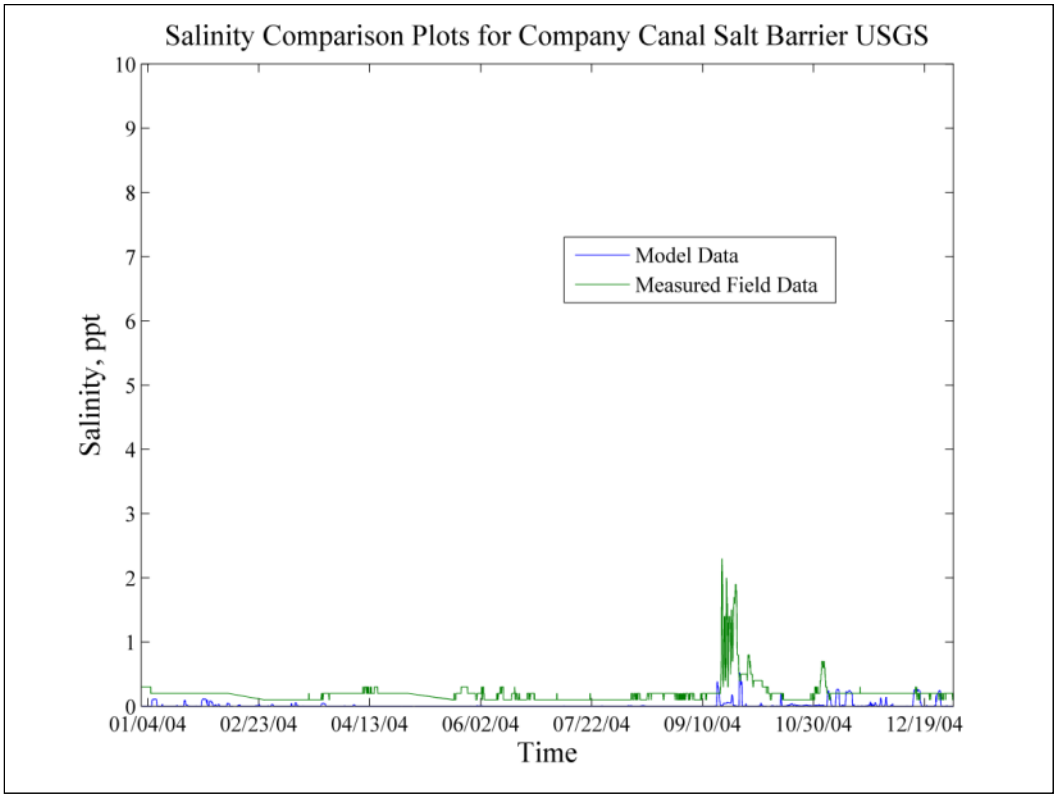

Figure 106. GIWW West of Minors Canal salinity comparisons.

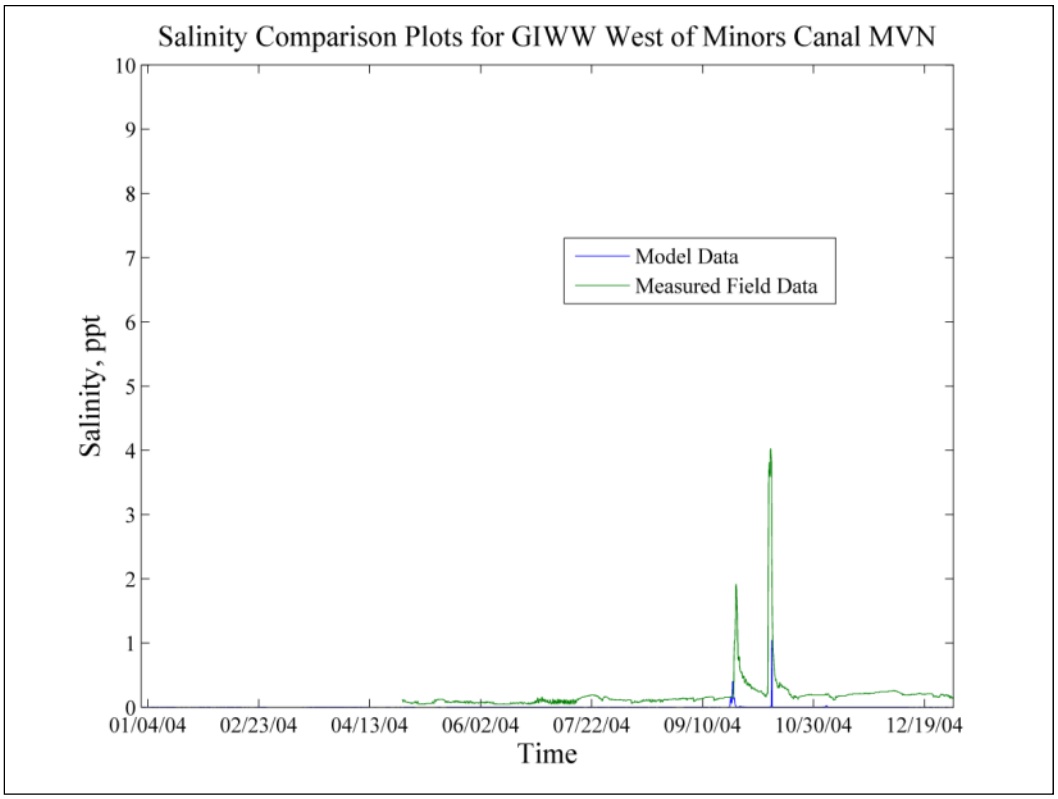

Figure 107. Falgout Canal salinity comparisons.

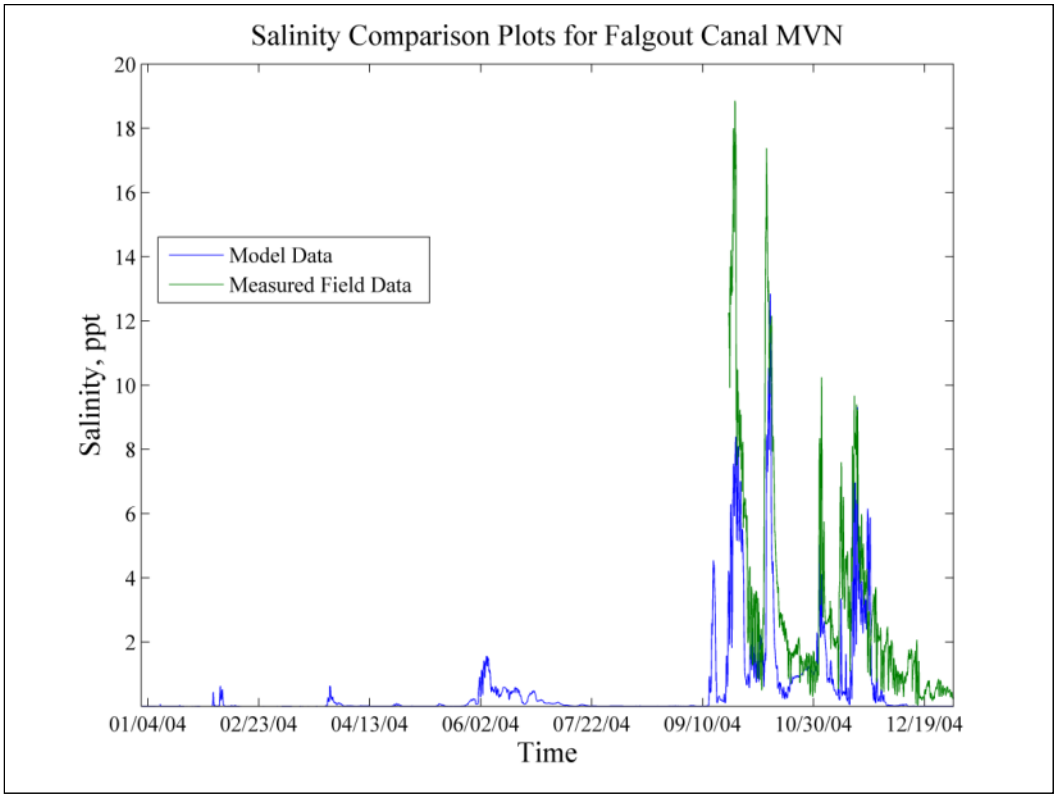

Figure 108. Bayou Dularge salinity comparisons.

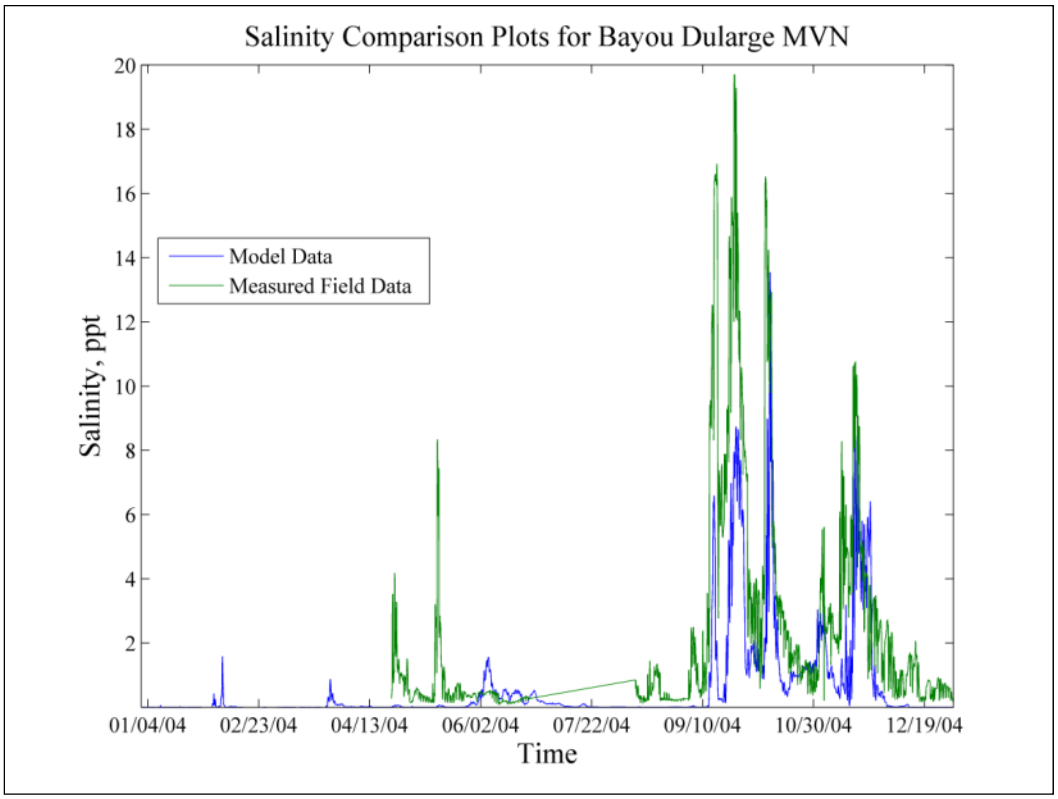

Figure 109. Bayou Grand Caillou salinity comparisons.

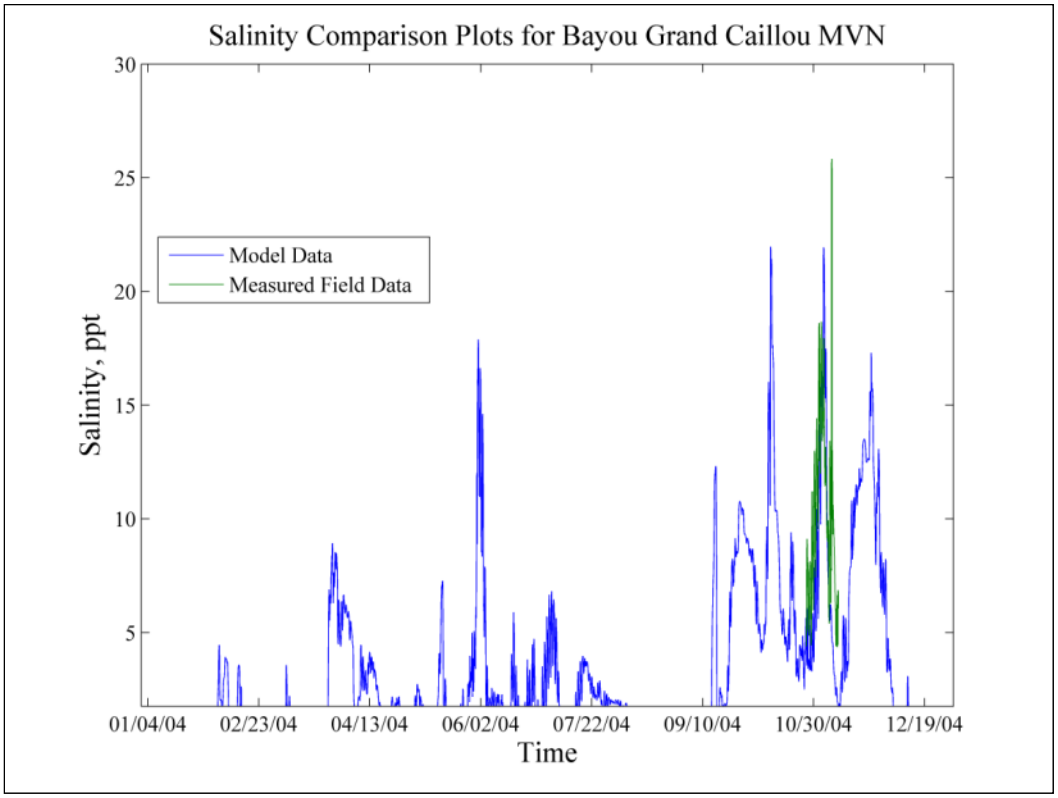

Figure 110. Bayou Petit Caillou salinity comparisons.

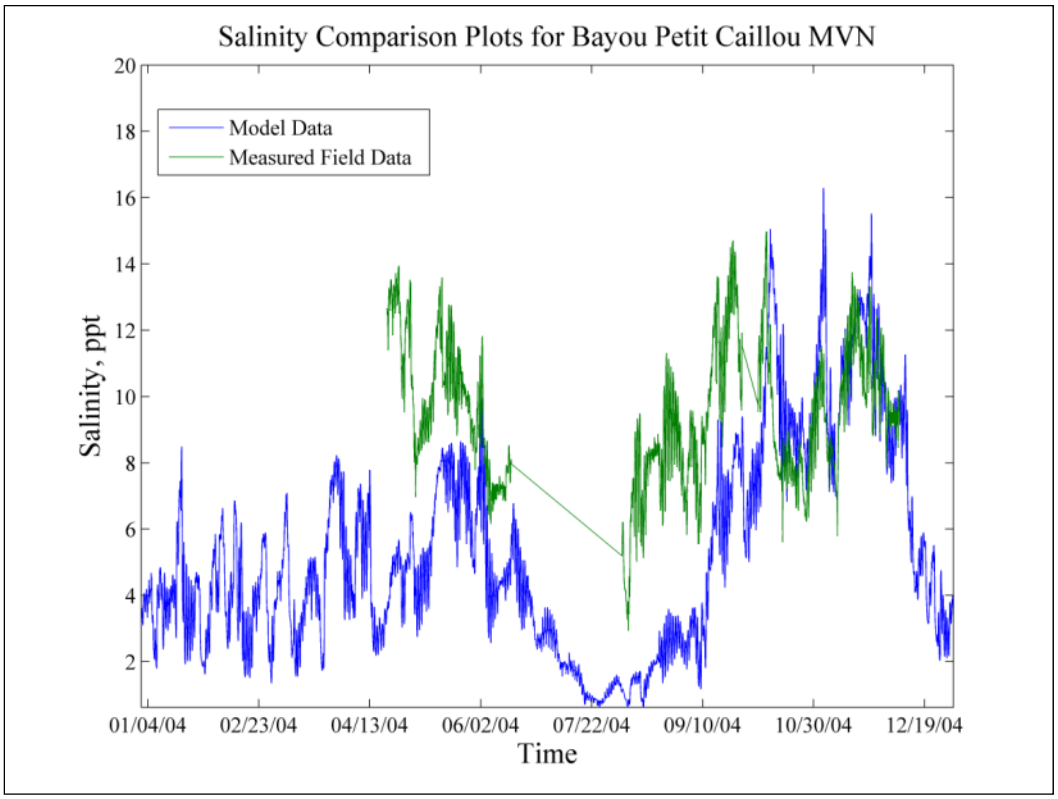

Figure 111. Bayou Terrebonne salinity comparisons.

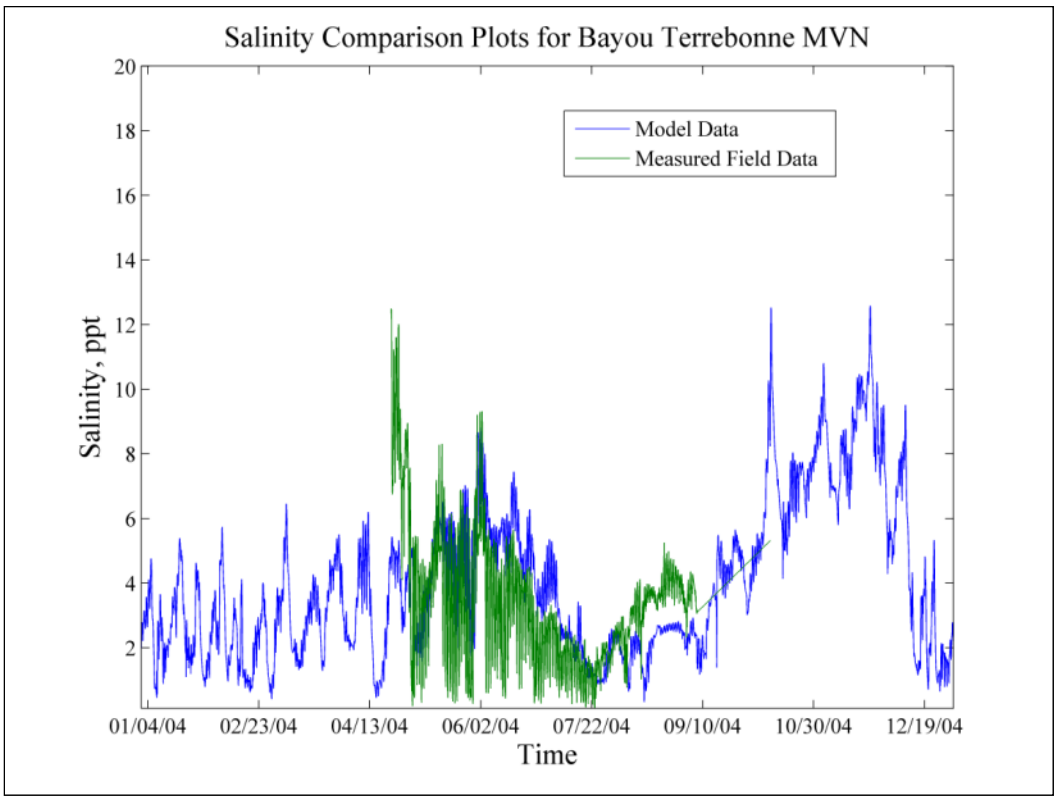

Figure 112. Humble Canal salinity comparisons.

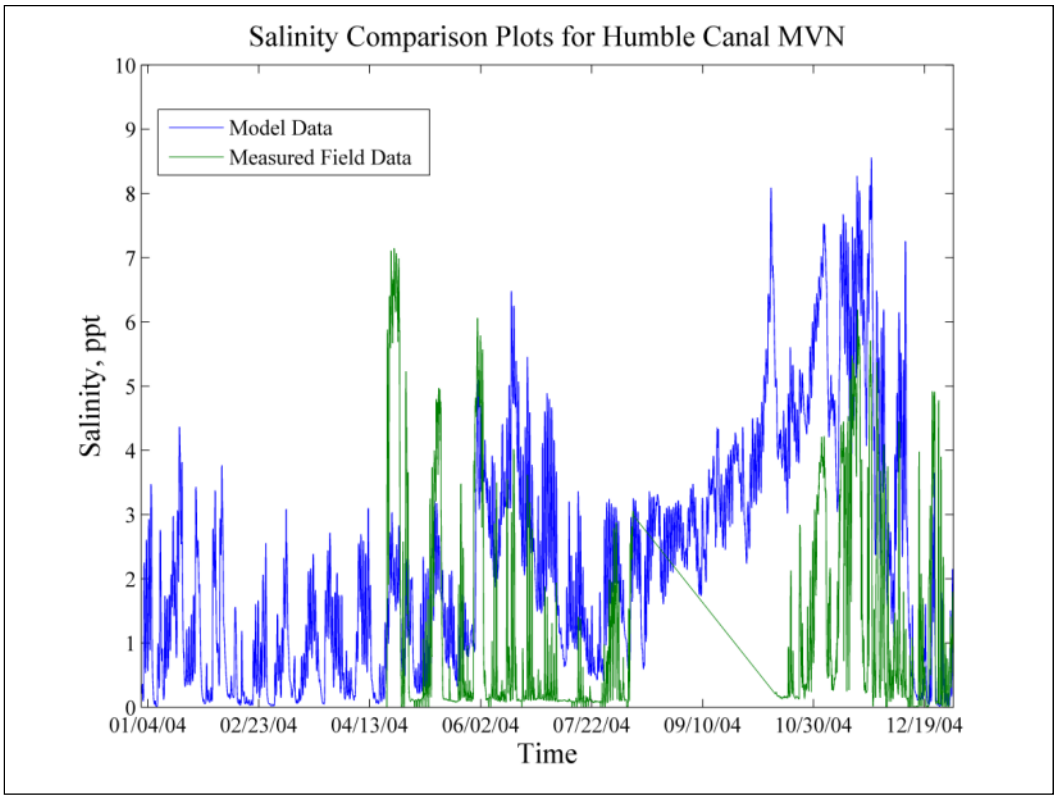

Figure 113. Pointe Aux Chenes salinity comparisons.

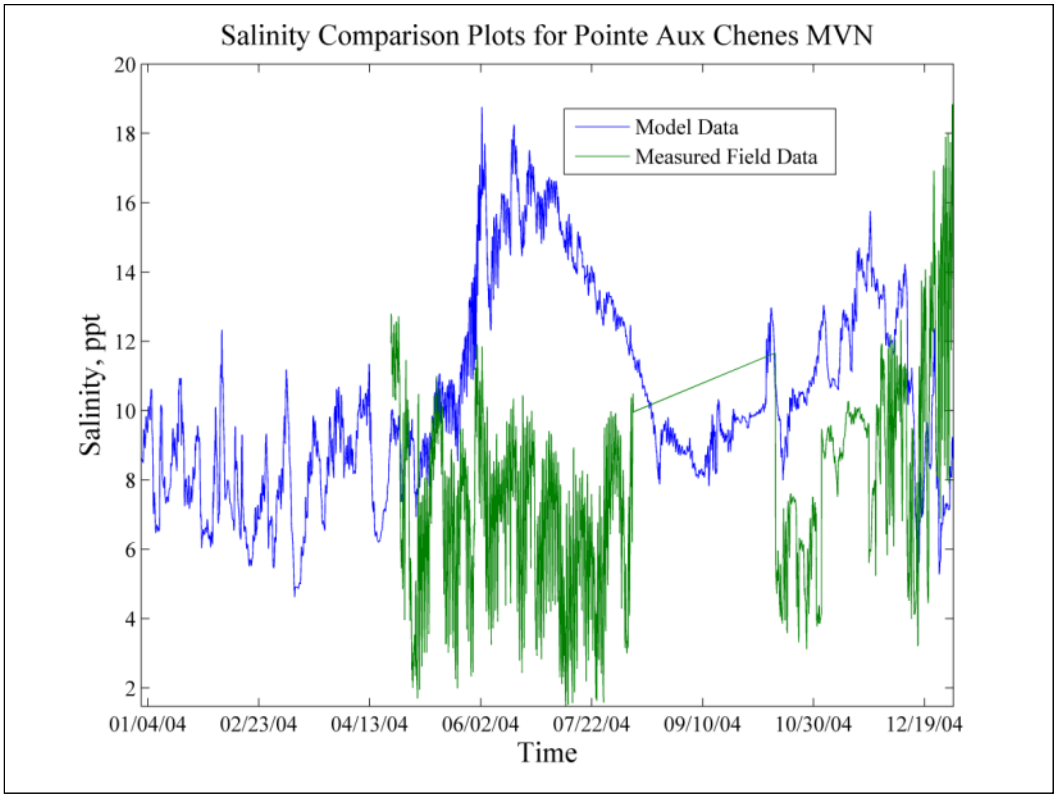

Figure 114. Grand Bayou Canal salinity comparisons.

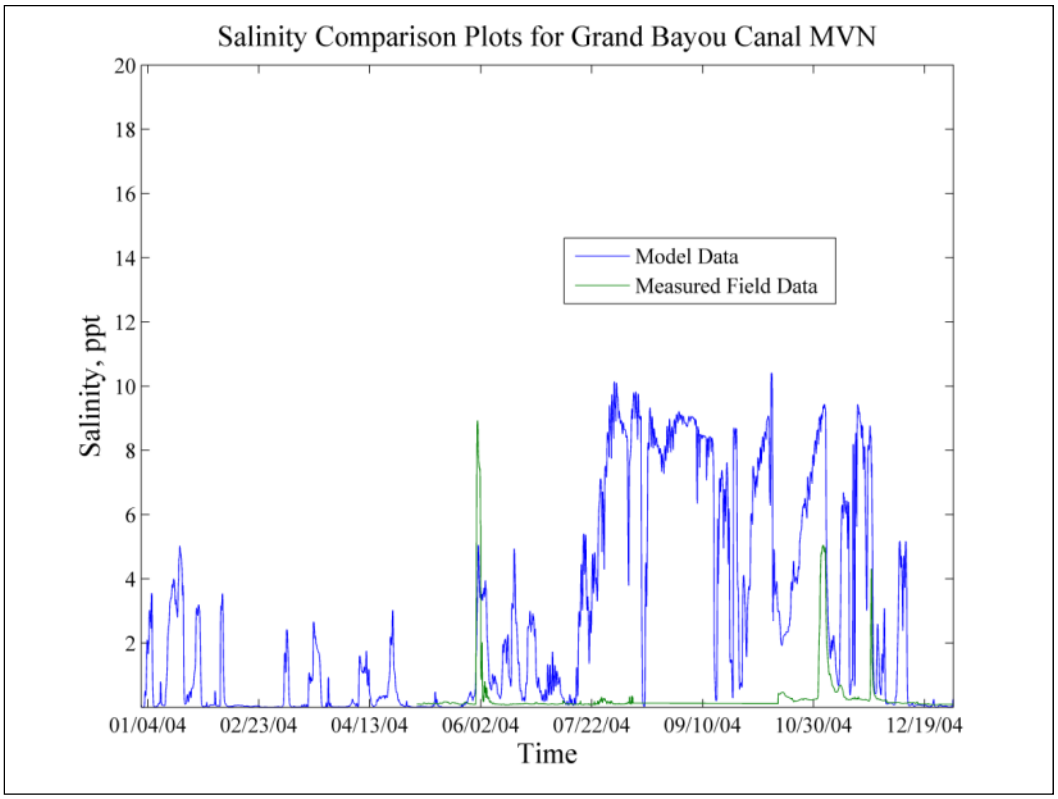

Appendix E: Alternative Configurations

The numerical model representation of each navigation and environmental structure is included in Figure 115 – Figure 137. The environmental structures consist of collections of culverts with the navigation structures consisting of different configurations of sluice and sector gates. Plan 1 has all structures in the open flow position. Plan 2 has all the navigation structures in the open position with all the environmental structures in the closed (no flow) position. Plan 3 has all structures in the open position with the exception of the Houma Navigational Canal structure and lock (both closed).

The Black Bayou Structure (S – 1) is a 17.07 m (56 ft) wide sector gate with a bottom elevation of -3.66 m (-12 ft), NAVD88(2004.65). The structure is shown in Figure 115.

Figure 115. Black Bayou Structure.

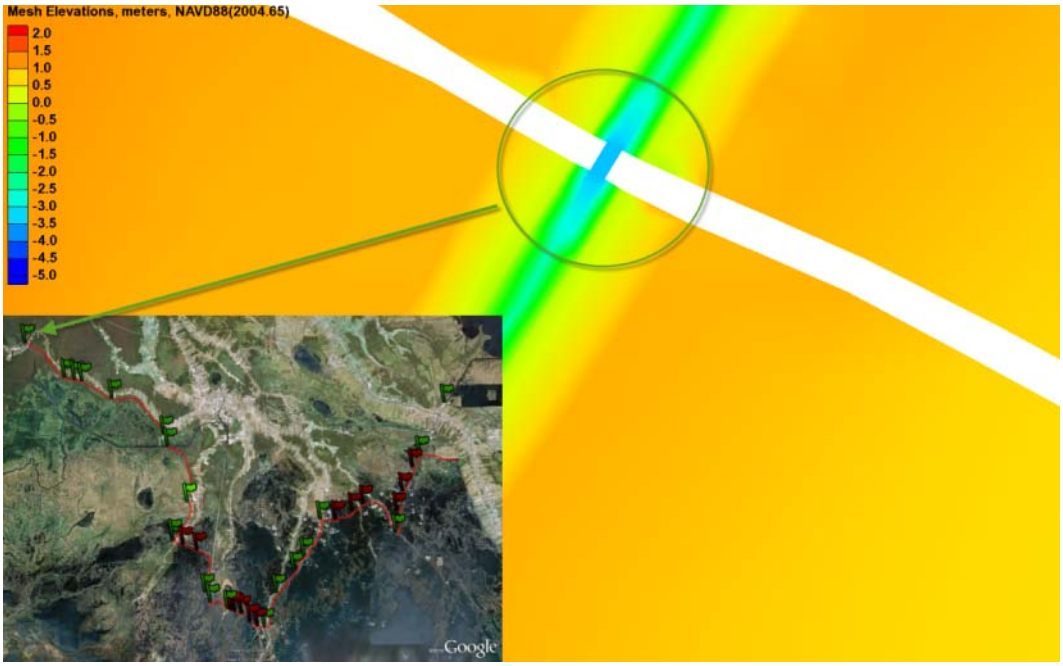

The West Shell Canal (S – 2) is a 10.67 m (35 ft) wide opening with a bottom elevation of -3.05 m (-10 ft), NAVD88(2004.65) and is shown as the left circle in Figure 116. The East Shell Canal (S – 3) is a 17.07 m (56 ft) wide opening with a bottom elevation of -3.66 m (-12 ft), NAVD88(2004.65) and is shown as the right circle in Figure 116.

Figure 116. Shell Structures.

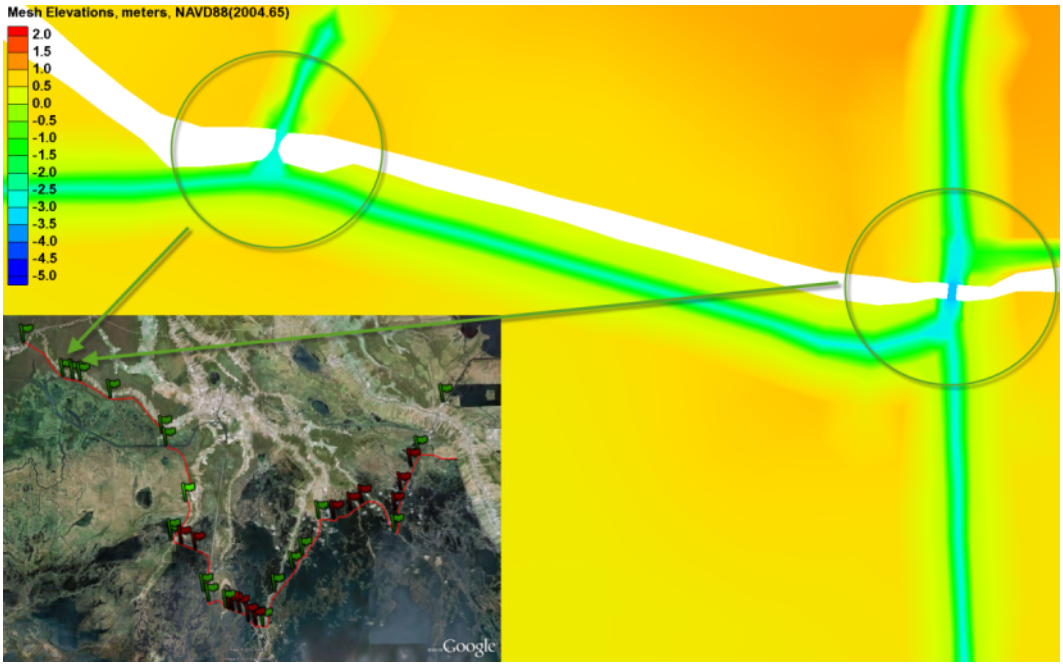

The Elliot Jones Canal (S – 4), shown in Figure 117, is a 6.10 m (20 ft) wide opening with a bottom elevation of -2.44 (-8 ft), NAVD88(2004.65).

Figure 117. Elliot Jones Structure.

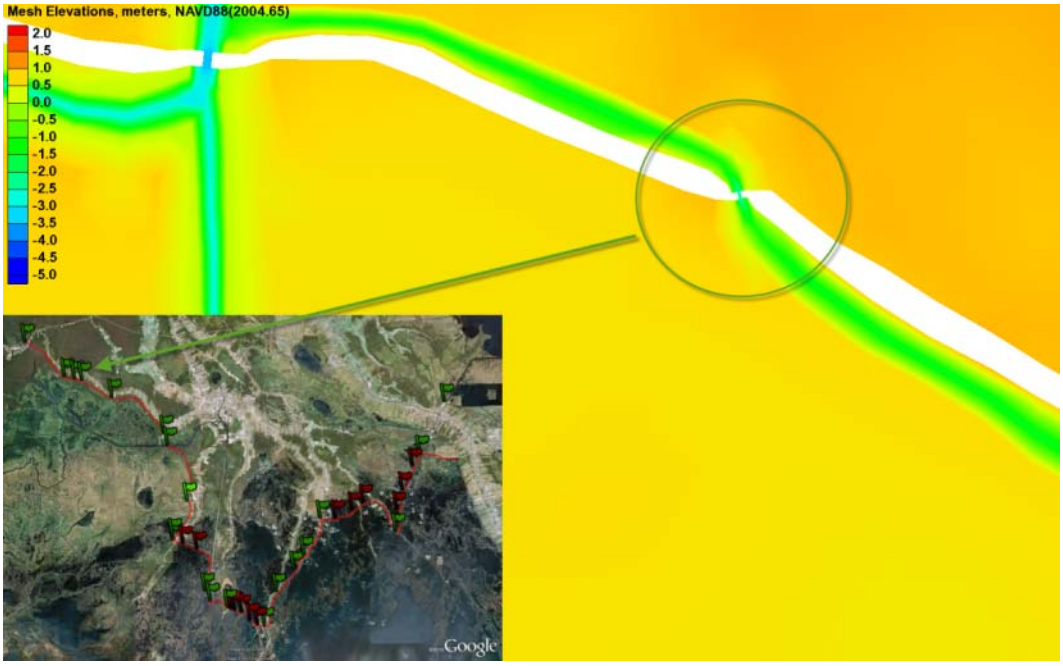

The NAFTA structure (S – 5) is a 17.07 m (56 ft) wide opening with a bottom elevation of -3.66 m (-12 ft), NAVD88(2004.65), and is shown in Figure 118.

Figure 118. NAFTA Structure.

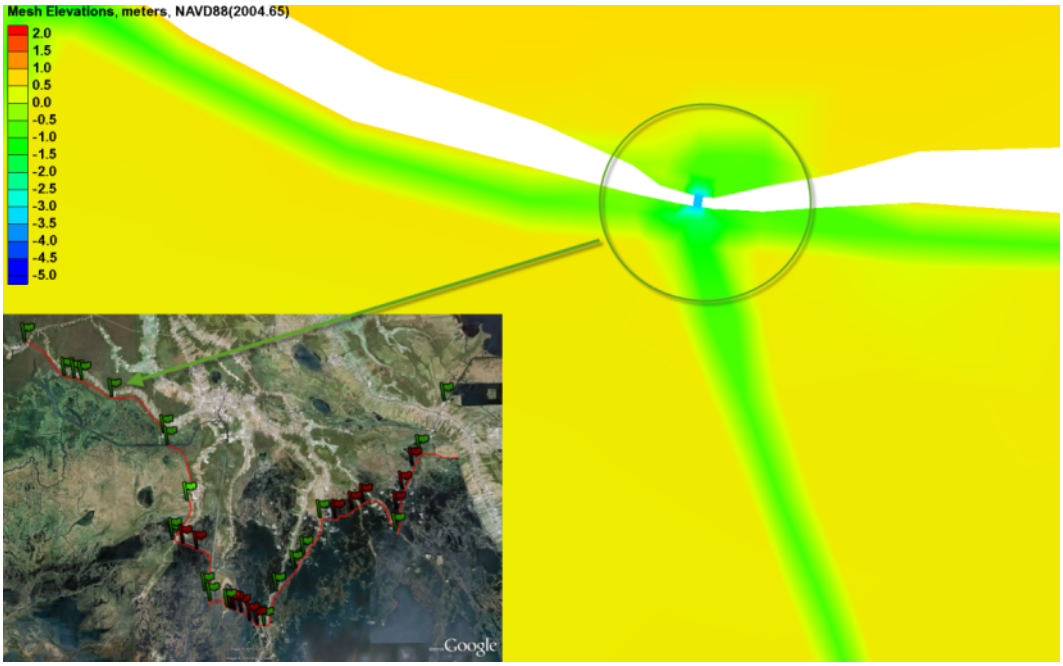

The Minors Canal structure (S – 6), circle in Figure 119, consists of one 17.07 m (56 ft) sector gate with a bottom elevation of -2.74 m (-9 ft), NAVD88(2004.65).

Figure 119. Model representation of the Minors Canal structure.

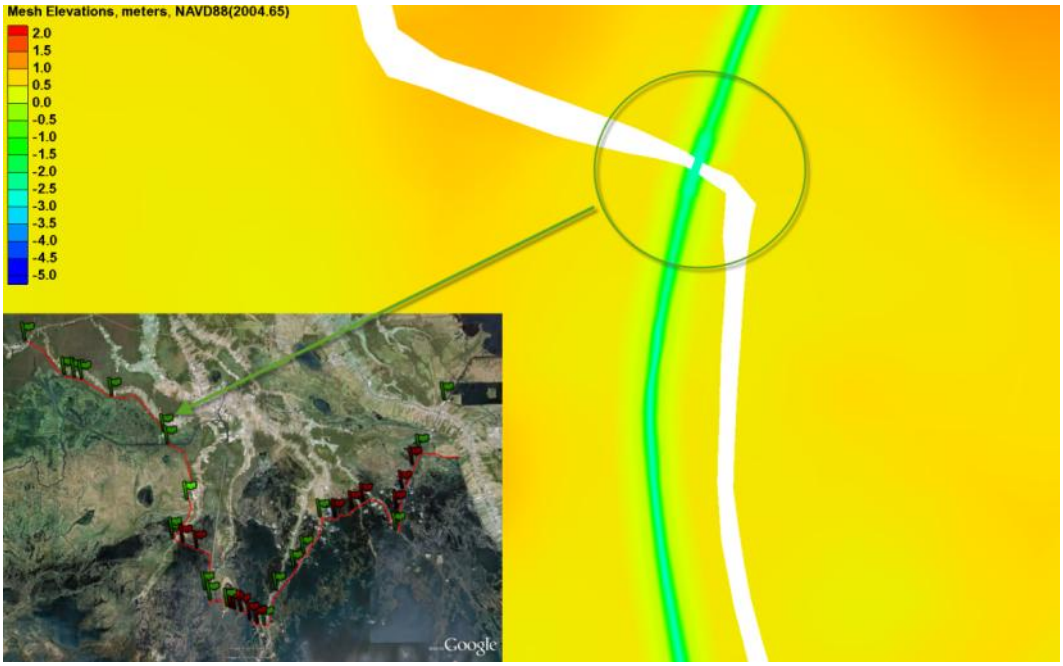

The structure located on the Gulf Intracoastal Waterway (GIWW) structure (S – 7) is shown in Figure 120. The structure consists of one 53.34 m (175 ft) sector gate with a bottom elevation of -4.88 m (-16 ft), NAVD88(2004.65), along with six 4.88 m (16 ft) wide sluice gates with bottom elevations of -3.96 m (-13 ft), NAVD88(2004.65), three on each side.

Figure 120. Model representation of the GIWW structure.

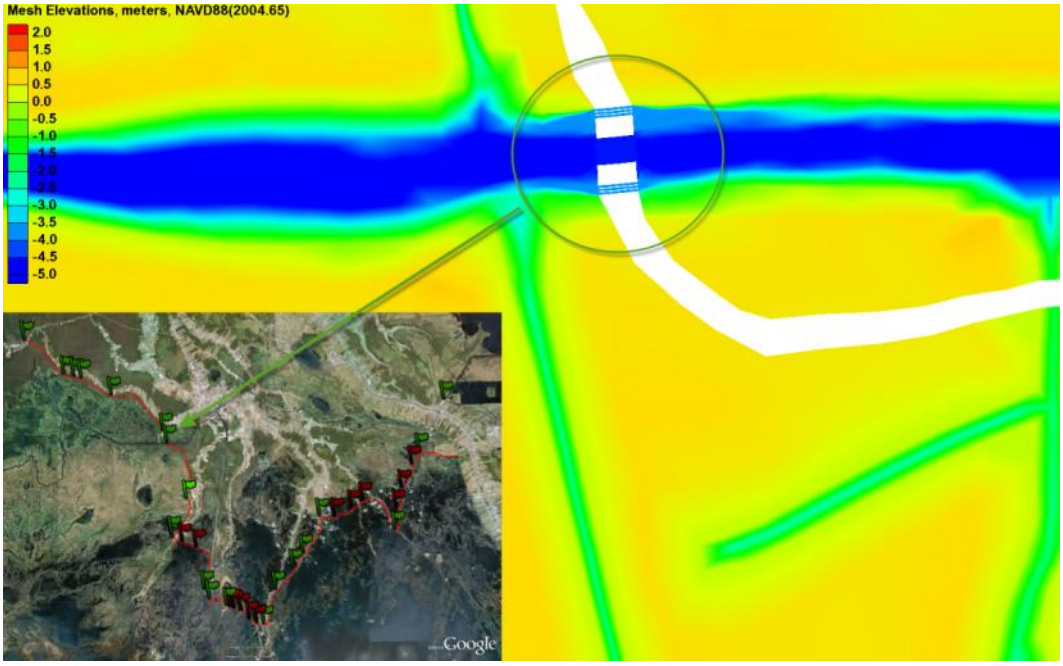

The formerly free-flowing Marmande Canal is now a 9.14 m (30 ft) wide structure (S – 8) with a bottom elevation of 1.83 m (-6 ft), NAVD88(2004.65). This structure representation is shown in Figure 121.

Figure 121. Model representation of the Marmande Canal culverts.

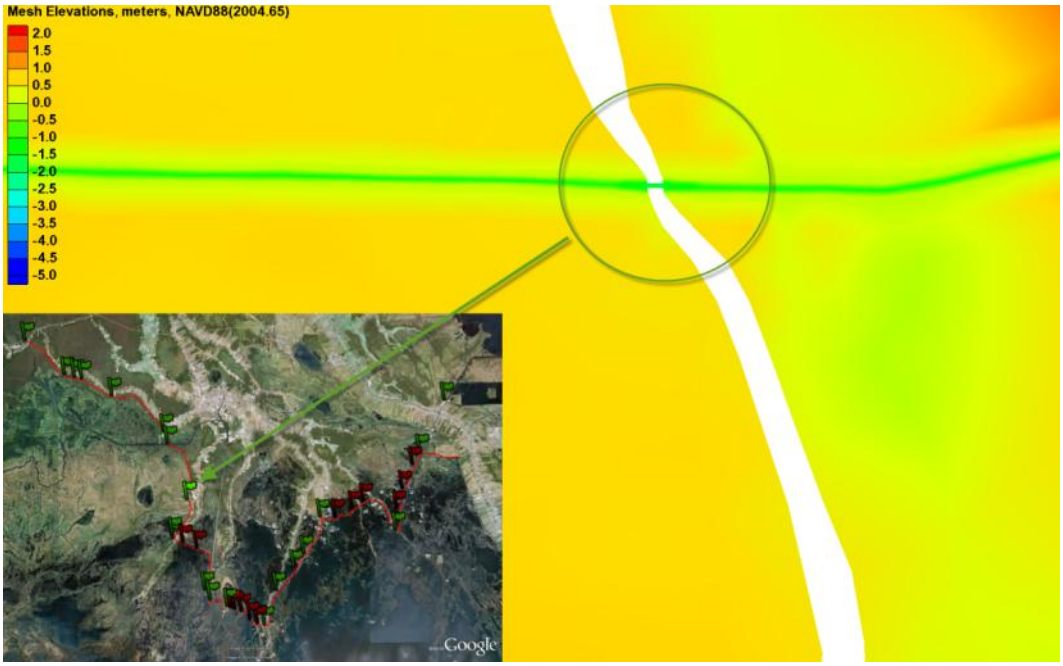

The Falgout Canal structure (S – 9), left circle, and the Bayou Dularge structure (S – 10), lower circle, are shown in Figure 122. The Falgout Canal structure consists of one 17.07 m (56 ft) sector gate and nine 4.88 m (16 ft) sluice gates with a -2.74 (-9 ft) NAVD88(2004.65) bottom elevation. The Bayou Dularge structure consists of one 17.07 m (56 ft) sector gate with a bottom elevation of -2.13 m (-7 ft), NAVD88(2004.65).

Figure 122. Model representation of the Falgout Canal and Bayou Dularge structures.

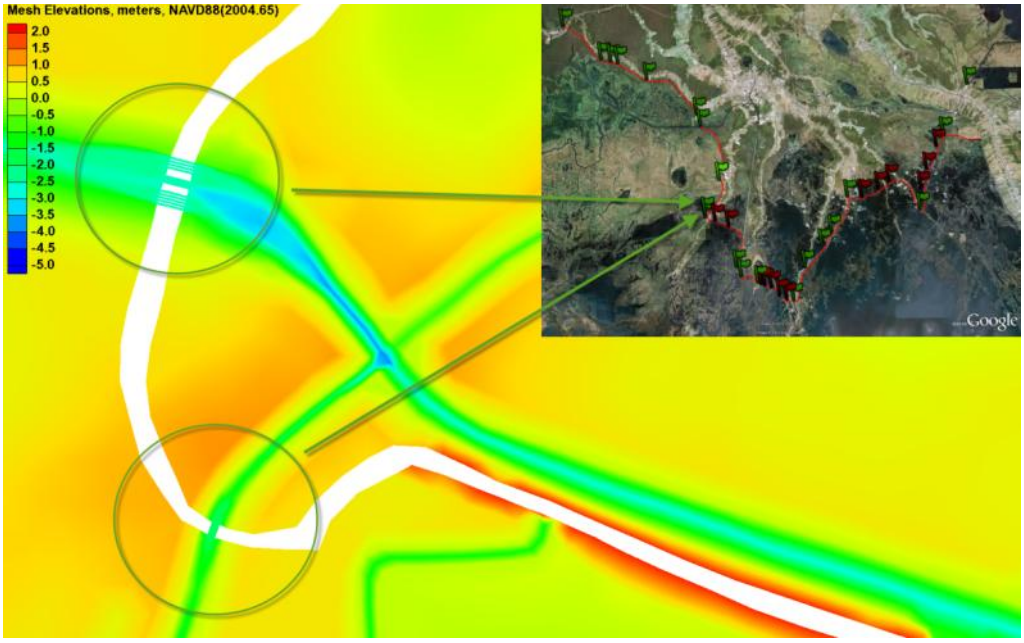

Two sets of nine culverts (1.83 m x 1.83 m) are located along Falgout Canal (E – 1 and E – 2). In the model, the two sets of culverts are represented as two single culverts with widths of 16.5 m (54 ft) and bottom elevation of -1.37 m (-4.5 ft), NAVD88(2004.65). This configuration is shown in Figure 123 (E – 1 is the left circle and E – 2 is the right circle). Plan 2 will have these culverts in the closed position.

Figure 123. Model representation of two sets of culverts located along Falgout Canal.

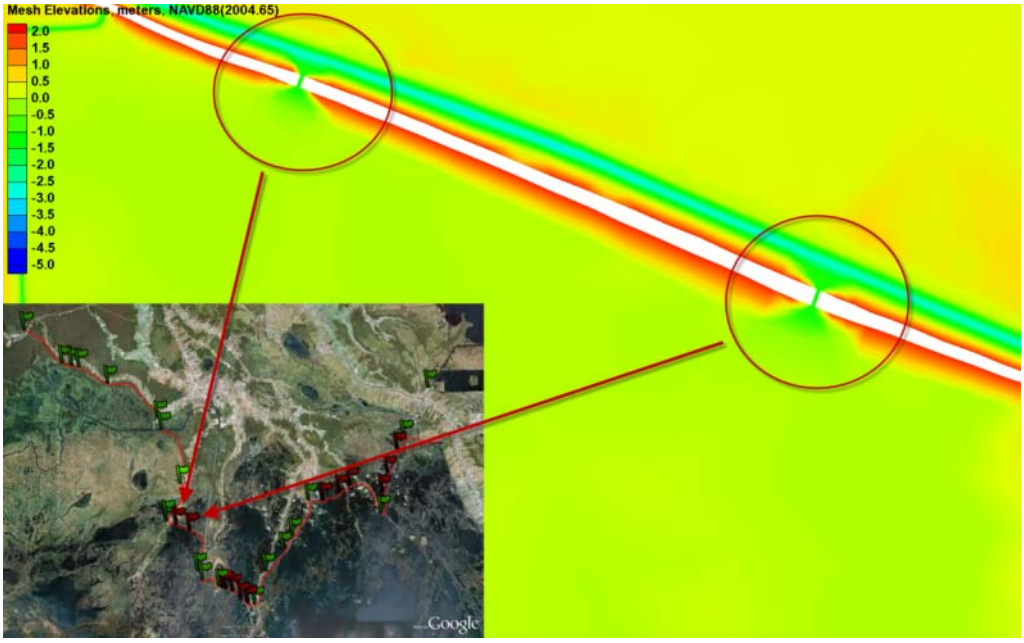

The Bayou Grand Caillou structure (S – 11), shown in Figure 124, consists of nine 4.88 m (16 ft) sluice gates and one 17.07 m (56 ft) sector gate. This structure had a bottom elevation of -3.66 m (-12 ft), NAVD88(2004.65).

Figure 124. Model representation of the Bayou Grand Caillou structure.

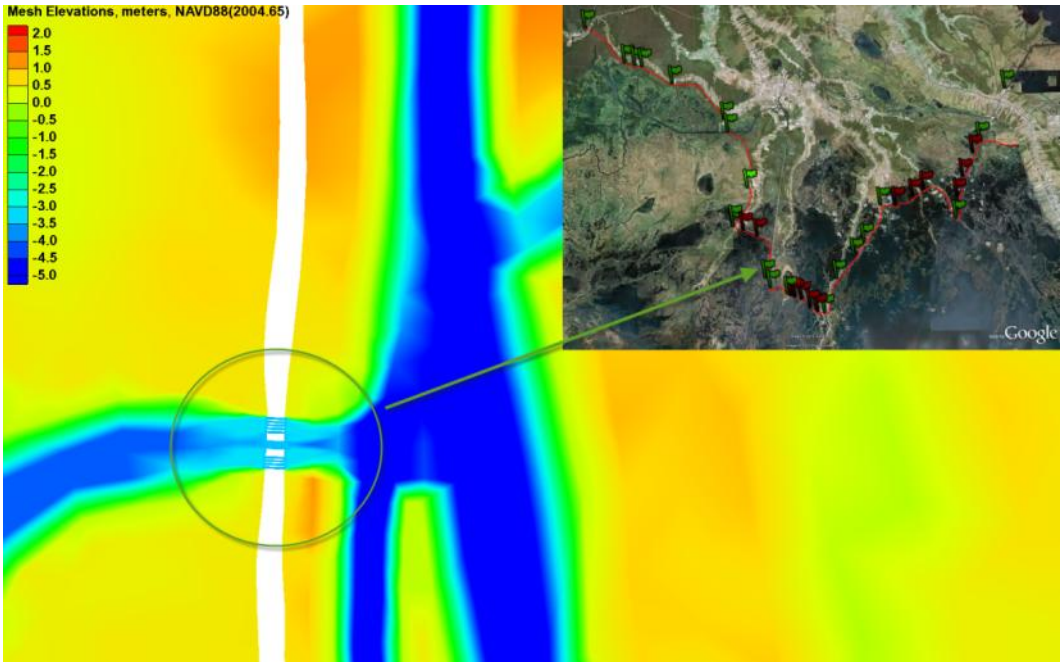

The Houma Navigation Canal structure (S – 12), Figure 125, consists of a 76.2 m (250 ft) wide structure and a 33.53 m (110 ft) wide lock, both with bottom elevations of -5.49 m (-18 ft), NAVD88(2004.65). The Houma Navigational Canal structure also consists of ten 3.05 m (10 ft) wide sluice gates with a 1.52 m (5 ft) opening from -0.61 m (-2 ft) to -2.13 m (-7 ft), NAVD88(2004.65). Plan 3 will have the Houma Navigation Canal structure and lock in the closed position.

Figure 125. Model representation of the Houma Navigation Canal structure and lock.

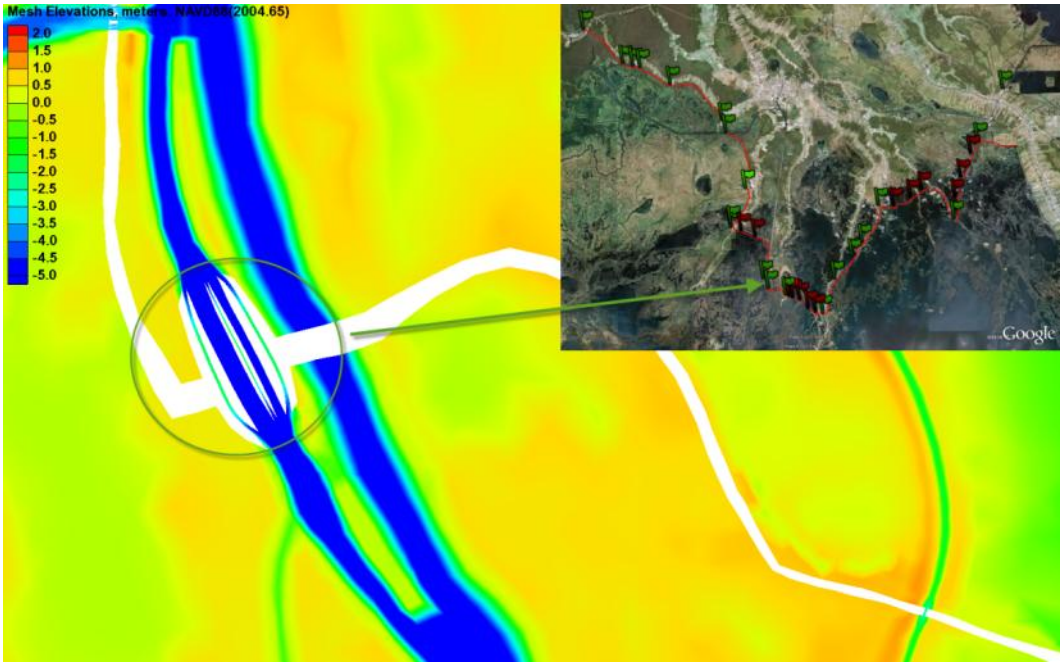

The structure located on Bayou Fourpoints (S – 13) (green circle on left in Figure 126) is a 9.14 m (30 ft) opening with a -2.44 m (-8 ft), NAVD88(2004.65) bottom elevation. A set of six culverts (E – 3) (1.83 m x 1.83 m) are located just east of Bayou Fourpoints (leftmost red circle in Figure 126). This configuration was represented in the model as a single culvert with a 11.0 m (36 ft) width and a bottom elevation of -1.37 m (-4.5 ft), NAVD88(2004.65). The two red circles to the right (E – 4 and E – 5) are two sets of four 1.83 m x 1.83 m culverts with a total width of 7.3 m (24 ft) and a bottom elevation of -1.37 m (-4.5 ft), NAVD88(2004.65). Plan 2 will have these culverts (E – 3, E – 4 and E – 5) in the closed position.

Figure 126. Model representation of the Bayou Fourpoints structure.

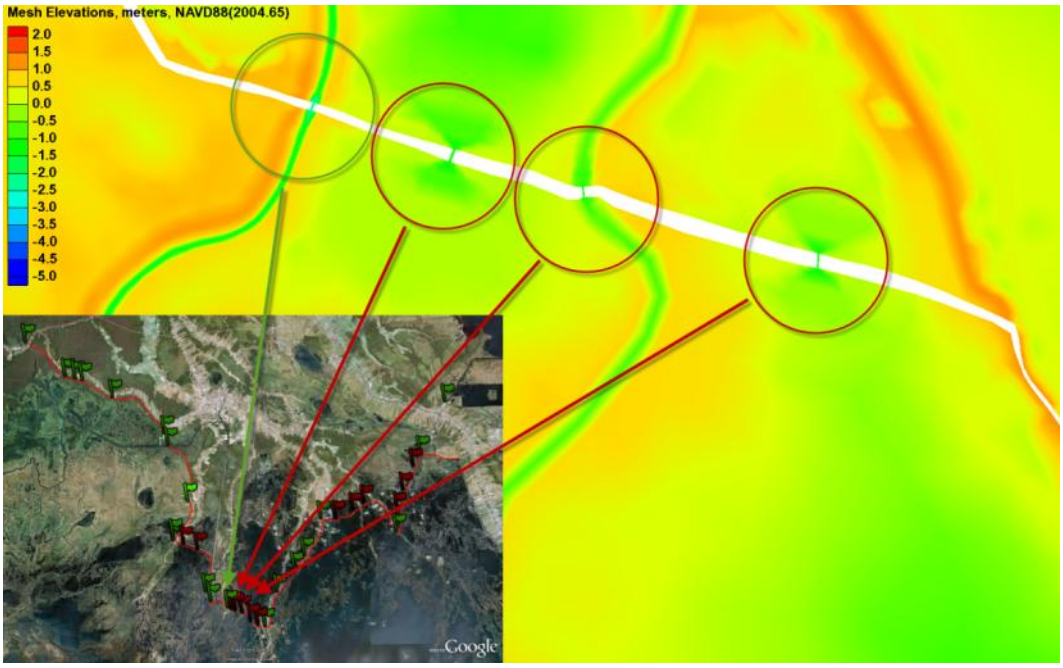

Two sets of culverts (E – 6 and E – 7) are located to the west of Bayou Petit Caillou (shown in Figure 127). The left circle (E – 6) is a single 1.83 m x 1.83 m culvert with a bottom elevation of -1.37 m (-4.5 ft), NAVD88(2004.65). The right circle (E – 7) is a set of a set of six 1.83 m x 1.83 m culverts with bottom elevations of -1.37 m (-4.5 ft), NAVD88(2004.65). This configuration is represented in the model as a single 11.0 m (36 ft) culvert. Plan 2 will have these culverts in the closed position.

Figure 127. Model representation of a set of culverts and Bayou Petit Caillou.

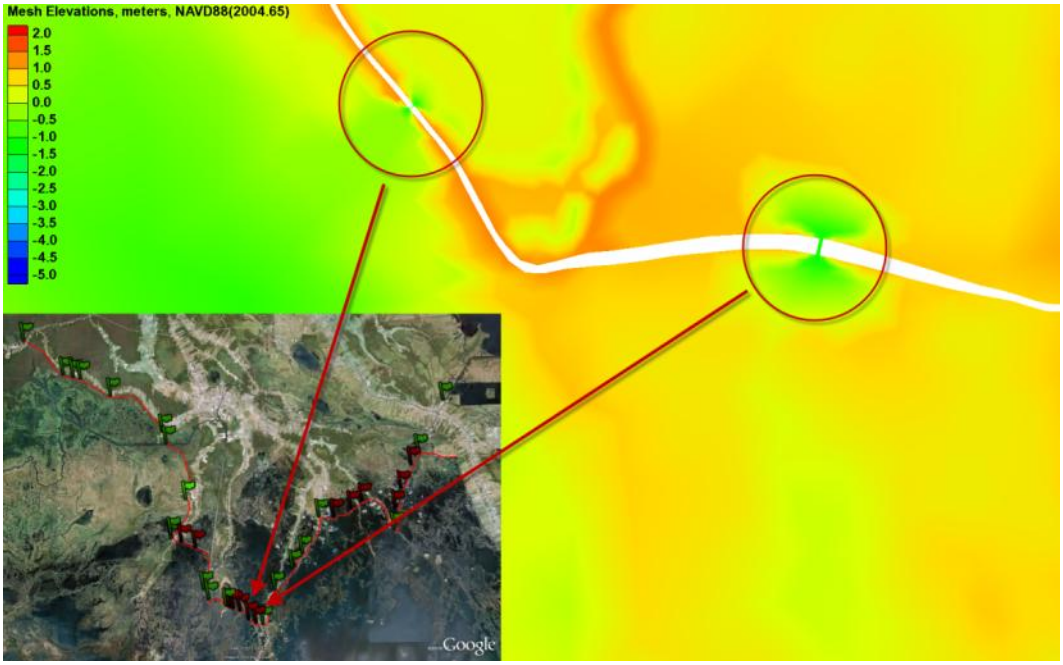

The Bayou Petit Caillou structure (S – 14), shown in Figure 128, is a 17.07 m (56 ft) wide sector gate and six 4.88 m (16 ft) wide sluice gates with bottom elevations of -2.44 m (-8 ft), NAVD88(2004.65).

Figure 128. Model representation of the Bayou Petit Caillou structure.

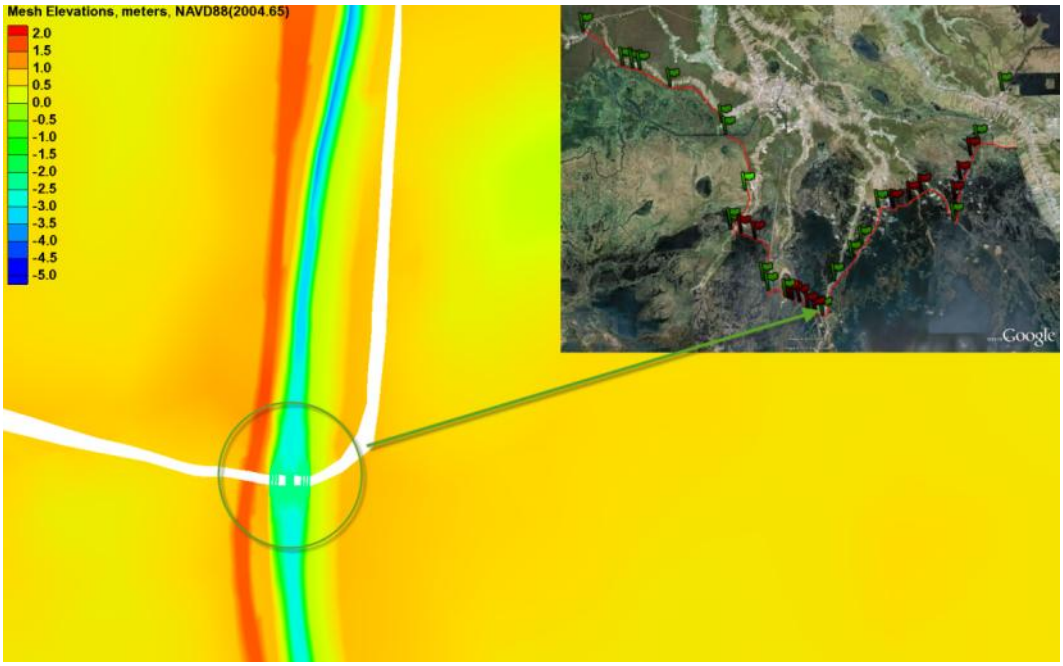

The Placid Canal structure (S – 15), shown in Figure 129, consists of one 17.07 m (56 ft) sector gate and six 4.88 m (16 ft) sluice gates with bottom elevations of -2.44 m (-8 ft), NAVD88(2004.65).

Figure 129. Model representation of the Placid Canal Structure.

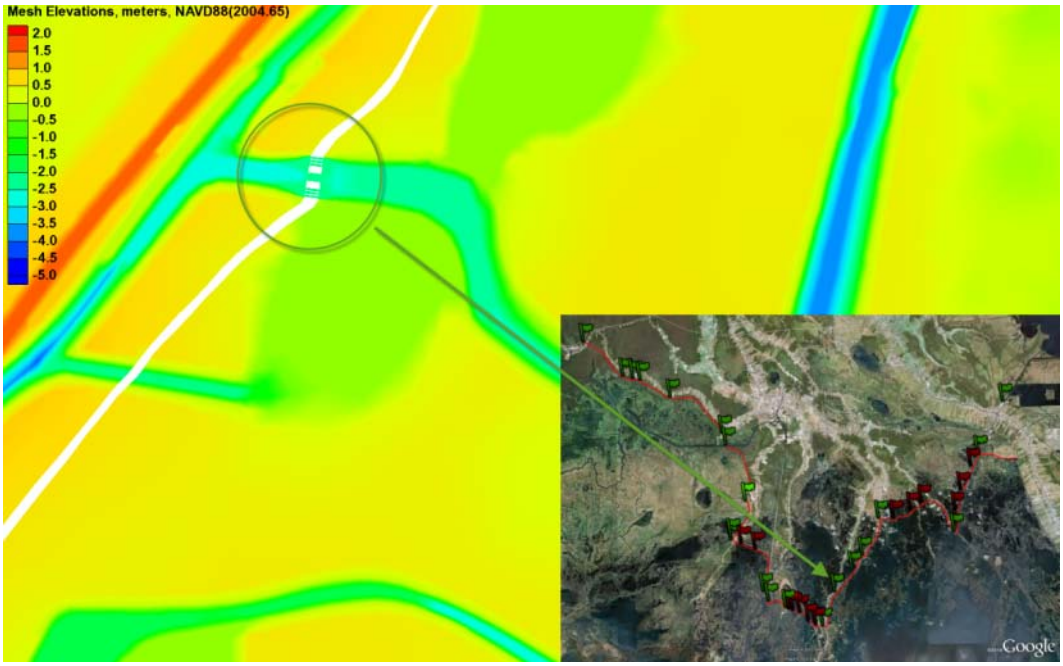

The Bush Canal structure (S – 16), shown in Figure 130, consists of nine 4.88 m (16 ft) sluice gates and one 17.07 m (56 ft) sector gate. This structure had a bottom elevation of -3.66 m (-12 ft), NAVD88(2004.65).

Figure 130. Model representation of the Bush Canal Structure.

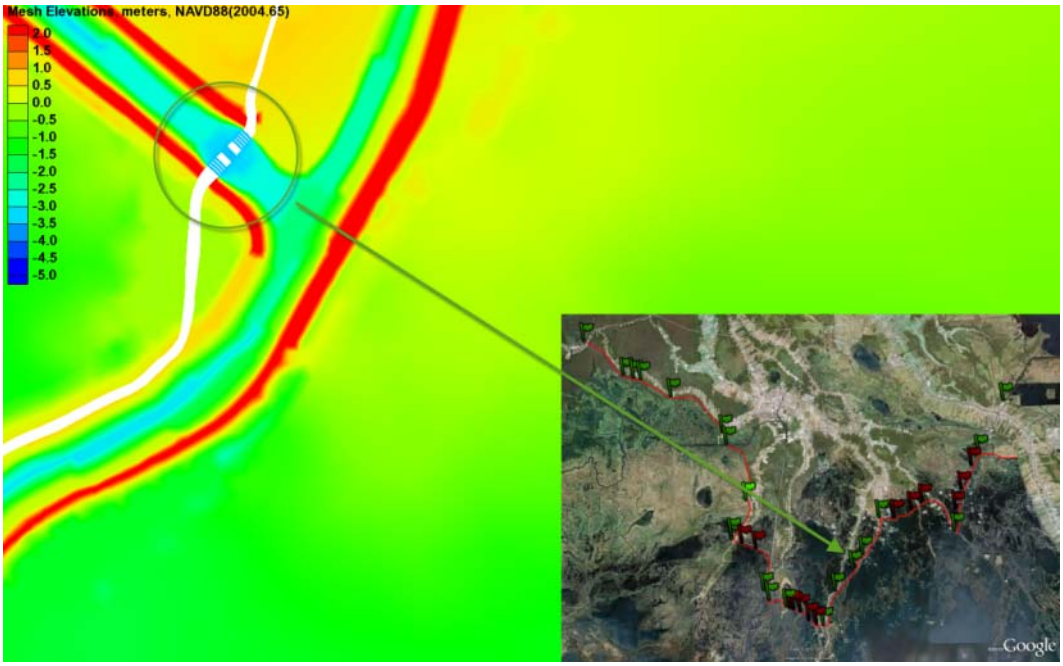

The Bayou Terrebonne structure (S – 17), shown in Figure 131, is a 17.07 m (56 ft) wide structure with a bottom elevation of -2.74 (-9 ft), NAVD88(2004.65).

Figure 131. Model representation of the Bayou Terrebonne structure.

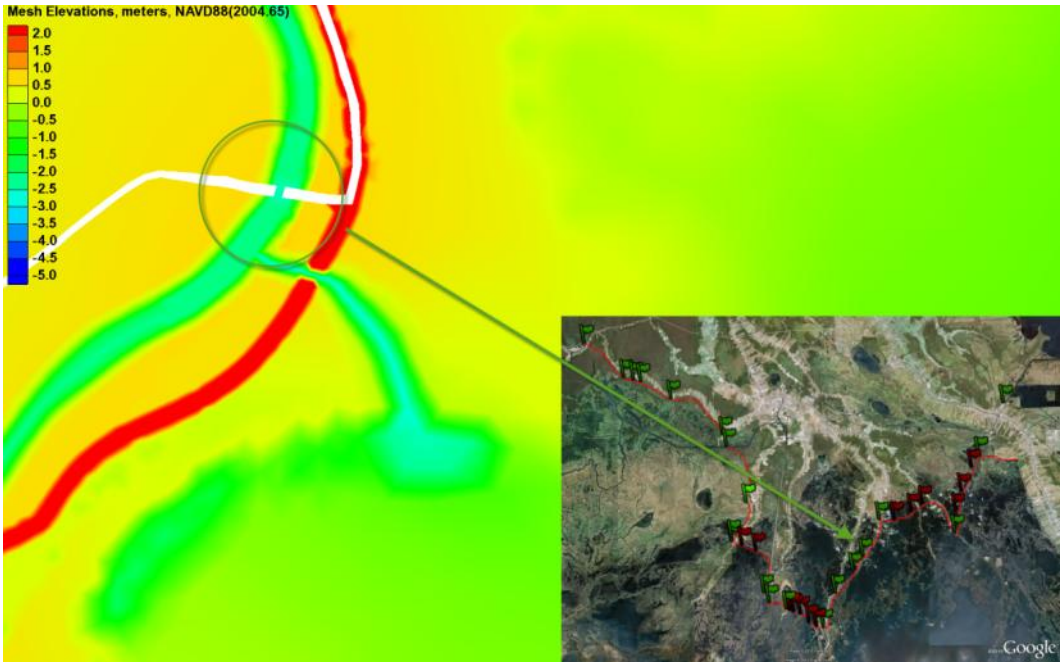

The Humble Canal structure (S – 18), shown in Figure 132, is a 17.07 m (56 ft) wide structure with a bottom elevation of -2.74 m (-9 ft), NAVD88(2004.65).

Figure 132. Model representation of the Humble Canal structure.

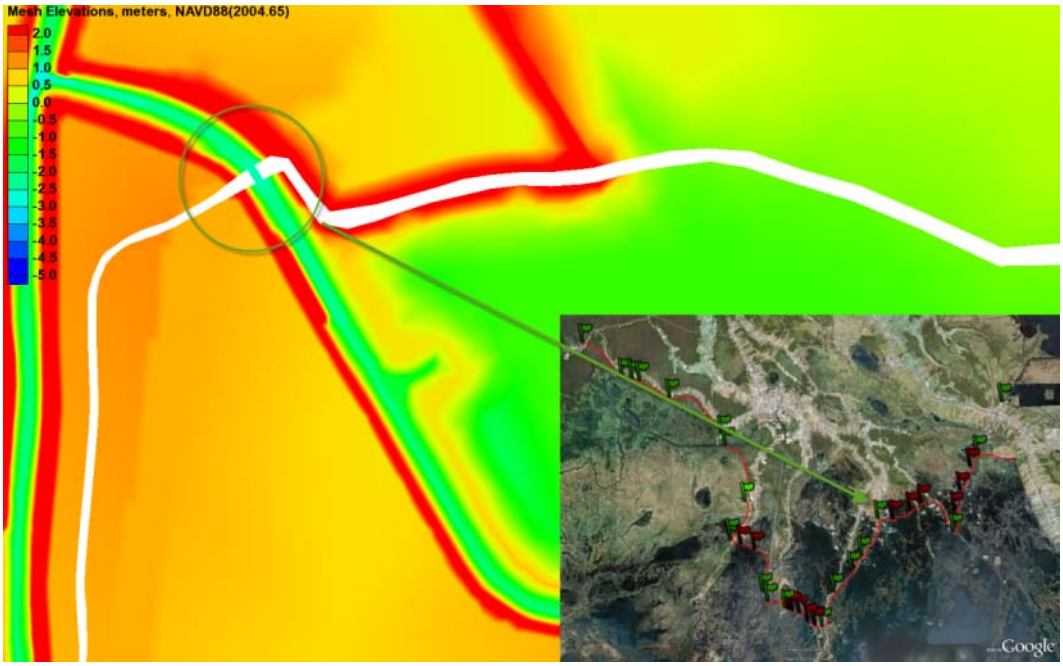

The three circles in Figure 133 are three sets of culverts (E – 8, E – 9 and E – 10) located in the Wonder Lake area (also known as the Montegut Wildlife Management Area). The left circle in Figure 133 (E – 8) consists of four 1.52 m x 3.05 m culverts that were represented in the model as a single culvert with a width of 12.2 m (40 ft) and a bottom elevation of -1.07 m (-3.5 ft), NAVD88(2004.65). The center circle in Figure 133 (E – 9) consists of four 1.52 m x 3.05 m culverts that are represented in the model as a single culvert with a 12.2 m (40 ft) width and a bottom elevation of -1.07 (-3.5 ft), NAVD88(2004.65). The right circle in Figure 133 (E – 10) is a set of five 1.52 m x 3.05 m culverts. This set was represented in the model as a single culvert with a width of 15.2 m (50 ft) and a bottom elevation of -1.07 m (-3.5 ft), NAVD88(2004.65). Plan 2 will have these three sets of culverts in the closed position.

Figure 133. Model representation of the Wonder Lake environmental structures.

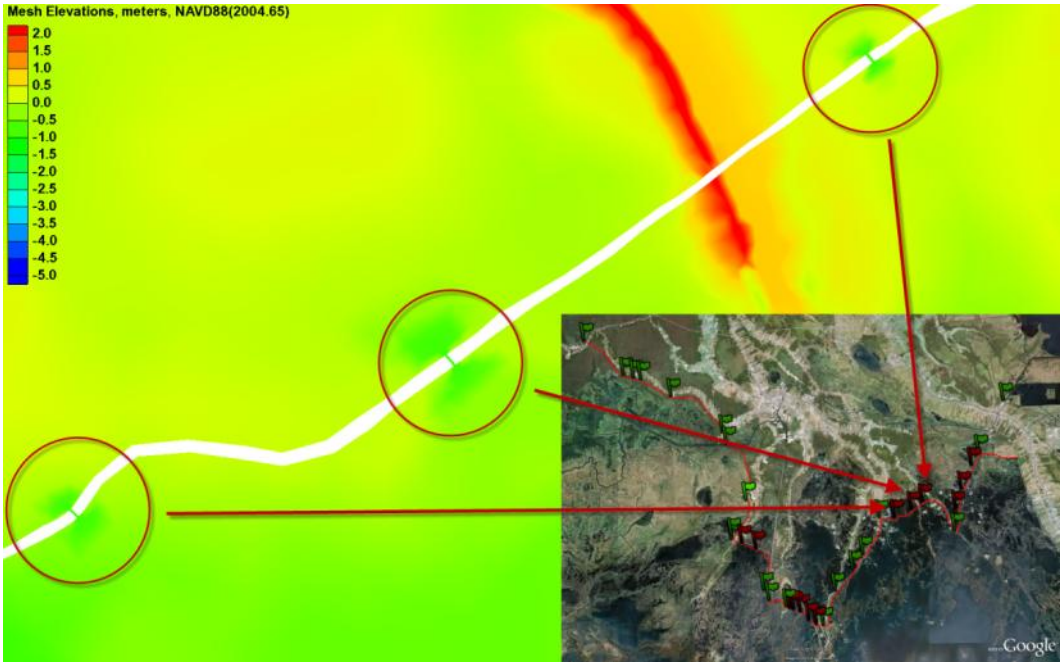

The Pointe Aux Chenes structure (S – 19), the green circle shown in Figure 134, has a 17.07 m (56 ft) width with a bottom elevation of -1.83 m (-6 ft), NAVD88(2004.65). Two 1.83 m x 1.83 m culverts (E – 11), red circle shown in Figure 134 located along Grand Bayou Canal, were represented as a single culvert with a width of 3.7 m (12 ft) and a bottom elevation of -1.37 m (-4.5 ft), NAVD88(2004.65). Plan 2 will have these culverts closed.

Figure 134. Model representation of the Pointe Aux Chenes structure and a set of culverts located to the north of the structure.

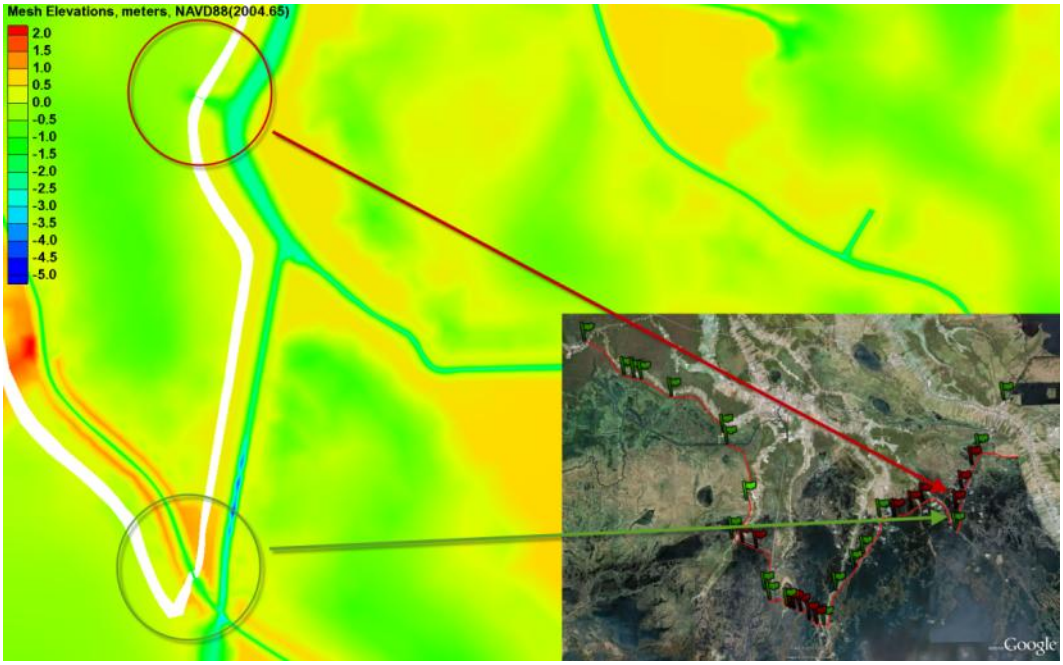

Two more sets of culverts, shown in Figure 135, are located along Grand Bayou Canal. The lower-left circle is a collection of two 1.83 m x 1.83 m culverts (E – 12) represented as a single culvert with a width of 3.7 m (12 ft) and a bottom elevation of -1.37 m (-4.5 ft), NAVD88(2004.65). The upper right circle in Figure 135 is a collection of six 1.83 m x 1.83 m culverts (E – 13) represented as a single culvert with a width of 11.0 m (36 ft) and a bottom elevation of -1.37 m (-4.5 ft), NAVD88(2004.65). Plan 2 will have these two sets of culverts in the closed position.

Figure 135. Model representation of two sets of culverts along Grand Bayou Canal.

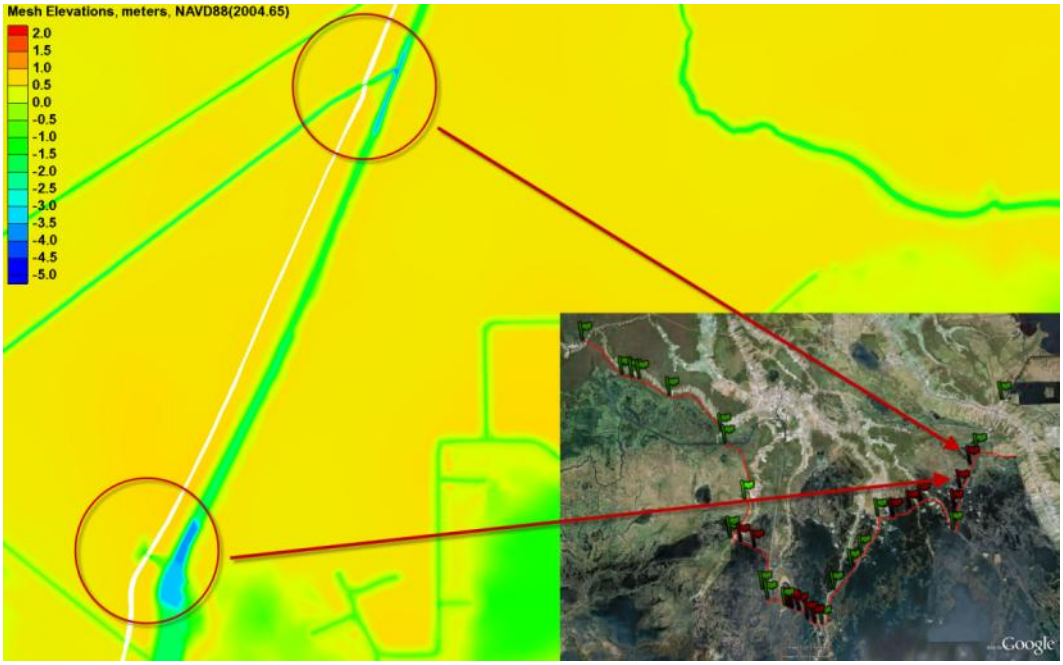

The Grand Bayou (S – 20) structure is shown in Figure 136. This structure is one 17.07 m (56 ft) wide sector gate with nine 4.88 m (16 ft) wide sluice gates with a bottom elevation of -2.74 m (-9 ft), NAVD88(2004.65).

Figure 136. Model representation of the Grand Bayou structure.

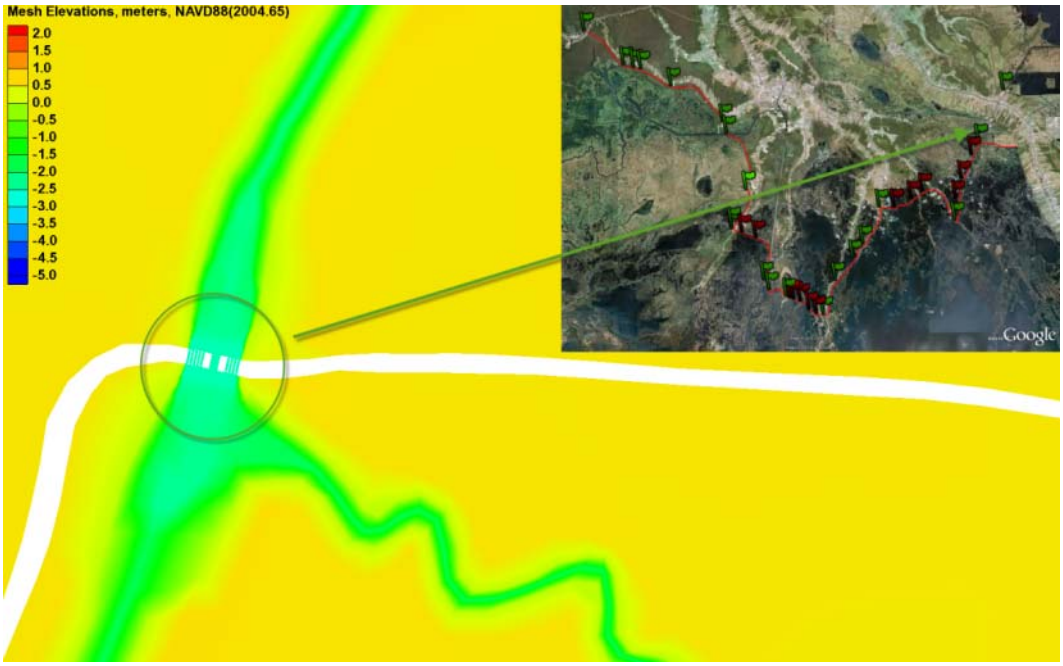

The GIWW at Larose structure (S – 21) is shown in Figure 137. This structure consists of a 53.34 m (175 ft) wide sector gate with a bottom elevation of -4.88 m (-16 ft), NAVD88(2004.65) and three 4.88 m (16 ft) wide sluice gates with bottom elevations of -3.05 m (-10 ft), NAVD88(2004.65).

Figure 137. Model representation of the GIWW at Larose structure.

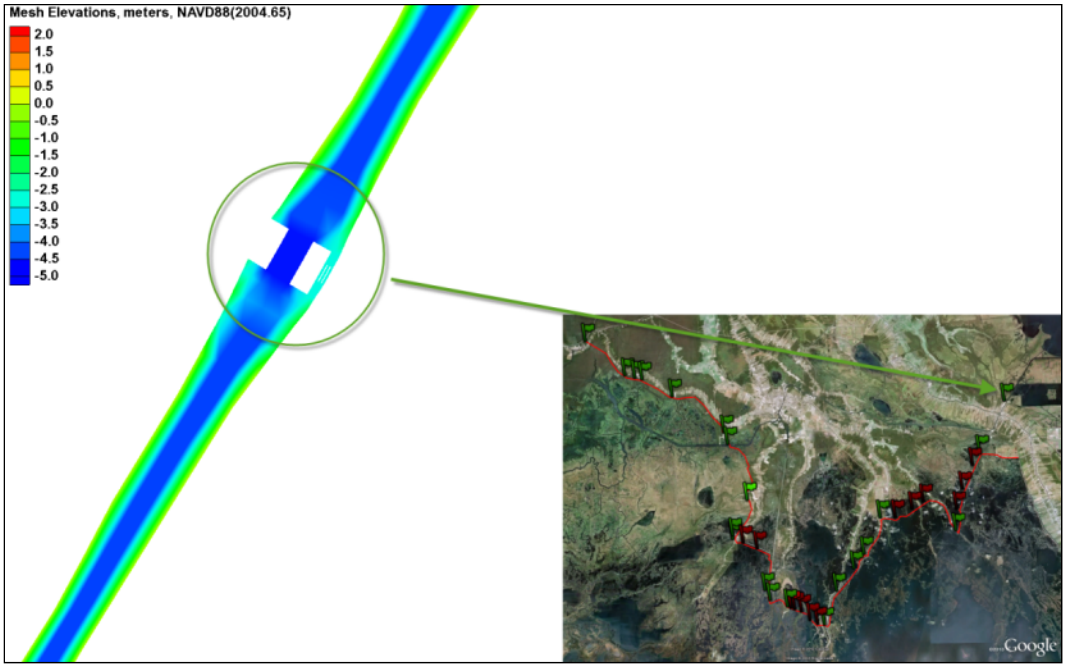

Appendix F: Average Salinities

A comparison was performed on the average salinity values for the base (without project) and plan conditions. These comparisons were performed for the vegetative growing season, March 1st to November 30th, along with yearly averaged values and are included as Figure 138 – Figure 179.

Figure 138. Baseline configuration salinities for the existing sea level for the growing season (March 1 to November 30).

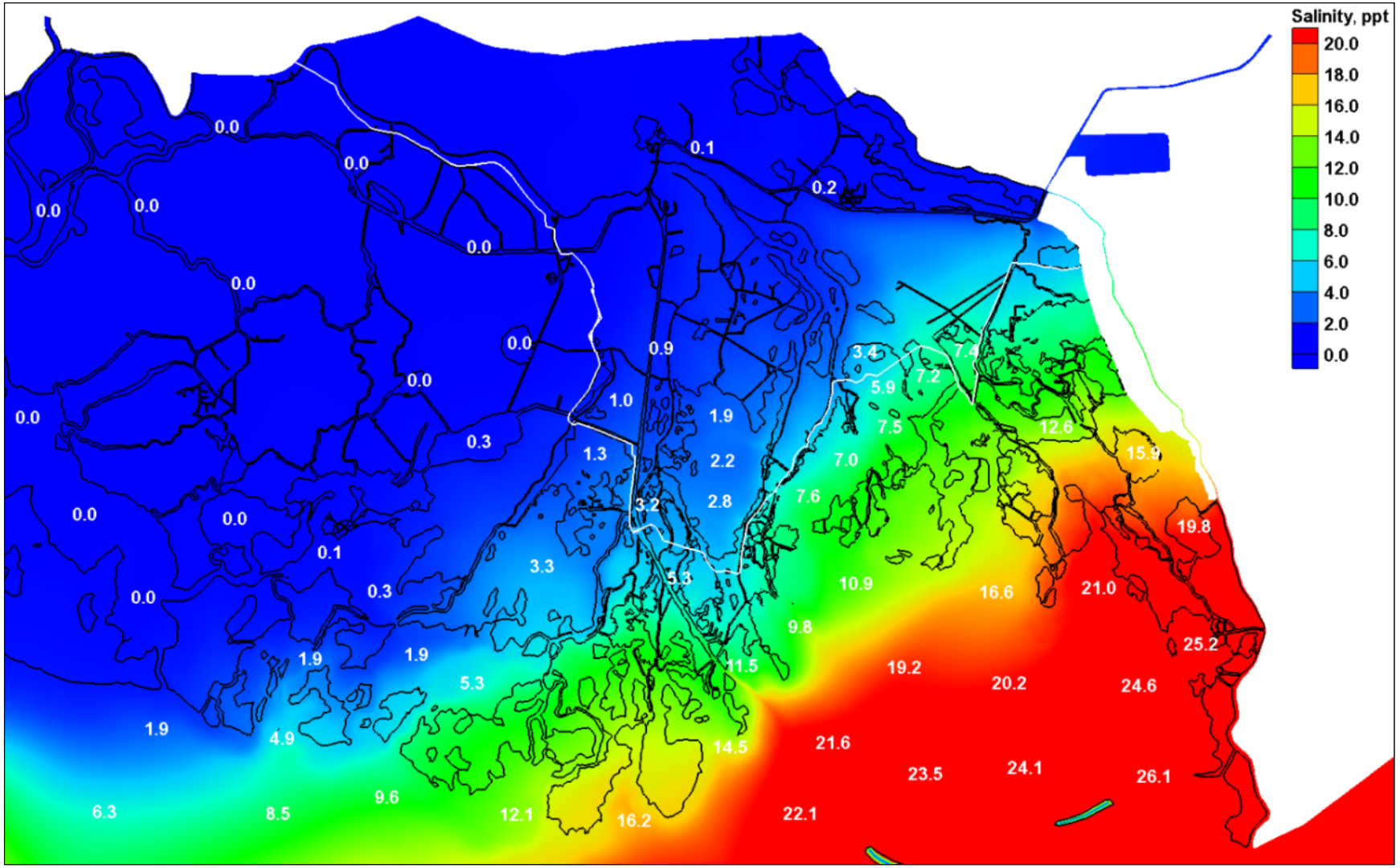

Figure 139. Plan 1 salinities for the existing sea level for the growing season (March to November 30).

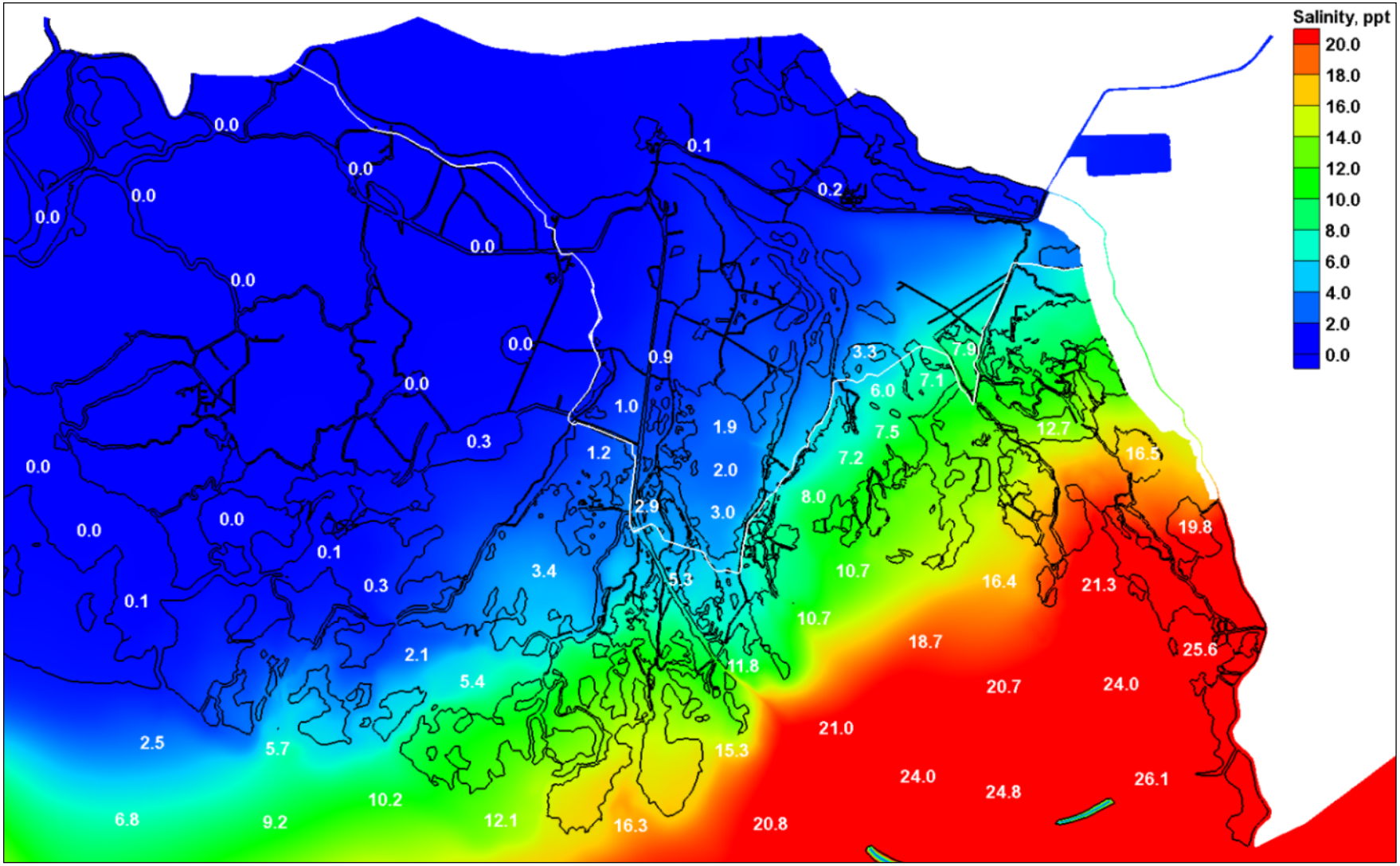

Figure 140. Plan 1 minus base configuration salinity differences for the existing sea level for the growing season (March 1 to November 30).

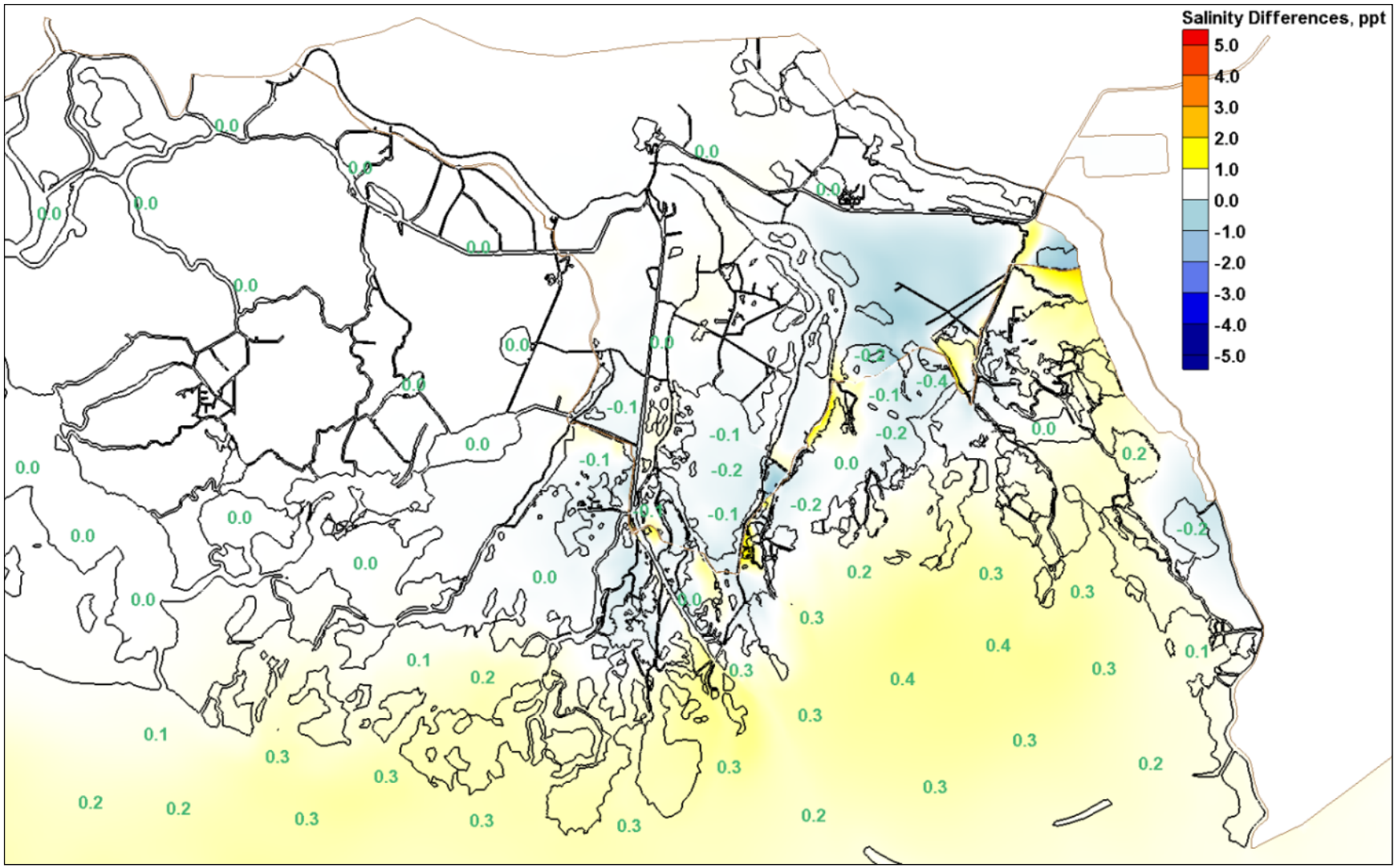

Figure 141. Plan 2 salinities for the existing sea level for the growing season (March 1 to November 30).

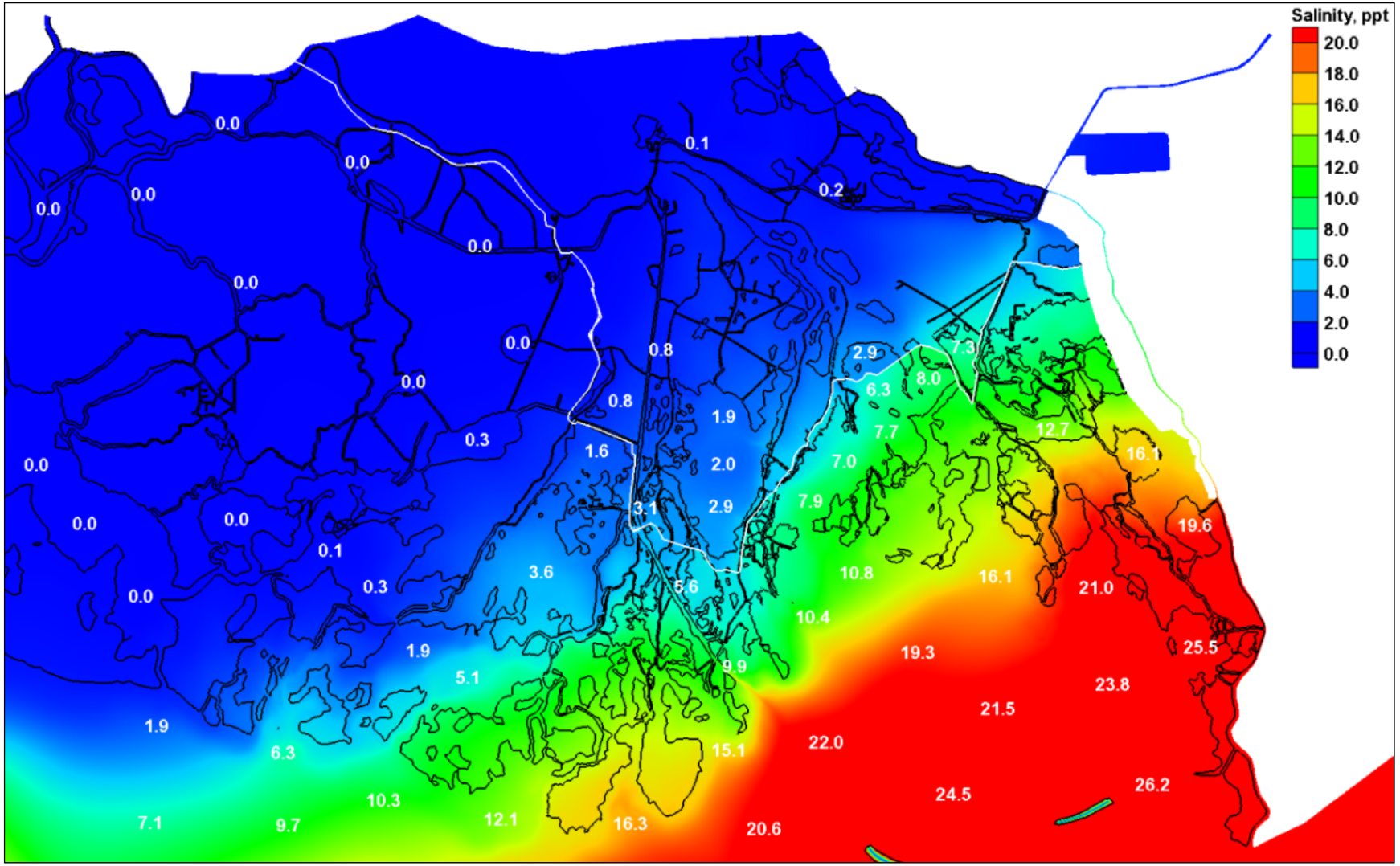

Figure 142. Plan 2 minus base configuration salinity differences for the existing sea level for the growing season (March 1 to November 30).

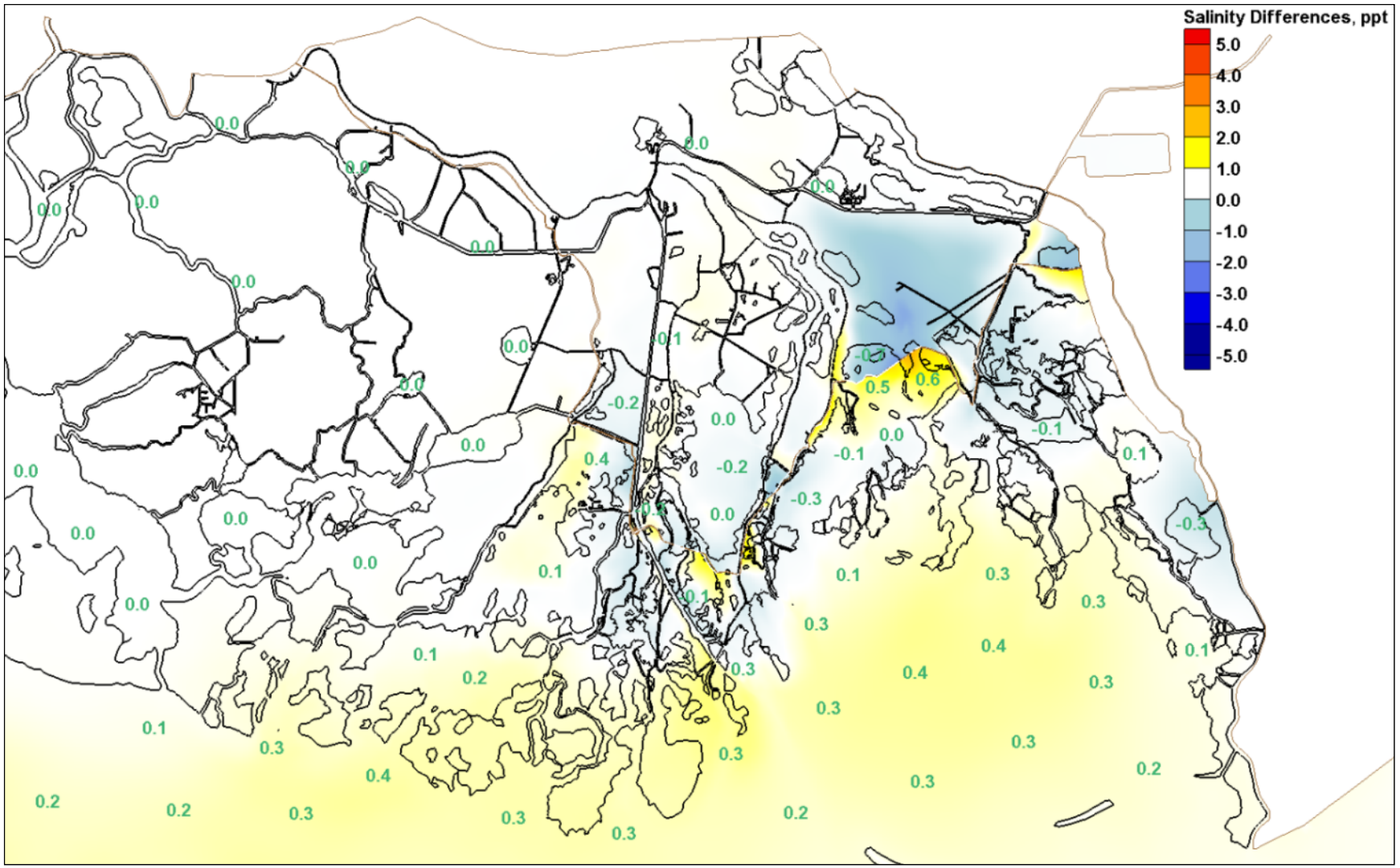

Figure 143. Plan 3 salinities for the existing sea level for the growing season (March 1 to November 30).

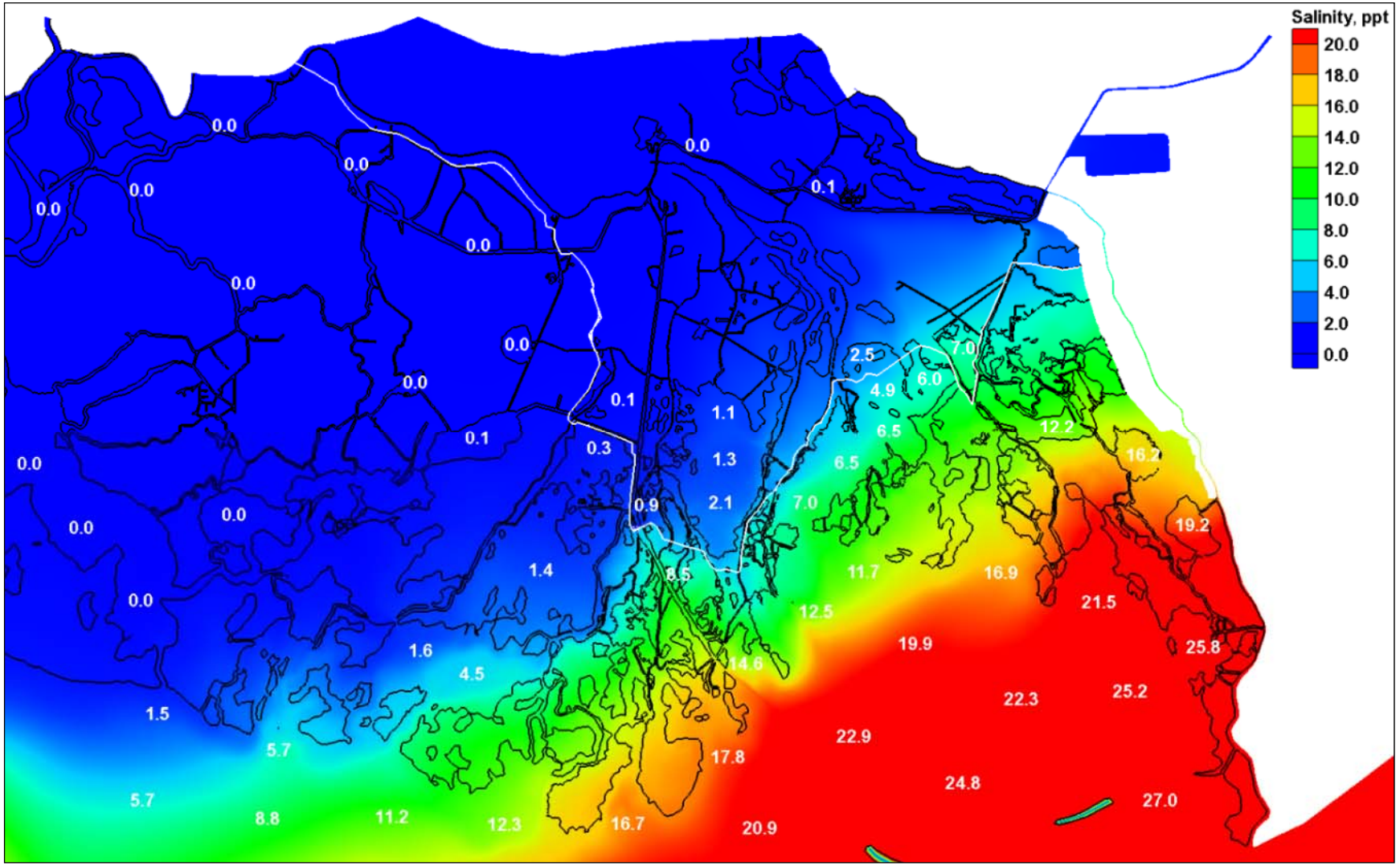

Figure 144. Plan 3 minus base configuration salinity differences for the existing sea level for the growing season (March 1 to November 30).

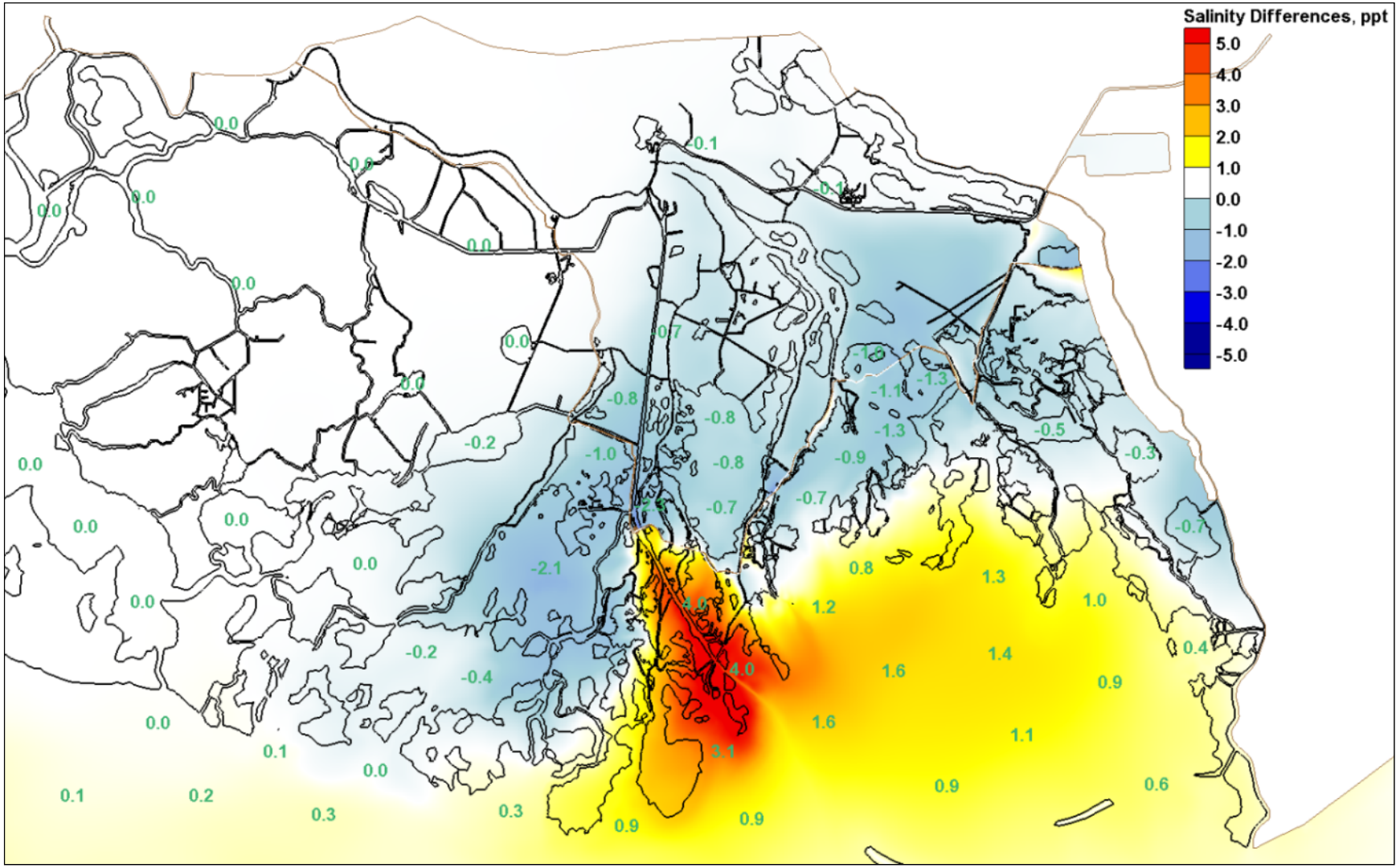

Figure 145. Base configuration salinities for the sea-level rise 1 scenario (0.738 m) for the growing season (March 1 to November 30).

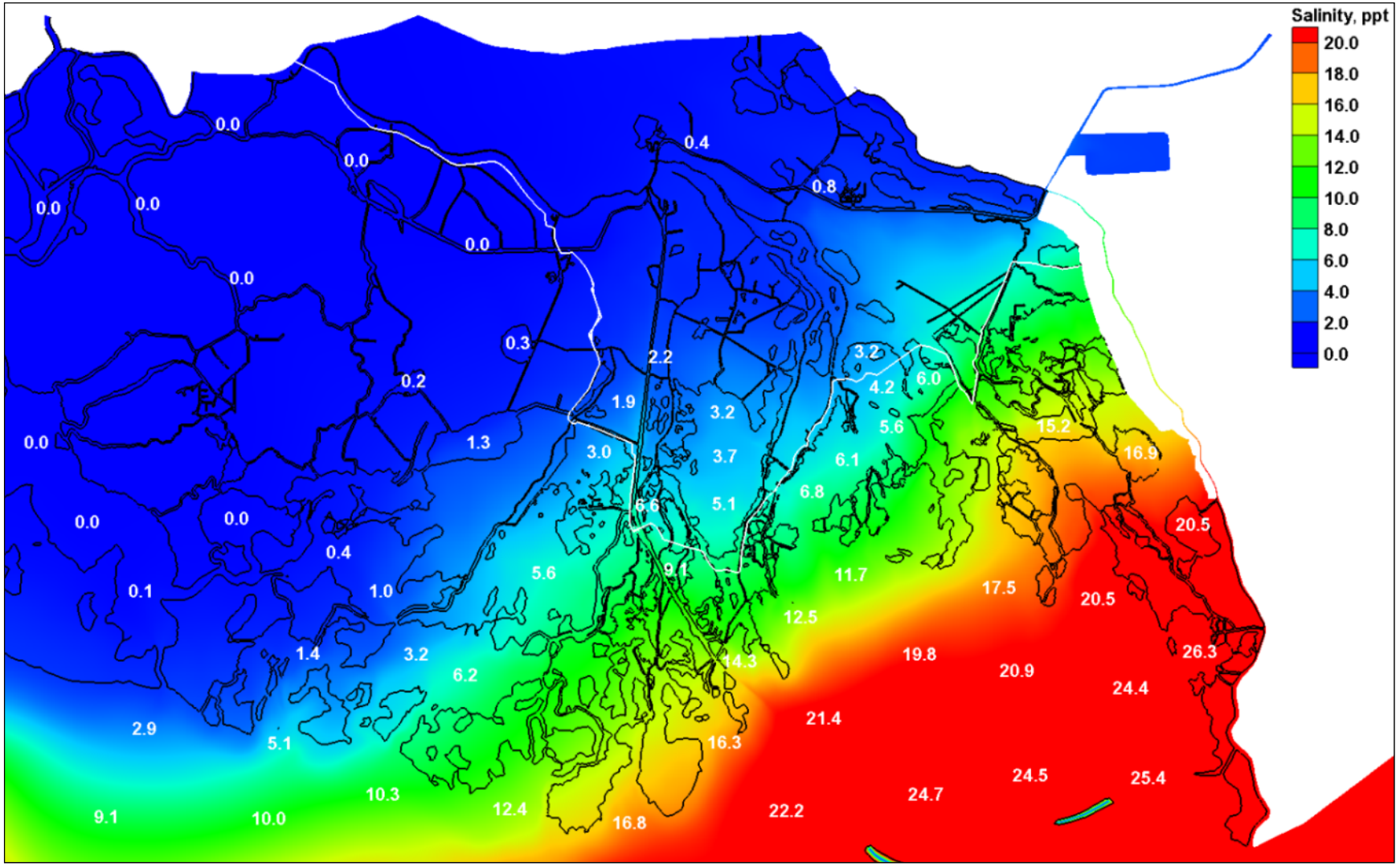

Figure 146. Plan 1 salinities for the sea-level rise 1 scenario (0.738 m) for the growing season (March 1 to November 30).

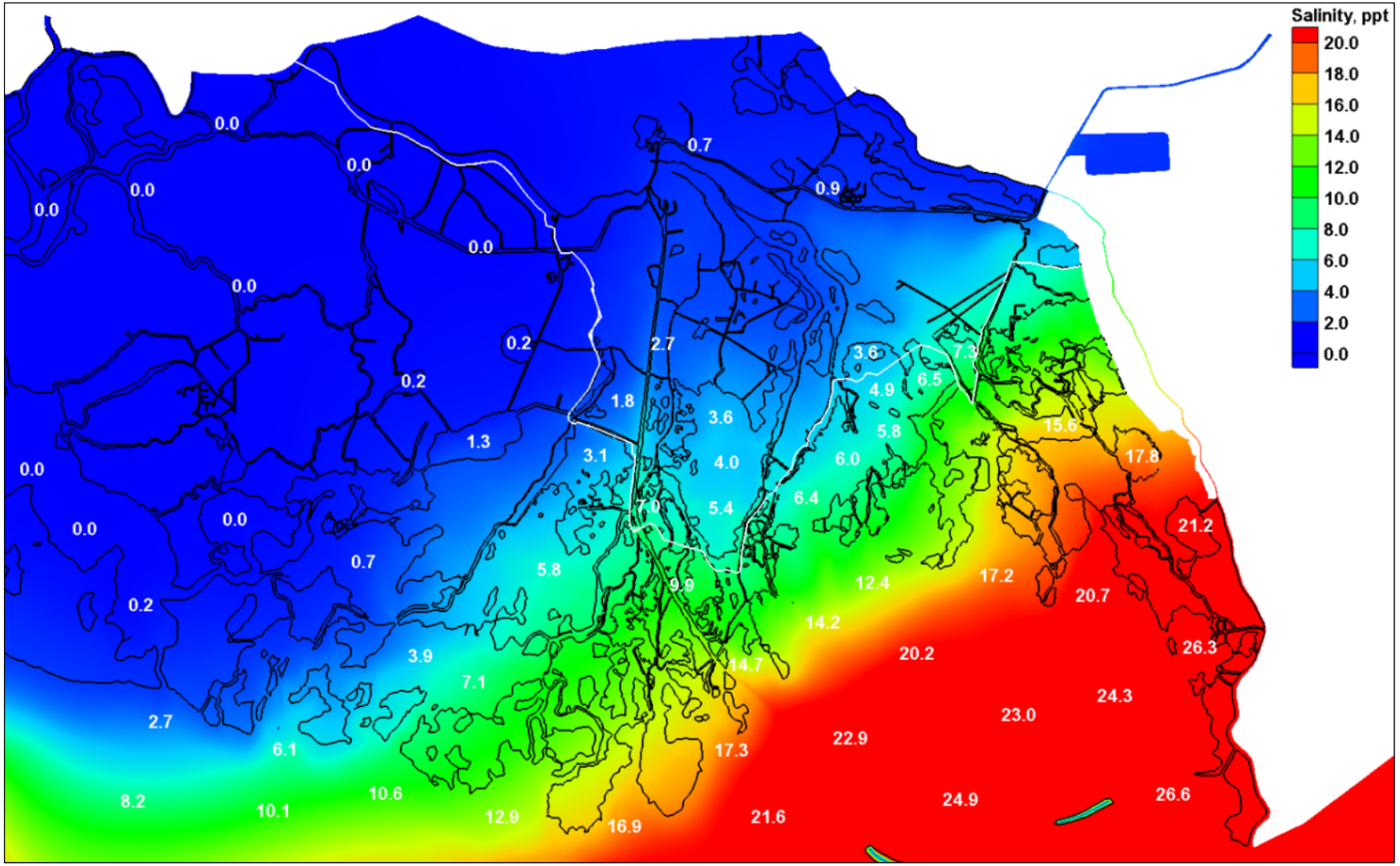

Figure 147. Plan 1 minus base configuration salinity differences for the sea-level rise 1 scenario (0.738 m) for the growing season (March 1 to November 30).

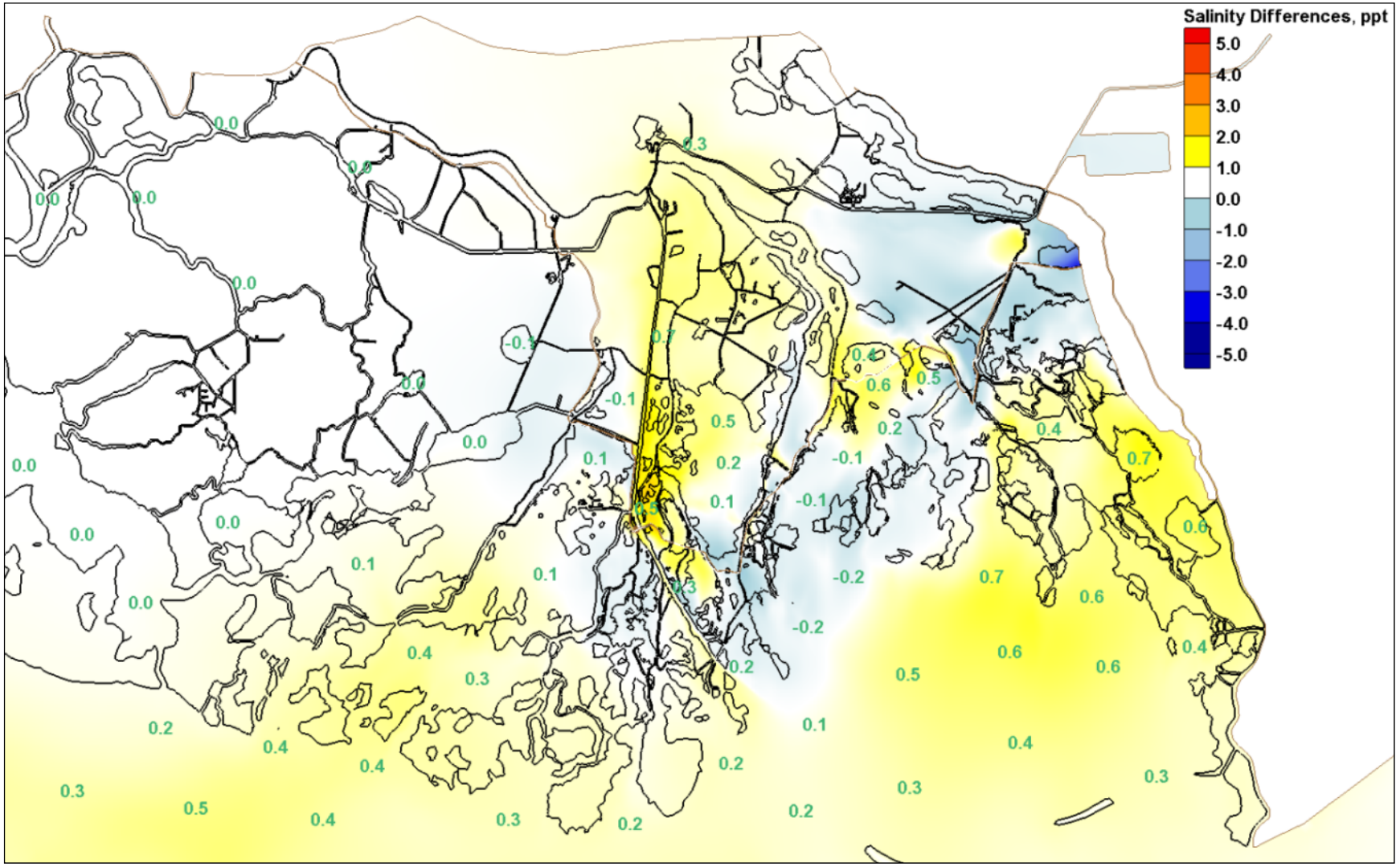

Figure 148. Plan 2 salinities for the sea-level rise 1 scenario (0.738 m) for the growing season (March 1 to November 30).

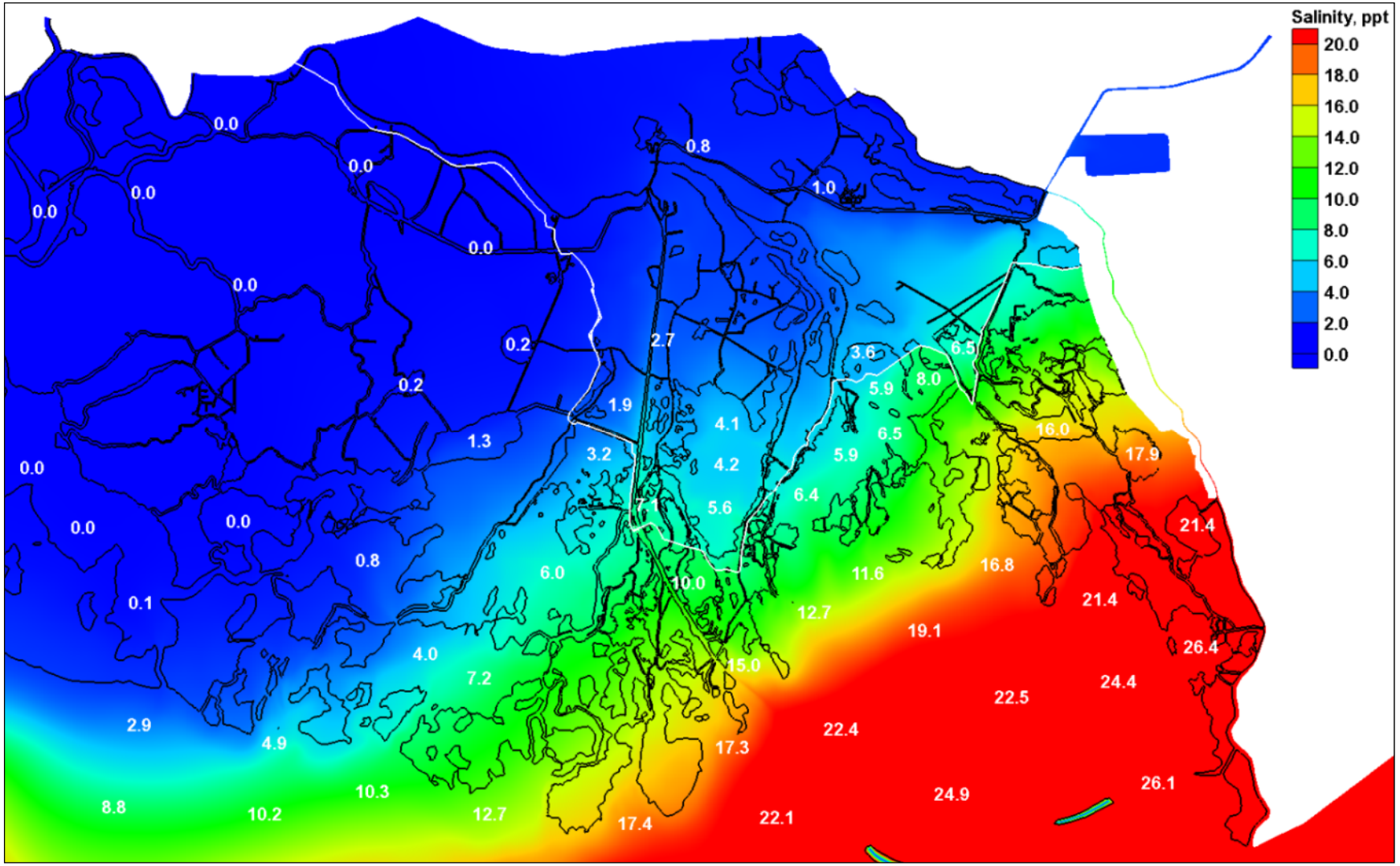

Figure 149. Plan 2 minus base configuration salinity differences for the sea-level rise 1 scenario (0.738 m) for the growing season (March 1 to November 30).

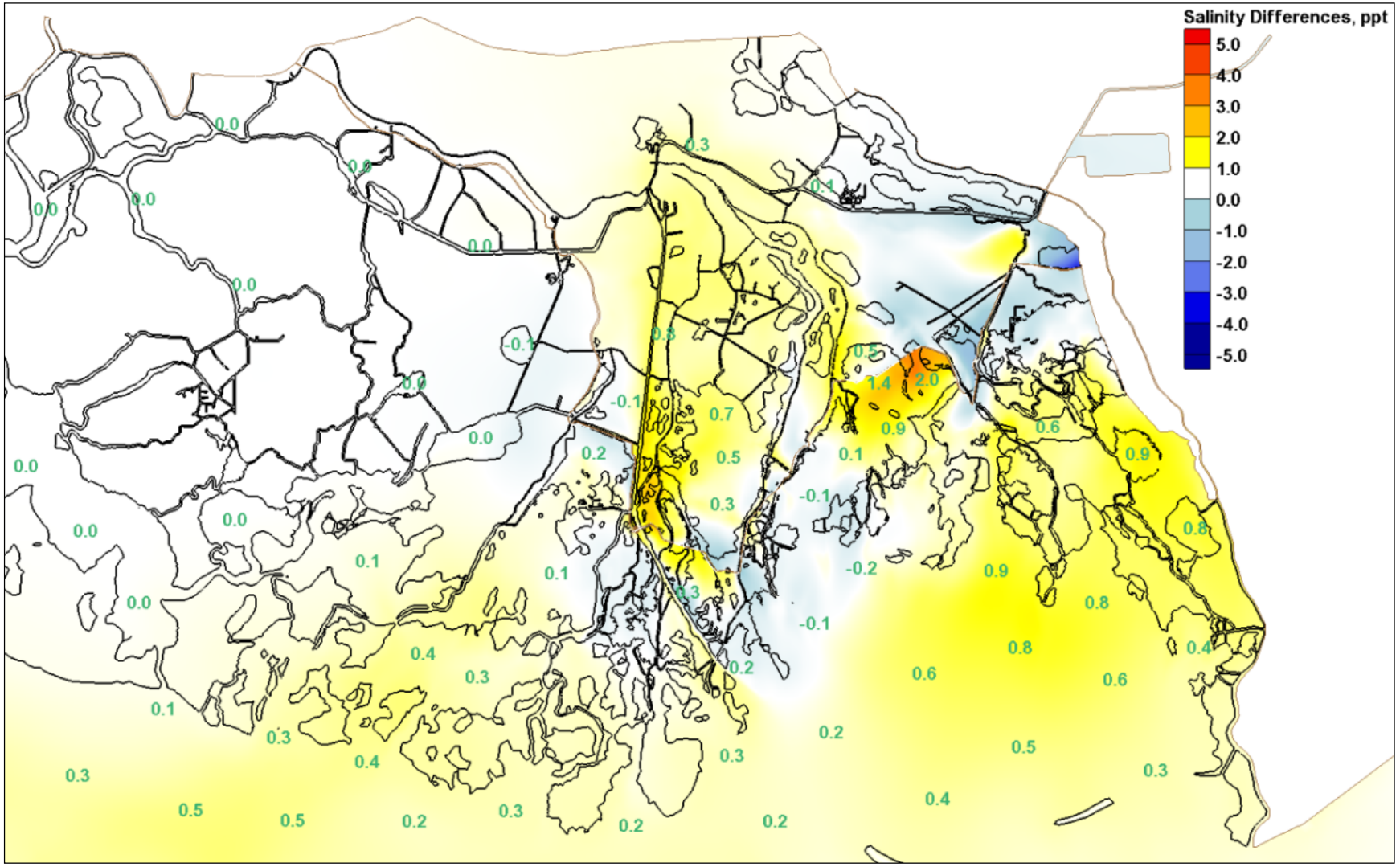

Figure 150. Plan 3 salinities for the sea-level rise 1 scenario (0.738 m) for the growing season (March 1 to November 30).

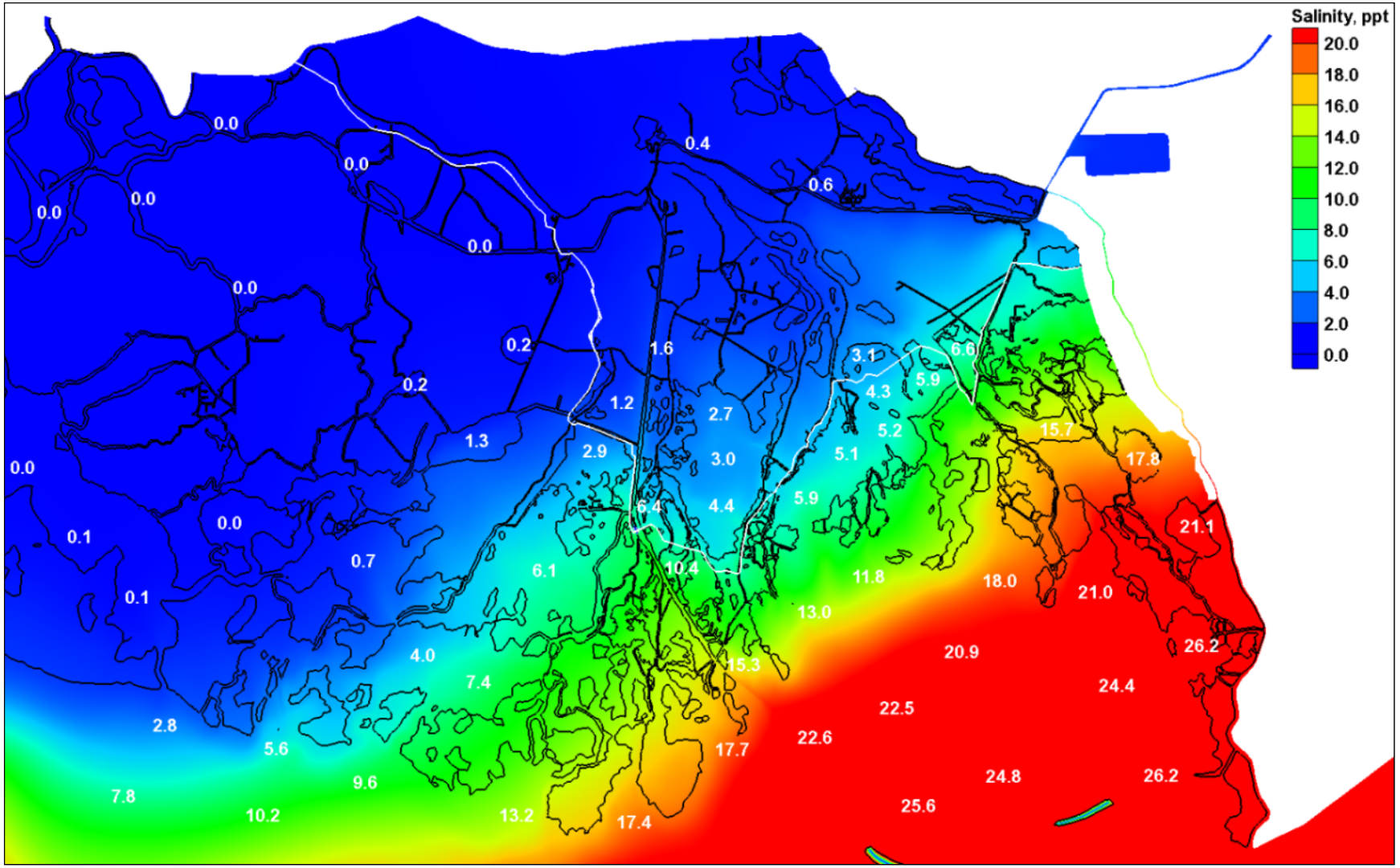

Figure 151. Plan 3 minus base configuration salinity differences for the sea-level rise 1 scenario (0.738 m) for the growing season (March 1 to November 30).

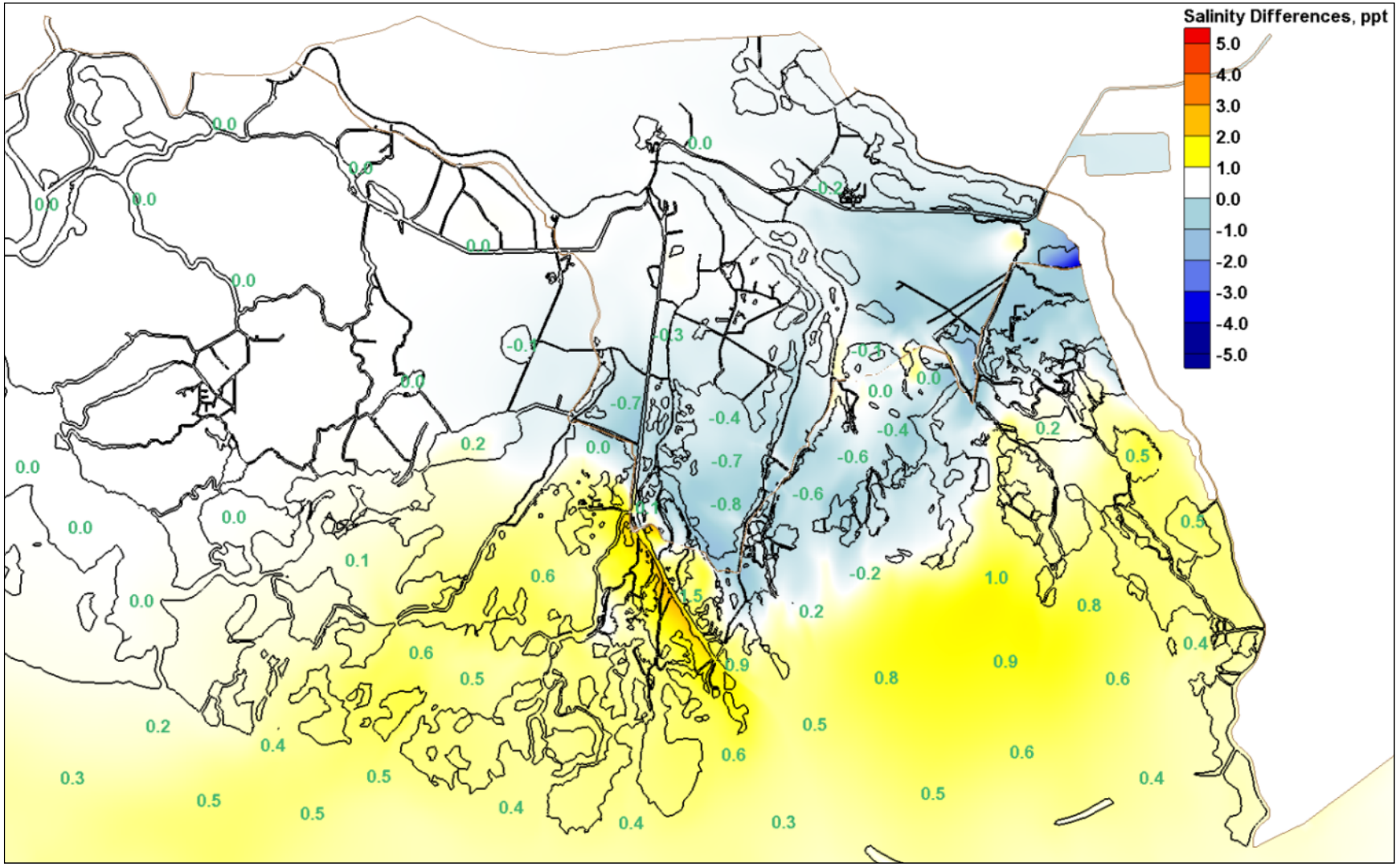

Figure 152. Base configuration salinities for the sea-level rise 2 scenario (1.45 m) for the growing season (March 1 to November 30).

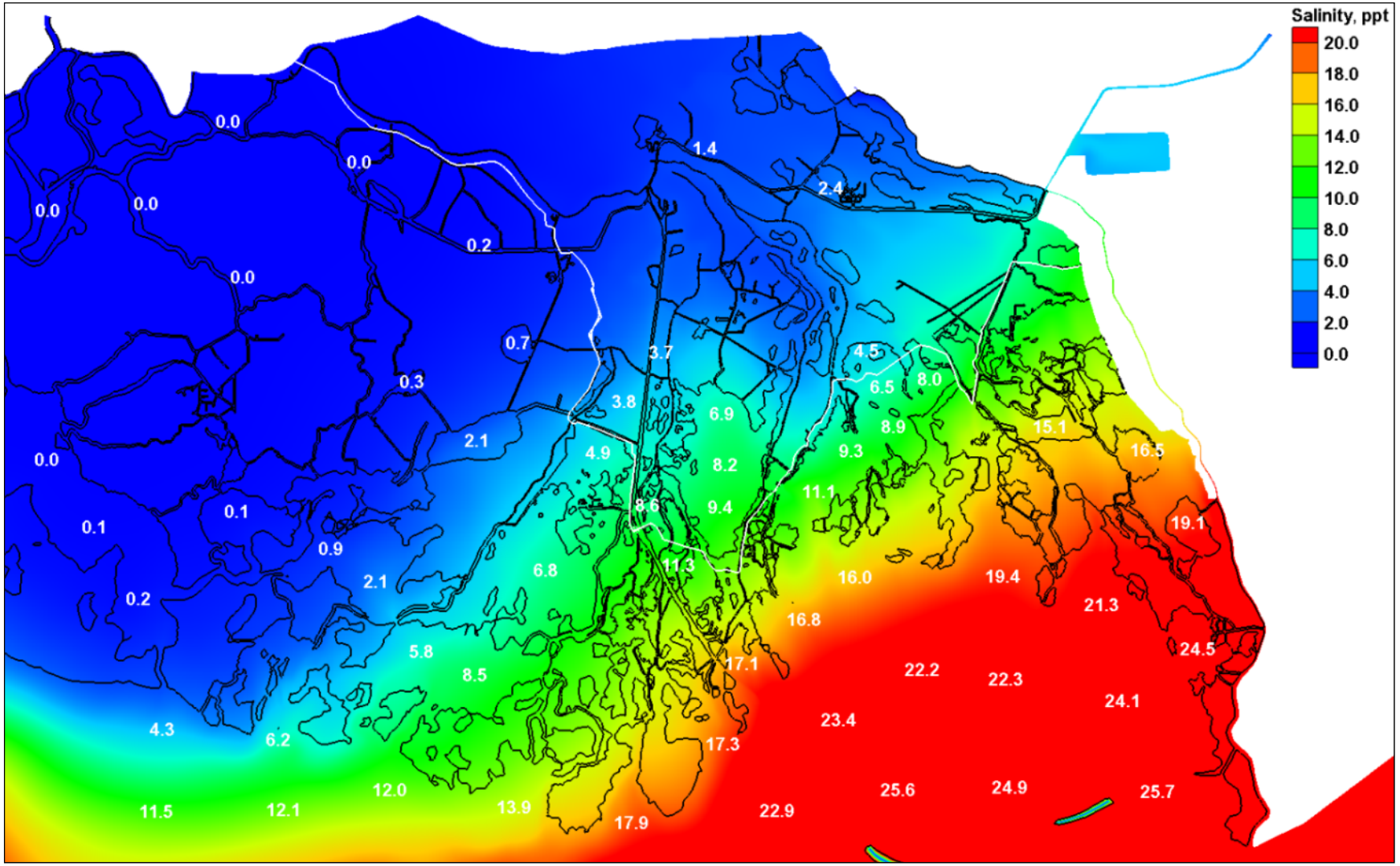

Figure 153. Plan 1 salinities for the sea-level rise 2 scenario (1.45 m) for the growing season (March 1 to November 30).

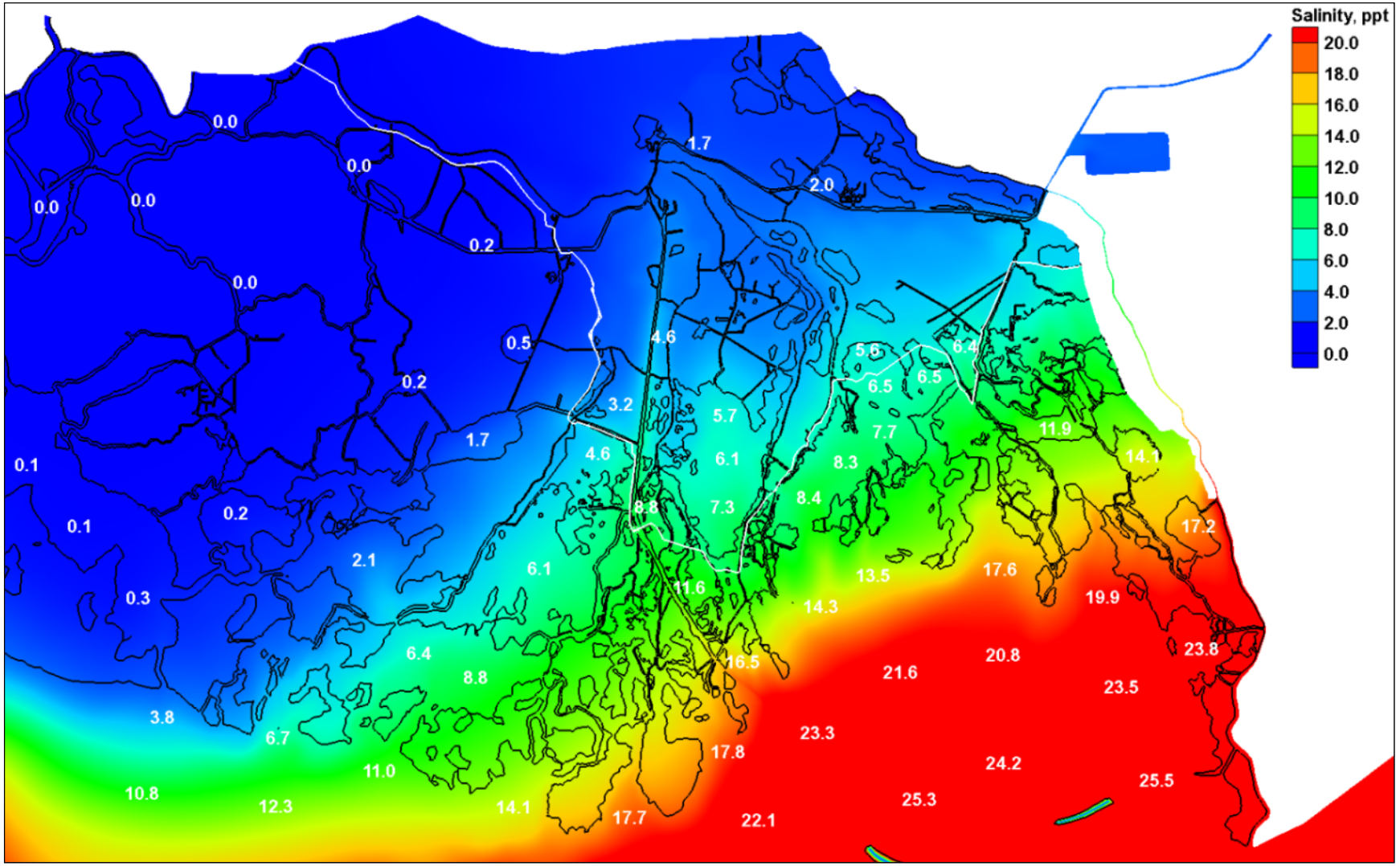

Figure 154. Plan 1 minus base configuration salinity differences for the sea-level rise 2 scenario (1.45 m) for the growing season (March 1 to November 30).

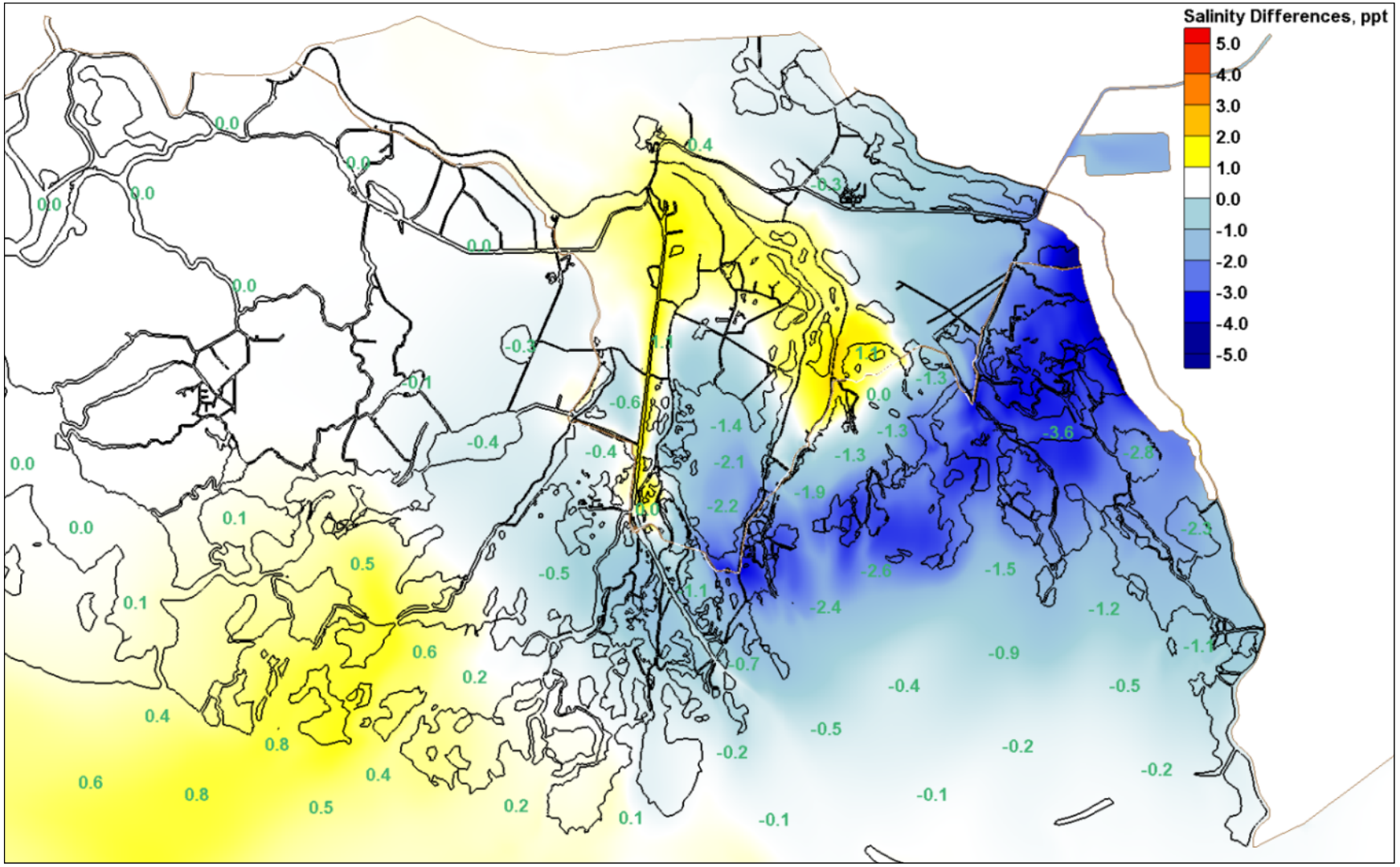

Figure 155. Plan 2 salinities for the sea-level rise 2 scenario (1.45 m) for the growing season (March 1 to November 30).

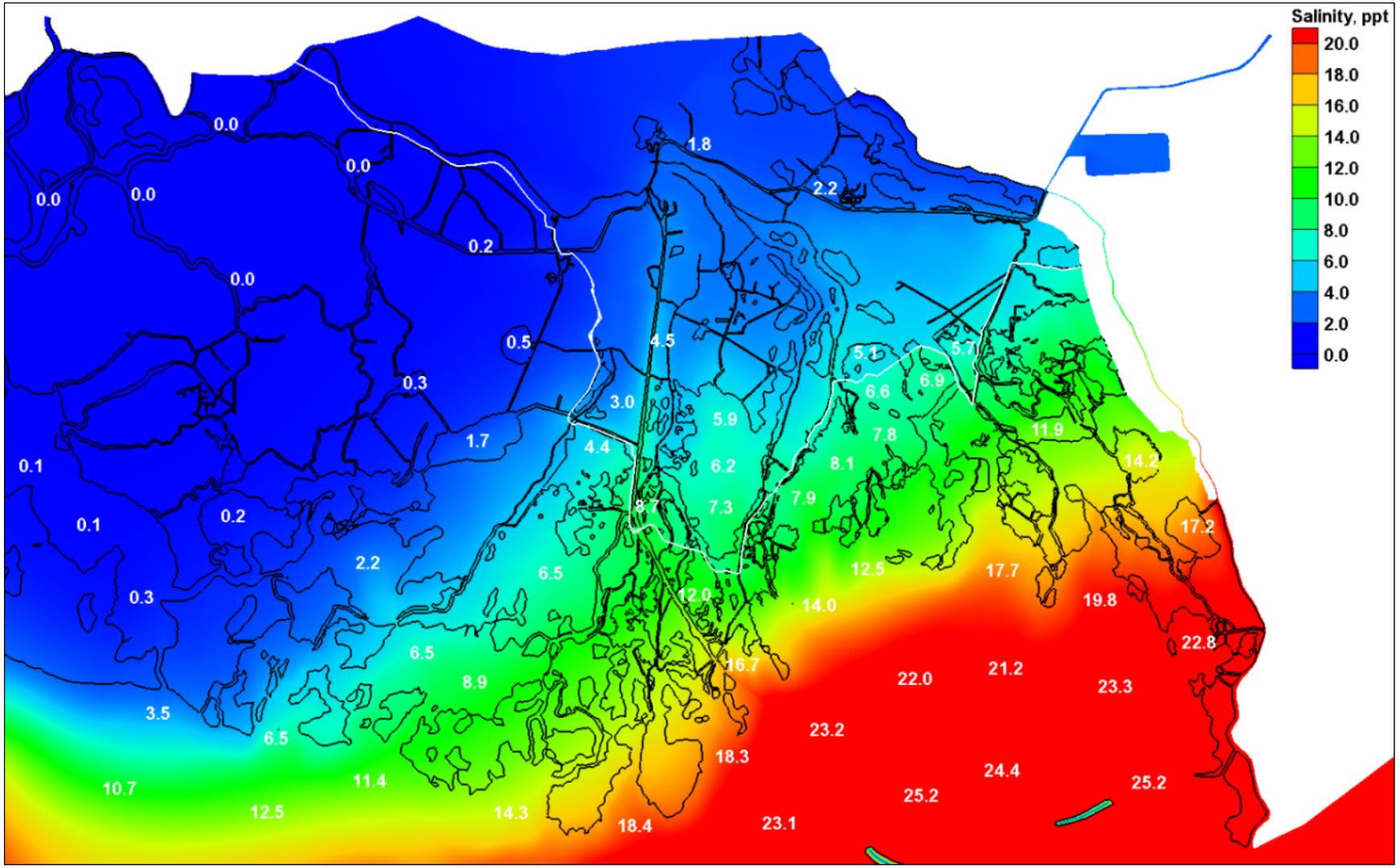

Figure 156. Plan 2 minus base configuration salinity differences for the sea-level rise 2 scenario (1.45 m) for the growing season (March 1 to November 30).

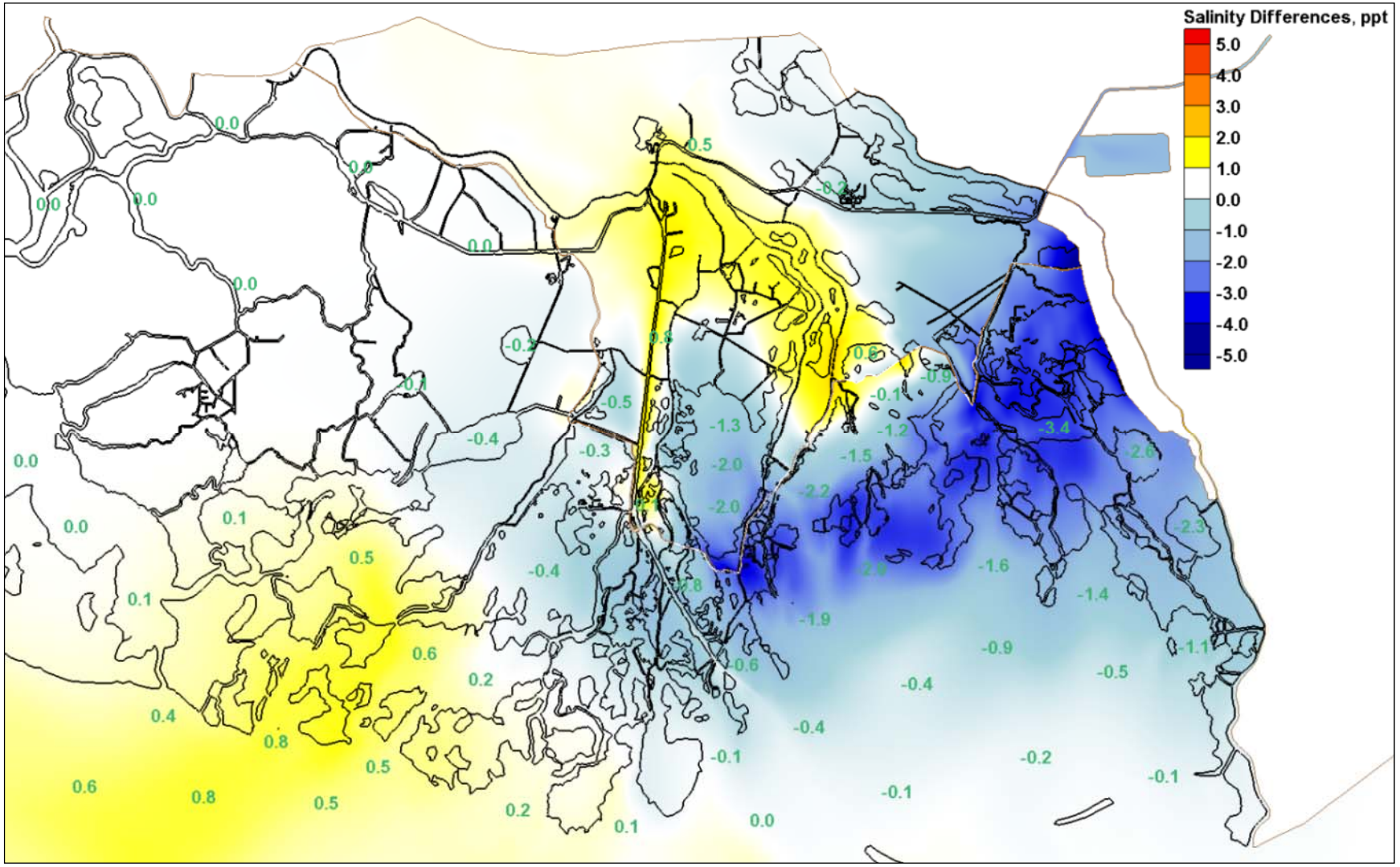

Figure 157. Plan 3 salinities for the sea-level rise 2 scenario (1.45 m) for the growing season (March 1 to November 30).

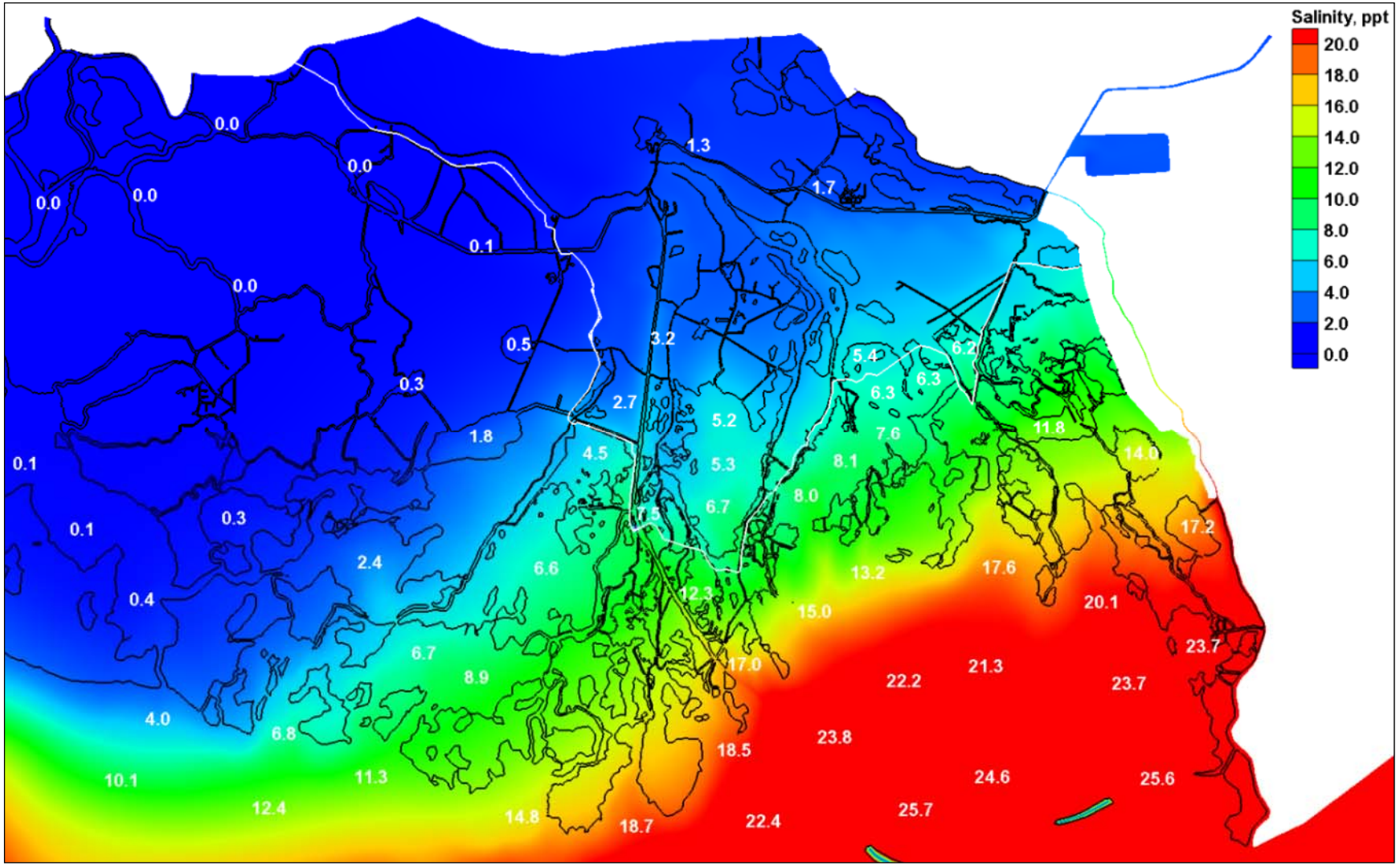

Figure 158. Plan 3 minus baseline salinity differences for the sea-level rise 2 scenario (1.45 m) for the growing season (March 1 to November 30).

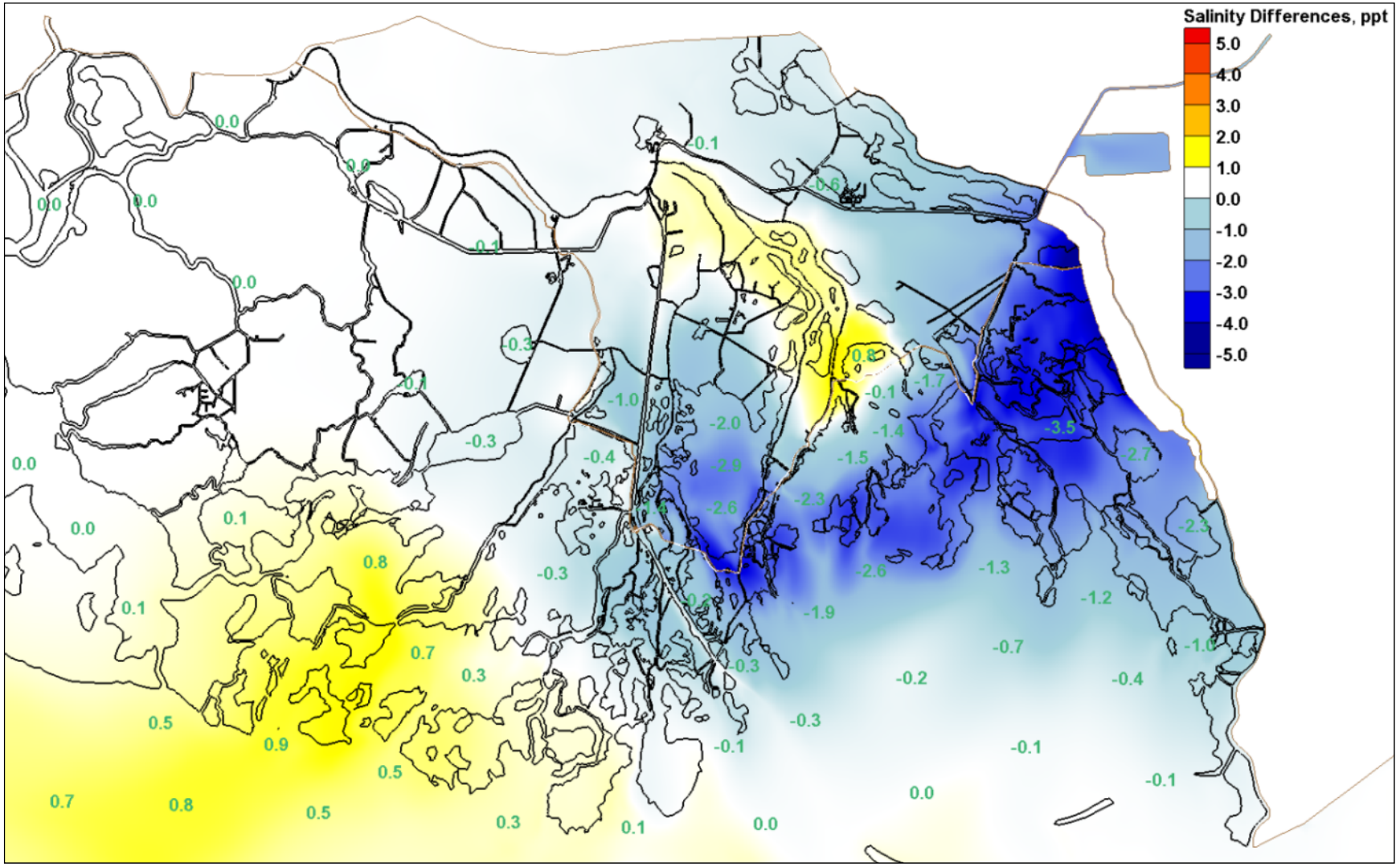

Figure 159. Base configuration yearly averaged salinity values for the existing sea level.

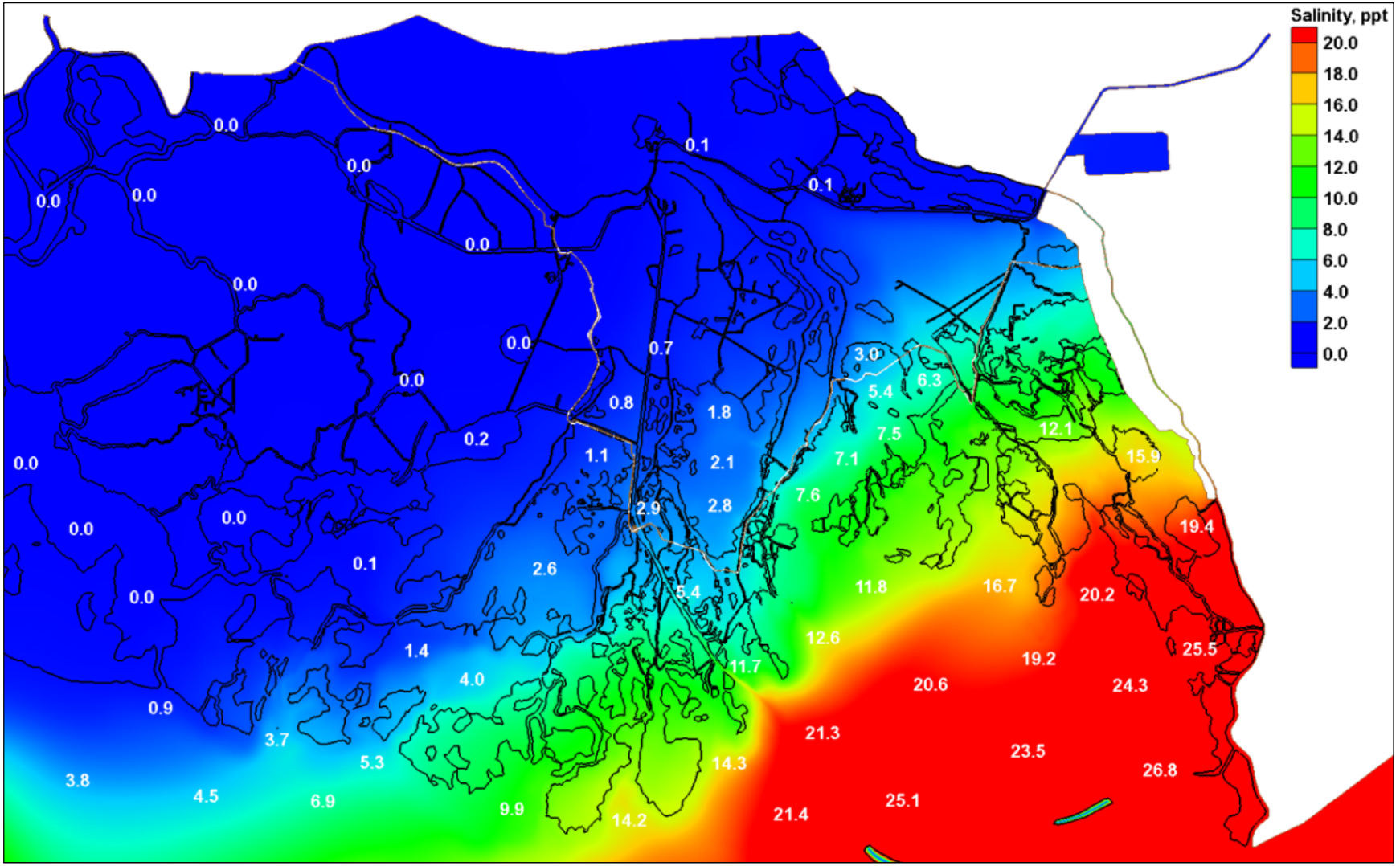

Figure 160. Plan 1 yearly averaged salinity values for the existing sea level.

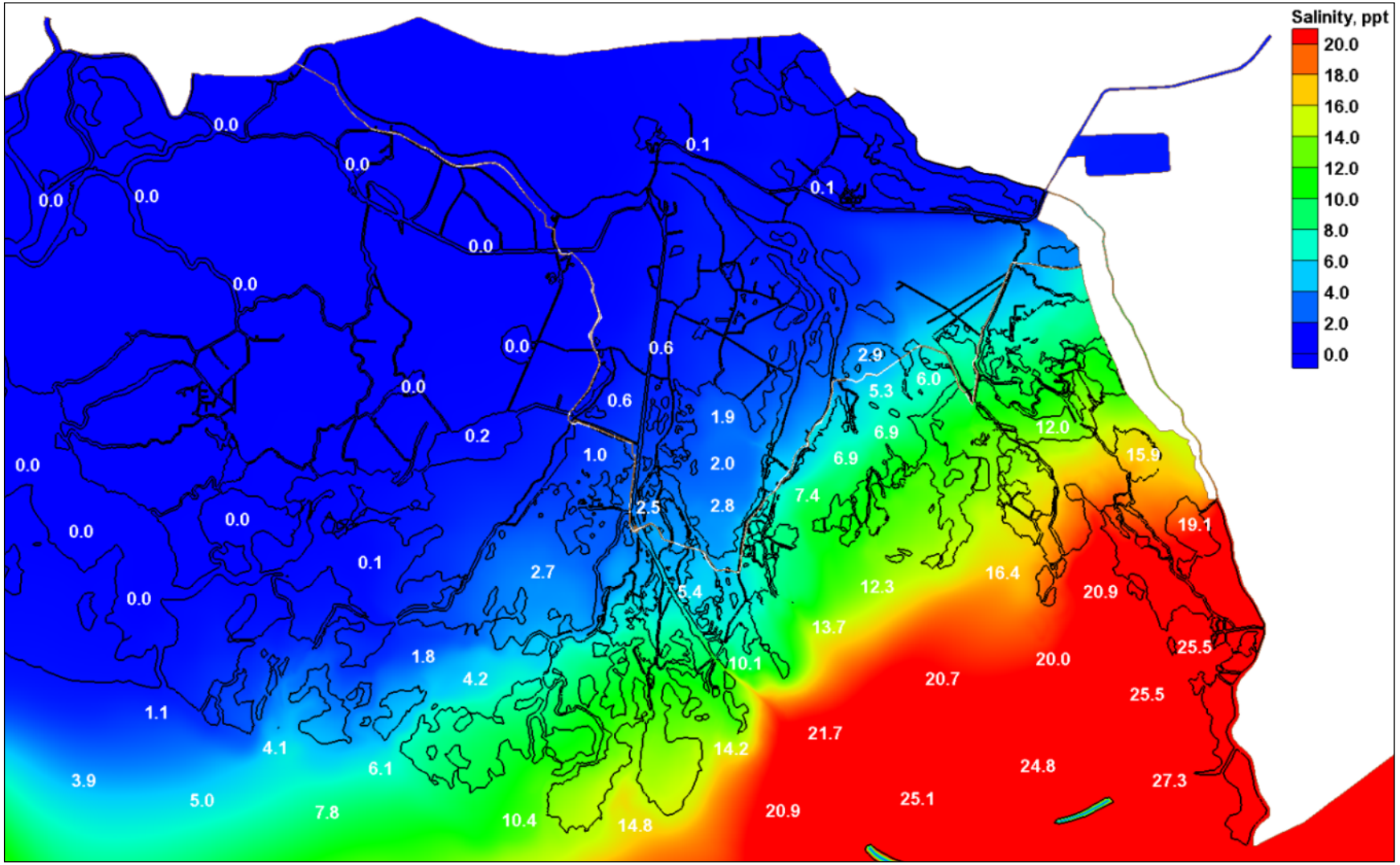

Figure 161. Plan 1 minus base configuration (yearly averaged salinities) differences for the existing sea level.

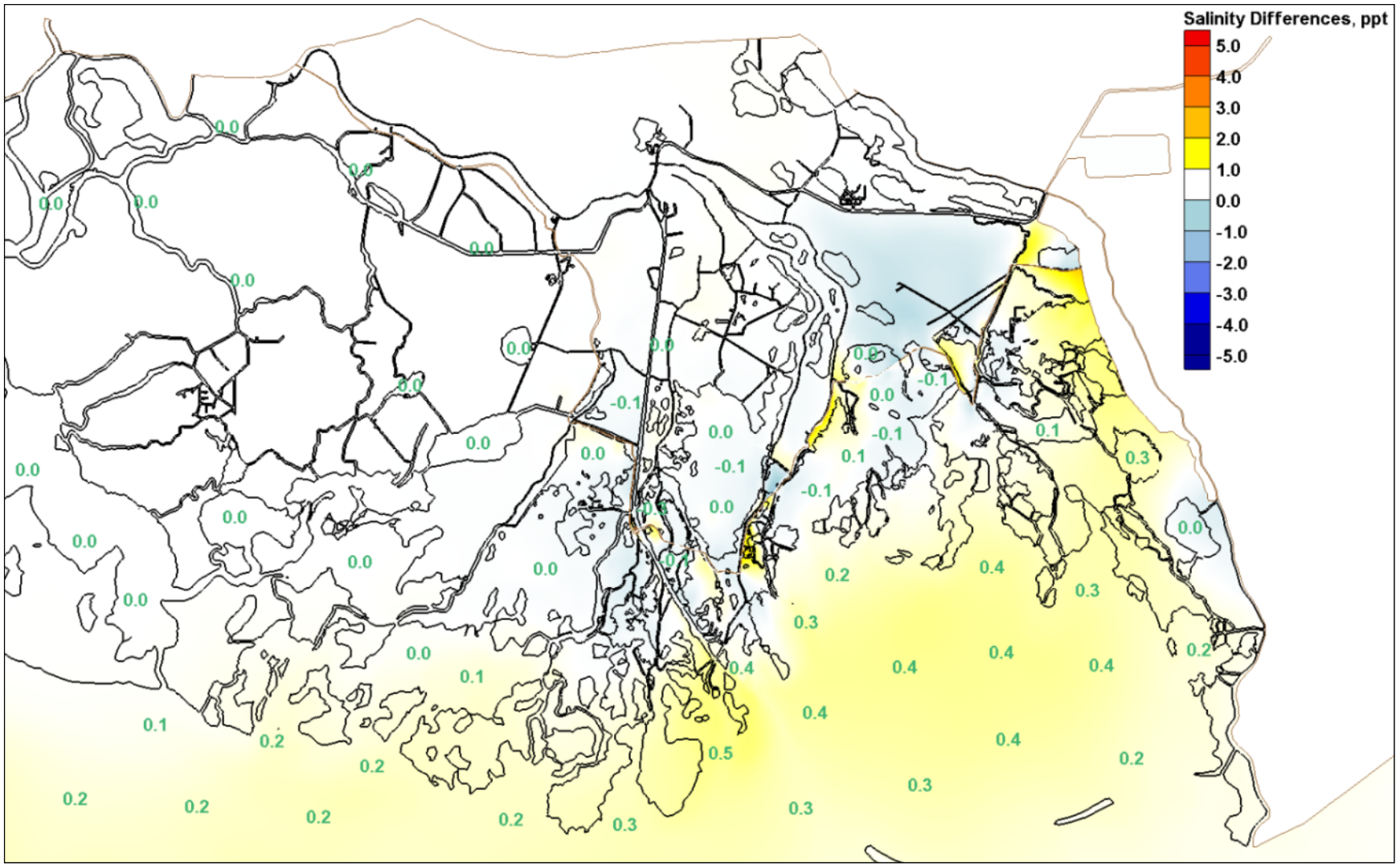

Figure 162. Plan 2 yearly averaged salinity values for the existing sea level.

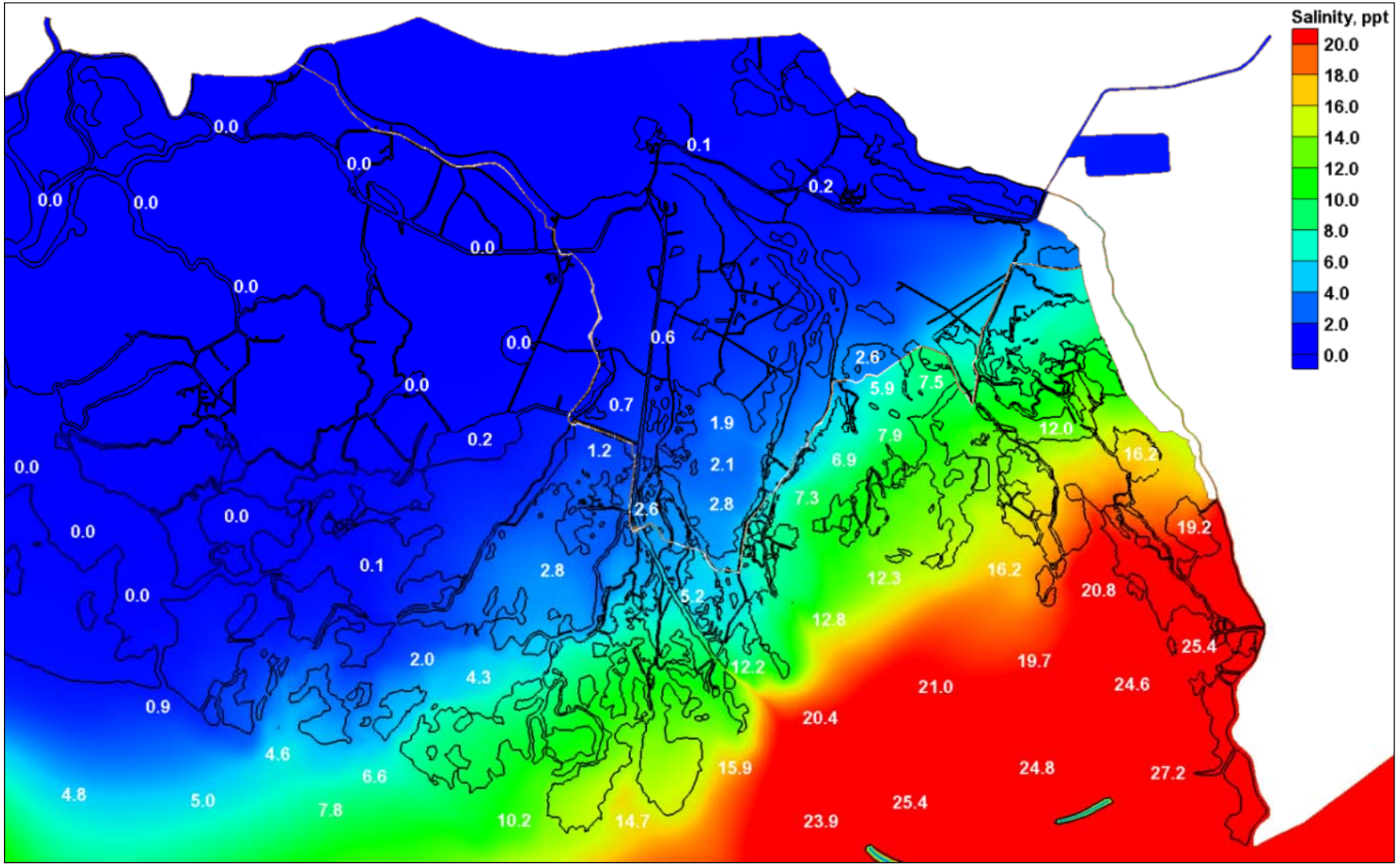

Figure 163. Plan 2 minus without project (yearly averaged salinities) differences for the existing sea level.

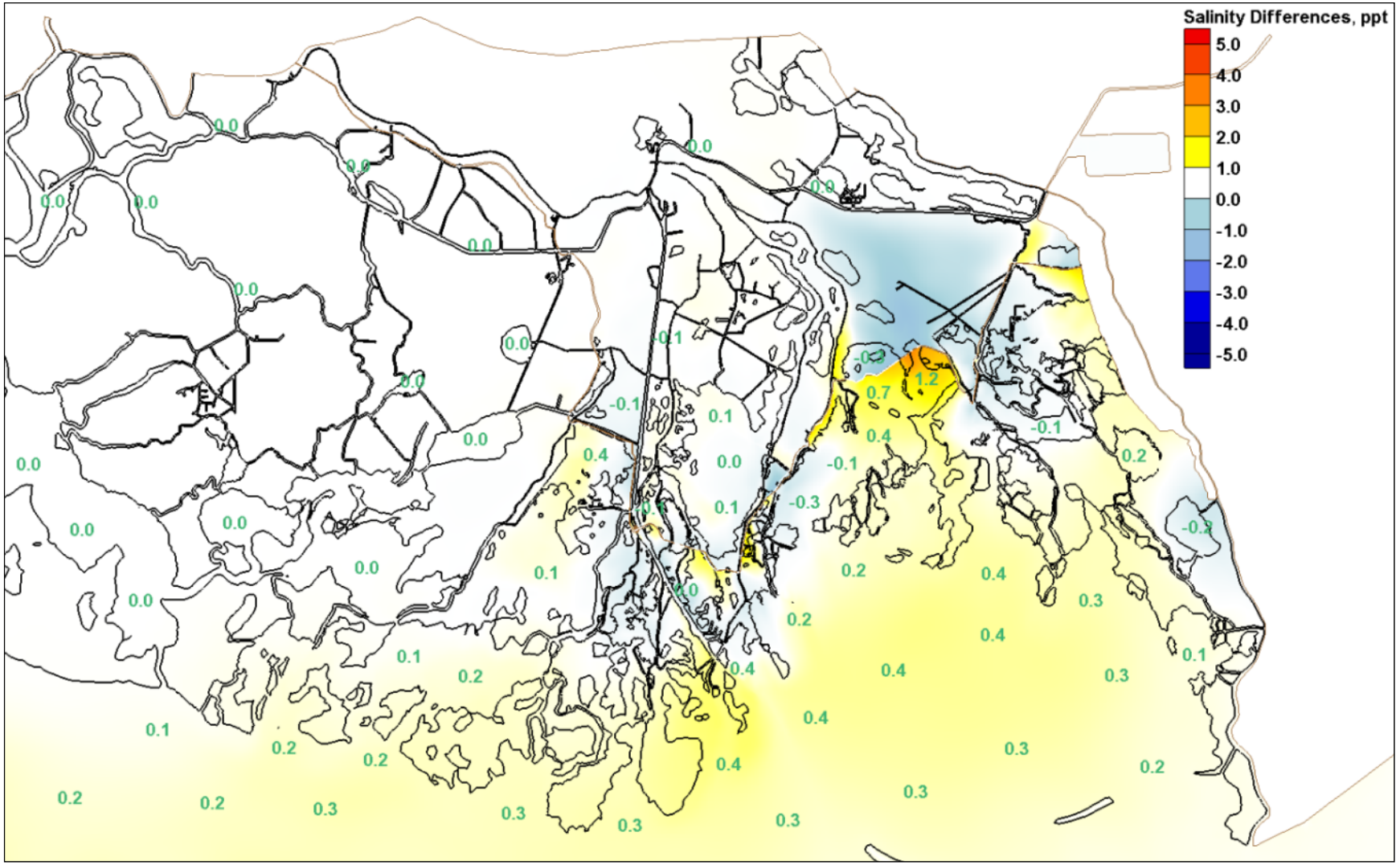

Figure 164. Plan 3 yearly averaged salinity values for the existing sea level.

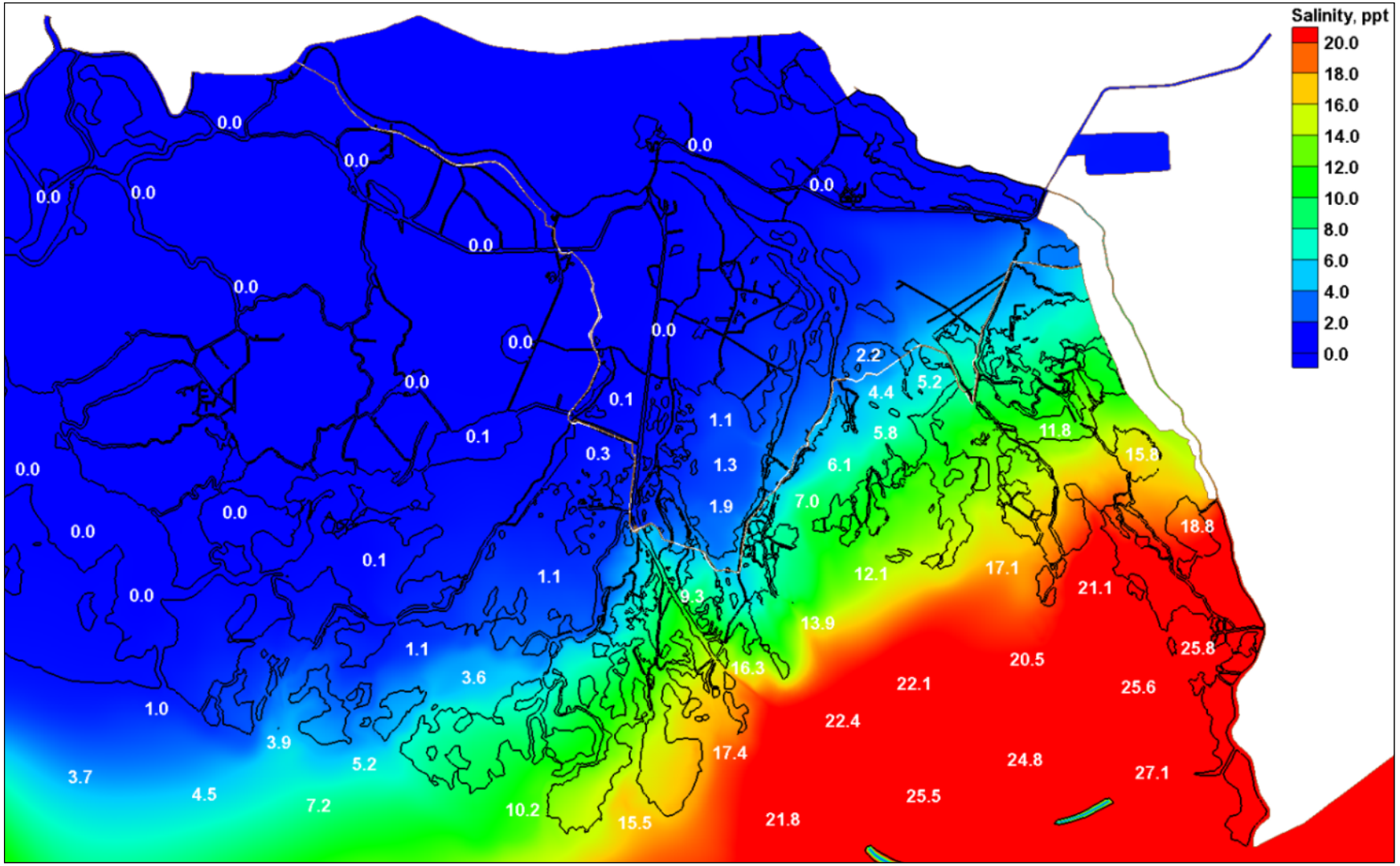

Figure 165. Plan 3 minus base configuration (yearly averaged salinities) differences for the existing sea level.

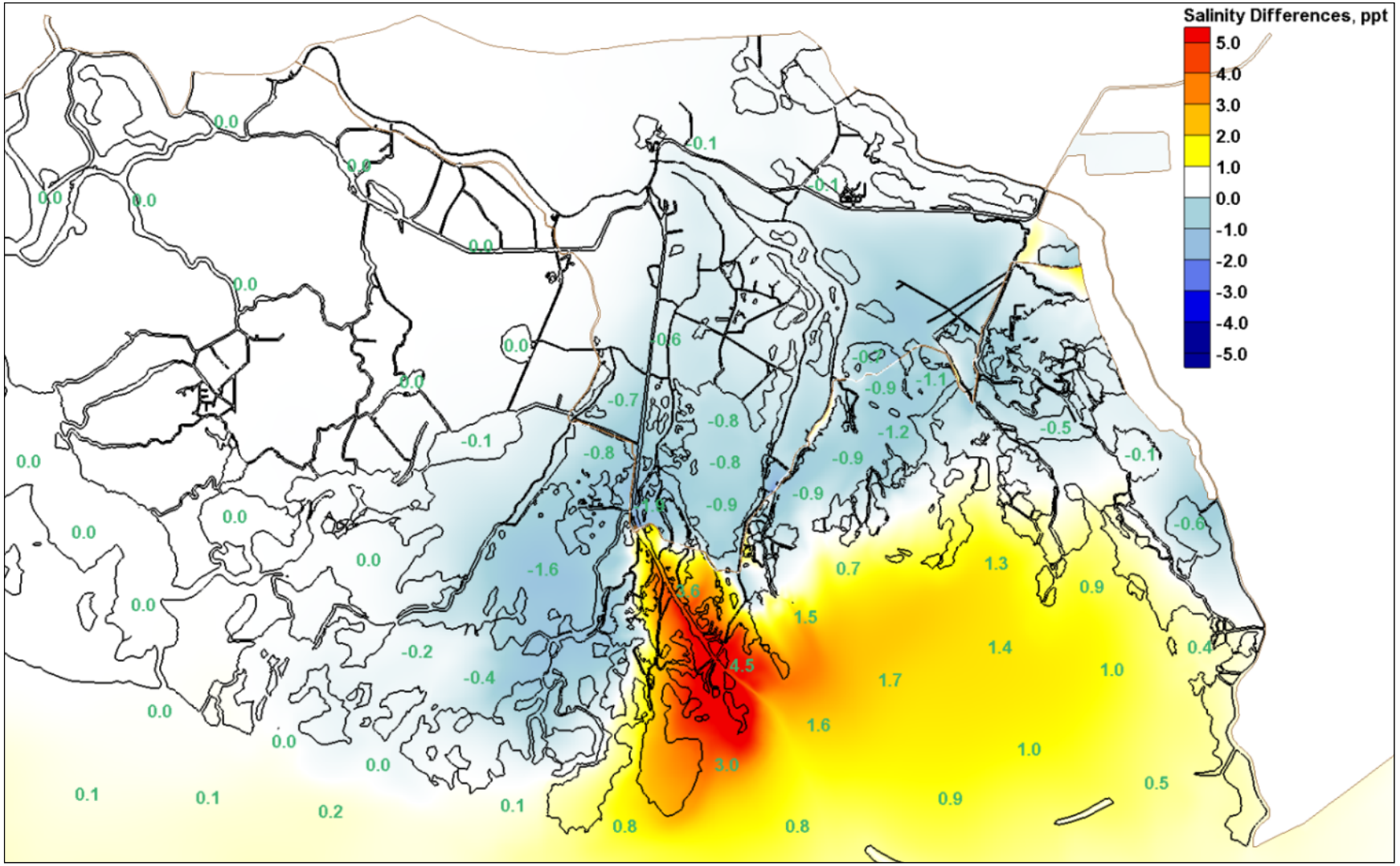

Figure 166. Base configuration yearly averaged salinity values for the sea-level rise 1 scenario (0.738 m).

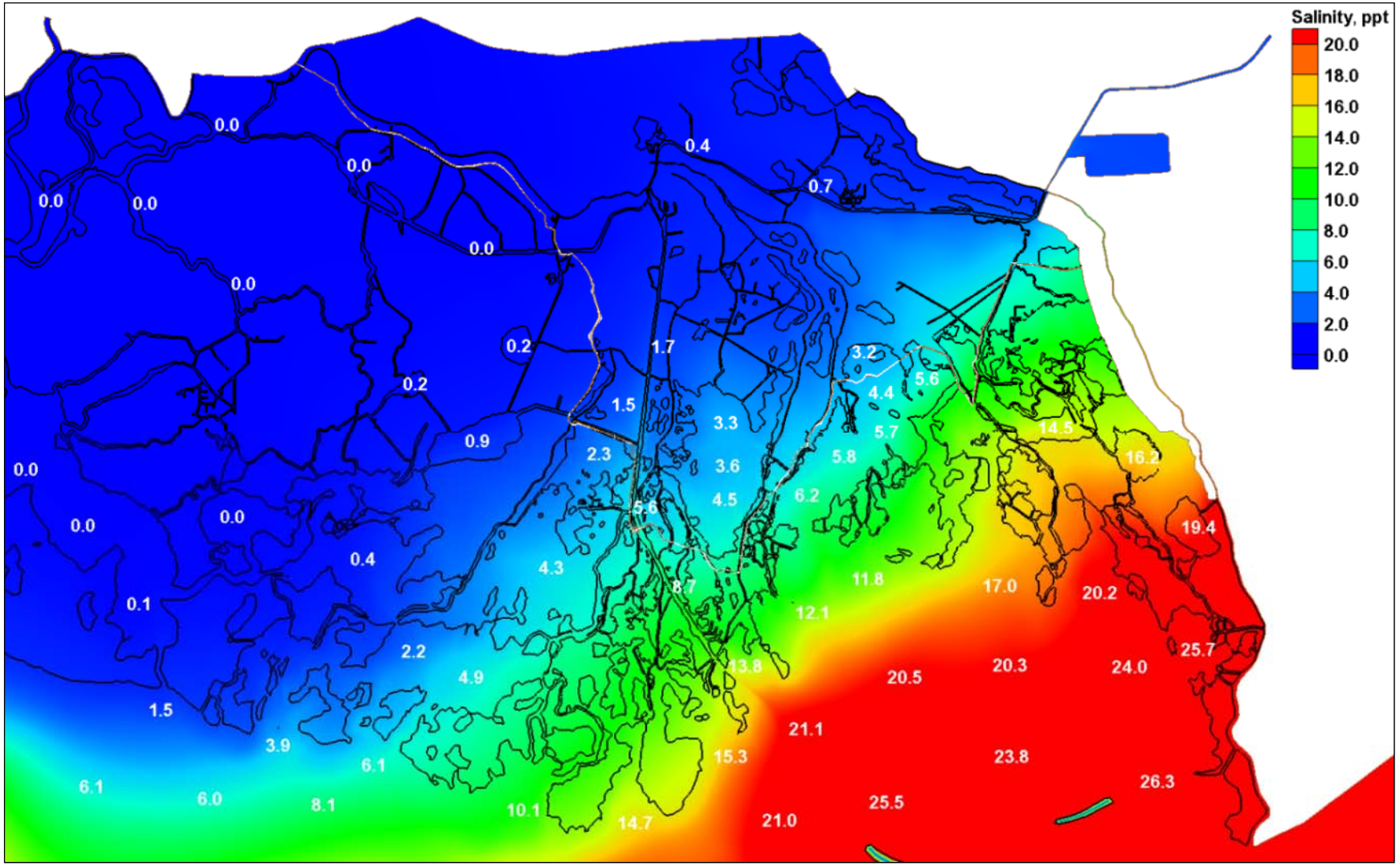

Figure 167. Plan 1 yearly averaged salinity values for the sea-level rise 1 scenario (0.738 m).

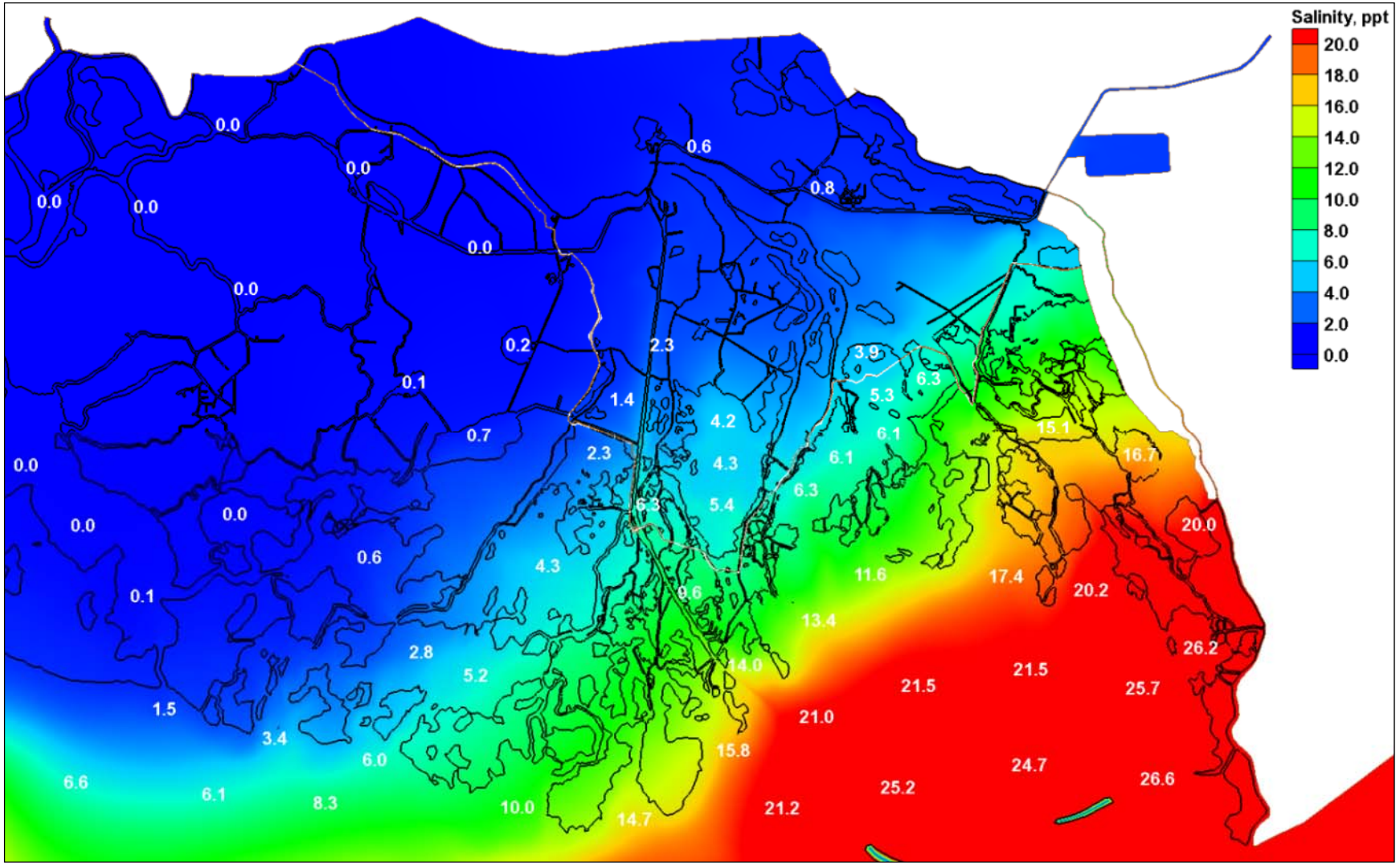

Figure 168. Plan 1 minus base configuration (yearly averaged salinities) differences for the sea-level rise 1 scenario (0.738 m).

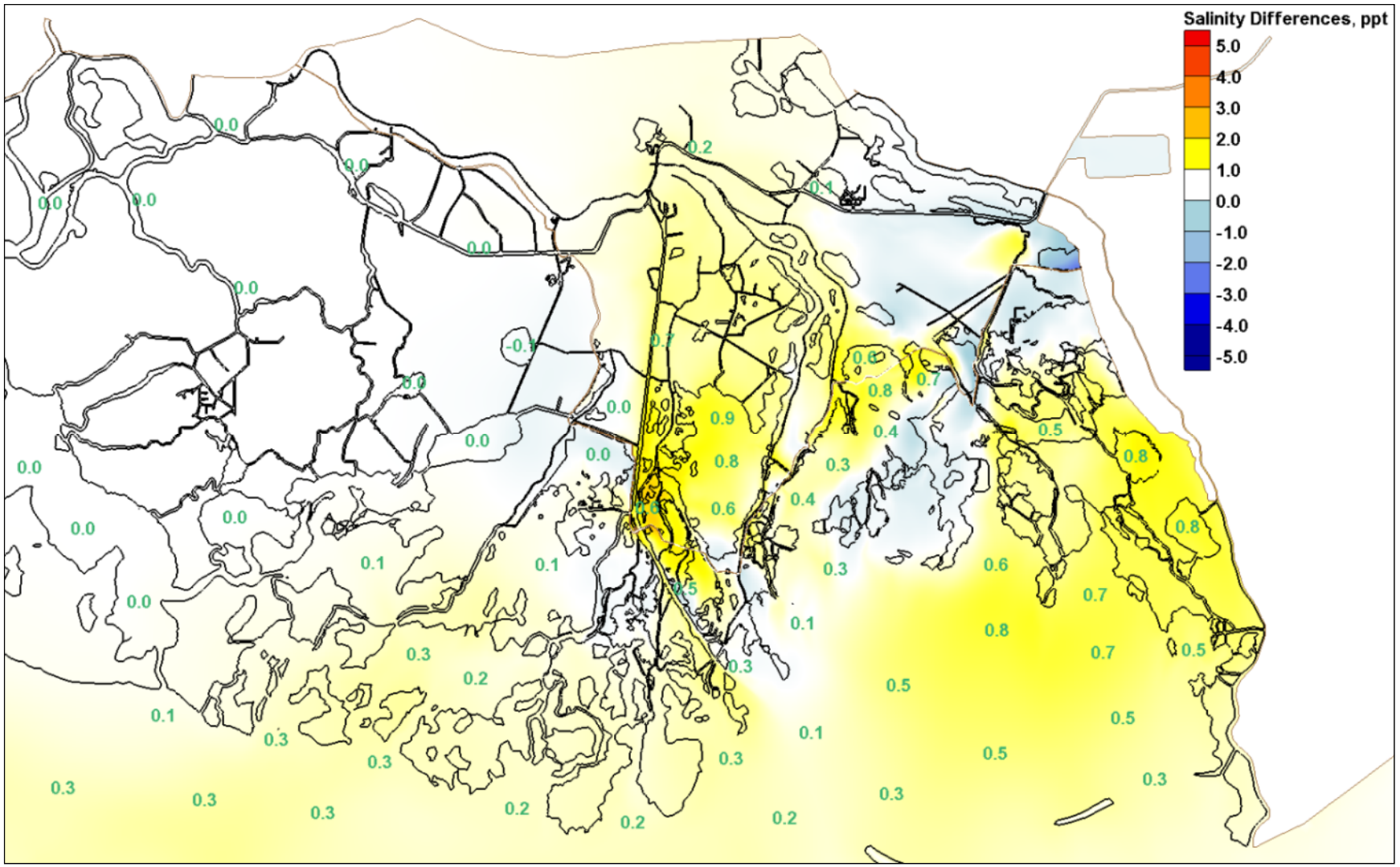

Figure 169. Plan 2 yearly averaged salinity values for the sea-level rise 1 scenario (0.738 m).

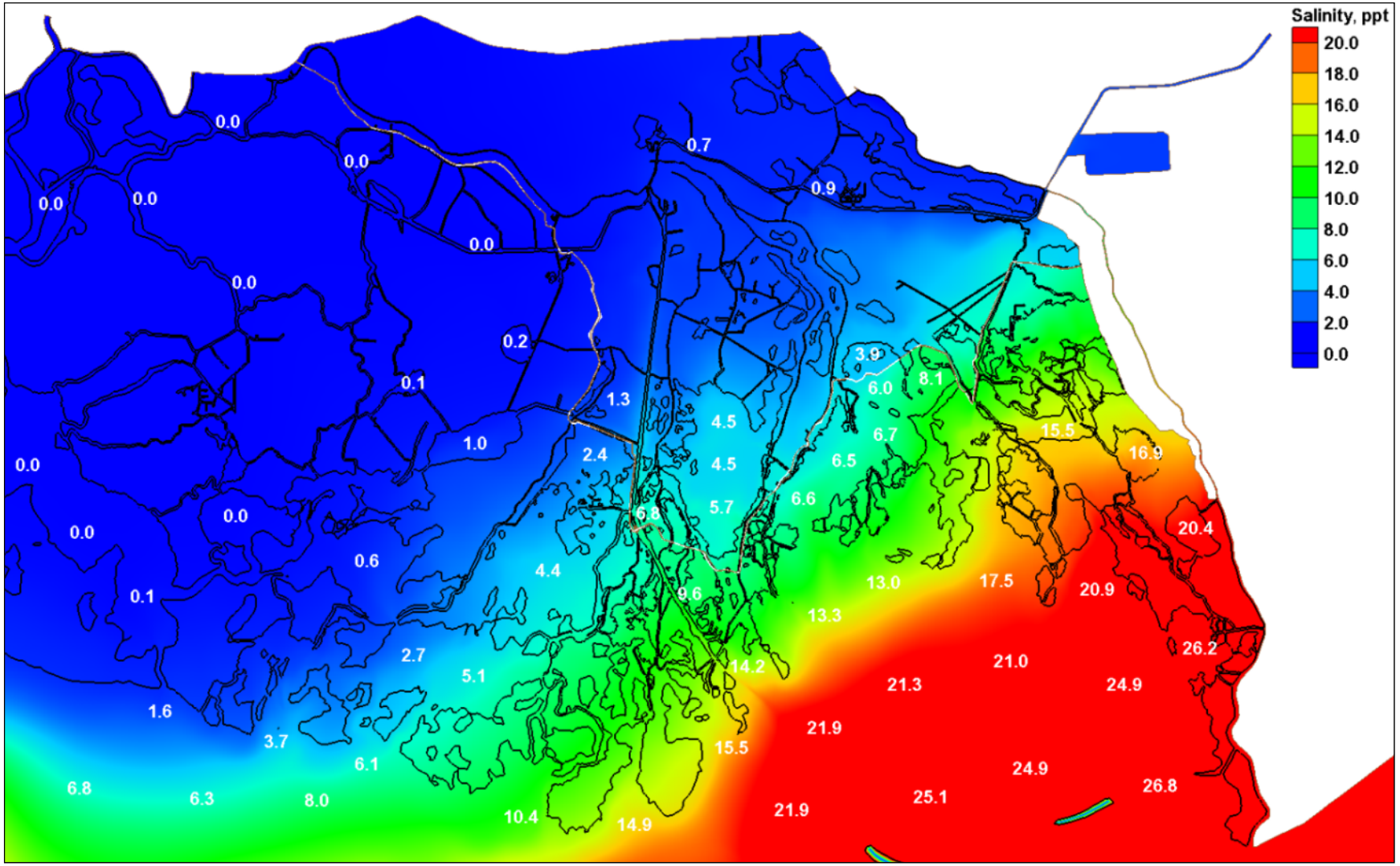

Figure 170. Plan 2 minus base configuration (yearly averaged salinities) differences for the sea-level rise 1 scenario (0.738 m).

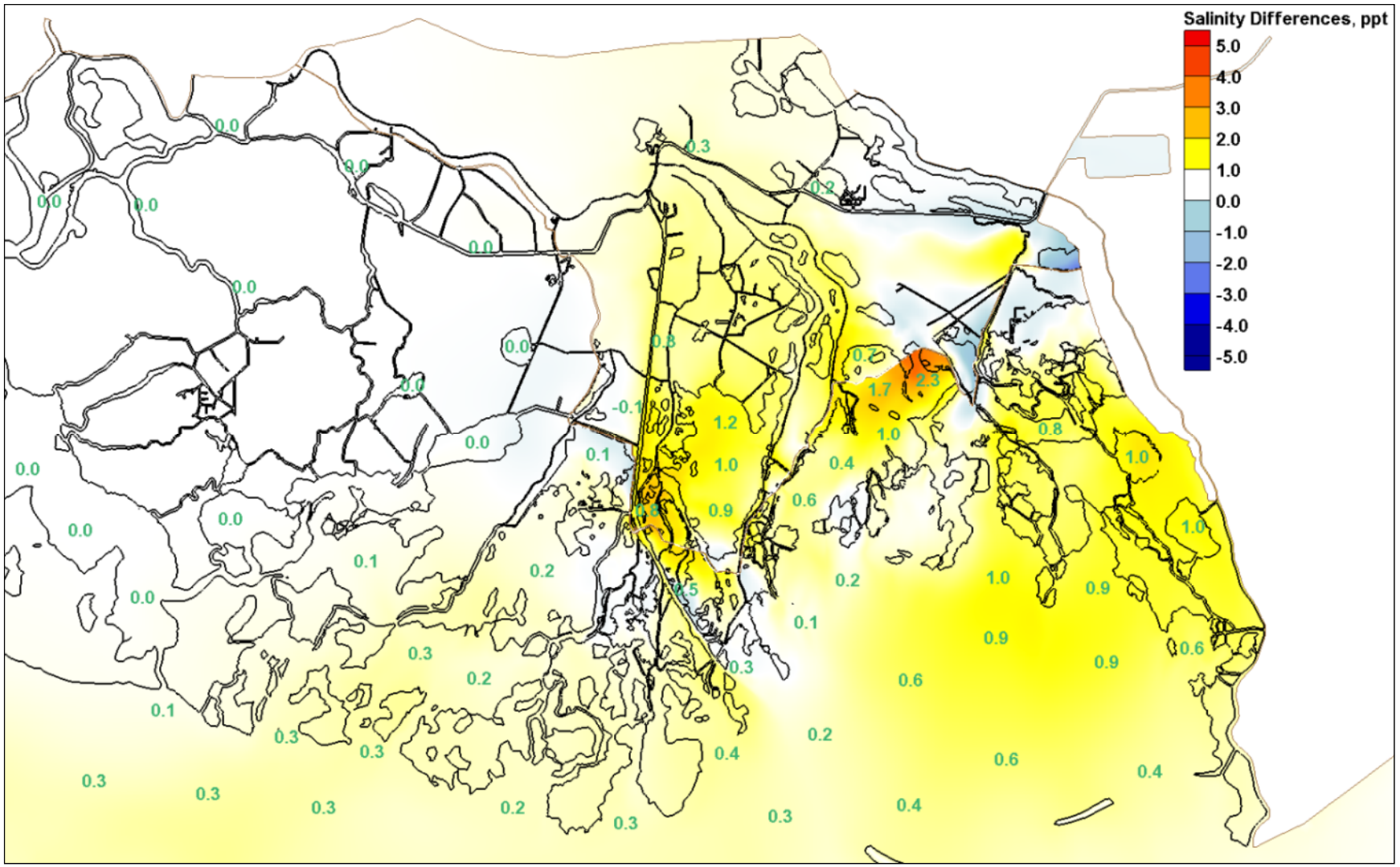

Figure 171. Plan 3 yearly averaged salinity values for the sea-level rise 1 scenario (0.738 m).

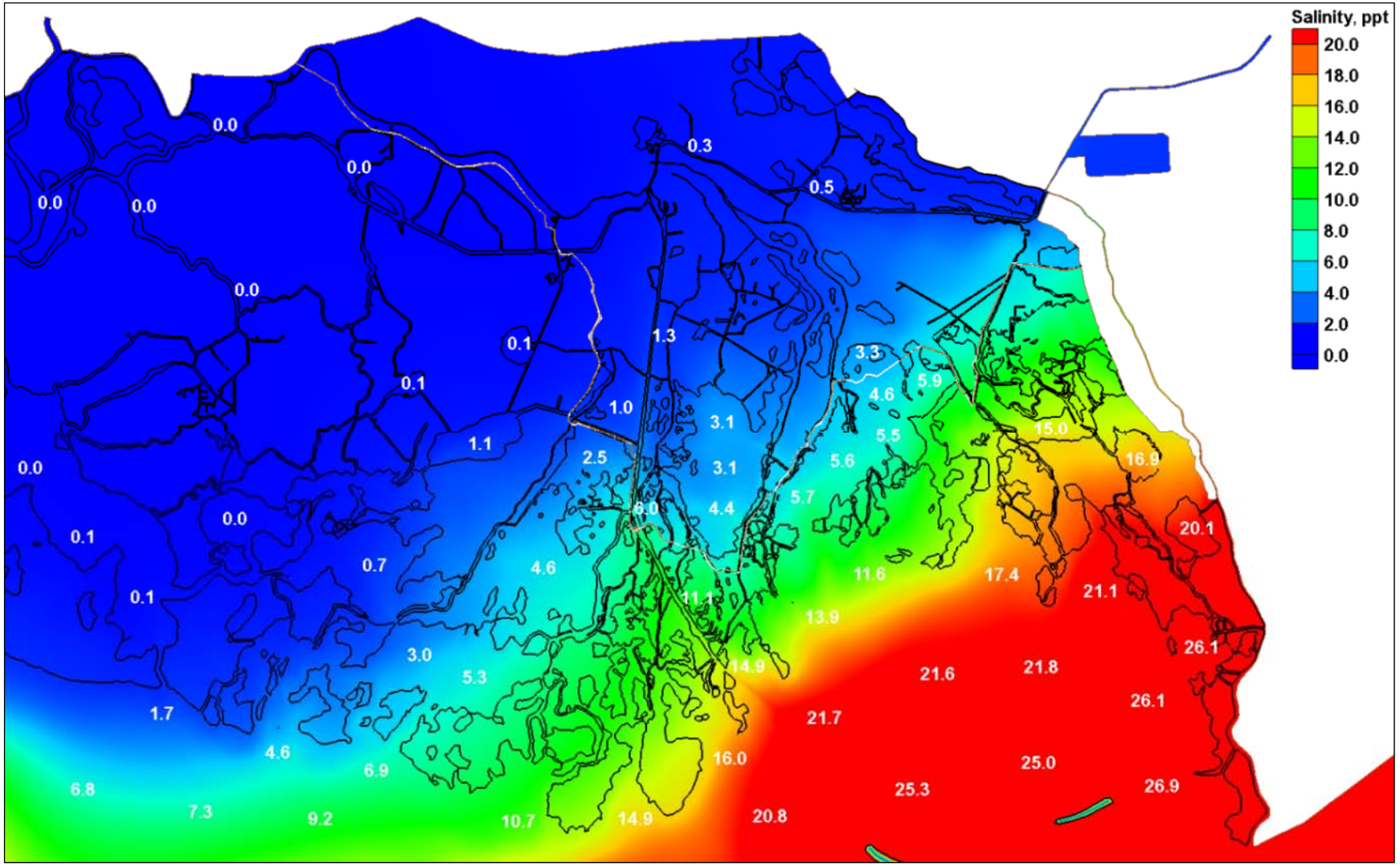

Figure 172. Plan 3 minus base configuration (yearly averaged salinities) differences for the sea-level rise 1 scenario (0.738 m).

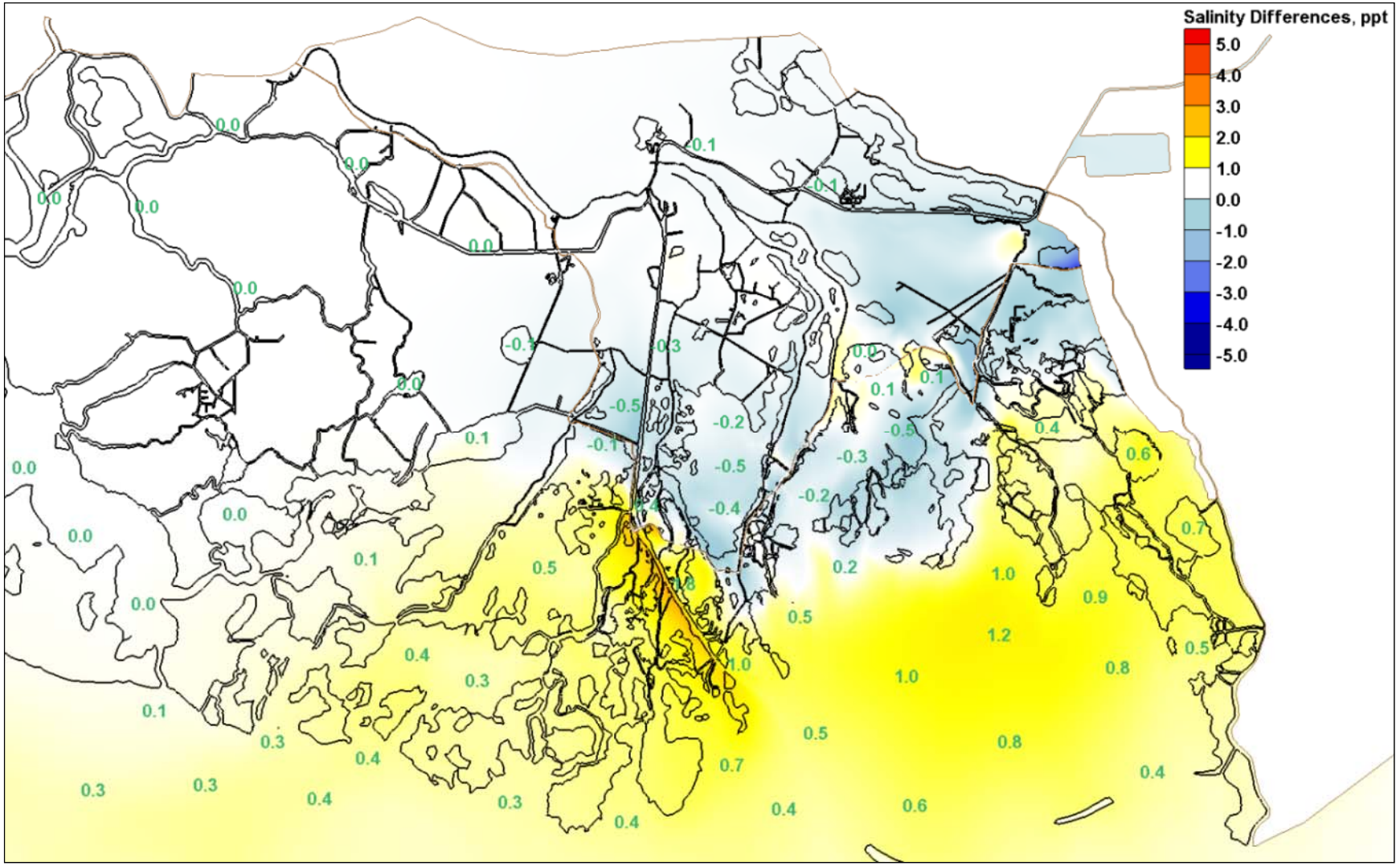

Figure 173. Base configuration yearly averaged salinity values for the sea-level rise 2 scenario (1.45 m).

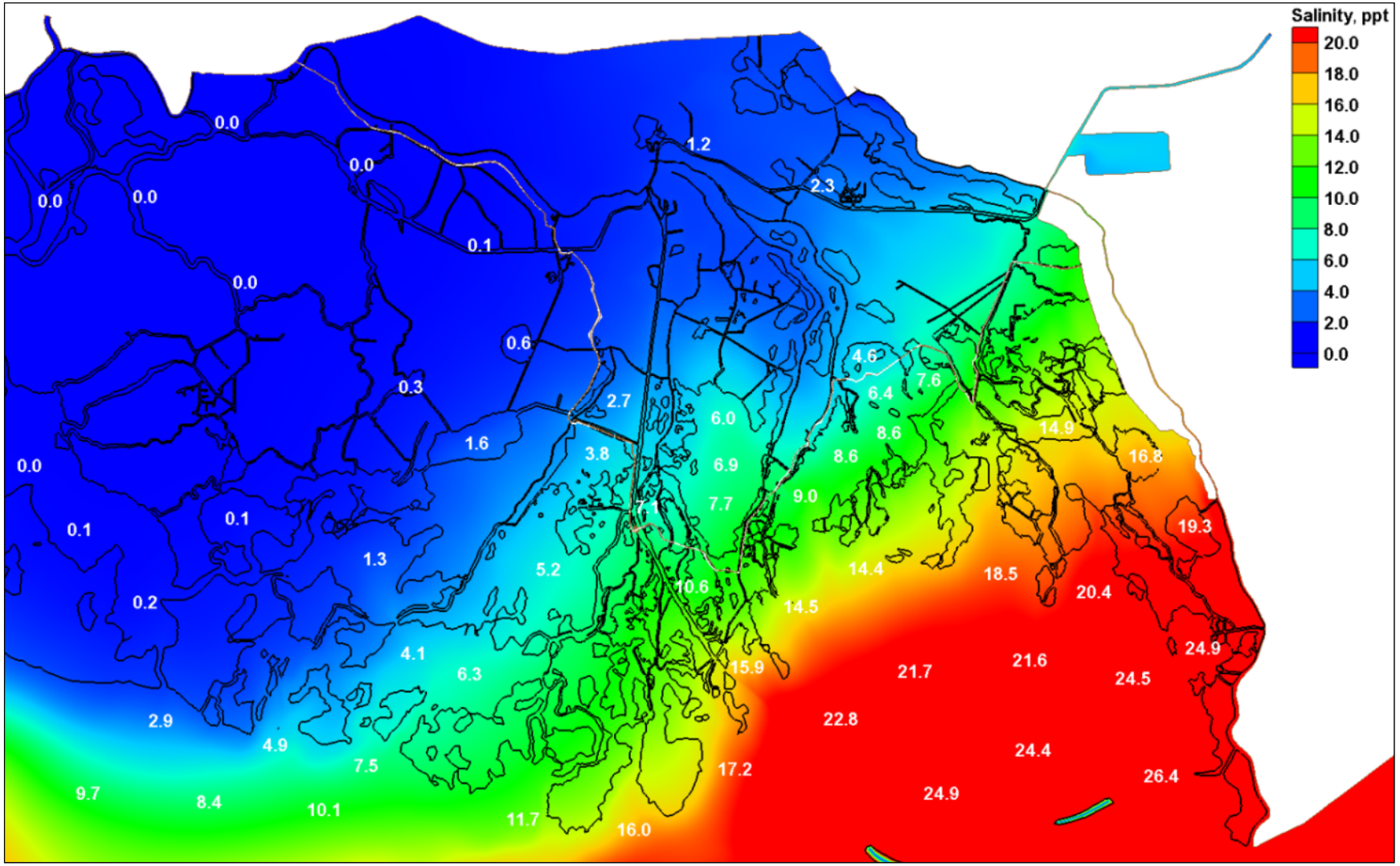

Figure 174. Plan 1 yearly averaged salinity values for the sea-level rise 2 scenario (1.45 m).

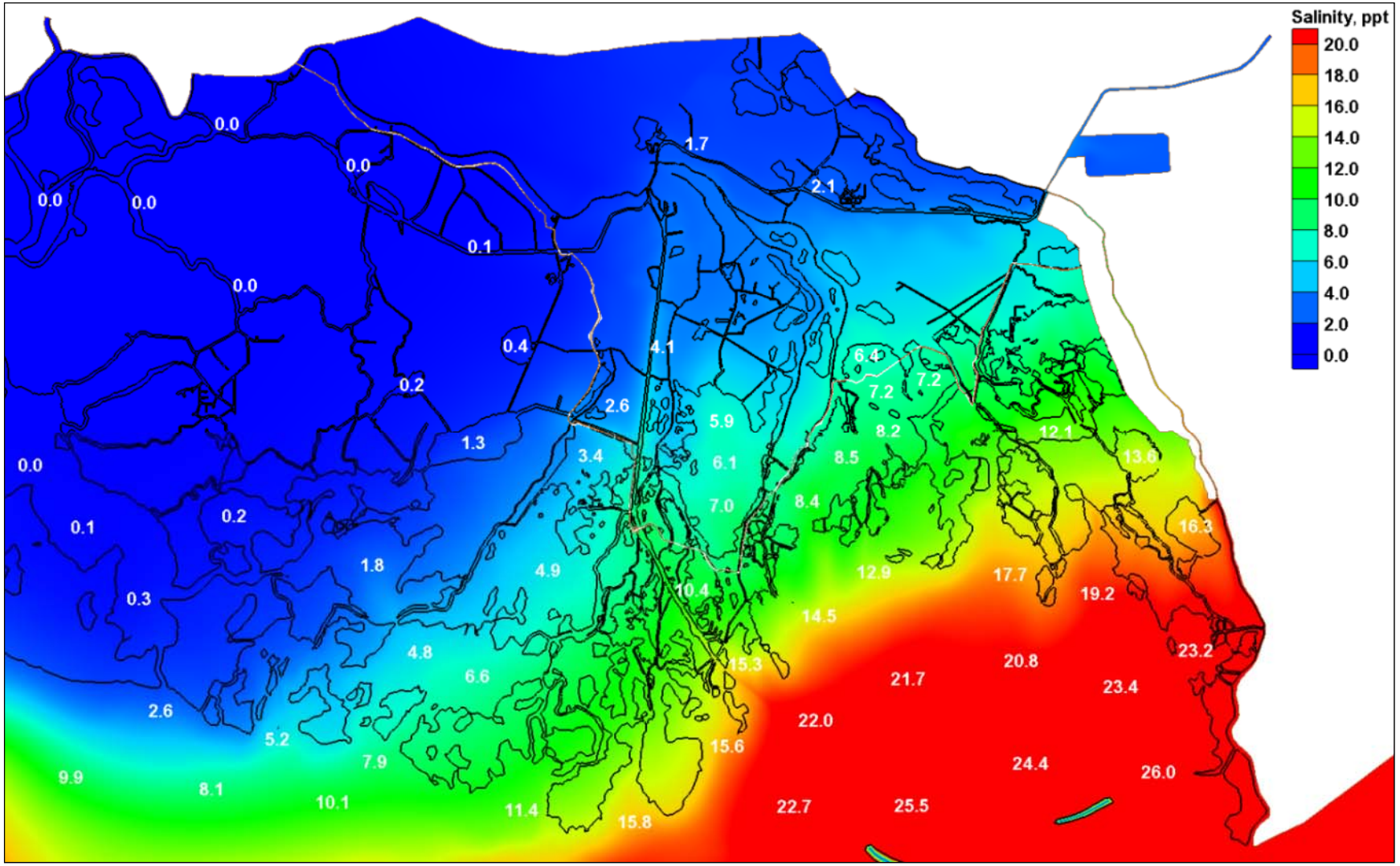

Figure 175. Plan 1 minus base configuration (yearly averaged salinities) differences for the sea-level rise 2 scenario (1.45 m).

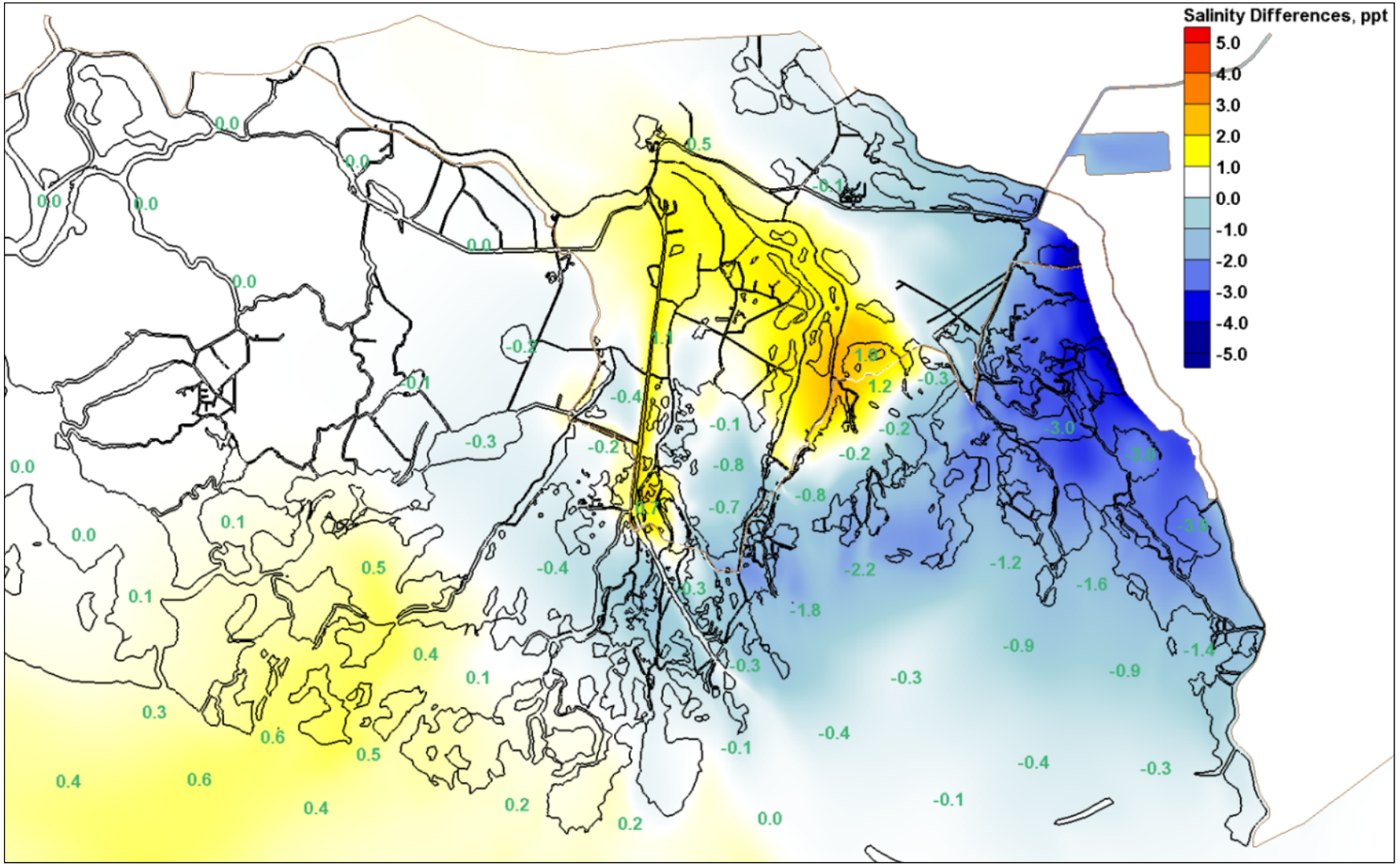

Figure 176. Plan 2 yearly averaged salinity values for the sea-level rise 2 scenario (1.45 m).

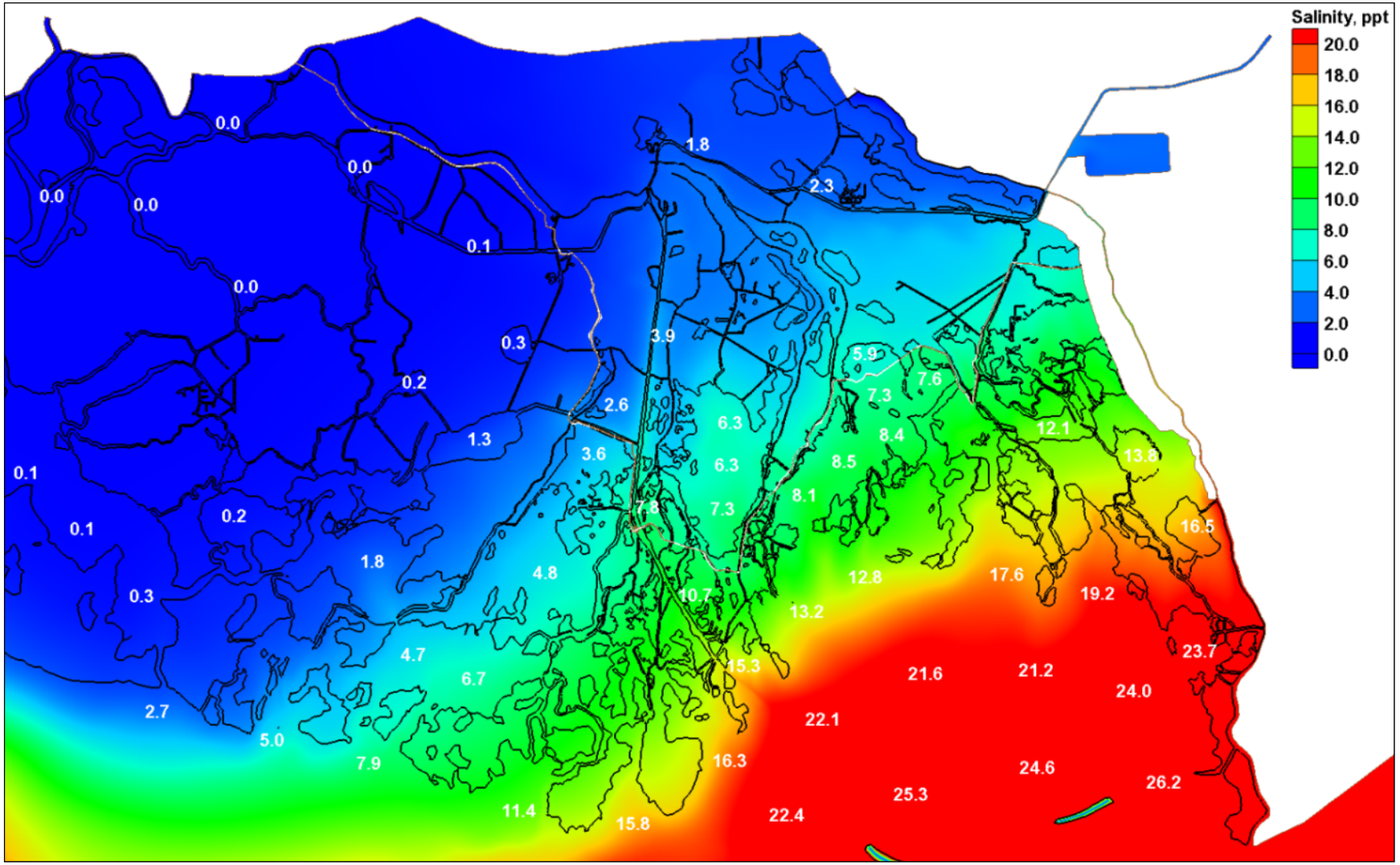

Figure 177. Plan 2 minus base configuration (yearly averaged salinities) differences for the sea-level rise 2 scenario (1.45 m).

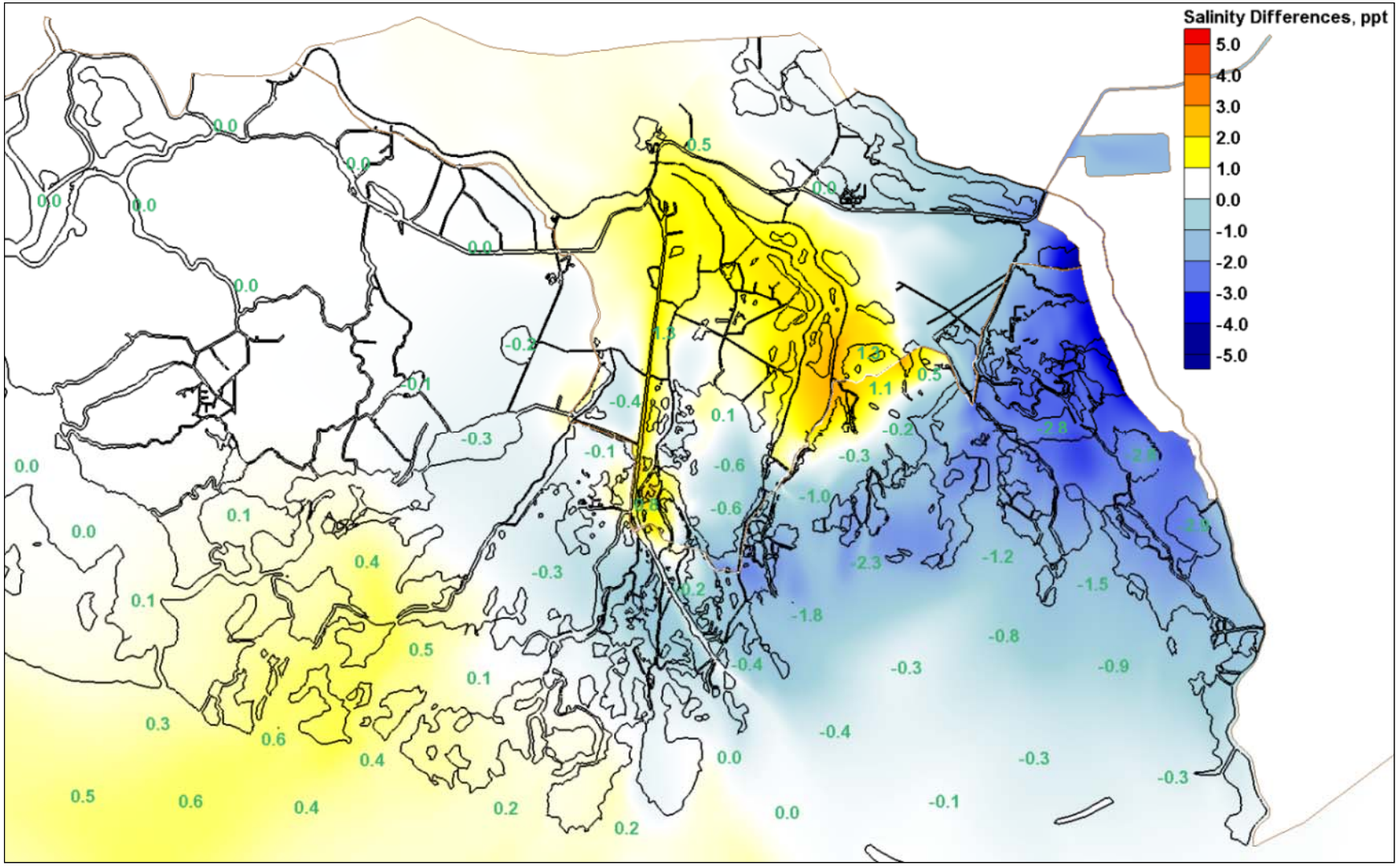

Figure 178. Plan 3 yearly averaged salinity values for the sea-level rise 2 scenario (1.45 m).

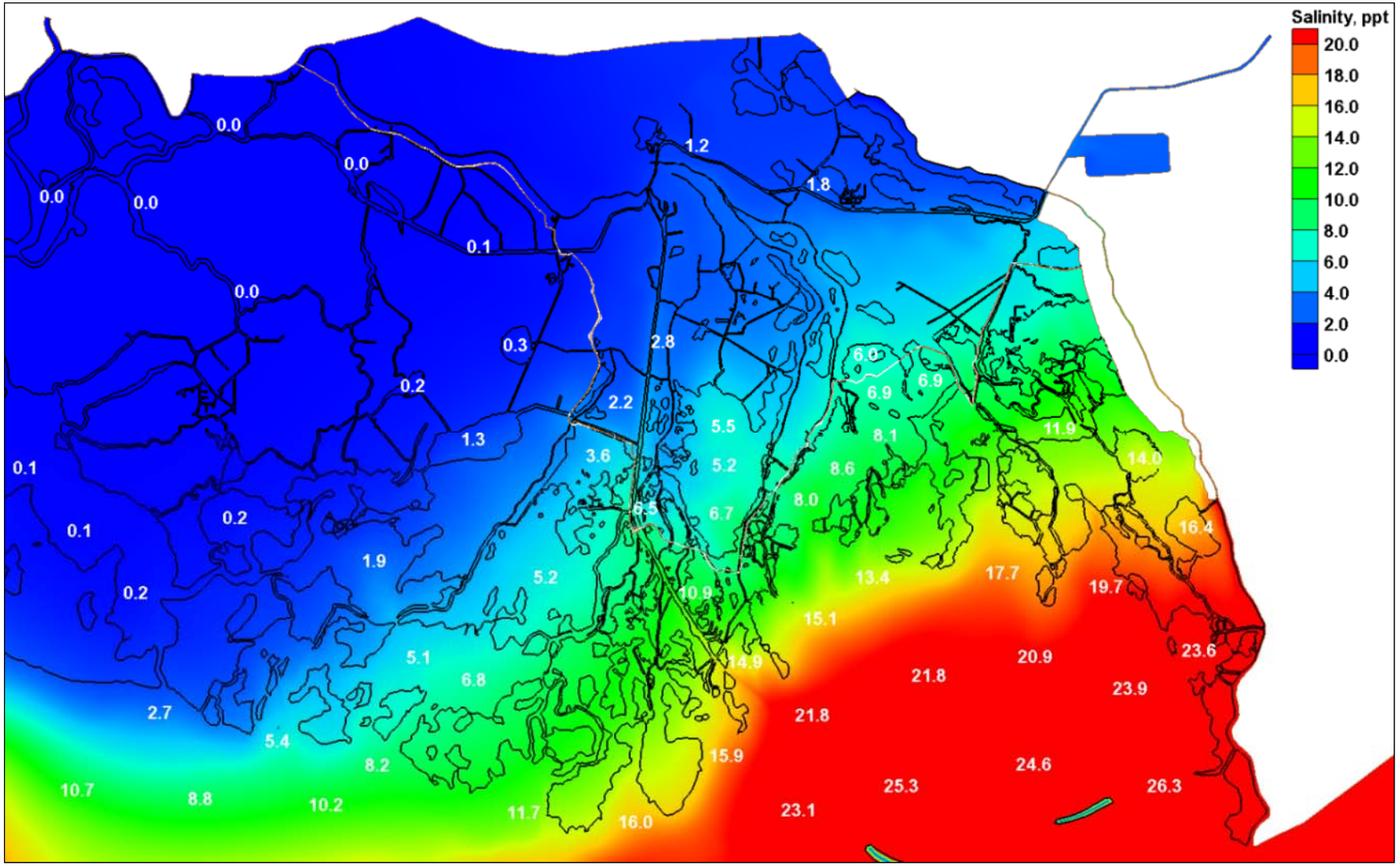

Figure 179. Plan 3 minus base configuration (yearly averaged salinities) differences for the sea-level rise 2 scenario (1.45 m).

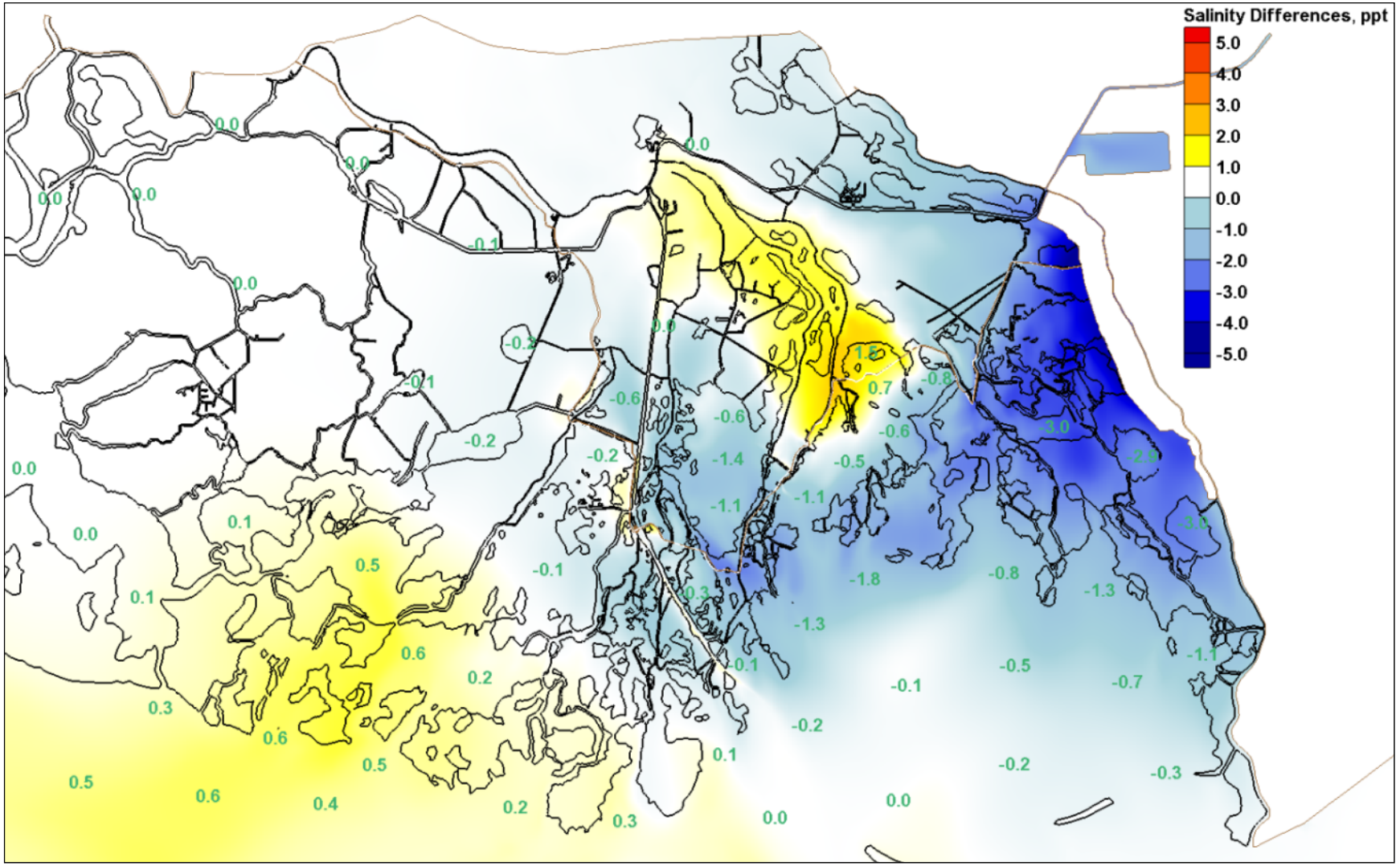

Appendix G: Point Comparisons

Figure 180 – Figure 253 display the impact of the levee system on the water level and salinity values for the discrete locations shown in Figure 50 – Figure 54, the coordinate locations of which are listed in Table 11. These figures present the minimum (top of blue bar), average (top of green bar) and maximum (top of maroon bar) values for each point for the base and all three plan configurations for all three sea-level scenarios.

Figure 180. Water-surface elevation and salinity comparisons at Point 1.

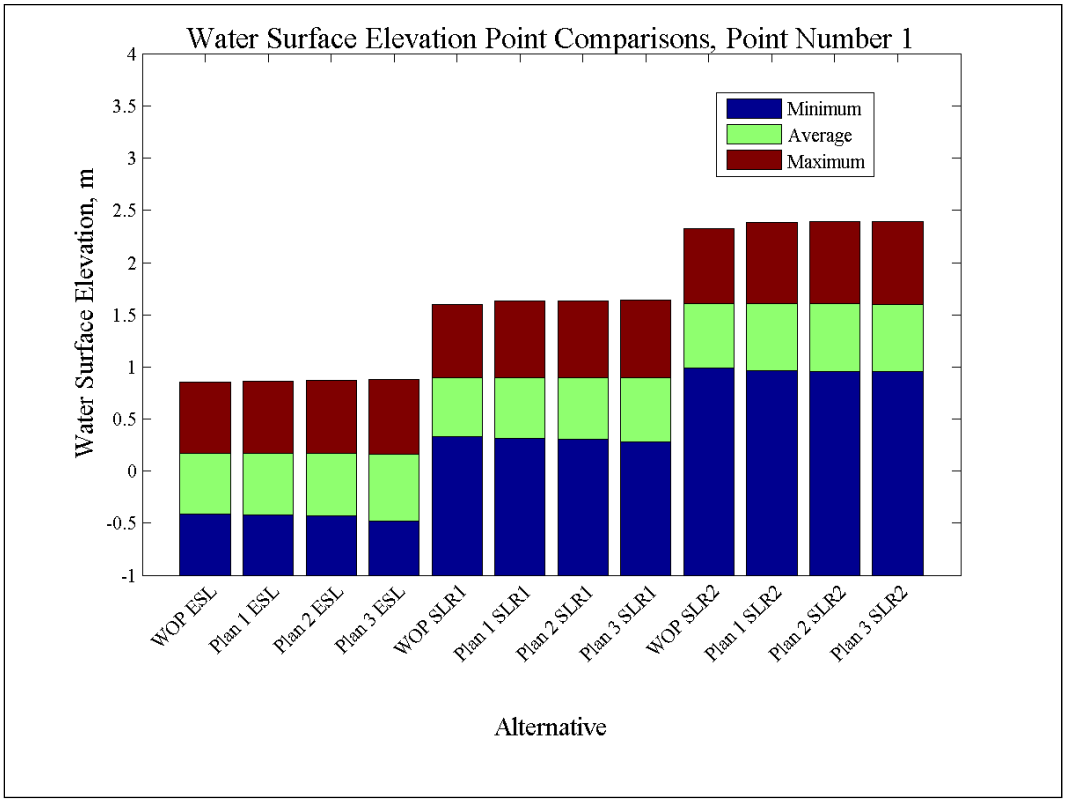

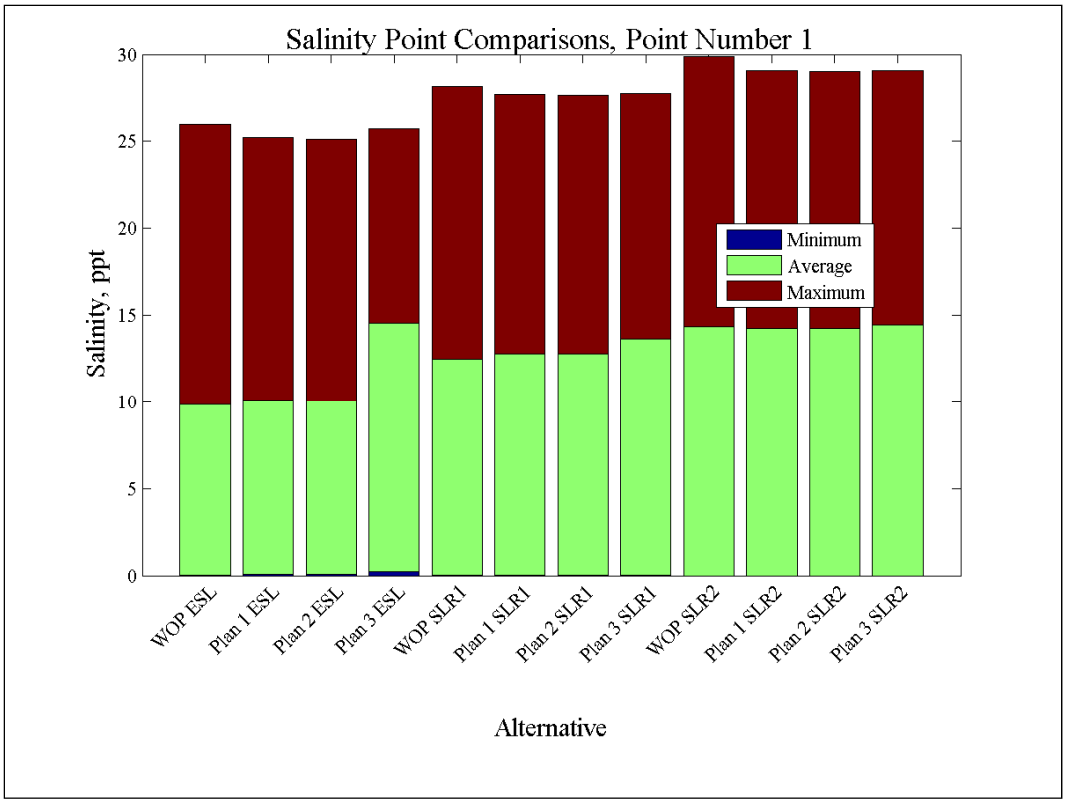

Figure 181. Water-surface elevation and salinity comparisons at Point 2.

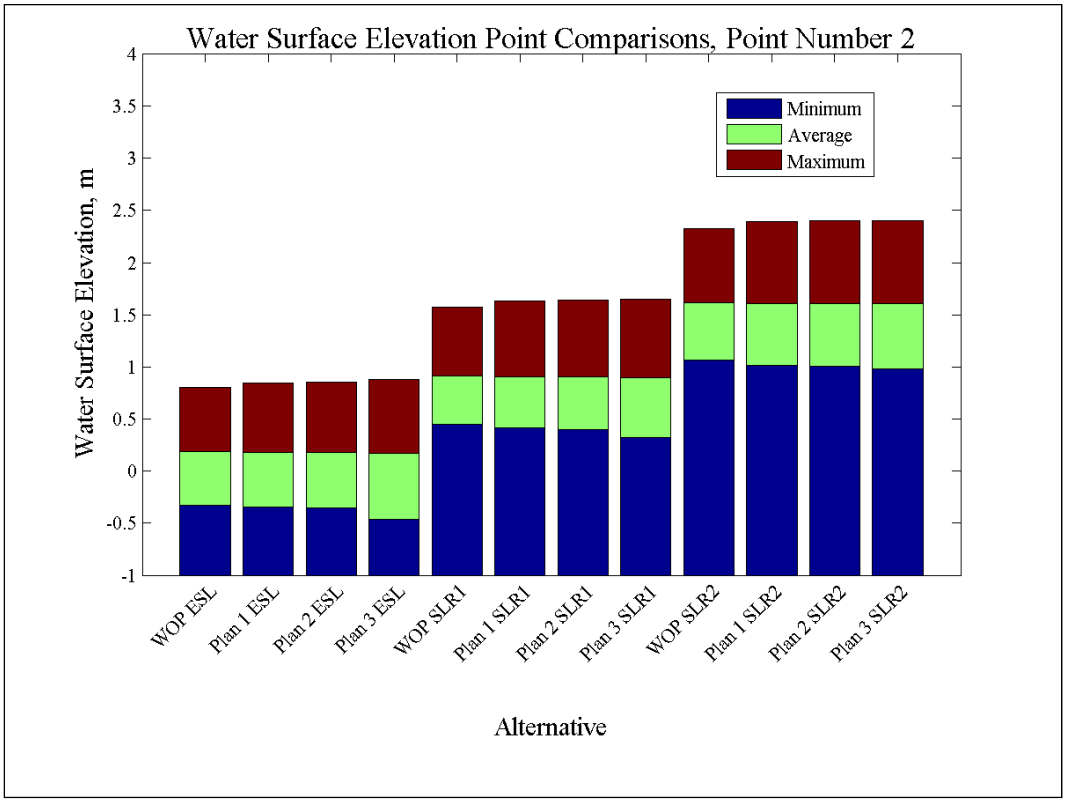

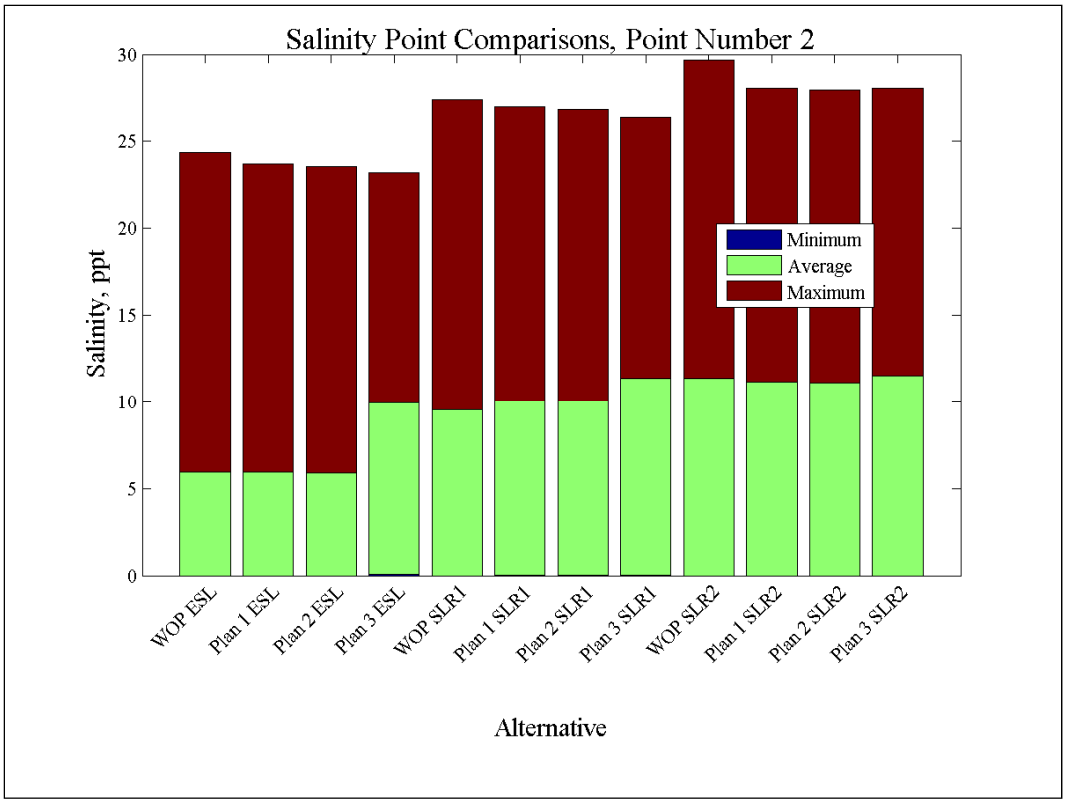

Figure 182. Water-surface elevation and salinity comparisons at Point 3.

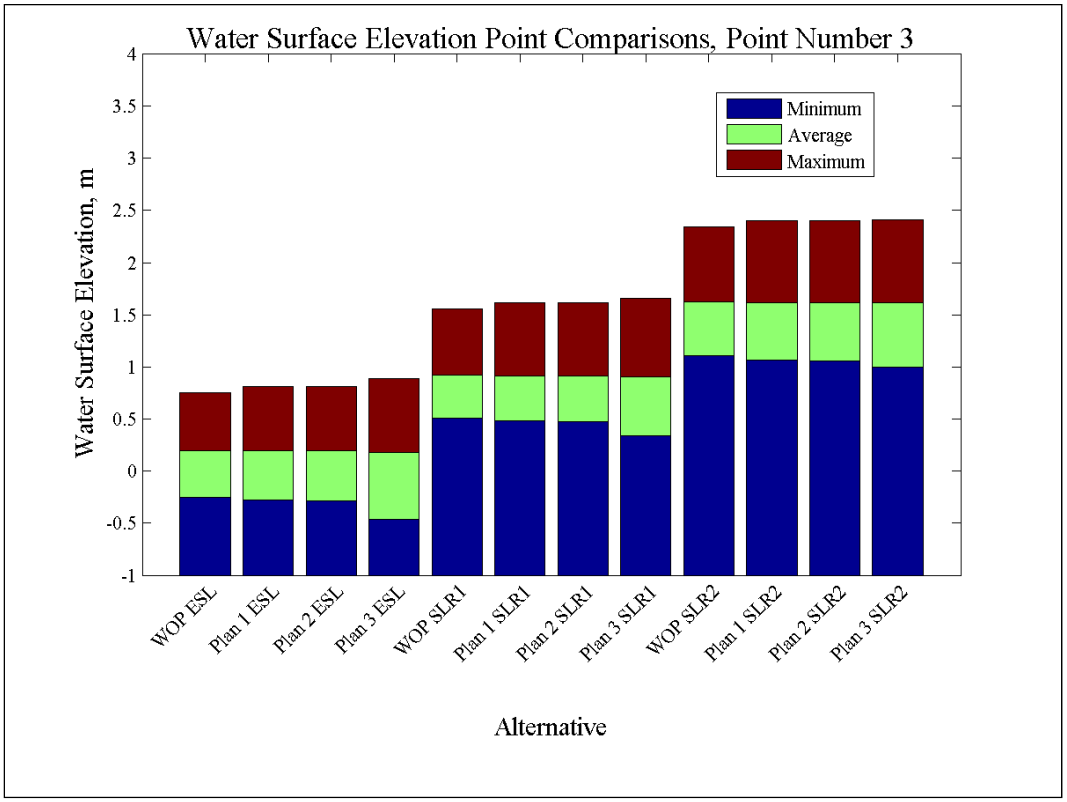

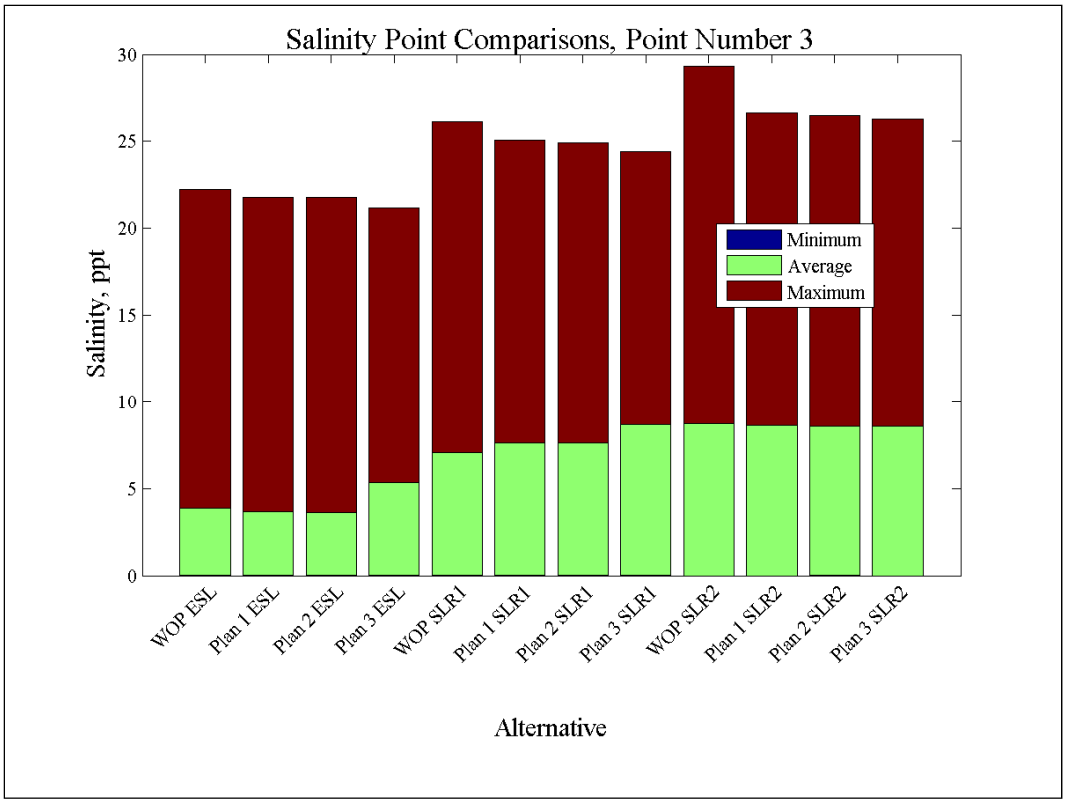

Figure 183. Water-surface elevation and salinity comparisons at Point 4.

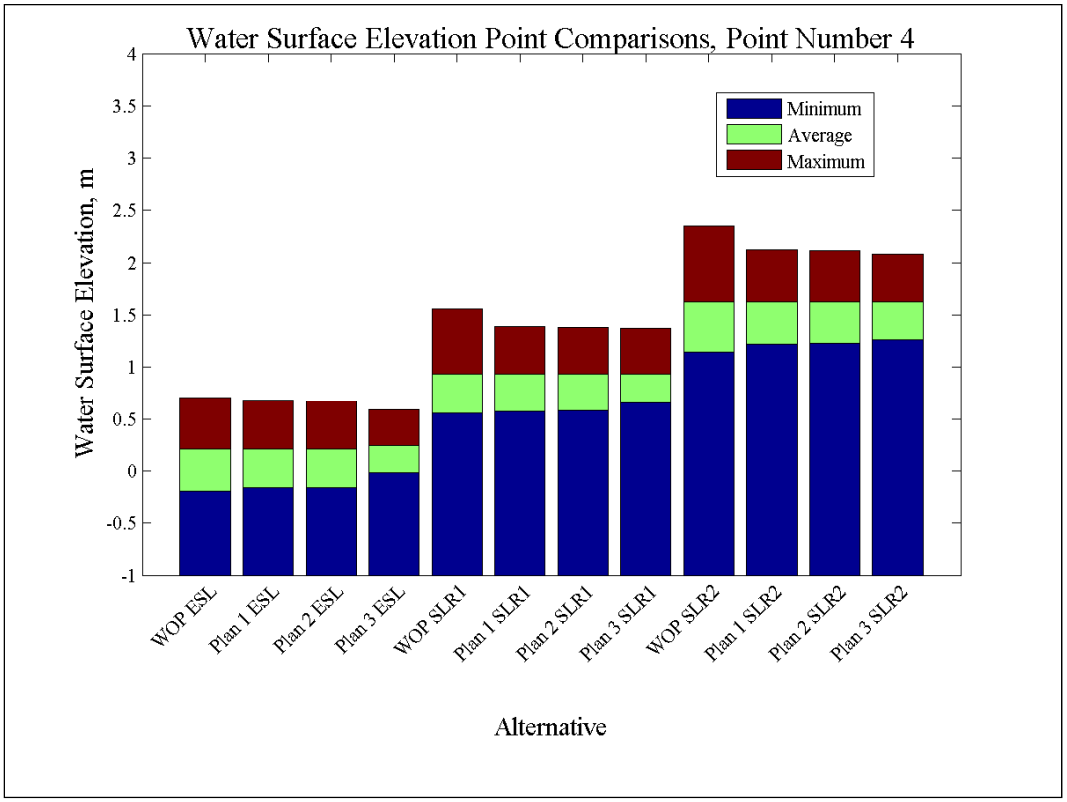

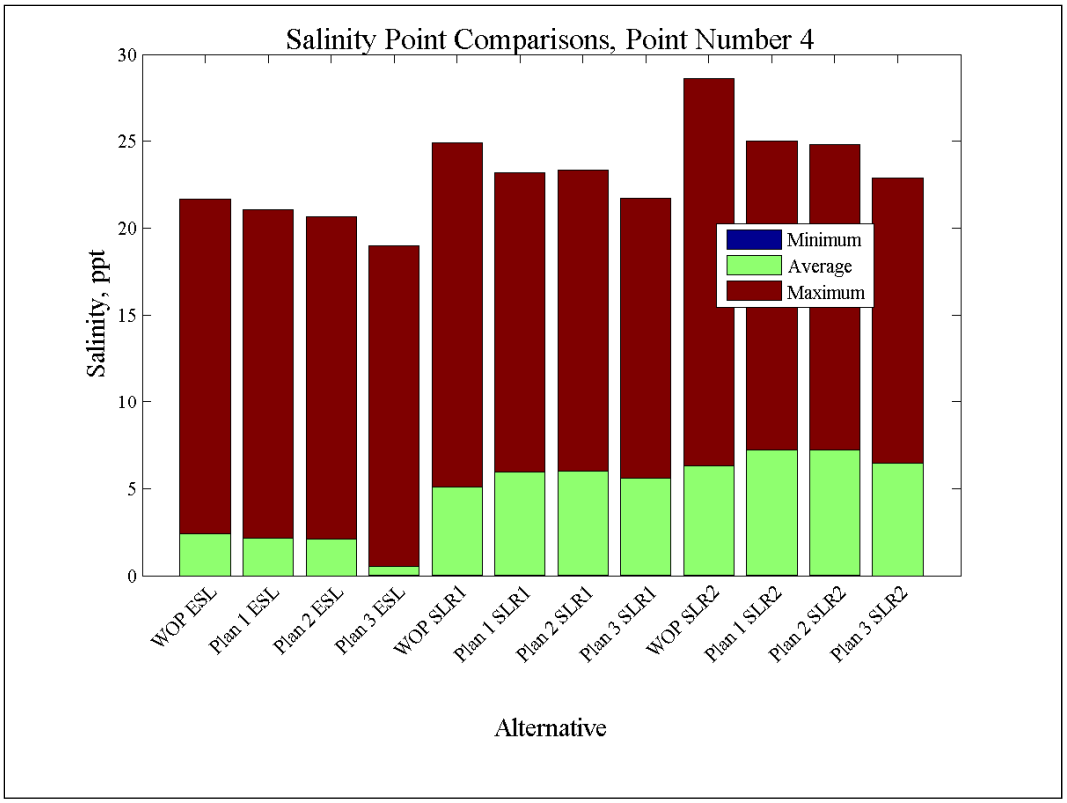

Figure 184. Water-surface elevation and salinity comparisons at Point 5.

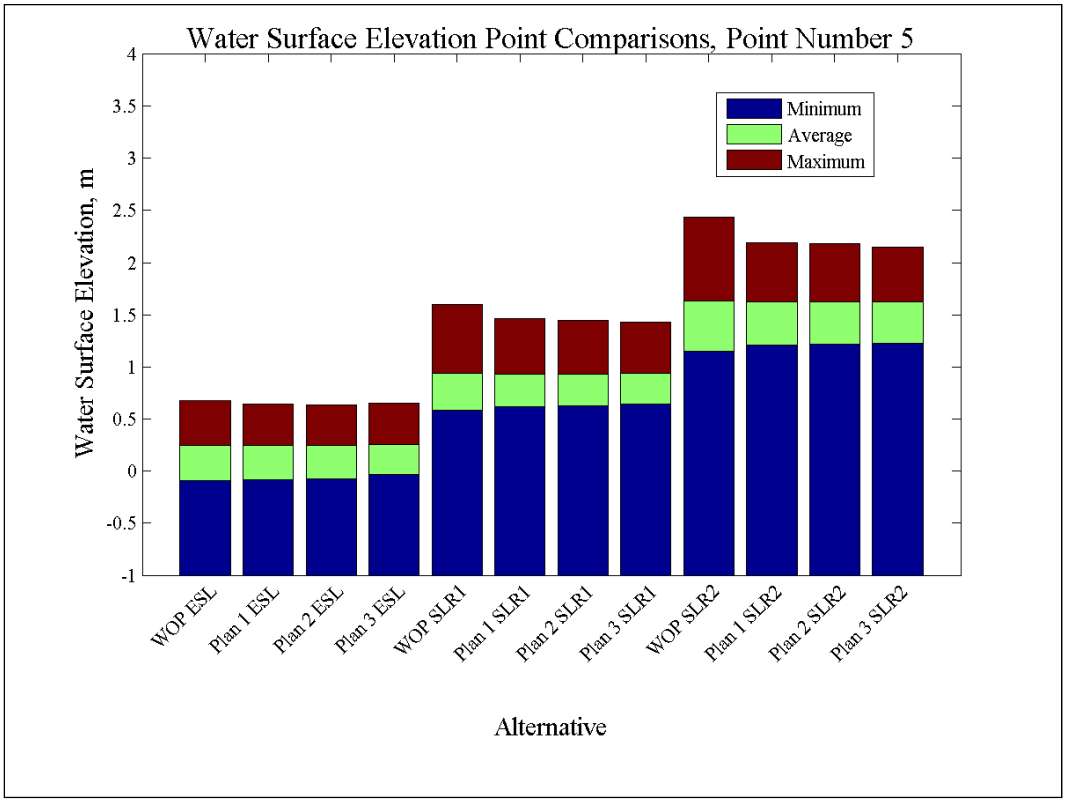

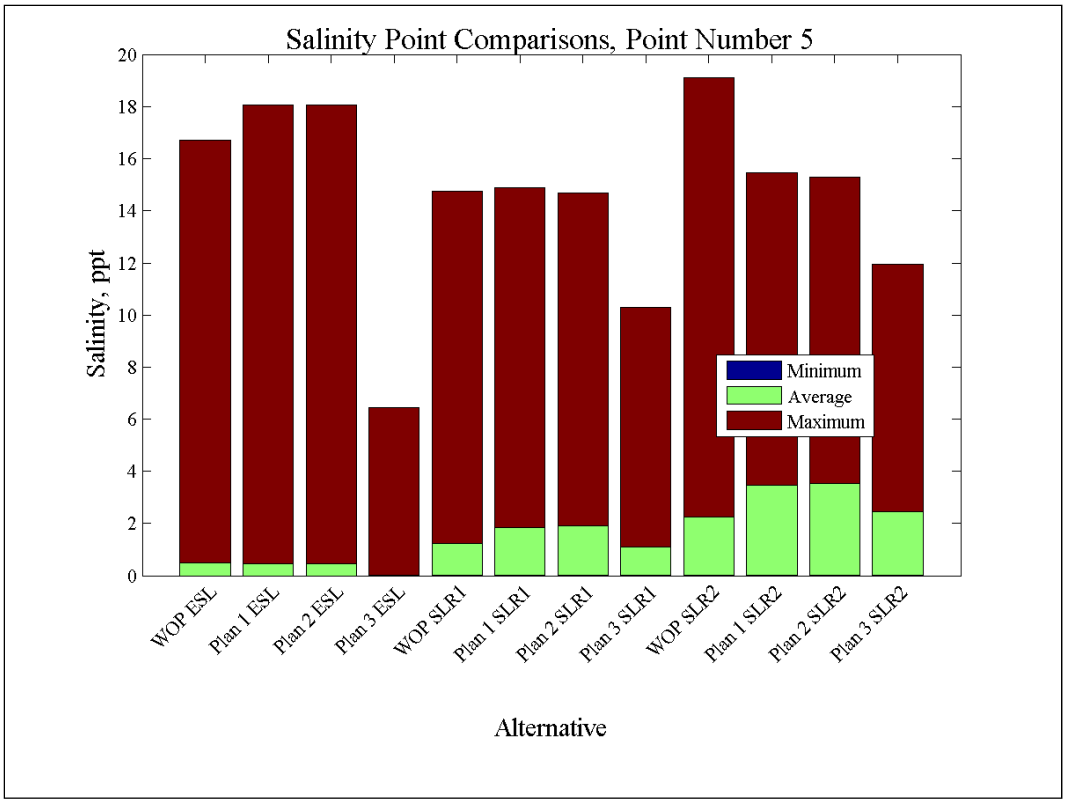

Figure 185. Water-surface elevation and salinity comparisons at Point 6.

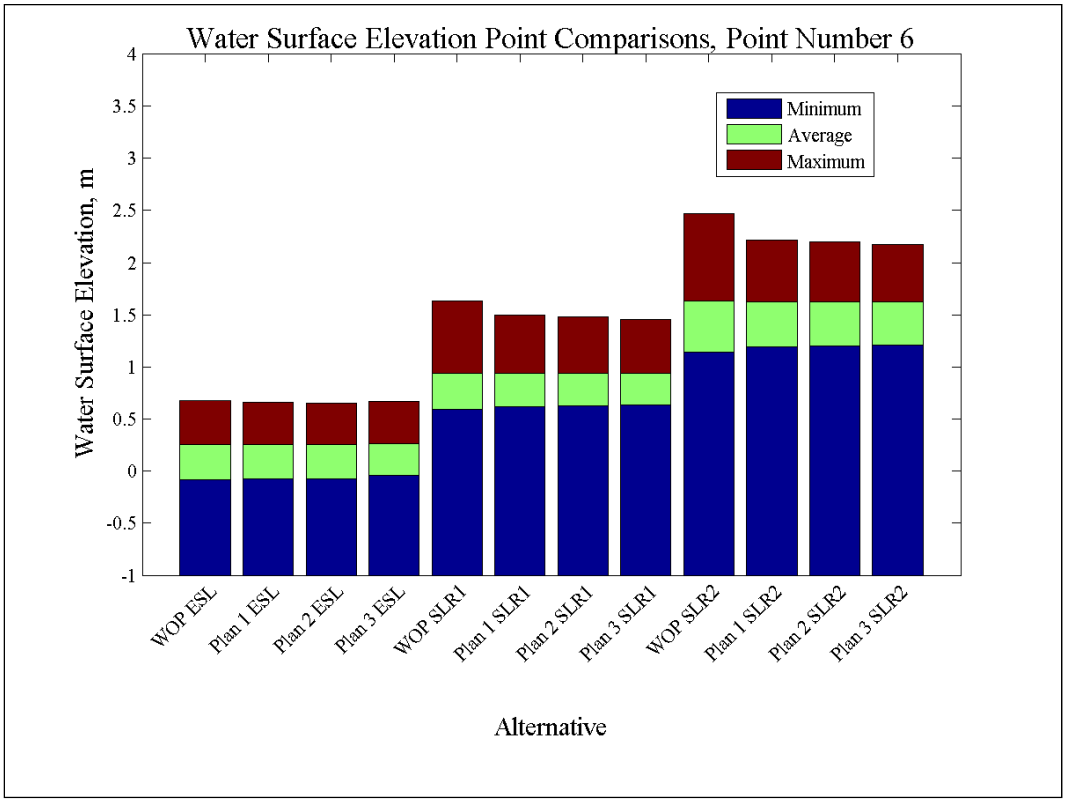

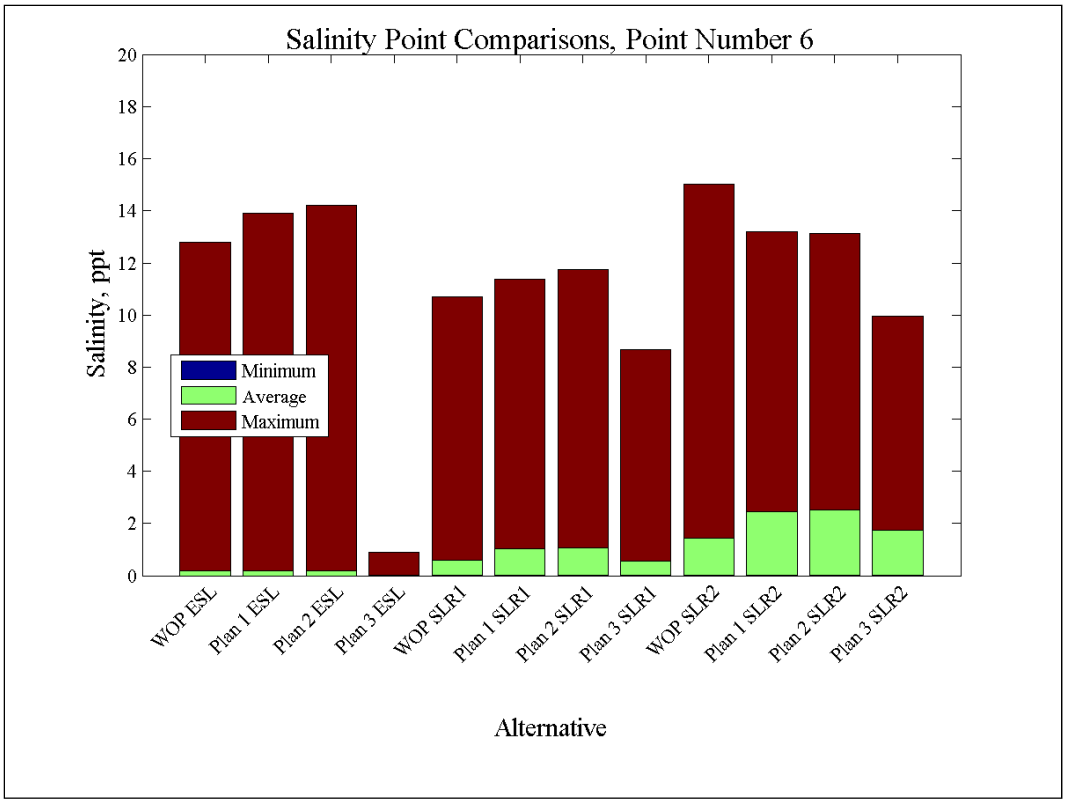

Figure 186. Water-surface elevation and salinity comparisons at Point 7.

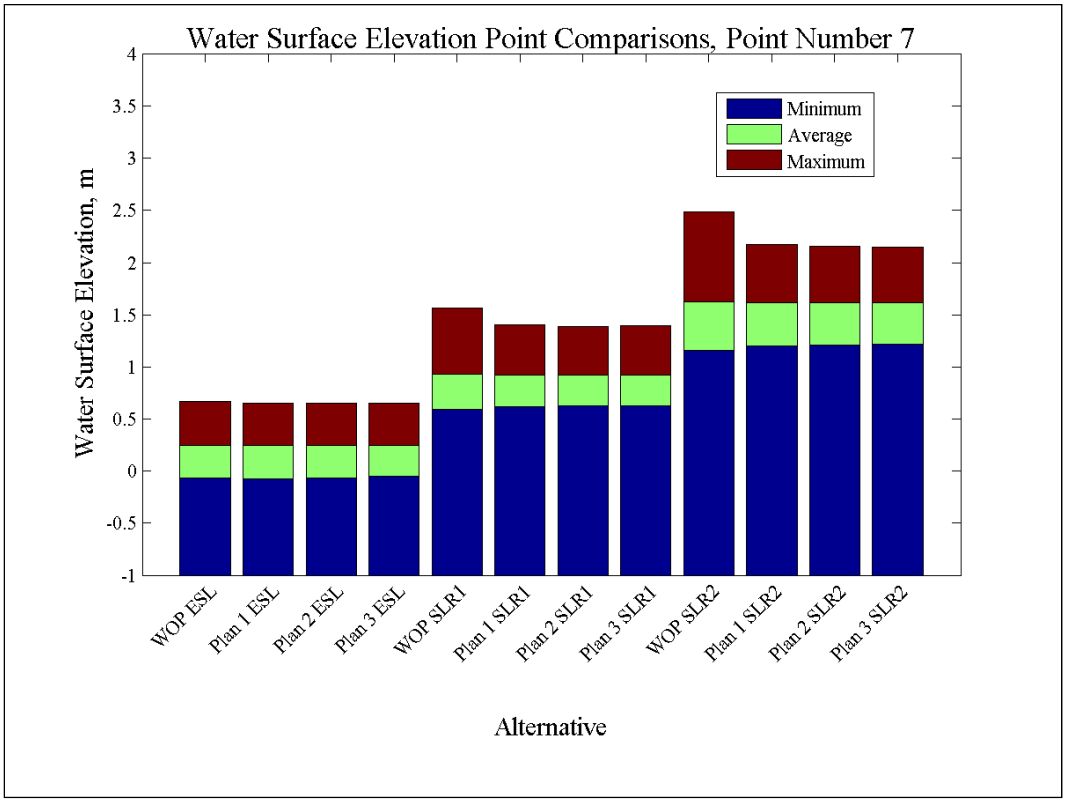

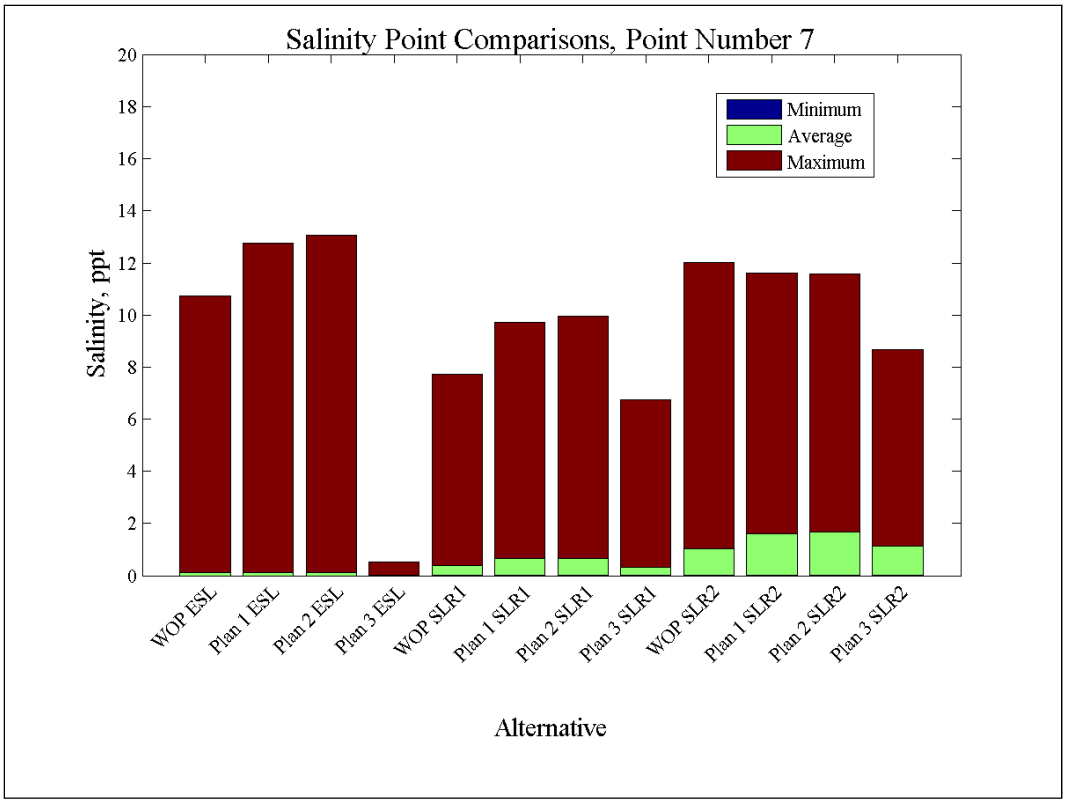

Figure 187. Water-surface elevation and salinity comparisons at Point 8.

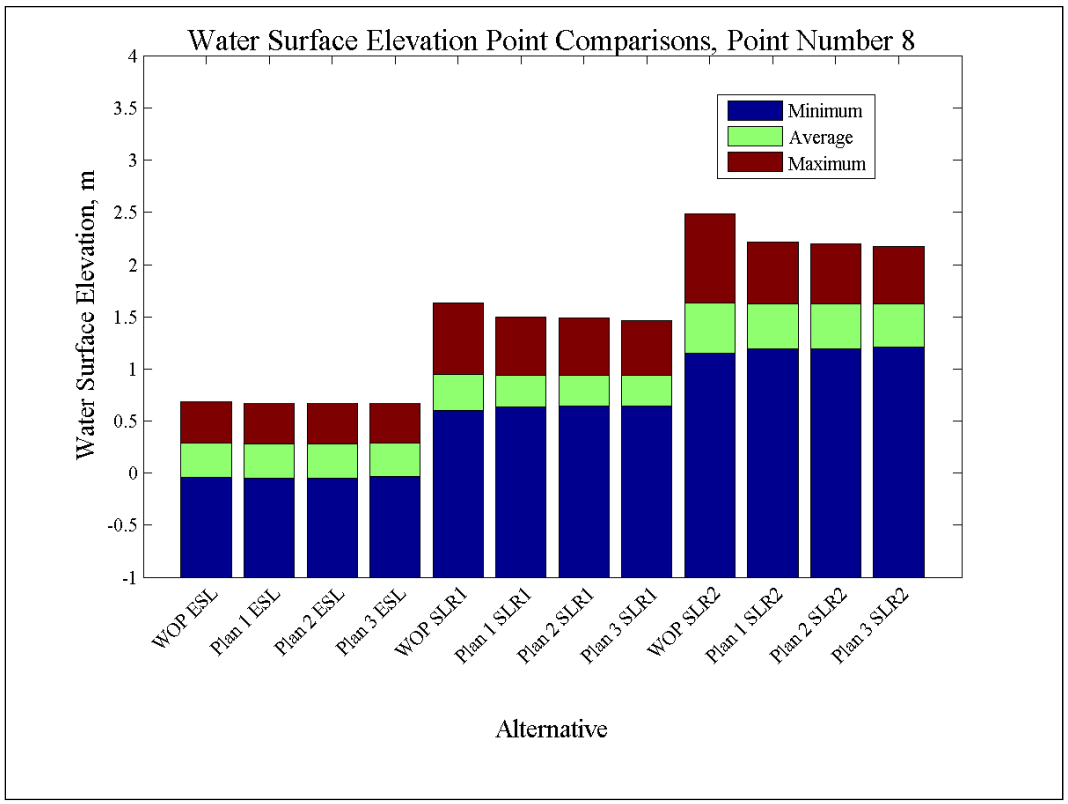

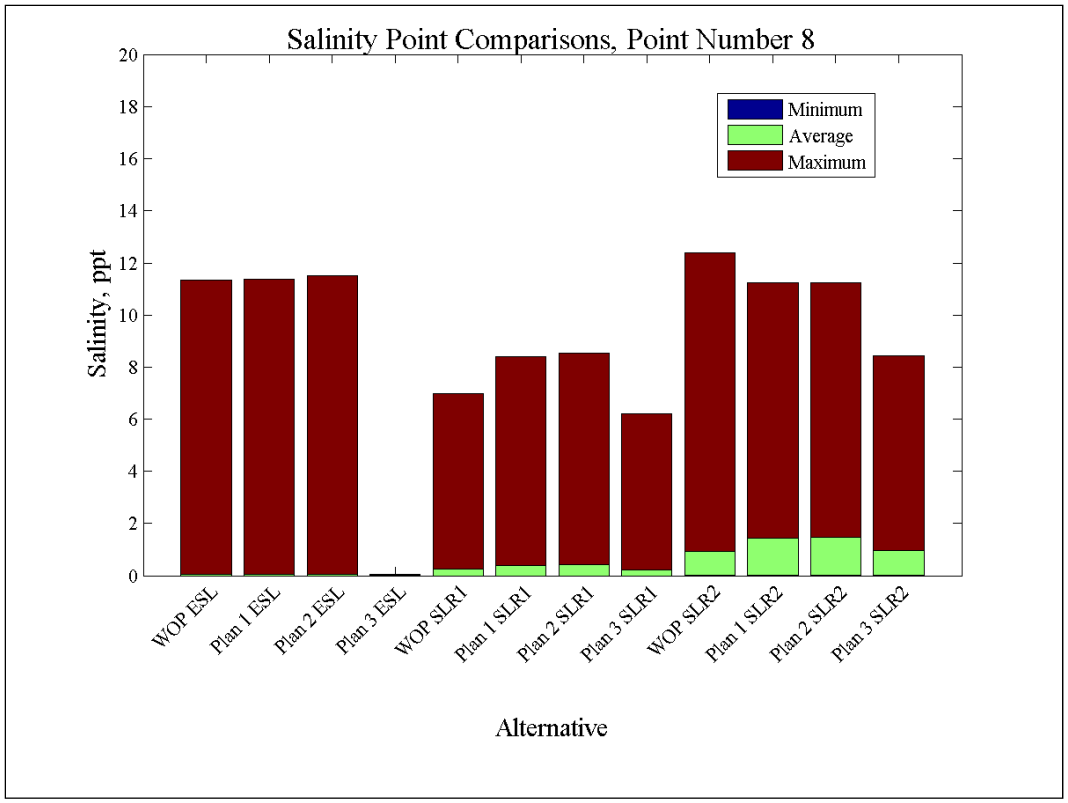

Figure 188. Water-surface elevation and salinity comparisons at Point 9.

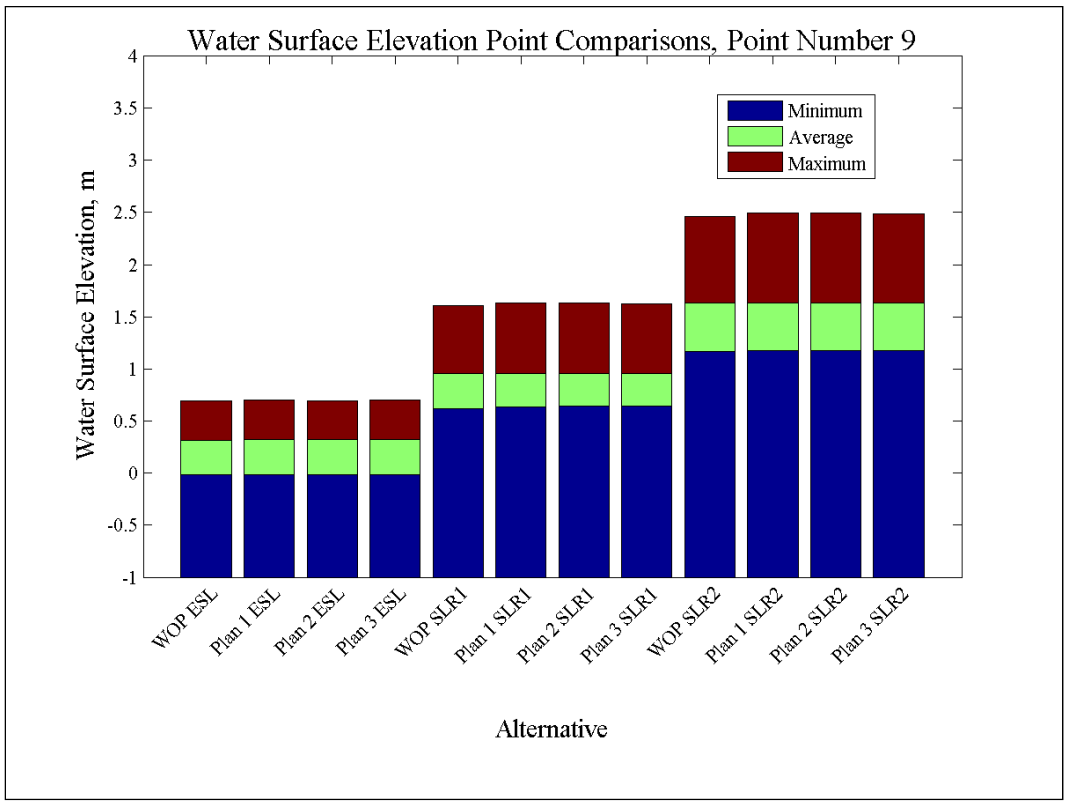

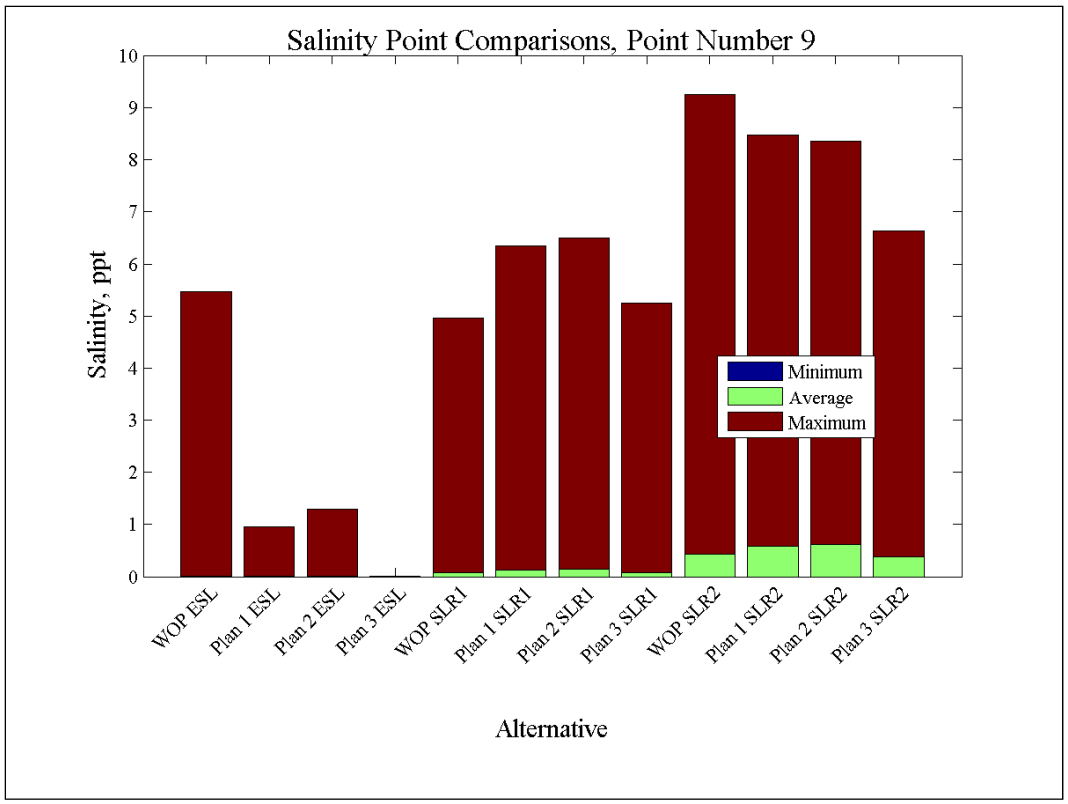

Figure 189. Water-surface elevation and salinity comparisons at Point 10.

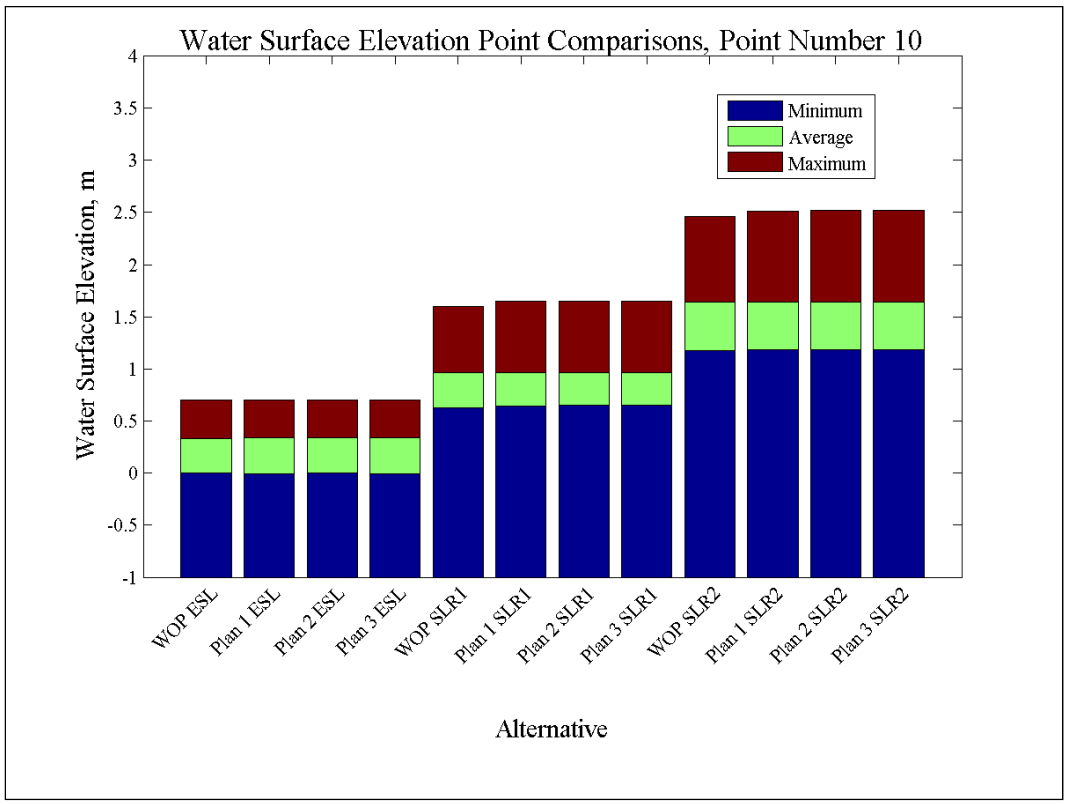

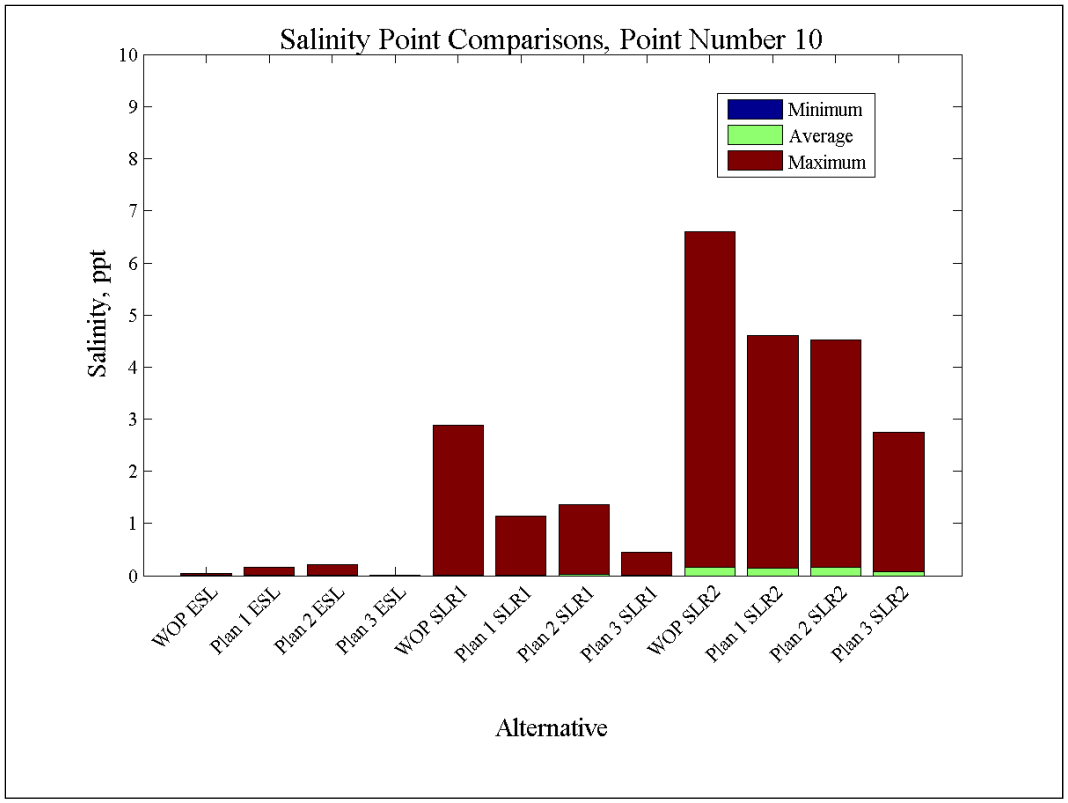

Figure 190. Water-surface elevation and salinity comparisons at Point 11.

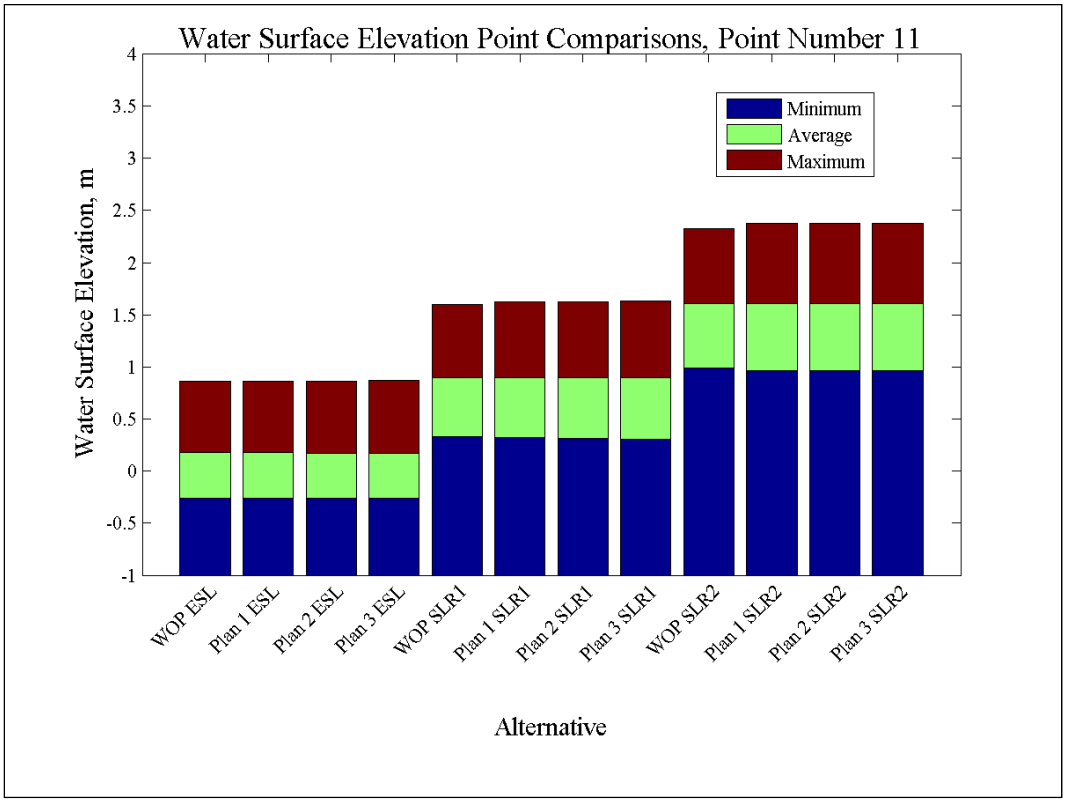

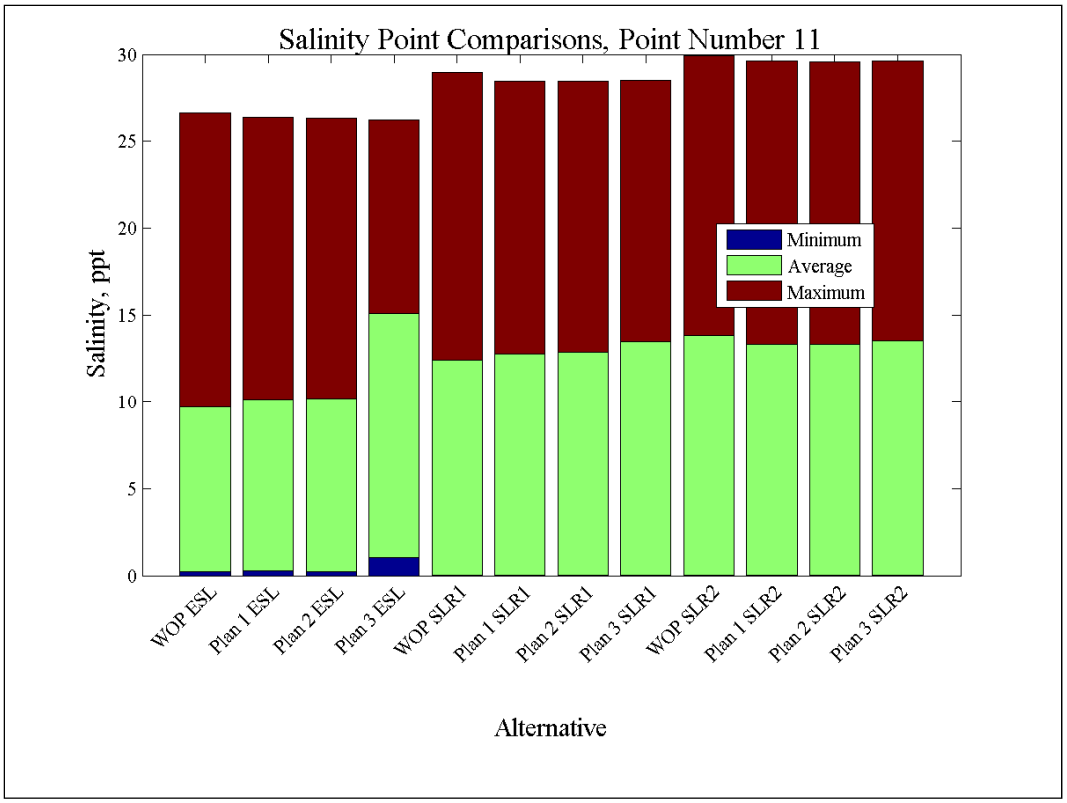

Figure 191. Water-surface elevation and salinity comparisons at Point 12.

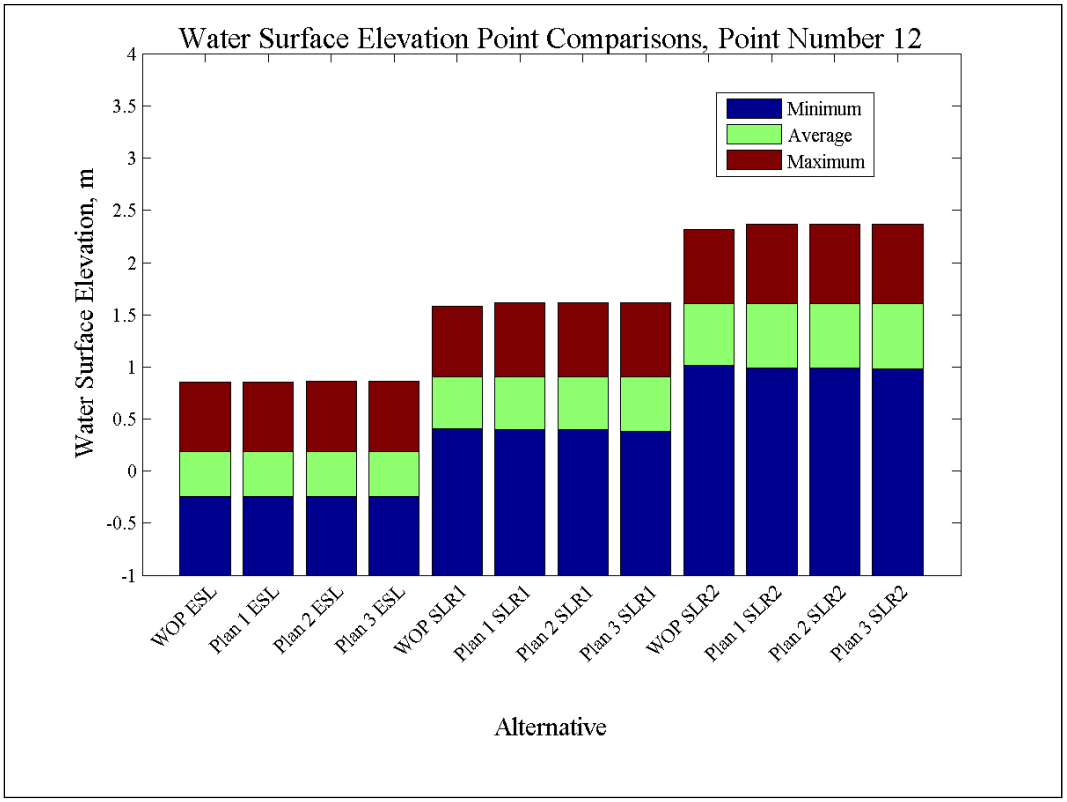

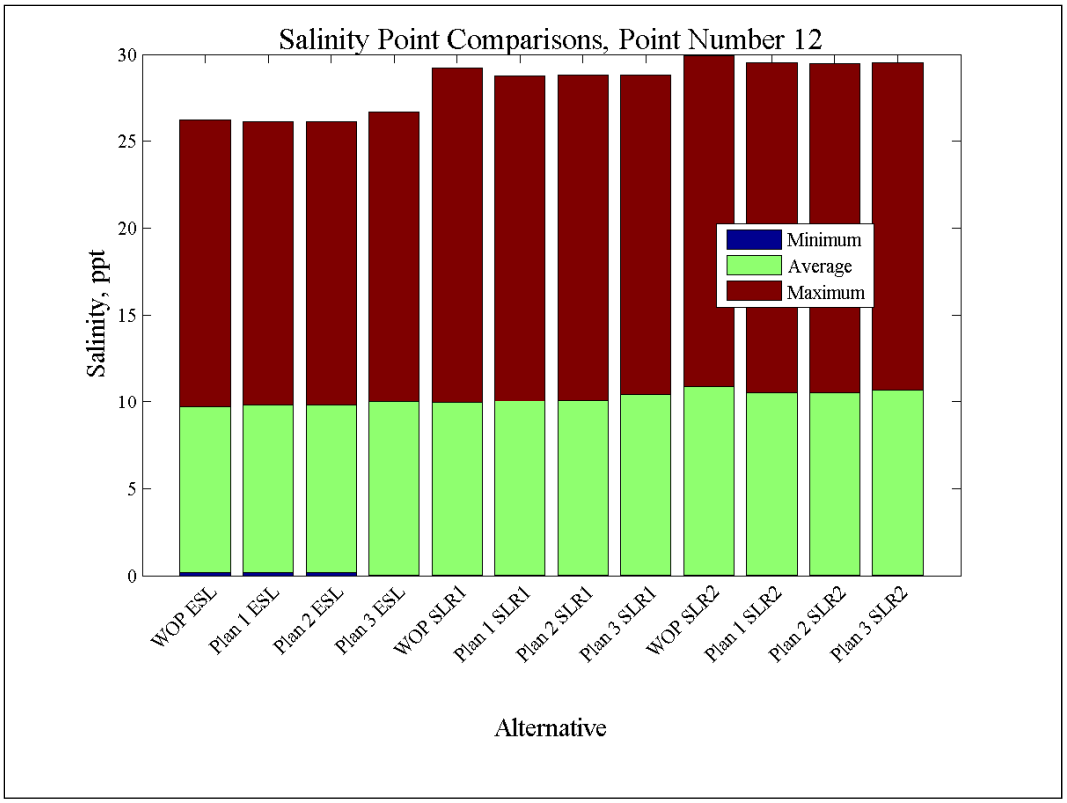

Figure 192. Water-surface elevation and salinity comparisons at Point 13.

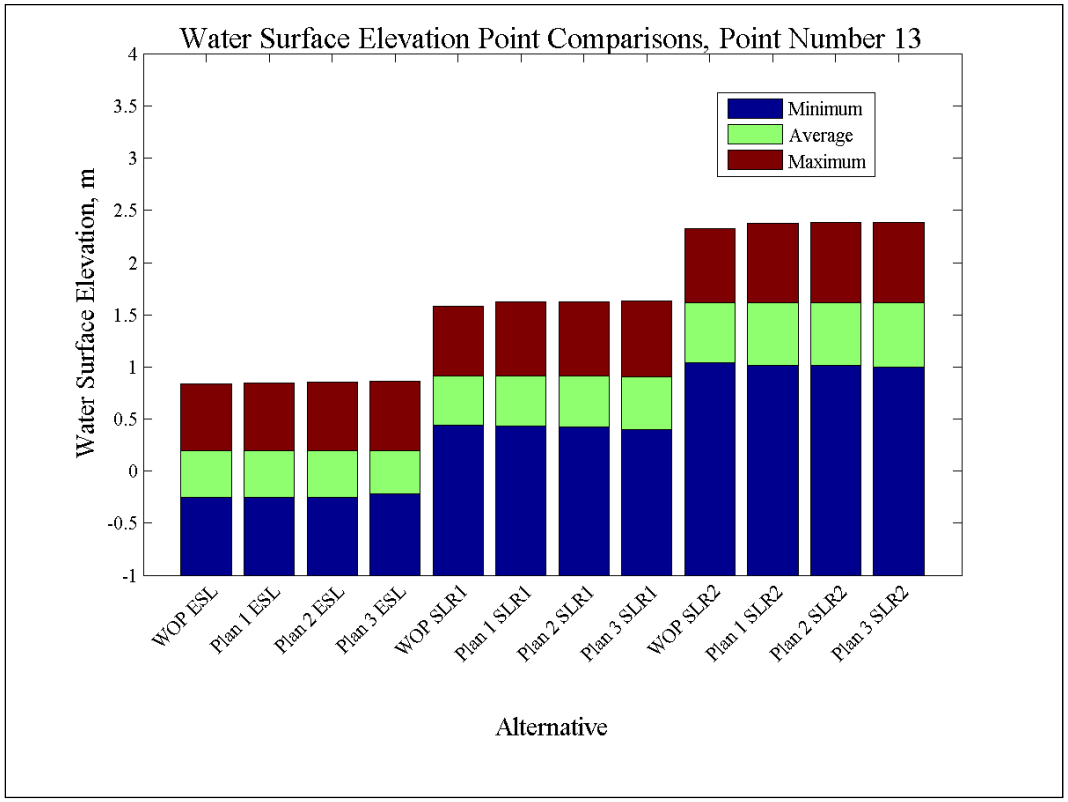

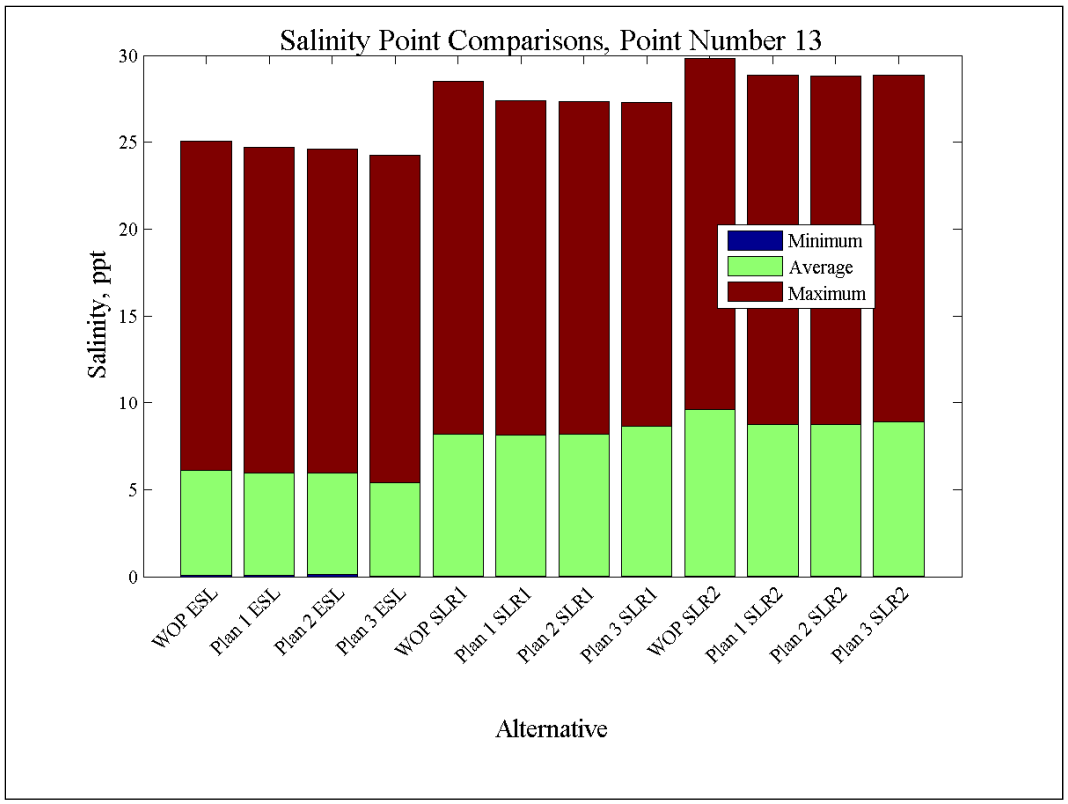

Figure 193. Water-surface elevation and salinity comparisons at Point 14.

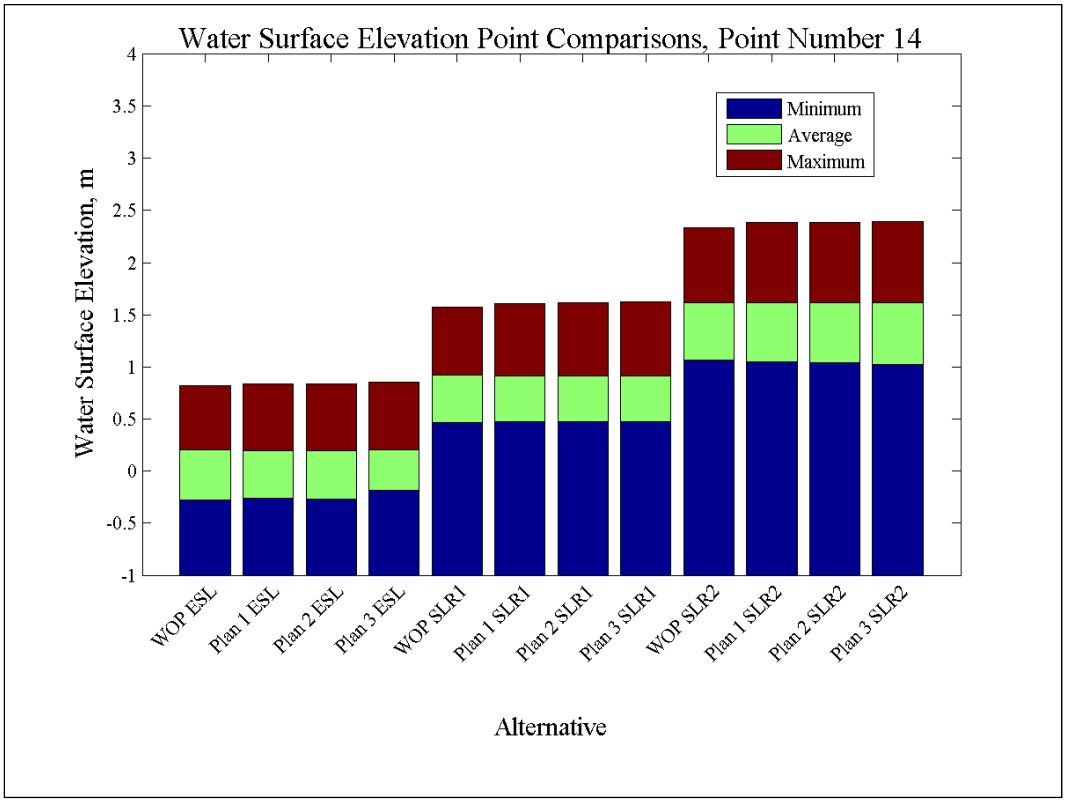

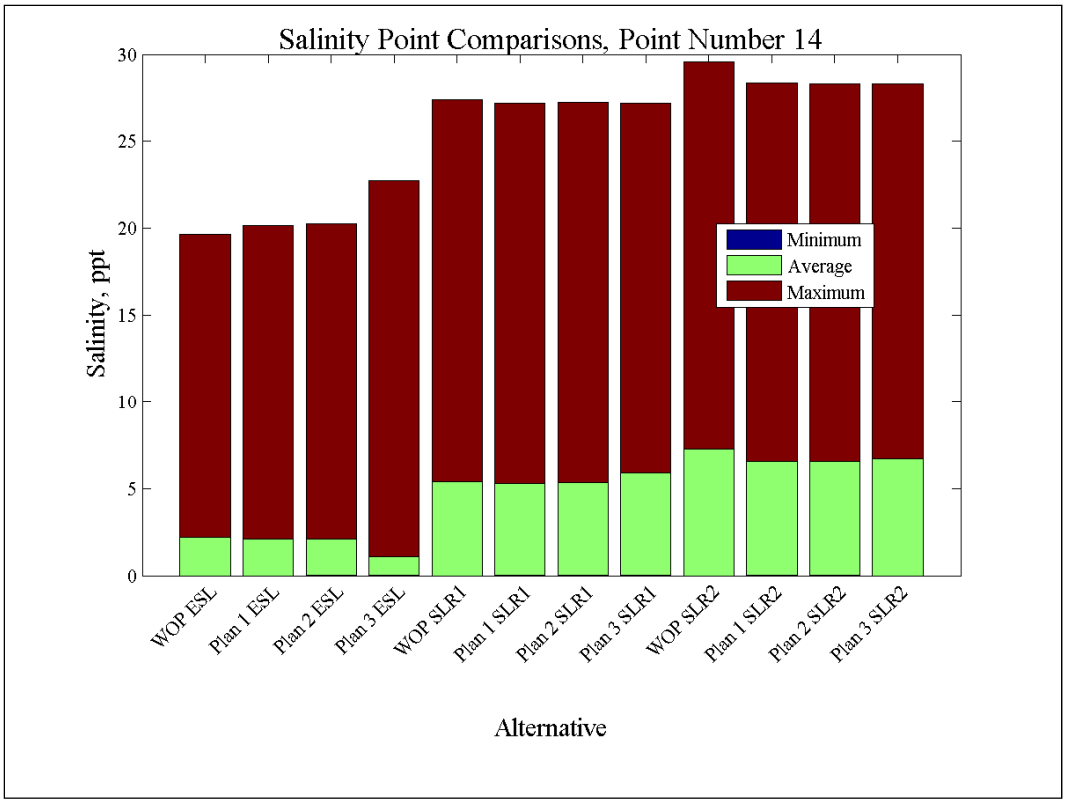

Figure 194. Water-surface elevation and salinity comparisons at Point 15.

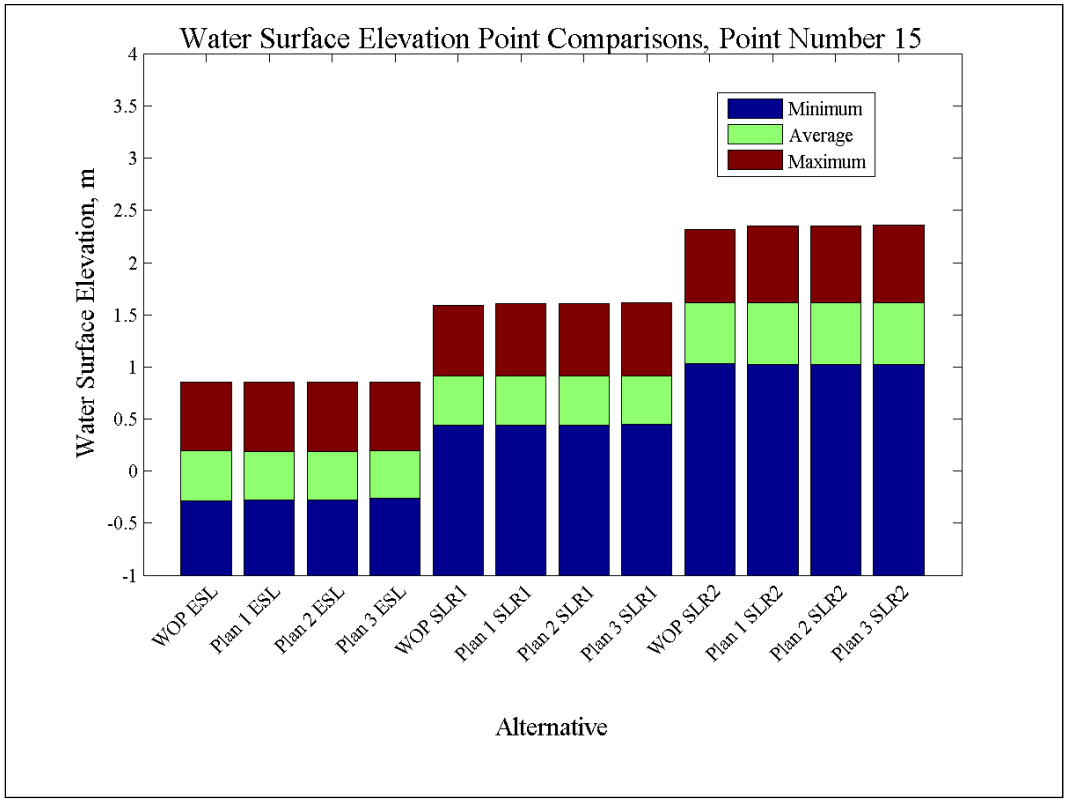

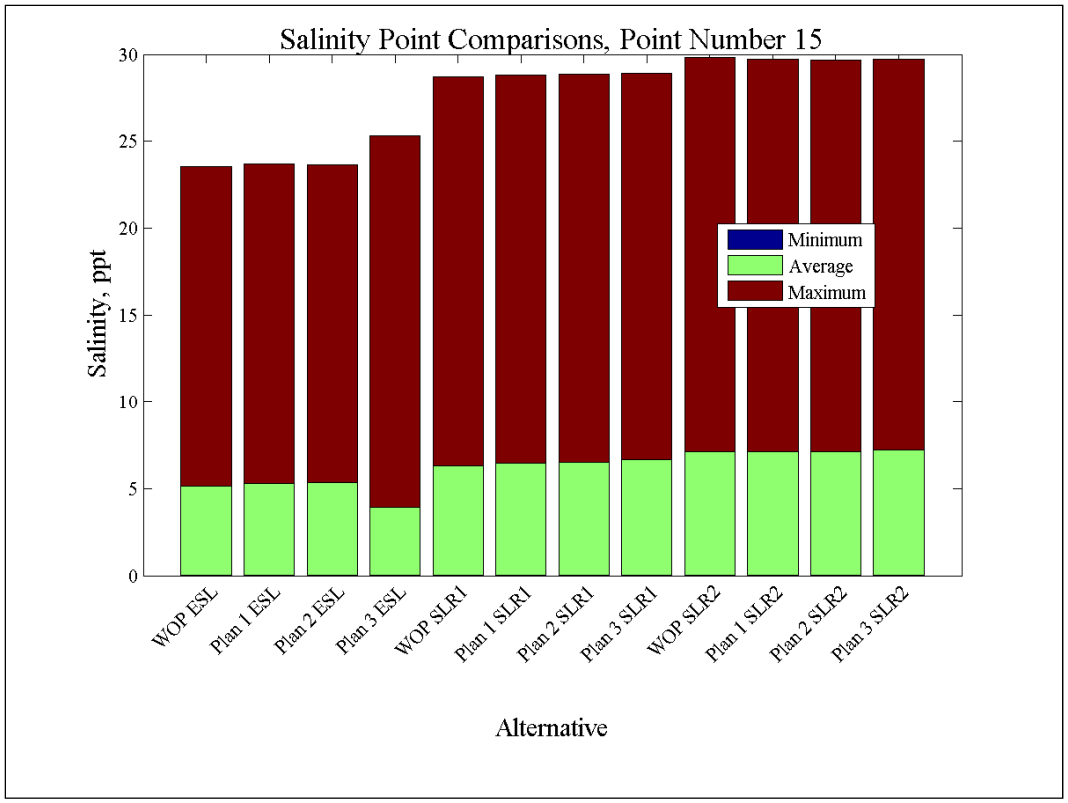

Figure 195. Water-surface elevation and salinity comparisons at Point 16.

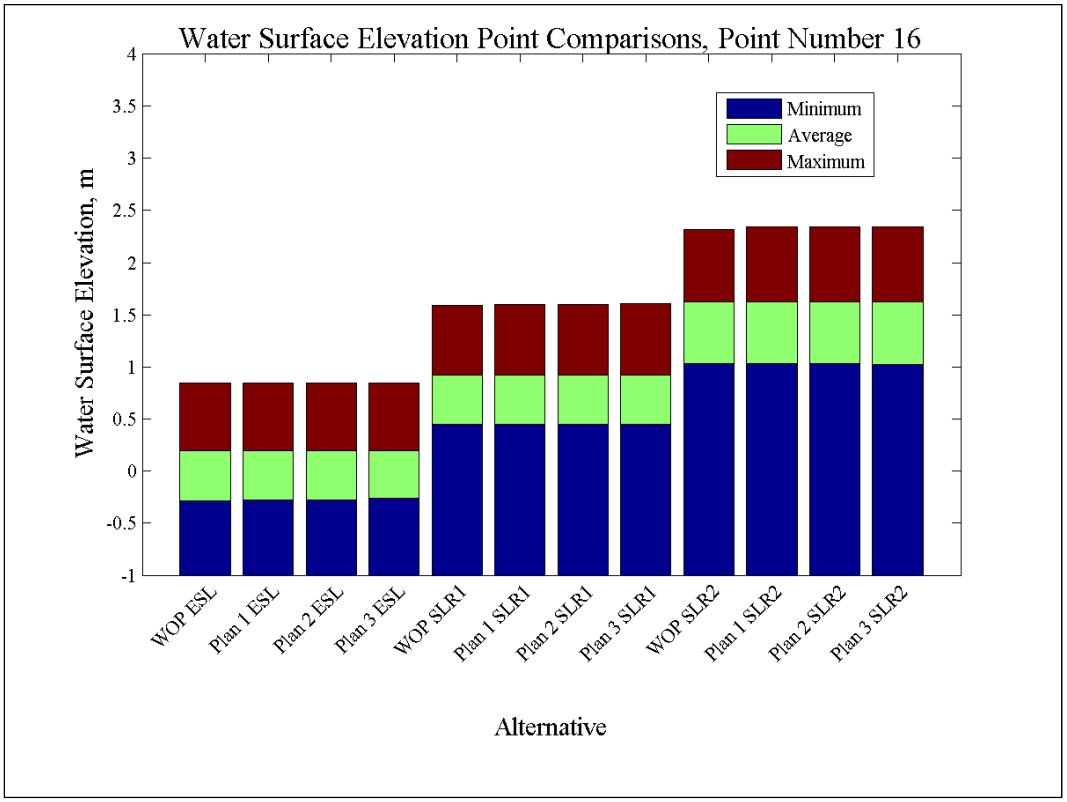

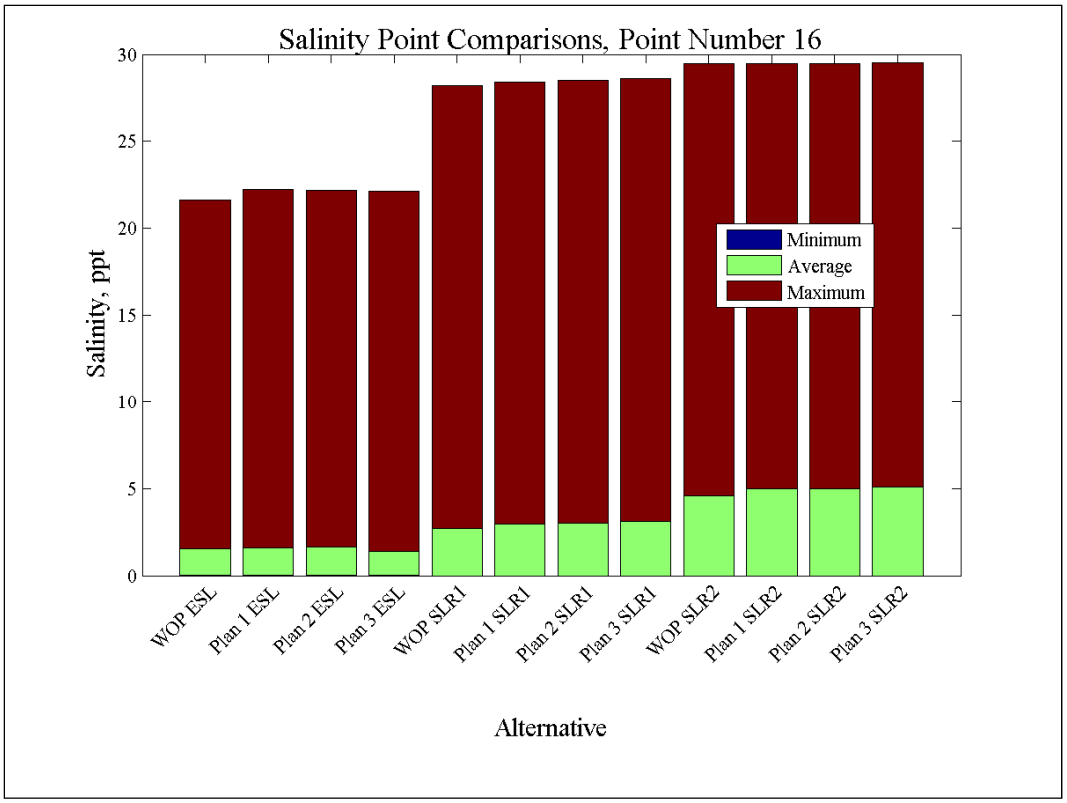

Figure 196. Water-surface elevation and salinity comparisons at Point 17.

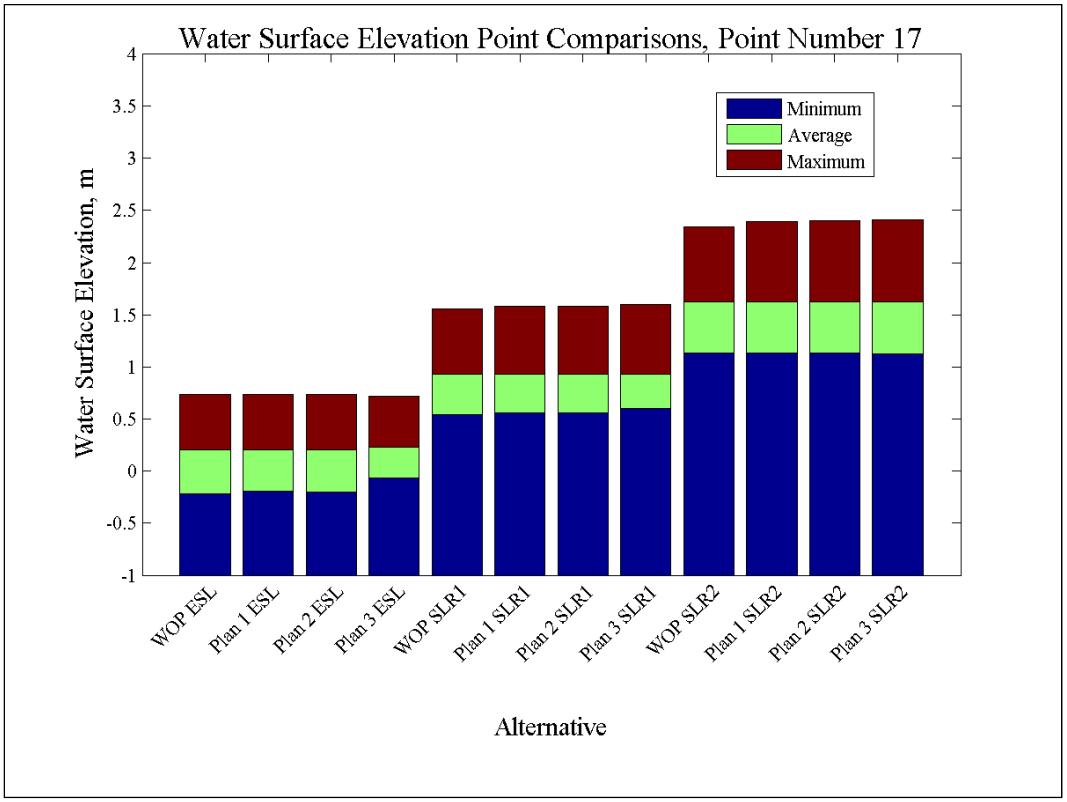

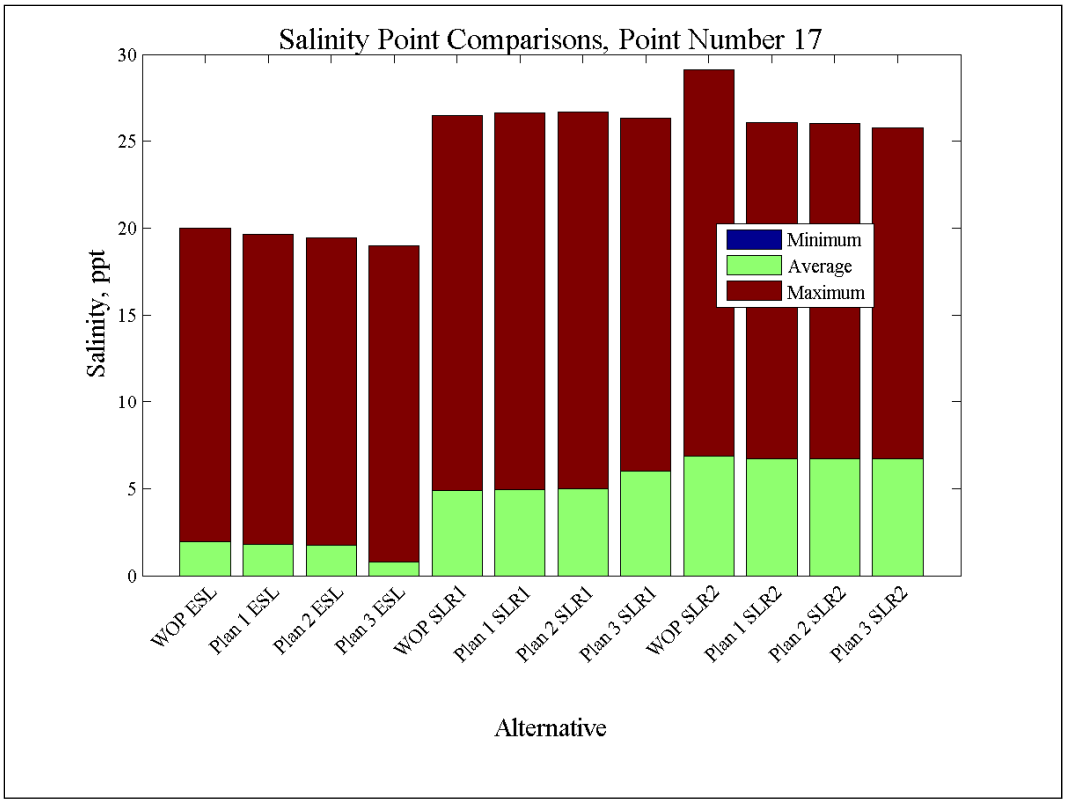

Figure 197. Water-surface elevation and salinity comparisons at Point 18.

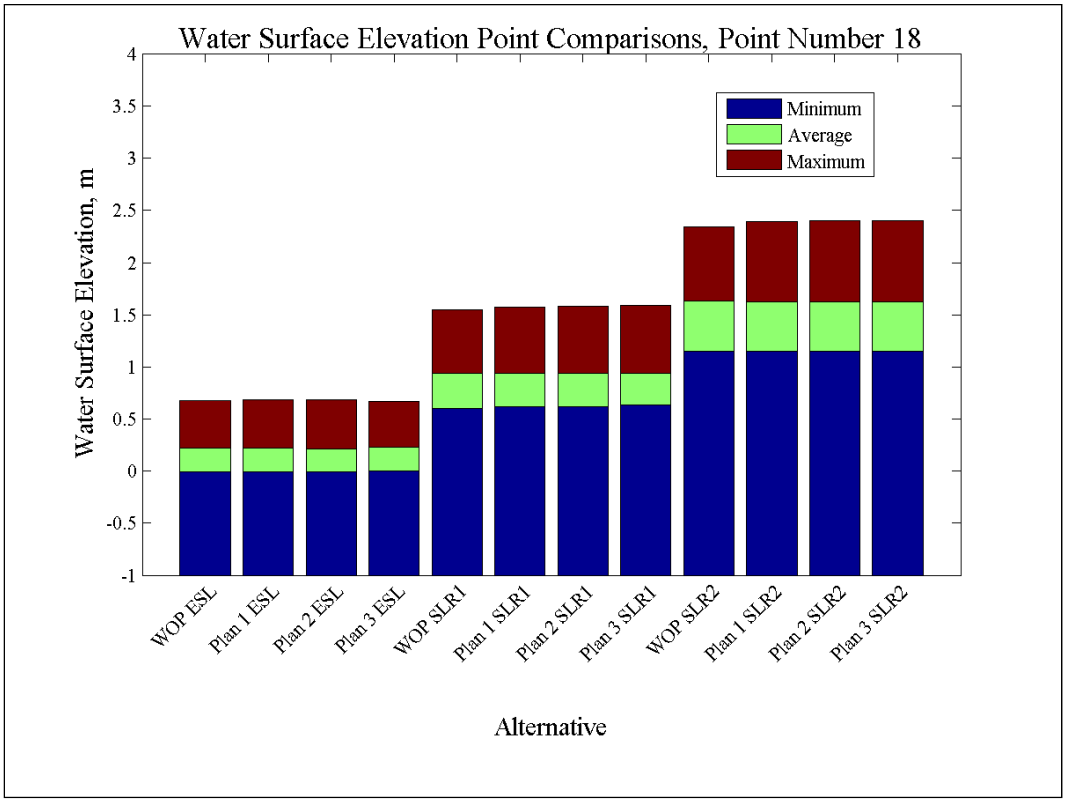

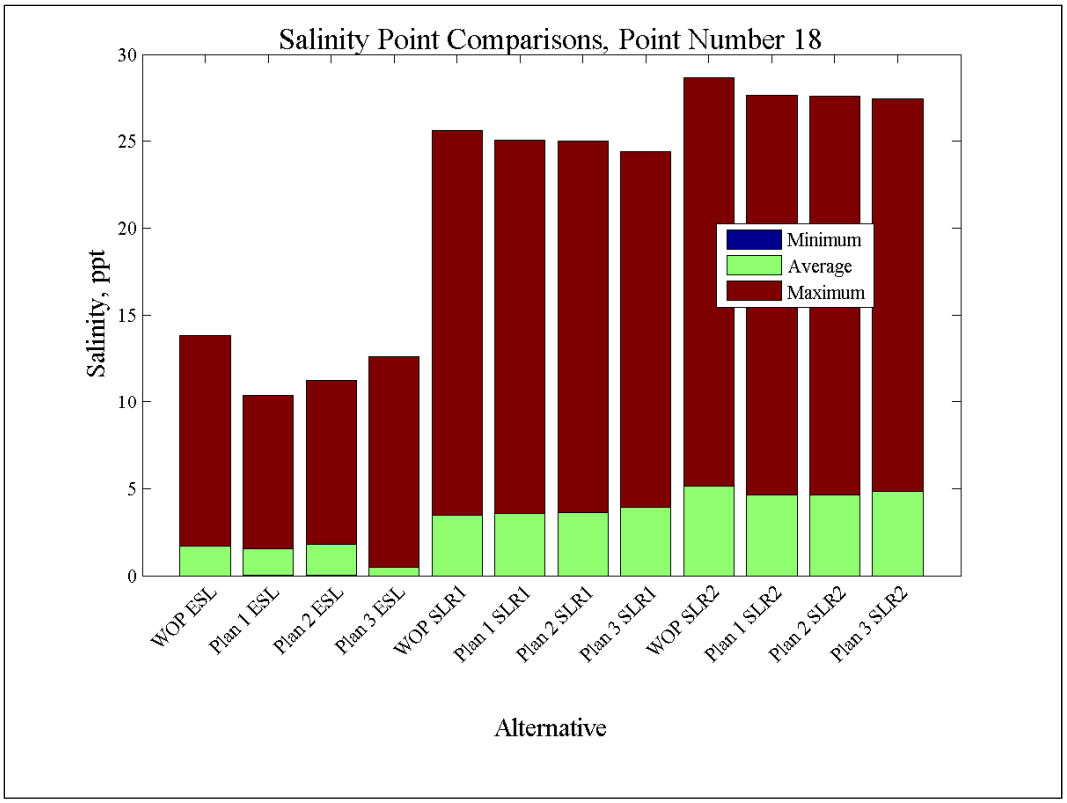

Figure 198. Water-surface elevation and salinity comparisons at Point 19.

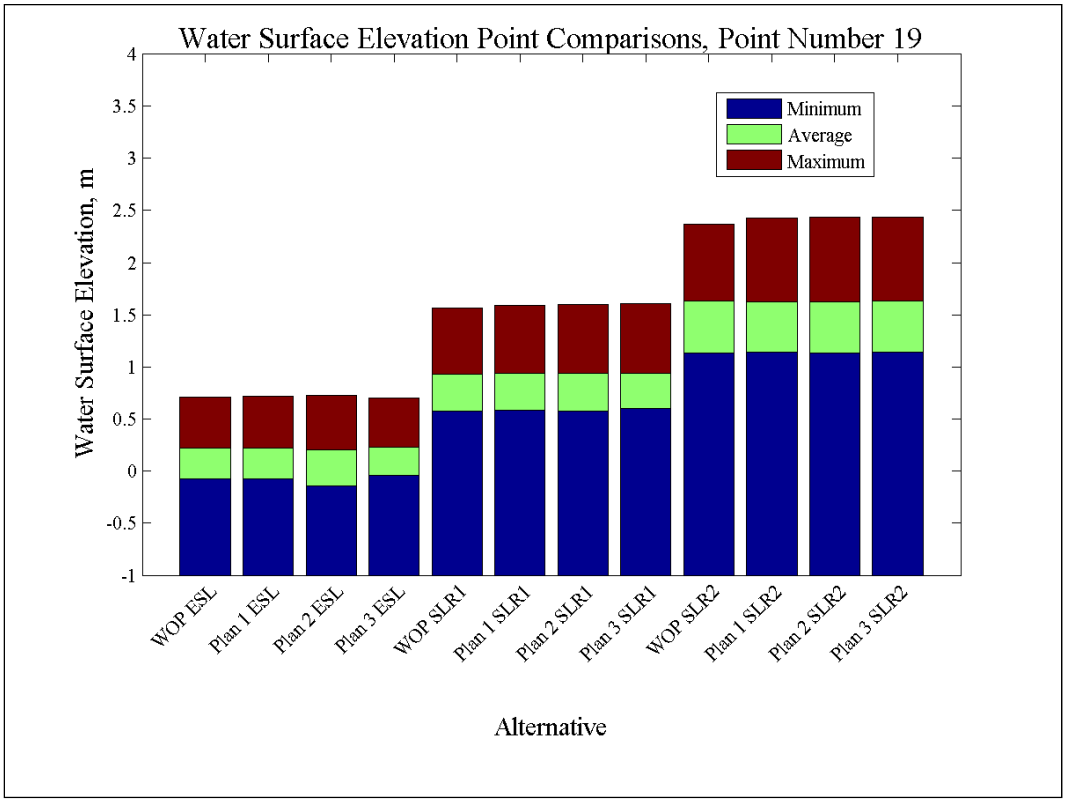

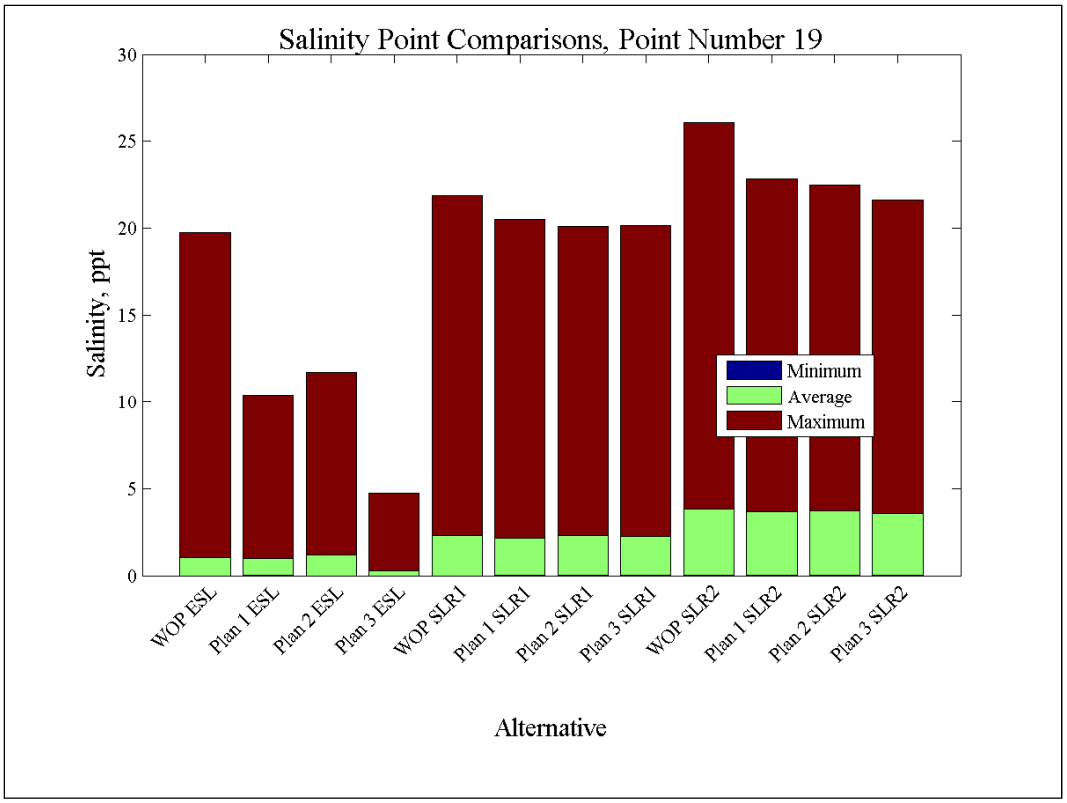

Figure 199. Water-surface elevation and salinity comparisons at Point 20.

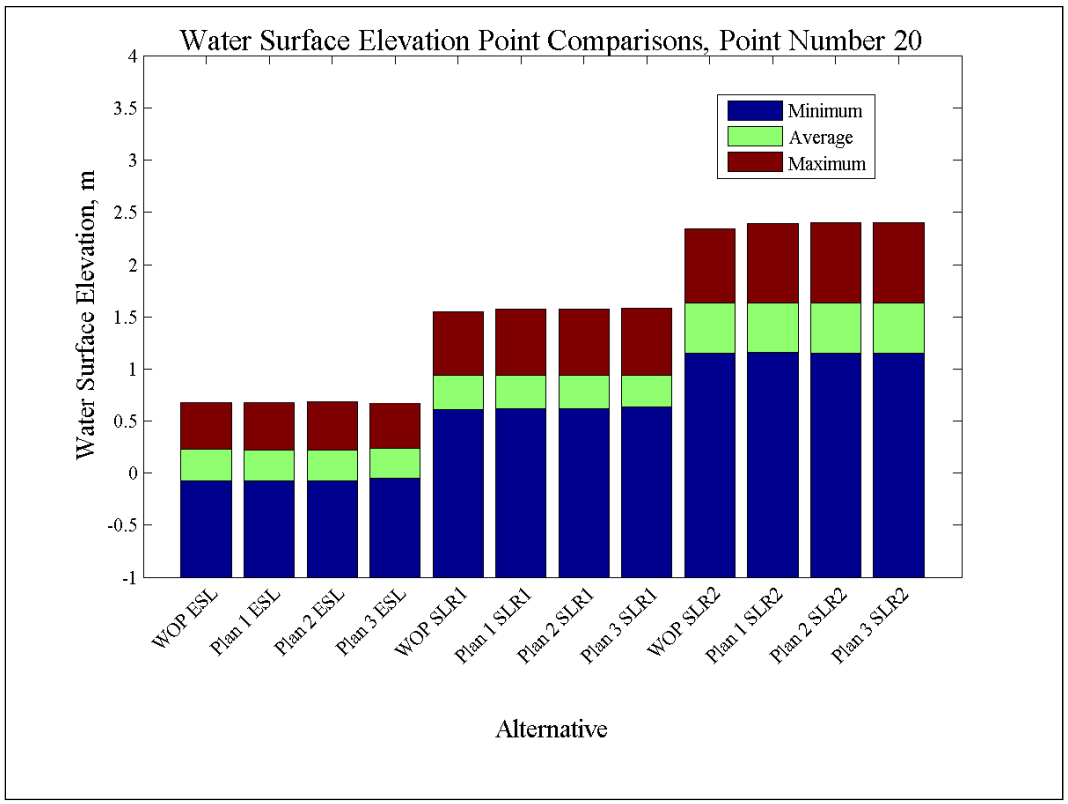

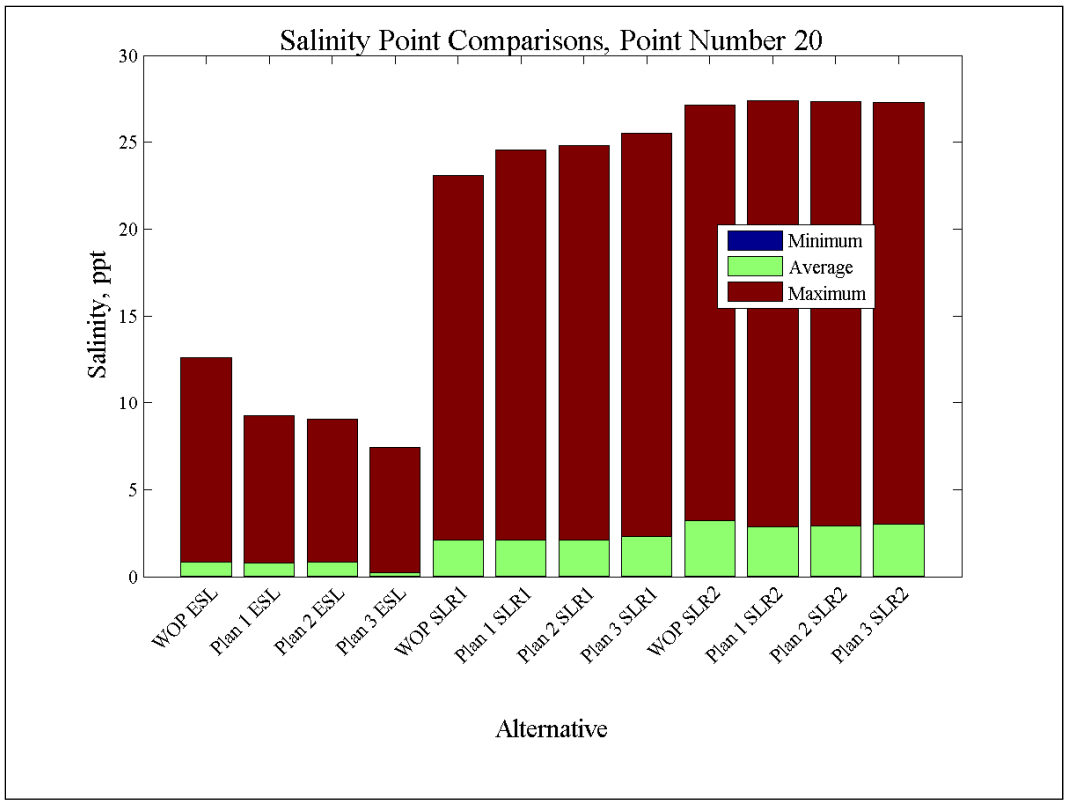

Figure 200. Water-surface elevation and salinity comparisons at Point 21.

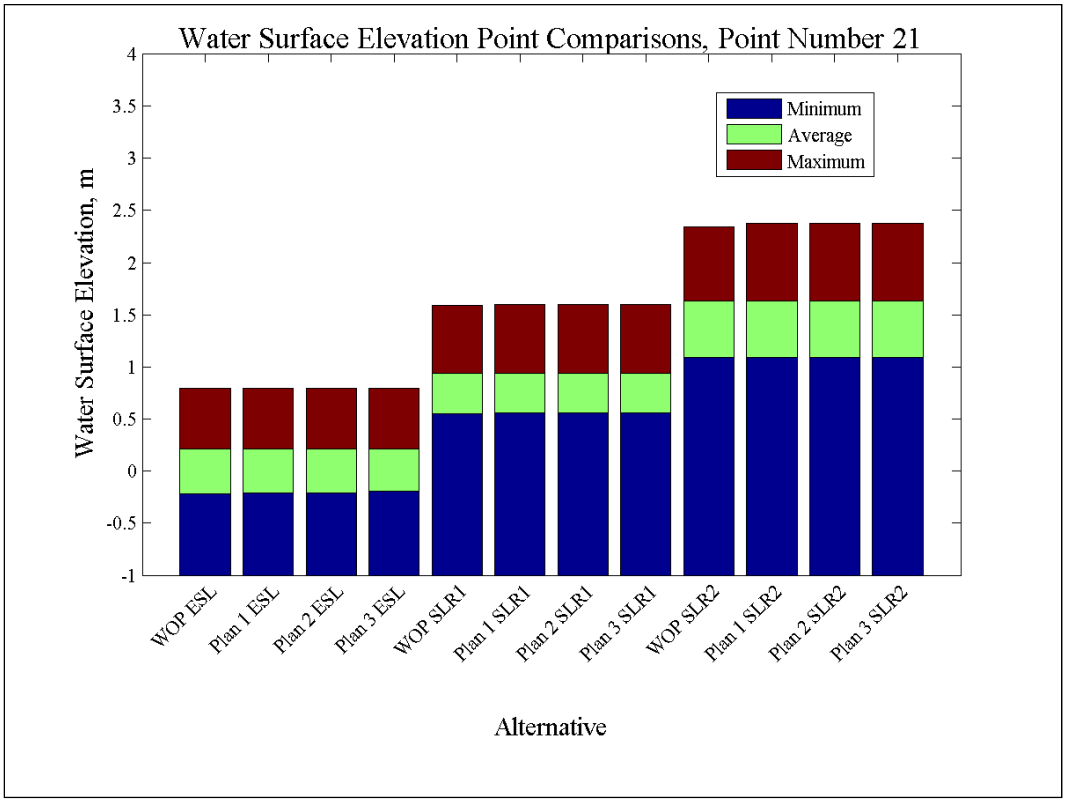

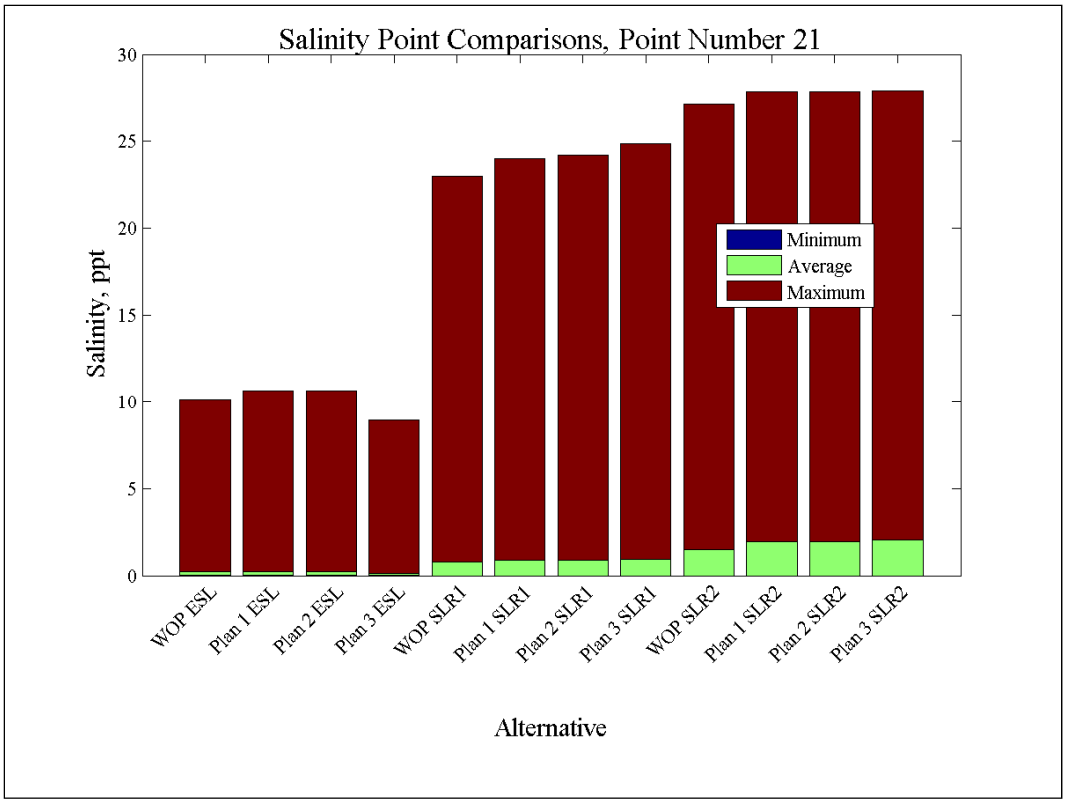

Figure 201. Water-surface elevation and salinity comparisons at Point 22.

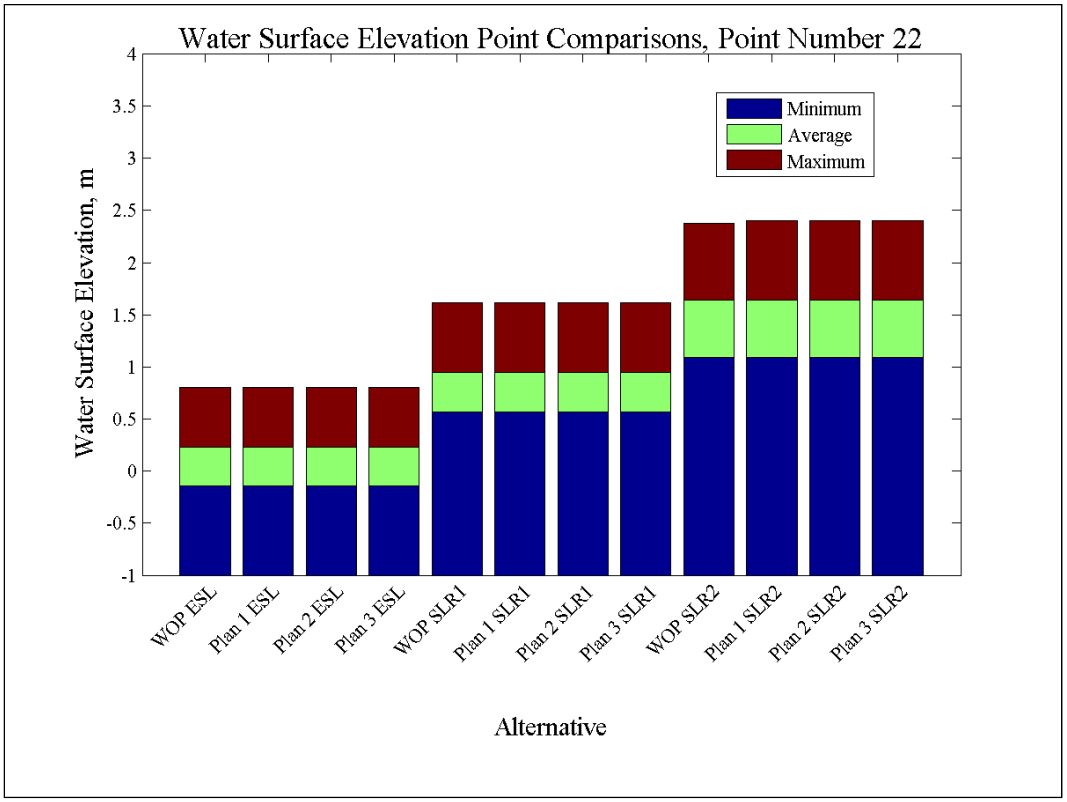

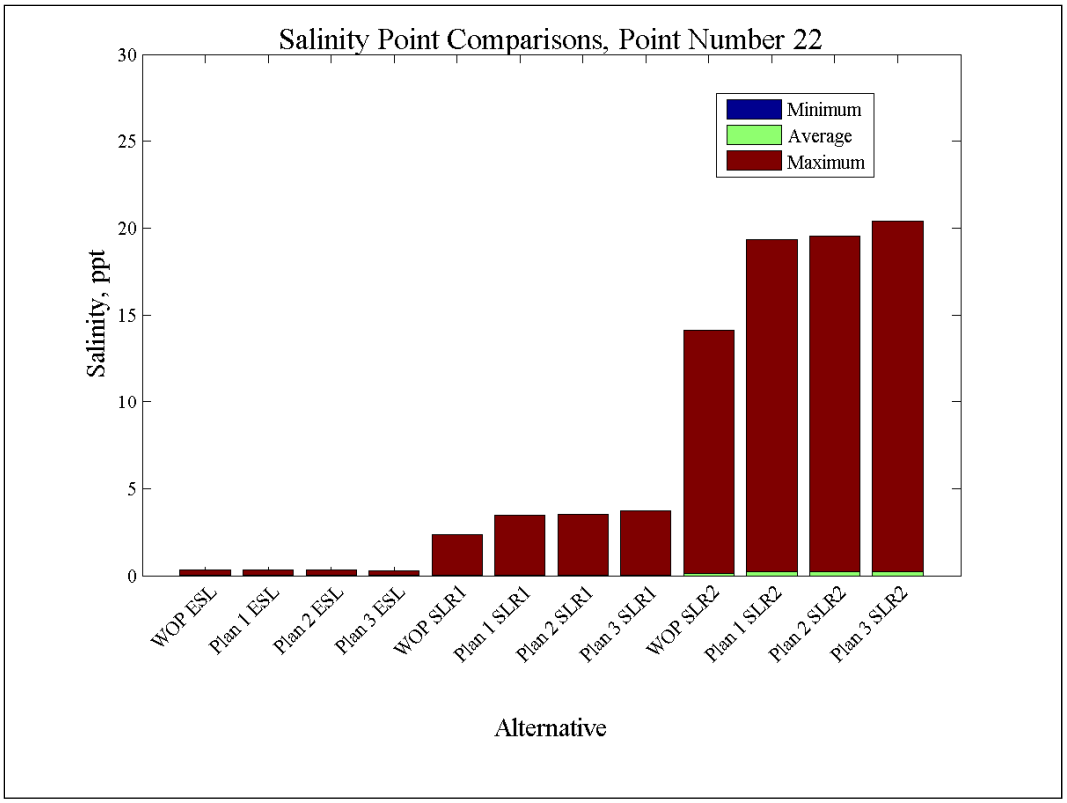

Figure 202. Water-surface elevation and salinity comparisons at Point 23.

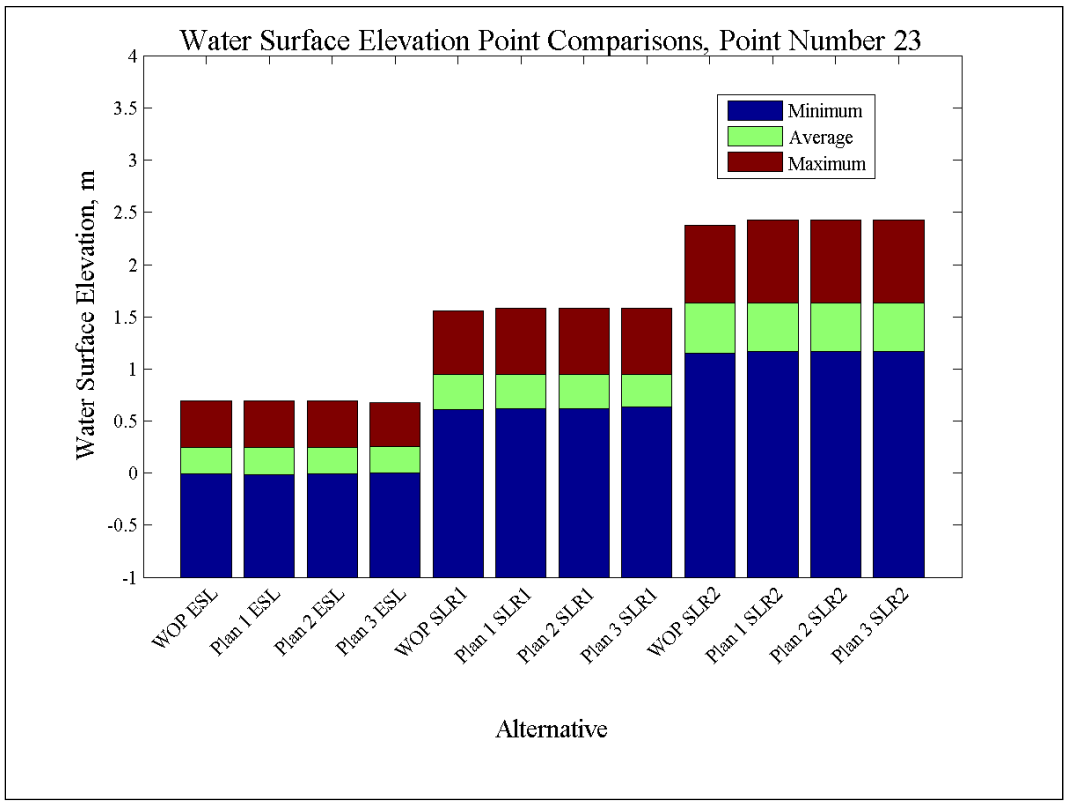

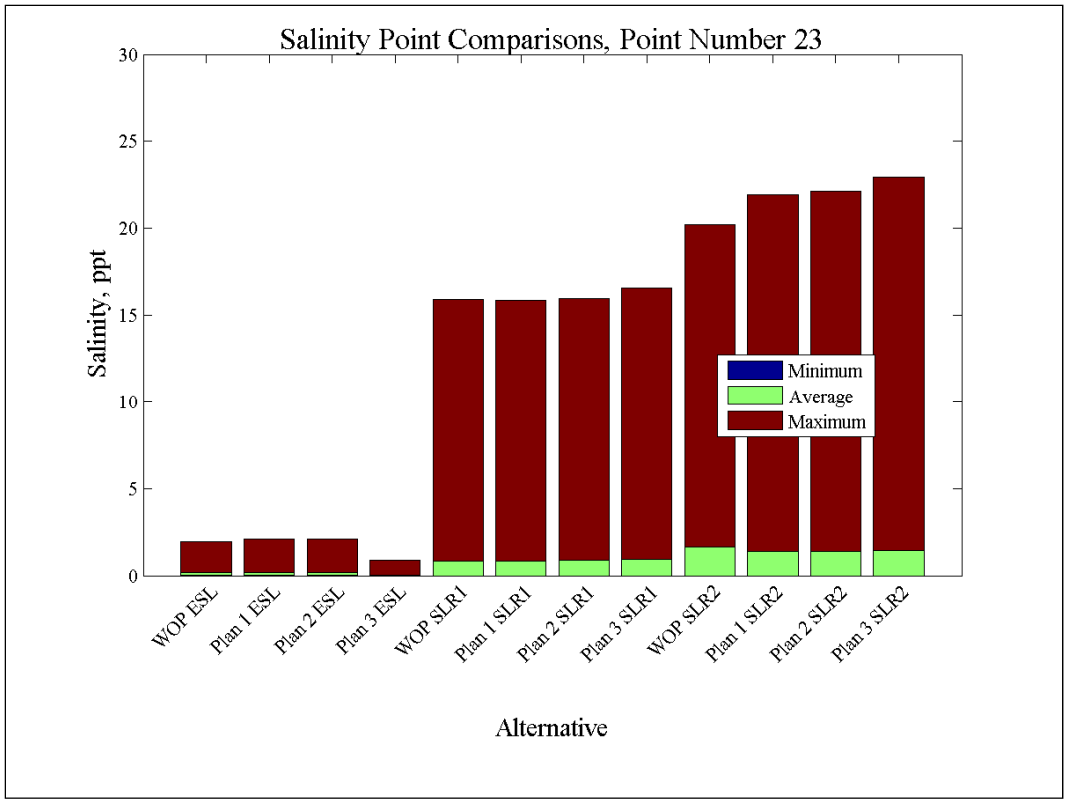

Figure 203. Water-surface elevation and salinity comparisons at Point 24.

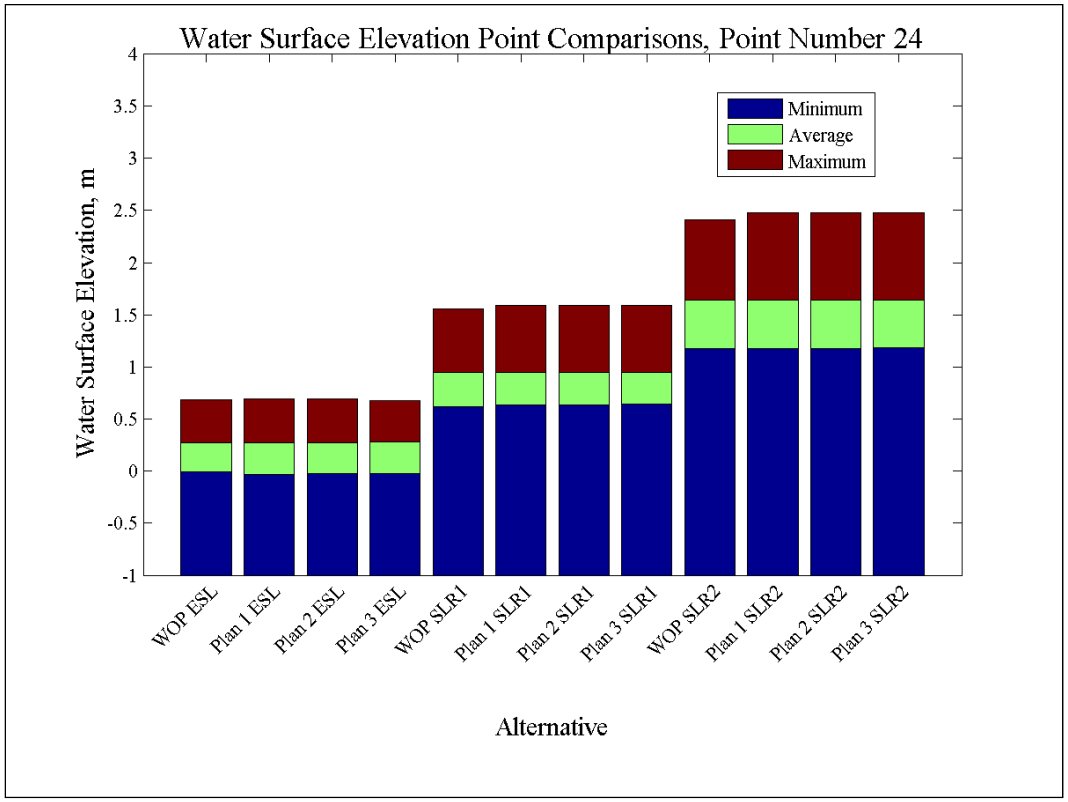

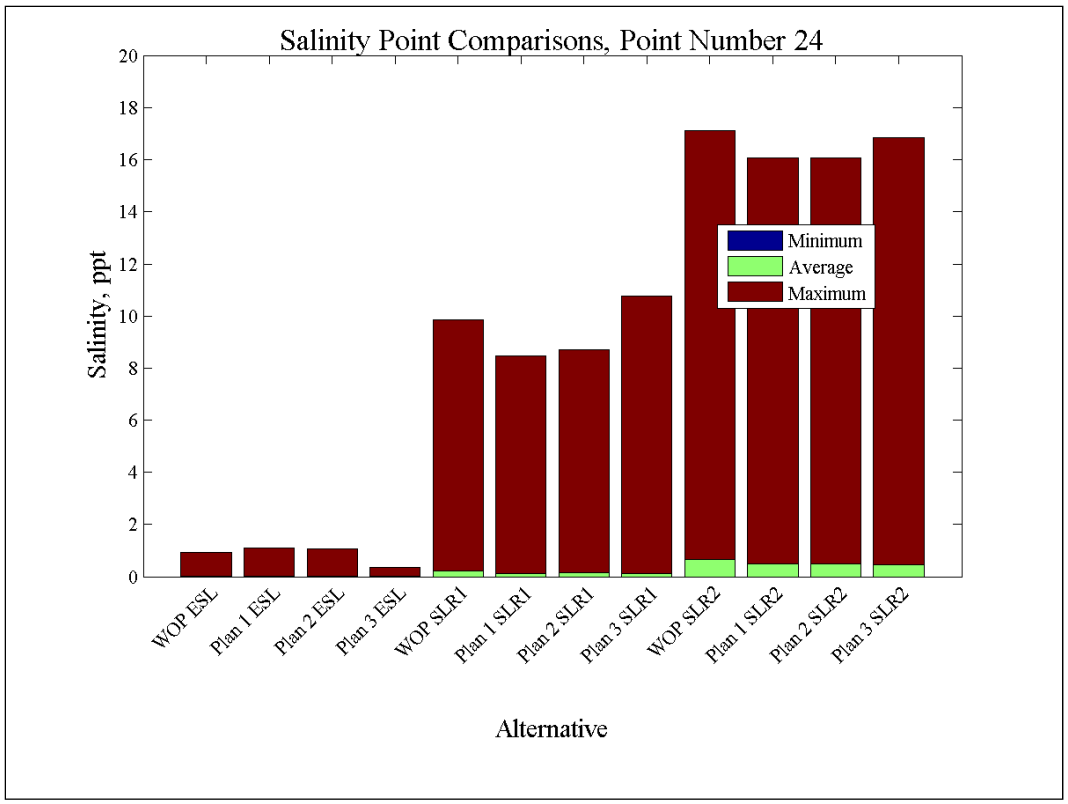

Figure 204. Water-surface elevation and salinity comparisons at Point 25.

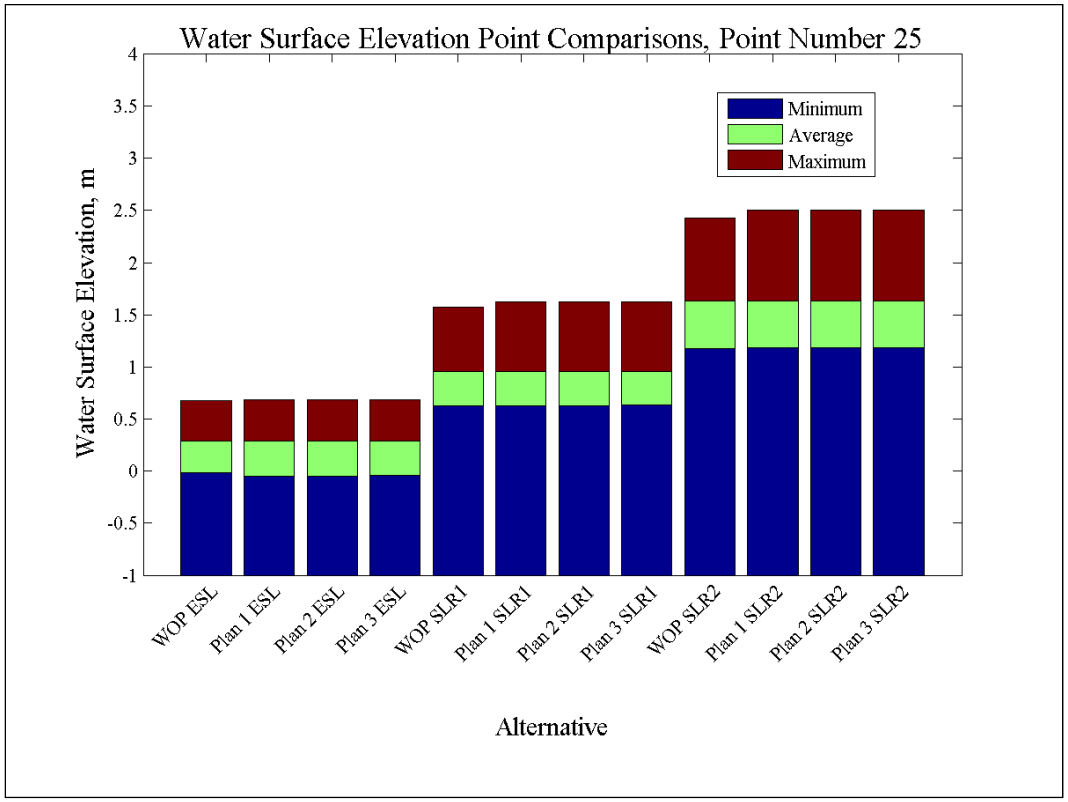

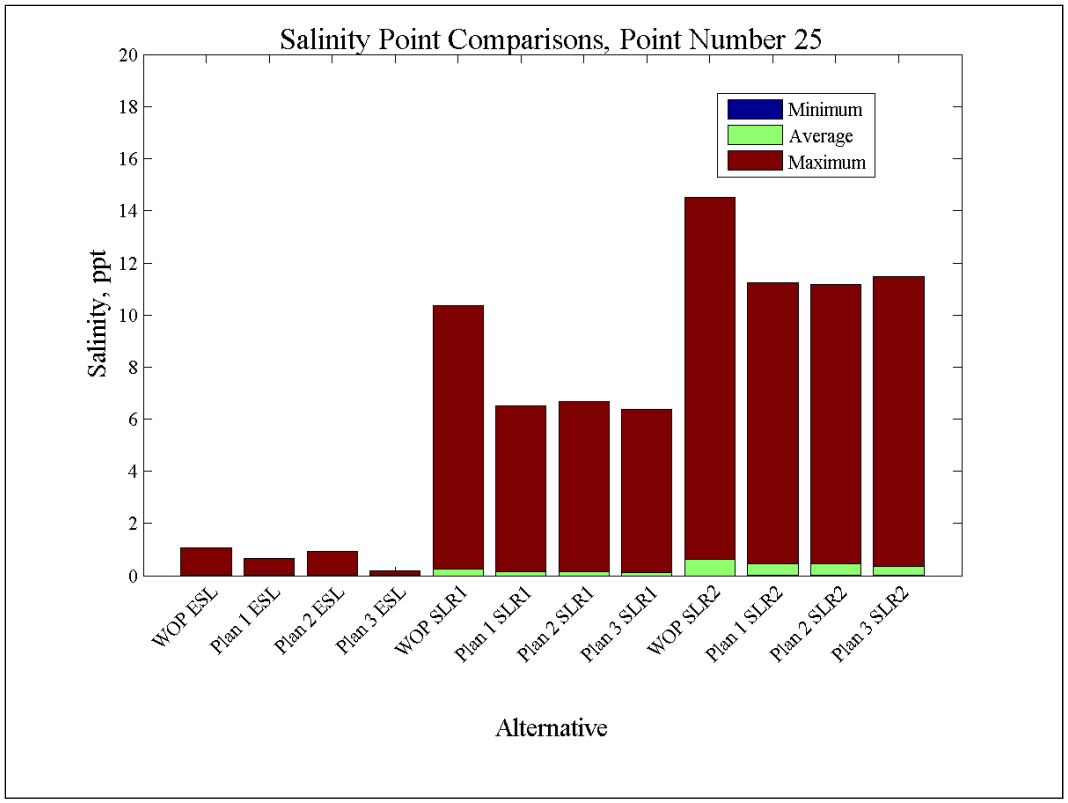

Figure 205. Water-surface elevation and salinity comparisons at Point 26.

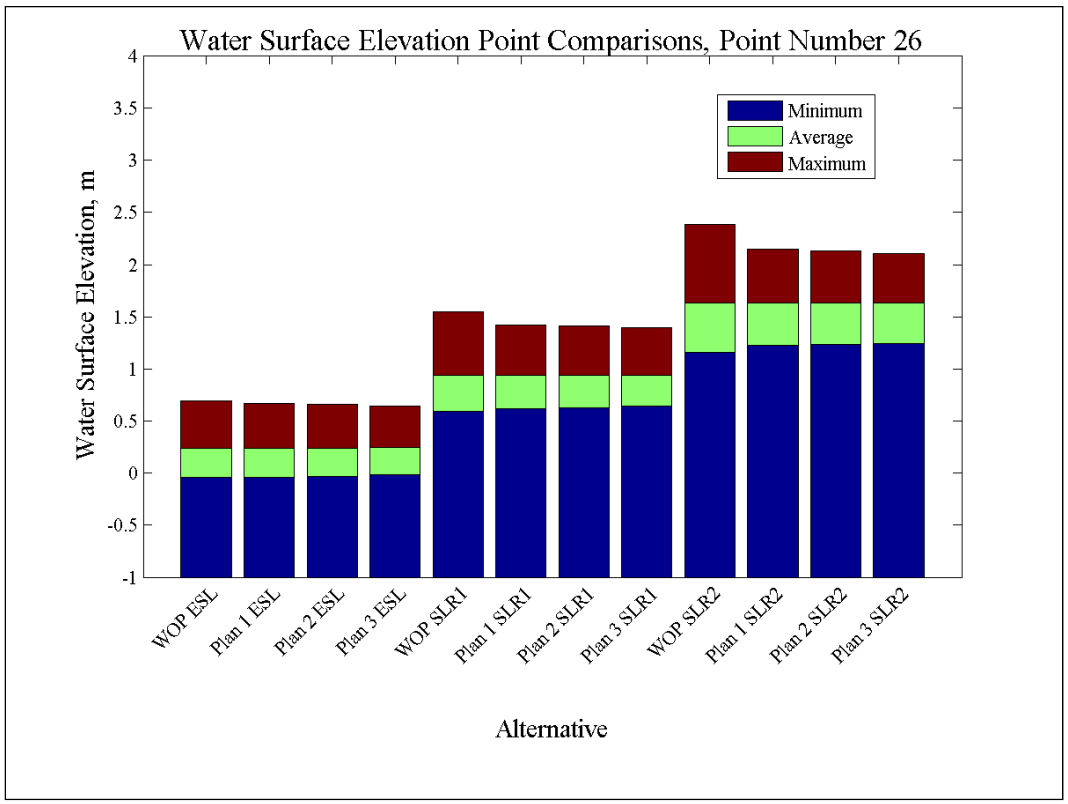

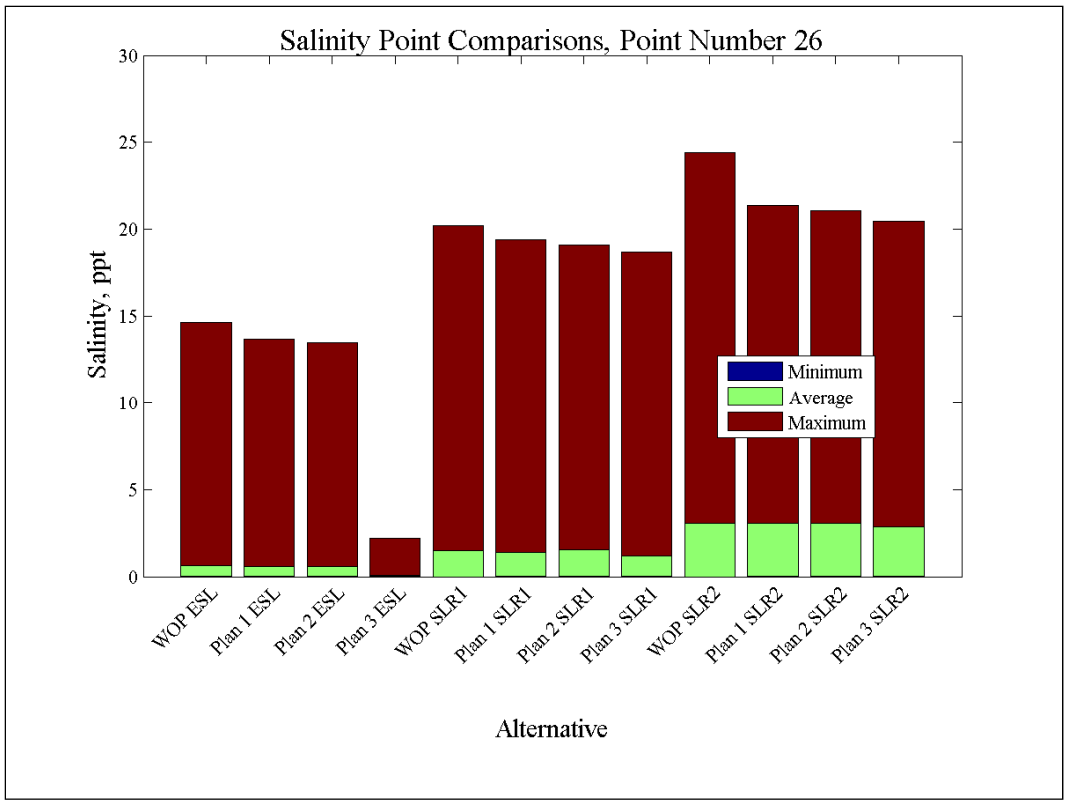

Figure 206. Water-surface elevation and salinity comparisons at Point 27.

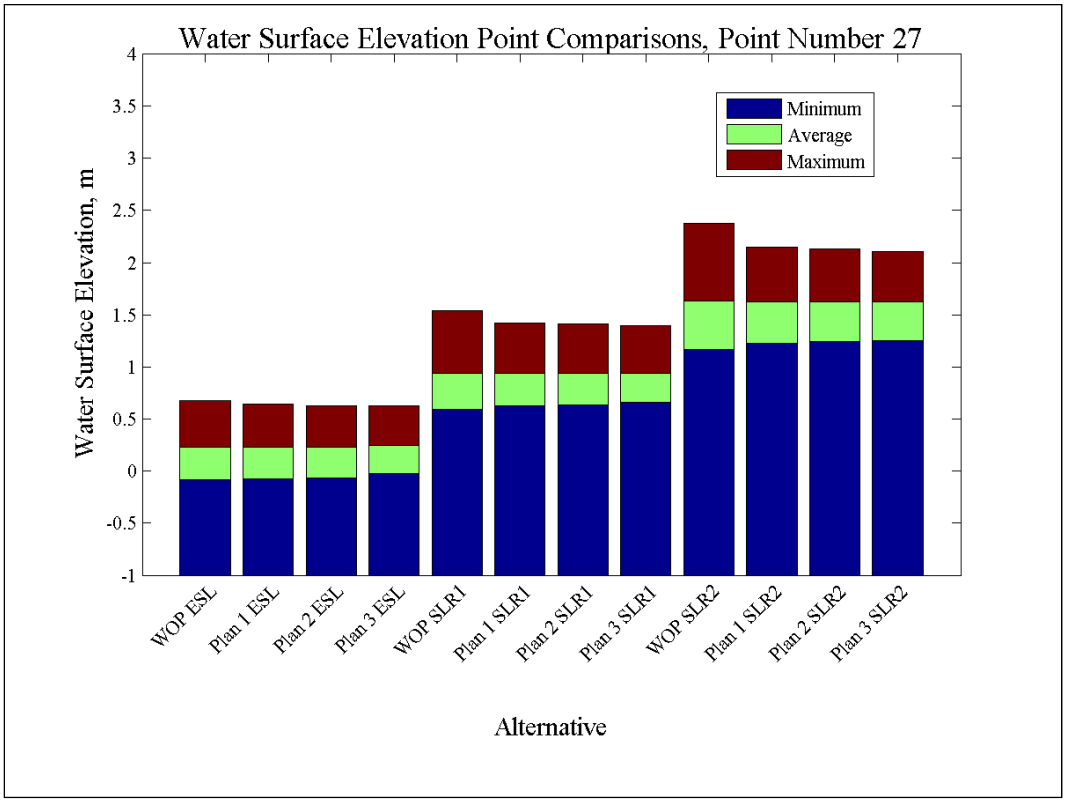

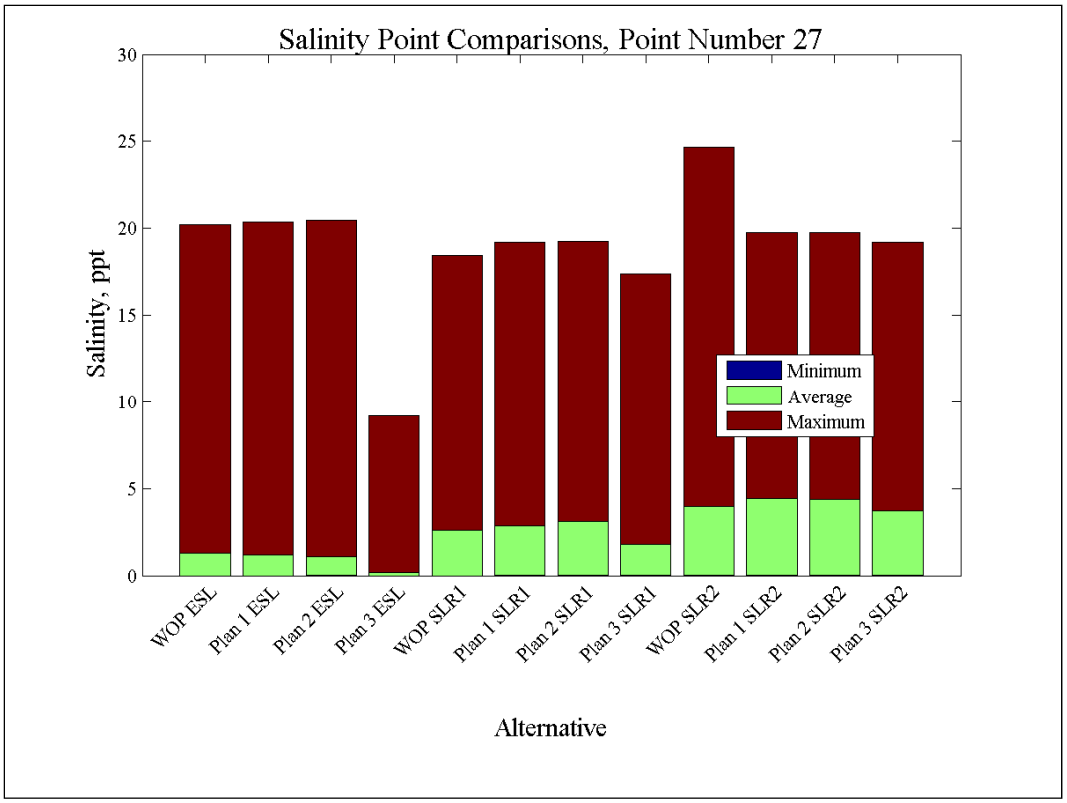

Figure 207. Water-surface elevation and salinity comparisons at Point 28.

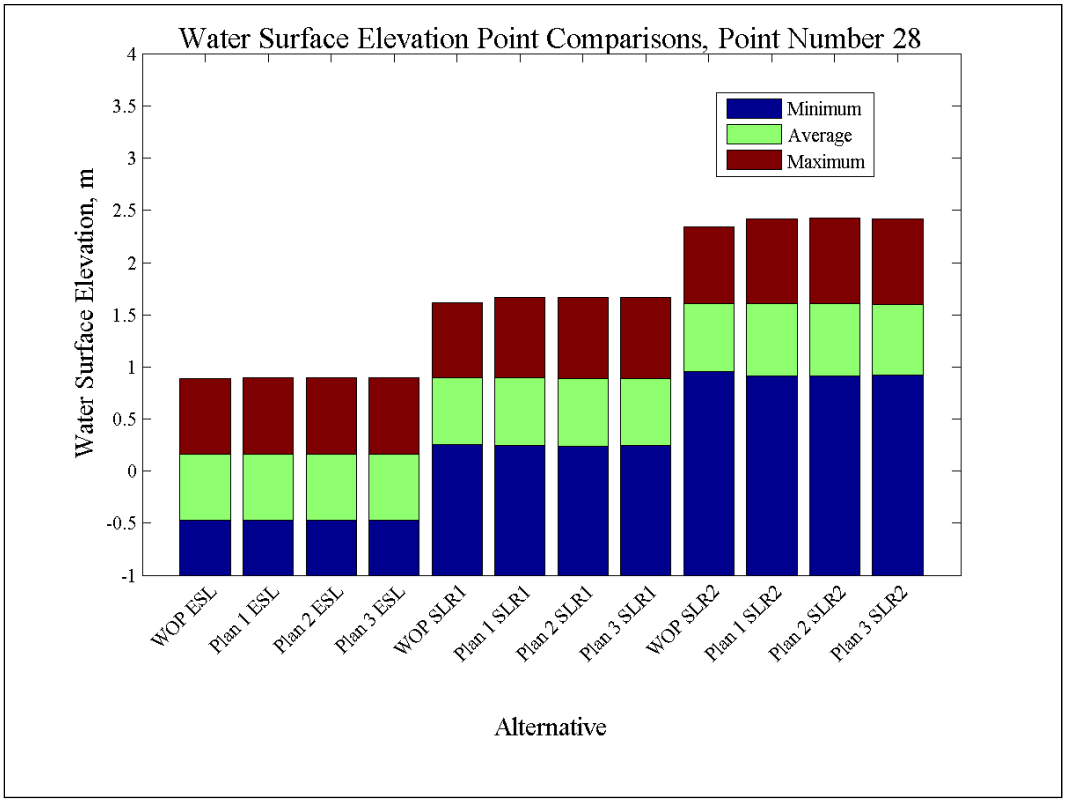

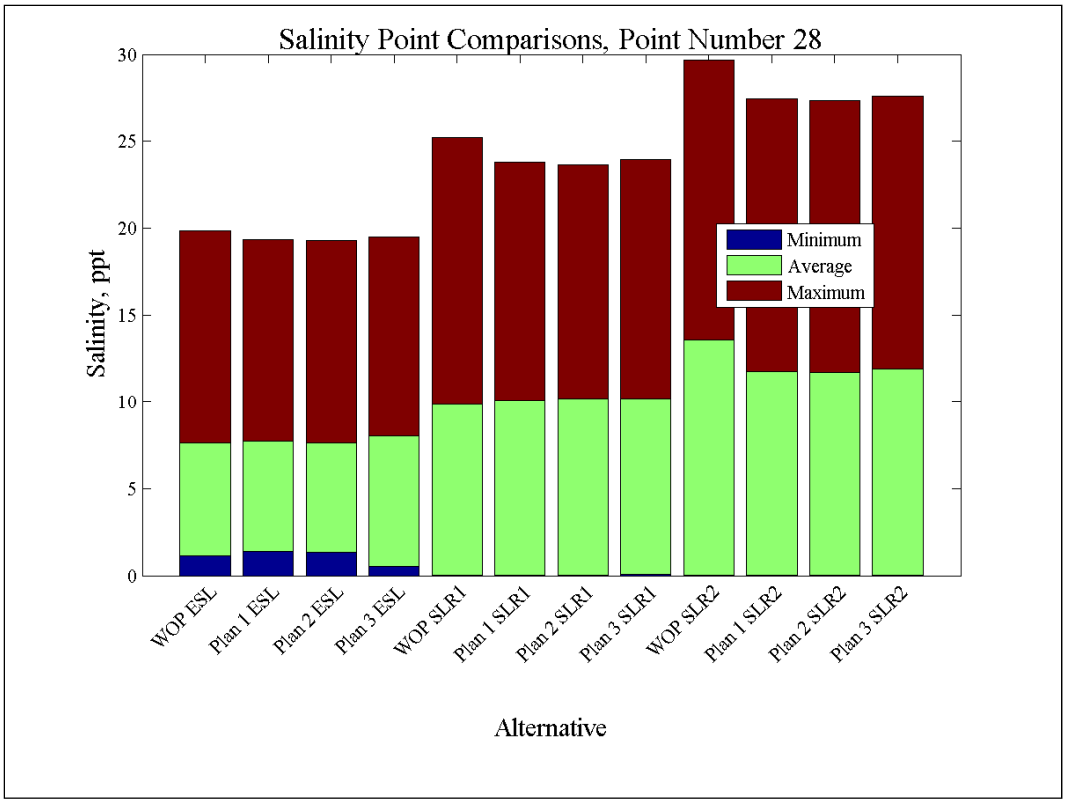

Figure 208. Water-surface elevation and salinity comparisons at Point 29.

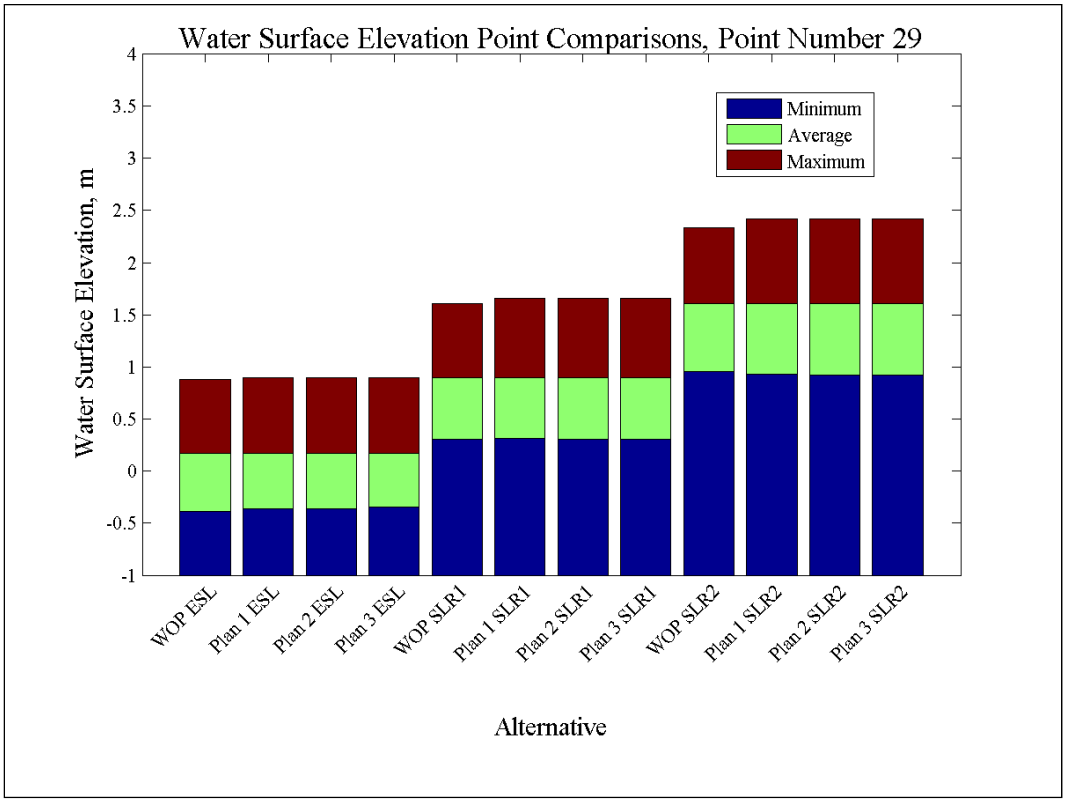

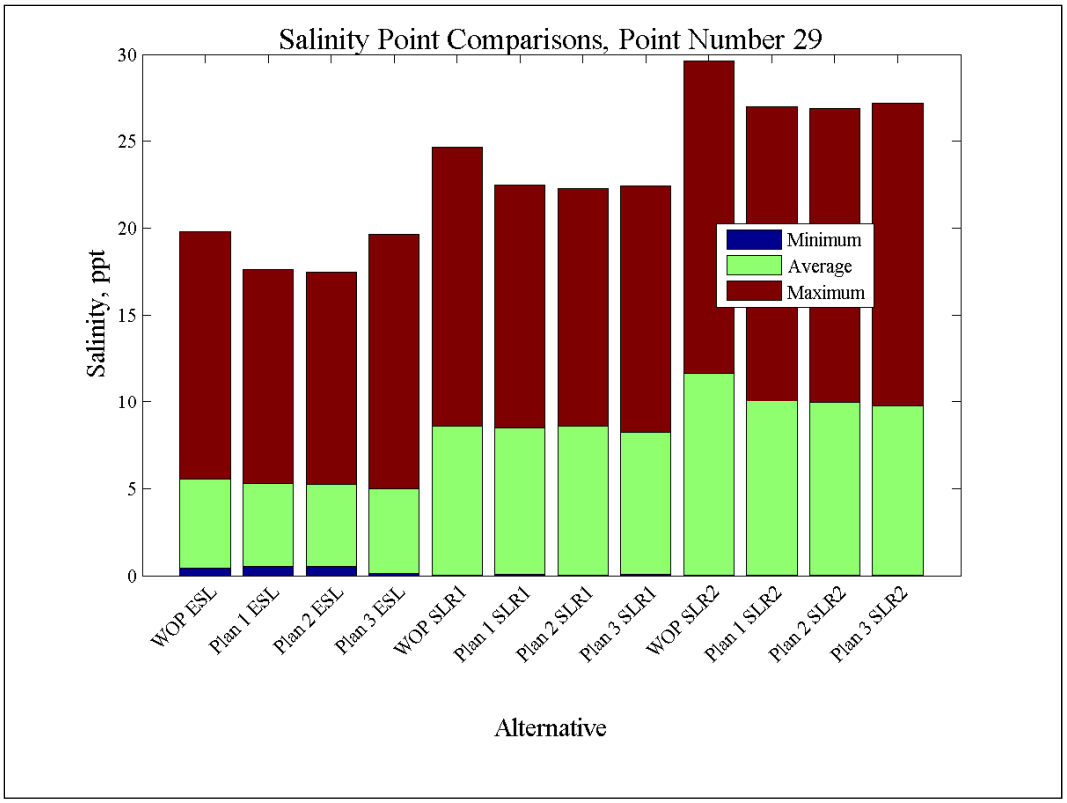

Figure 209. Water-surface elevation and salinity comparisons at Point 30.

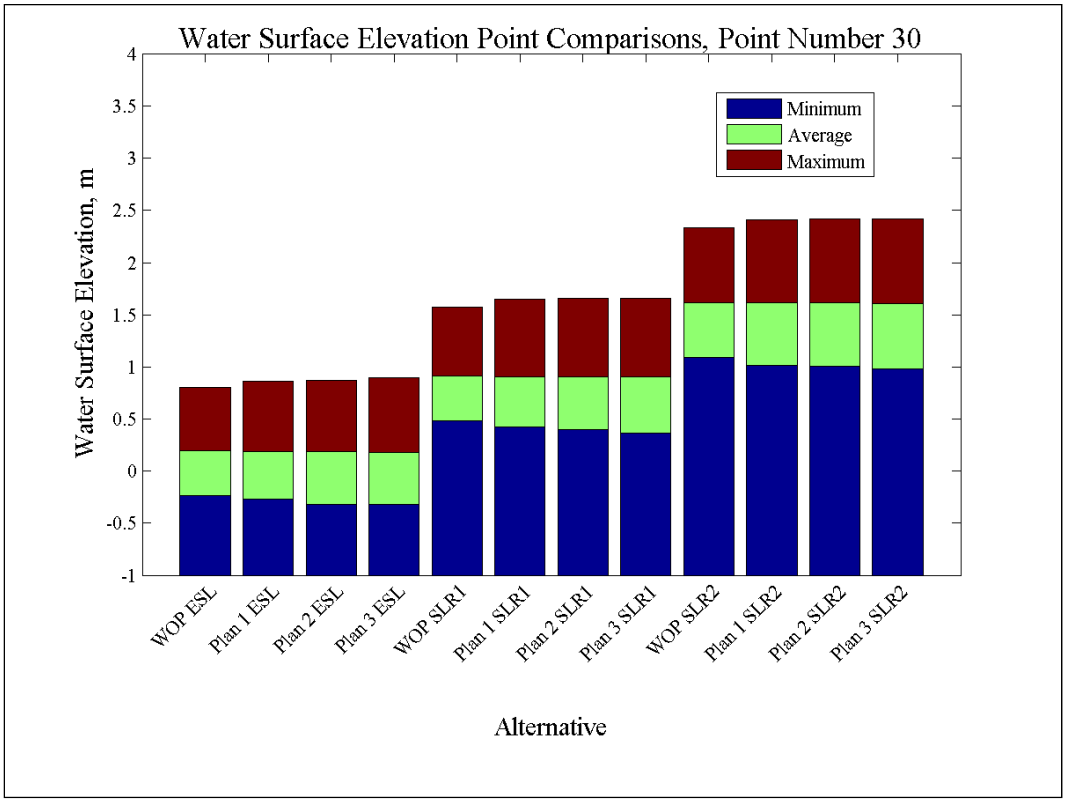

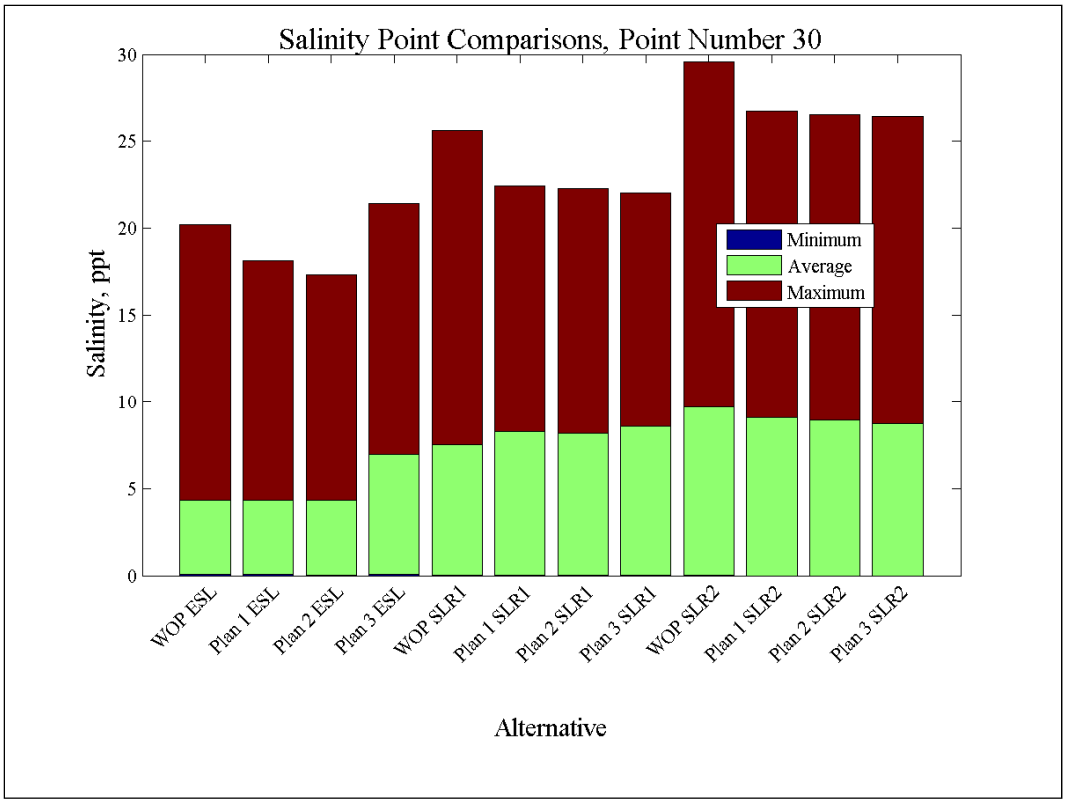

Figure 210. Water-surface elevation and salinity comparisons at Point 31.

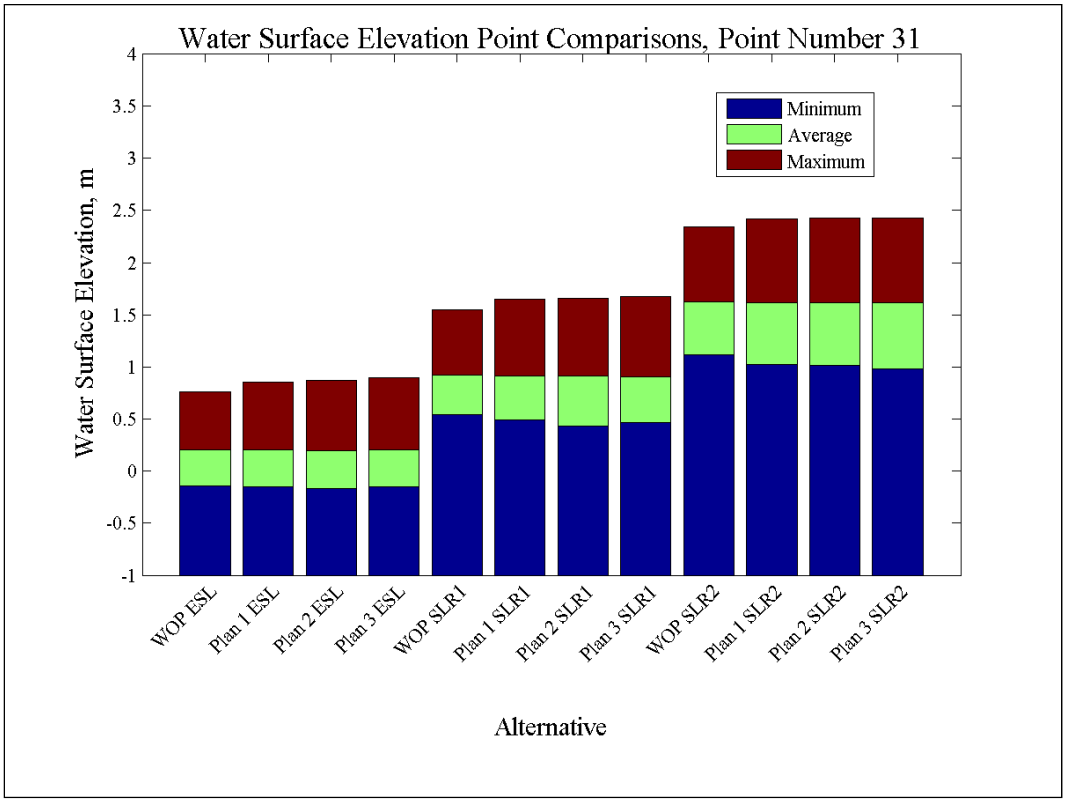

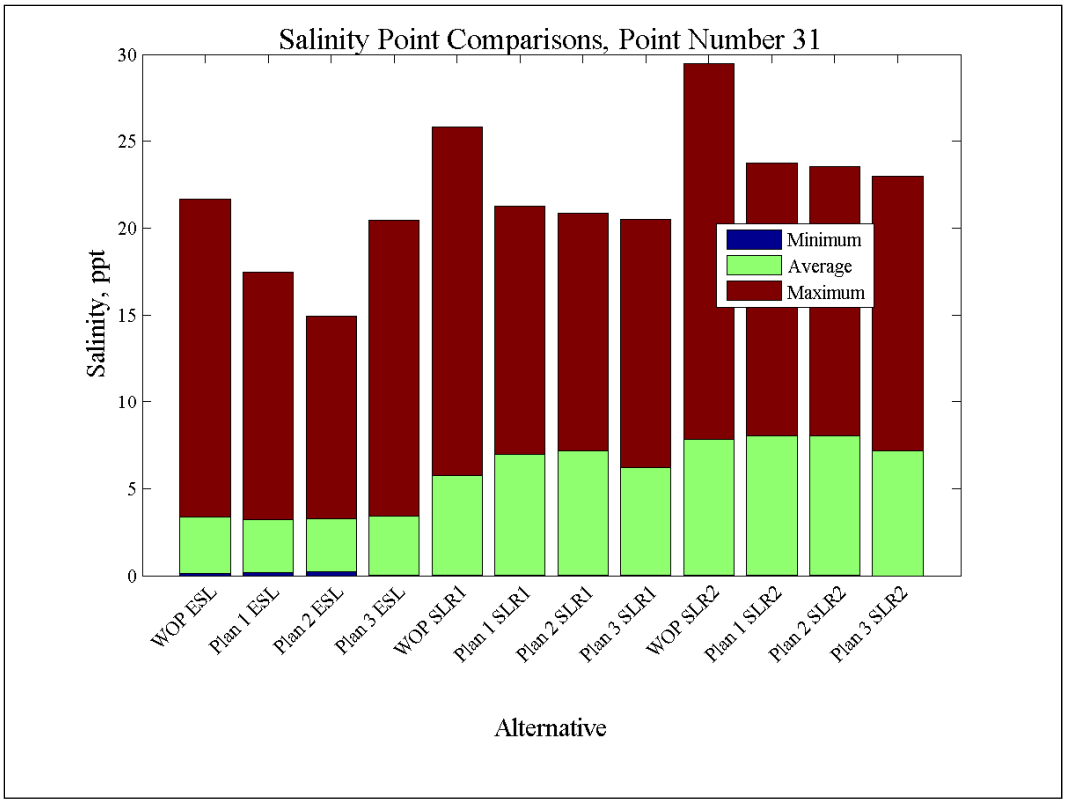

Figure 211. Water-surface elevation and salinity comparisons at Point 32.

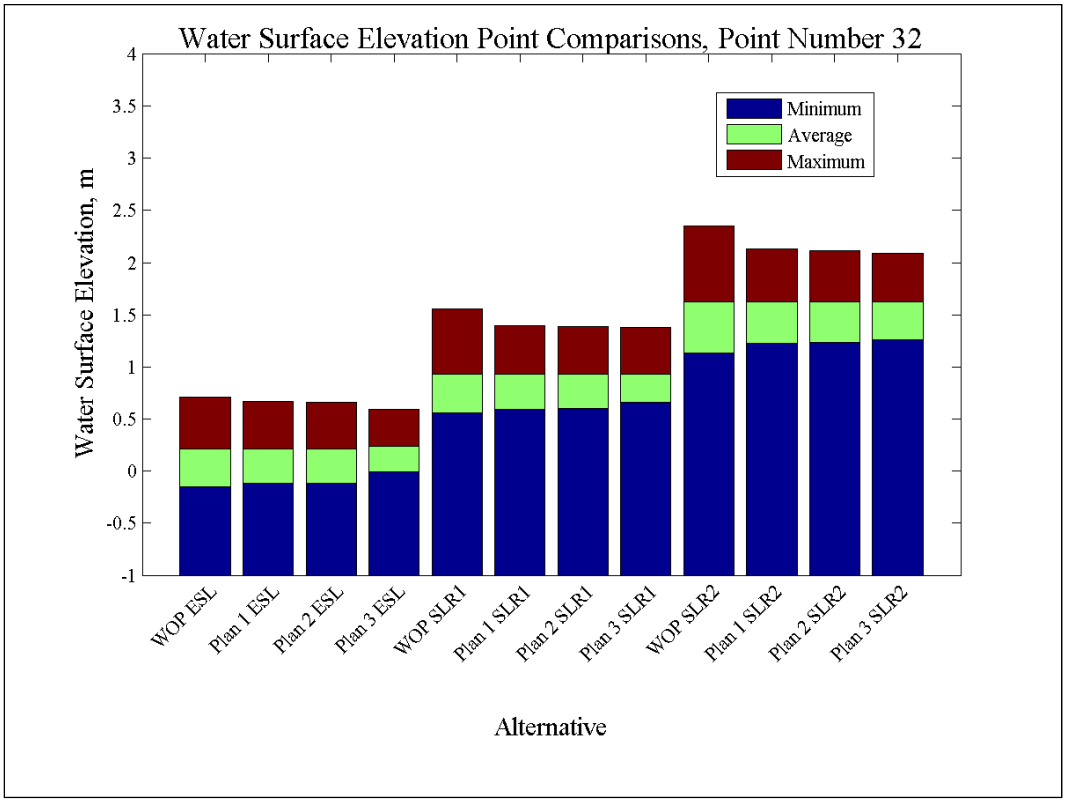

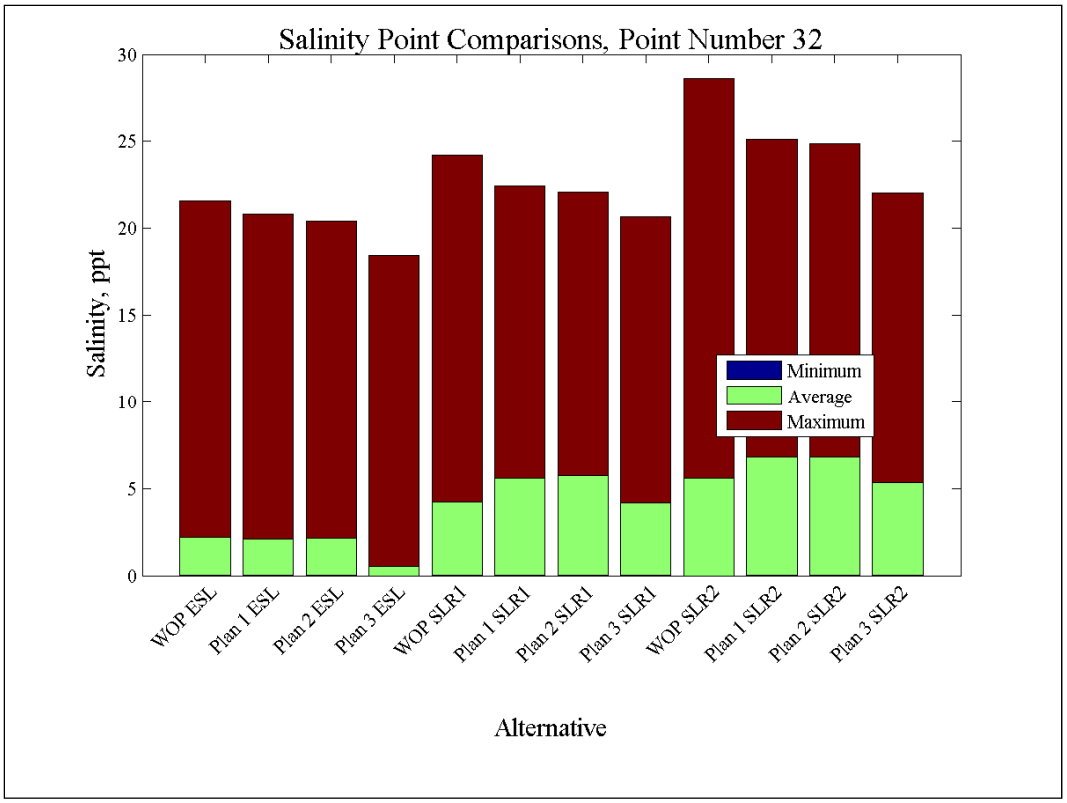

Figure 212. Water-surface elevation and salinity comparisons at Point 33.

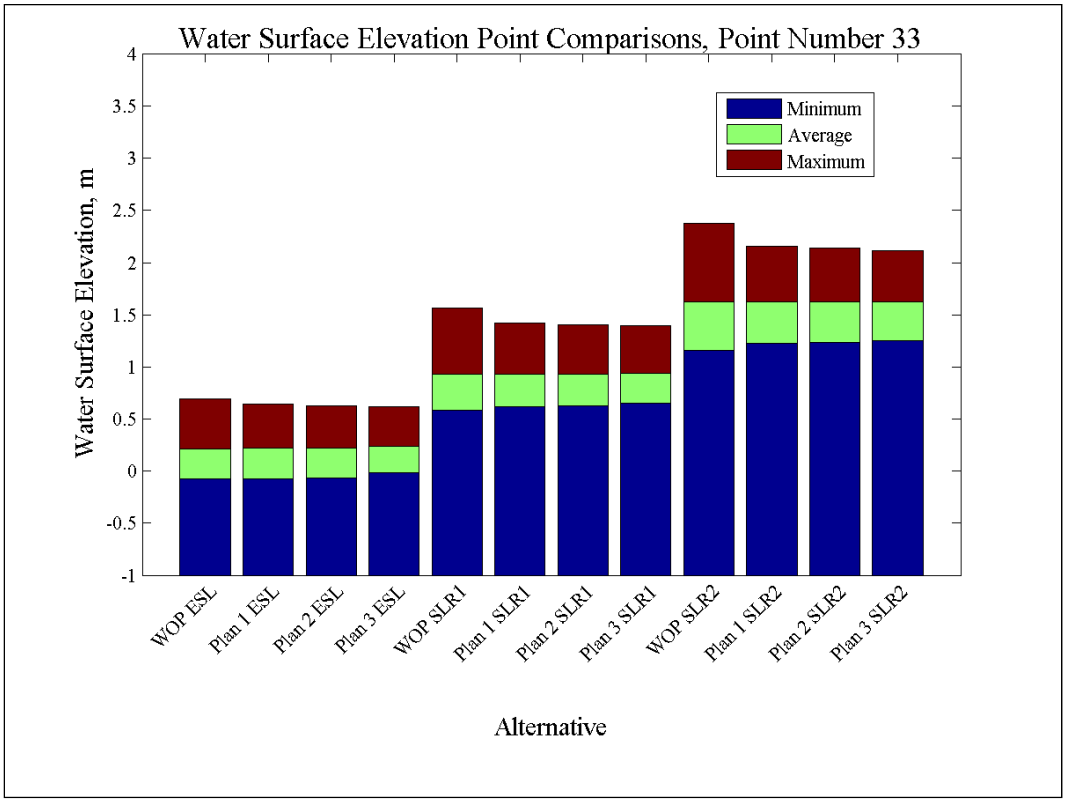

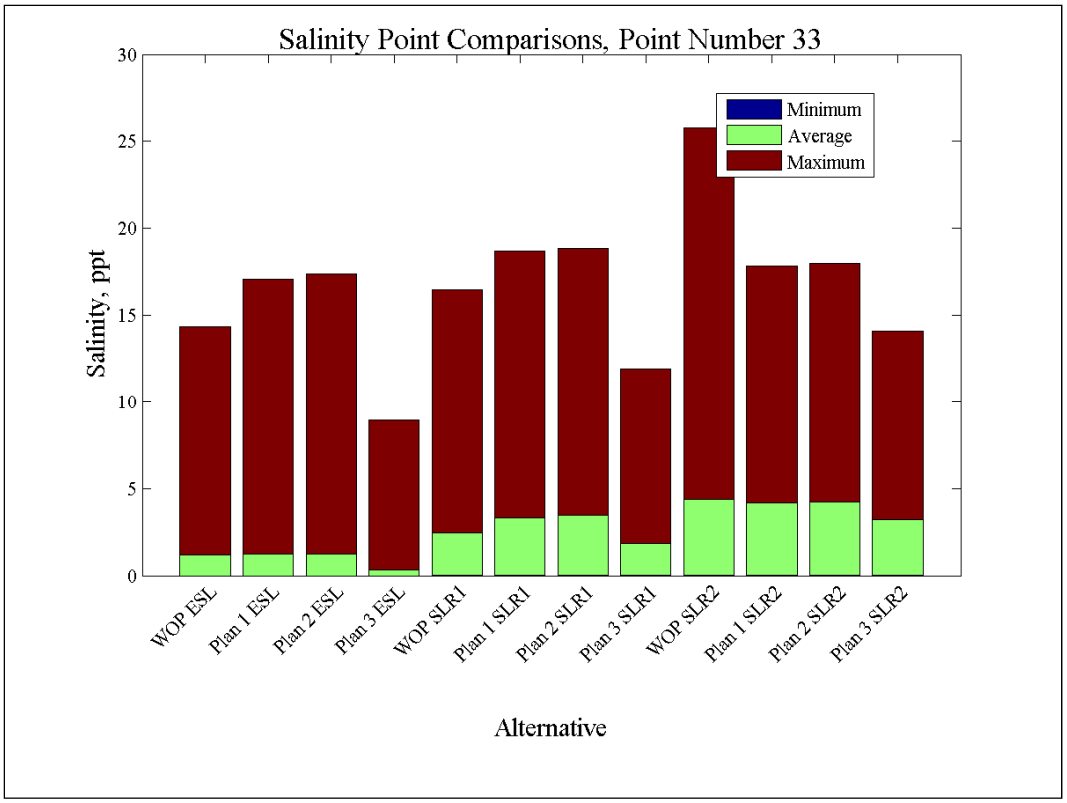

Figure 213. Water-surface elevation and salinity comparisons at Point 34.

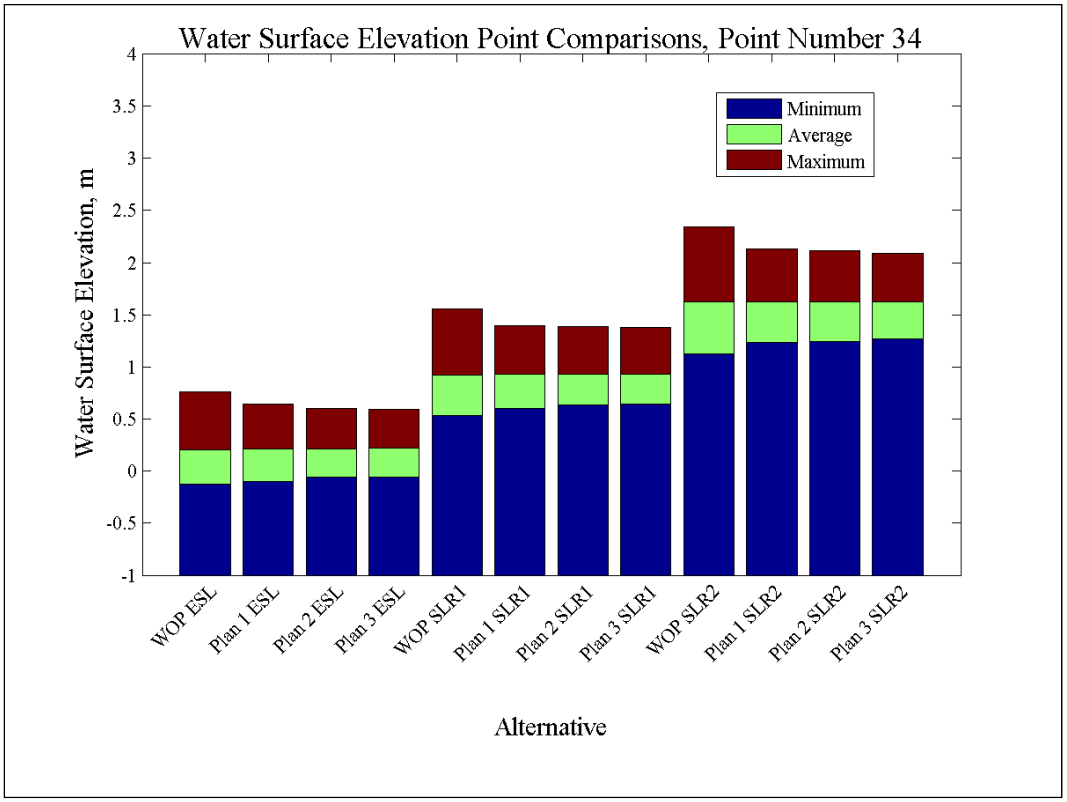

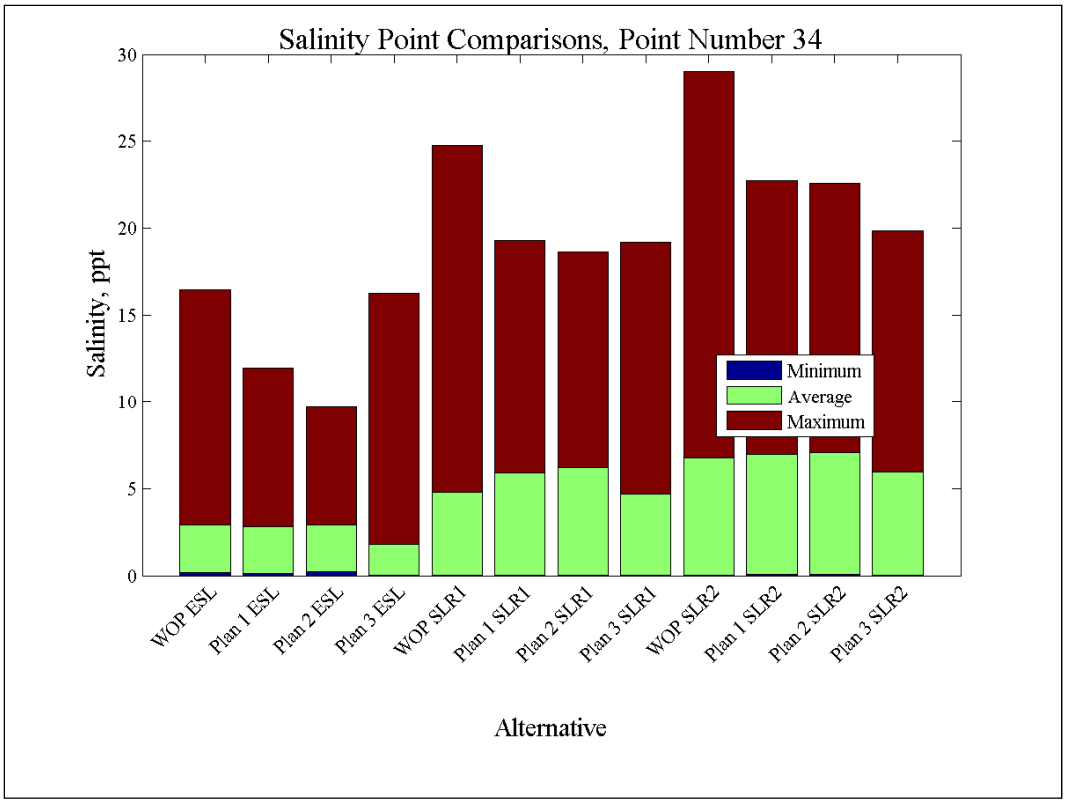

Figure 214. Water-surface elevation and salinity comparisons at Point 35.

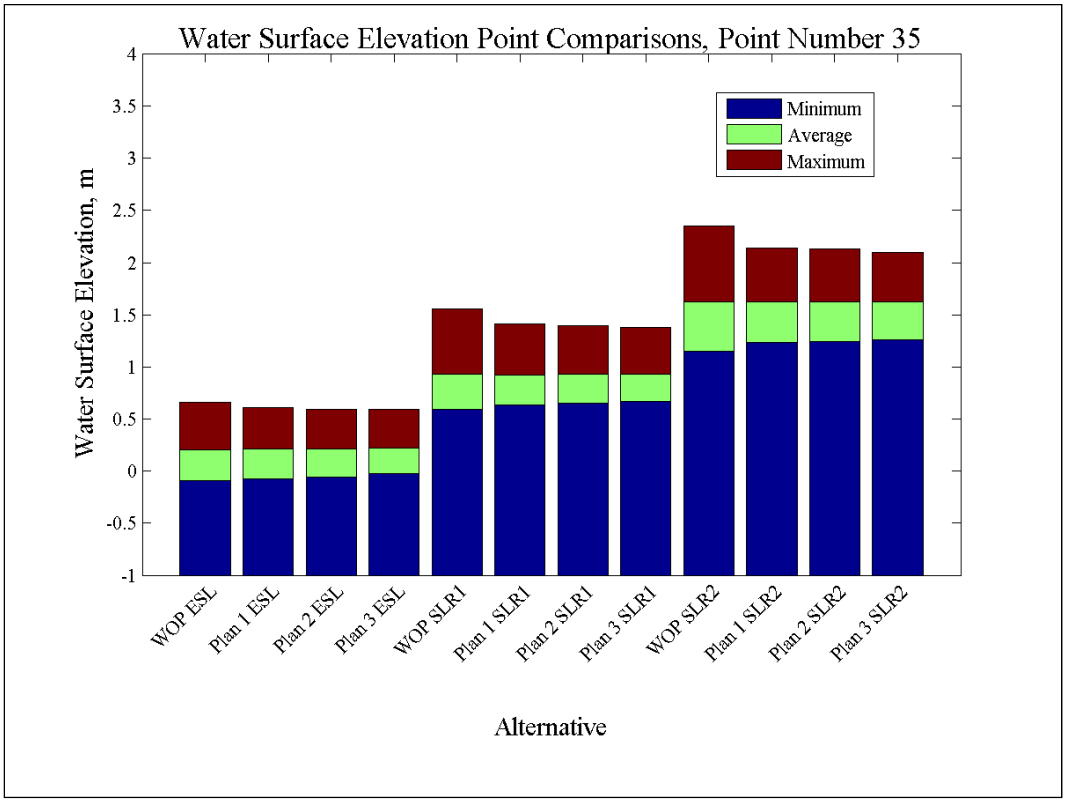

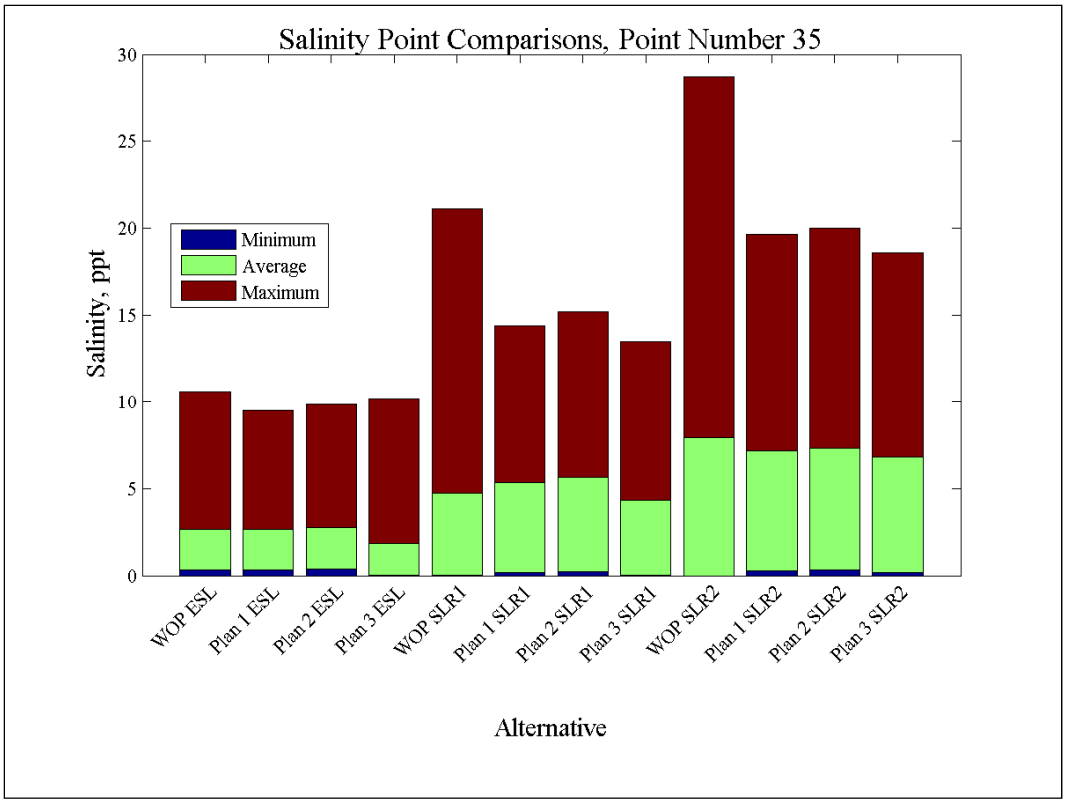

Figure 215. Water-surface elevation and salinity comparisons at Point 36.

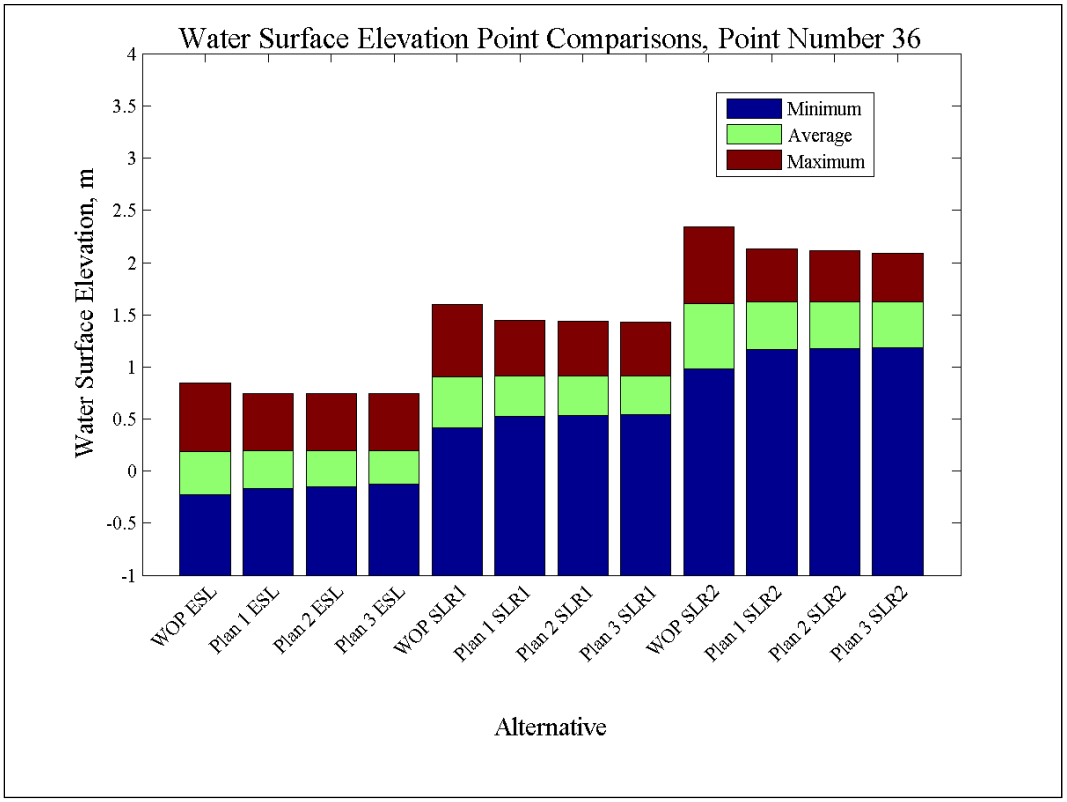

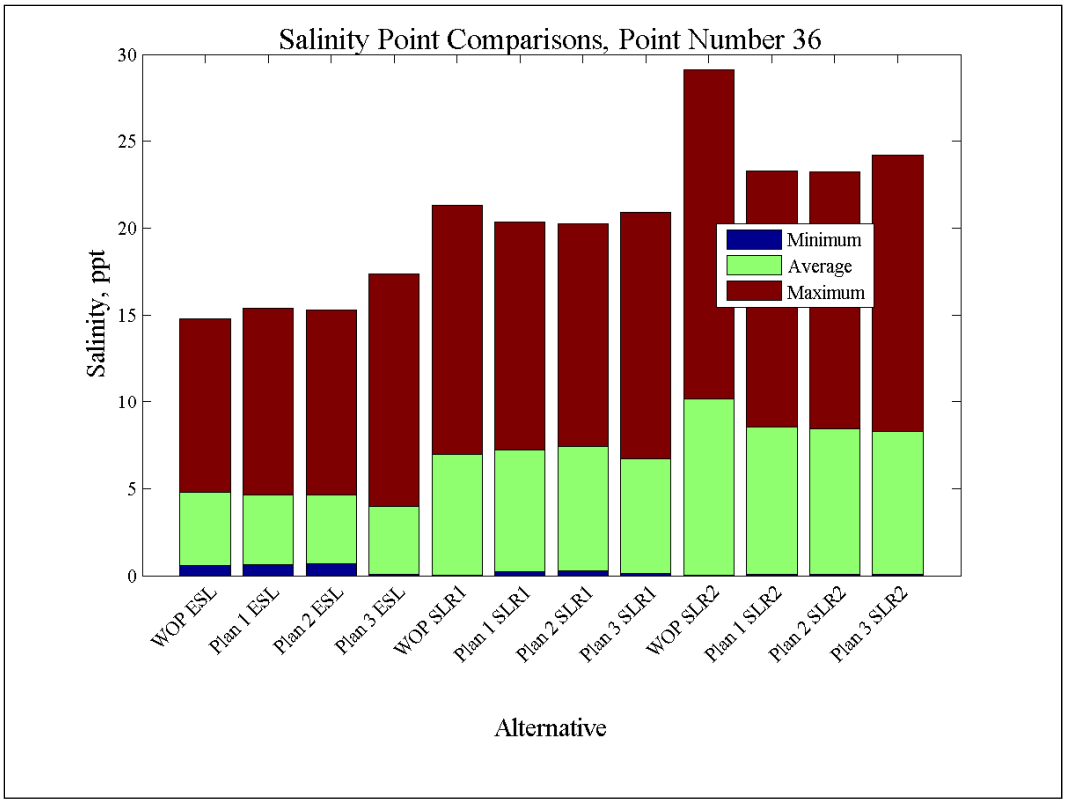

Figure 216. Water-surface elevation and salinity comparisons at Point 37.

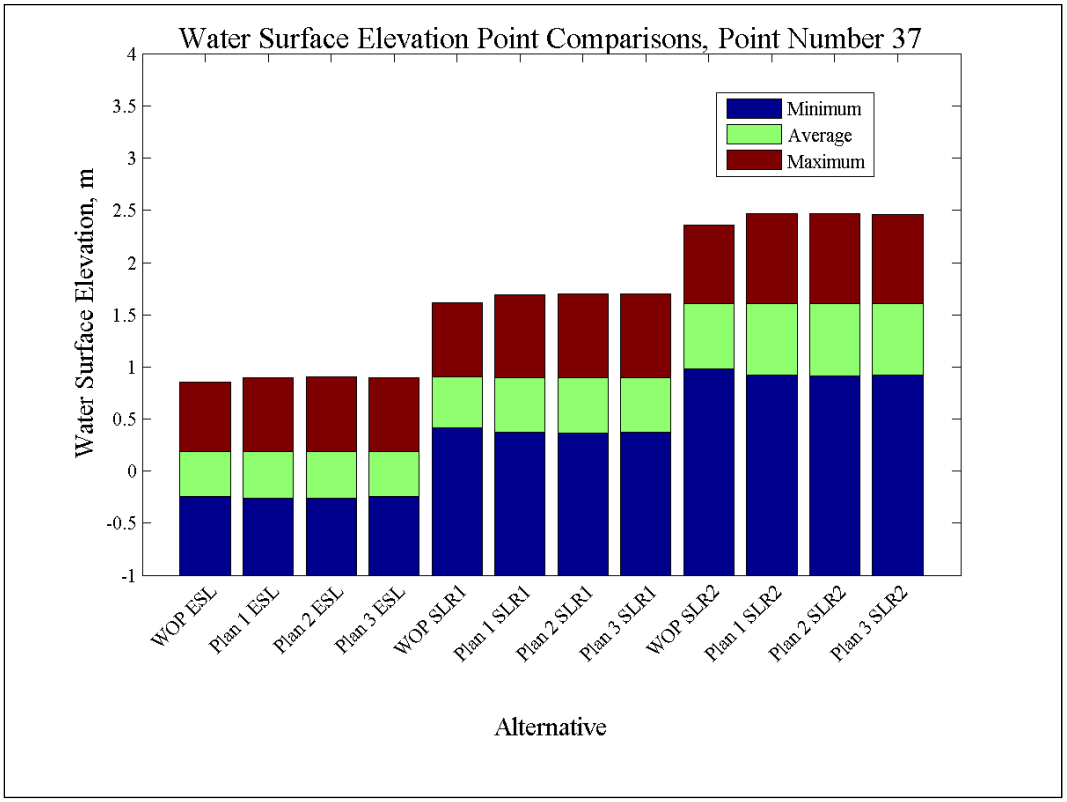

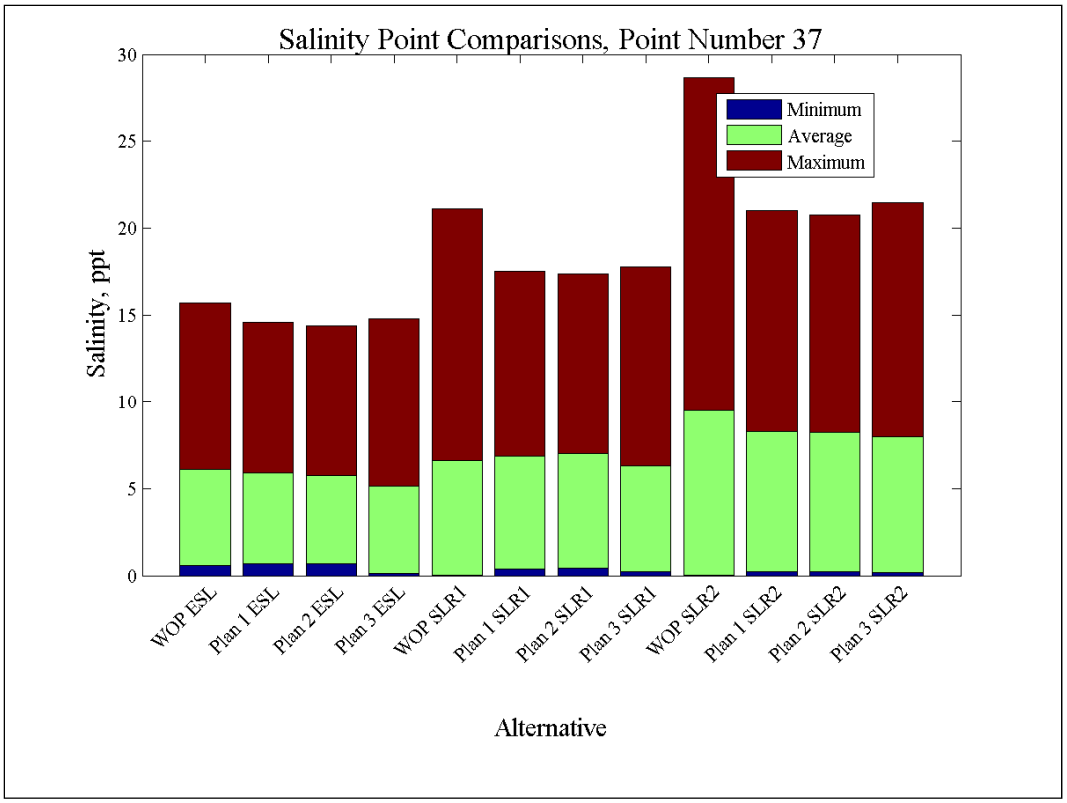

Figure 217. Water-surface elevation and salinity comparisons at Point 38.

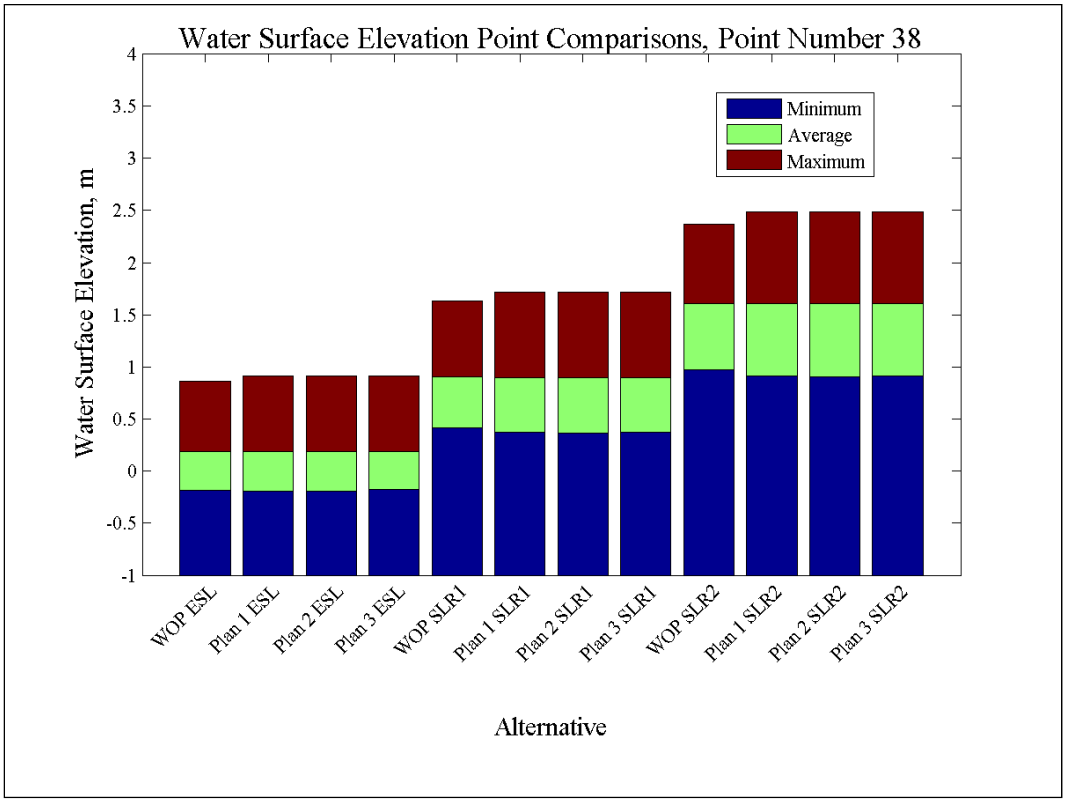

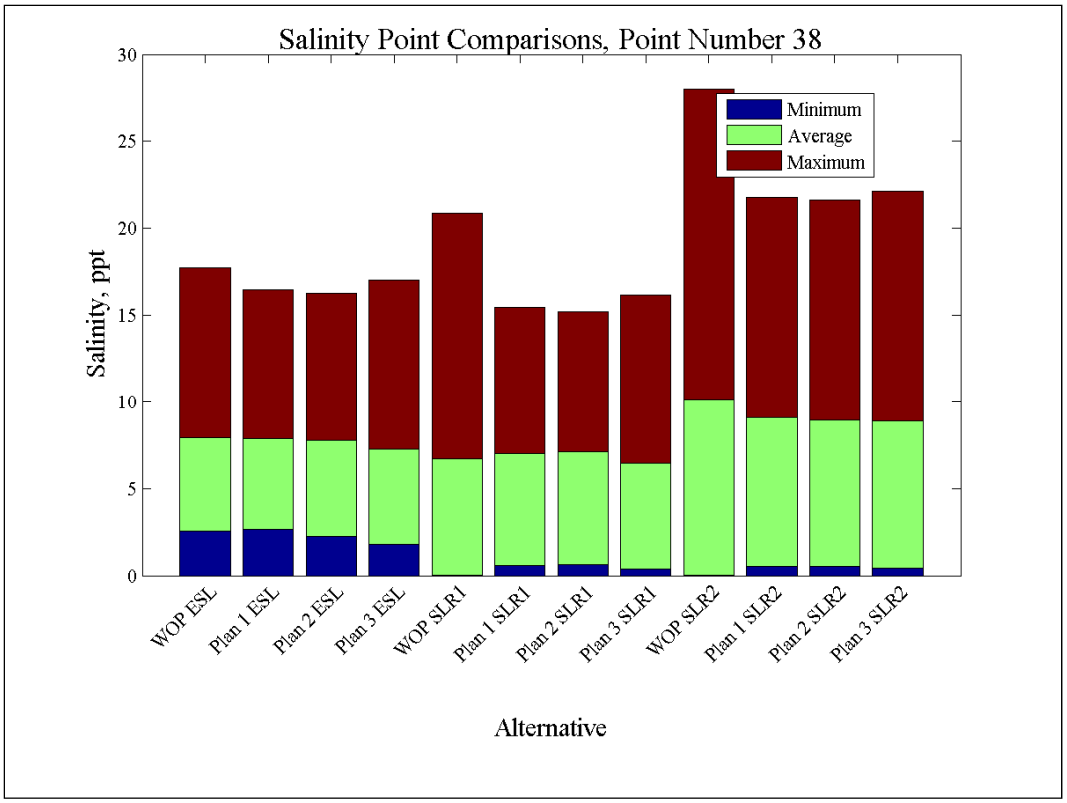

Figure 218. Water-surface elevation and salinity comparisons at Point 39.

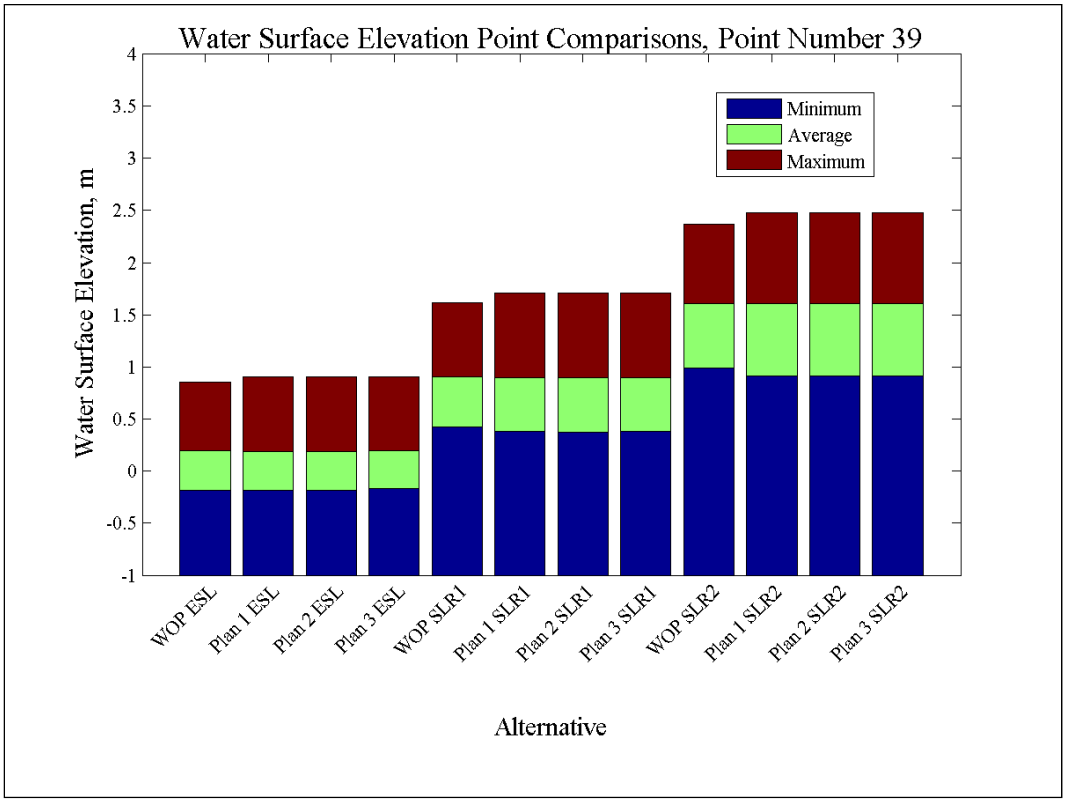

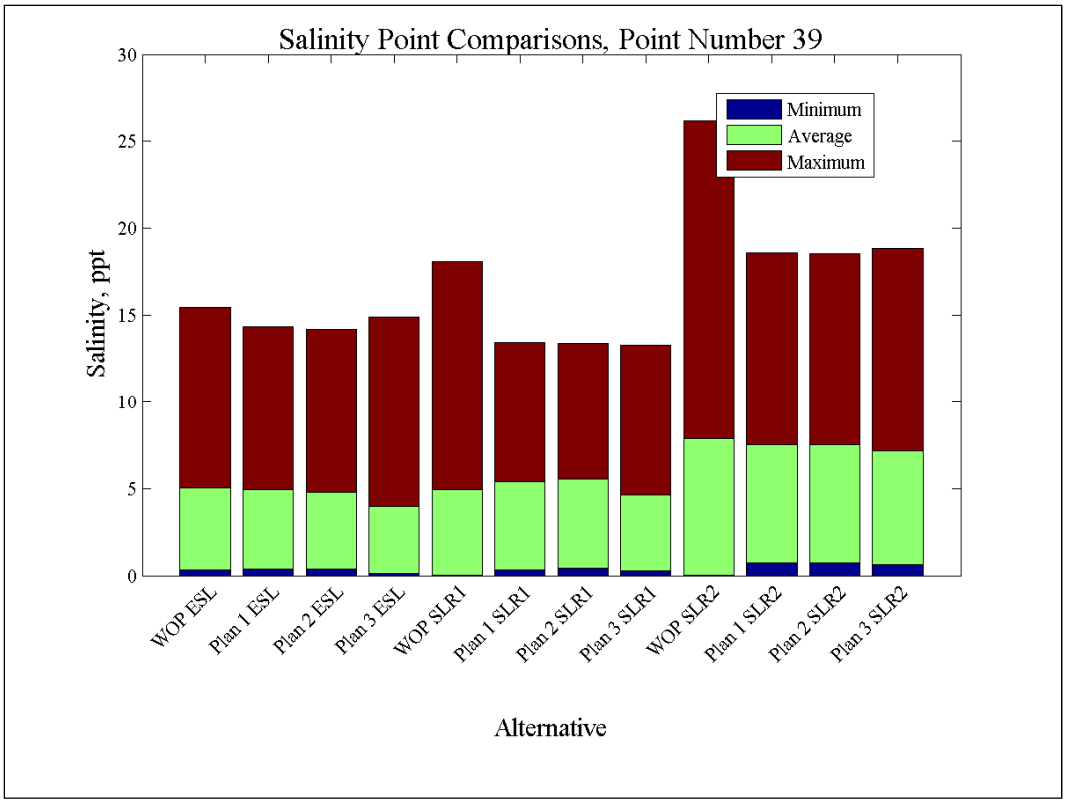

Figure 219. Water-surface elevation and salinity comparisons at Point 40.

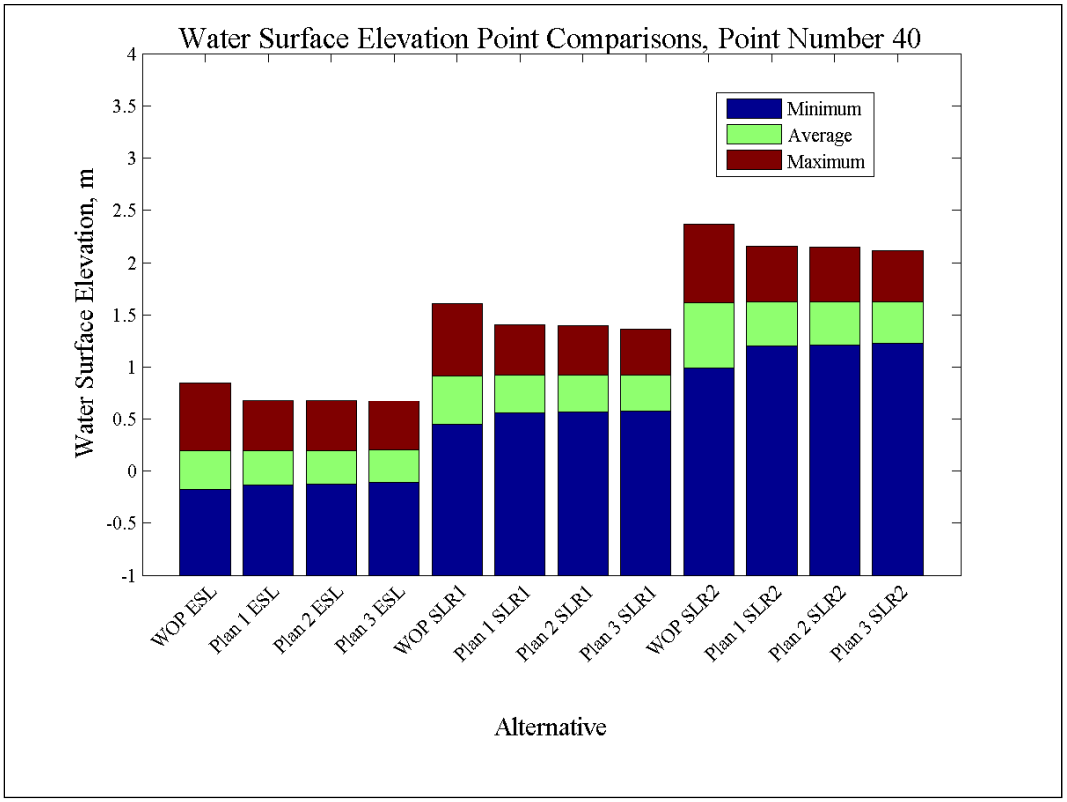

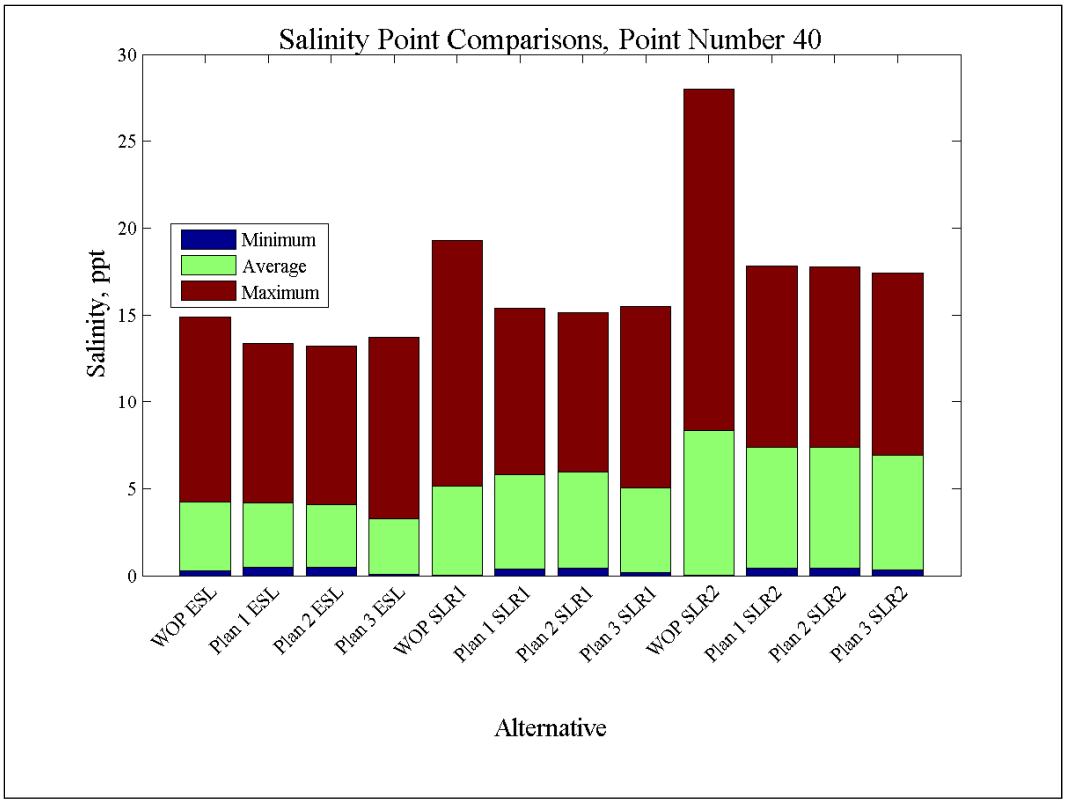

Figure 220. Water-surface elevation and salinity comparisons at Point 41.

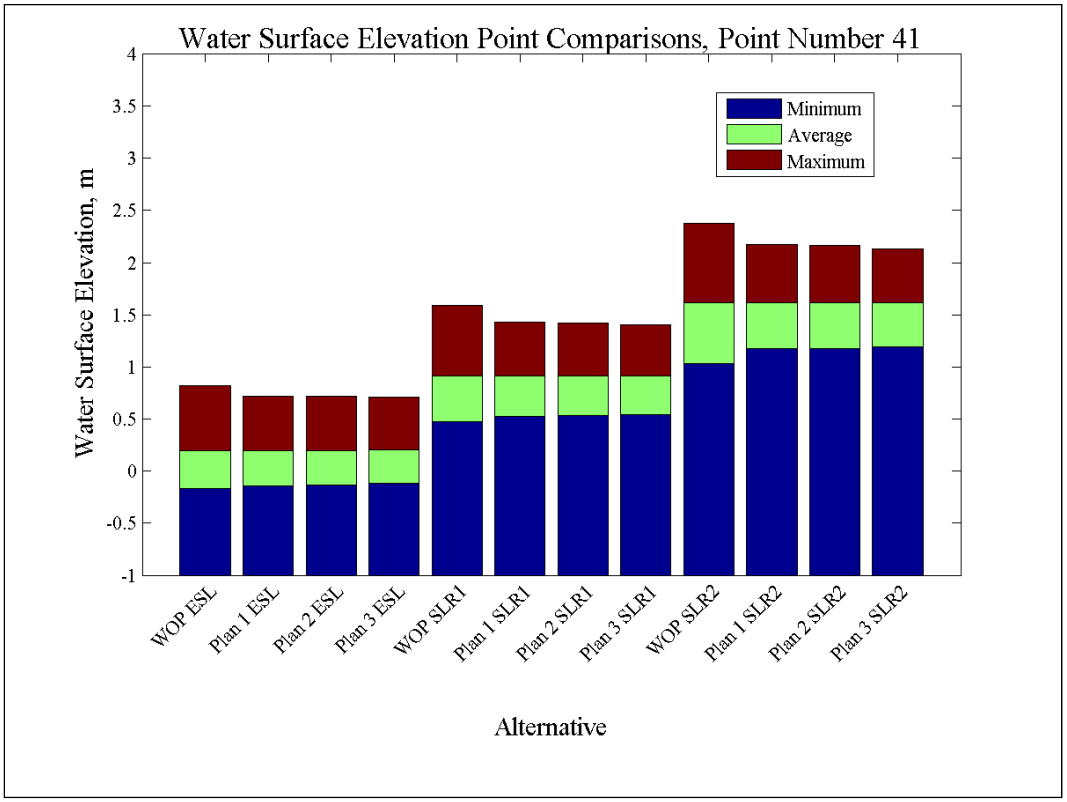

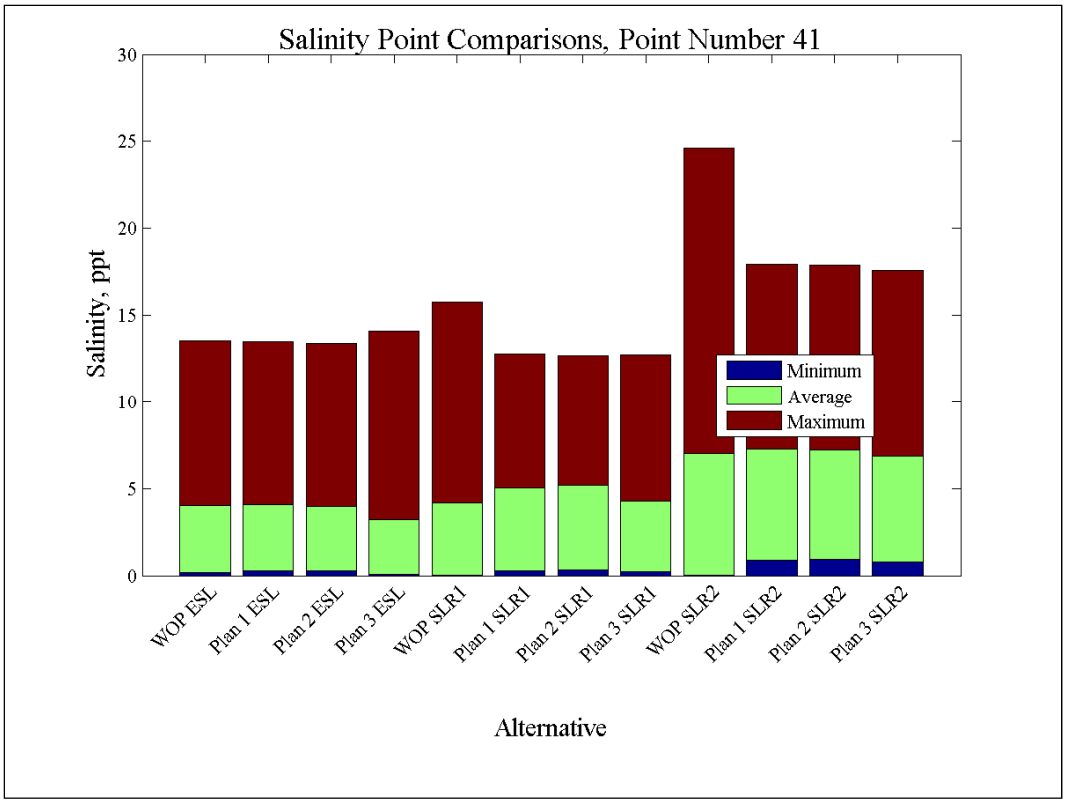

Figure 221. Water-surface elevation and salinity comparisons at Point 42.

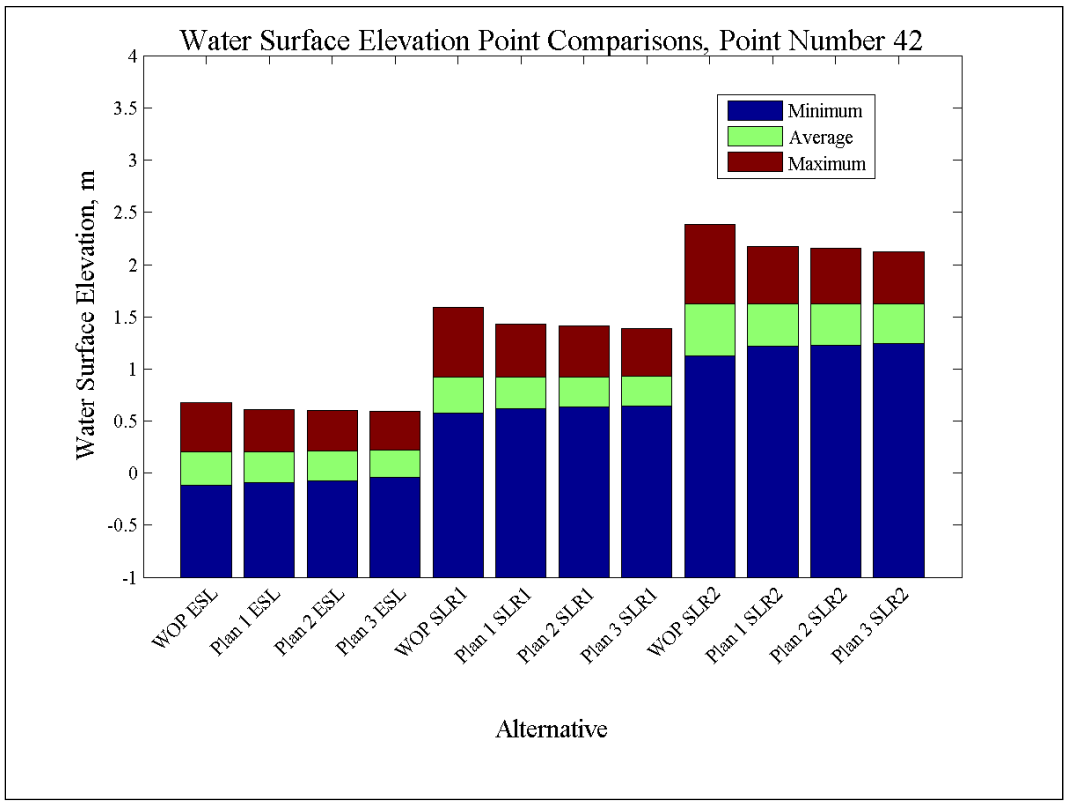

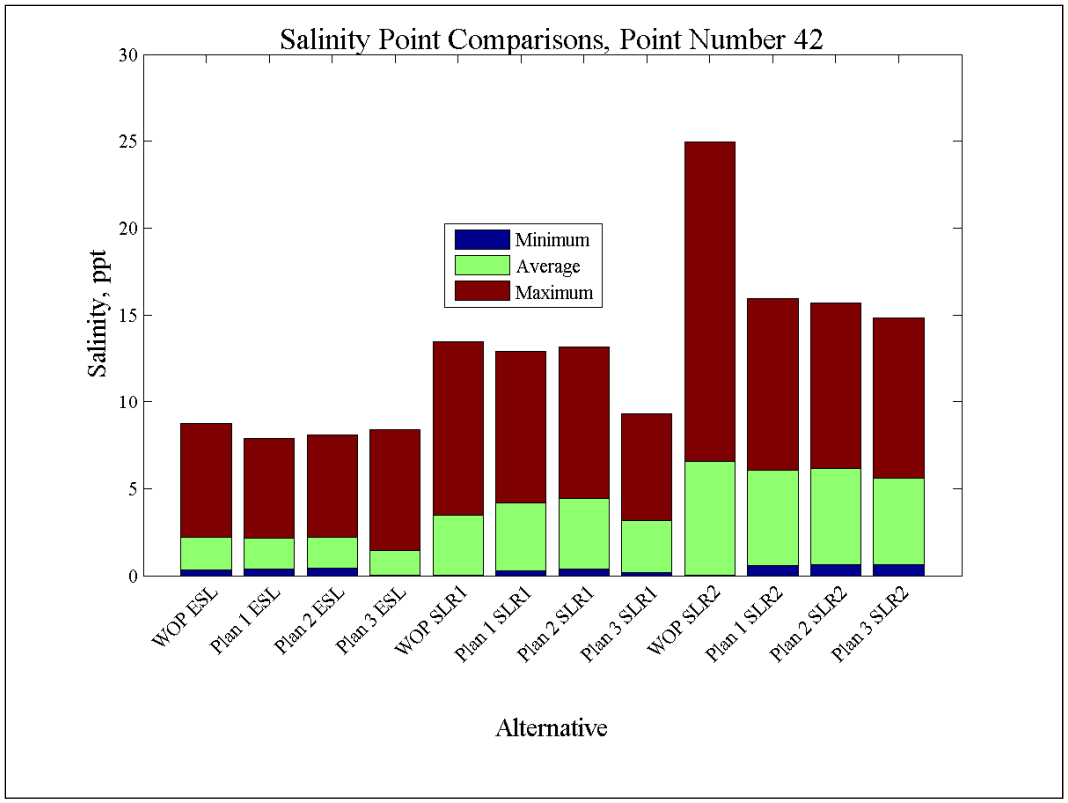

Figure 222. Water-surface elevation and salinity comparisons at Point 43.

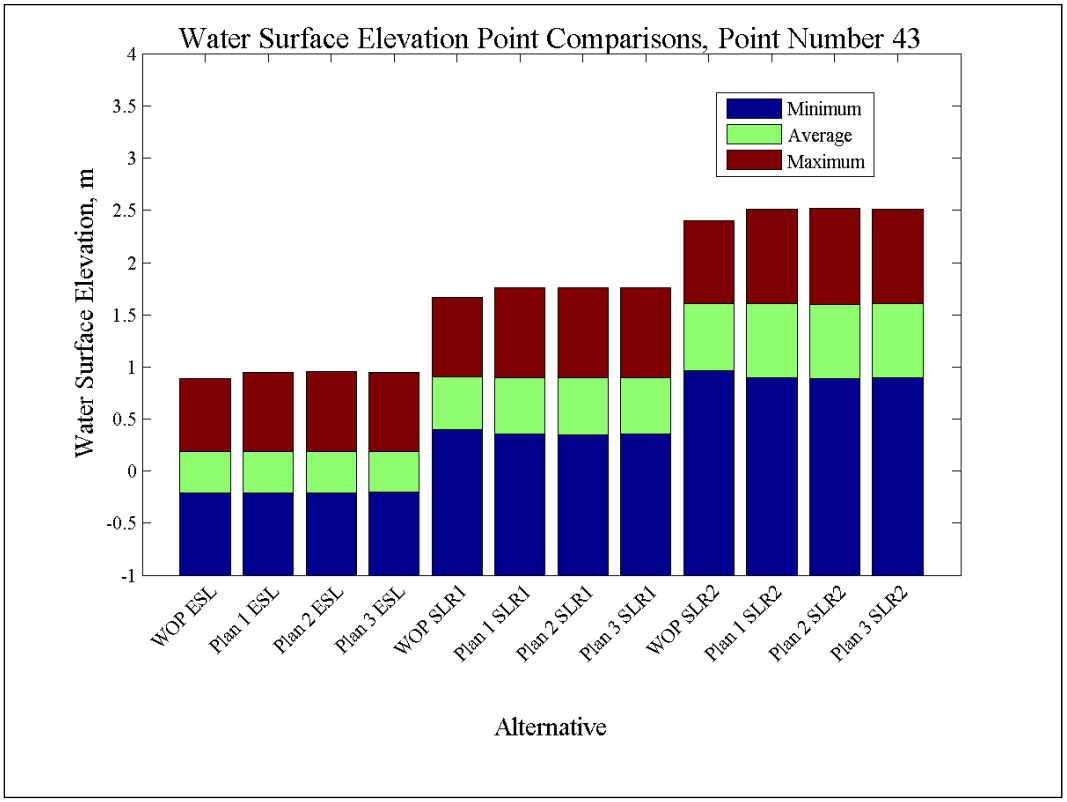

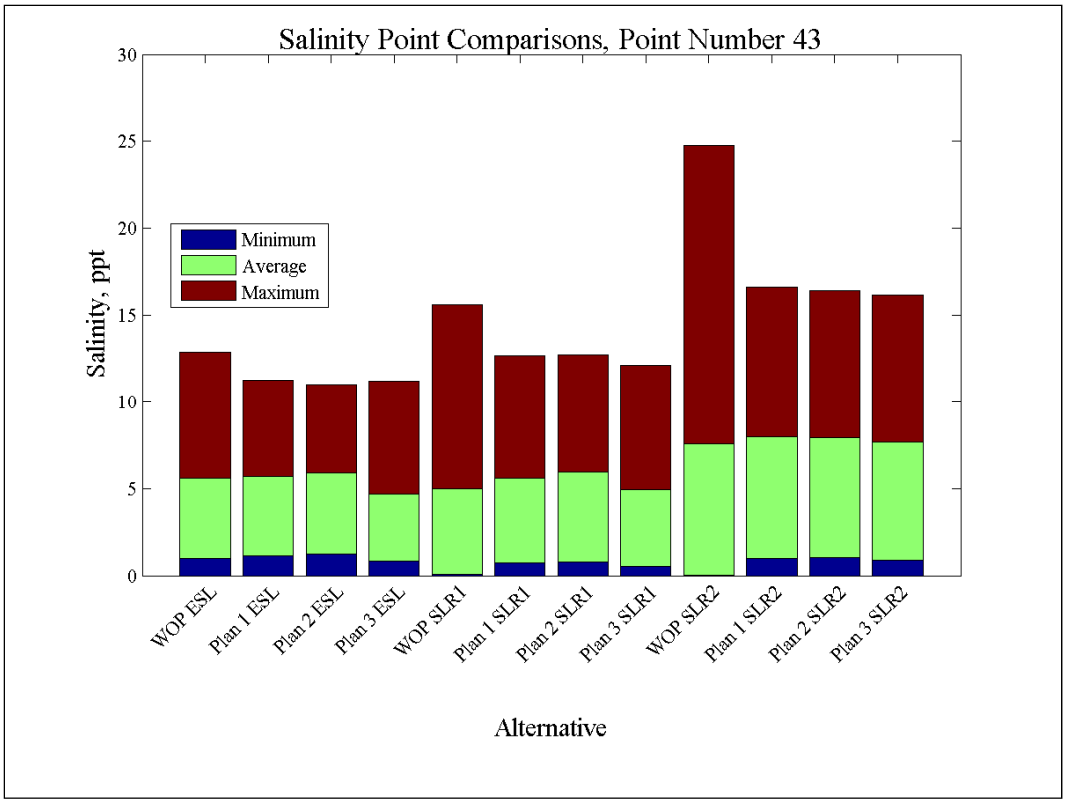

Figure 223. Water-surface elevation and salinity comparisons at Point 44.

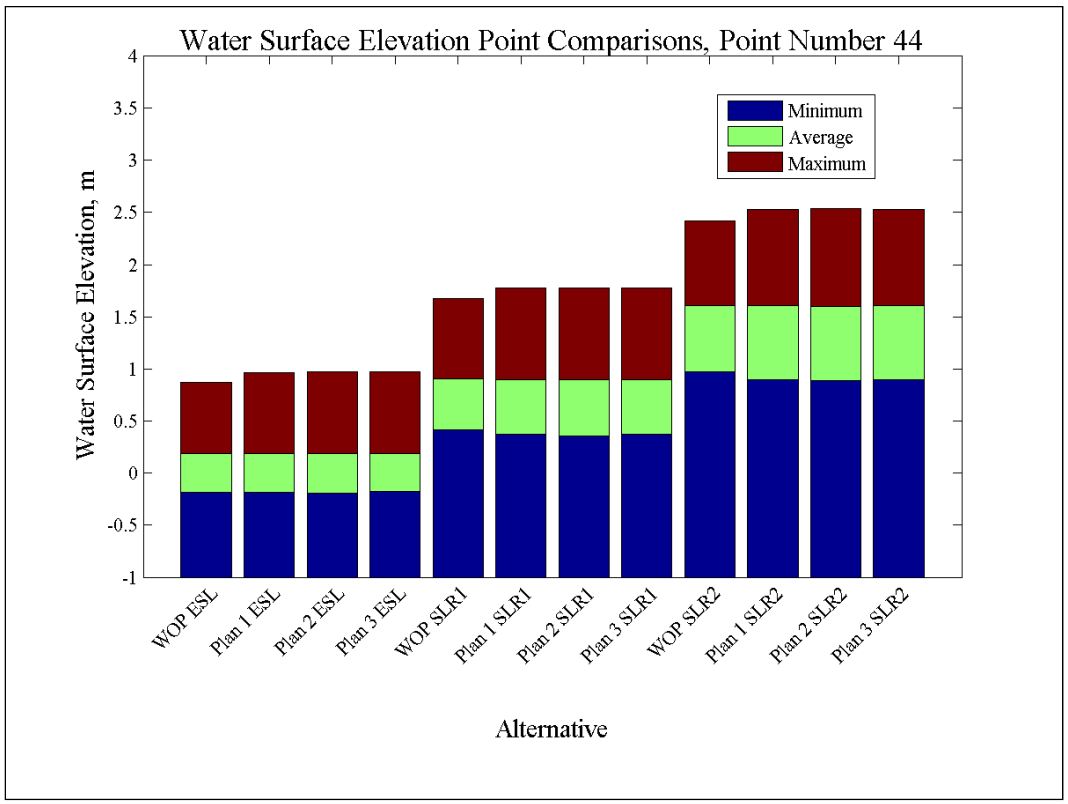

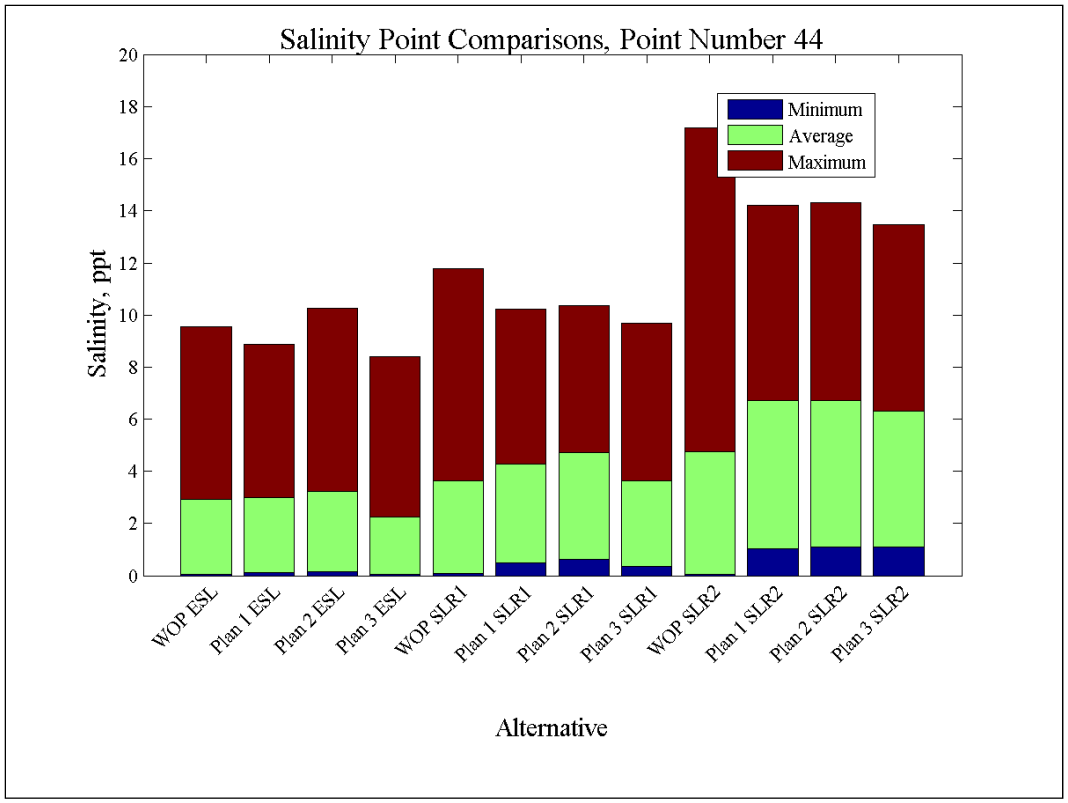

Figure 224. Water-surface elevation and salinity comparisons at Point 45.

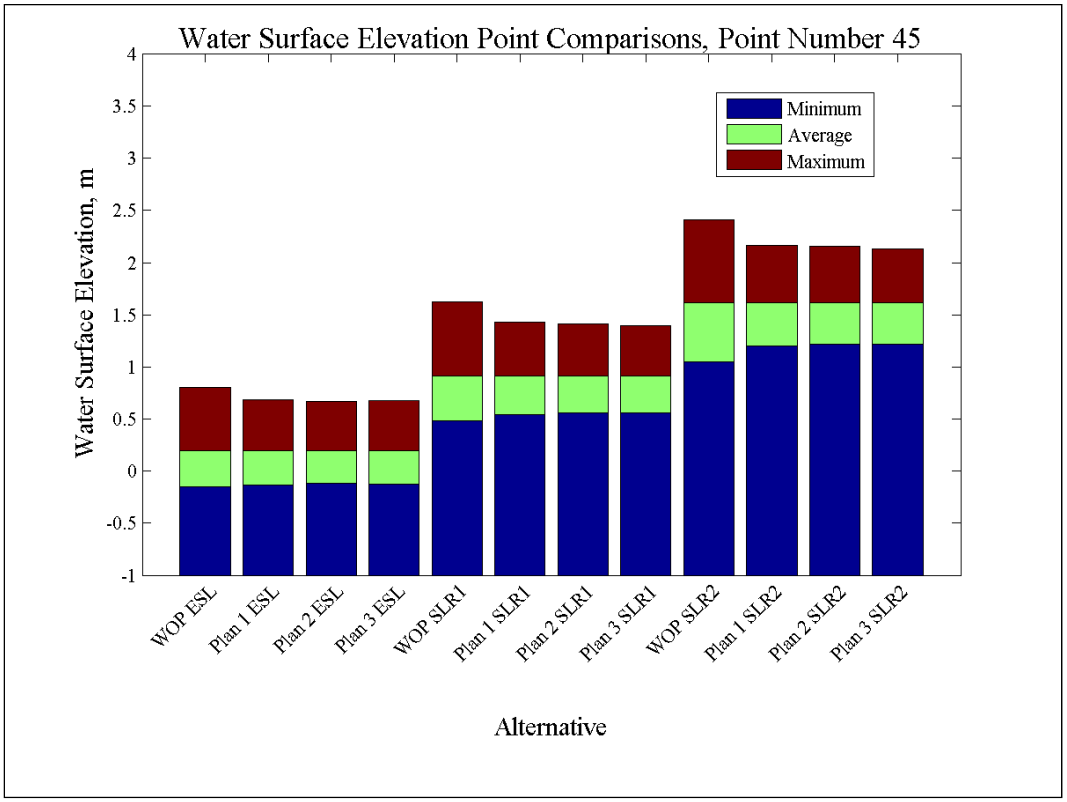

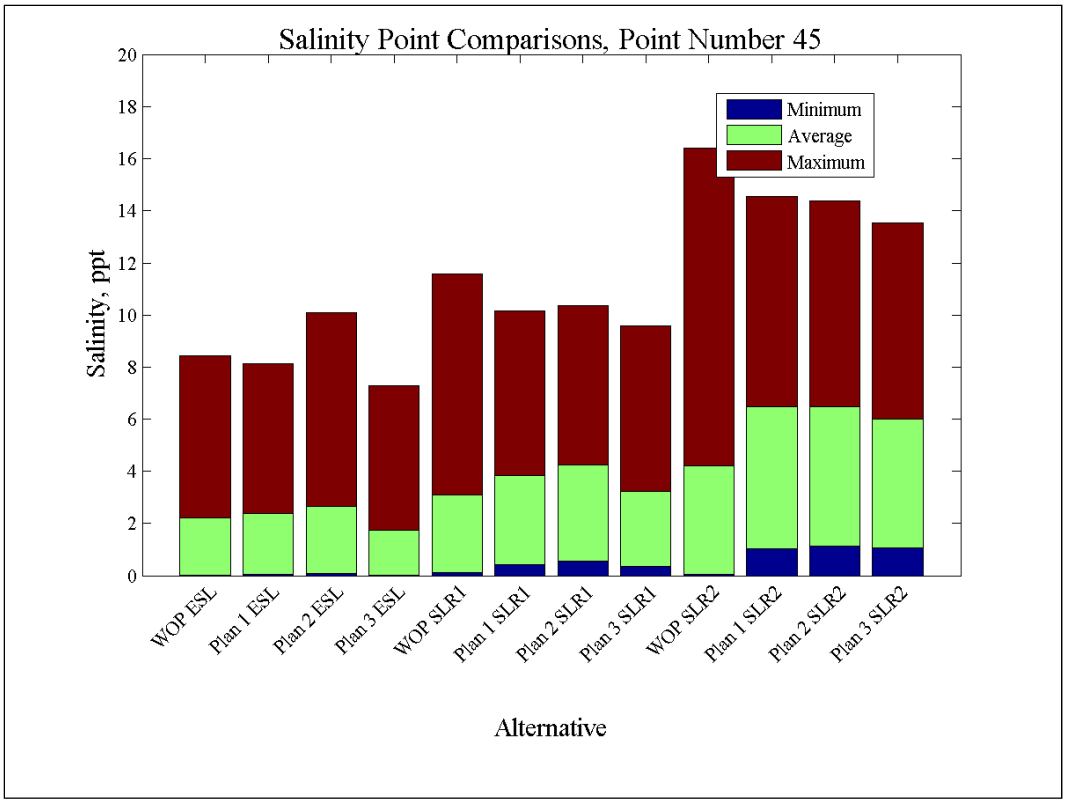

Figure 225. Water-surface elevation and salinity comparisons at Point 46.

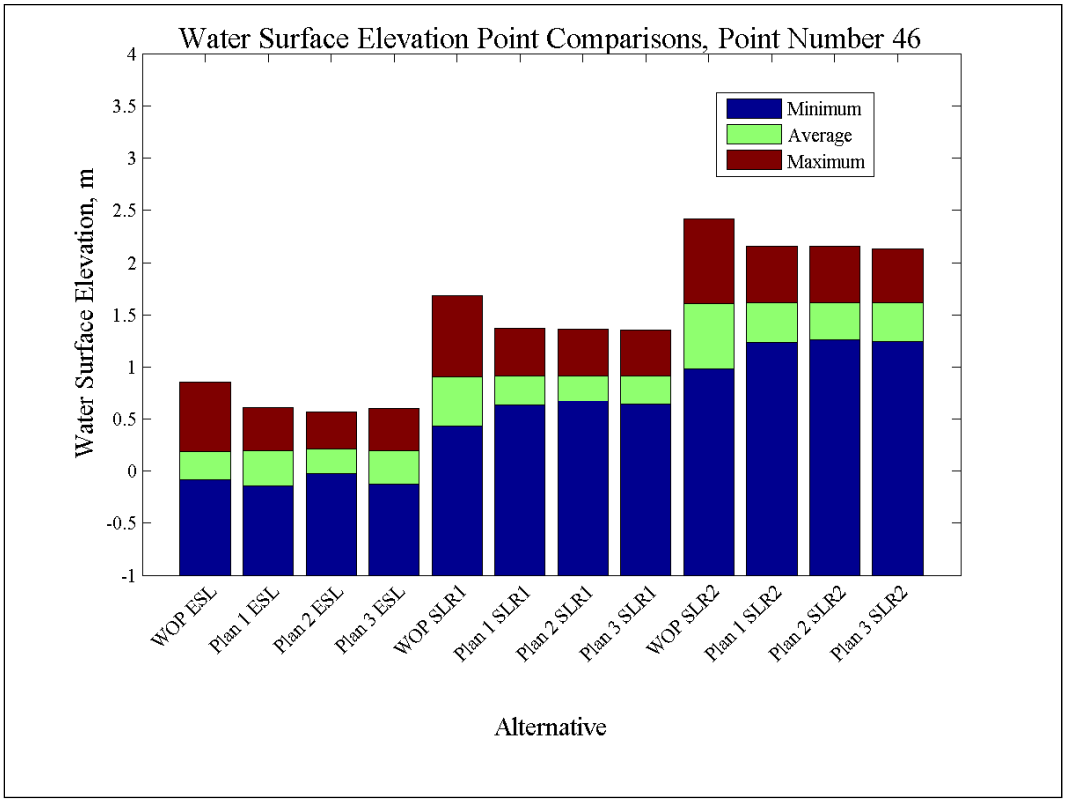

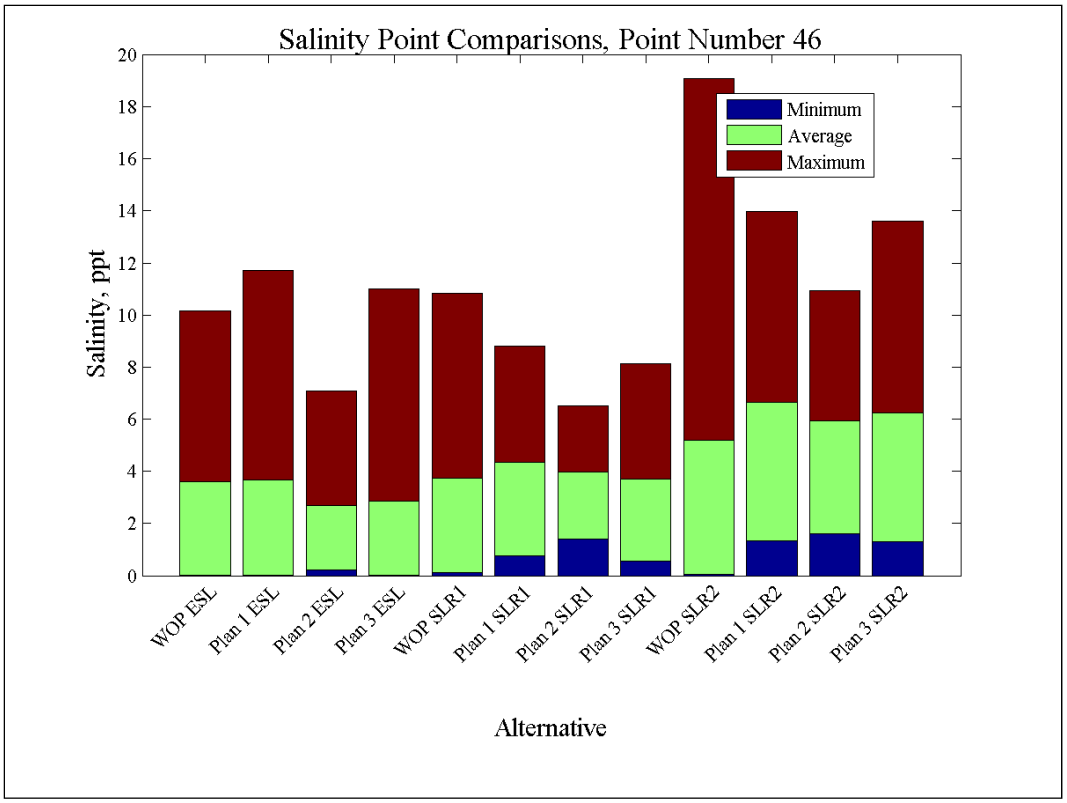

Figure 226. Water-surface elevation and salinity comparisons at Point 47.

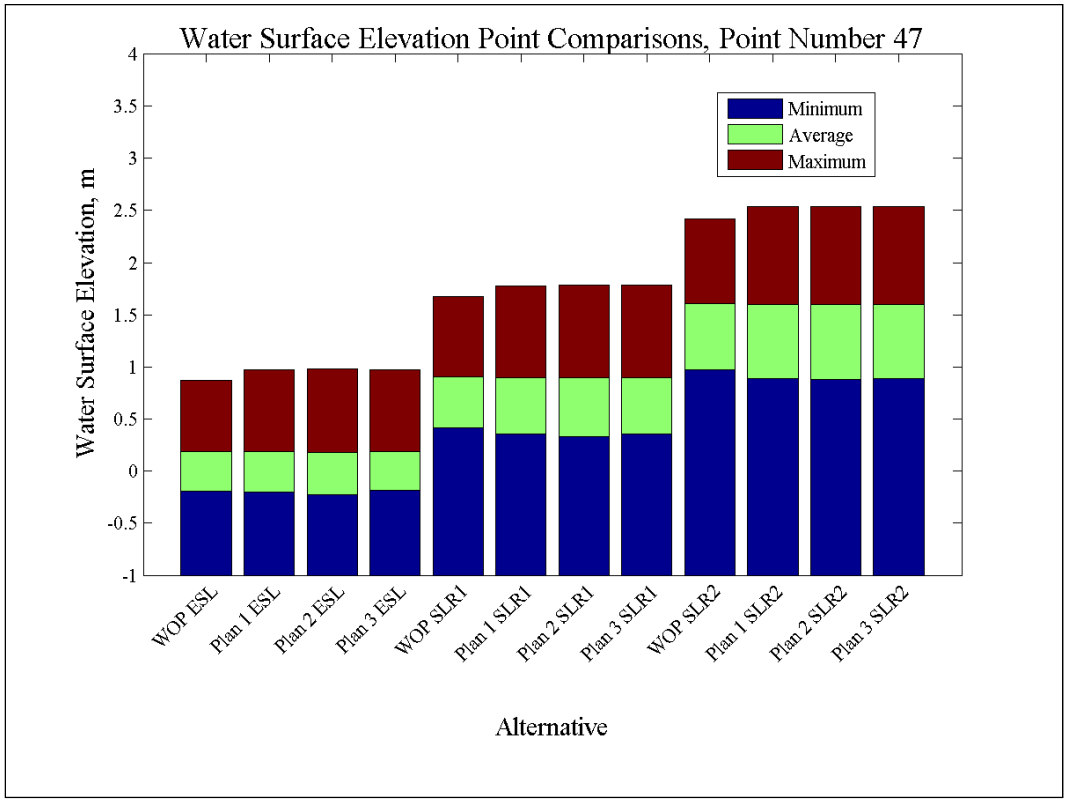

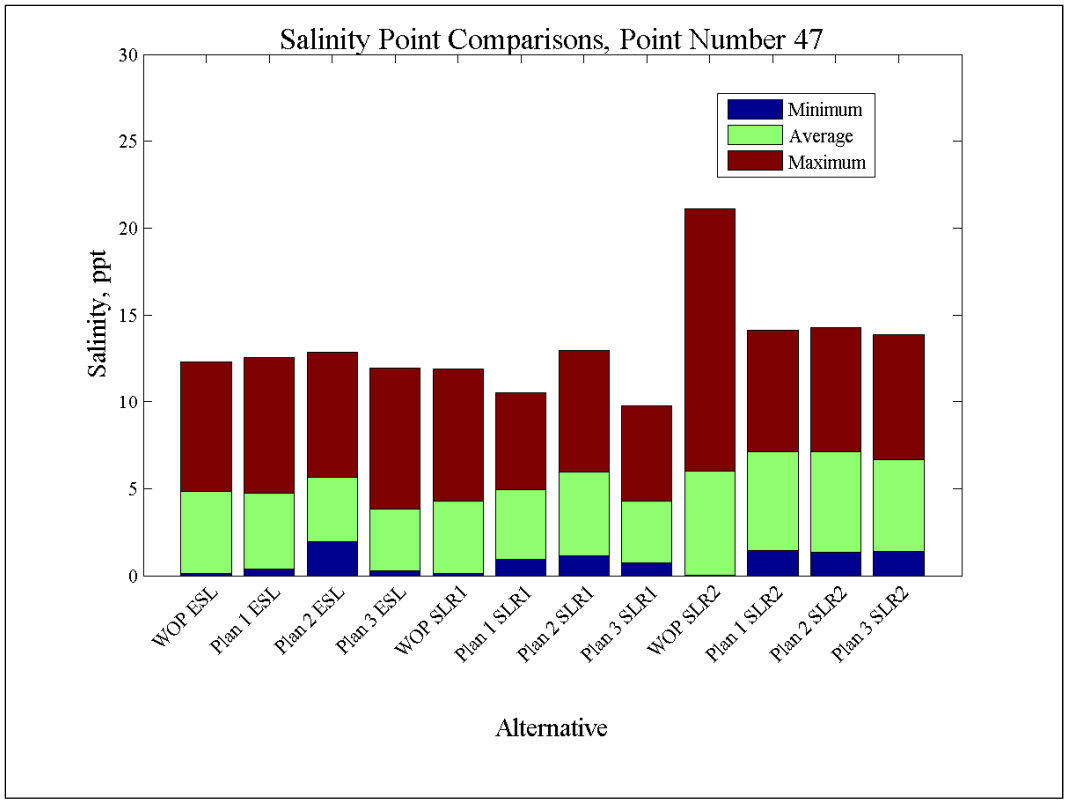

Figure 227. Water-surface elevation and salinity comparisons at Point 48.

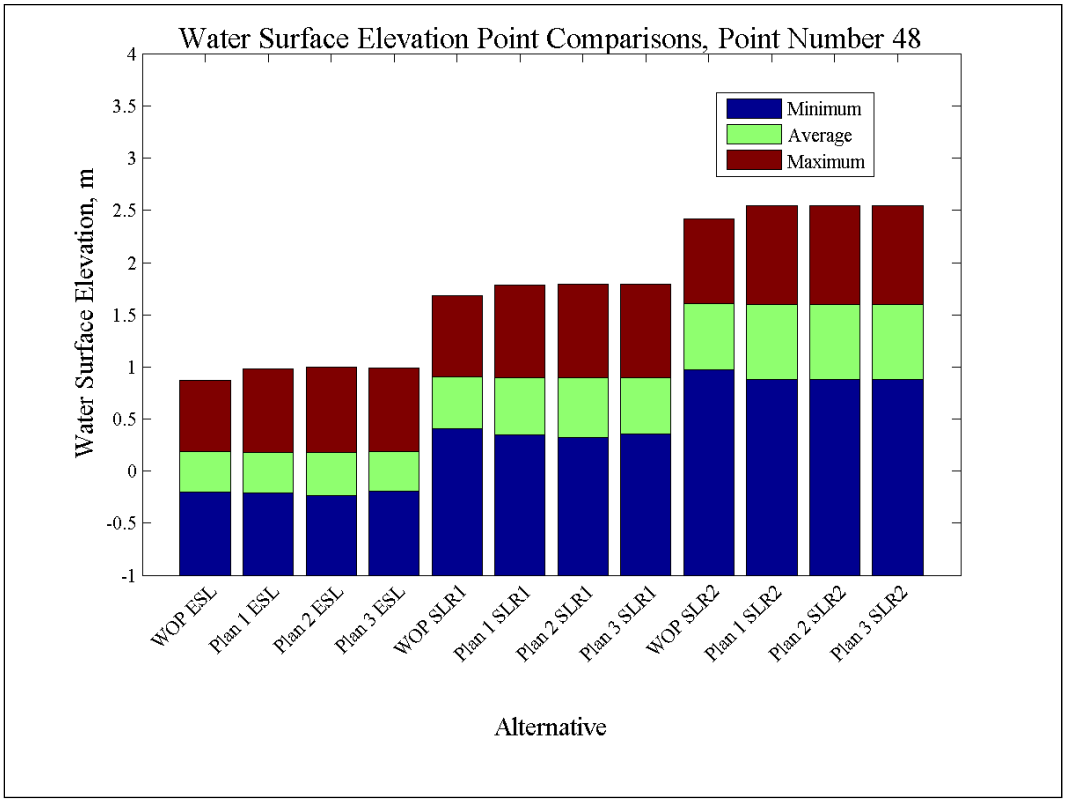

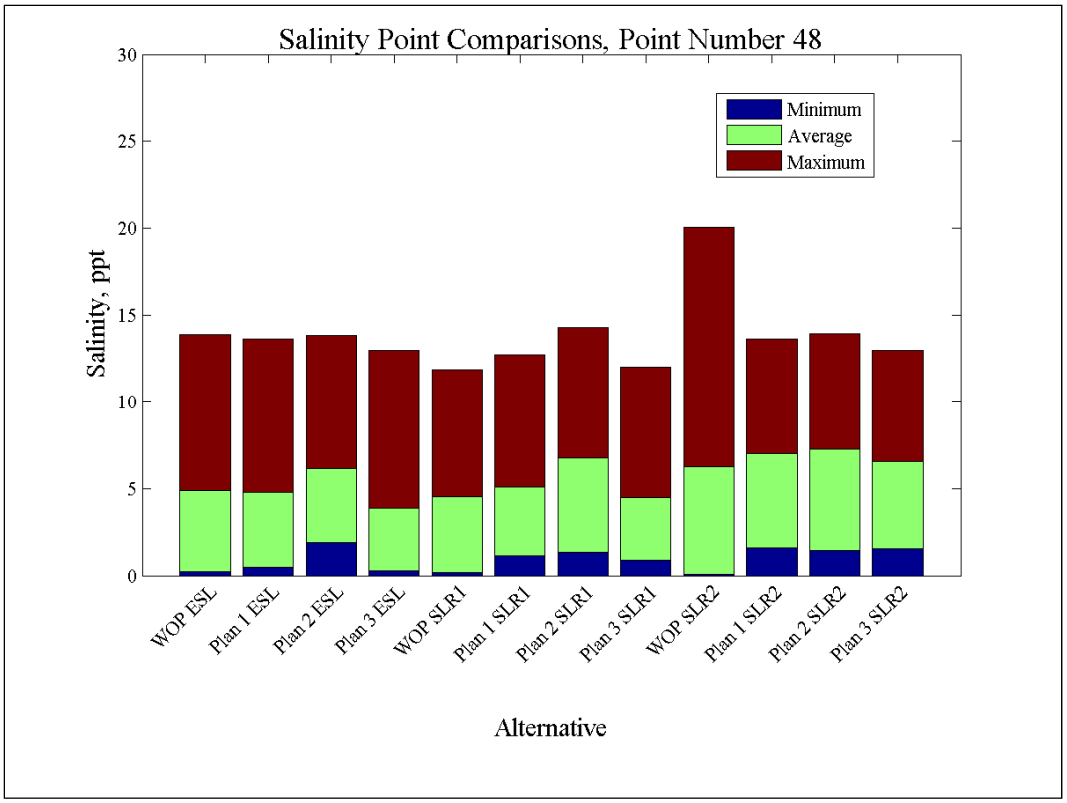

Figure 228. Water-surface elevation and salinity comparisons at Point 49.

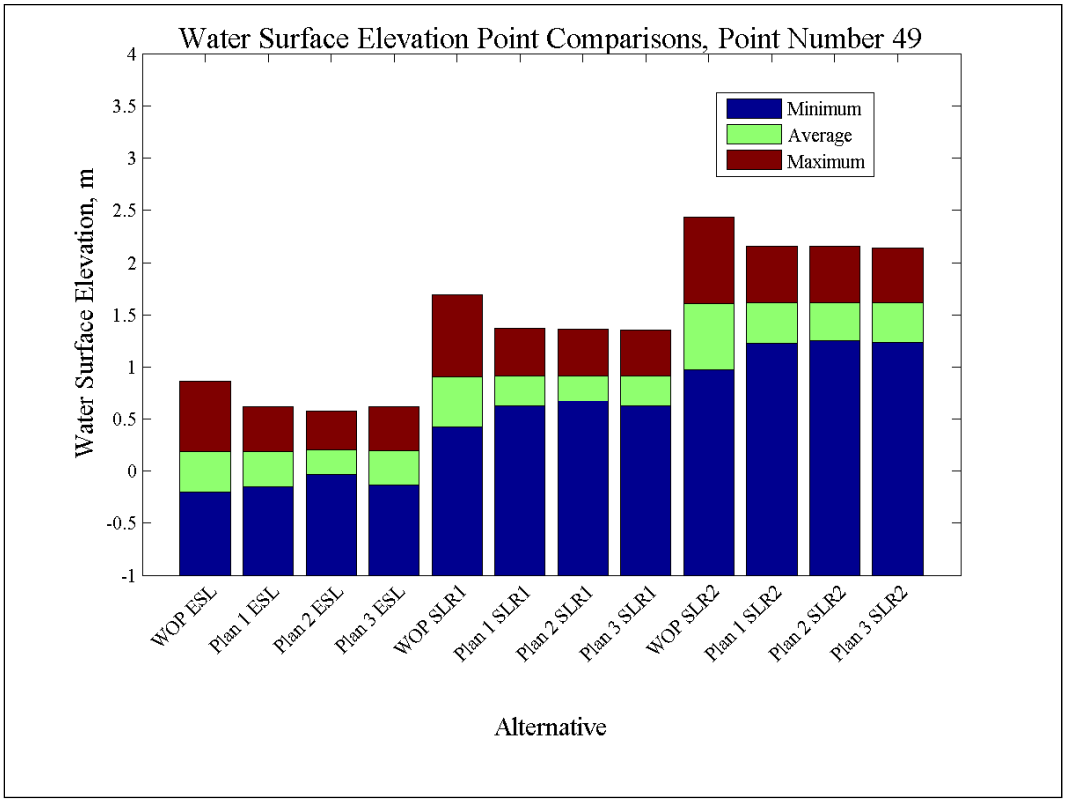

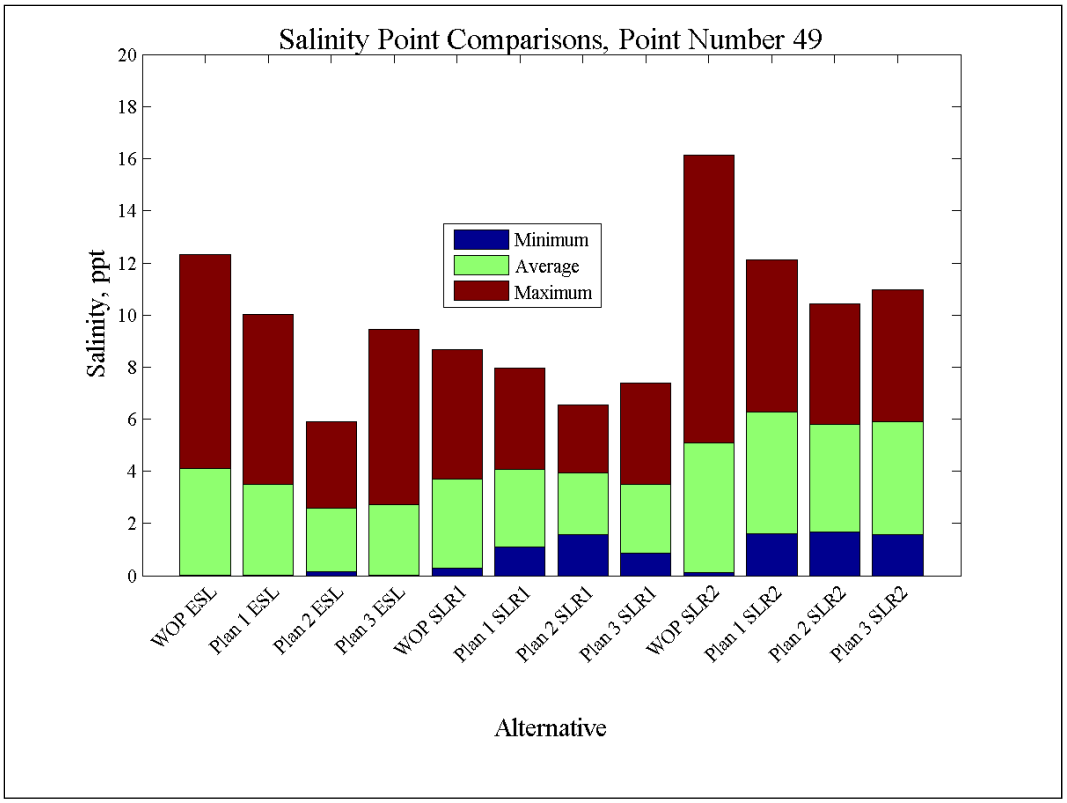

Figure 229. Water-surface elevation and salinity comparisons at Point 50.

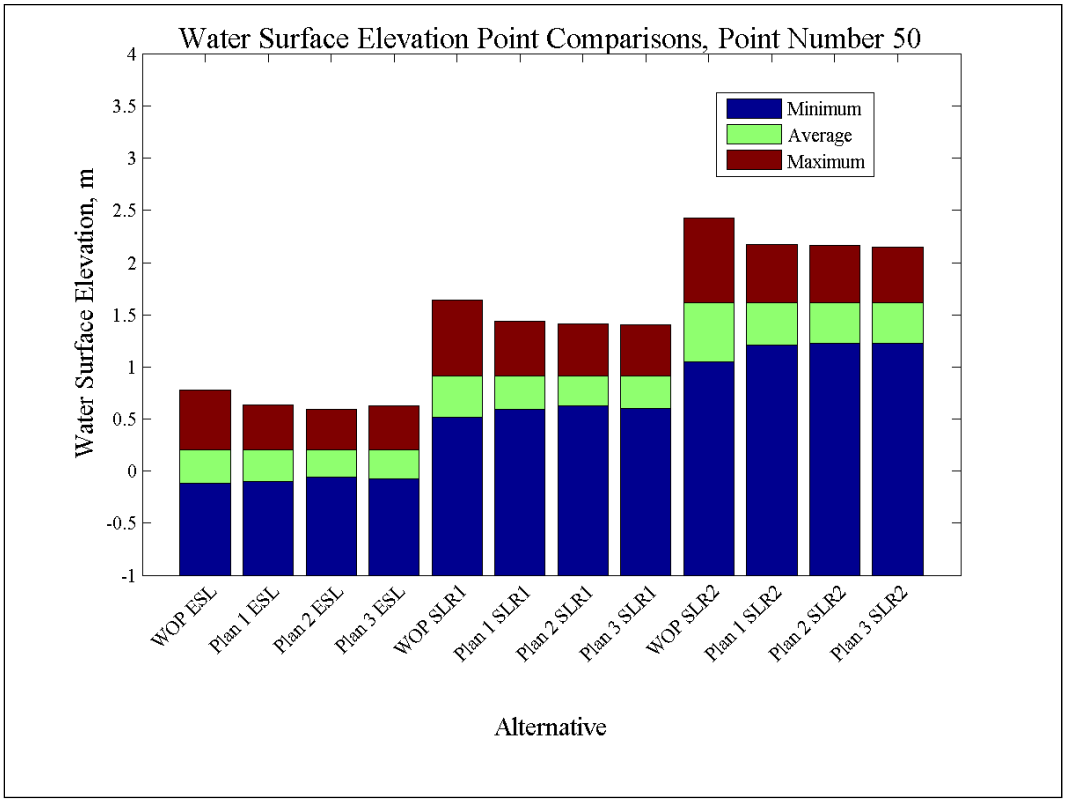

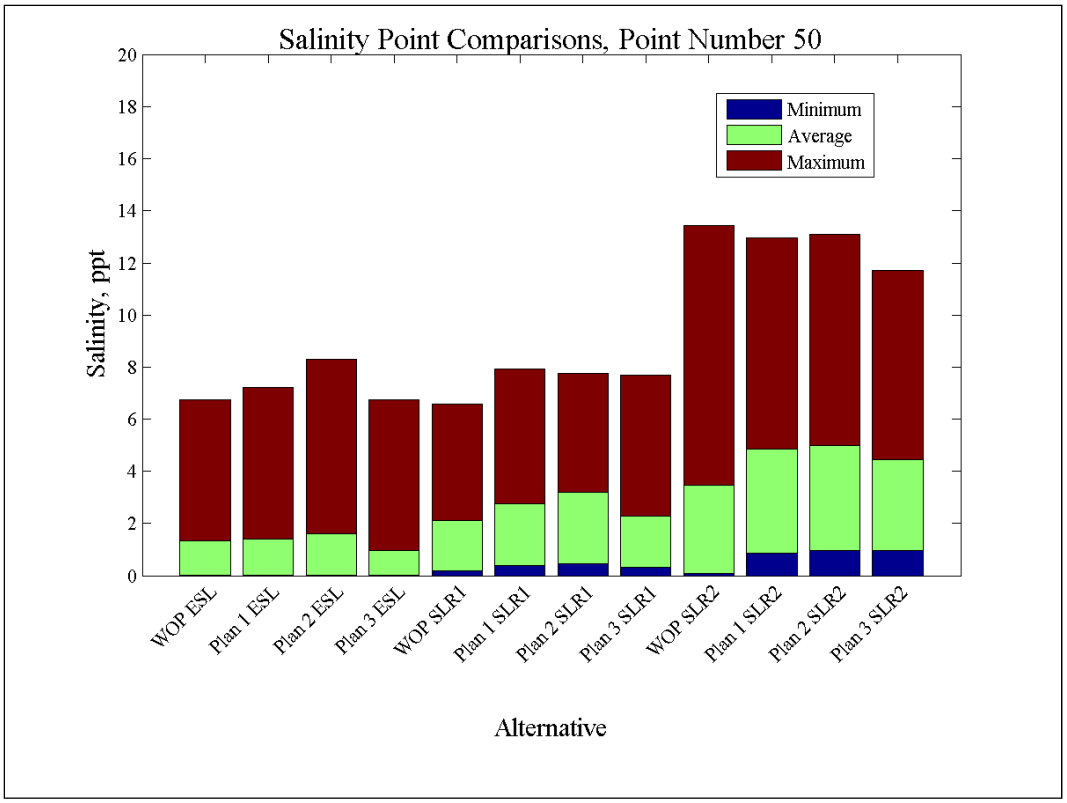

Figure 230. Water-surface elevation and salinity comparisons at Point 51.

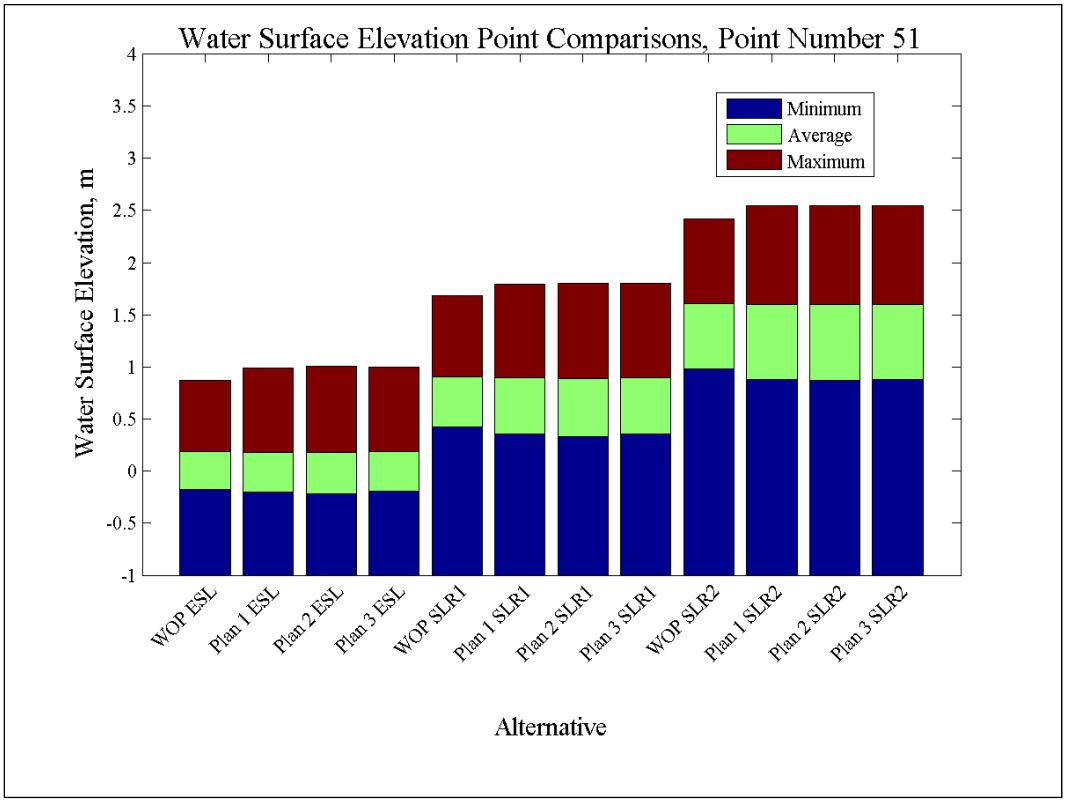

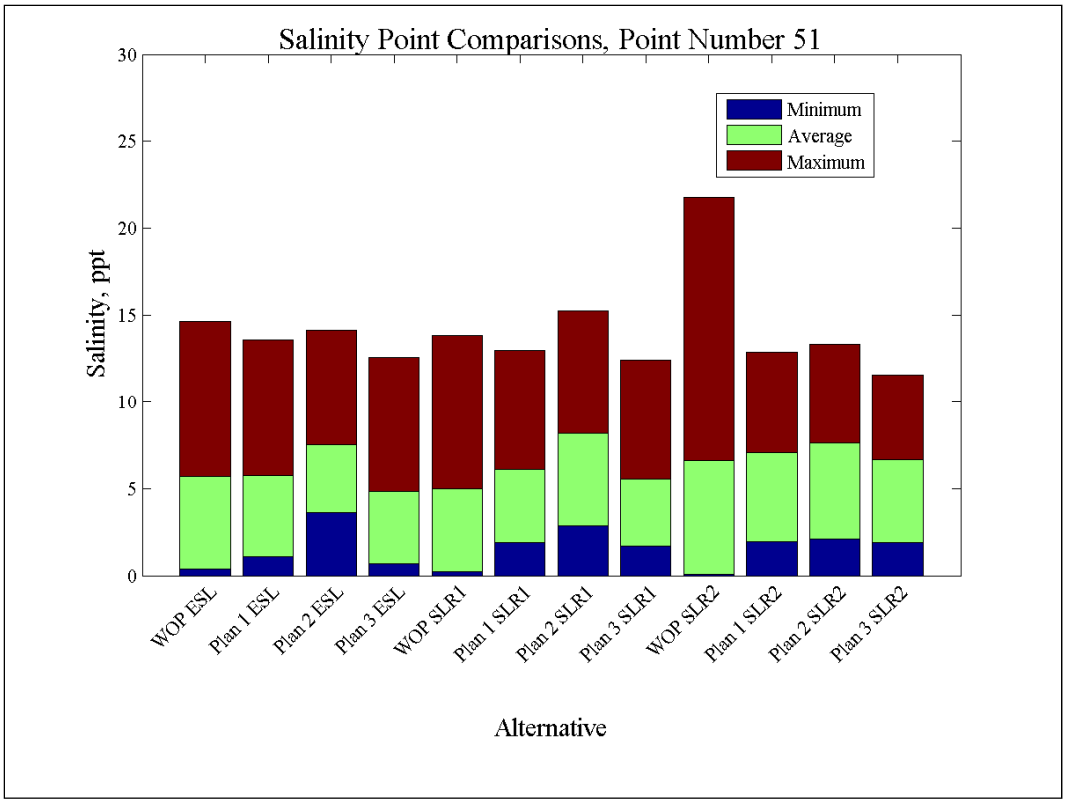

Figure 231. Water-surface elevation and salinity comparisons at Point 52.

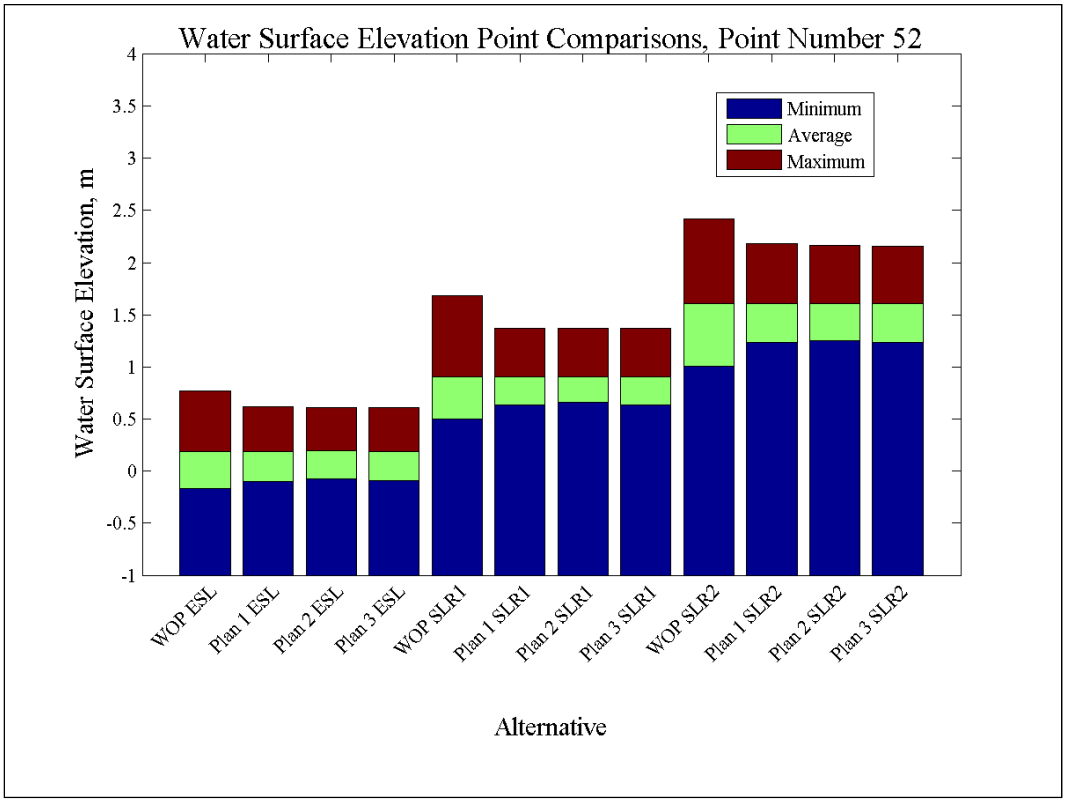

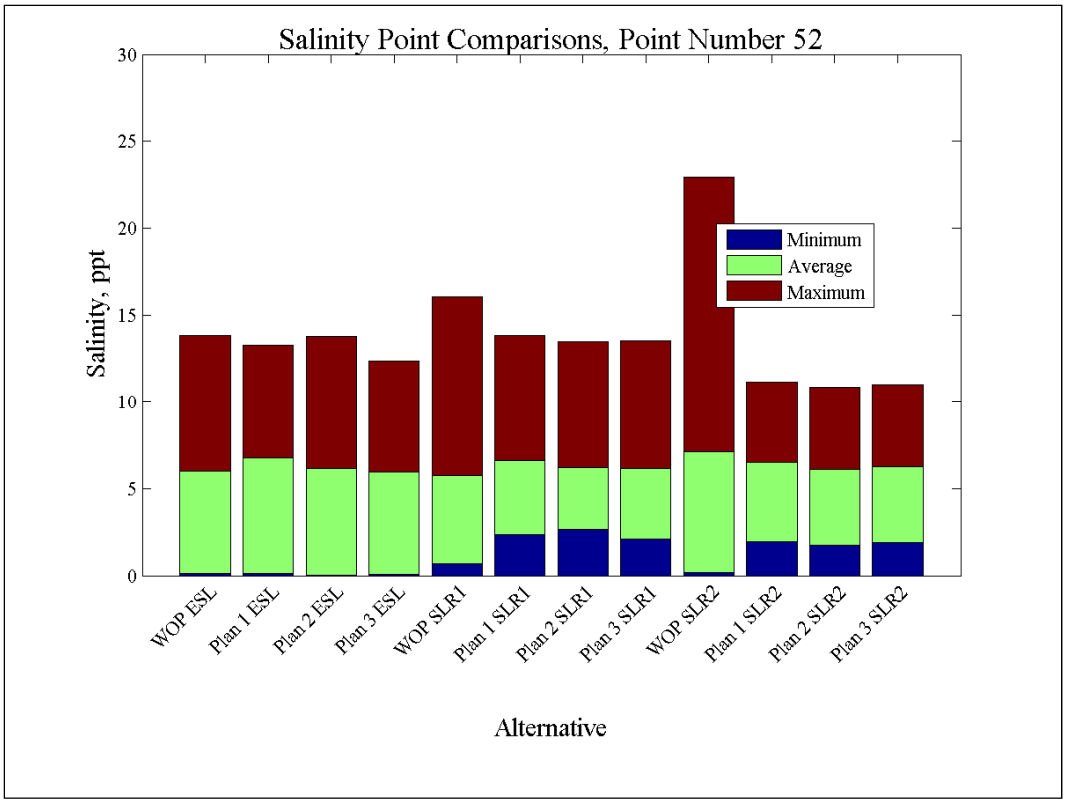

Figure 232. Water-surface elevation and salinity comparisons at Point 53.

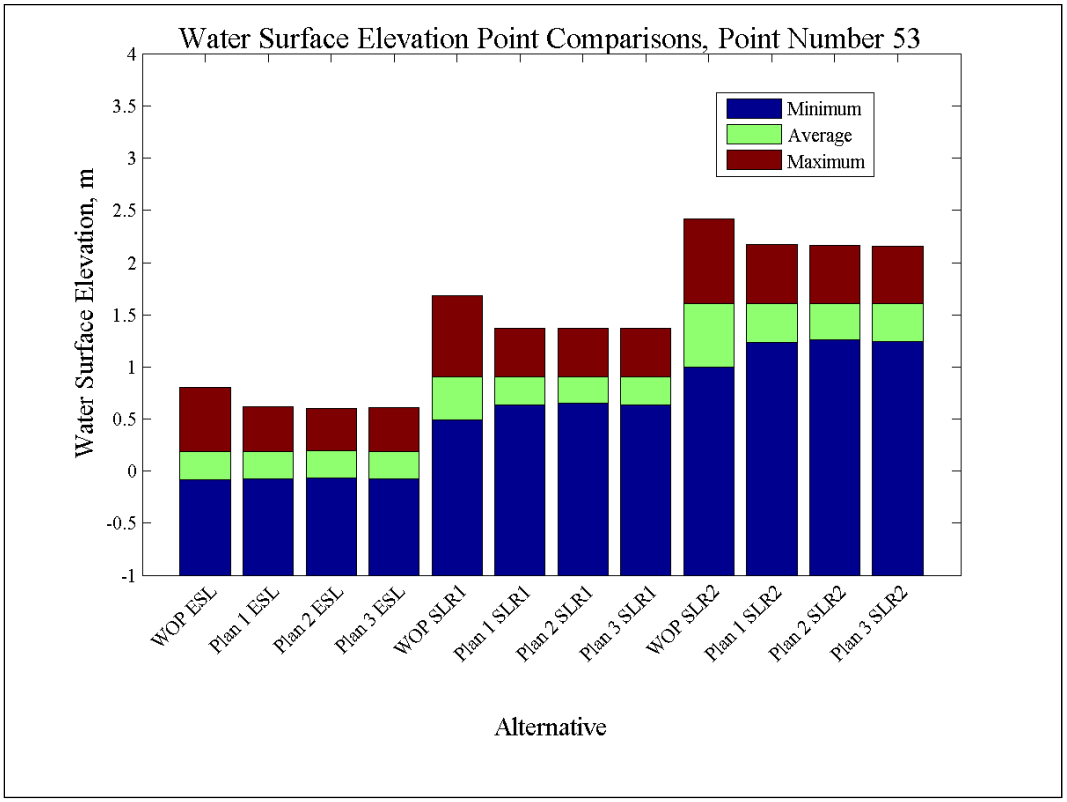

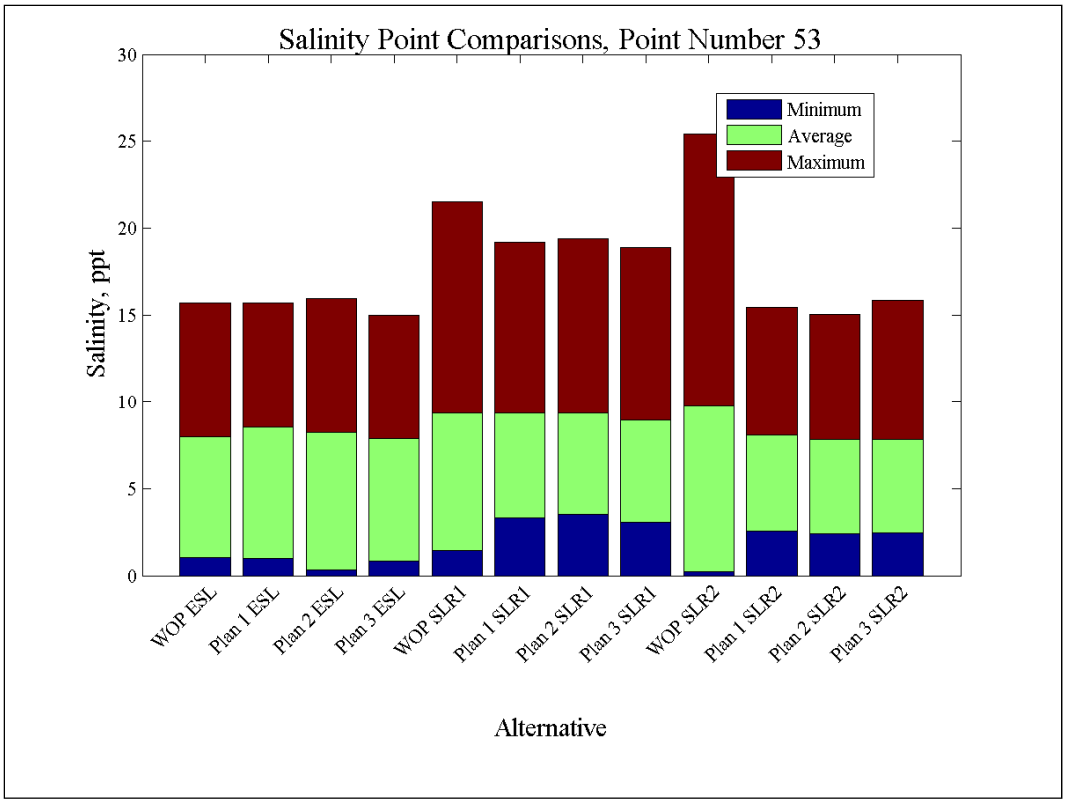

Figure 233. Water-surface elevation and salinity comparisons at Point 54.

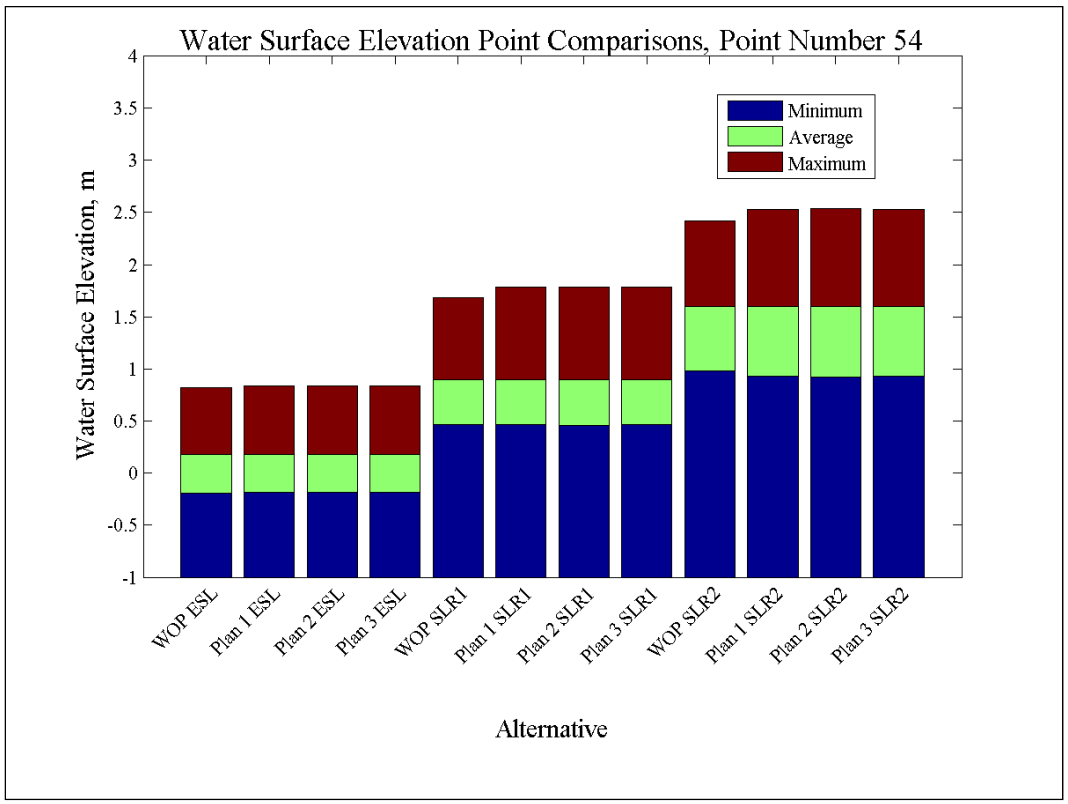

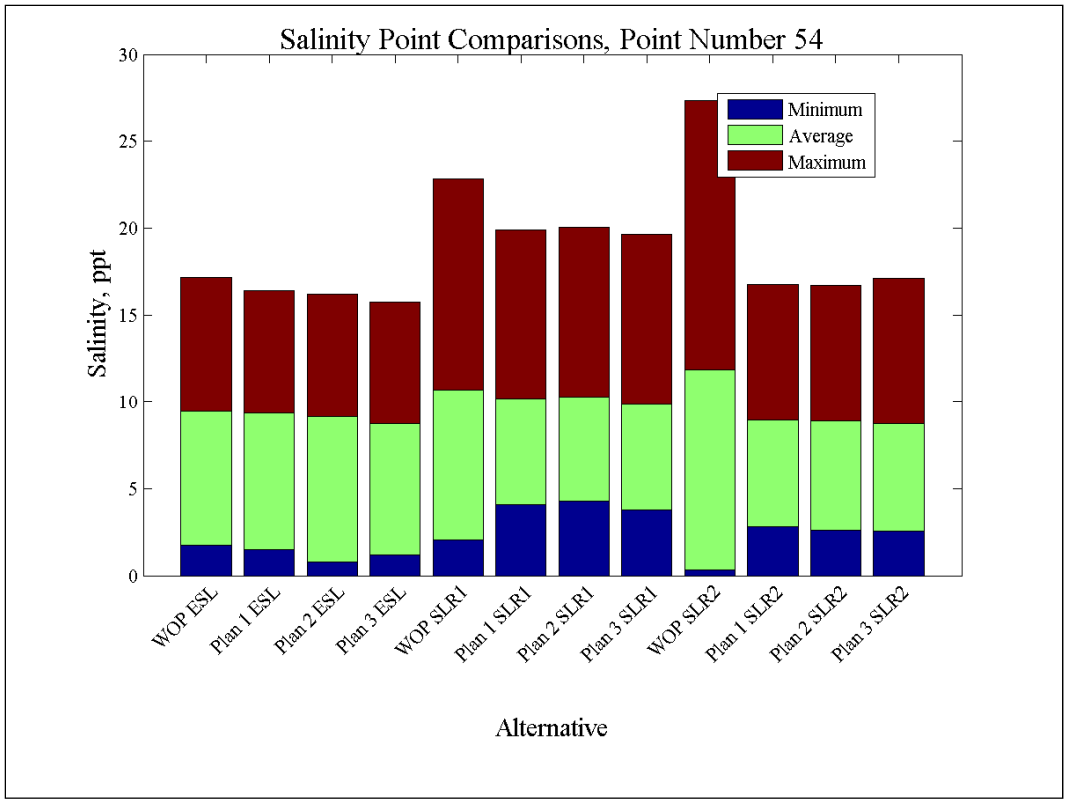

Figure 234. Water-surface elevation and salinity comparisons at Point 55.

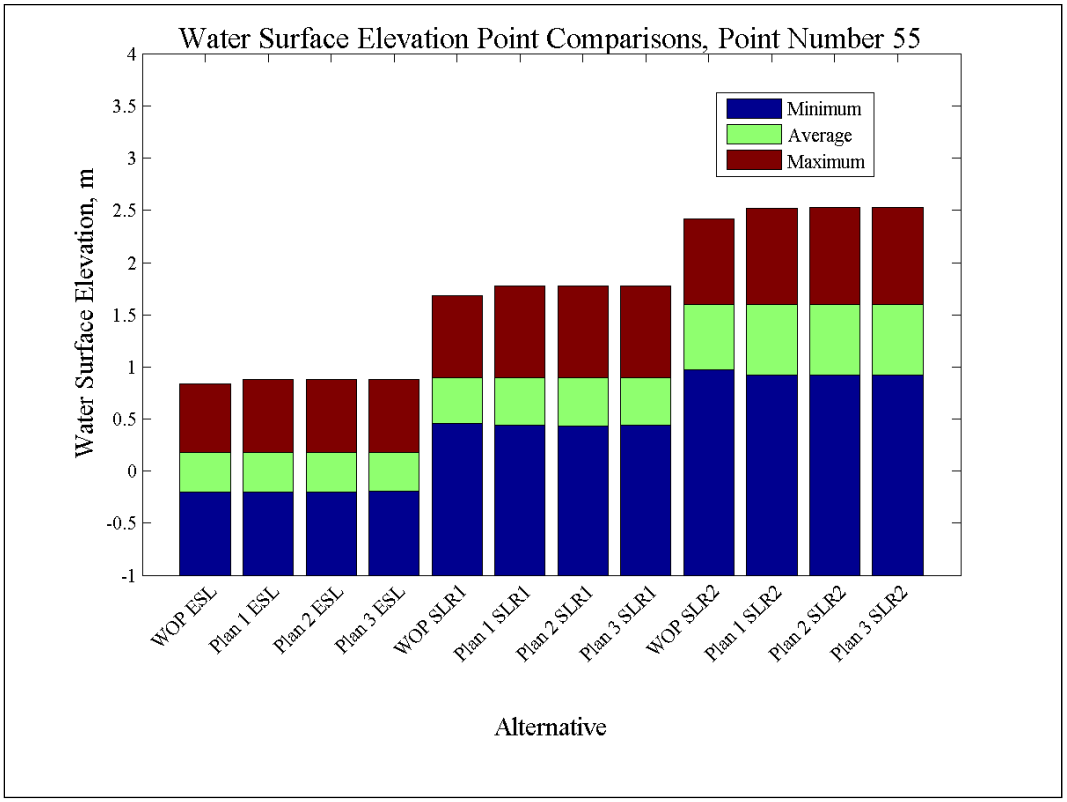

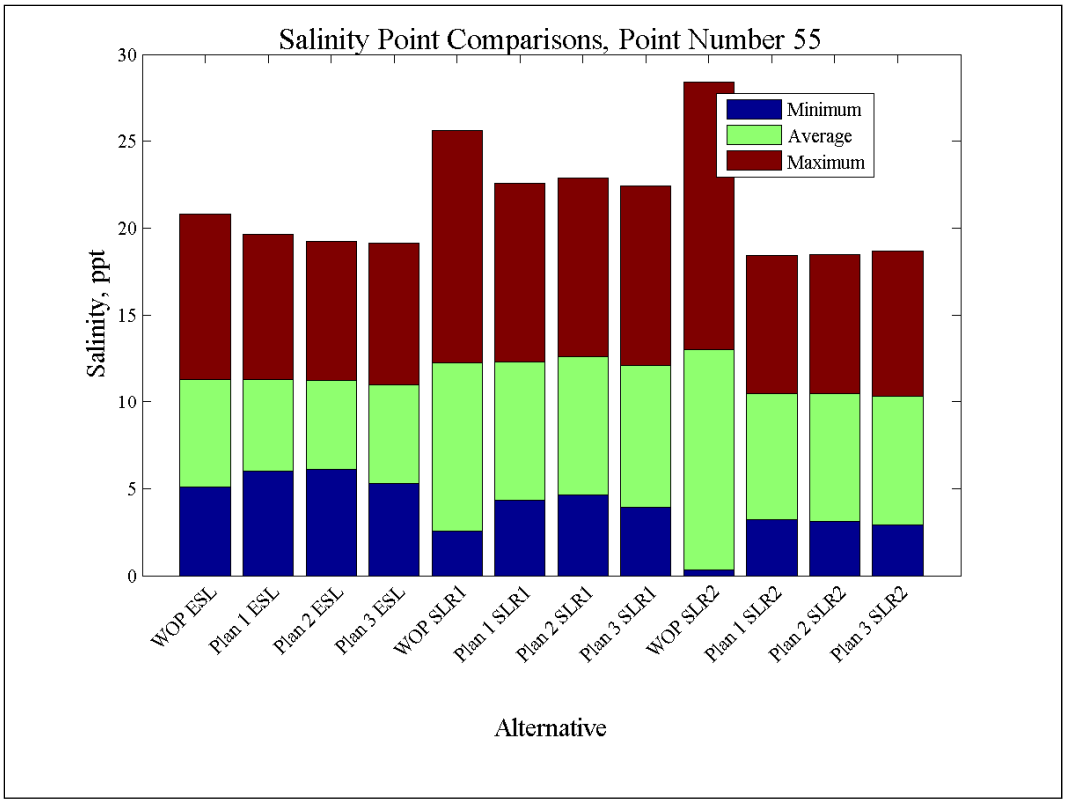

Figure 235. Water-surface elevation and salinity comparisons at Point 56.

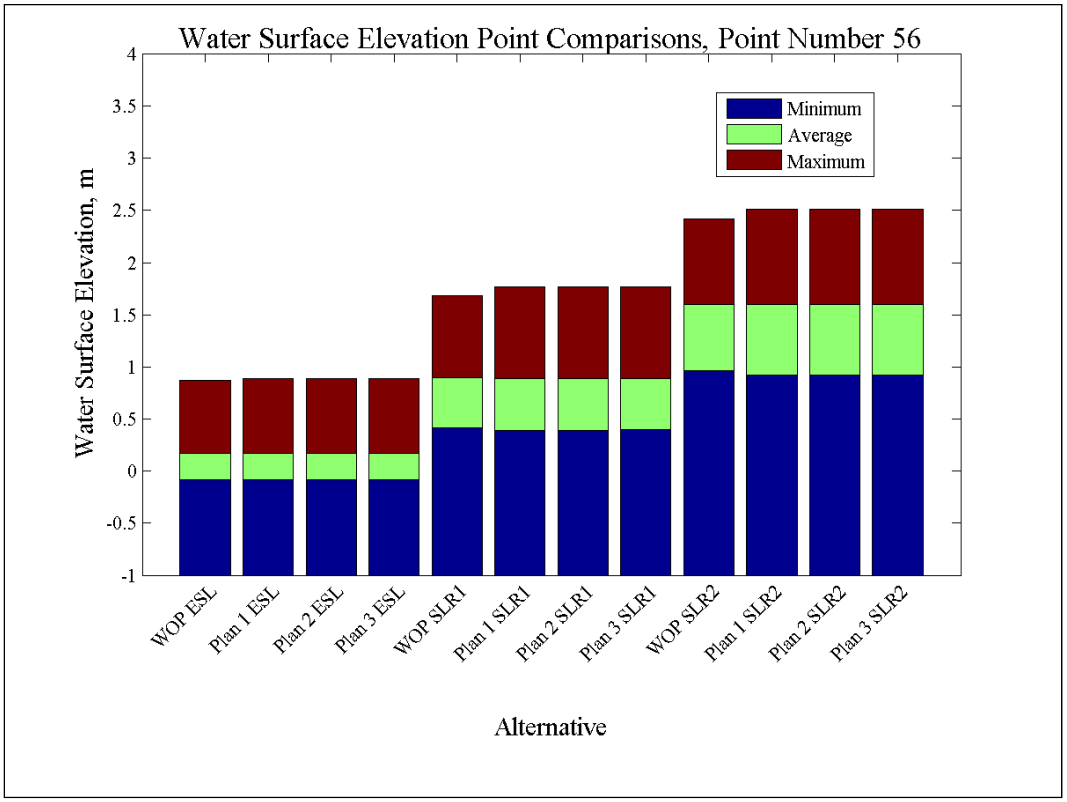

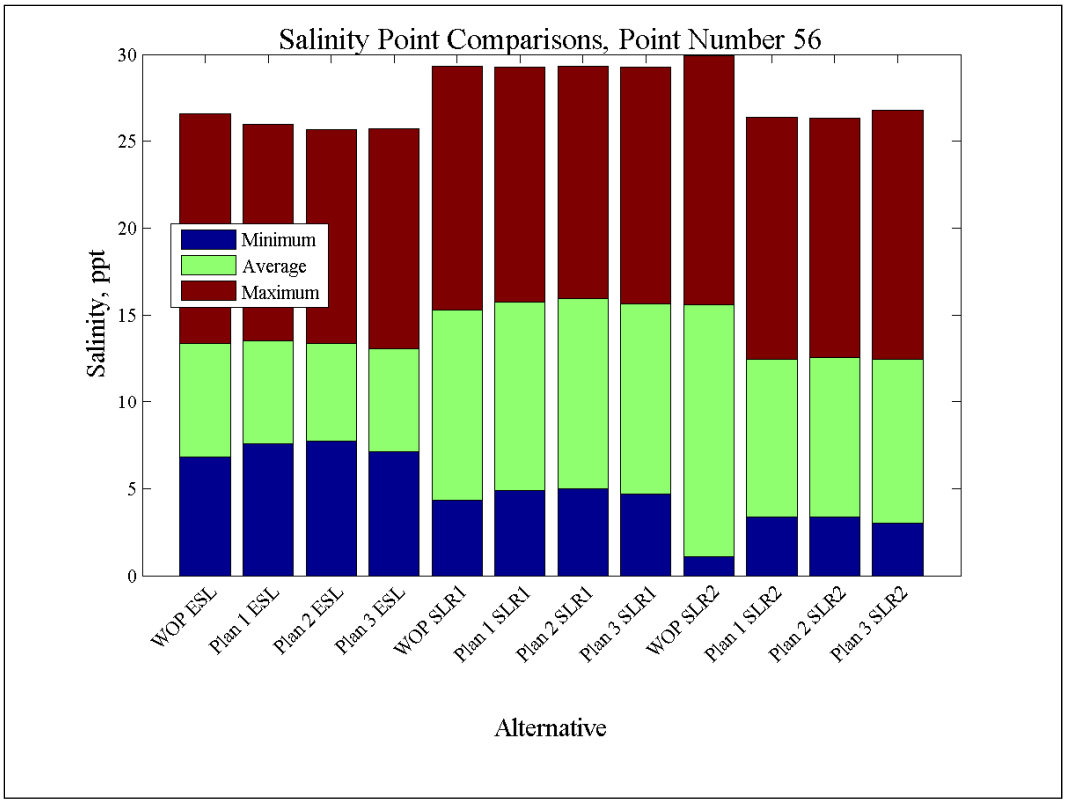

Figure 236. Water-surface elevation and salinity comparisons at Point 57.

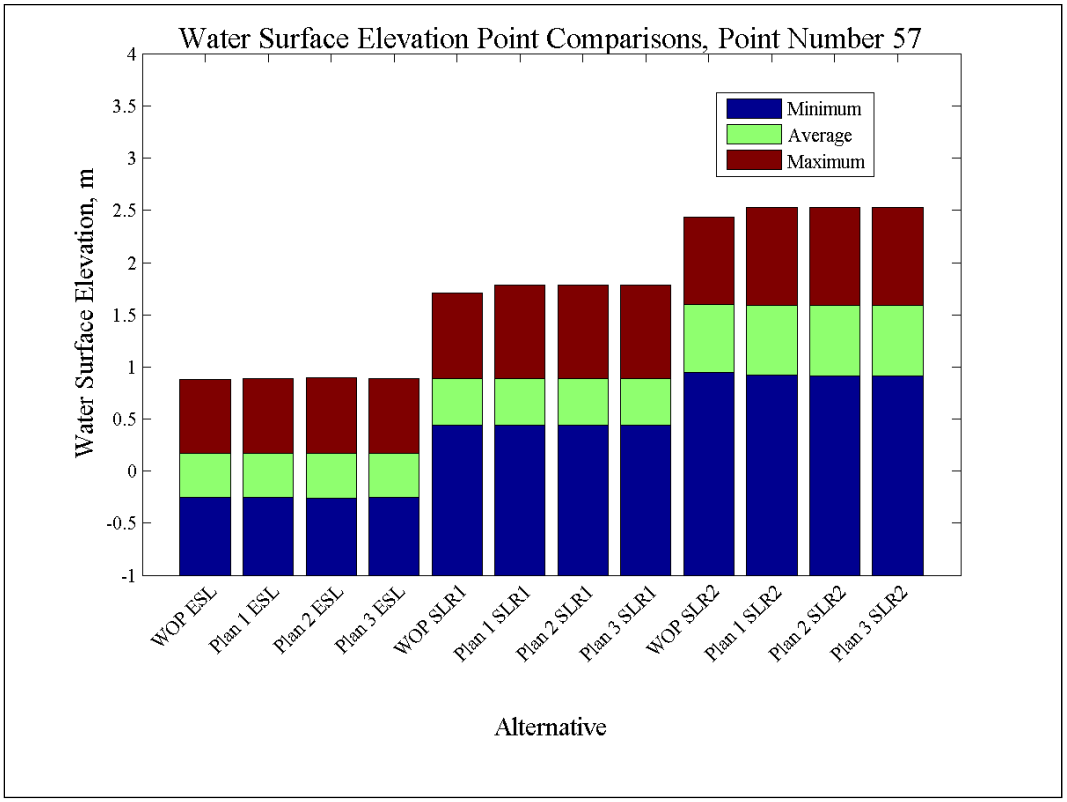

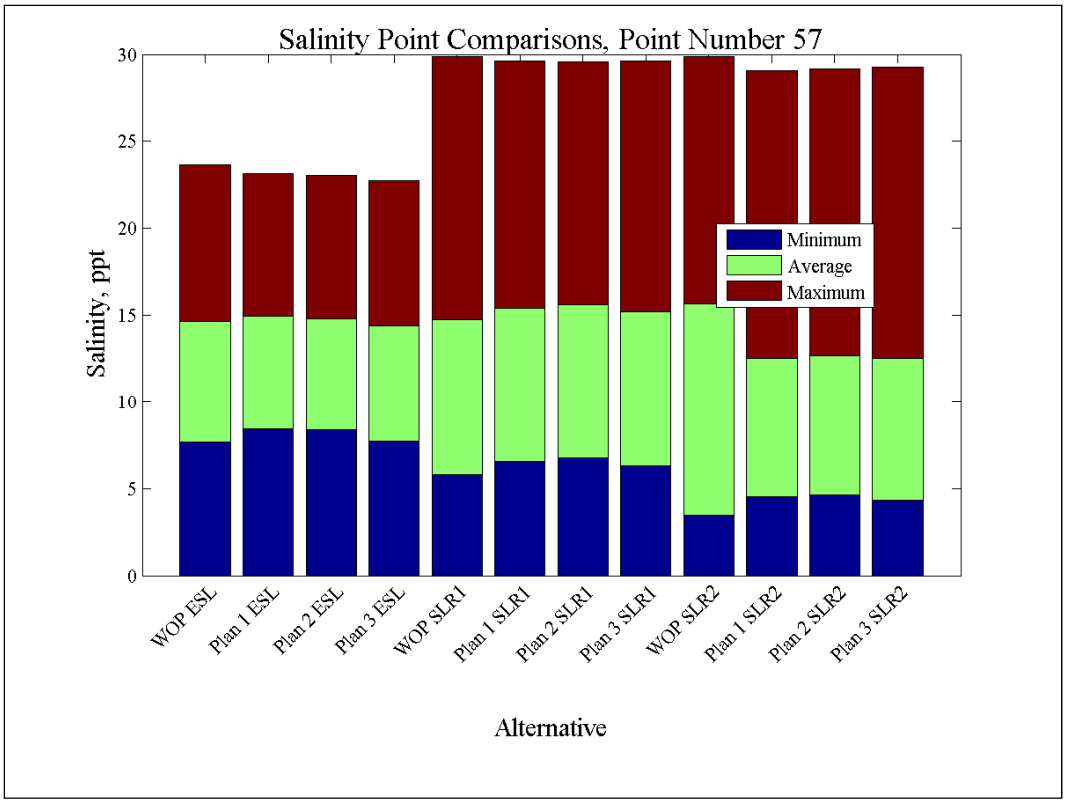

Figure 237. Water-surface elevation and salinity comparisons at Point 58.

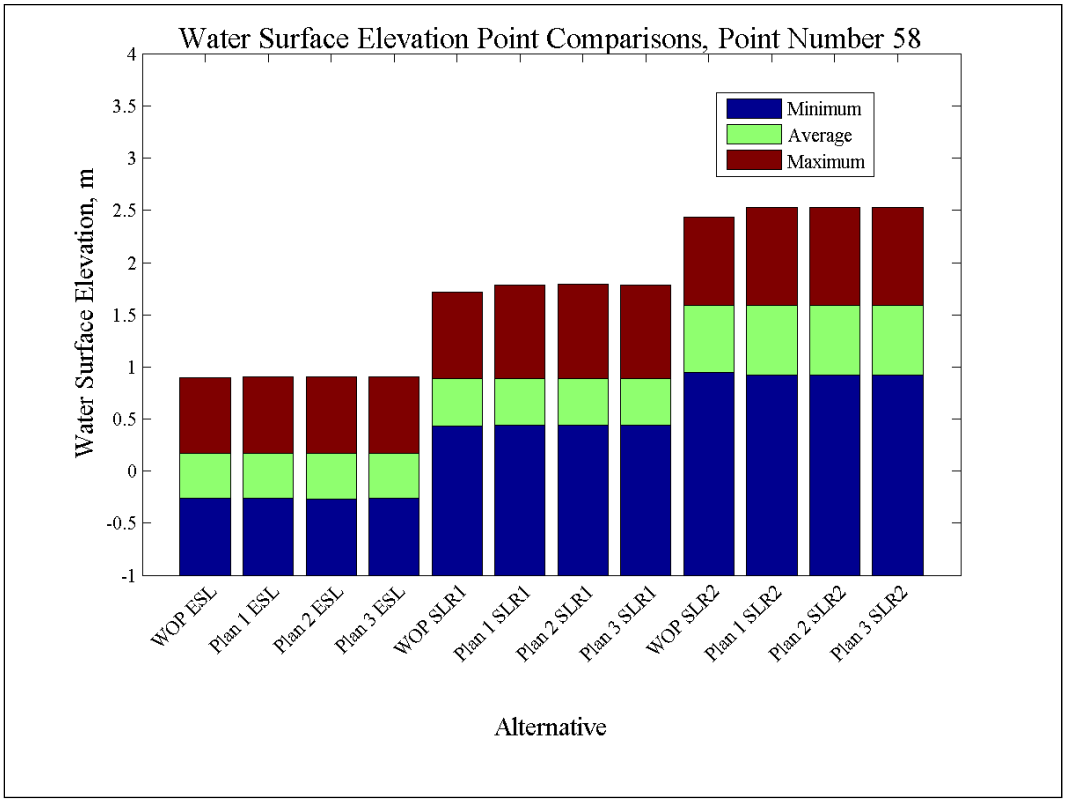

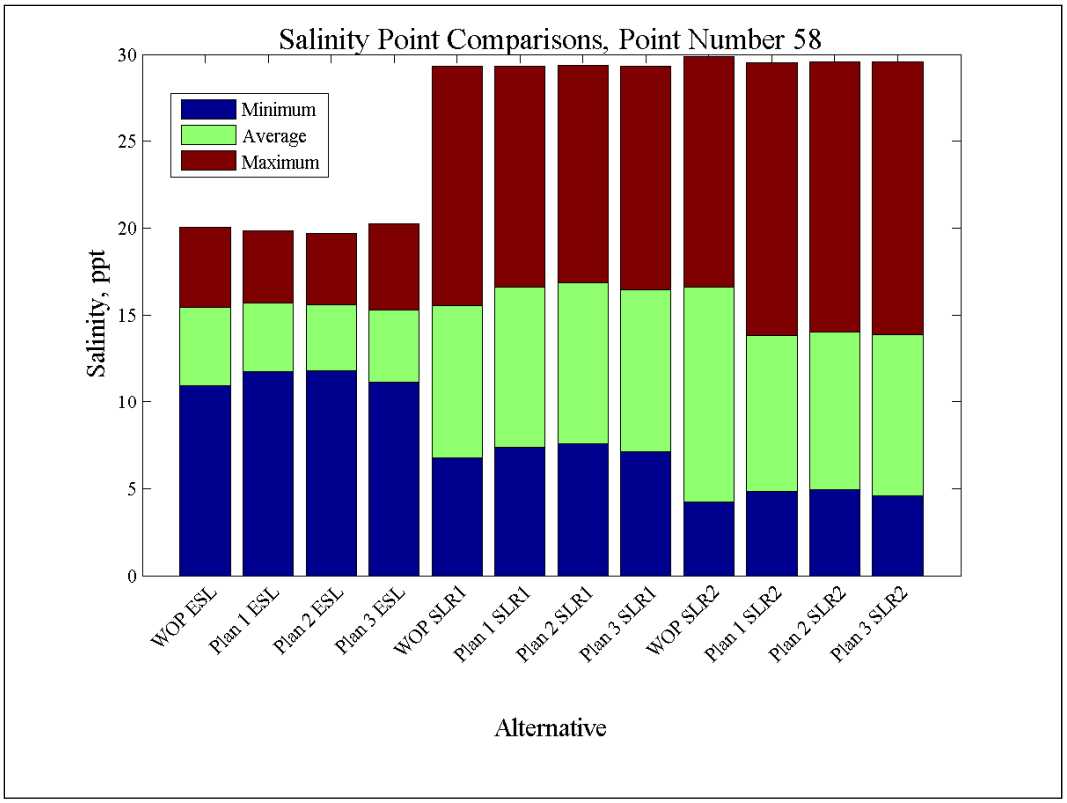

Figure 238. Water-surface elevation and salinity comparisons at Point 59.

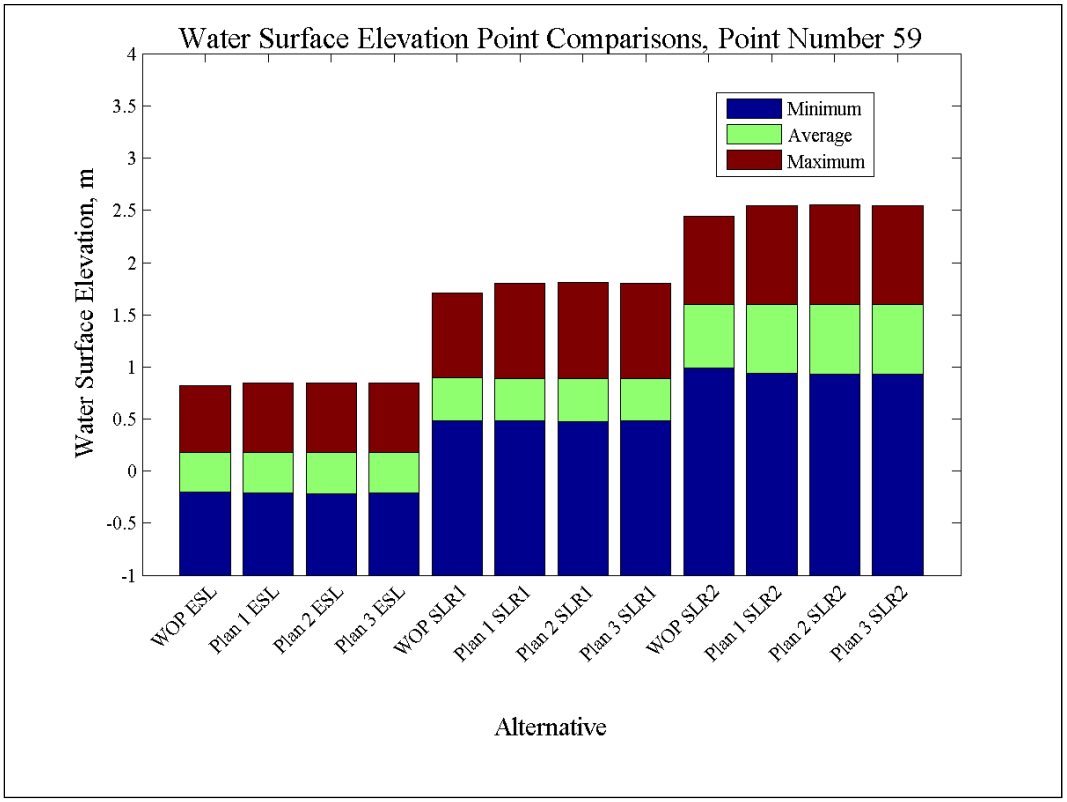

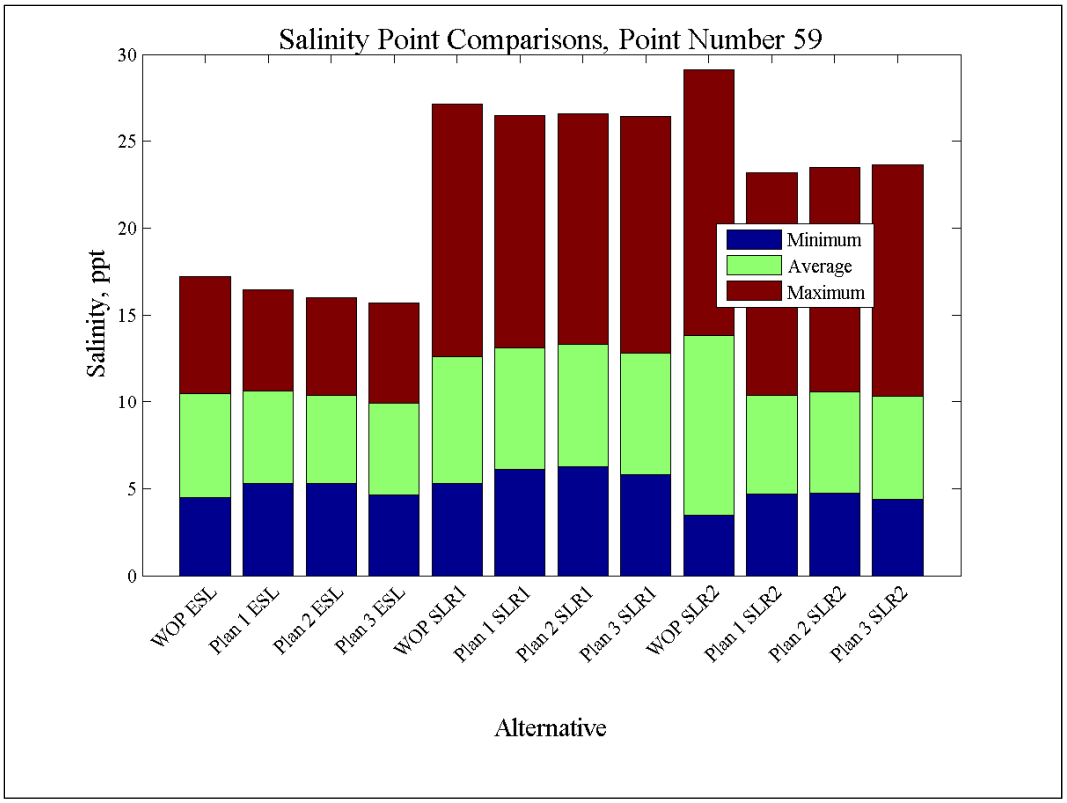

Figure 239. Water-surface elevation and salinity comparisons at Point 60.

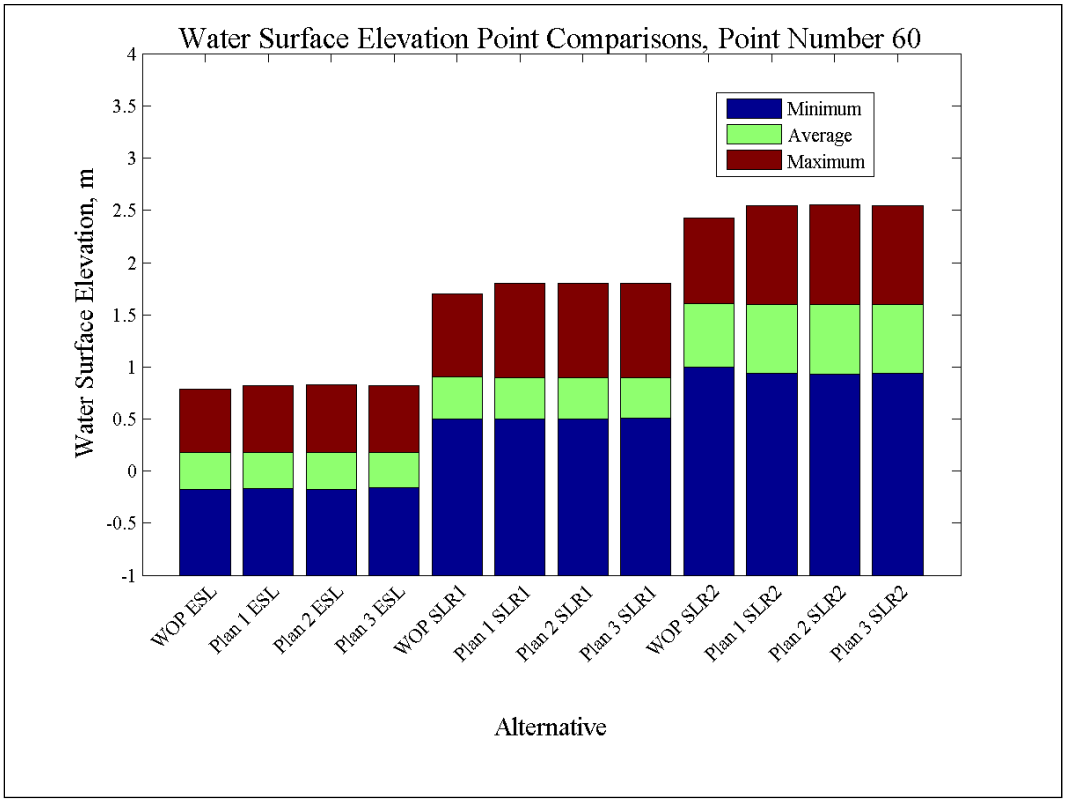

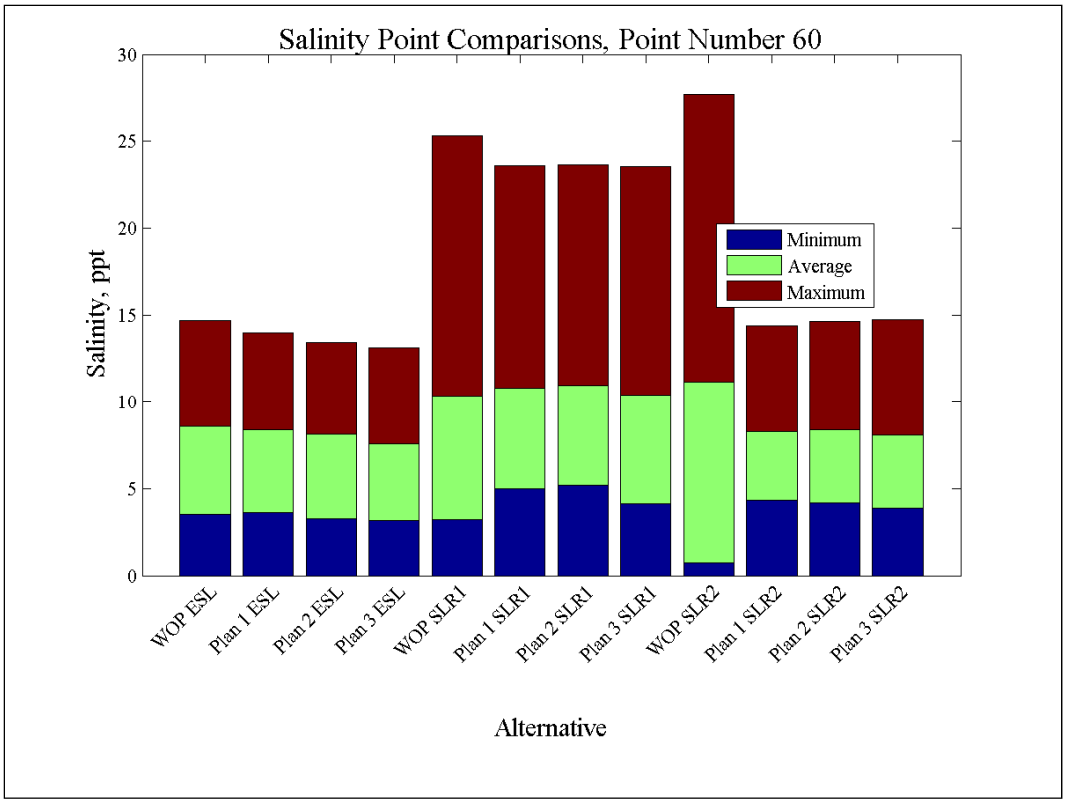

Figure 240. Water-surface elevation and salinity comparisons at Point 61.

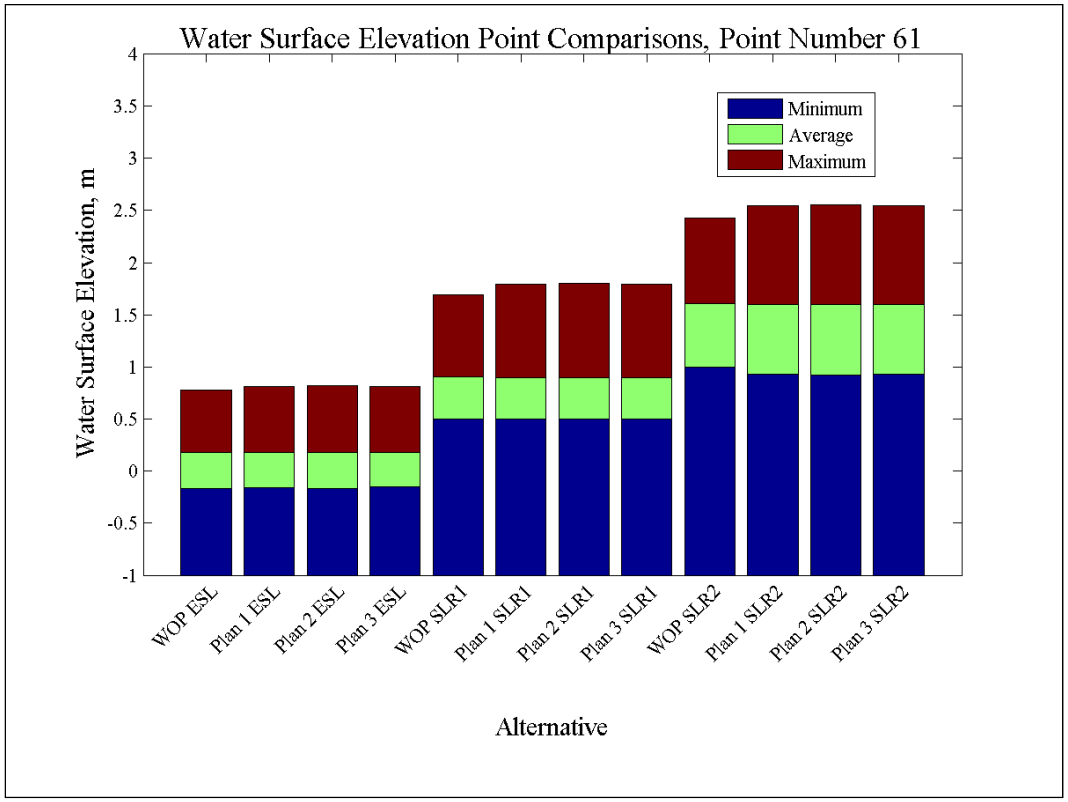

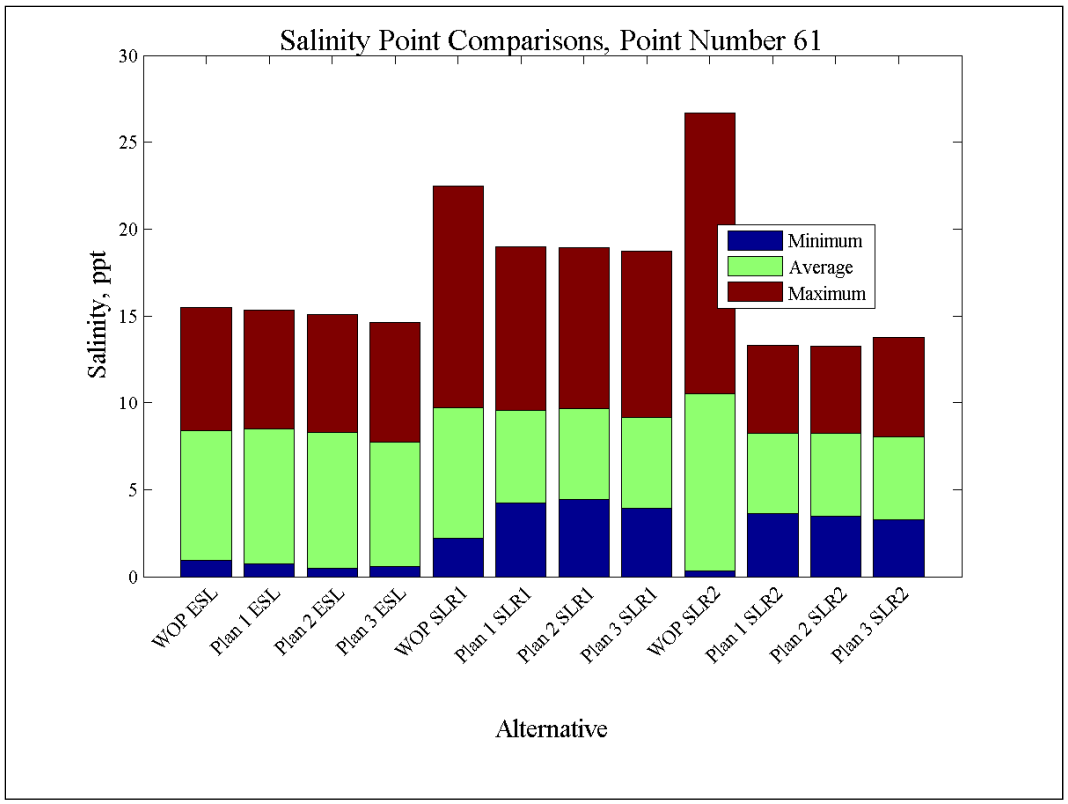

Figure 241. Water-surface elevation and salinity comparisons at Point 62.

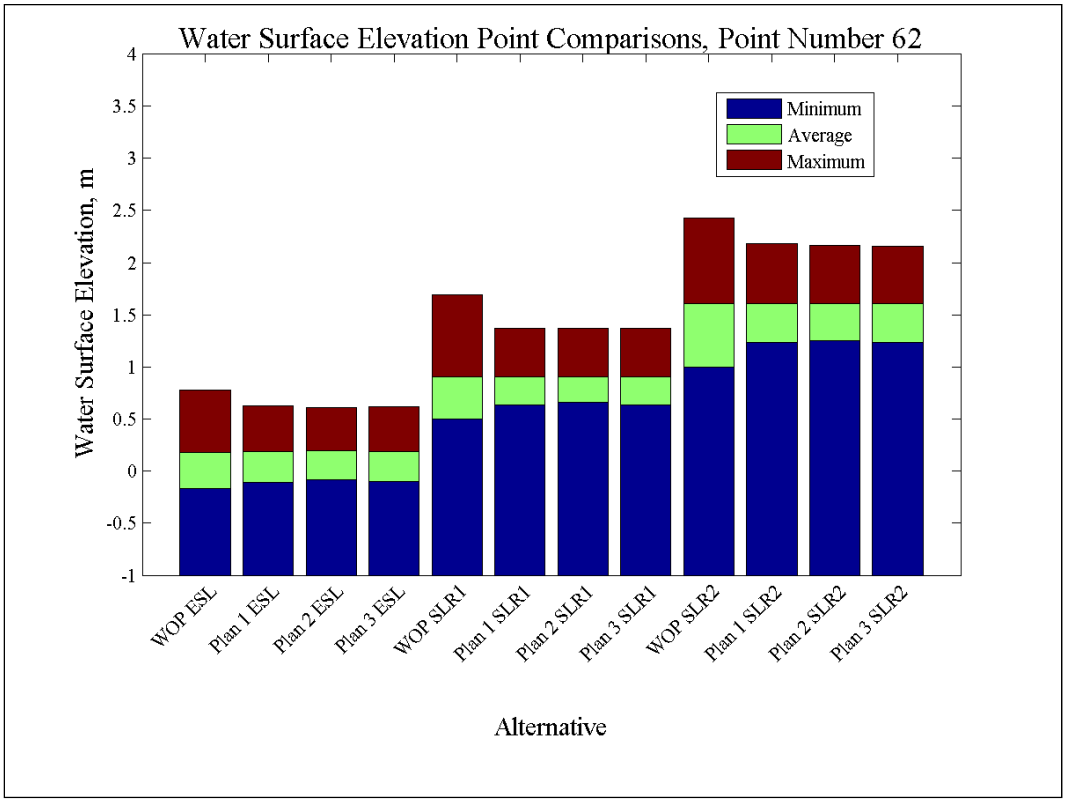

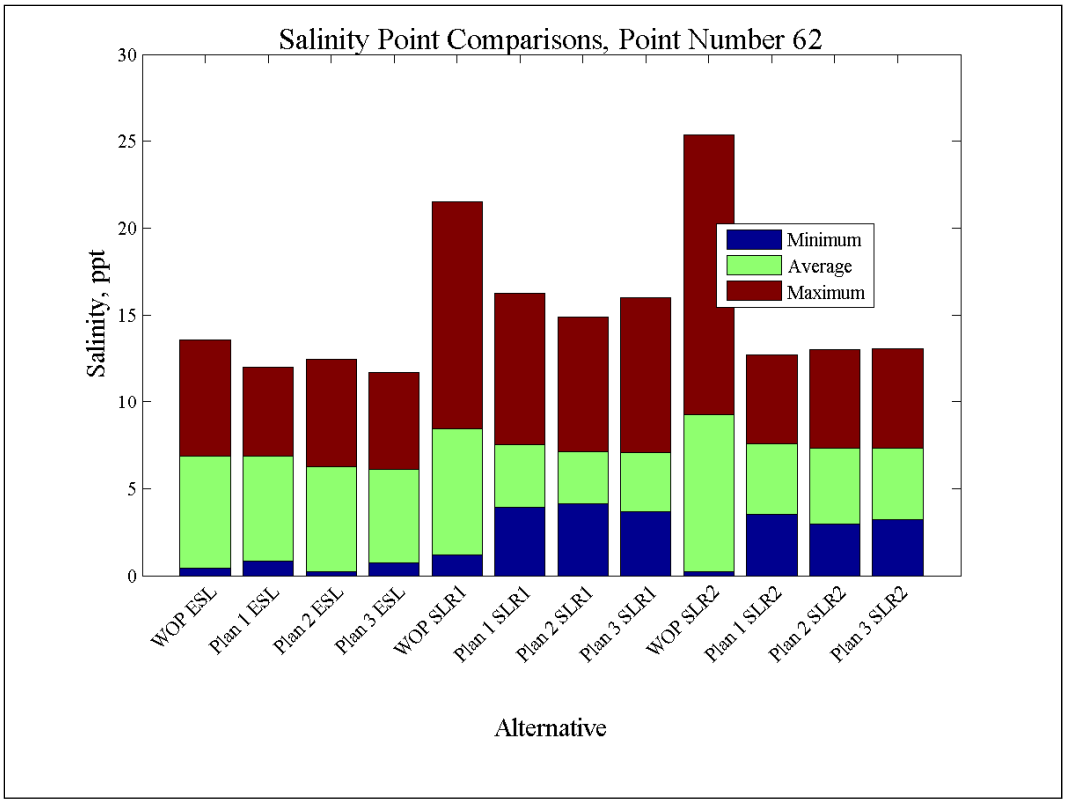

Figure 242. Water-surface elevation and salinity comparisons at Point 63.

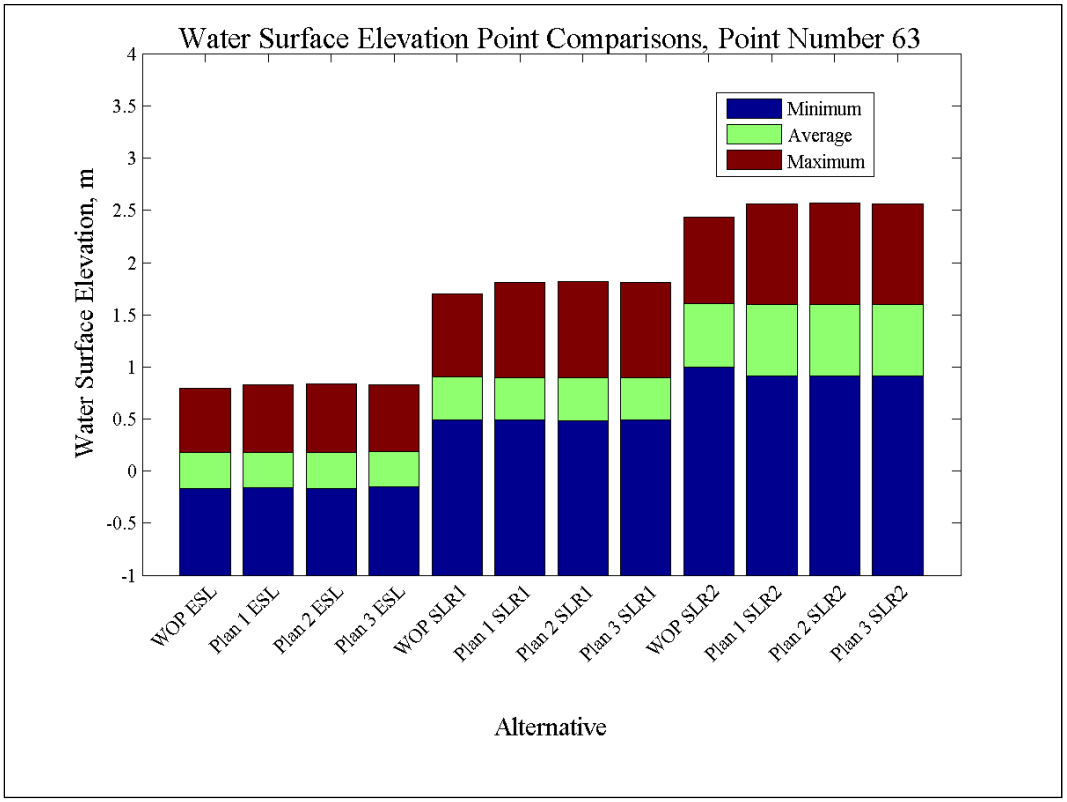

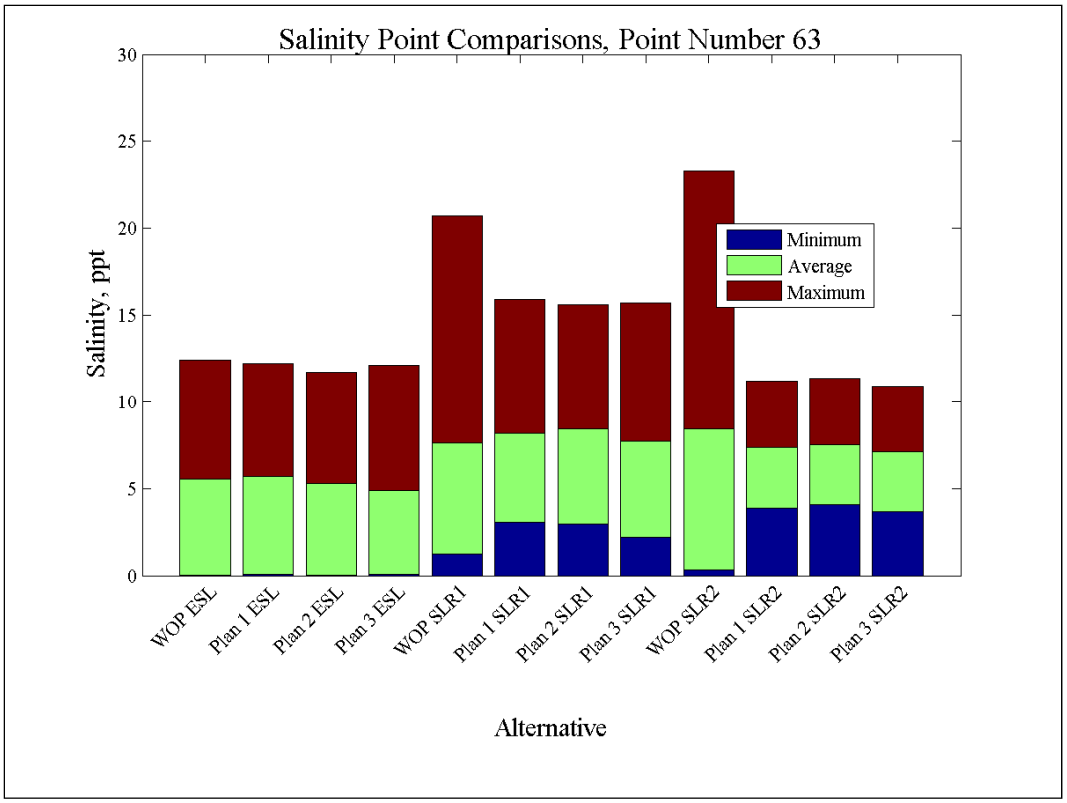

Figure 243. Water-surface elevation and salinity comparisons at Point 64.

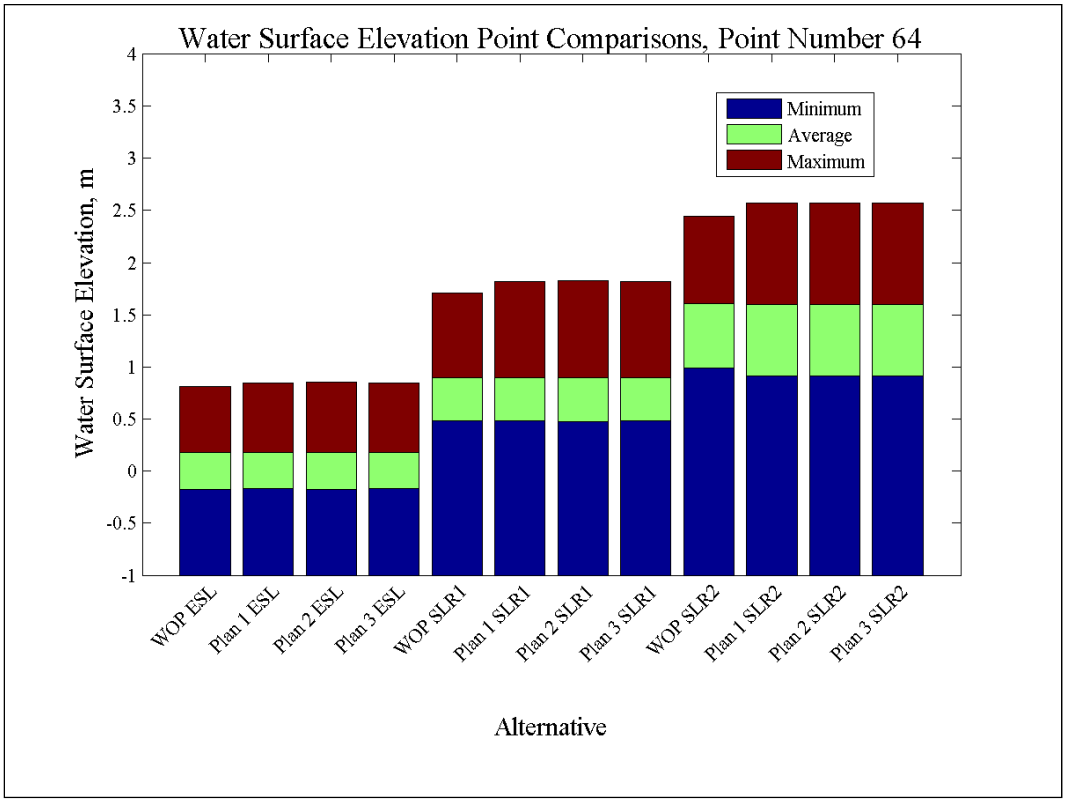

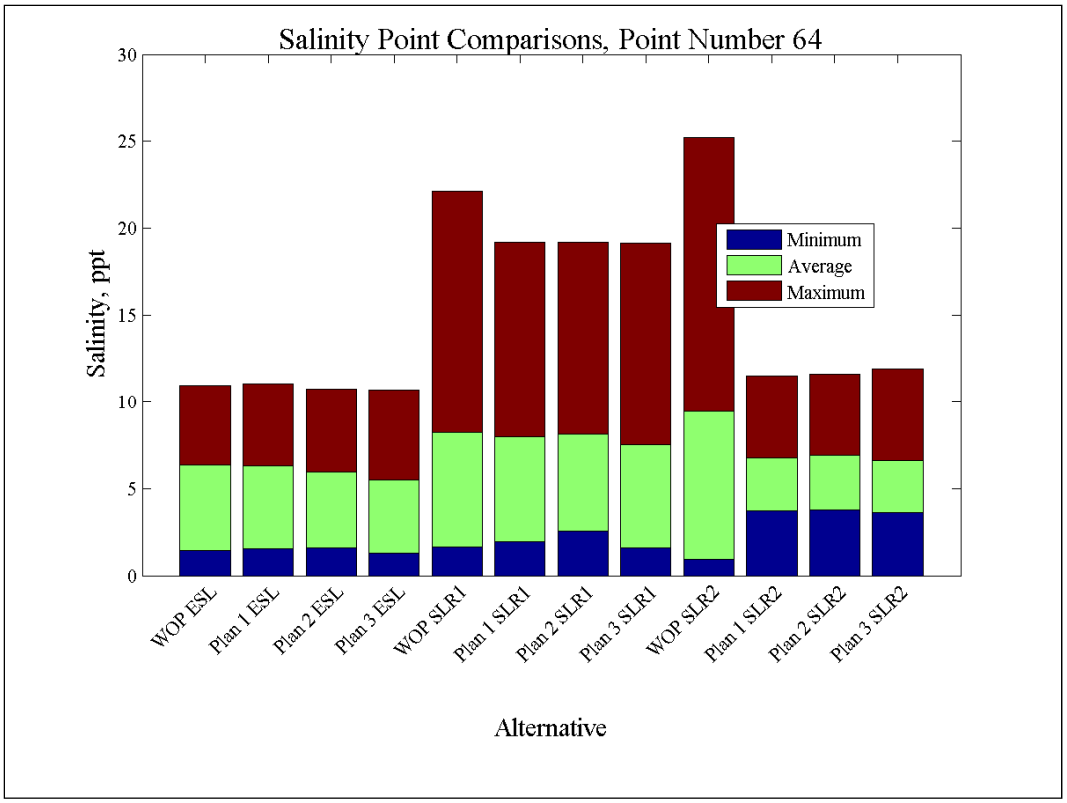

Figure 244. Water-surface elevation and salinity comparisons at Point 65.

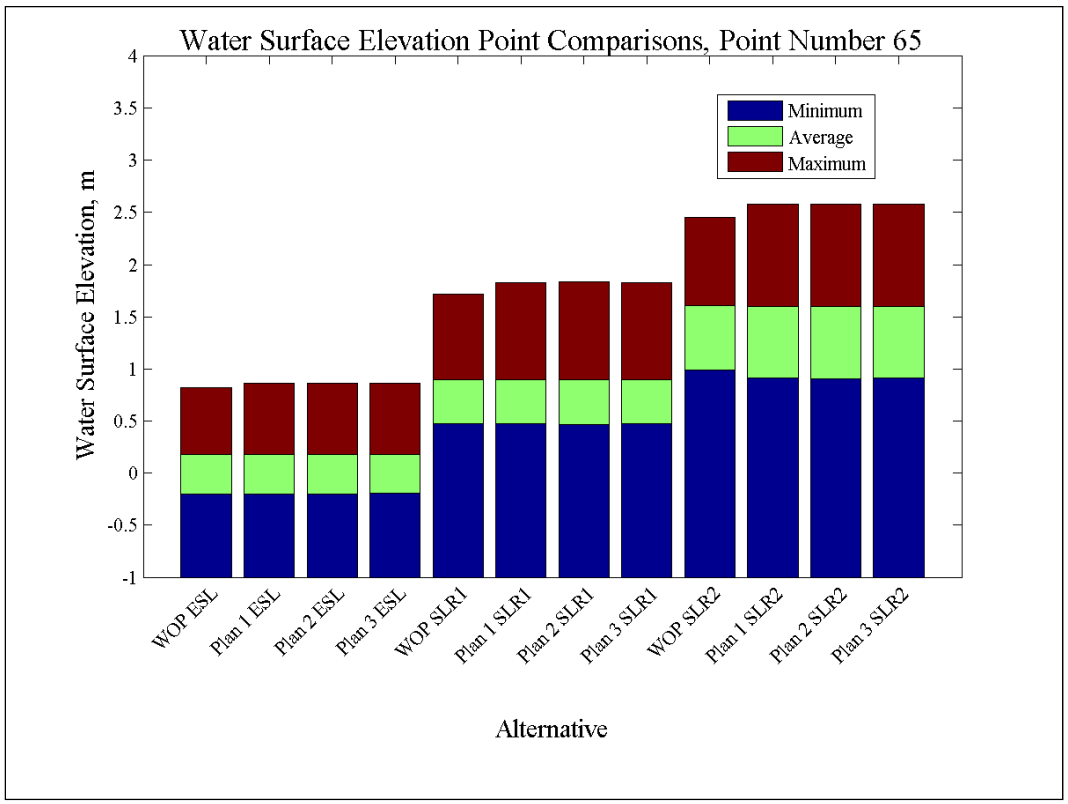

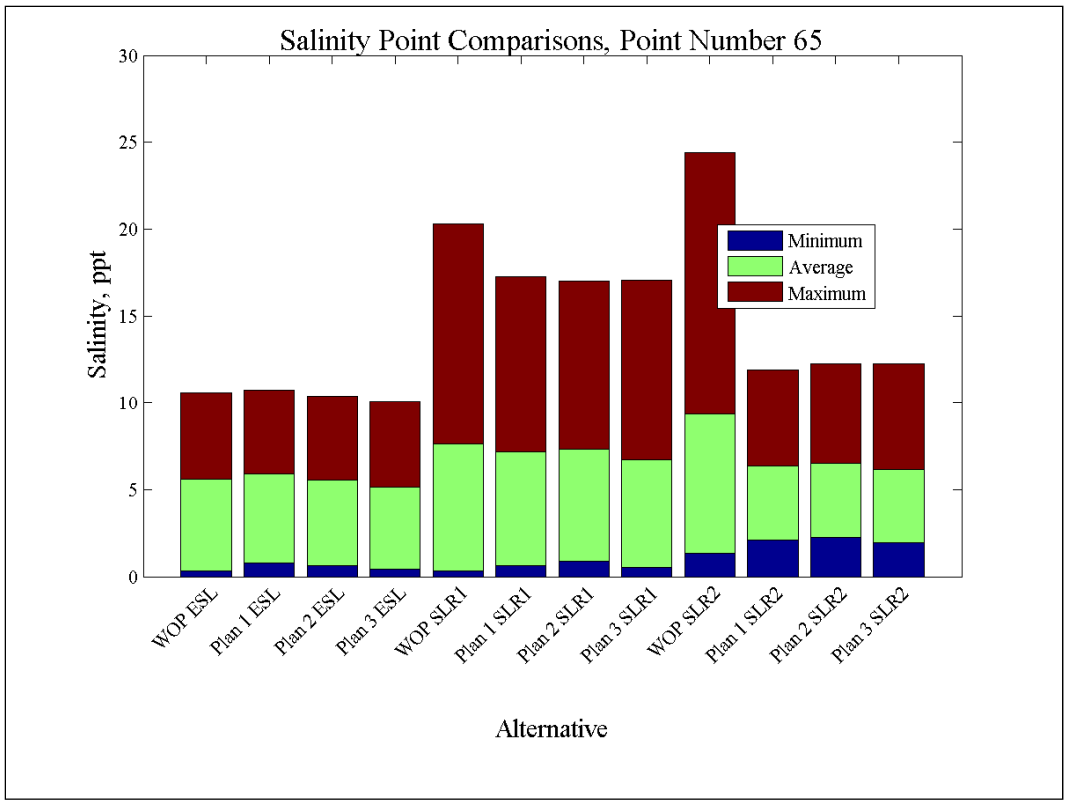

Figure 245. Water-surface elevation and salinity comparisons at Point 66.

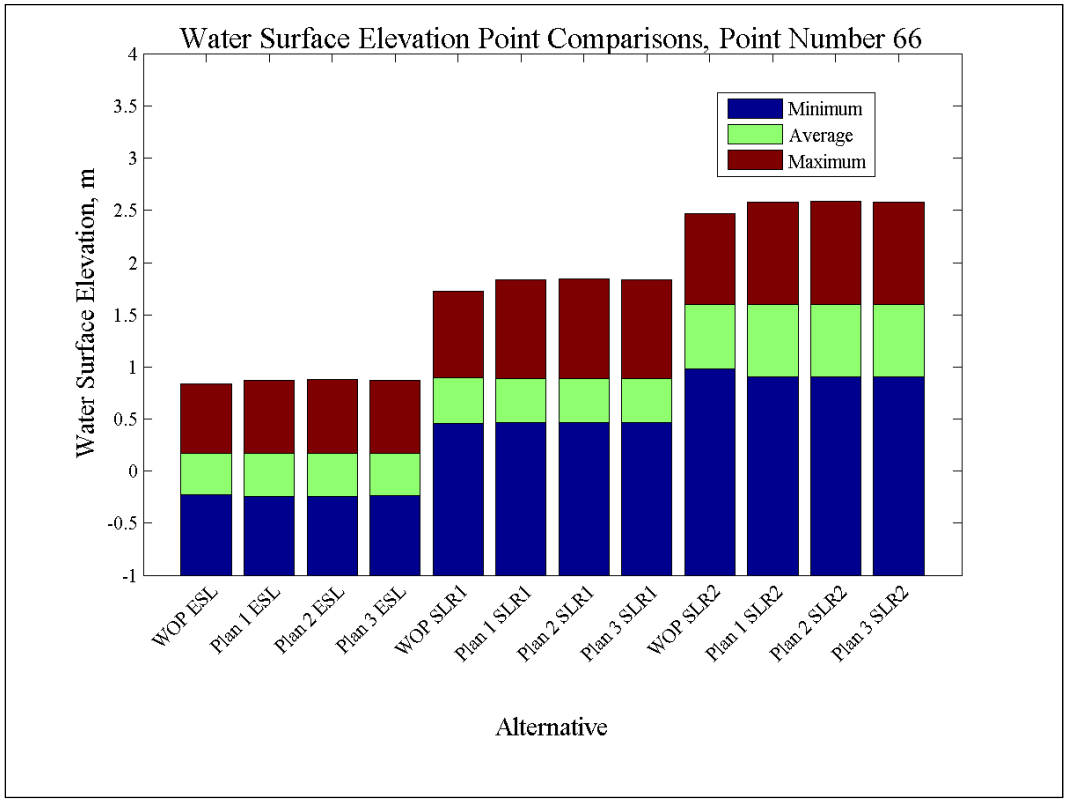

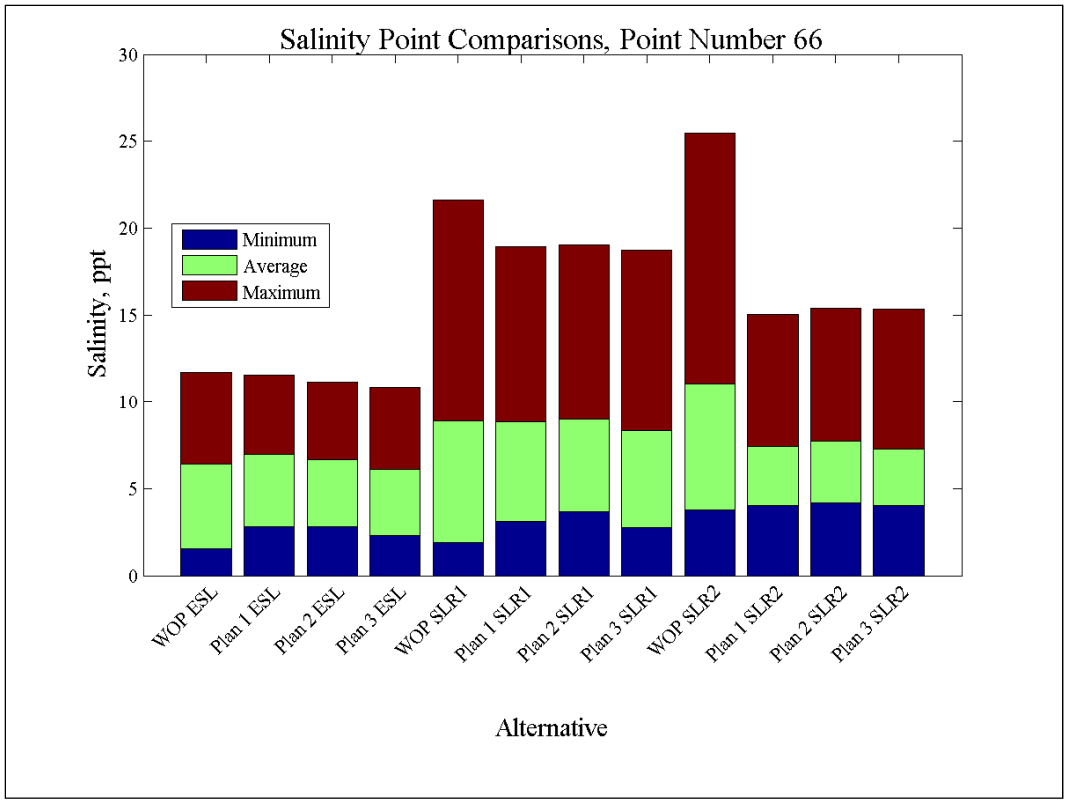

Figure 246. Water-surface elevation and salinity comparisons at Point 67.

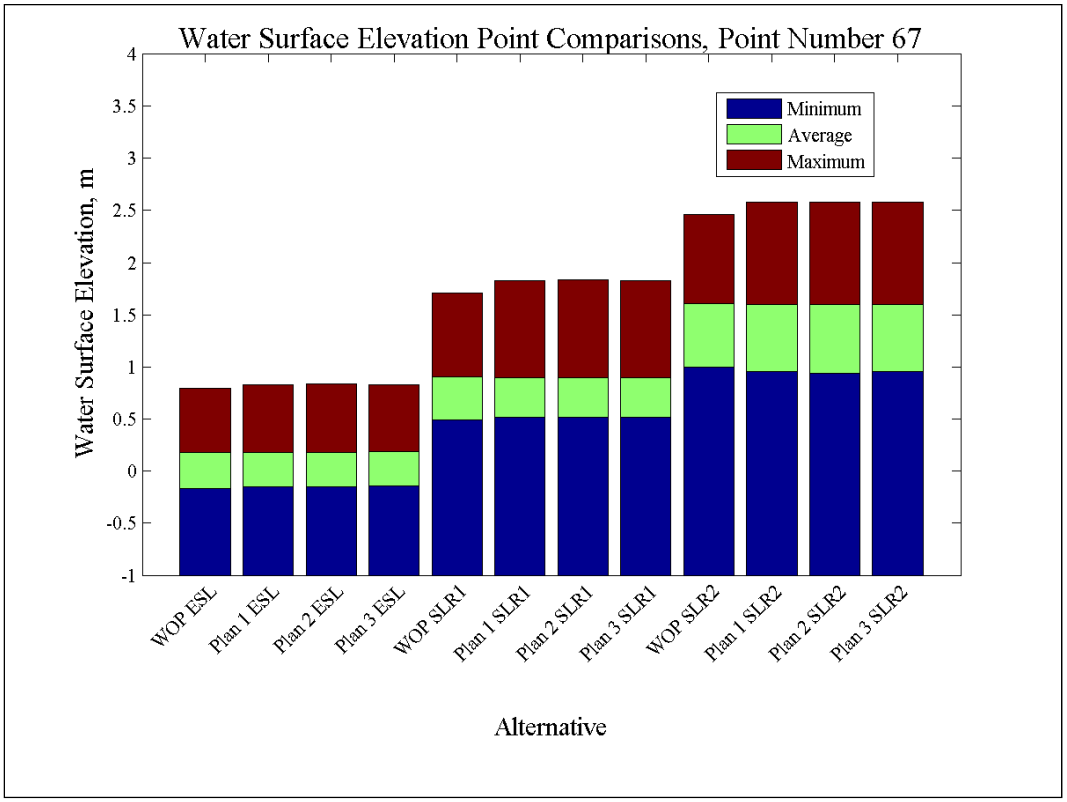

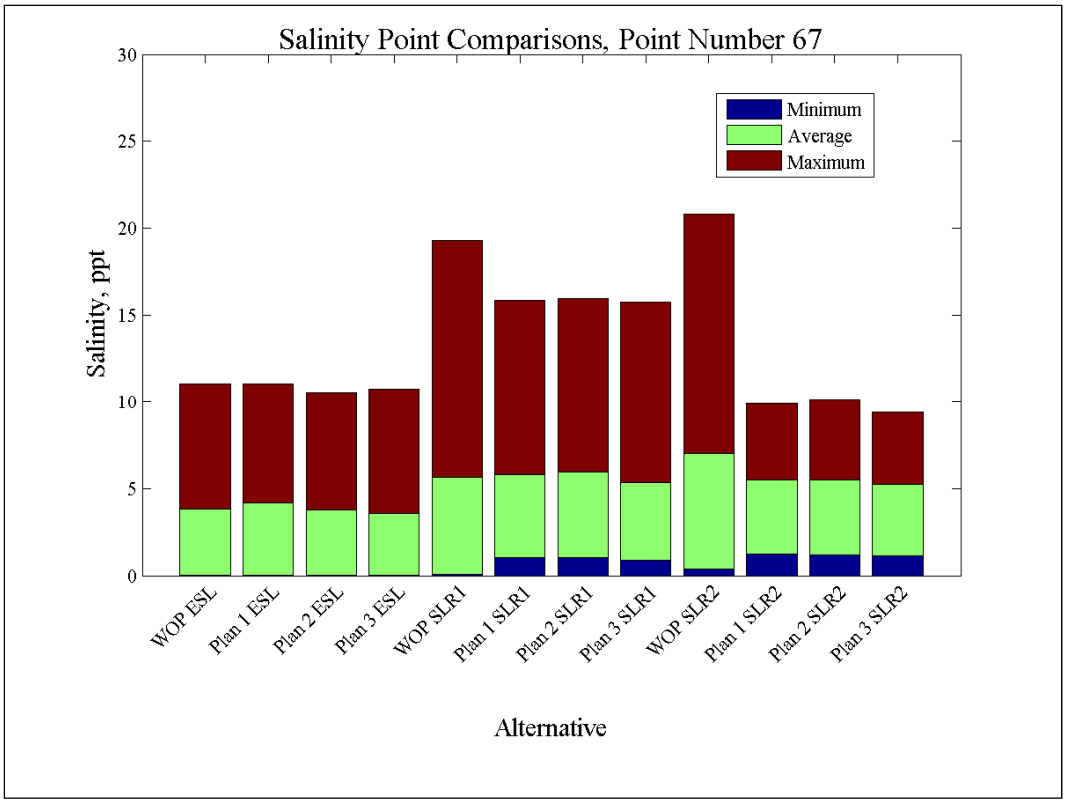

Figure 247. Water-surface elevation and salinity comparisons at Point 68.

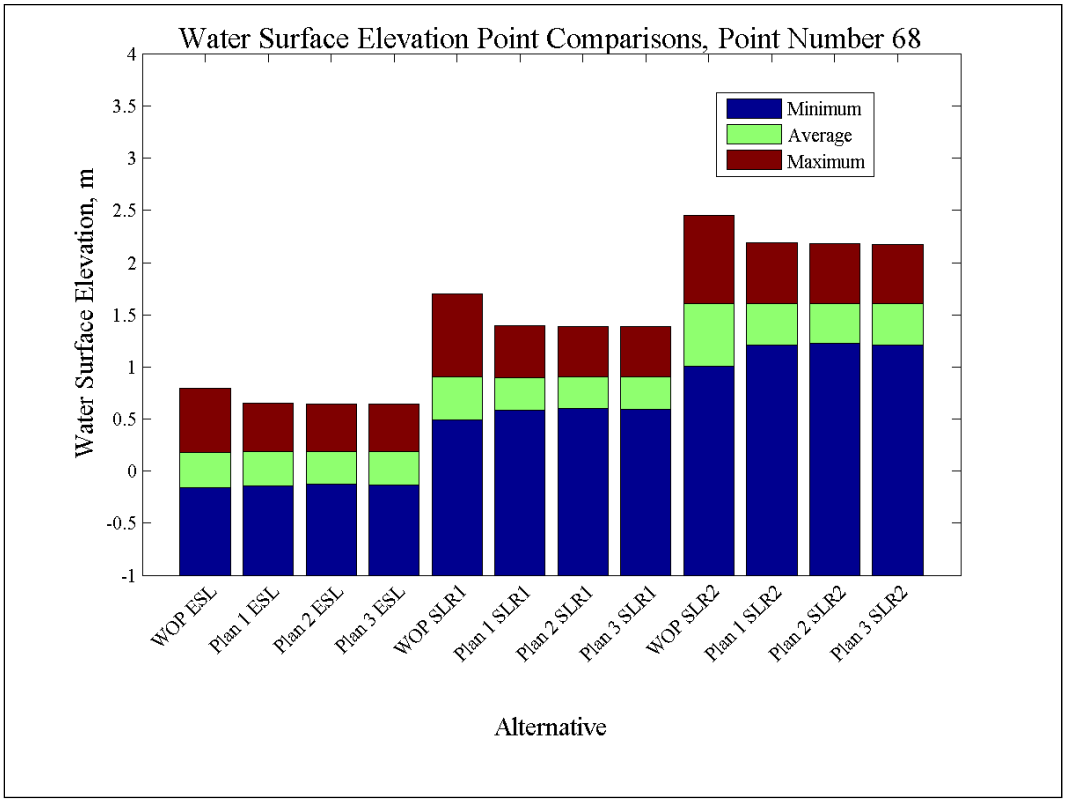

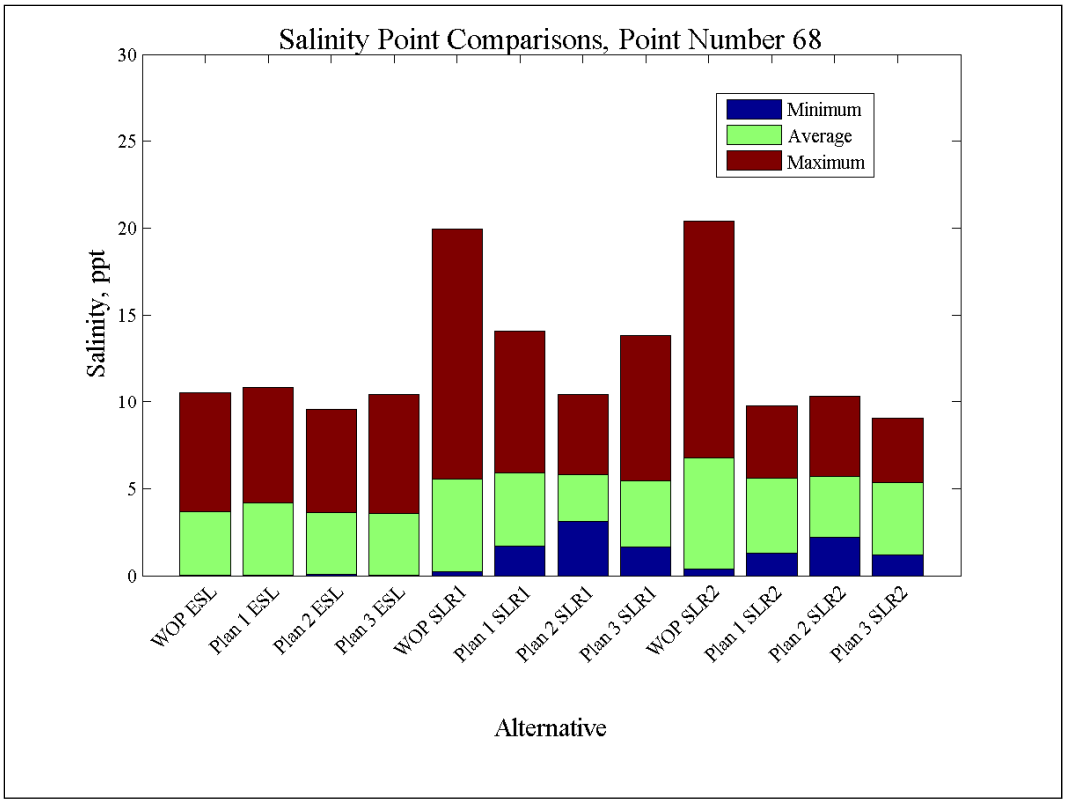

Figure 248. Water-surface elevation and salinity comparisons at Point 69.

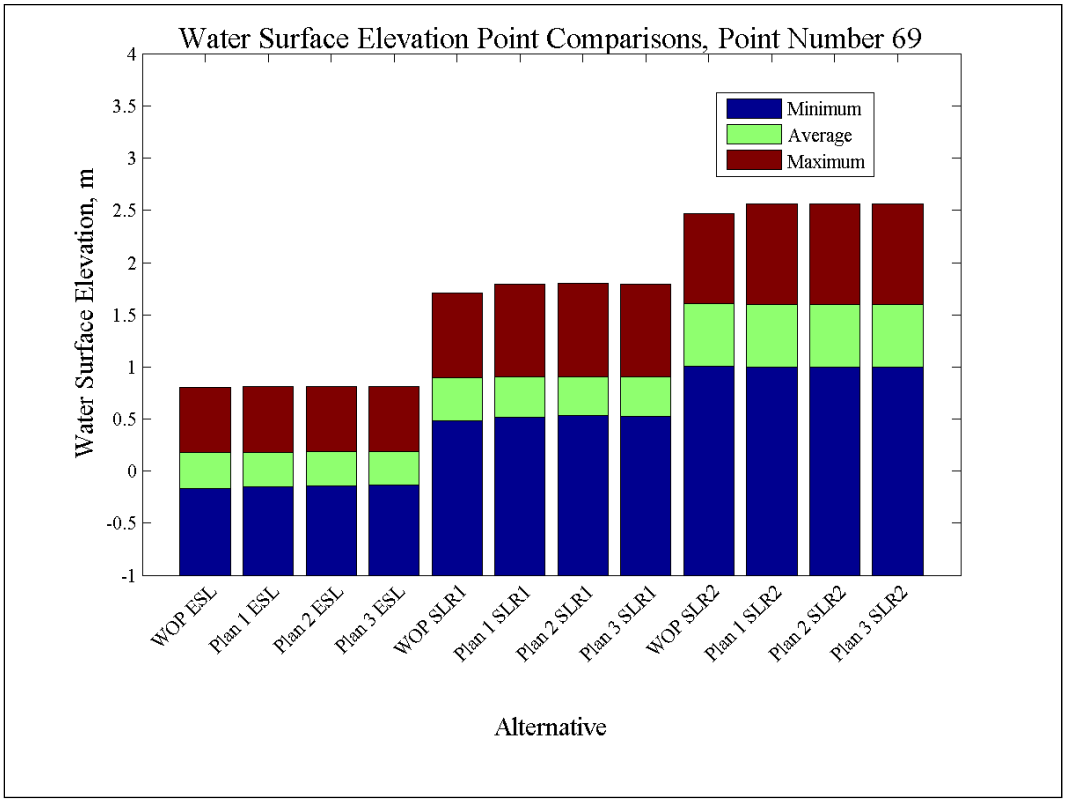

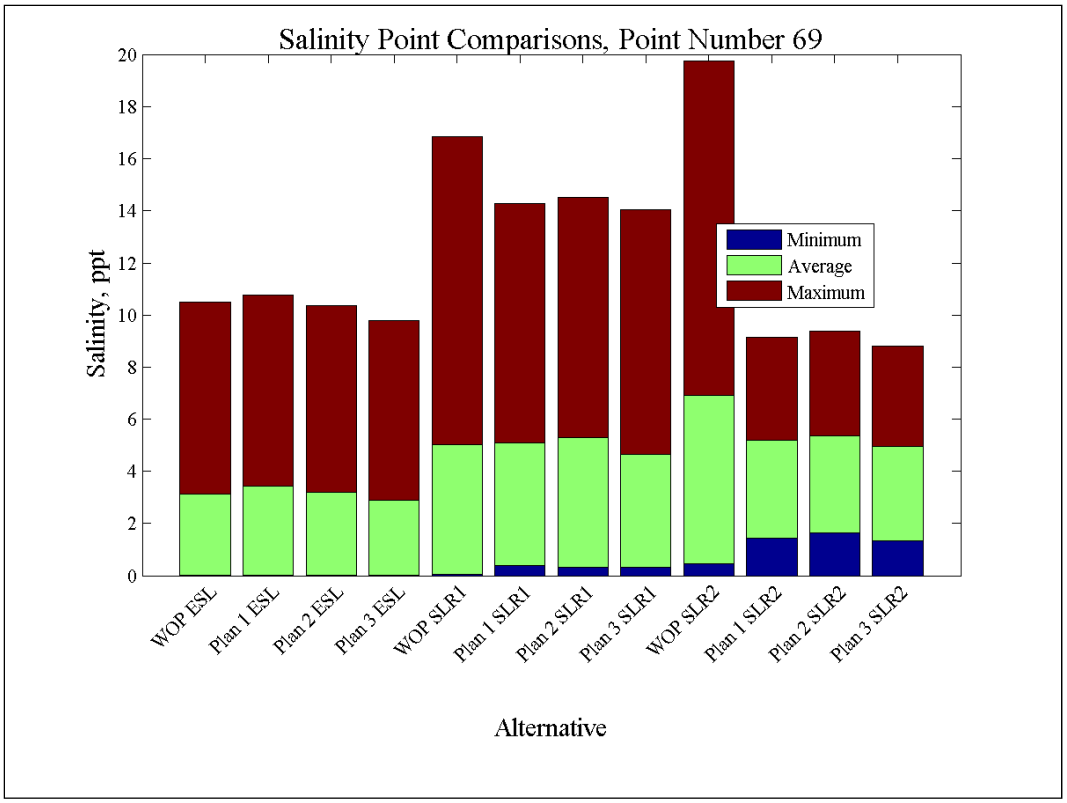

Figure 249. Water-surface elevation and salinity comparisons at Point 70.

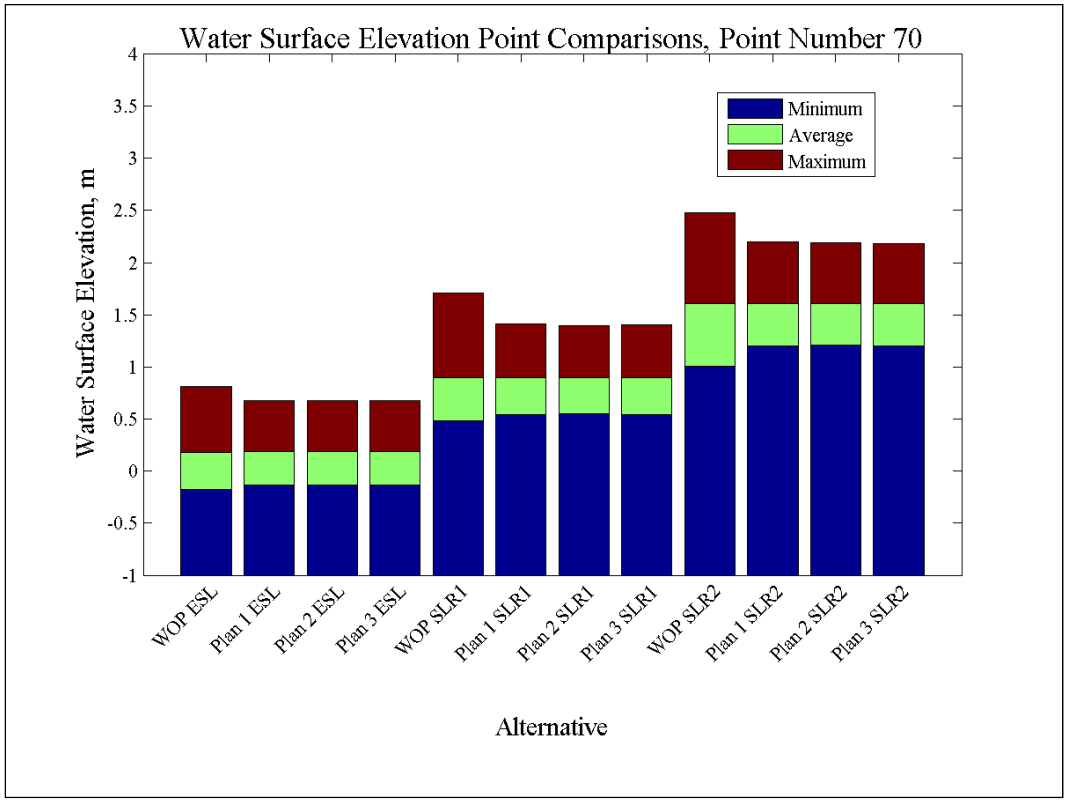

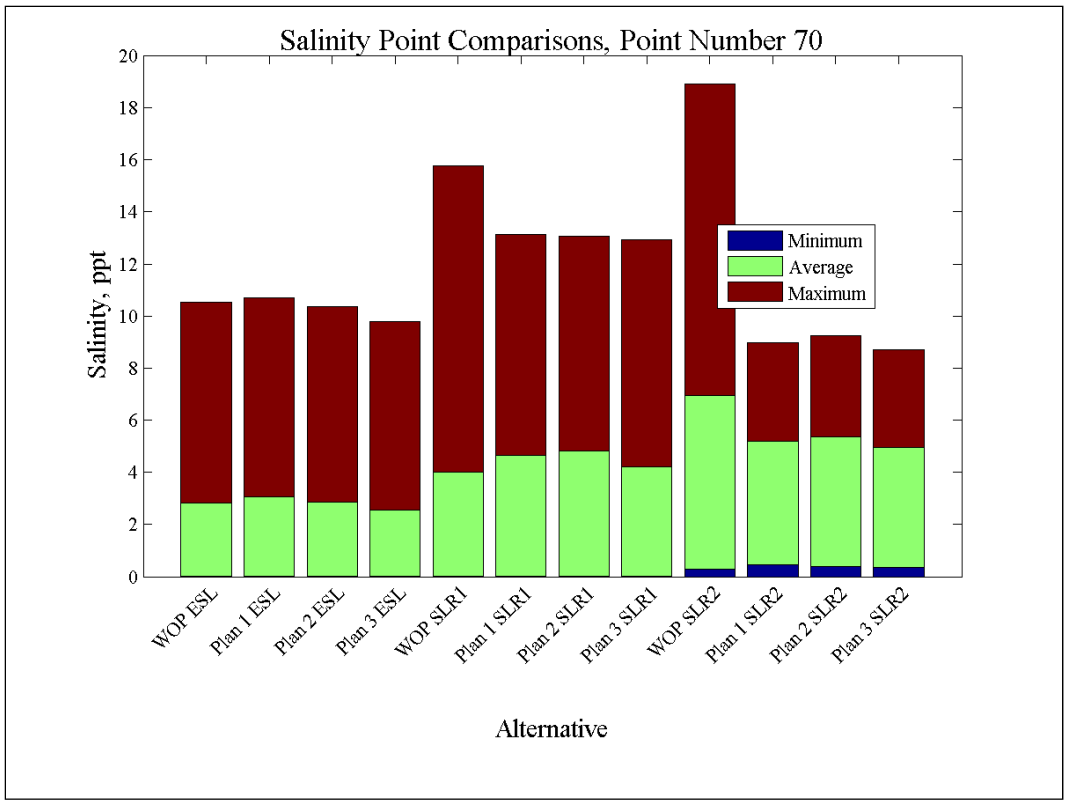

Figure 250. Water-surface elevation and salinity comparisons at Point 71.

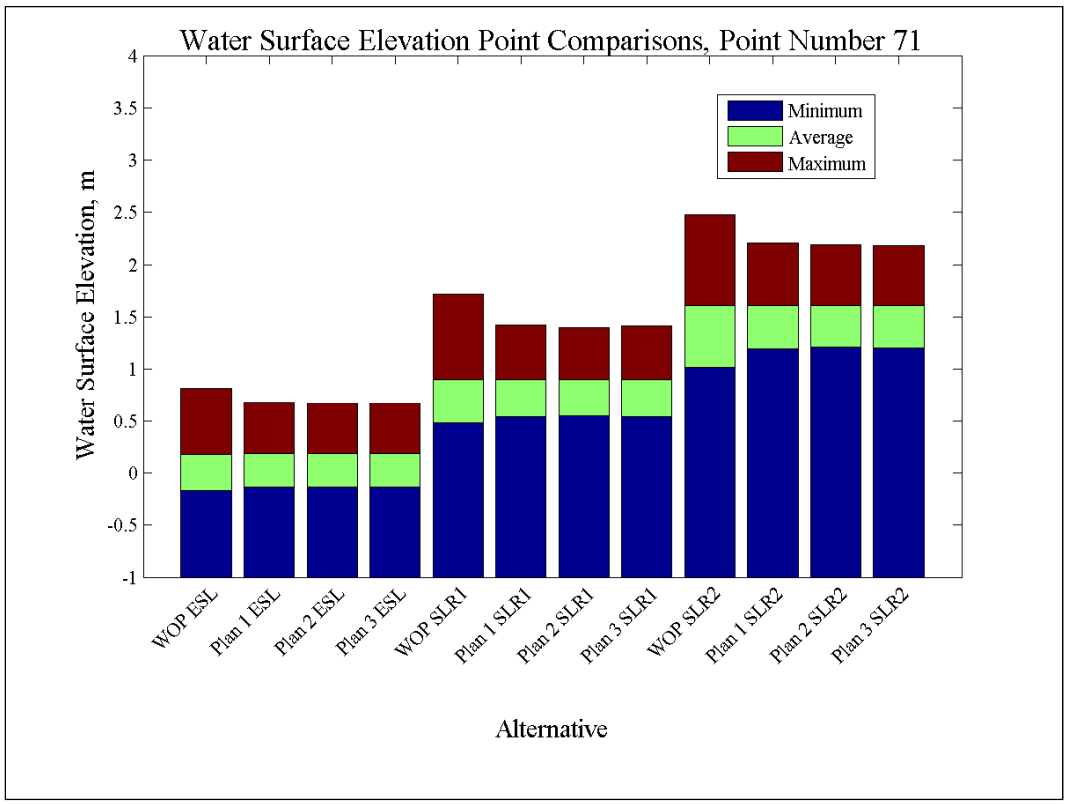

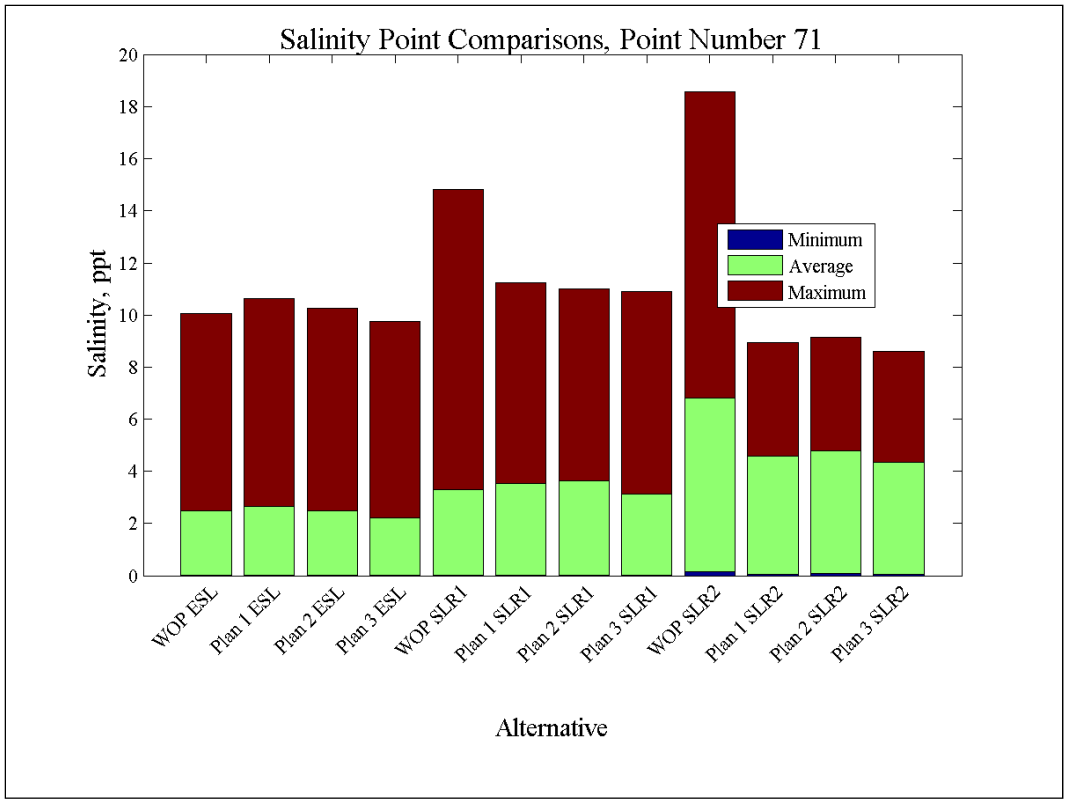

Figure 251. Water-surface elevation and salinity comparisons at Point 72.

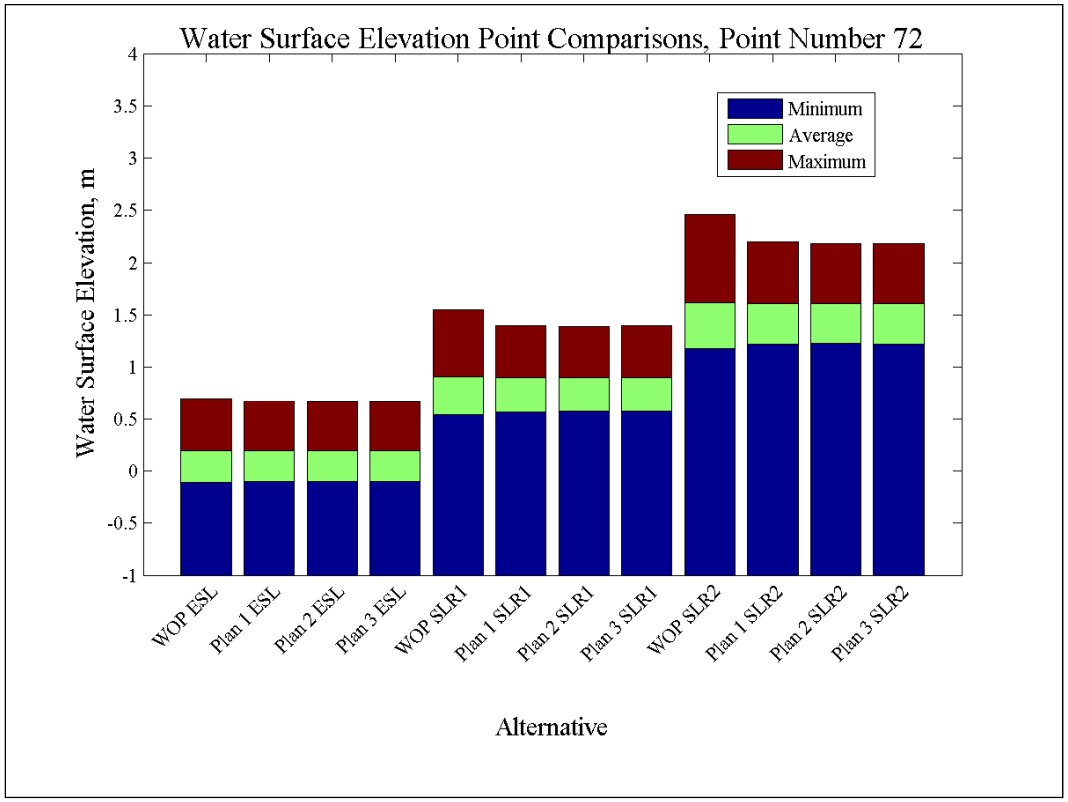

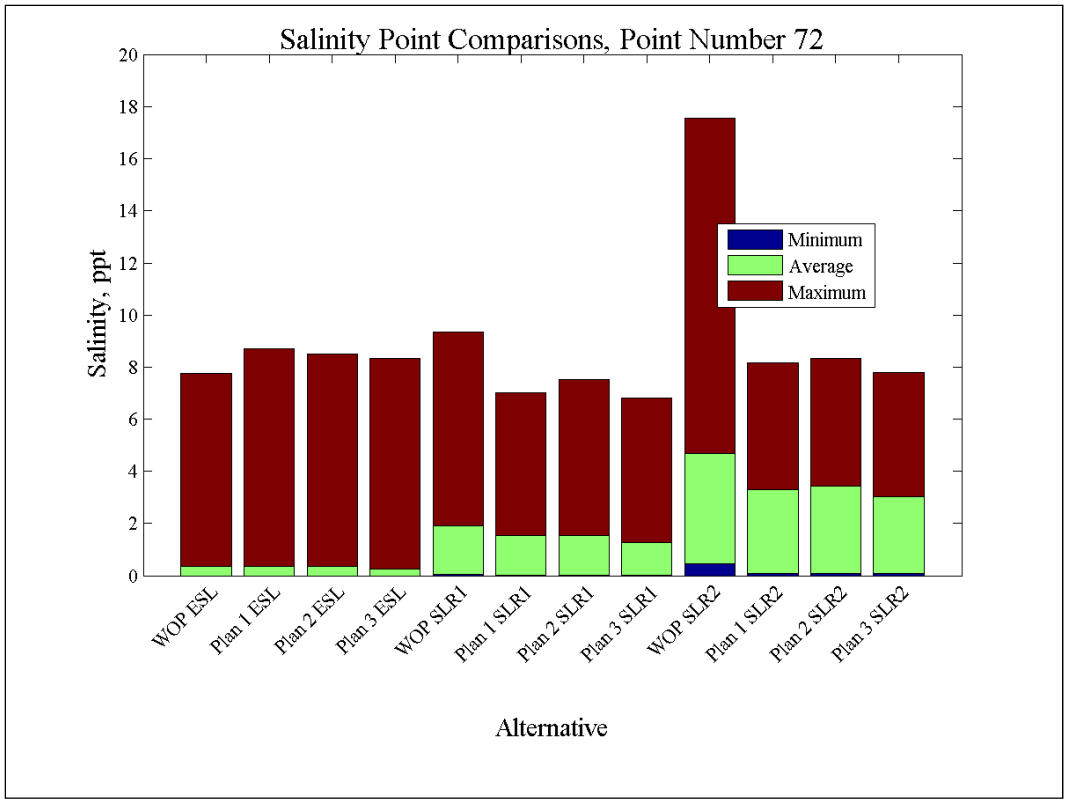

Figure 252. Water-surface elevation and salinity comparisons at Point 73.

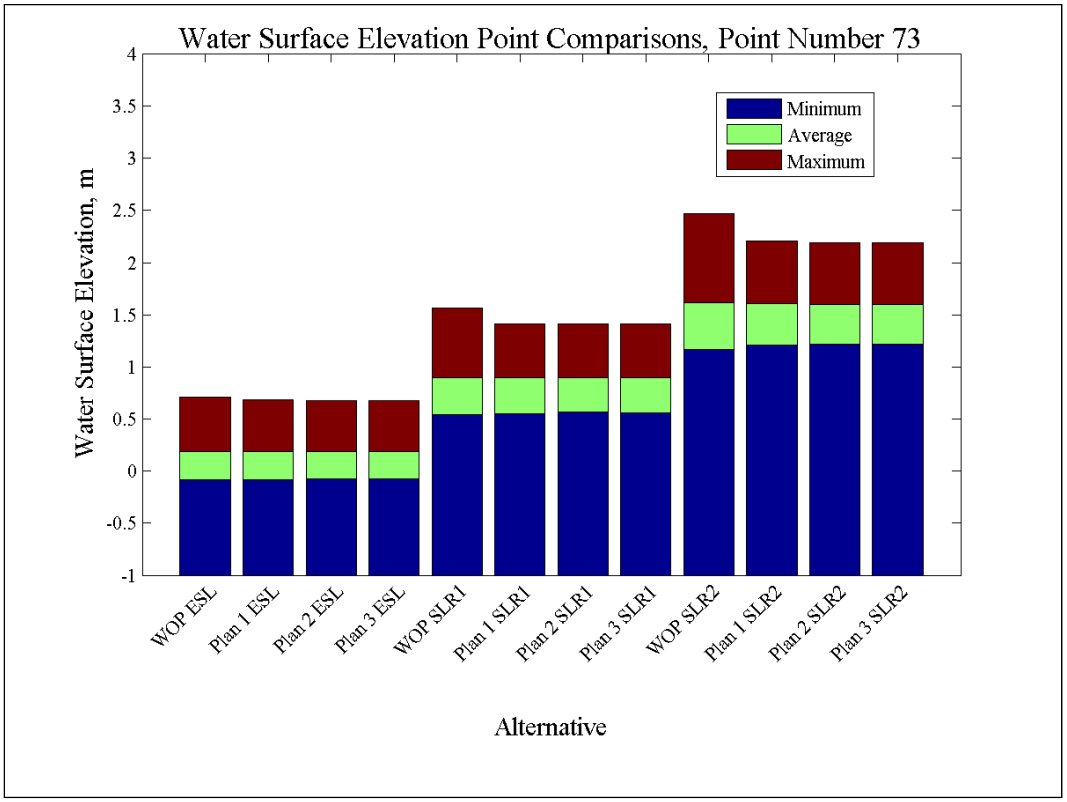

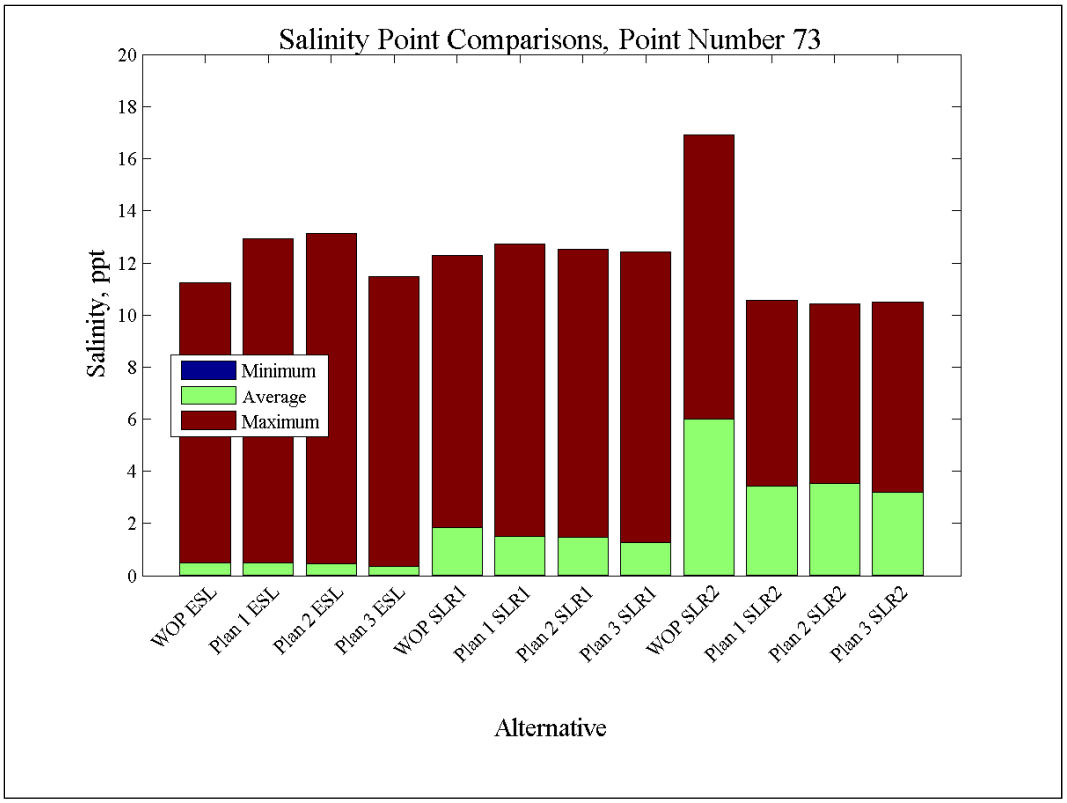

Figure 253. Water-surface elevation and salinity comparisons at Point 74.

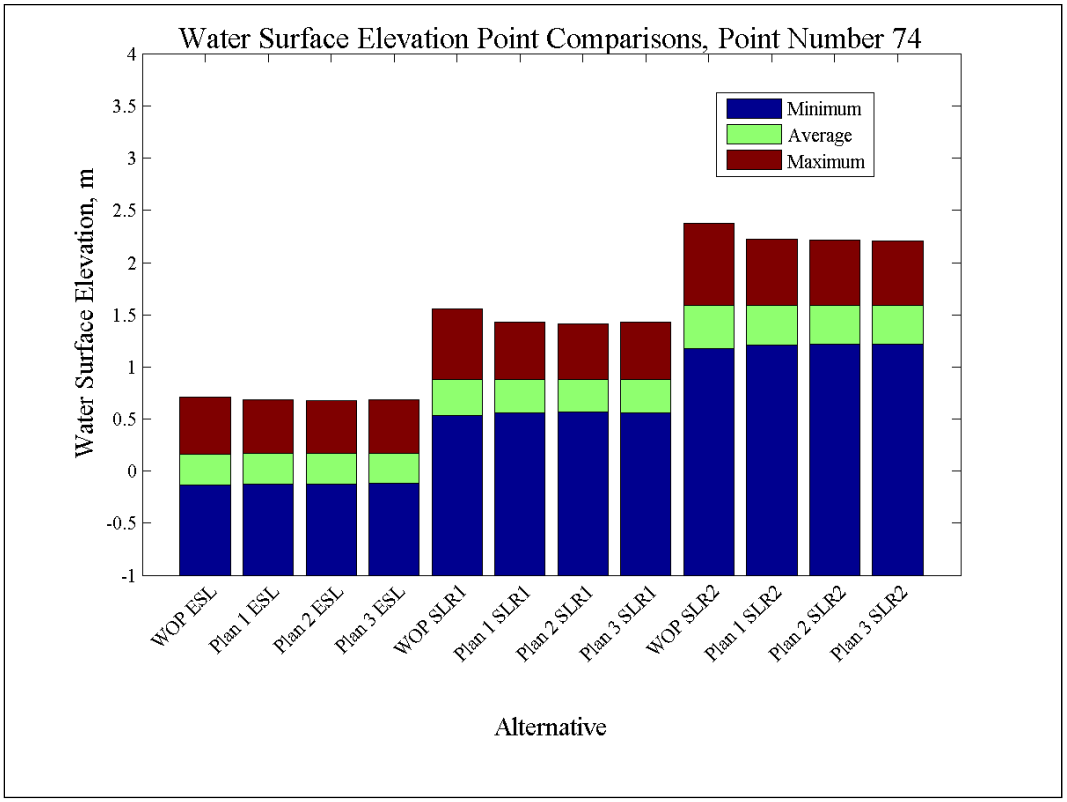

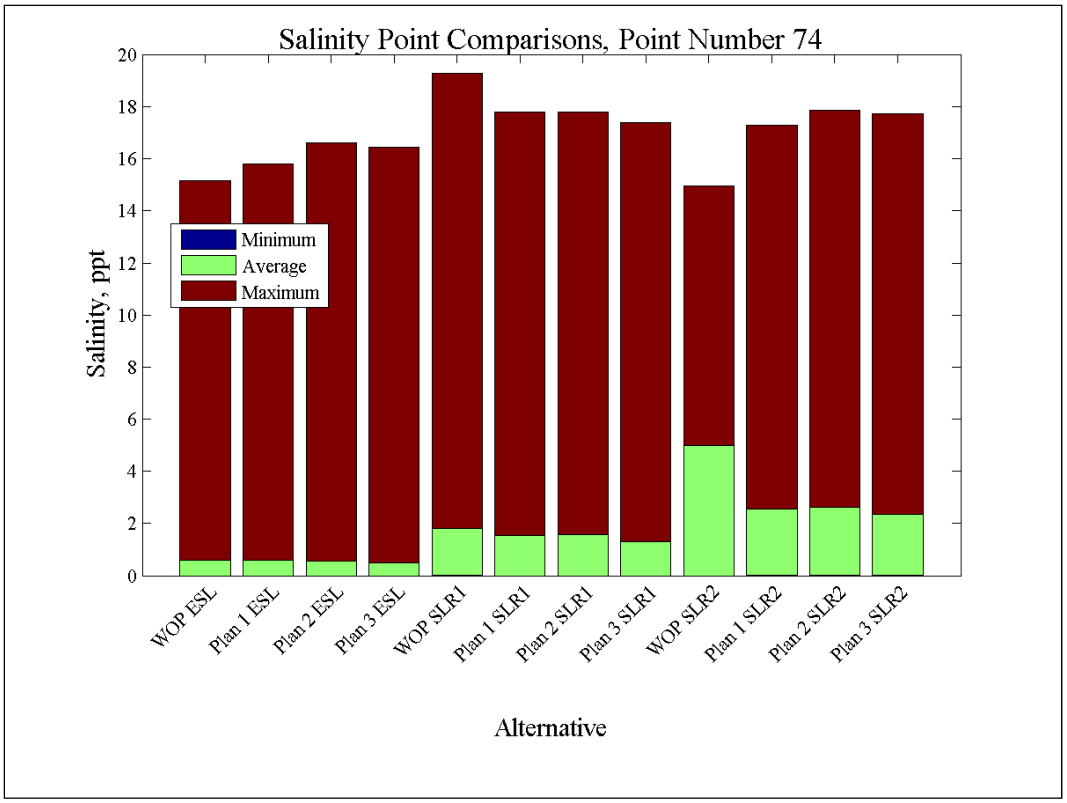

REPORT DOCUMENTATION PAGE

Form Approved
OMB No. 0704-0188

1. REPORT DATE *(DD-MM-YYYY)*	2. REPORT TYPE	3. DATES COVERED *(From - To)*
August 2013	Final	

4. TITLE AND SUBTITLE
Hydrodynamic and Salinity Transport Modeling of the Morganza to the Gulf of Mexico Study Area

5a. CONTRACT NUMBER

5b. GRANT NUMBER

5c. PROGRAM ELEMENT NUMBER

6. AUTHOR(S)
Tate O. McAlpin, Joseph V. Letter, Jr., Gaurav Savant, and Fulton C. Carson

5d. PROJECT NUMBER

5e. TASK NUMBER
MIPR W42HEM03376317

5f. WORK UNIT NUMBER

7. PERFORMING ORGANIZATION NAME(S) AND ADDRESS(ES)
US Army Engineer Research and Development Center
Coastal and Hydraulics Laboratory
3909 Halls Ferry Road
Vicksburg, MS 39180

8. PERFORMING ORGANIZATION REPORT NUMBER
ERDC/CHL TR-13-7

9. SPONSORING / MONITORING AGENCY NAME(S) AND ADDRESS(ES)
US Army Engineer District New Orleans
7400 Leake Ave.
New Orleans, LA 70118-3651

10. SPONSOR/MONITOR'S ACRONYM(S)
MVN

11. SPONSOR/MONITOR'S REPORT NUMBER(S)

12. DISTRIBUTION / AVAILABILITY STATEMENT
Approved for public release; distribution is unlimited.

13. SUPPLEMENTARY NOTES

14. ABSTRACT

This report documents the development of a hydrodynamic and salinity transport model for the Morganza to the Gulf of Mexico study area. The model domain encompasses a significant portion of the Louisiana coastline, extending from Bayou Lafourche (eastern boundary) to the Vermilion Bay (western boundary). This report details the creation of the mesh and all boundary conditions. Also included are model-versus-field comparisons, exhibiting the model's ability to accurately represent the behavior of the system. The validated model (for hydrodynamics and salinity) detailed in this report was utilized to determine approximate base-versus-plan differences for the proposed Morganza to the Gulf of Mexico levee system, including the impacts associated with sea-level rise.

15. SUBJECT TERMS
Adaptive Hydraulics (AdH), Morganza to the Gulf of Mexico, hydrodynamics, salinity transport modeling

16. SECURITY CLASSIFICATION OF:			17. LIMITATION OF ABSTRACT	18. NUMBER OF PAGES	19a. NAME OF RESPONSIBLE PERSON
a. REPORT	b. ABSTRACT	c. THIS PAGE			19b. TELEPHONE NUMBER *(include area code)*
Unclassified	Unclassified	Unclassified		319	